ABSTRACT

Title of Document: EFFECTS OF WINGWALL CONFIGURATIONS ON THE BEHAVIOR OF INTEGRAL ABUTMENT BRIDGES

Andreas Paraschos, Doctor of Philosophy, 2016

Dissertation Directed By: Professor Amde M. Amde
Department of Civil and Environmental Engineering

This research includes parametric studies performed with the use of three-dimensional nonlinear finite element models in order to investigate the effects of cantilever wingwall configurations on the behavior of integral abutment bridges located on straight alignment and zero skew. The parametric studies include all three types of cantilever wingwalls; inline, flared, and U-shaped wingwalls. Bridges analyzed vary in length from 100 to 1200 feet. Soil-structure and soil-pile interaction are included in the analysis. Loadings include dead load in combination with temperature loads in both rising and falling temperatures. Plasticity in the integral abutment piles is investigated by means of nonlinear plasticity models. Cracking in the abutments and stresses in the reinforcing steel are investigated by means of nonlinear concrete models. The effects of wingwall configurations are assessed in terms of stresses in the integral abutment piles, cracking in the abutment walls, stresses in the reinforcing steel of abutment walls, and axial forces induced in the steel girders.

The models developed are analyzed for three types of soil behind the abutments and wingwalls; dense sand, medium dense sand, and loose sand. In addition, the models consider both the case of presence and absence of predrilled holes at the top nine feet of

piles. The soil around the piles below the predrilled holes consists of very stiff clay. The results indicate that for the stresses in the piles, the critical load is temperature contraction and the most critical parameter is the use of predrilled holes. However, for both the stresses in the reinforcing steel and the axial forces induced in the girders, the critical load is temperature expansion and the critical parameter is the bridge length. In addition, the results indicate that the use of cantilever wingwalls in integral abutment bridges results in an increase in the magnitude of axial forces in the steel girders during temperature expansion and generation of pile plasticity at shorter bridge lengths compared to bridges built without cantilever wingwalls.

EFFECTS OF WINGWALL CONFIGURATIONS ON THE BEHAVIOR OF INTEGRAL ABUTMENT BRIDGES

By

Andreas Paraschos

Dissertation submitted to the Faculty of the Graduate School of the
University of Maryland, College Park, in partial fulfillment
of the requirements for the degree of
Doctor of Philosophy
2016

Advisory Committee:

Professor Amde M. Amde, Advisor and chair
Professor Chung C. Fu
Professor Sherif M. Aggour
Professor Bital M. Ayyub
Professor Sung W. Lee

Acknowledgments

I would like to express my special thanks to Professor Amde M. Amde, Ph.D., P.E. of the University of Maryland at College Park for his enthusiastic support throughout the course of this research study. I would like to thank him for his technical advice and guidance throughout the development of this research study.

Table of Contents

Acknowledgements ii

Table of Contents iii

List of Tables vii

List of Figures x

List of Symbols xx

List of Abbreviations xxvii

Chapter 1 Introduction 1

1.1. Background 1
1.1.1. Bridge Engineering 1
1.1.2. Bridge Classifications 2
1.1.3. Conventional Girder Bridges 10
1.1.4. Integral Abutment Bridges 13
1.1.5. Semi-Integral Abutment Bridges 14
1.2. Scope of Work 16
1.3. Objective 16
1.4. Significance of Work 16
1.5. Document Organization 17

Chapter 2 Overview of Integral Abutment Bridges 19

2.1. Introduction 19
2.2. Evolution of Integral Abutment Bridges 20
2.3. Advantages of Integral Abutment Bridges 24
2.4. Limitations on the Use of Integral Abutment Bridges 28

Chapter 3 Literature Review on Integral Abutment Bridges 32

3.1. Introduction 32
3.2. Parameters that Influence the Behavior of Integral Abutment Bridges 32
3.2.1. Loads 33
3.2.2. Skew 50
3.2.3. Curvature 54
3.2.4. Soil-Structure Interaction 55
3.2.5. Soil-Pile Interaction 58

3.2.6. Flexibility of Substructure 62
3.2.7. Foundation Systems 67
3.2.8. Approach Slabs 70
3.2.9. Wingwalls 74
3.2.10. Bridge Length and Movement Limitations 77
3.2.11. Type of Superstructure 79
3.2.12. Construction Sequence 79

Chapter 4 Survey on Integral Abutment Bridges 82

4.1. Introduction 82
4.2. Survey Questions Related to Design Parameters of Use of Integral Abutment Bridges 83
4.3. Survey Questions Related to Status of Use, Problems, and Costs of Integral Abutment Bridges 97

Chapter 5 Selection of Parameters for the Parametric Studies 111

Chapter 6 Parametric Studies 130

6.1. Introduction 130
6.2. Objective of the Parametric Studies 130
6.3. Parametric Studies 130
6.3.1. Bridge Length 130
6.3.2. Span Layout 133
6.3.3. Range and Values of Selected Parameters 133

Chapter 7 Modeling of Soil-Structure Interaction 141

7.1. Introduction 141
7.2. Lateral Earth Pressure 141
7.3. Lateral Earth Pressure Theories 144
7.3.1. Classical Lateral Earth Pressure Theories 144
7.3.2. Other Earth Pressure Theories 148
7.3.3. Seismic Earth Pressures 148
7.4. Lateral Earth Pressures on Bridge Abutments 149
7.4.1. Lateral Earth Pressures on Integral Abutments 149
7.5. Soil Constitutive Models 159
7.5.1. Most Commonly Used Soil Constitutive Models 160
7.5.1.1. Mohr Coulomb Model 160
7.5.1.2. Duncan-Chang Hyperbolic Model 161
7.5.1.3. Drucker-Prager Model and Extended Drucker-Prager Model 163
7.5.1.4. Cam Clay Model and Modified Cam-Clay Model 165
7.5.1.5. Plaxis Hardening Soil Model 166

7.5.2. Selection of Soil Constitutive Model 168
7.5.3. Soil Constitutive Models for Integral Abutment Bridges 170
7.6. Modeling of Soil-Structure Interaction 172
7.6.1. Soil-Structure Modeling Approaches 172
7.6.1.1. Winkler Springs Method 172
7.6.1.2. Interface Element Method 174
7.6.1.3. Contact Analysis Method 180
7.7. Modeling of Soil-Structure Interaction of Integral Abutment Bridges 183
7.8. Modeling of Soil-Structure Interaction for this Research Study 186

Chapter 8 Modeling of Soil-Pile Interaction 188

8.1. Introduction 188
8.2. Modeling of Soil-Pile Interaction 188
8.3. Modified Ramberg-Osgood Model 190
8.4. Analytical Forms of Soil-Pile Interaction Curves 194
8.5. Soil-Pile Interaction Curves 202

Chapter 9 Structural Modeling and Analysis 209

9.1. Introduction 209
9.2. Finite Element Analysis Three-Dimensional Models 209
9.2.1. Modeling Approach 209
9.2.2. Geometric Models 210
9.2.3. ANSYS Elements used in Structural Analyses 211
9.2.4. Element Size 215
9.2.5. Finite Element Models 215
9.3. Structural and Material Modeling 222
9.4. Nonlinear Structural Analysis - Plasticity Model 223
9.4.1. Plasticity Model Theory 223
9.4.1.1. Rate-Independent Plasticity 223
9.4.1.2. Yield Criterion 224
9.4.1.3. Flow Rule 227
9.4.1.4. Hardening Rule 228
9.4.2. Modeling of Plasticity in ANSYS for this study 230
9.4.2.1. Definition of elastic material properties 230
9.4.2.2. Definition of plastic parameters 231
9.4.2.3. Nonlinear solution 231
9.4.2.4. Output from plasticity analysis 233
9.5. Nonlinear Structural Analysis - Concrete Model 235
9.5.1. Academic Research Applications of the Nonlinear ANSYS Concrete Model 236
9.5.2. The Concrete Material Model in ANSYS 237

9.5.3. Modeling of Concrete using Finite Elements 240
9.5.3.1. Discrete Crack Models 240
9.5.3.2. Smeared Crack Models 241
9.5.3.3. Uses of Discrete and Smeared Crack Models 242
9.5.4. Modeling of Steel Reinforcement using Finite Elements 243
9.5.5. Finite Element Modeling using the ANSYS Concrete Model for this Study 245
9.5.5.1. Definition of elastic and plastic properties 245
9.5.5.2. Nonlinear solution 248
9.5.5.3. Output from nonlinear concrete analysis 248
9.6. Validation of Finite Element Models 250

Chapter 10 Results of Parametric Studies 251

10.1. Introduction 251
10.2. Effects of Cantilever Wingwalls on Pile Stresses 252
10.3. Cracking Pattern in Integral Abutments 264
10.4. Stresses in the Reinforcing Steel of Integral Abutments with no Cantilever Wingwalls 267
10.5. Stresses in the Reinforcing Steel of Integral Abutments with Inline Cantilever Wingwalls 272
10.6. Effects of Cantilever Wingwalls on Bridge Superstructure 276
10.7. Ranking of Parameters on the Basis of their Impact on Bridge Elements 286

Chapter 11 Summary of Results, Conclusions, and Recommendations 287

Appendix A Integral Abutment Bridge Survey Questionnaire 295

Appendix B Calculation of Ramberg-Osgood Parameters for HP10X57 and HP12X84 Piles in Loose Sand and Very Stiff Soil 298

Appendix C Calculation of Tangent Modulus for the Nonlinear Plasticity Model 315

References 317

List of Tables

Table 1-1 Span range of various types of bridges

Table 3-1 Maximum allowable limits (Kunin and Alampalli, 1999)

Table 4-1 Integral abutment bridge length limits (ft) with steel girder superstructure

Table 4-2 Integral abutment bridge length limits (ft) with prestressed concrete superstructure

Table 4-3 Integral abutment bridge length limits (ft) with cast-in-place concrete superstructure

Table 4-4 Normal distribution curve results

Table 5-1 Parameters for the research study on wingwall configurations

Table 6-1 Range and values of selected parameters

Table 7-1 Approximate horizontal displacement of a wall to activate active and passive earth pressure conditions (Clough and Duncan 1991)

Table 7-2 Other earth pressure theories

Table 7-3 Common relations for Ks (Sadrekarini and Akbarzad 2009)

Table 8-1 Analytical forms of P-y curves (Greimann et al. 1984)

Table 8-2 Analytical forms of f-z curves (Amde et al. 1987)

Table 8-3 Analytical forms of q-z curves (Amde et al. 1987)

Table 8-4 Spring stiffnesses Kh, Kv, and Kq (Amde et al. 1987)

Table 8-5 Ramberg-Osgood parameters for HP10X57 and HP12X84 piles in loose sand

Table 8-6 Ramberg-Osgood parameters for HP10X57 and HP12X84 piles in very stiff clay

Table 8-7 List of soil-pile interaction curves for the research study

Table 9-1 ANSYS elements used in the finite element analysis models

Table 9-2 ANSYS elements' representation of bridge structural elements

Table 9-3 Element size of structural elements in ANSYS models

Table 9-4 Size of smallest and largest ANSYS finite element models

Table 9-5 Differences between isotropic and kinematic hardening

Table 9-6 Recommendations for use of discrete and smeared crack models (Jendele et al. 2001)

Table 9-7 Material properties defined in the ANSYS concrete model

Table 9-8 Real constants for steel reinforcement

Table 10-1 Bridge length at onset of pile plasticity during temperature contraction No predrilled holes Vs predrilled holes comparison

Table 10-2 Bridge length at onset of pile plasticity during temperature expansion No predrilled holes Vs predrilled holes comparison

Table 10-3 Bridge length at onset of pile plasticity with predrilled holes DL+TC Vs DL+TE comparison

Table 10-4 Bridge length at onset of pile plasticity - No predrilled holes DL+TC Vs DL+TE comparison

Table 10-5 Comparison of equivalent plastic strain EPEQ in a 1200-feet-long bridge No predrilled holes Vs predrilled holes comparison

Table 10-6 Comparison of 2-lane bridges Vs 4-lane bridge in terms of equivalent plastic strain EPEQ in the piles

Table 10-7 Maximum stress in the integral abutment reinforcing steel during temperature expansion with medium dense sand backfill soil and no cantilever wingwalls

Table 10-8 Maximum stress in the integral abutment reinforcing steel during temperature contraction with medium dense sand backfill soil and no cantilever wingwalls

Table 10-9 Bridge length (feet) at onset of yielding of reinforcing steel

Table 10-10 Summary of percentage increase in the magnitude of axial forces introduced into the steel girders

Table 10-11 Effect of the three types of cantilever wingwalls on the magnitude of axial forces introduced into the steel girders

Table 10-12 Ranking of parameters on the basis of their impact on bridge elements

Table C-1 Mechanical properties of ASTM A709 Grade 50

List of Figures

Figure 1-1 Types of movable bridges

Figure 1-2 Types of fixed bridges

Figure 1-3 Bridge types in the United States

Figure 1-4 Superstructure material of in-service bridges

Figure 1-5 Bridge superstructure material trends

Figure 1-6 Maximum span length (ft) of in-service bridges

Figure 1-7 Conventional girder bridge (Greimann et al. 1987)

Figure 1-8 Elements of a conventional girder bridge (Chen and Duan 2000)

Figure 1-9 Stub abutment

Figure 1-10 Cantilever abutment

Figure 1-11 Gravity abutment

Figure 1-12 Counterfort abutment

Figure 1-13 Integral abutment bridge

Figure 1-14 Integral abutment bridge elevation and section view

Figure 1-15 New York State DOT steel superstructure integral abutment

Figure 1-16 New York State DOT semi-integral abutment

Figure 2-1 Bridge bent damaged by a leaking expansion joint

Figure 2-2 Damaged bridge joint

Figure 2-3 Corroded bridge bearing

Figure 2-4 Corroded bridge girder

Figure 2-5 Evolution of integral abutment bridges in the United States

Figure 2-6 Year of construction of highway bridges in the United States (Alampalli 2009)

Figure 2-7 Causes of bridge failures in the United States

Figure 2-8 Appropriate integral abutment bridge layout

Figure 2-9 Inappropriate integral abutment bridge layout

Figure 2-10 Minimum cover over the bottom of the integral abutment

Figure 3-1 AASHTO LRFD HL-93 live load

Figure 3-2 AASHTO HS25 truck load

Figure 3-3 AASHTO HS25 lane load

Figure 3-4 Effects of primary loads, shrinkage, and creep on the superstructure of a hybrid integral bridge (Thippeswamy and GangaRao 1995)

Figure 3-5 Pile orientation in skewed bridges cases 2a and 2b (Greimann et al. 1983)

Figure 3-6 Pile orientation in skewed bridges cases 1a and 1b (Greimann et al. 1983)

Figure 3-7 Pile orientation in skewed bridges (Najib 2002; Najib and Amde 2010)

Figure 3-8 Predrilled hole detail (Yang et al. 1982)

Figure 3-9 Equivalent radius of HP section

Figure 3-10 Strong-axis bending pile orientation

Figure 3-11 Weak-axis bending pile orientation

Figure 3-12 Connection of approach slab to bridge deck (standard Nevada detail)

Figure 3-13 Connection of approach slab to integral abutment (standard Ohio detail)

Figure 3-14 Sleeper slab at the connection of approach slab and roadway pavement

Figure 3-15 Cantilevered inline wingwall (White 2008)

Figure 3-16 Cantilevered U-shaped wingwall (White 2008)

Figure 3-17 Cantilevered flared wingwall (White 2008)

Figure 3-18 Step 1: Placement of abutment embankment

Figure 3-19 Step 2: Excavation for abutment pile cap

Figure 3-20 Step 3: Driving of integral abutment piles

Figure 3-21 Step 4: Construction of integral abutment pile cap

Figure 3-22 Step 5: Construction of deck slab and end diaphragm at abutment

Figure 3-23 Step 6: Placement of backfill and construction of approach slab

Figure 4-1 Type of superstructure for integral abutment bridges

Figure 4-2 Alignment

Figure 4-3 Maximum skew angle for integral abutment bridges

Figure 4-4 Bridge length limits (ft) for zero skew

Figure 4-5 Average bridge length limits (ft) for various skew angles

Figure 4-6 Standard deviation for various skew angles

Figure 4-7 Types of foundations for integral abutment bridges

Figure 4-8 Secondary lateral loads accounted for in pile design

Figure 4-9 Types of wingwalls used with integral abutment bridges

Figure 4-10 Status of use of integral abutment bridges

Figure 4-11 Status of problems with integral abutment bridges

Figure 4-12 Status of comparative construction costs of integral abutment and conventional bridges

Figure 4-13 Status of comparative maintenance costs of integral abutment and conventional bridges

Figure 5-1 Definition of cantilever wingwall length

Figure 6-1 Normal distribution length for length of steel girder integral abutment bridges

Figure 6-2 Soil profile

Figure 7-1 Relationship between displacement and earth pressure

Figure 7-2 Categories of lateral earth pressure

Figure 7-3 Relationship between wall movement and earth pressure (Clough and Duncan 1991)

Figure 7-4 Coulomb theory for active and passive earth pressures

Figure 7-5 Rankine's earth pressure theory (Ou 2006)

Figure 7-6 Comparison of logarithmic spiral and Coulomb's failure surfaces for active conditions (Clough and Duncan 1991)

Figure 7-7 Comparison of logarithmic spiral and Coulomb's failure surfaces for passive conditions (Ou 2006)

Figure 7-8 Canadian Foundation Engineering Manual (1992)

Figure 7-9 Husain and Bagnaroil (1996)

Figure 7-10 Massachusetts DOT Manual (2009)

Figure 7-11 Comparison of abutment displacement to height ratio (Δ/H) versus temperature variation (ΔT) using various methods

Figure 7-12 Earth pressure distribution according to Hassiotis and Xiong (2007)

Figure 7-13 Earth pressure distribution according to the Swedish Bridge Code

Figure 7-14 Earth pressure distribution according to the British Code BA42

Figure 7-15 Earth pressure distribution according to Sanford and Elgaaly (1993)

Figure 7-16 Parameters used for the derivation of Figure 7-17 that depicts earth pressure distribution from various sources (Flener 2004)

Figure 7-17 Comparison of earth pressure distributions behind bridge abutments from different sources

Figure 7-18 Elastic-perfectly plastic assumption of Mohr-Coulomb model (Kok et al. 2009)

Figure 7-19 The Mohr-Coulomb yield surface in principal stress space

Figure 7-20 Hyperbolic stress-strain relation in primary loading for a standard drained triaxial test (Schanz et al. 1999)

Figure 7-21 Mohr-Coulomb (M-C) and Drucker-Prager (D-P) models in the deviatoric

Figure 7-22 Deviatoric plane

Figure 7-23 Mohr-Coulomb, Drucker–Prager, and Extended Drucker-Prager models in the deviatoric plane

Figure 7-24 Critical State Line (Utomo et al. 2007)

Figure 7-25 Yield surface of Cam Clay (dotted line) and Modified Cam Clay (solid line) (Matsuoka and Sun 2006)

Figure 7-26 Representation of total yield contour of the Hardening Soil Model in principal stress space for cohesionless soil (Schanz et al. 1999)

Figure 7-27 Stiffness parameters used in the Hardening Soil model (Obrzud 2010)

Figure 7-28 The location of the representative soil element behind a typical integral abutment (Bloodworth et al. 2012)

Figure 7-29 Winkler Spring Model

Figure 7-30 Goodman's zero thickness interface element (Mayer and Gaul 2008)

Figure 7-31 Goodman's zero thickness interface element and stiffness matrix (Gomez 2000)

Figure 7-32 Thin layer interface element (Mayer and Gaul 2008)

Figure 7-33 Comparison of zero thickness and thin layer interface elements

Figure 7-34 Coulomb friction model (Hibbitt et al. 2002)

Figure 7-35 Use of the Winkler Springs method by Doust (2011)

Figure 7-36 Use of the Interface Element method by Arsoy et al. (2002)

Figure 7-37 Integral abutment movement due to thermal expansion and contraction (David and Forth 2011)

Figure 7-38 Gap between the integral abutment and backfill due to cyclic pressure on the soil over period of time (David and Forth 2011)

Figure 7-39 Force-Displacement curves for the 9-feet high integral abutment with medium dense sand as the backfill soil material

Figure 8-1 Soil springs for soil-pile interaction (Thanasattayawibul 2006)

Figure 8-2 Modified Ramberg-Osgood P-y curve (Amde et al. 1987)

Figure 8-3 Non-dimensional form of the modified Ramberg-Osgood P-y equation (Amde et al. 1987)

Figure 8-4 Non-dimensional form of the modified Ramberg-Osgood f-z equation (Vijayvergiya 1977)

Figure 8-5 f-z curve (Mosher and Dawkins 2000)

Figure 8-6 Shear strength reduction factor (Tomlinson 1957)

Figure 8-7 P-y curves for HP10X57 piles in loose sand

Figure 8-8 P-y curves for HP12X84 piles in loose sand

Figure 8-9 P-y curve for HP10X57 and HP12X84 piles in very stiff clay

Figure 8-10 f-z curve for HP10X57 and HP12X84 piles in loose sand

Figure 8-11 f-z curve for HP10X57 and HP12X84 piles in very stiff clay

Figure 8-12 f/fmax - Z curve for HP10X57 and HP12X84 piles in loose sand

Figure 8-13 f/fmax - Z curve for HP10X57 and HP12X84 piles in very stiff clay

Figure 8-14 q-z curve for HP10X57 and HP12X84 piles in loose sand

Figure 8-15 q-z curve for HP10X57 and HP12X84 piles in very stiff clay

Figure 8-16 q/qmax - Z curve for HP10X57 and HP12X84 piles in loose sand

Figure 8-17 q/qmax - Z curve for HP10X57 and HP12X84 piles in very stiff clay

Figure 9-1 Geometric model of an integral abutment bridge with flared cantilever wingwalls

Figure 9-2 Schematic of integral abutment bridge finite element analysis model

Figure 9-3 Schematic of connection of steel girder to deck slab (Chung and Sotelino 2006)

Figure 9-4 Finite element model of an integral abutment bridge with no cantilever wingwalls

Figure 9-5 Finite element model of an integral abutment bridge with inline cantilever wingwalls

Figure 9-6 Finite element model of an integral abutment bridge with flared cantilever wingwalls at 45 degrees

Figure 9-7 Finite element model of an integral abutment bridge with U-shape cantilever wingwalls at 45 degrees

Figure 9-8 View of deck slab and steel girders' finite element mesh

Figure 9-9 View of pile finite element mesh

Figure 9-10 View of soil-structure and soil-pile interaction

Figure 9-11 View of temperature load during thermal expansion

Figure 9-12 Stress-strain behavior of each of the plasticity options (ANSYS Mechanical APDL and Mechanical Applications Theory Reference 2010)

Figure 9-13 Von Mises criterion for different stress conditions (Wikipedia)

Figure 9-14 Comparison between Von Mises and Tresca criteria (Wikipedia)

Figure 9-15 Isotropic hardening rule (ANSYS Training Material 2010)

Figure 9-16 Stress-strain diagram of isotropic hardening behavior (ANSYS Training Material 2010)

Figure 9-17 Kinematic hardening rule (ANSYS Training Material 2010)

Figure 9-18 Stress-strain diagram of kinematic hardening behavior (ANSYS Training Material 2010)

Figure 9-19 Definition of bilinear isotropic hardening material in ANSYS

Figure 9-20 Traditional Newton-Raphson Method versus Arc-Length Method (ANSYS Mechanical APDL Structural Analysis Guide 2010)

Figure 9-21 Load steps, substeps, and time (ANSYS Mechanical APDL Structural Analysis Guide 2010)

Figure 9-22 Contour of the von Mises equivalent stress SEQV for the case of 1200-feet-long bridge with 10-feet flared cantilever wingwalls

Figure 9-23 Contour of the equivalent plastic strain EPEQ for the case of 1200-feet-long bridge with 10-feet flared cantilever wingwalls

Figure 9-24 Typical uniaxial compressive and tensile stress-strain curve for concrete (Bangash 1989)

Figure 9-25 Three-dimensional failure surface for concrete (ANSYS Mechanical APDL and Mechanical Applications Theory Reference 2010)

Figure 9-26 Early discrete crack modeling (De Borst et al. 2004)

Figure 9-27 Identification of rebar in concrete with discrete reinforcement modeling (Tavarez 2001)

Figure 9-28 Identification of rebar in concrete with smeared reinforcement modeling (Tavarez 2001)

Figure 9-29 Finite element meshes with discrete and smeared reinforcement (Barbosa and Riberio 1998)

Figure 9-30 Stress-strain curve for steel reinforcement

Figure 9-31 Cracking pattern in the integral abutment of an 800-feet-long bridge during temperature expansion (DL+TE)

Figure 9-32 Stresses in the abutment and wingwall rebar of a 400-feet-long bridge with 24-feet-long wingwalls during temperature contraction (DL+TC)

Figure 10-1 Bridge length at onset of pile plasticity during temperature contraction No predrilled holes Vs predrilled holes comparison

Figure 10-2 Bridge length at onset of pile plasticity during temperature expansion No predrilled holes Vs predrilled holes comparison

Figure 10-3 Bridge length at onset of pile plasticity with predrilled holes DL+TC Vs DL+TE comparison

Figure 10-4 Bridge length at onset of pile plasticity - No predrilled holes DL+TC Vs DL+TE comparison

Figure 10-5 Percentage increase in equivalent plastic strain EPEQ for 2-lane bridges 430-feet bridge Vs 1200-feet bridge

Figure 10-6 Comparison of equivalent plastic strain EPEQ in a 1200-feet-long bridge No predrilled holes Vs predrilled holes comparison

Figure 10-7 Percentage increase in equivalent plastic strain EPEQ in a 1200-feet-long bridge - No predrilled holes Vs predrilled holes comparison

Figure 10-8 Contour of the Von Mises equivalent stress SEQV for piles for the most critical scenario during temperature contraction DL+TC

Figure 10-9 Contour of the equivalent plastic strain EPEQ for piles for the most critical scenario during temperature contraction DL+TC

Figure 10-10 Comparison of 2-lane bridges Vs 4-lane bridge in terms of equivalent plastic strain EPEQ in the piles

Figure 10-11 Evolution of cracking pattern in integral abutments with predrilled holes at top nine feet of piles

Figure 10-12 Evolution of cracking pattern in integral abutments with no predrilled holes at top nine feet of piles

Figure 10-13 Cracking in a 1200-feet-long bridge with 24-feet-long inline cantilever wingwalls

Figure 10-14 Abutment rebar modeled with LINK8 spar elements

Figure 10-15 Maximum stress in the integral abutment reinforcing steel during temperature expansion with medium dense sand backfill soil and no cantilever wingwalls

Figure 10-16 Stress in the integral abutment reinforcing steel of 1000-feet-long bridge during temperature expansion with predrilled holes and medium dense sand backfill soil, but no cantilever wingwalls

Figure 10-17 Average stress in the integral abutment reinforcing steel during temperature contraction with medium dense sand backfill soil and no cantilever wingwalls

Figure 10-18 Stress in the abutment and wingwall reinforcing steel of 1100-feet-long integral abutment bridge with dense sand backfill soil, predrilled holes at the top nine feet of piles, and inline cantilever wingwalls during temperature expansion

Figure 10-19 Girder axial forces during temperature expansion using dense sand backfill soil and no predrilled holes at the top nine feet of piles

Figure 10-20 Percentage change in the magnitude of girder axial forces compared to bridges with no wingwalls during temperature expansion using dense sand backfill soil and no predrilled holes at the top nine feet of piles

Figure 10-21 Girder axial forces during temperature expansion using dense sand backfill soil and predrilled holes at the top nine feet of piles

Figure 10-22 Percentage change in the magnitude of girder axial forces compared to bridges with no wingwalls during temperature expansion using dense sand backfill soil and predrilled holes at the top nine feet of piles

Figure 10-23 Girder axial forces during temperature expansion using medium dense sand backfill soil and no predrilled holes at the top nine feet of piles

Figure 10-24 Percentage change in the magnitude of girder axial forces compared to bridges with no wingwalls during temperature expansion using medium dense sand backfill soil and no predrilled holes at the top nine feet of piles

Figure 10-25 Girder axial forces during temperature expansion using medium dense sand backfill soil and predrilled holes at the top nine feet of piles

Figure 10-26 Percentage change in the magnitude of girder axial forces compared to bridges with no wingwalls during temperature expansion using medium dense sand backfill soil and predrilled holes at the top nine feet of piles

Figure 10-27 Girder axial forces during temperature expansion using loose sand backfill soil and no predrilled holes at the top nine feet of piles

Figure 10-28 Percentage change in the magnitude of girder axial forces compared to bridges with no wingwalls during temperature expansion using loose sand backfill soil and no predrilled holes at the top nine feet of piles

Figure 10-29 Girder axial forces during temperature expansion using loose sand backfill soil and predrilled holes at the top nine feet of piles

Figure 10-30 Percentage change in the magnitude of girder axial forces compared to bridges with no wingwalls during temperature expansion using loose sand backfill soil and predrilled holes at the top nine feet of piles

Figure C-1 True stress-true strain curve of low carbon steel

List of Symbols

B	pile width
B	footing width
BR	vehicular braking force
C	cohesion
Ca	adhesion between soil and pile
Cu	undrained cohesion of clay
CE	vehicular centrifugal force from vehicles on a curved roadway
CR	creep of concrete
CT	vehicular collision force on abutments or piers due to vehicles or trains
Cu	undrained cohesion of clay
CV	vessel collision force due to aberrant ships or barges
DC	dead load of structural components and nonstructural attachments
DD	downdrag
DL	dead load
DW	dead load of wearing surfaces and utilities
E	modulus of elasticity
EH	horizontal earth pressure
EI	flexural rigidity
EL	locked-in or residual force effects resulting from the construction process, including the secondary forces from post-tensioning (which are not gravitational dead loads)
EPEQ	equivalent plastic strain

EQ earthquake loads

ES earth pressure from a permanent earth surcharge such as an embankment

EV vertical pressure of earth fill

EX modulus of elasticity

Eoed oedometer loading stiffness modulus

Es modulus of elasticity of soil

E_T tangent modulus

Eur triaxial unloading-reloading stiffness

E_{50} triaxial loading stiffness

F force

FR friction forces on sliding surfaces from structure movements

Fy yield strength

G shear modulus

H abutment height

IC ice load

IM dynamic load allowance

J empirical dimensionless soil parameter

J Jacobian

J_2 second invariant of the deviatoric stress

K earth pressure coefficient

Ka coefficient of active earth pressure

Kh initial lateral stiffness of the soil

Kn normal interface stiffness

Ko coefficient of at rest earth pressure

Kp coefficient of passive earth pressure

Kq initial vertical stiffness of the soil at the pile tip

Ks interface shear stiffness

Ks1 coefficient of subgrade reaction of soil for a plate 1 foot wide

Kv initial vertical stiffness of the soil

L distance

L length

LL vehicular live load

LS live load surcharge

N average standard penetration test (SPT) blow count

Ncorr corrected standard penetration (SPT) test blow count

P lateral soil resistance

P contact pressure

PL pedestrian live load

PRXY Poisson's ratio

Pu ultimate lateral soil resistance at depth z along the pile length

SE settlement effects due to settlement of substructure units on the superstructure

SEQV von Mises equivalent stress

SH shrinkage

STCCC shear transfer coefficient for closed crack

STCUC shear transfer coefficient for open crack

TC temperature contraction

TE temperature expansion

TG temperature gradient due to exposure of the bridge to solar radiation

TU uniform temperature change due to seasonal variation

UCS uniaxial crushing stress

UTCS uniaxial tensile cracking stress

UTS ultimate tensile strength

Vs Poisson's ratio of soil

WA water load resulting from differential water levels, stream flow or buoyancy

WL wind load on live load

WS wind load on structure

Z vertical pile displacement

Z pile tip displacement

Zc vertical pile displacement needed to mobilize the maximum friction force f_{max}

Zc pile tip displacement needed to mobilize the maximum soil resistance at the pile tip q_{max}

a coefficient of thermal expansion and contraction

a shear strength reduction factor

a soil parameter

b_f flange width of steel H pile

d section depth of steel H pile

d abutment displacement

d element thickness

f friction force mobilized at the pile/soil interface

f_1 biaxial crushing stress under the ambient hydrostatic stress state

f_2 uniaxial crushing stress under the ambient hydrostatic stress state

f_c uniaxial crushing stress

f_{cb} biaxial crushing stress

f_{max} maximum friction force mobilized at the pile/soil interface

f_r modulus of rupture

f_t uniaxial tensile cracking stress

f_y yield stress

l element length

lg gross perimeter of the pile

n shape parameter

n_h constant of subgrade reaction

p mean stress

q deviatoric stress

q soil resistance mobilized at the pile tip

q_{max} maximum soil resistance at the pile tip

s deviatoric stress

x depth from the top surface of soil

y lateral displacement of pile

y settlement

y_u lateral displacement of the pile that is associated with an elastic-plastic soil material when the resistance P equals the resistance Pu

y_{50} displacement at one-half of the ultimate soil reaction

β soil parameter

βG	reduced shear modulus
γ	unit weight of soil
γ'	submerged unit weight of soil
δ	soil-wall friction angle
Δ	abutment movement
Δ	abutment displacement
ΔL	elongation
ΔT	temperature change
ΔT	temperature variation
Δn	displacement normal to the interface
Δs	displacement along the interface
ε_{50}	strain of clay at 50 percent of soil strength
ε_{cu}	ultimate strain
$\varepsilon_{elastic}$	true total strain at yield
$\varepsilon_{true\ total}$	true total strain at ultimate tensile strength
μ	coefficient of friction
μ	non-dimensional soil mass per unit length
μE	reduced elastic modulus
ν	Poisson's ratio
π	ratio of a circle's circumference to its diameter and equal to 3.14
σ_1	maximum principal stress
σ_2	intermediate principal stress
σ_3	minimum principal stress

σ_{cu} peak compressive stress

σ_e von Mises equivalent stress

σ_h ambient hydrostatic stress state

σ_m mean or hydrostatic stress

σ_n normal stress acting on the interface

σ_{tu} maximum tensile strength of concrete

σ_y yield stress, material yield parameter

τ shear stress

Φ angle of internal friction of soil

Ψ dilatancy angle

°F degrees Fahrenheit

List of Abbreviations

3-D	Three-dimensional
AASHTO	American Association of State Highway and Transportation Officials
ACI	American Concrete Institute
AISC	American Institute of Steel Construction
ANISO	Anisotropic
APDL	ANSYS Parametric Design Language
A.R.	Aspect Ratio
ASCE	American Society of Civil Engineers
ASME	American Society of Mechanical Engineers
ASTM	American Society for Testing and Materials
BISO	Bilinear Isotropic Hardening
BKIN	Bilinear Kinematic Hardening
BSCE	Boston Society of Civil Engineers
Caltrans	California Department of Transportation
CC	Cam Clay
CFEM	Canadian Foundation Engineering Manual
CPU	Computer Processing Unit
CSL	Critical State Line
CTRE	Center for Transportation Research and Education
DM	Design Manual
DOF	Degree of Freedom

DOT	Department of Transportation
D-P, DP	Drucker-Prager
EF	Each Face
EPS	Expanded Polystyrene
F	Fahrenheit
FDM	Finite Difference Method
FE	Finite Element
FEA	Finite Element Analysis
FHWA	Federal Highway Administration
FLAC	Fast Lagrangian Analysis of Continua
GUI	Graphical User Interface
HL	Highway Load
HS	Highway Semitrailer
IABSE	International Association for Bridge and Structural Engineering
IHRB	Iowa Highway Research Board
K	Kip
Klf	Kips per linear foot
KN	Kilonewton
LRFD	Load and Resistance Factor Design
MassDOT	Massachusetts Department of Transportation
Max.	Maximum
M-C	Mohr-Coulomb
MCC	Modified Cam Clay

MISO	Multilinear Isotropic Hardening
MKIN	Multilinear Kinematic Hardening
MnDOT	Minnesota Department of Transportation
M-O	Mononobe-Okabe
MSE	Mechanically Stabilized Earth
NAVFAC	Naval Facilities Engineering Command
NBI	National Bridge Inventory
NC	Normally Consolidated
NCHRP	National Cooperative Highway Research Program
NHI	National Highway Institute
NJDOT	New Jersey Department of Transportation
No.	Number
NSBA	National Steel Bridge Alliance
NYSDOT	New York State Department of Transportation
OC	Overconsolidated
PCA	Portland Cement Association
PCI	Prestressed Concrete Institute
PS	Prestressed
RC	Reinforced Concrete
RD	Research & Development
SSI	Soil-Structure Interaction
TR	Transportation Research
TRB	Transportation Research Board

Vol.	Volume
VRTC	Virginia Research Transportation Council
WW	Wingwall
et al.	and others
ft	feet
in.	inch
ksi	Kips per square inch
lbs	pounds
m	meters
pcf	pounds per cubic feet
psi	pounds per square inch
pp.	pages

Chapter 1

Introduction

1.1. Background

An integral abutment is a structure where the bridge superstructure (beams and deck) is directly connected to the abutments. During thermal expansion and contraction, the superstructure and abutments move together into and away from the backfill. There are no bearings at the abutments and no expansion joints in the bridge deck.

Integral abutment bridges have been used for decades in the United States. Colorado was the first state to build integral abutments in 1920 followed by Massachusetts, Kansas, Ohio, Oregon, Pennsylvania, and South Dakota in the 1930s and 1940s (Kunin and Alampalli 1999; Burke 1990). As a result of their excellent performance over the years, forty-one states are now using integral abutment bridges. More than 6,955 integral abutment bridges have been built since 1995 raising the total number of integral abutment bridges in the United States to over 13,230 (Maruri and Petro 2004). However, these numbers are probably an underestimate considering the fact that the National Bridge Inventory (NBI) data, which is kept by all the states with information about their bridges, does not differentiate between the different types of abutments and most states do not have other methods for maintaining an inventory of bridges or integral abutments.

Use of integral abutments reduces initial costs because of the elimination of bearings and expansion joints. It also reduces life-cycle costs by minimizing maintenance costs since there is no need to repair any damage from leaking joints. Integral bridges remain in service for longer periods of time with only moderate maintenance and occasional repairs. In addition, they exhibit superior earthquake performance compared to conventional bridges. For these reasons, the current policy of the vast majority of states is to build integral abutment bridges whenever possible.

1.1.1. Bridge Engineering

Bridge Engineering is the branch of engineering that deals with bridges, which are the key elements of the transportation infrastructure. The Federal Highway Administration (FHWA) defines bridges as structures with at least 20 feet of length along the roadway centerline spanning bodies of water, valleys, or highways and afford passage for pedestrians, vehicles, bicycles, and railroads. Structures with length less than 20 feet are classified as culverts. The structural and hydraulic design of bridges is substantially different from culverts, as are construction methods, maintenance requirements, and inspection procedures. All bridges are listed in the National Bridge Inventory (NBI), a database comprised of each state's department of transportation (DOT) bridge inventory.

1.1.2. Bridge Classifications

There are several ways to classify bridge structures:

- ✯ Classification by structural form
- ✯ Classification by type of traffic usage
- ✯ Classification by superstructure material
- ✯ Classification by span length
- ✯ Classification by alignment

(1) Classification by structural form

Depending on whether spans are fixed or movable, bridges are classified either as movable or fixed.

Movable Bridges are bridges having one or more spans capable of being raised, turned, translated or slid from their normal location to provide for the passage of boats or ships for navigation. The typical movable bridge types are bascule, swing, and vertical lift.

Fixed Bridges are bridges without any movable span. There are ten basic types of fixed bridges: Slab, girder, girder and floorbeam, tee beam, box beam, frame, truss, arch, suspension, and cable-stayed.

The December 2010 FHWA Bridge Programs National Bridge Inventory (NBI) Data shows a total of 473,571 bridges. This includes 472,726 fixed bridges (99.8 percent) and 845 movable bridges (0.2 percent).

Movable Bridges

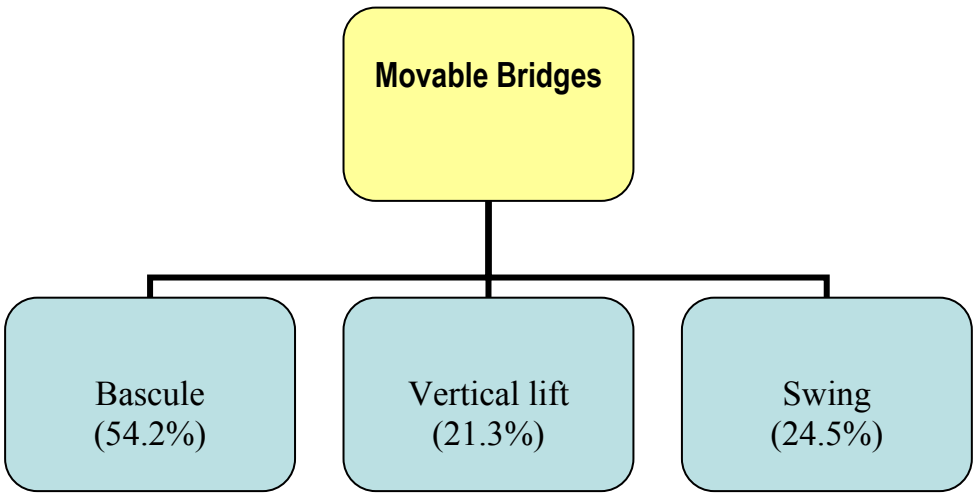

Figure 1-1 Types of movable bridges

Bascule bridges: Bascule bridges are the most common type of movable bridge (Figure 1-1). They pivot upward from a horizontal axis to open. Highway bascules can be either single or double leaf; however, railroad bascules are almost always single leaf so that the heavy railroad live load and impact are taken on fixed substructure elements. Bascule is the French word for teeter-totter, or seesaw.

Vertical lift bridges: Movable bridges in which the span moves up and down without rotating, remaining parallel to the roadway.

Swing bridges: Movable bridges in which the swing bridge, the movable span pivots in the horizontal plane. This type of bridge is built infrequently now, but there are many existing swing bridges that may require rehabilitation.

Fixed Bridges

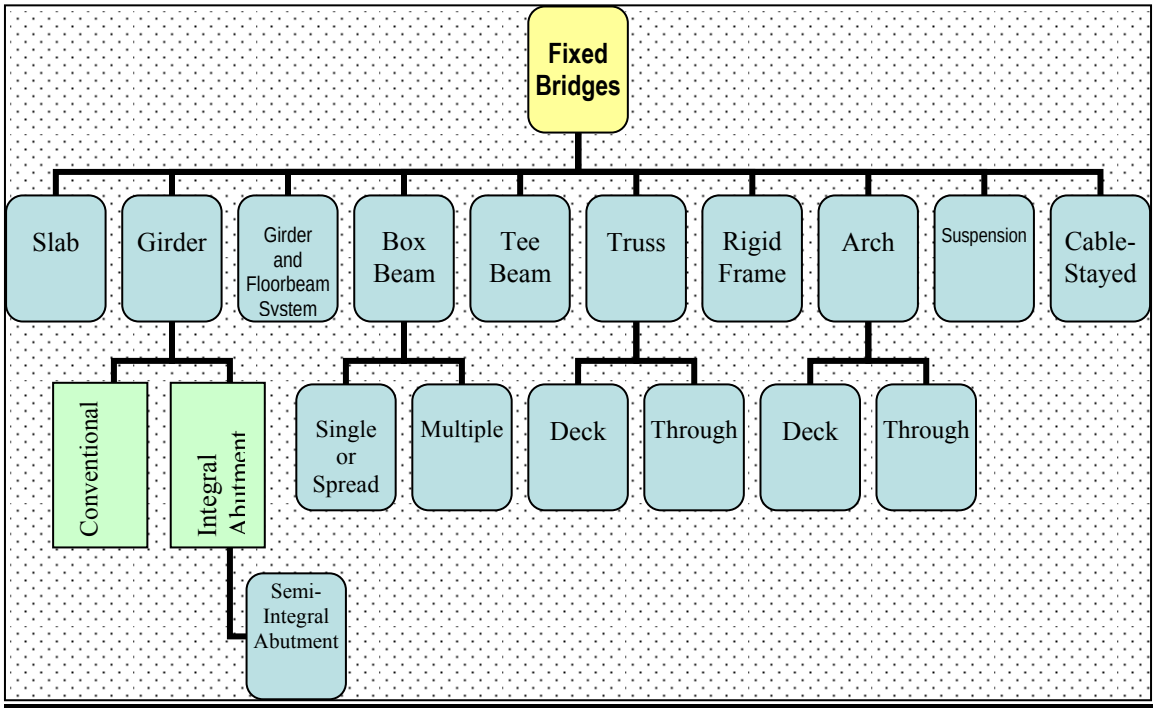

Figure 1-2 Types of fixed bridges

Slab Bridges

Slab bridges are bridges in which the superstructure is composed of single or multiple slabs.

Girder Bridges
Girder bridges are the most common type of bridge (Figure 1-3). They consist of multiple longitudinal members, which directly support the deck slab. Steel members may be either rolled beams or plate girders, depending on span. Prestressed I-girders are also used. Depending on the presence of expansion joints and bearings at the abutments, girder bridges can be classified either as (a) **conventional bridges:** girder bridges with expansion joints in the bridge deck and bearings at the abutments. The ends of girders are supported on the bearings placed on top of the abutments, or (b) **integral abutment bridges:** girder bridges with no expansion joints in the bridge deck and no bearings at the abutments. The ends of girders are integral with the abutments.

Girder and Floorbeam System Bridges
Bridges where the deck slab is supported by floorbeams transverse to the main members, with smaller section stringers spanning between the floorbeams. Usually, there are only two main member sections, but three are sometimes seen on wide bridges. The main girders are almost always riveted or welded plate girders. Floorbeams may be plate girders or rolled sections, while stringers are almost always rolled sections.

Tee Beam Bridges
Bridges with a monolithic concrete deck and beam system formed in the shape of the letter "T".

Box Beam Bridges
Bridges where the deck slab is supported by box beams, which are hollow structural sections having a square, rectangular, or trapezoidal cross section. There are two types of box beam bridges: (a) **multiple box beam bridges:** multiple, longitudinal, voided, prestressed concrete longitudinal beams are placed directly adjacent to each other, and are then post-tensioned together with transverse tendons. Distinct joints separating members can be seen from below. A concrete wearing surface is applied. Note that there is no structural deck for this type, even though the wearing course may be designed to act compositely with the beams, and (b) **single or spread box beam bridges:** they consist of prestressed concrete or steel sections with a trapezoidal or rectangular cross-section. Spread boxes have a structural deck spanning between them.

Rigid Frame Bridges
A rigid frame bridge is one in which the piers and girder are one solid structure. The horizontal and vertical/inclined units of a frame are a rigidly-connected unit, which resists moments and shears. Frames may have either vertical or slanted legs.

Truss Bridges
Truss bridge is a bridge supported by trusses. Depending on the position of the deck relative to the truss, truss bridges can be classified either as (a) **deck truss bridges**: truss bridges in which the deck is located at the same level as the top chord, or (b) **through truss bridges**: truss bridges in which the deck is located either between the trusses or at the lower chord level.

Arch Bridges
An arch bridge is a type of bridge that relies on a curved, semi-circular structure for its support. Depending on the position of the deck relative to the arch, arch bridges can be classified either as (a) **deck arch bridges**: arch bridges in which the deck is located above the top of the arch, or (b)t**hrough arch bridges**: arch bridges in which the deck is placed between the arches.

Suspension Bridges
Bridges where the support is provided by two large wire cables on either side of the roadway. These cables are draped over towers and anchored into concrete blocks embedded into rock at each end. Suspension bridges are used to span wide openings. The structural deck and floor system are supported by vertical cables, which are fastened to the main cables. The deck is often provided with a stiffening truss to reduce the flexibility of the roadway.

Cable-stayed Bridges
Bridges where the superstructure is directly supported by diagonal cables attached to towers at the main piers.

The graph in Figure 1-3 is derived from the December 2010 FHWA Bridge Programs NBI Data. Girder bridges are the most common type of bridge; 13,230 or 5.3 percent of the 249,165 girder bridges are integral abutment bridges (Maruri and Petro 2004).

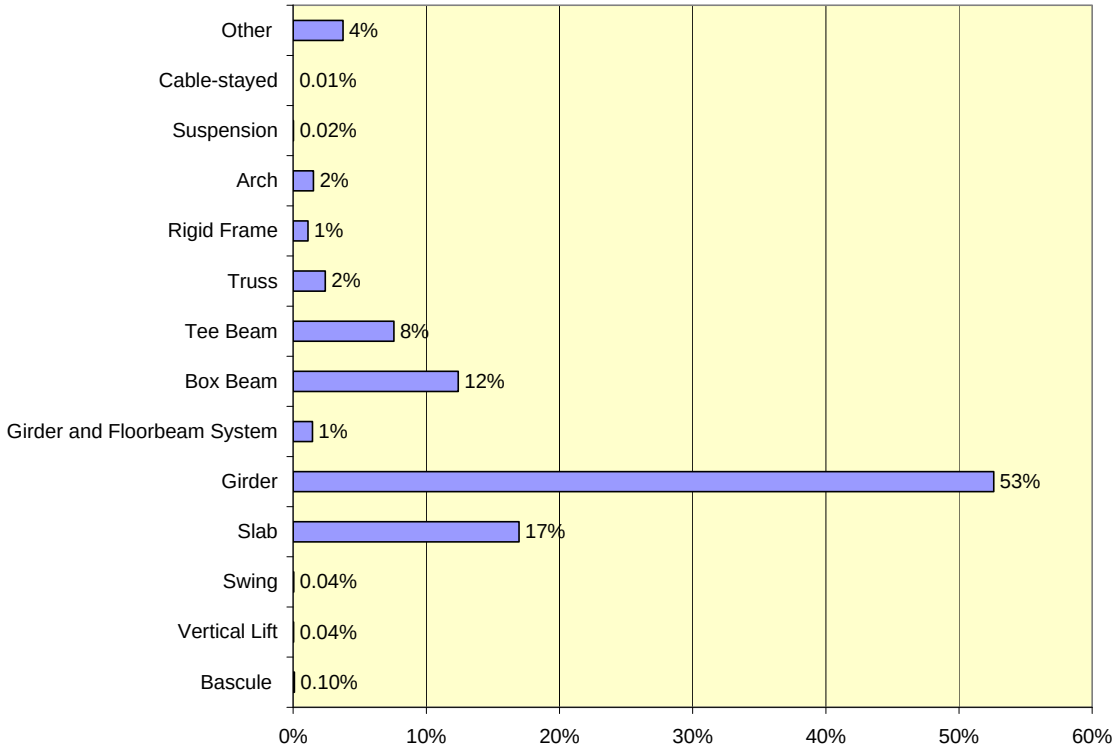

Figure 1-3 Bridge types in the United States

(2) Classification by type of traffic usage

Depending on the type of traffic usage, bridges are classified as:

- Highway bridges: Bridges carrying vehicular traffic
- Pedestrian bridges: Bridges carrying pedestrian traffic
- Railroad bridges: Bridges carrying railroad traffic.

(3) Classification by superstructure material

Depending on the superstructure material, bridges are classified as steel, reinforced concrete, prestressed concrete, and timber. According to the FHWA Bridge Programs NBI 2010 Data that accounts all bridges in service regardless of the year built,

- Steel bridges constitute 30.6 percent of the bridge inventory
- Reinforced concrete bridges constitute 41.6 percent of the bridge inventory
- Prestressed concrete bridges constitute 23.2 percent of the bridge inventory
- Timber bridges constitute 4 percent of the bridge inventory

In addition, masonry, aluminum, wrought iron, cast iron, and composite bridges constitute 0.6 percent of the bridge inventory and classified as "other".

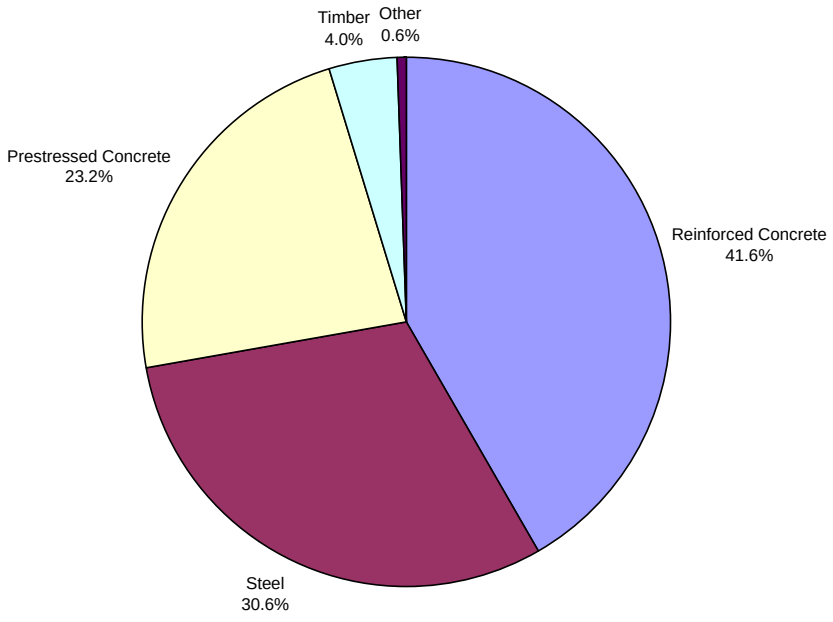

Figure 1-4 Superstructure material of in-service bridges

Many of the in–service bridges were built in the early 1900s. The emergence of prestressed concrete in the 1950s took a market share from the other bridge materials. In fact, approximately 50 percent of new bridges are built with prestressed concrete (Figure 1-5), thus making prestressed concrete the dominant material of today's bridge industry.

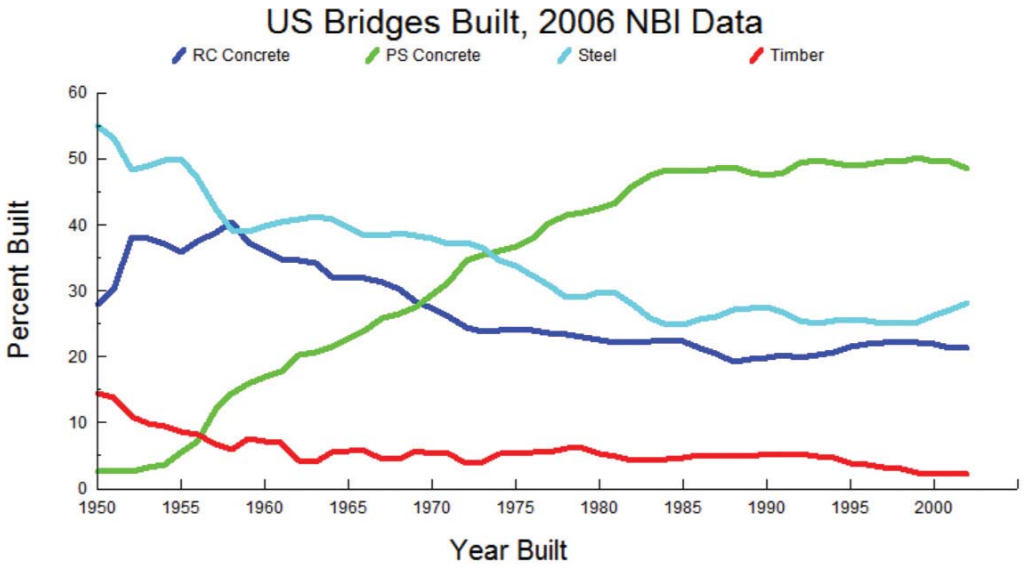

Figure 1-5 Bridge superstructure material trends

(4) Classification by span length

Depending on the length of maximum span, bridges are classified as short span, medium span, and long-span bridges.

- **Short span bridges:** Bridges with their longest span equal to or less than 125 feet.
- **Medium-span bridges**: Bridges with their longest span in the range of 125 feet to 400 feet in length
- **Long-span bridges:** Bridges with one or more spans more than 400 feet in length

Figure 1-6 is based on data furnished in the August 2008 PCA publication "Material Usage and Condition of Existing Bridges in the U.S." The graph indicates that 88.3 percent of bridges have maximum spans 100 feet or less and 56.5 percent of bridges have maximum spans 50 feet or less. In fact, only 1.1 percent of bridges have maximum spans longer than 200 feet.

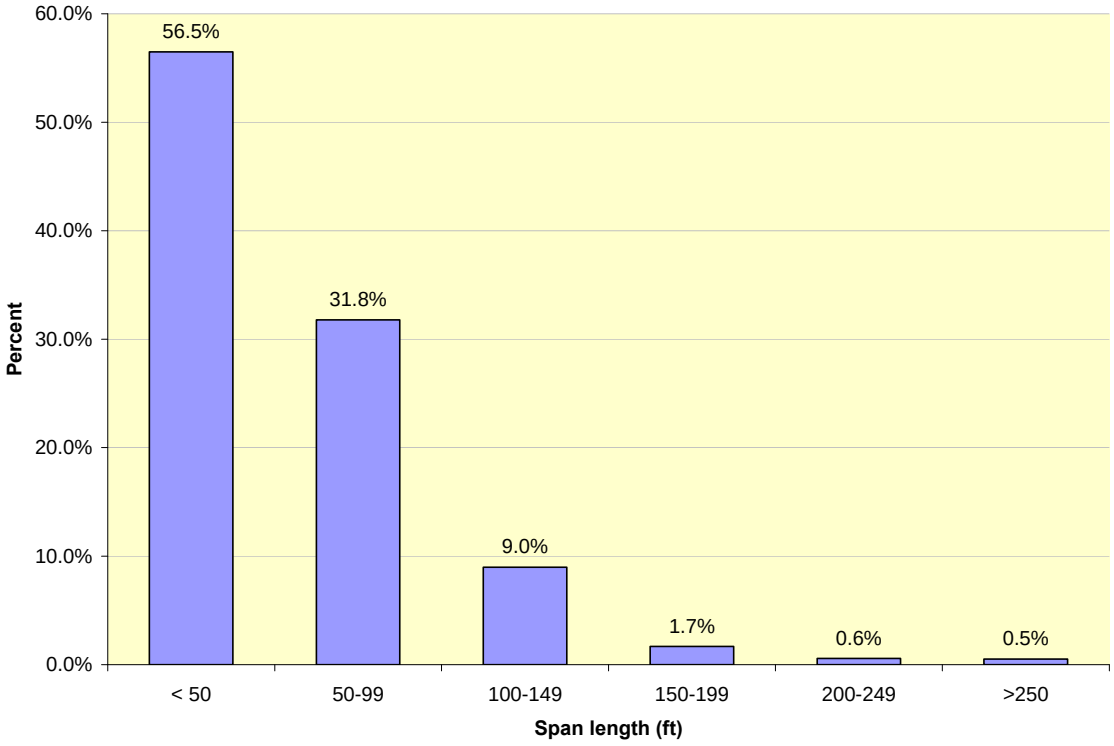

Figure 1-6 Maximum span length (ft) of in-service bridges

Bridge span length varies depending on the bridge's structural form. Table 1-1 illustrates the span range associated with the various types of bridges.

Table 1-1 Span range of various types of bridges

Bridge Type	Span Range (feet)
Slab	0-50
Rolled Beam Bridges (Steel I-Beam)	40-100
Precast Prestressed Girder (a) Precast Box Girder (b) Precast AASHTO I-Girder (c) Tee Beams	40-150
Welded Steel Plate Girder	100-400
Post Tensioned Spliced Girder	180-300
Segmental Girder	200-600
Steel Box Girder	200-600
Truss	500-1200
Arch	500-1200
Cable-Stayed	600-2800
Suspension	1500 to over 4000

(5) Classification by alignment

Bridges are integrated parts of the highway system. As such, they are designed to match the roadway alignment. Bridge alignment is described in terms of both the horizontal and vertical alignment. A vertical alignment is tied to a corresponding horizontal alignment with each alignment anchored together by a common stationing.

Horizontal alignment is the path which defines the geometry of the bridge in plan. This alignment can be represented by a straight tangent, circular curve, or a spiral, that is, a curve with a constantly changing radius. **Vertical alignment** is the path which defines the geometry of a bridge in elevation. A vertical alignment can be represented by a single tangent at a given grade, a vertical curve, or a combination. The vertical alignment greatly affects the vertical clearance of the bridge, which should satisfy code-specified minimum clearances.

The ideal alignment for a bridge structure is not only to be on tangent throughout its entire length, but also to continue the said tangent quite a distance away from the bridge at each end if such can be accomplished without sacrificing the overall geometric design of the highway. Tangent alignment affords easier bridge construction resulting in lower structure cost. In areas where it is not feasible to build structures on a tangent alignment, curved structures are the solution. Although tightly curved alignments can significantly restrict the type of superstructure and sharp curves constitute an invitation for derailment, the number of curved bridges has continued to increase. This is due to the fact that state DOTs find it is more economical to align the bridge to the roadway than align the roadway to the bridge. In fact, one-quarter of steel girder bridges are horizontally-curved steel girder bridges.

Skew

Bridges are also built on a skew if necessary to match alignment of roadways, railroad tracks, or stream flow; skew is the acute angle formed by the intersection of a line normal to the centerline of a roadway with a line parallel to the face of the abutments or piers. Bridges can be designed to accommodate the skew; however, skews are limited to the minimum angle practicable. Skewed bridges that have horizontal curvature require special geometric and structural design.

1.1.3. Conventional Girder Bridges

Conventional girder bridges are girder bridges built with expansion joints in the bridge deck and bearings at the abutments. The ends of girders are supported on the bearings placed on top of the abutments (Figure 1-7). The elements of a conventional girder bridge are shown in Figure 1-8.

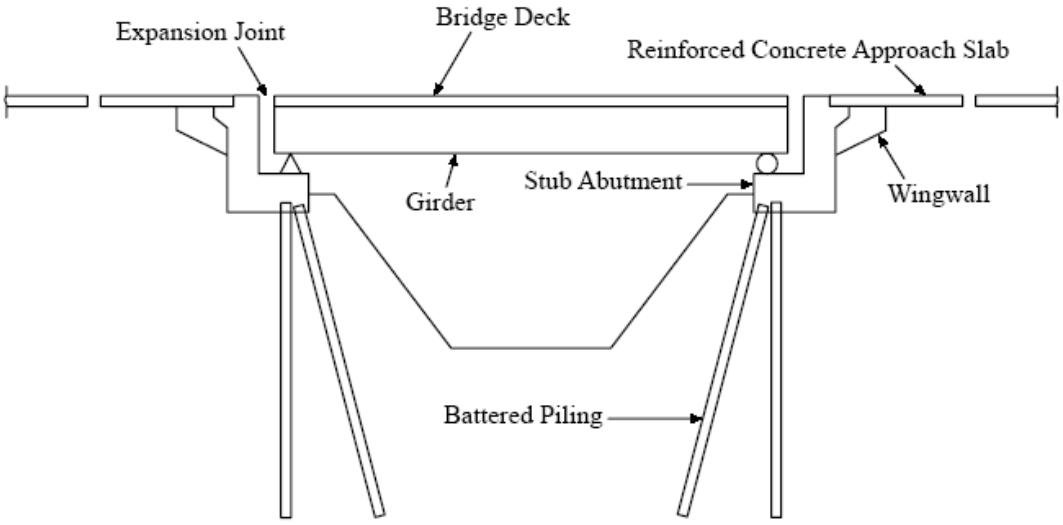

Figure 1-7 Conventional girder bridge (Greimann et al. 1987)

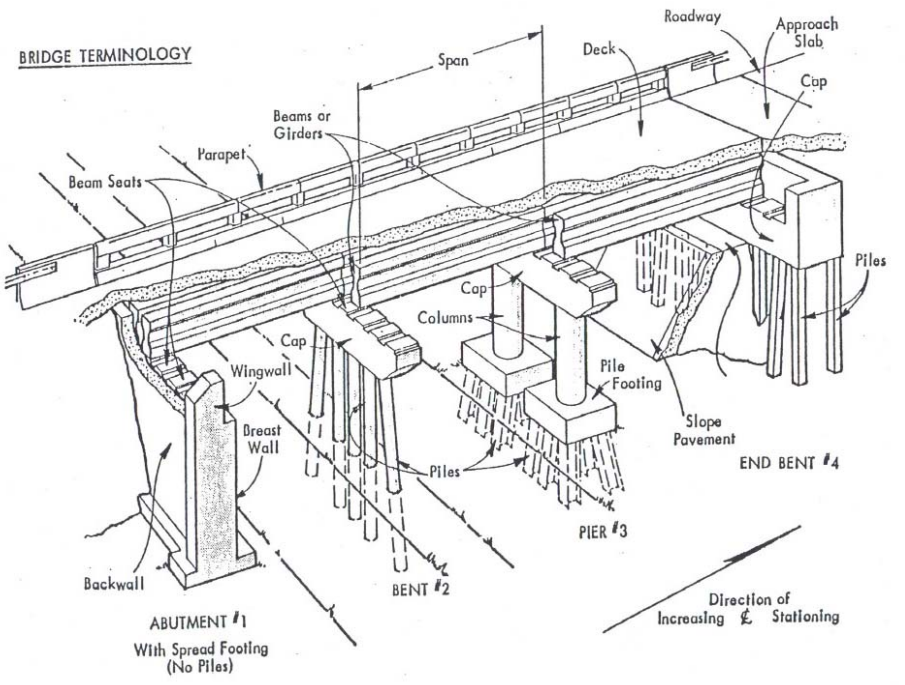

Figure 1-8 Elements of a conventional girder bridge (Chen and Duan 2000)

Abutments in conventional bridges have both expansion joints and bearings. The basic types of abutments in conventional bridges are: (1) stub abutments, (2) cantilever abutments, (3) gravity abutments, and (4) counterfort abutments.

Stub abutments (Figure 1-9) have a backwall with a maximum height of approximately 10 feet. The superstructure members are supported on individual pedestals

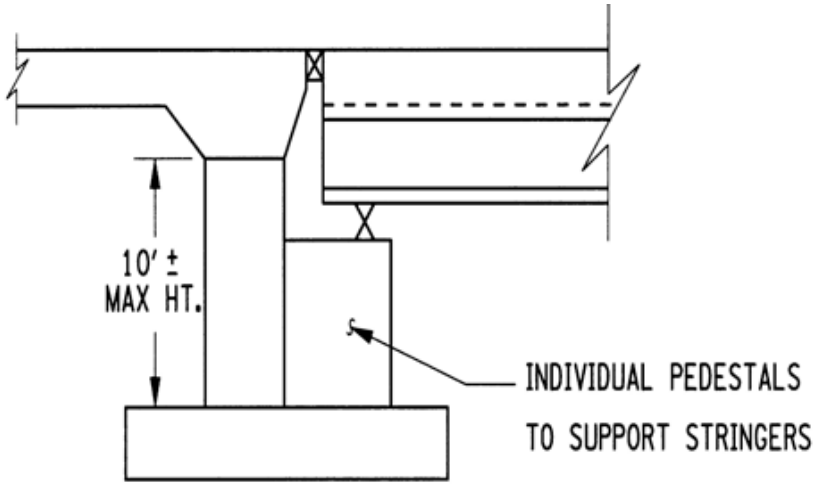

Figure 1-9 Stub abutment

Cantilever Abutments (Figure 1-10) are used when the height of the backwall required exceeds the limits of a stub abutment. The superstructure is supported on a continuous bridge seat.

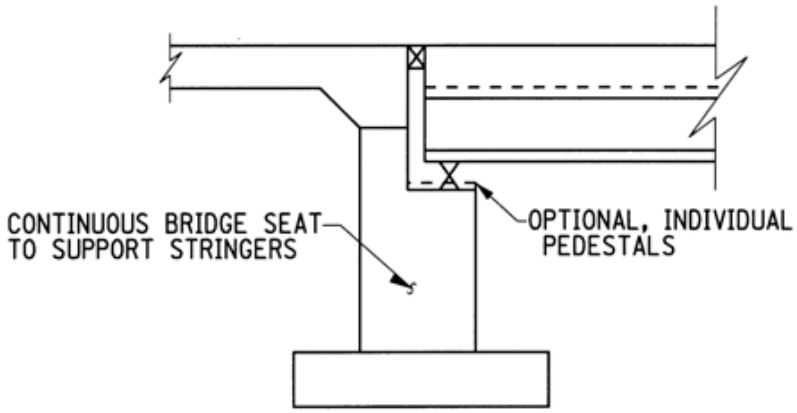

Figure 1-10 Cantilever abutment

Gravity abutments (Figure 1-11) derive their ability to resist applied loads primarily from their size and weight.

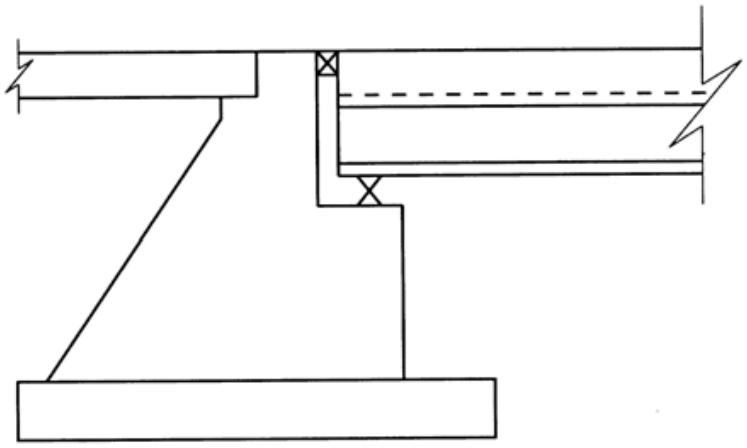

Figure 1-11 Gravity abutment

Counterfort abutments (Figure 1-12) have bracket-like elements which project from the fill side of the backwalls. They provide additional resistance against overturning. The backwall is designed as a horizontal beam between counterforts.

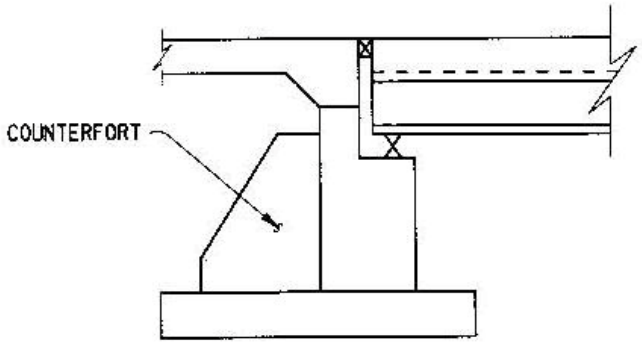

Figure 1-12 Counterfort abutment

1.1.4. Integral Abutment Bridges

Integral abutment bridges are girder bridges with no expansion joints in the bridge deck and no bearings at the abutments (Figures 1-13 and 1-14).

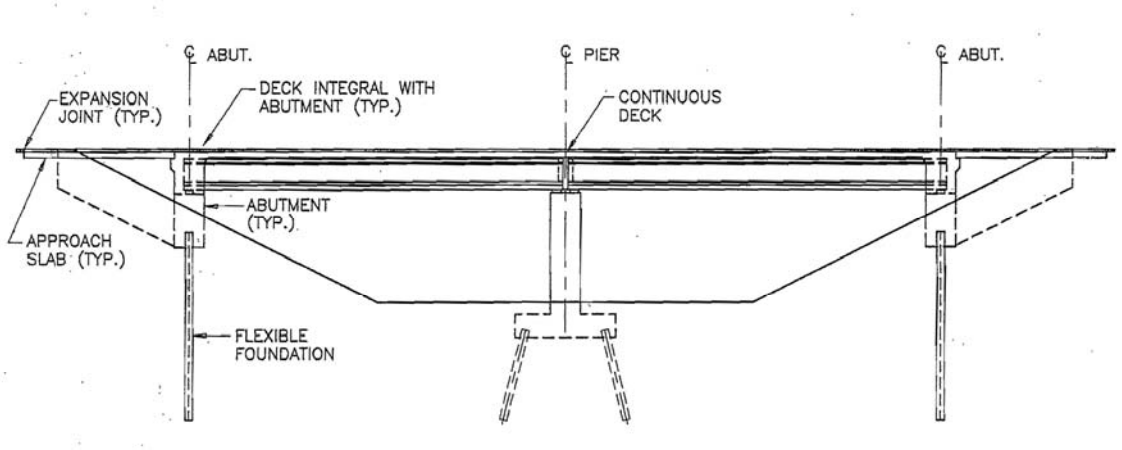

Figure 1-13 Integral abutment bridge

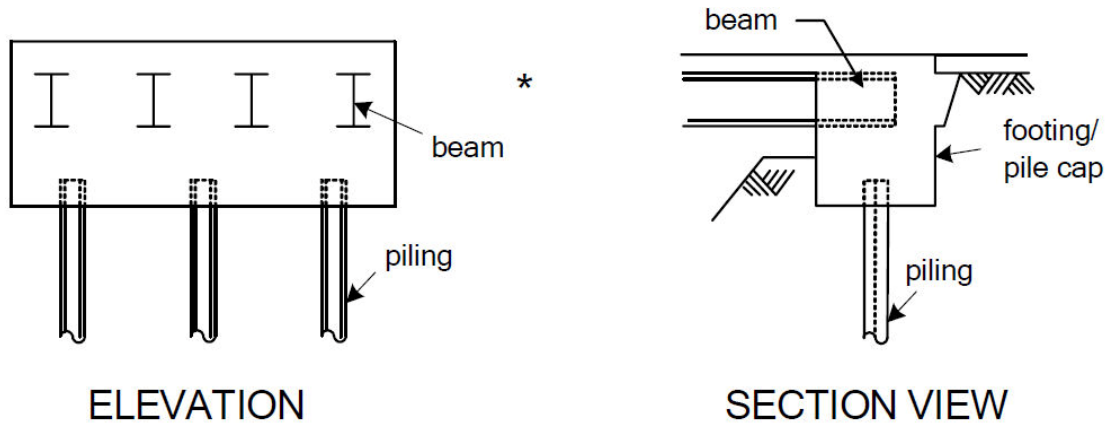

Figure 1-14 Integral abutment bridge elevation and section view

The ends of girders are integral with the abutments, so the name integral abutments. At the integral abutment locations the girders are cast into a concrete end diaphragm, which is rigidly connected to a concrete pile cap. The pile cap is supported by a single row of vertical piles (Figures 1-15). Pile stiffness and flexibility accommodate thermal expansion and contraction of the superstructure.

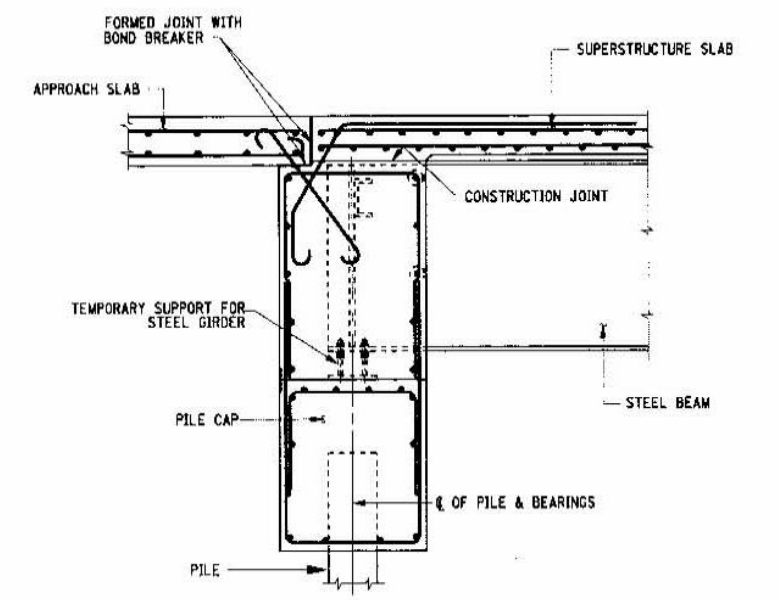

Figure 1-15 New York State DOT steel superstructure integral abutment

Integral abutment bridges differ from conventional bridges and rigid frame bridges in the manner superstructure movement is accommodated. The superstructure movement is due to temperature changes, creep, and shrinkage and is primarily horizontal translation. An integral abutment bridge accommodates superstructure movement by flexure of the piling and the use of cycle-control (expansion) joints at the roadway end of the approach slabs. Conventional bridges accommodate superstructure movement by means of deck expansion joints combined with fixed and expansion bearings. Rigid frame bridges accommodate the effects of temperature change, creep, and shrinkage with full height abutment walls that are fixed or pinned at the footing level.

Use of integral abutment bridges offers numerous advantages over conventional bridges (Chapter 2). As a result, the current policy of the majority of states is to build integral abutment bridges whenever possible. However, there are limitations on the use of integral abutments (Chapter 2). In those instances, state transportation departments recommend the use of semi-integral abutment bridges as the second option with conventional bridges as the third option.

1.1.5. Semi-Integral Abutment Bridges

Semi-integral abutment bridges have no expansion joints in the bridge deck and the superstructure is not rigidly connected to its substructure. The beams extend over the abutment cap, embedded in a backwall (Figure 1-16), and are supported on bearings placed on the abutment cap. This abutment style fits certain conditions that prevent the use of full integral abutments; high abutments that require more than one row of piling, abutments either founded on rock or shallow depth to bedrock, and geometric constraints

calling for higher skews. In addition, semi-integral abutment bridges can accommodate longer bridge lengths than full integral abutments.

The basic feature of the semi-integral abutment detail different from the integral abutment detail is that the superstructure moves longitudinally on elastomeric bearings almost independent of rigid abutment foundations. As a result, the superstructure behavior is independent of the foundation type. Consequently, large spread footings or multiple rows of piles that include battered can be used. In addition, the foundation may be founded on bedrock Superstructure deformations are not transmitted to the foundations and the substructure stiffness does not restrain the superstructure. Construction is more straightforward than for fully integral abutments, while seismic behavior is robust.

Semi-integral abutment bridges have no expansion joints in the bridge deck. Only the backwall portion of the substructure is directly connected to the superstructure. The beams rest on bearings, which rest on the abutment stem. The superstructure, backwall, and approach slab move together into and away from the backfill during thermal expansion and contraction.

Semi-integral abutment structures have been successfully used in many states since the 1970s. In addition, their construction cost is lower compared to conventional abutments with deck joints.

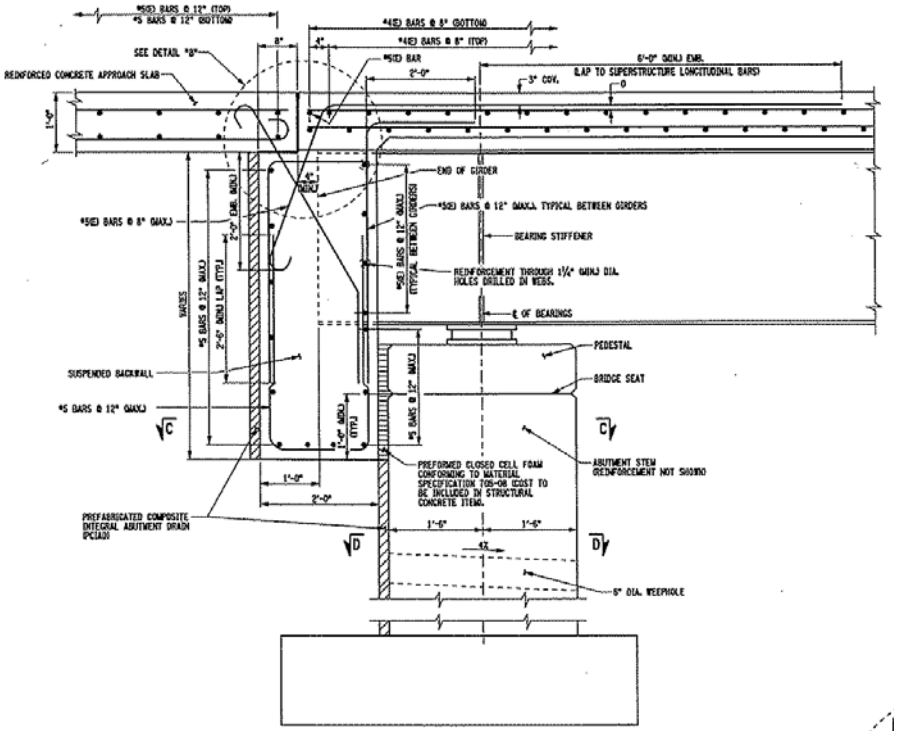

Figure 1-16 New York State DOT semi-integral abutment

1.2. Scope of Work

The scope of work of this study is to investigate the effects of cantilever wingwall configurations on the behavior of integral abutment bridges located on straight alignment. The study presents an overview of integral abutment bridges; it discusses their evolution, their advantages over conventional bridges and their limitations. It includes a literature review of the parameters that influence their behavior and presents the results of a survey of all fifty state departments of transportation in the United States that reflect the current state-of-practice of integral abutment bridges. However, the main focus of this research study are the parametric studies that investigate the effects of cantilever wingwall configurations on the behavior of integral abutment bridges located on straight alignment. The research utilizes three-dimensional nonlinear finite element models; each model incorporates the entire bridge structure, which includes the bridge superstructure, substructure and foundation as well as the soil behind the abutments and wingwalls and around the piles. More specific finite element models for nonlinear pile and nonlinear reinforced concrete analyses are also developed for this research. The effects of cantilever wingwall configurations on skewed integral abutment bridges and bridges on horizontally-curved alignment are not a part of this study.

1.3. Objective

The objective of this research study is to enhance the status of knowledge on the issue of the effects of cantilever wingwalls on the behavior of integral abutment bridges located on straight alignment and zero skew. The conclusions of this study might be used by state agencies as part of their design guidelines for integral abutment bridges.

1.4. Significance of Work

The significance of this research study lies in the fact that by expanding the use of integral abutments, either by building new bridges with integral abutments or retrofitting existing bridges to eliminate deck joints and bearings at the abutments, results in substantial savings in both bridge construction and maintenance costs compared to conventional bridges. Taking into consideration that (1) girder bridges constitute 53 percent of the U.S. bridge inventory, (2) only 5.3 percent of girder bridges are built with integral abutments, (3) ninety percent of the nation's bridges have length of 300 ft or less (Burke 2009) and eighty percent of bridges in the National Bridge Inventory have length of 180 feet or less (Wasserman and Walker 1996; Mistry 2005), a serious argument can be made that there is a potential for substantial savings in both bridge construction and maintenance costs by expanding the use of integral abutment bridges. This can be accomplished by conducting more research on integral abutment bridges in order to eliminate or reduce the number of limitations currently imposed on the use of integral abutment bridges.

In addition, in order to insure safe and reliable performance, integral abutment bridges should be designed as a complete system that works together, rather than as a series of individual components that happen to be connected. Each component should be investigated as to how it affects the overall structure.

Wingwalls are considered part of the bridge substructure only if they are integral with the abutment. In this case, the wingwalls are called cantilever wingwalls. When there is an expansion or construction joint between the abutment and the wingwall, the wingwall is called independent wingwall and is not a part of the bridge substructure. However, use of independent wingwalls with integral abutments is less common (Figure 4-9) because their use creates interaction problems with the integral bridge and complex joints are required. This is due to the fact that while integral abutments are constantly moving (rotating and translating) the independent wingwalls are typically static. Any joint between the two will need to accommodate the movements and there is a risk of differential settlement occurring. Consequently, cantilever wingwalls are much more commonly used with integral abutment bridges than independent wingwalls.

The issue with the use of cantilever wingwalls with integral abutment bridges is the following: Current bridge design procedures used by bridge engineers to design integral abutment bridges built with cantilever wingwalls start with girder design, continue with superstructure design, abutment design, pile design, and end with the design of the cantilever wingwalls. The design procedure does not cycle back to include the effects of wingwall forces on the other bridge elements previously designed. Although wingwalls are not primary load-carrying members of integral abutment bridges their connection to the abutment stem might have an impact on other bridge elements; bridge superstructure, piles, and the integral abutment. The purpose of this study is to investigate those effects and draw conclusions based on the results of the analysis. The significance of this study lies in the fact that the conclusions of this study might lead to elimination of any limitations on the use of cantilever wingwalls on integral abutments or to a significant reduction of those limitations. Conversely, it might lead to further limitations on their use depending on the results of this study.

1.5. Document Organization

The study consists of eleven chapters. The first chapter provides background information on bridge engineering, bridge classifications, conventional girder bridges, integral abutment bridges, and semi-integral abutment bridges. It describes the scope and objectives of this research and explains its significance. The second chapter provides an overview of integral abutment bridges, their evolution, advantages over conventional bridges as well as their limitations. The third chapter presents an extensive literature review on the parameters that influence the behavior of integral abutment bridges. This includes a total of 12 parameters. The fourth chapter presents the results of a national survey on integral abutment bridges that was conducted as part of this research study. The results of the survey reveal the state-of-practice on integral abutment bridges in the United States. The fifth chapter presents the parameters selected for the purpose of this

research and the sixth chapter elaborates on the parametric studies conducted as part of this research. The seventh and eighth chapters are devoted to the modelling of soil-structure and soil-pile interaction respectively. The ninth chapter elaborates on both the structural modeling as well as the types of structural analyses performed. The tenth chapter presents detailed results of the parametric studies. The last chapter presents a summary of both the results and conclusions of this study along with recommendations for future research.

Chapter 2

Overview of Integral Abutment Bridges

2.1. Introduction

Integral abutments got their name because the abutment structure is made integral with the superstructure elements. Bridges with integral abutments are called integral abutment bridges; there are no bearings at the abutments and no expansion joints in the bridge deck. Integral abutment bridges accommodate superstructure movements by flexure of the piling and by provision of cycle-control (expansion) joints at the roadway end of the approach slabs. Due to the elimination of the bridge deck expansion joints, construction and maintenance costs are reduced. The integral abutment bridge concept is based on the assumption that due to the flexibility of piles thermal stresses are transferred to the substructure by way of a rigid connection between the superstructure and substructure meaning the temperature change causes the abutment to translate without rotation. The concrete abutment contains sufficient bulk to be considered rigid. A connection with the ends of the girders is provided by rigidly connecting the girders and by encasing them in reinforced concrete. This provides for full transfer of temperature variation and live load rotational displacements from the superstructure to the piles through the abutment. The abutment wall simply acts as a rigid link between the superstructure and the piles (Husain and Bagnariol 1996).

Integral abutment bridges have been used for decades in the United States. Colorado was the first state to build integral abutments in 1920 followed by Massachusetts, Kansas, Ohio, Oregon, Pennsylvania, and South Dakota in the 1930s and 1940s (Kunin and Alampalli 1999; Burke 1990). As a result of their excellent performance over the years, the current policy of the majority of states is to build integral abutment bridges whenever possible. In fact, AASHTO/NSBA (2011) states that full integral abutments on piles is the most efficient design in most situations and every effort should be made to achieve full integral construction.

This chapter presents an overview of integral abutment bridges. It begins with a discussion on the evolution of integral abutment bridges in the United States, elaborates on the advantages of integral abutment bridges over conventional bridges, and concludes with the limitations on the use of integral abutment bridges.

2.2. Evolution of Integral Abutment Bridges

Early bridge structures were designed as a series of simple spans. The introduction of the Moment Distribution Method developed by Professor Hardy Cross in 1932 allowed structural engineers to eliminate deck joints and one line of bearing devices at piers, and design bridges as continuous structures. As a result of the continuity and negative moments over the interior supports, midspan positive moments were reduced, which in turn led to the construction of longer bridges. Concrete bridge decks, however, experience expansion and contraction as a result of exposure to the environment and the imposition of loads. This led to the provision of deck joints to accommodate bridge deck expansion and contraction.

Unfortunately, the introduction of deck joints creates many problems to bridge owners. Joints are expensive to buy, install, maintain, and repair. Repair costs are high. Besides, joints leak over time, allowing the deicing chemicals used to lower the freezing point of water to attack the girders (Figure 2-4), bearings (Figure 2-3), and supporting reinforced concrete substructures (Figure 2-1). The result is corrosion and deterioration of girders and bearings as well as scaling and spalling of piers and pier caps along with corrosion of reinforcing steel in those members (Amde and Greimann 1988). Bearings are generally much more durable than expansion joints. But, they are also expensive to buy and install and costly to replace. Over time steel bearings tip over and seize up due to loss of lubrication or buildup of corrosion. Elastomeric bearings can split and rupture due to unanticipated movements. Because of these problems, it is necessary to continuously inspect, maintain, and periodically replace the joints. In short, use of expansion joints and bearings to accommodate thermal movement requires maintenance work, even if they are correctly designed and detailed.

Figure 2-1 Bridge bent damaged by a leaking expansion joint

Figure 2-2 Damaged bridge joint

Figure 2-3 Corroded bridge bearing

Figure 2-4 Corroded bridge girder

Integral abutments eliminate the need to provide deck joints. In addition, they can save bridge owners a considerable amount of money, time, and inconvenience compared to conventional abutments. Because of these advantages, states began building integral abutments. Colorado was the first state to build integral abutments in 1920. Massachusetts, Kansas, Ohio, Oregon, Pennsylvania, and South Dakota followed in the 1930s and 1940s (Kunin and Alampalli 1999; Burke 1990). California, New Mexico, and Wyoming built integral abutment bridges in the 1950s. With the National Interstate Highway System construction boom in the late 1950s and mid-'60s. Minnesota, Tennessee, North Dakota, Iowa, Wisconsin, and Washington began moving toward continuous bridges with integral abutments, as standard construction practice. A testament of their excellent performance over the years is the fact that the current policy of the majority of states is to build integral abutment bridges whenever possible. In fact, forty-one states are now using integral abutment bridges. In addition, eight states have more than 1,000 integral abutment bridges; this includes Missouri with more than 4,000 integral abutment bridges and Tennessee with more than 2,000 integral abutment bridges. The nine states that do not use integral abutments are: Alabama, Alaska, Arizona, Delaware, Florida, Louisiana, Mississippi, Texas, and Washington. The evolution of integral abutment bridges over the years is illustrated in Figure 2-5.

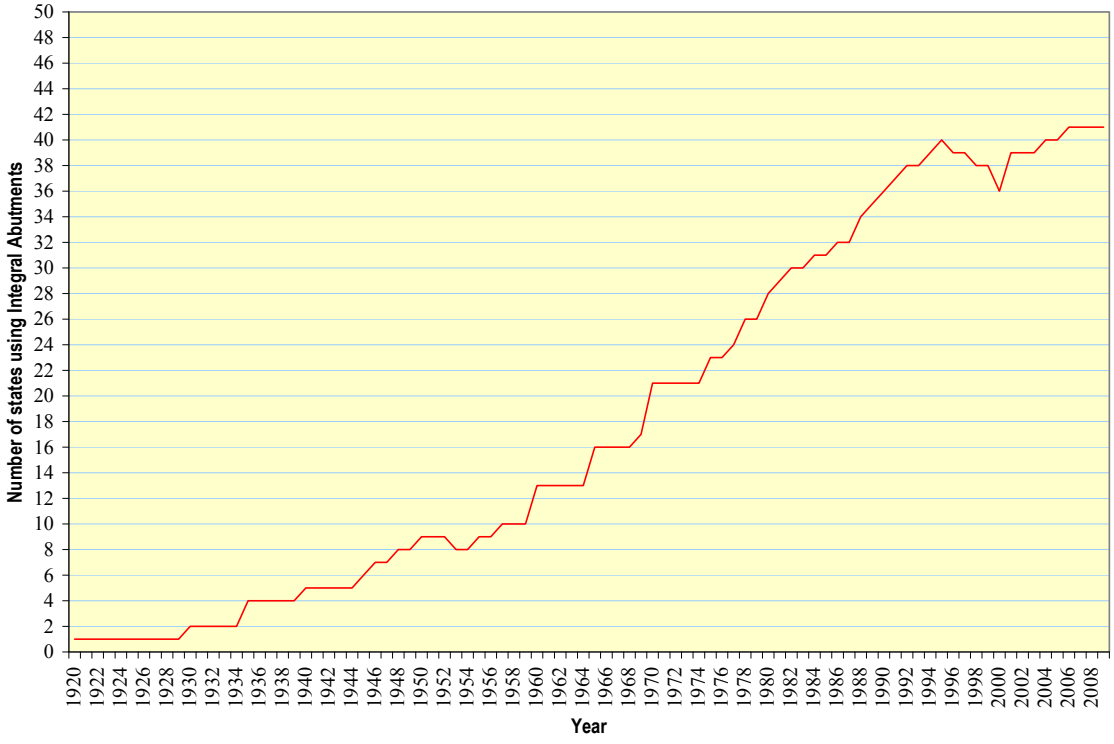

Figure 2-5 Evolution of integral abutment bridges in the United States (Paraschos and Amde 2010, 2011)

State transportation departments set maximum lengths for the integral abutment bridges in their states as illustrated in Tables 4-1, 4-2, and 4-3. However, a number of states allow the use of integral abutment bridges with lengths exceeding those limits provided that an appropriate rigorous detailed structural analysis is performed. As a result, the state of Colorado has the longest steel girder integral bridge in the United States; its length is 1,044 feet. It also has the longest cast-in-place concrete integral bridge with a length of 952 feet. Meanwhile, the State Route 50 Bridge in Hickman County, Tennessee is the longest precast concrete integral bridge in the United States with a length of 1,175 feet.

2.3. Advantages of Integral Abutment Bridges

Integral abutment bridges offer significant advantages over conventional bridges:

- Lower construction costs compared to conventional bridge structures because of the elimination of deck expansion joints and bearings at the abutments. Additional cost savings come from the elimination of cofferdams and from using less concrete and reinforcing steel in the substructure and superstructure. Furthermore, integral abutments have a typical height that is less than that of conventional abutments, reducing the quantity of excavation and backfill materials. In addition, integral abutments require fewer piles for support than do conventional abutments. The responses of the fifty state transportation departments to the survey on integral abutment bridges (Chapter 4) confirms the fact that the vast majority of Departments of Transportation incur lower construction costs with the use of integral abutment bridges compared to conventional bridges.

- Expedite bridge construction compared to conventional bridge structures. Only one row of vertical piles is used meaning fewer piles need to be driven. Because of the elimination of the footing, cofferdams for footing excavation and construction are not needed (Mistry 2005). The entire end diaphragm/backwall can be cast simultaneously with less forming, eliminating the need to form bridge seats. Furthermore, expansion joints and bearings are eliminated. As a result, delays associated with the installation of bearings and expansion joints do not occur. Taking into consideration the fact that the construction of a conventional bridge substructure (abutments and piers) consumes 60 to 70 percent of the time required to construct a bridge (Sprinkel 1978), the advantage of building integral abutment bridges in reference to construction duration becomes obvious.

- Provide significant maintenance cost savings over the life of the structure because of reduced maintenance costs associated with deck expansion joints and bearings (Walker 2013). This is due to minimization of inspection and maintenance operations required. In conventional bridges, much of the cost of maintenance is related to repair of damage at expansion joints and deterioration of both superstructure and substructure from deicing chemicals. According to Maruri and Petro (2004), once joints start leaking account for 70 percent of the deterioration that occurs at the ends of girders, piers, and abutment seats. The responses of the fifty state transportation departments to the survey on integral abutment bridges (Chapter 4) indicate that all states incur lower maintenance costs with the use of integral abutment bridges compared to conventional bridges.

- Minimized traffic disturbances during the course of the life of the bridge due to reduced maintenance requirements.

- Show superior performance when compared to conventional bridges of similar age and exposure (Alampalli and Yannotti 1999; Yannotti et al. 2005). In addition, they

have longer service lives compared to conventional bridges (Burke 1990; Xanthakos 1996). This is due to the fact that they incur less damage during the course of their service life due to elimination of corrosion of girders and reinforcing steel caused by leaking joints loaded with deicing chemicals. According to Barbaccia (2014), 80 percent of state transportation departments cite corrosion, age, and traffic as the top three contributing factors causing the most damage onto the nation's bridges.

- Easier to maintain than conventional bridge structures because of the elimination of the continuous maintenance required for both deck expansion joints and bearings (Mourad and Tabsh 1999).

- Provide enhanced protection for weathering steel girders (Wasserman and Walker 1996). According to FHWA Technical Advisory T 5140.22, the cost effectiveness of weathering steel as a bridge material has been demonstrated in both short-term and long-term savings. The combination of weathering steel and integral abutments offers long-term durability and low maintenance cost.

- Offer a convenient bridge replacement option at a time when 12 percent of the bridges in the United States are classified as *structurally deficient* and their average age is 42 years as shown in Figure 2-6. Integral abutments do not require the typical large footings and battered piles associated with conventional bridges. As a result, they can be built behind existing bridge foundations eliminating the need for additional foundation excavation (Hassiotis and Roman 2005). Conversely, they can be built around the existing foundations without any requirement for complete removal of existing structural elements (Mistry 2005).

- Impact loads (dynamic effects of live load) are reduced because the smooth uninterrupted deck of the integral bridge improves vehicular riding quality (Mistry 2005)and diminishes vehicular impact stress levels.

- Provide enhanced seismic performance compared to conventional bridges (Greimann et al. 1987; Hoppe and Gomez 1996). According to the 1986 Federal Highway Administration report FHWA-RD-86-102, integral abutment bridges are the preferred structures for the most seismically-active regions of the nation. Itani and Pekcan (2011) argue that the seismic performance of integral abutment bridges is better compared to conventional bridges in terms of both overall displacements and forces. In fact, integral abutment bridges have consistently performed well in actual seismic events (Lam and Martin 1986). This is attributed to the elimination of bearings and expansion joints, which are elements of serious concern in earthquake-prone areas. Use of integral abutments eliminates the most common cause of damage to bridges in seismic events, loss of girder support. Furthermore, the dampening effect arising from soil-structure interaction reduces the seismic demand on intermediate substructure columns and footings (Wasserman and Walker 1996; Wasserman 2007).

- Provide a reserve live load capacity to resist potentially damaging overloads that represent 10 percent of bridge failures in the United States (Figure 2-7). This is possible because loads are distributed through the continuous and full-depth end diaphragm at bridge ends (Wasserman and Walker 1996).

- Offer design efficiencies in substructure design due to the increase in the number of supports over which longitudinal and transverse superstructure loads may be distributed (Walker 2013). For example, the longitudinal load distribution for the bent supporting a two-span bridge is reduced by 67 percent when integral abutments are used in the place of abutments with expansion bearings. Depending whether fixed or expansion bearings are used at the abutments, transverse loadings on the same bent can be reduced by 67 percent as well (Wasserman 2007).

- Allow a lower continuous-span ratio and therefore shorter end spans: In multi-span bridges with equal spans, the sagging moment at the midspan of the end span is largest. In order to achieve optimal economical design, the magnitude of this moment is reduced by decreasing the end span to 0.75 of inner spans. The NYSDOT Bridge Manual indicates that for optimal economic design, three-span bridges should be designed with a span ratio of 0.75:1.0:0.75, four-span bridges with a span ratio of 0.8:1.0:1.0:0.8, and five-span bridges with a span ratio of 0.6:0.8:1.0:0.8:0.6. Problem is, using shorter end spans may result in uplift at the end-span supports, which will require the use of either tie-down systems or anchoring of the end spans; both of which are expensive operations. A cheaper alternative is the use of integral abutments. According to Wasserman (2007), integral abutments eliminate uplift by using their weight as a counterweight. The National Steel Bridge Alliance (NSBA) Steel Bridge Design Handbook states that end spans shorter than 0.6 times the adjacent interior span can be used for integral abutment bridges. In fact, Harvey and Kennedy (2002) report the use of a span ratio of 0.25:1.0:0.25 for the Forbidden Plateau Underpass steel integral abutment bridge, a part of the Vancouver Island Highway Project completed in 2001. Use of such broad span ratios allows for longer interior spans over roadways and rivers. This arrangement can accommodate environmental restrictions for bridges spanning over waterways, which may include environmentally-sensitive areas. In addition, constructing fewer or no piers within the water allows a wider flood section that can better handle flood conditions. Furthermore, constructing foundations in waterways escalates construction costs because of the need to include the costs for cofferdams, dewatering, and barge mounted equipment (NSBA Steel Bridge Design Handbook).

- Lead to reduced environmental impacts (Allen 2010) compared to conventional abutments. Integral abutments are located farther away from the streams, which minimizes the effects on stream water. In addition, a longer superstructure allows more room below for wildlife passages.

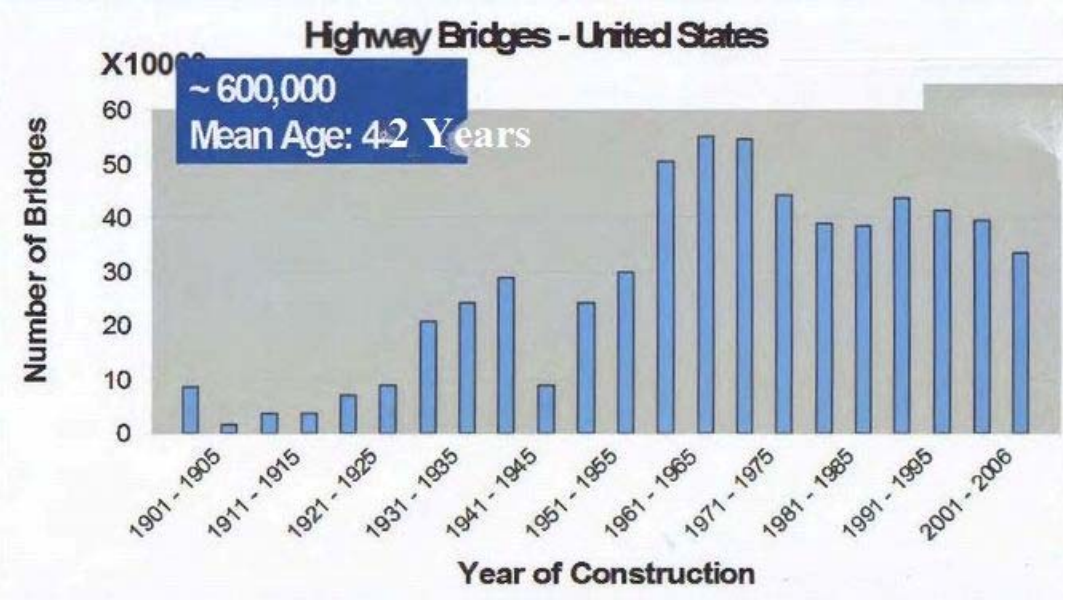

Figure 2-6 Year of construction of highway bridges in the United States (Alampalli 2009)

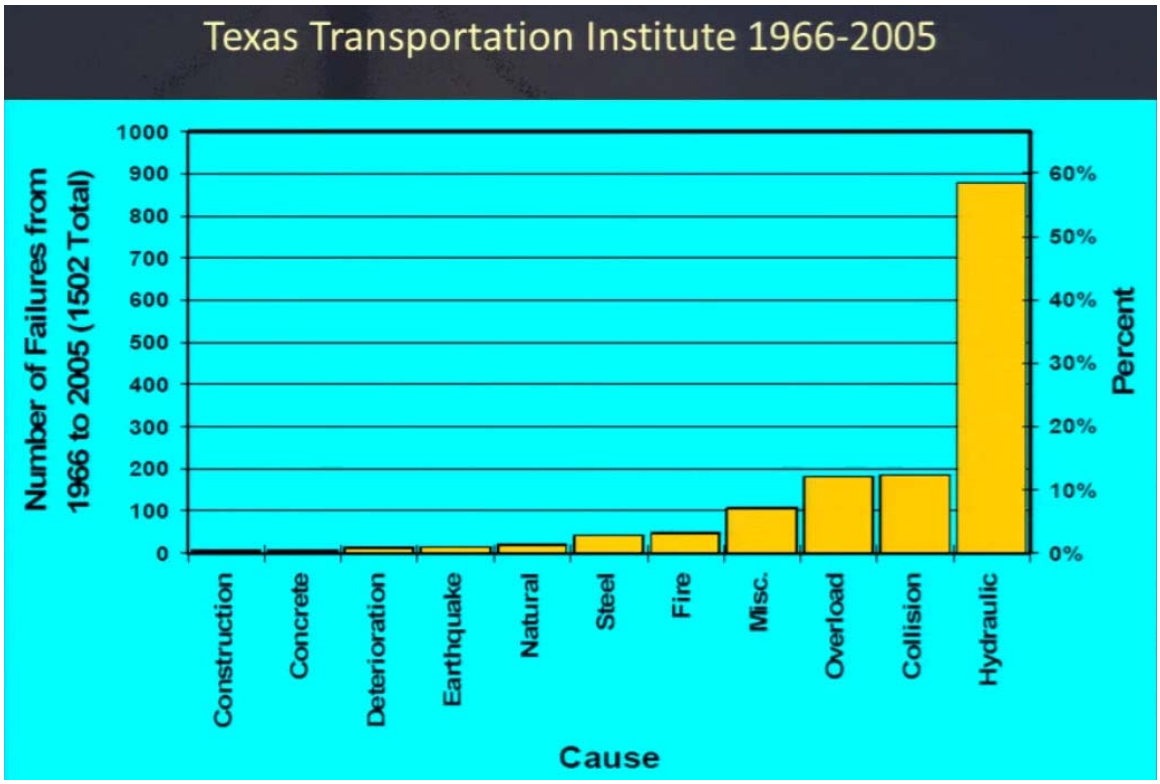

Figure 2-7 Causes of bridge failures in the United States

2.4. Limitations on the Use of Integral Abutment Bridges

The use of integral abutment bridges has its limitations. The purpose of these limitations is to reduce the magnitude of stresses in the piles of integral abutments and the magnitude of passive earth pressures behind the integral abutments. A major reason for this conservatism is the fact that there has been very little verification of the behavior of integral abutment bridges or direct evaluation of the validity of design assumptions through field monitoring (Bonczar et al. 2005). The list of limitations includes:

- Limitations on bridge length; each state sets its own bridge length limits as evidenced by the responses to the survey on integral abutment bridges (Chapter 4). According to FHWA National Bridge Inventory (NBI) Data Dictionary, bridge length is the distance from back to back of abutment backwalls measured along the centerline of the roadway. Length limits for integral abutment bridges vary by superstructure material (Chapter 4).

- Limitations on skew; each state sets its own limits on skew as evidenced by the responses to the survey on integral abutment bridges (Chapter 4).

- Limitations on the amount of allowable thermal movement (Kunin and Alampalli 1999).

- Limitations on horizontal alignment; only a limited number of states allow integral abutment bridges on horizontally-curved alignment (Chapter 4).

- Limitations on the height of integral abutments (Kunin and Alampalli 1999). Integral abutment height is the vertical distance from the top of the deck to the bottom of the pile cap (Figure 1-15). The intent of keeping the abutment as short as possible is to reduce the magnitude of earth pressures exerted on the abutments. However, a minimum penetration of abutment into the backfill for frost protection should be provided (Husain and Bagnariol 1996). This is accomplished by providing a minimum fill cover over the bottom of the abutment (MassDOT 2009) as shown in Figure 2-10.

- Limitations on backfill material: compacted backfill behind integral abutments is the preferred option of the vast majority of states (Chapter 4). The backfill shall be non-cohesive, well-graded, and free draining (White 2012). Flowable fill has very high passive pressure resistance and it should not be used behind integral abutments as per Federal Highway Administration Report FHWA-IF-09-010.

.

- Provisions for approach slabs (Burke 1993) to prevent vehicular compaction of backfill adjacent to abutments, that is, to eliminate live load surcharging of backfill, and to minimize the adverse effect of consolidating backfill and approach embankments on movement of vehicular traffic. In addition, the continual cyclic movement of integral bridges requires anchoring of the approach slabs to the

bridges; otherwise continual bridge movement and joint infiltration will shift slabs toward the flexible approach pavement, away from abutments.

- Provisions for cycle-control (expansion) joints at the roadway end of the approach slabs in order to accommodate the cyclic thermal movement of the bridge resulting from temperature variations (Burke 1993). In addition, the cycle-control joints shall be located beyond the end of wingwalls requiring an approach slab of appropriate length (Hartt et al. 2006).

- Limitations on both pile material and size of piles supporting the integral abutments (Burke 1993).

- Limitations on the use of piles under wingwalls as evidenced by the responses to the survey on integral abutment bridges (Chapter 4).

- Limitations based on type of soil present at the bridge site; if the soil in the site is susceptible to liquefaction, integral abutment bridges are not suitable for the site. According to the response of Alaska DOT to the survey on integral abutment bridges (Chapter 4), "slender end-bearing piles in liquefiable soils are vulnerable to instability as liquefaction reduces the soil support, rendering the piles as effectively unsupported slender columns."

- Provisions for predrilled holes around piles in stiff soil conditions. The holes which are sufficiently deep and wide, are filled with loose granular soil to increase pile flexibility. Use of predrilled holes reduces bending stresses in the piles and increases their vertical load capacity (Yang et al. 1985; Greimann et al. 1986; Greimann and Amde 1988; Faraji 1997; Najib 2002; Khodair and Hassiotis 2003).

- Use of minimum length of piling. This is due to the fact that the overall length of a pile is relevant to the pile's flexibility and its ability to accommodate abutment movement—the longer the pile, the more flexible is (GangaRao et al. 1996) and the higher is its lateral load carrying capacity (Begum and Muthukkumaran 2008). Therefore, there is a need to ensure that
  - The piles have sufficient flexibility to accommodate the horizontal displacements of the superstructure (Mistry 2005) and that the depth of overburden provides fixed support conditions. This precludes the use of integral abutments where the depth to bedrock is considered shallow, less than 13 feet from the ground surface (Hartt et al. 2006) or where piles cannot be driven through at least 10 to 15 feet of overburden (Burke 1993; Hoppe and Gomez 1996). Others (Vermont Agency of Transportation Integral Abutment Bridge Design Guidelines) stipulate a minimum pile embedment length of 16 feet below the bottom of the pile cap. For instances where one abutment is founded directly on bedrock, but there is sufficient depth for piles to flex at the other abutment, the abutment on bedrock may simply be considered the center of the bridge and piles at the other abutment can be checked for thermal movement based on the entire length of the bridge, rather than half the length (Dunker and Abu-Hawash 2005).

- The anticipated scour at the abutments is within the limits of piles regardless of whether countermeasures have been installed (Virginia DOT 2007). When scour is anticipated in addition to erosion prevention using rip-rap, the pile length shall be extended beyond the depth of computed maximum scour to ensure sufficient pile embedment (Kunin and Alampalli 2000) and the stability of the structure (Vermont Agency of Transportation Integral Abutment Bridge Design Guidelines).

- Need for an appropriate layout as illustrated in Figure 2-8 as opposed to Figure 2-9

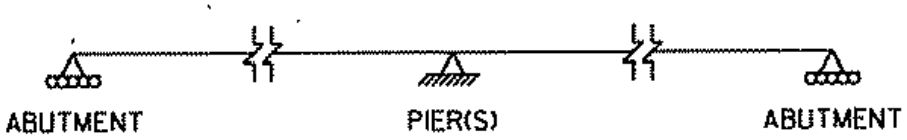

Figure 2-8 Appropriate integral abutment bridge layout

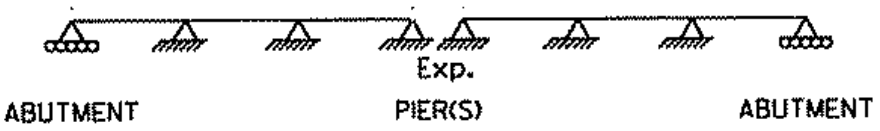

Figure 2-9 Inappropriate integral abutment bridge layout

- Span arrangement and interior bearing selection should be such that approximately equal movement will occur at each abutment (Amde and Greimann 1988) to balance the passive pressures. This can be achieved with a symmetrical or close to symmetrical layout. For this reason (a) for the case of an even number of continuous spans, fixed bearings at the center pier shall be used, and (b) for the case of an odd number of continuous spans, fixed bearings at both center piers shall be used. (Virginia DOT 2007).

- Integral abutments are of equal height so lateral loads are balanced and to protect against sidesway (Crovo 1998; Husain and Bagnariol 2000). This is due to the fact that a difference in abutment heights causes more movement to take place at the shorter abutment during both thermal expansion and thermal contraction (Knickerbocker et al. 2005; MassDOT 2009).

- The difference in elevation between the integral abutments shall not exceed five percent of the bridge length (Amde and Greimann 1988; Crovo 1998).

- Construction of integral abutment bridges shall be performed with an appropriate construction sequence (Burke 1999; Harvey and Kennedy 2002; Wasserman 2007).

- Use of open steel grid, concrete-filled steel grid, and timber bridge decks is unsuitable for integral abutment bridges (GangaRao et al. 1996).

- Stage construction is not allowed when integral abutments are used (Amde and Greimann 1988).

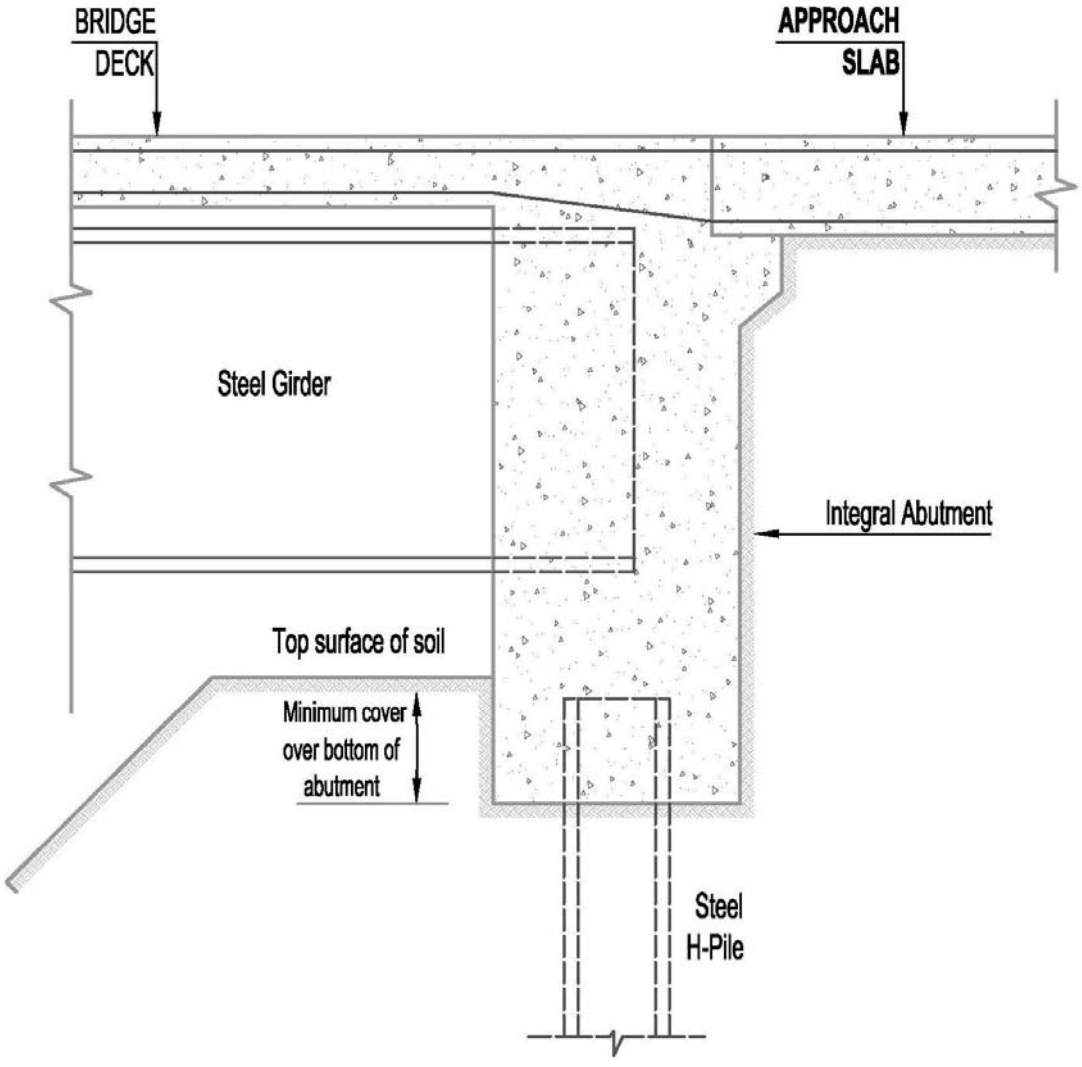

Figure 2-10 Minimum cover over the bottom of the integral abutment

Chapter 3

Literature Review on Integral Abutment Bridges

3.1. Introduction

Integral abutment bridges are single or multiple span bridges in which the superstructure is cast integrally with the substructure. There are no bearings at the abutments and no expansion joints in the bridge deck. The performance of integral abutment bridges depends on many variables. Because of the complex interactions between these variables, there is no consensus in the engineering community about the behavior of integral abutment bridges. In fact, there are no national specifications on integral abutment bridges. Instead, each state has developed its own guidelines for integral abutment bridge design (Chapter 4).

This chapter discusses the parameters that affect the behavior of integral abutment bridges.

3.2. Parameters that Influence the Behavior of Integral Abutment Bridges

This part of the study on integral abutment bridges looks into the parameters that influence the behavior of integral abutment bridges:

- Loads
- Skew
- Curvature
- Soil-structure interaction
- Soil-pile interaction
- Flexibility of substructure
- Foundation system
- Approach slabs
- Wingwalls
- Bridge length and movement limitations
- Type of superstructure
- Construction sequence

3.2.1. Loads

Depending on whether the loading can lead to a progressive collapse of a highway bridge, loads are classified either as primary or secondary. Primary loads include the dead loads, gravity vehicular live load, and earthquake loads. Secondary loads include the force effects due to superimposed deformations (thermal, creep, shrinkage, and settlement loads); earth pressures; wind loads; vehicular loads due to longitudinal (braking) forces, centrifugal forces, and collision forces; water and stream loads; and pedestrian live loads.

Primary loads

Primary loads are loads that can lead to a progressive collapse of a bridge structure. This includes dead loads, gravity live load, and earthquake loads.

With respect to primary loads, the type of connection that exists between the superstructure and its foundation mainly affects the seismic loading. In general, integral abutments are preferred in more active seismic regions and have performed well in actual seismic events (Lam and Martin 1986). They are advantageous because they eliminate the possibility of girder support loss, the most common cause of damage to a bridge during a seismic event. Integral abutments also offer significant material reduction by eliminating the need for large bridge seats and restrainers (Hoppe and Gomez 1996; Wasserman and Walker 1996; Faraji 1997; Goel 1997).

Dead load

Dead load is the permanent weight of all structural and nonstructural components of a bridge, including the appurtenances and utilities attached to the bridge, earth cover, wearing surfaces, future overlays and planned widenings. In the LRFD Specification, the component dead load (denoted as DC) is assumed to consist of all the structure dead load except for non-integral wearing surfaces and any specified utility loads (denoted as DW).

The following unit weights are used to calculate the dead load (AASHTO LRFD Bridge Design Specifications, 7th edition, 2014):

Steel	490 pcf
Hard wood	60 pcf
Soft wood	50 pcf
Concrete normal weight with f"c up to 5 Ksi	145 pcf
Concrete normal weight with f"c higher than 5 Ksi	[140+ f"c(Ksi)] pcf
Compacted sand, silt or clay	120 pcf
Loose sand, silt, or gravel	100 pcf
Salt water	62.4 pcf
Bituminous wearing surface	140 pcf

The dead load on the abutments of integral abutment bridges are distributed equally to all integral abutment piles.

Live load

Currently, the AASHTO LRFD Bridge Design Specifications is the design document used to design new and replacement highway bridges while the AASHTO Standard Specifications for Highway Bridges continue to be used as the design document for highway bridge repairs and rehabilitations. The LRFD vehicular live load model is the HL-93 live load (Figure 3-1). The AASHTO Standard Specifications live load model is the most critical of the HS25 truck load (Figure 3-2) and HS25 lane load (Figure 3-3). The first edition of the AASHTO LRFD Specifications was published in 1994 and the latest edition (7th edition) in 2014. The first edition of the AASHTO Standard Specifications was published in 1931 and the last edition (17th edition) in 2002.

The AASHTO LRFD HL-93 live load consists of two parts: either a design truck or a design tandem each combined with a design lane load. The truck is essentially the same as the axle load portion of the HS20-44 truck, and the design tandem is the same as a military load with the exception of the axle weights, which are 25 kips each rather than 24 kips. The design lane load is a uniform load of 0.64 k/ft

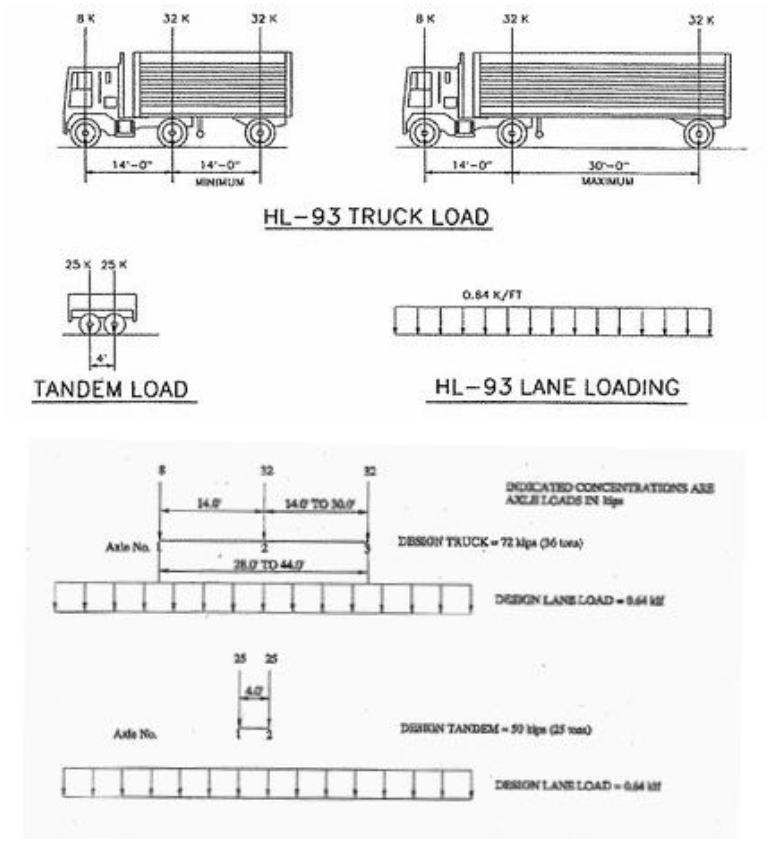

Figure 3-1 AASHTO LRFD HL-93 live load

The AASHTO HS25 truck (Figure 3-2) is 25 percent heavier than the HS20 truck and consists of a two-axle tractor truck with a one-axle semitrailer. The semitrailer axle weighs 10 kips; consists of two wheel loads 5 kips each spaced at 6 feet. The two tractor axles weigh 40 kips each; they consist of two wheel loads 20 kips each spaced at 6 feet.

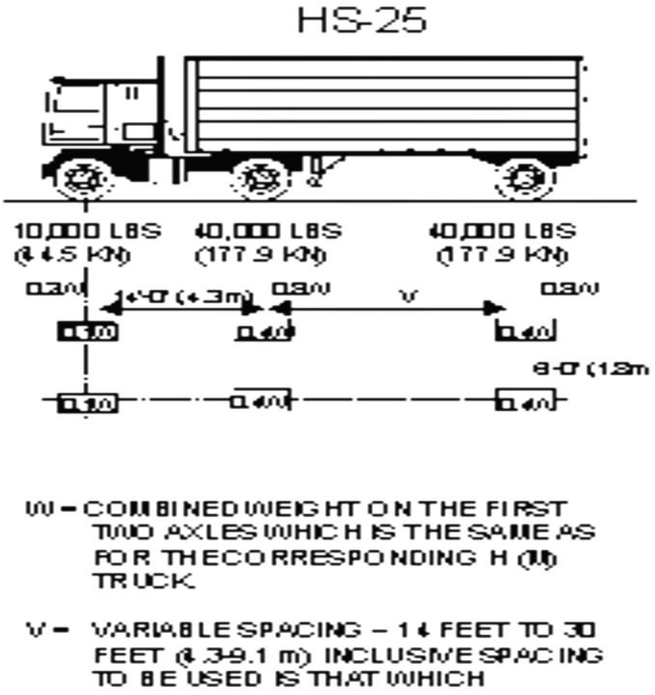

Figure 3-2 AASHTO HS25 truck load

Lane loads were adopted by AASHTO to provide a simpler method of calculating moments and shears. These loads are intended to represent a line of medium-weight traffic with a heavy truck positioned somewhere in the line in such a way as to produce the maximum stress in the component being designed. Both the uniform and the concentrated loads are assumed to be transversely distributed a 10-foot width. Lane loading is a better live load model for long spans where a string of vehicles may be critical. Lane loading fills the need to have more than one design truck per lane regardless of span length and number of spans. The HS25 lane loading is shown in Figure 3-3

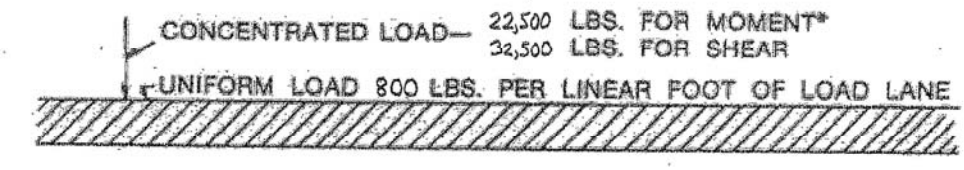

Figure 3-3 AASHTO HS25 lane load

The live load models used in both the AASHTO LRFD and the AASHTO Standard Specifications are fictitious loads generating stresses that cannot be exceeded by any real truck or series of trucks. The AASHTO truck loads are model vehicles that do not resemble any real vehicle. Only one truck per lane is used in the analysis for spans up to 200 feet. The truck is placed in such a way as to produce maximum stress in the component being designed; for example, bridge girders.

According to the AASHTO Standard Specifications, the most critical of truck loading and lane loadings is used in design. In general, lane loadings govern the design of bridges with longer spans.

- For simple spans, truck loading governs up to 144'-10" for moment, and up to 127'-3" for shear.
- For negative moment in continuous spans, lane loading governs for spans over 45 feet.
- For positive moment in continuous spans, lane loading governs for spans over 110 feet.

The live load models in the AASHTO LRFD Bridge Design Specifications and the AASHTO Standard Specifications for Highway Bridges differ in many aspects. The most significant differences are:

1. The basic live load designation in the AASHTO Standard Specifications is HS25. The basic live load designation in the AASHTO LRFD Design Specifications is HL-93

2. The live load in the AASHTO Standard Specifications consists of either a truck load or a lane load and concentrated loads. The live load in the AASHTO LRFD Design Specifications consists of a design truck or tandem, combined with a lane load.

3. The maximum negative live load moment in the AASHTO Standard Specifications is calculated by combining the two concentrated loads with lane load. The maximum negative live load moment in the AASHTO LRFD Design Specifications is calculated by combining 90 percent of the effect of two design trucks at a specified distance with 90 percent of the lane load.

4. The AASHTO Standard Specifications uses the term "impact" for the dynamic interaction between the bridge and the moving vehicles. The AASHTO LRFD Design Specifications use the term "dynamic load allowance".

5. In the AASHTO Standard Specifications, impact is applied to the entire live load. On the other hand, in the AASHTO LRFD Design Specifications, dynamic load allowance is only applied to the vehicles of the HL-93 live load model— the design truck or the design tandem—not the design lane load. The dynamic load allowance is fixed at 15 percent for the fatigue and fracture limit states and at 33 percent for all other limit states.

6. Live load distribution, which refers to the amount of load resisted by individual bridge girders is calculated using different distribution factors for both shear and moment in AASHTO LRFD Specifications compared to AASHTO Standard Specifications.

7. The multiple presence of live load on a bridge is accounted in the AASHTO Standard Specifications with the use of reduction factors that vary depending on the number of loaded traffic lanes. On the other hand, the AASHTO LRFD Specifications provide a multiple presence factor to account for this scenario.

Interestingly, neither the AASHTO LRFD Bridge Design Specifications nor the AASHTO Standard Specifications have any provisions for the calculation of live load effects in integral abutment bridge components that includes the girders, abutments, and piles. As a result, the current state of practice is to use the live load distribution equations of conventional (jointed) bridges to design the girders and calculate the live load effects in the abutments and piles of integral abutment bridges. Dicleli and Erhan (2009) conducted finite element analyses to obtain the live load distribution factors for the prestressed concrete girders of single-span integral abutment bridges with no skew. The live load distribution factors of the same bridges were also calculated using the AASHTO LRFD live load distribution factors that apply to conventional bridges. The comparison indicated a good agreement for the interior girder shear, but significant difference for the girder moment and exterior girder shear especially for short spans. For these cases, the live load distribution factors calculated from the finite element analyses were smaller than those stipulated in the AASHTO LRFD Bridge Design Specifications. As a result, the authors developed live load distribution formulas and correction factors for the current AASHTO LRFD live load distribution equations to accurately estimate girder live load shears and moments. In addition, a research study conducted by Dicleli and Erhan (2008) revealed that the effects of abutment soil-structure interaction and substructure properties on the distribution of live load among girders of integral abutment bridges are negligible. The study also revealed that abutment soil-structure interaction has a significant effect on the live load distribution factors for the abutment, but negligible effect on piles. However, abutment height has a considerable effect on the distribution factors calculated for the abutment and pile moments while wingwalls have only a negligible effect on the live load distribution factors of all integral abutment bridge components.

The issue on whether dynamic load allowance shall apply to foundation components of integral abutment bridges located entirely below ground level is also unsettled. While the AASHTO LRFD Specifications stipulate that the dynamic load allowance (IM) shall not apply to foundation components entirely below ground level, several states including Iowa, Massachusetts, and New Jersey among others require the designer to include the dynamic load allowance for the entire length of integral abutment piles. The rationale for this requirement is that the piles are almost attached to the superstructure; therefore, the top portions of the piles do no benefit from the dampening effect of the soil as per Federal Highway Administration report FHWA NHI-04-043.

Earthquake loads

Seible et al. (2008) note that earthquake loads can cause progressive collapse of bridges. Consequently, earthquake loads are classified as primary loads. AASHTO makes specific recommendations with respect to seismic analysis and design of bridges. The objective of the recommendations is not to design bridges to resist all potential seismic loads with no damage, but to minimize damage to a level below that associated with failure. Furthermore, each state has its own standards for seismic design of bridges that reflect the earthquake hazard and earthquake risk associated with each geographical region of the state. State code provisions for seismic design are more specific than the national code provisions.

Several states have specific modeling procedures and standard details for seismic analysis and design of integral abutment bridges. For example, Massachusetts evaluates seismic loadings on integral abutment bridges using finite element analysis. Oregon includes hooked dowels in the approach slab to restrain earthquake movement with respect to the bridge (Kunin and Alampalli 1999). In addition, researchers such as Lam and Martin (1986) suggest that integral abutment bridges be proportioned to limit displacements to four inches or less in order to minimize damage from earthquakes.

Seismic analysis of bridges is performed with the use of computer software. The basic modeling objective in seismic bridge analysis is to provide the simplest mathematical formulation of the true bridge behavior. This will lead to a reasonable quantification of bridge seismic response in terms of overall structural displacements, member forces, and deformations. For integral abutment bridges that means inclusion of soil-structure interaction. This requires the creation of a computer model that will determine the interactions between the bridge, the abutments and the foundation and calculate the forces that will be used for the design of the bridge. The model will allow for nonlinear behavior of the piles and the intermediate piers. It will also include nonlinear soil springs to describe the response of the soil behind the abutment walls as well as the response of the soil around the piles. Currently, only a handful of states require that soil-structure interaction (SSI)) be included in the seismic analysis of integral abutment bridges.

There are three methods of seismic analysis of bridges:

- Equivalent static analysis: An approximate linear elastic analysis method most often used on simple bridges.

- Linear dynamic analysis: Response spectrum analysis and/or linear elastic time history analysis.

- Nonlinear analysis using performance-based design: A more advanced approach that includes static pushover analysis and/or nonlinear time history analysis both of which produced a more accurate structural response of a bridge compared to the other methods of seismic analysis.

The selection of the appropriate method of seismic analysis for a particular bridge structure depends on several factors such as the seismic classification of the bridge. Most states classify bridges either as critical or essential based on certain parameters.

Seismic analysis of bridges requires that the period and damping ratio be determined for each significant mode of vibration. (Goel 1997) measured the vibration properties of a two-span concrete bridge from its motions recorded during acttual earthquake events and used the data to investigate how abutment participation affects the vibration properties of bridges with integral abutments. Among the findings was that the period of vibration elongated by a factor of over two and the damping ratio increased by 5 to 10 percent as the intensity of ground shaking increased from low level to intense level. According to Goel (1997), the changes in the magnitude of period of vibration and damping ratio were caused by increased abutment participation in the form of soil-structure interaction.

The seismic response of bridges with integral abutments is mainly dominated by the abutment-soil interaction in the longitudinal direction and soil-pile interaction in the transverse direction (Itani and Pekcan 2011; Bao and Rietz 2013). The response reduces the seismic demand on the piers and their foundations, but places larger demand on the integral abutment piles since they will be subjected to large cyclic deformations.

Secondary loads

Secondary loads are loads that do not lead to a progressive collapse of a bridge structure. This includes the force effects due to superimposed deformations (thermal, creep, shrinkage, and settlement loads); earth pressures; wind loads; vehicular loads due to longitudinal (braking) forces, centrifugal forces, and collision forces; water and stream loads; and pedestrian live loads. In reference to integral abutment bridges, the most significant loads are those due to superimposed deformations and the earth pressures. Even so, Burke (1993) reports that the sum of the effects of these loads, that is, the sum of thermal, creep, shrinkage, settlement, and earth pressures is very small in comparison to the effects of primary loads for bridges with a length of less than 300 feet. As a result, the effects of secondary loads for bridges up to 300 feet in length can be ignored with the exception of single span bridges and the continuity connection of continuous spans. However, the effects of secondary loads shall be considered for all bridges longer than 300 feet.

Thermal load

The behavior of an integral abutment bridge depends on the extent of temperature variation. According to Harvey and Kennedy (2002), daily temperature variations have the greatest influence on the behavior of integral abutment bridges. Nicholson (1998) states that the response of bridge abutments to temperature variation is the most important difference between integral bridges and jointed bridges. Both daily and

seasonal temperature changes affect integral bridges and cause the bridge to expand during temperature increases and to contract during temperature decreases. This cyclic behavior results in lateral displacements that must be accommodated by the pile/abutment system. These movements can cause changes in the stresses and strains in the piles supporting the abutments. They can affect the magnitude and distribution of the soil pressures on the abutments, diaphragms and wingwalls. They can also cause changes in the movement of the approach slabs, and cause settlements near the abutments. In addition to lateral displacements and forces, nonlinear thermal gradients through the depth of the superstructure induce stresses in the bridge components. This is due to the fact that the centroid of the temperature distribution curve does not coincide with the centroid of the beam cross-section.

Thermal Expansion

High stresses can develop in the components of an integral bridge as the structure undergoes the thermal length changes of its bridge deck. Differences often exist in measured and theoretical temperature-induced length changes. This is the chief reason why integral bridges in some states have performed satisfactorily even though structural analysis indicated there should have been thermal stress problems. These differences can be traced to errors in the value of the coefficient of thermal expansion, temperature gradients across the bridge cross sections, and resistance to movement provided by the abutment system and the soil pressure, which depends on the soil-structure interaction.

Coefficient of Thermal Expansion

Researchers believe that the reason behind the difference between the measured thermal length change of a bridge and its theoretical thermal length change lies in the value of coefficient of thermal expansion. The coefficient of thermal expansion of concrete is a function of cement quality, aggregates, mix proportions, temperature, humidity, and concrete age. As a result, its value can be very different than the value of 0.000006 per degree Fahrenheit prescribed in the AASHTO Specifications and routinely used in the design practice. Girton et al (1991) found that the coefficient for the bridges in their study ranged from 0.0000045 per degree Fahrenheit to 0.000005 per degree Fahrenheit. In addition, Construction Technology Laboratories researchers (Oesterle et al. 1998) experimentally determined an average coefficient of thermal expansion equal to 0.0000049 per degree Fahrenheit.

Because thermal movements of integral bridges are a key parameter of their behavior, it is important to make an accurate estimate of the coefficient of thermal expansion. The American Concrete Institute (ACI) publication ACI 209R provides an empirical equation to estimate the coefficient of thermal expansion of concrete based on the environmental conditions and aggregate characteristics. Methods developed by Emanuel and Hulsey (1977) may also be used to make an accurate estimate when the concrete mix design is known.

Temperature Range

There is a lag between the ambient air temperature and the temperature of the bridge components, which affects the design temperature range of the bridge. The lag is primarily affected by the materials used in bridge construction. Hybrid bridges such as steel girders and a concrete deck tend to follow the extremes of ambient temperature more closely than concrete structures. This can be attributed to the larger thermal mass of concrete structures and the difference in thermal conductivity and diffusivity between steel and concrete. This is reflected in the AASHTO LRFD Bridge Design Specifications, which stipulate larger design temperature ranges for metal bridge structures compared to concrete bridge structures. Thus, for a moderate climate, the temperature range for concrete bridge superstructures is 10 to 80°F and for steel bridge superstructures 0 to 120°F. For a cold climate, the temperature range for concrete bridge superstructures is 0 to 80°F and for steel bridge superstructures -30 to 120°F. Thus, for a 100-feet long steel integral abutment bridge located in a cold climate with the beams set at either of the temperature extremes, the amount of thermal movement as given by the equation

$$\Delta L = (a)(L)(\Delta T)$$

where, ΔL is the amount of thermal movement
a is the coefficient of thermal expansion and contraction
L is the length of the bridge superstructure
ΔT is the temperature range

Thus,

$\Delta L = (0.0000060)(100x12)(70) = 0.504"$ concrete superstructure in moderate climate
$\Delta L = (0.0000065)(100x12)(120) = 0.936"$ steel superstructure in moderate climate
$\Delta L = (0.0000060)(100x12)(80) = 0.576"$ concrete superstructure in cold climate
$\Delta L = (0.0000065)(100x12)(150) = 1.170"$ steel superstructure in cold climate
The calculated thermal movement ΔL is distributed equally to both integral abutments.

Integral abutment bridges are designed for the same range of temperatures as conventional bridges. However, a number of researchers suggest that the temperature ranges given by AASHTO are not accurate enough for integral bridge design and that temperature ranges should be determined on a regional or local level. Flores (1994) compared the temperature ranges from several studies to the AASHTO temperature recommendations. The results indicated that the AASHTO temperature ranges were too conservative for steel girder bridges while underestimated the temperature range for concrete bridges. Huang et al. (2004) reached the same conclusion investigating the behavior of concrete integral bridges in Minnesota; while the temperature range for concrete bridge superstructures in cold climate stipulated in the AASHTO LRFD Specifications is 80°F their research indicated that the appropriate temperature range for the design of concrete bridges in Minnesota should be 130°F.

Jorgenson (1983) monitored an integral bridge with a concrete deck and concrete box girders to determine, in part, how the lag in bridge temperature affected the design temperature range. He proposed calculating the design temperature range as the temperature difference between dawn on the hottest and coldest day of the year and adding one-third of the difference between the maximum temperature and the temperature at dawn during the hottest day of the year.

Thermal Gradients

Temperatures throughout a bridge structure are not uniform because of varying rates of heat transfer of different materials, heat sources, and varying exposure to direct solar radiation. As a result, the centroid of the temperature distribution curve does not coincide with the centroid of the beam cross-section. This results in thermal gradients through the depth of the superstructure. These thermal gradients induce stresses in the bridge components. The stresses induced by thermal gradients have been compared to those caused by creep and shrinkage (Arsoy et al. 1999; Burke 1993), which are typically ignored. However, Hoppe and Gomez (1996) noted that the stresses in steel girders caused by daily temperature fluctuations might be more critical than the compressive forces caused by the restraining force of the backfill.

The magnitude of the stresses induced by thermal gradients depends on the thermal gradient distribution, the relative flexibility of the abutment with respect to the superstructure, and the materials used in the bridge superstructure (concrete or steel girders).

There is fairly wide agreement that temperature gradient distributions are nonlinear through the depth of the superstructure (Russell and Girken 1994). However, Girton et al (1991) measured a bilinear distribution consisting of moderate temperature gradients in prestressed concrete girders with a steep temperature gradient in the slab.

The effect of asphalt topping on the thermal gradient distribution is not clear. It is logical to assume that the dark surface absorbs more solar radiation than a concrete surface and, therefore, create a larger thermal gradient in the superstructure. However, it has been reported that asphalt surfacing acts as insulation and actually reduces the maximum temperature in the deck concrete (Potgieter and Gamble 1989). Elbadry and Ghali (1983) conducted a numerical analysis and found that an asphalt topping increases the temperature-induced stresses in the concrete deck. Clearly, additional studies are needed to clarify the effect of asphalt topping on the magnitude and distribution of temperature-induced stresses in the concrete deck.

The magnitude of the stresses induced by thermal gradients also depends on the relative flexibility of the abutment with respect to the superstructure. As pile/abutment systems become more flexible, they provide less restraint against induced superstructure curvature. As a result, gradient-induced axial and bending stresses in the superstructure are reduced. Thippeswamy et al (1994) conducted a two dimensional frame analysis of a

hybrid bridge and abutment and measured the effects of thermal gradients on the maximum moments. They found that as the flexibility of the abutment increased, that is, as the ratio of superstructure to substructure stiffness became bigger, the bending stresses at midspan due to the thermal gradient decreased.

Superstructure material affects the magnitude of the stresses induced in the bridge by thermal gradients. Burke (1993) found that for concrete structures in moderate climates, the moments induced by thermal gradients can be ignored. However, Thippeswamy and GangaRao (1995) conducted a two-dimensional frame analysis of five steel girder integral bridges and found that a thermal gradient of 30°F through the depth of the superstructure produced considerable tensile stresses at the superstructure/abutment joint. In other words, stresses induced by thermal gradients in steel superstructures shall be considered in the analysis.

However, thermal gradients in the superstructure do not have a significant effect on the stresses in the piles or footings. Thippeswamy and GangaRao (1995) found that thermal gradient-induced stresses were negligible in foundation systems consisting of piles or flexible spread footings.

Effect of soil on bridge length expansion

The soil behind the abutment wall provides restraint against thermal expansion that affect the overall length change of the bridge. In turn, it induces secondary stresses in the structure. However, the restraint provided by abutment wall backfill is usually considered ineffective in reducing the free thermal expansion of the superstructure because the superstructure to abutment stiffness ratio in the direction of bridge expansion is high, and the reactive soil pressure at the top of the wall is low. Observations of integral bridges have confirmed that the soil restraint does not significantly reduce the expansion of the bridge.

Several bridges monitored by Lawver et al. (2000) exhibited nearly free expansion behavior. The theoretical unrestrained length change nearly matched the measured length change for the 216-feet prestressed concrete bridge investigated when using a coefficient of thermal expansion of 0.000006 per degree Fahrenheit and the temperature change measured at the girders. The theoretical length change also nearly matched the measured length change in a study conducted by Girton et al (1991).Elgaaly et al (1992) measured strains in the steel frame of an integral bridge and found good correlation with free thermal expansion of the bridge. Construction Technology Laboratories (Oesterle et al. 1998) found that the restraint provided by the soil had a negligible effect on thermal expansion of the bridge in their study. Finally, Sayers (2000) conducted a finite element analysis that varied soil stiffness behind the abutment wall and at the level of the piles. The overall change in bridge length was relatively unaffected by the original stiffness of the soils at the piles.

Although it does not appear that restraint from soils significantly influences the overall expansion of the superstructure, varying soil properties at each end of a bridge can have a significant impact on the distribution of the length change. Jorgenson (1983) measured an abutment movement of 1.96 inches on one side of the bridge while the opposite abutment moved 0.74 inches. This was attributed to the difference in effective soil stiffness. Thomas (1999) also measured unequal abutment movement. The south end of the bridge experienced a decreased rate of expansion as the temperature rose and the north end experienced an increased rate of expansion, but the net expansion of the bridge maintained a linear relationship with the change in temperature. Thomas hypothesized that the non-uniformity was due to increasing backfill stiffness behind the south abutment as the abutment expanded.

Creep and Shrinkage loads

Creep and shrinkage effects are interrelated. Conventional practice also assumes that because creep and shrinkage stresses have opposite effects, they cancel each other out. Consequently, their effects are ignored in the analysis and design of conventional bridges. However, the assumption that creep and shrinkage forces tend to cancel each other out does not appear to be valid for hybrid integral bridges, that is, integral bridges with steel superstructure and a composite concrete deck. Results from numerical analysis indicate that the effects can be additive in certain regions of integral bridges that consist of steel girders and a concrete deck. This is reflected in the fifth edition of AASHTO LRFD Bridge Design Specifications section 11.6.1.3, which stipulates that in addition to the thermal deformations, integral abutments shall be designed to resist and/or absorb the creep and shrinkage deformations of the superstructure.

Creep

Creep is long-term deformation under sustained load. Creep stresses are caused by a decrease in the stiffness of the material over time. Thippeswamy and GangaRao (1995) conducted numerical analysis of five integral bridges that consisted of steel superstructure with composite concrete deck in order to study the effects of creep in stresses in the concrete deck and steel girders. For the integral bridges supported on piles, creep decreased the compressive dead load stress in the steel girder at the abutment by 10 percent. However, for integral bridges on spread footings, creep decreased the compressive dead load stress in the steel girder at the abutment by 40 percent. There was no comparison to the live load stresses in the numerical analysis. The results of the numerical analysis also indicated that at mid-span, the creep stresses decreased the compressive dead load stress and increased the tensile dead load stress. Over the piers, tensile dead load stress was significantly reduced while the compressive stress in the steel increased. The results of the numerical analysis also indicated that creep stresses were greater in the fixed spread-footing model and were lower for hinged-spread footings and piles. The overall effect of creep was a reduction of stresses in the concrete deck and an increase of stresses in the steel girders.

Siros and Spyrakos (1995) conducted a numerical analysis of a hybrid integral bridge to compare the creep stresses to the dead load stresses in both the concrete deck and the steel. They found out that the creep stresses in the concrete deck were between 26 and 55 percent of the dead load stresses. The creep stresses in the steel were between 2 and 21 percent of the dead load stresses. But since Thippeswamy and GangaRao's (1995) indicate that creep stresses reduce the magnitude of the stresses in the concrete deck, the high percentages in the deck are not a concern. However, creep adds to the steel stresses at the bottom of the superstructure. In fact, creep stresses in the steel girders are in the range of 1 to 9 percent of the allowable steel stress.

Shrinkage

Shrinkage is reduction of volume due to evaporation that occurs as concrete cures and loses moisture. Because steel girders restrain the free shrinkage of the concrete deck, bridges composed of cast-in-place deck and steel girders exhibit a non-uniform shrinkage. Tensile shrinkage stresses develop in the concrete and compressive shrinkage stresses develop in the steel girders. Research by Thippeswamy and GangaRao (1995) confirms this behavior. While tensile shrinkage stresses of the order of 290 psi were observed in the concrete deck, shrinkage compressive stresses of the order of 4,000 psi were observed in the steel girders. The shrinkage of the deck concrete also produced small tensile stresses in the girder at the connection of the superstructure to the abutment.

As shown in Figure 3-4, stresses caused by shrinkage in hybrid integral bridges are opposite in sign to dead and live load stresses at mid-span, but have the same sign as dead and live load stresses in the negative moment regions over the piers. At the connection of the superstructure with the abutment, the shrinkage tensile stresses are additive to dead and live load stresses at the top of the joint, but opposite in sign at the bottom of the joint.

Combined Effect of Creep and Shrinkage

The assumption that creep and shrinkage forces tend to cancel each other out does not appear to be valid for integral bridges with a steel superstructure and composite concrete deck. Figure 3-4 shows that creep and shrinkage stresses are similar in sign at the top of the superstructure at mid-span and at the bottom of the structure over piers. In addition, at locations where the stresses are opposite in sign, they are not equal. As shown in Figure 3-4, the creep and shrinkage stresses are much larger than the primary load stresses in the girder at the abutment. As a result, there is a change of stress from compression to tension at the abutment. At mid-span, the combined tensile stresses from creep and shrinkage at the top of the slab reduce the magnitude of the compressive stress from primary loads. The other significant effect is that the compressive stress in the girder over piers increased by 20 percent due to the combined effects of creep and shrinkage.

Burke (1993) and Fennema et al. (2005) studied the effects of creep and shrinkage on integral bridges with concrete girders. Burke (1993) indicates that creep has the opposite effect of shrinkage at all locations while Fennema et al. (2005) indicate that creep and shrinkage may play a significant role in the axial response of the girders.

There is limited information available on the presence of shrinkage and creep stresses in the foundation system. Thippeswamy and GangaRao (1995) indicate that shrinkage stresses at the foundations are negligible for all footing systems except for fixed spread footings.

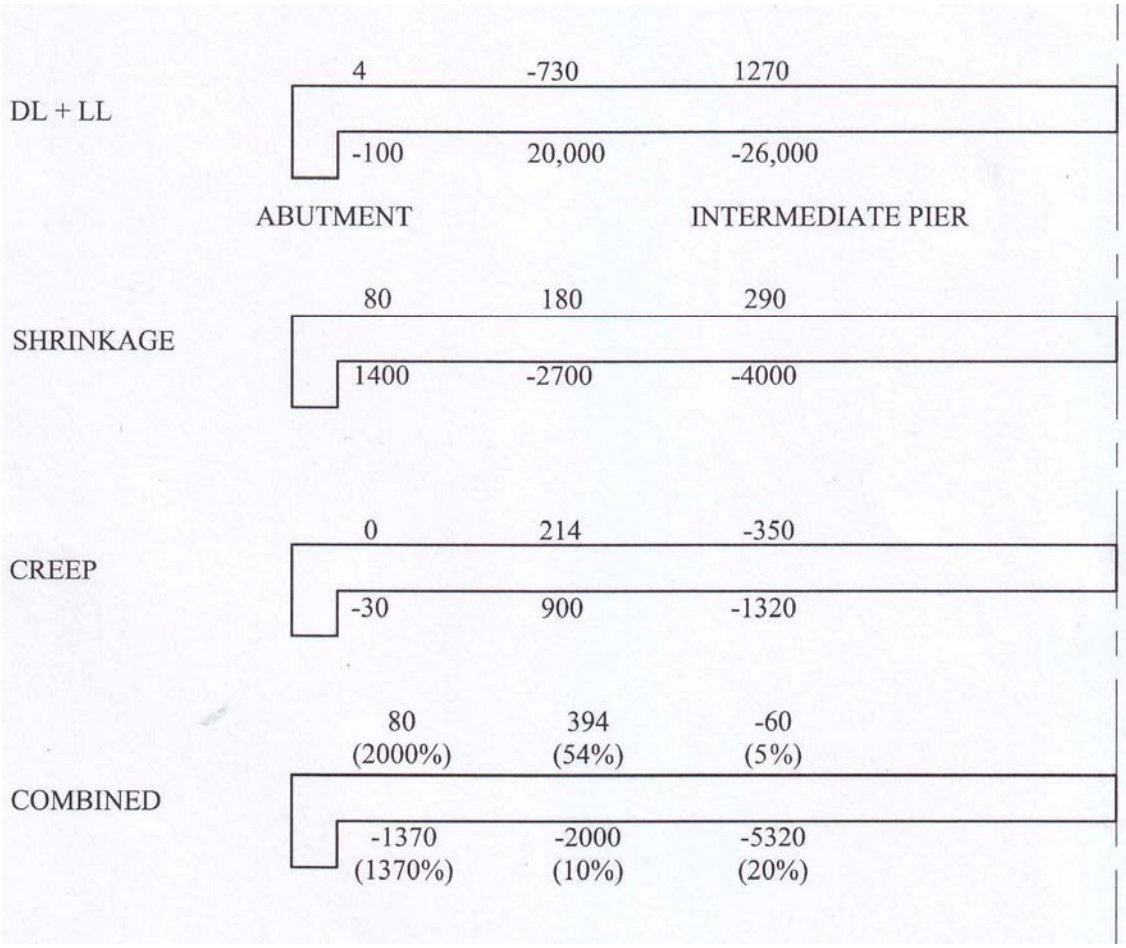

Figure 3-4 Effects of primary loads, shrinkage, and creep on the superstructure of a hybrid integral bridge (Thippeswamy and GangaRao 1995)

Settlement load

Settlement of integral abutments is typically the result of cyclic loading of the soil and the vertical loads on the abutments or approach slab. Washout and scour also cause settlements in bridges spanning bodies of water or bridges with a defective means of preventing significant amounts of water from infiltrating the backfill. The effects of settlements on the stresses in integral bridges have not been thoroughly studied, and the available information is somewhat conflicting (Wiss, Janney, Elstner Associates, Inc. 2002).

A study by Moulton et al. (1981) determined that for two and four-span steel stringer bridges, a differential settlement of 1 inch or more would produce unacceptable stresses for spans of up to 50 feet. Effects of a 3-inch settlement were small for bridges with 100 to 200 feet spans and negligible for bridges with spans greater than 200 feet. He concluded that the settlement stresses in single-span bridges are insignificant and can be

disregarded in analysis and design. In addition, Chen (1997) suggests that for differential settlements less than 1.5 inches, the induced secondary moments can be ignored.

Integral bridges supported on spread footings appear to develop high stresses in the superstructure at the abutment joint whereas integral bridges supported on flexible piles develop much lower stresses under the same settlement. It is not entirely clear why the same settlement produces different stresses in the superstructure, although it is likely related to the stiffness and deflected shape of the abutment system. Thippeswamy and GangaRao (1995) conducted a numerical analysis and reported that the stresses in the superstructure at the abutment due to settlement of the spread footing were nearly a quarter of the dead load stress and had the same effect as primary loads. On the other hand, the settlement stresses were very small at the superstructure/abutment joint and at the bottom of the abutment for integral bridges supported on piles.

Greimann et al. (1986) conducted a numerical analysis of the effects of abutment pile settlement. The load-settlement curves were unaffected by pile orientation, thermal movements of the superstructure, or the presence of backfill behind the abutment wall. However, piles were unable to carry substantial additional load when the vertical settlement reached the range of 0.25 inches leading to the conclusion that the maximum allowable settlement of integral abutment piles should be limited to 0.25 inches.

Earth Pressures

The magnitude and distribution of soil pressures exerted on integral abutments is a complex issue because soil pressures change significantly when the integral abutment moves due to seasonal and daily cycles of expansion and contraction of the bridge deck. Over time, the magnitude of soil pressures escalates due to densification of the retained soil (England and Dunstan 1994) - this built-up of lateral earth pressures is referred to as "soil ratcheting." The fact is confirmed by Hassiotis et al. (2006) and Xu et al. (2007). Both researchers indicate that the earth pressures behind integral abutments increases over time with expansion-contraction cycles and eventually reaches states of stress close to full passive and active pressures (Xu et al. 2007) or higher than the usual design values (Hassiotis et al. 2006). Both the magnitude and distribution of soil pressures depends on the deflected shape of the abutment wall. Pressure distribution is inherently nonlinear despite the fact that a linear distribution is often assumed in design.

Bending moments induced by passive pressures on abutments counteract the dead and live load bending moments in simple spans. Therefore, overestimating passive pressures is not necessarily a conservative approach if the bridge behaves as a simple span. For continuous-span bridges, the negative moments are increased at abutments and are reduced at piers for two and three-span bridges, and center span positive moments of three-span bridges are slightly increased (Burke 1993). Chen (1997) and Burke (1993) recommend that only two-thirds of the full passive pressures be used in modest length bridges and that the passive pressures can be ignored completely in short single and multiple-span bridges.

Several other studies confirm that near full passive pressures occur against the abutment wall and piles during periods of bridge expansion (Ting and Faraji 1998). The Massachusetts Highway Department (Crovo 1998) found that near the ground surface, full passive resistance was nearly achieved for a thermal movement of 0.5 inch at each footing-supported abutment. At greater depths, the full passive pressure was approached even for small horizontal displacements.

Sandford and Elgaaly (1993) measured soil pressures on a 23-feet high abutment wall resting on spread footings. The pressure approached at rest pressures during periods of contraction. During periods of expansion, combining the passive pressure distribution over the top third of the wall with a transition to the active pressure case at the base of the wall gave a conservative envelope for the measured soil pressure. This recognizes the larger movement of the top of the wall into the backfill and the lack of movement at the bottom of the wall.

Numerical analysis conducted by Wood and Nash (2000) indicates that the shape of the soil pressure distribution is controlled by the relative stiffness of fill and abutment while the magnitude of the stress distribution is primarily controlled by the stiffness of the fill. As the ratio of the soil stiffness to abutment stiffness increased, the peak of the stress distribution moved towards the top of the wall. A nine-fold increase in the fill stiffness increased the maximum moment in the abutment wall by a factor of 1.5, and a ten-fold decrease in the abutment stiffness produced a reduction in moment by a factor of about two. Thus, there is a nonlinear relationship between relative stiffness and resultant abutment moment. Other parameters, such as soil friction angle, had very little effect on the earth pressures or abutment moments.

3.2.2. Skew

Skew is a challenge for both conventional bridges and integral abutment bridges. However, the skew of integral bridges is a concern to structural engineers because of the effect of skew on soil pressures behind the abutments. Research indicates that higher skew angles result in lateral displacements of the abutment wall towards the acute side of the bridge. As a result, high stresses in the superstructure and substructure develop near the obtuse corners of skewed integral abutment bridges.

Effect of skew on pile stresses

Skewed integral abutment bridges generate thermally-induced biaxial bending stresses in the piles. Greimann et al. (1983) conducted a research on the effect of skew on pile stresses. Thus, they investigated the pile orientations shown in Figures 3-5 and 3-6. Cases 1a and 2a indicate piles oriented in weak-axis bending (Figure 3-9) while cases 1b and 2b indicate piles oriented in strong-axis bending (Figure 3-8). The results of their research show that the stresses in piles 2a and 2b are much higher compared to the stresses in piles 1a and 1b. In fact, the stresses in piles 1a and 1b are close in magnitude with piles supporting integral abutments without skew.

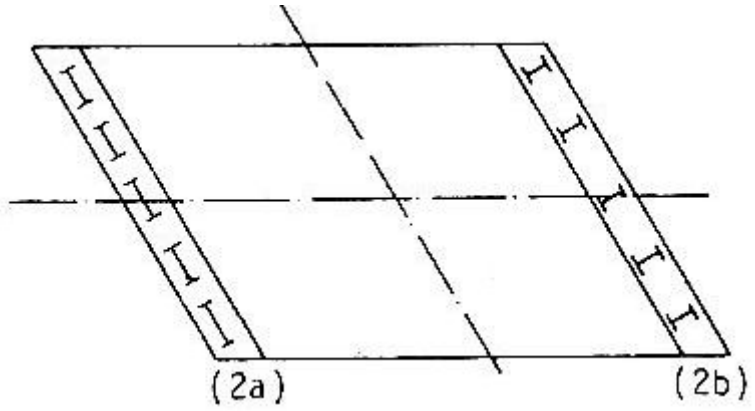

Figure 3-5 Pile orientation in skewed bridges cases 2a and 2b (Greimann et al. 1983)

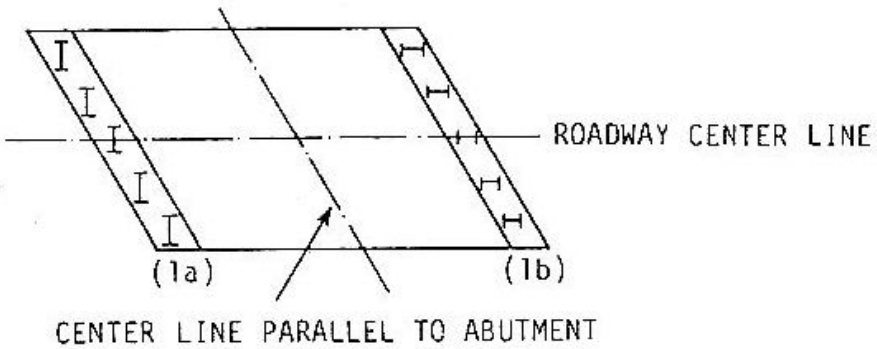

Figure 3-6 Pile orientation in skewed bridges cases 1a and 1b (Greimann et al. 1983)

Najib (2002) as well as Najib and Amde (2010) investigated only piles oriented in weak-axis bending, that is, cases 1a and 2a shown in Figures 3-5 and 3-6. The two cases investigated are shown in plan in Figure 3-7 and include (a) piles whose web is parallel to the abutment line, and (b) piles whose web is perpendicular to the roadway and bridge centerline. The results indicate that the effect of skew is less pronounced for piles oriented with their webs perpendicular to the roadway and bridge centerline. These results are in line with the research conducted by Greimann et al. (1983) as well as Amde and Greimann (1988). According to Amde and Greimann (1988) "when steel H-piles are used, the web of the pile should be perpendicular to the centerline of the stringer regardless of the skew."

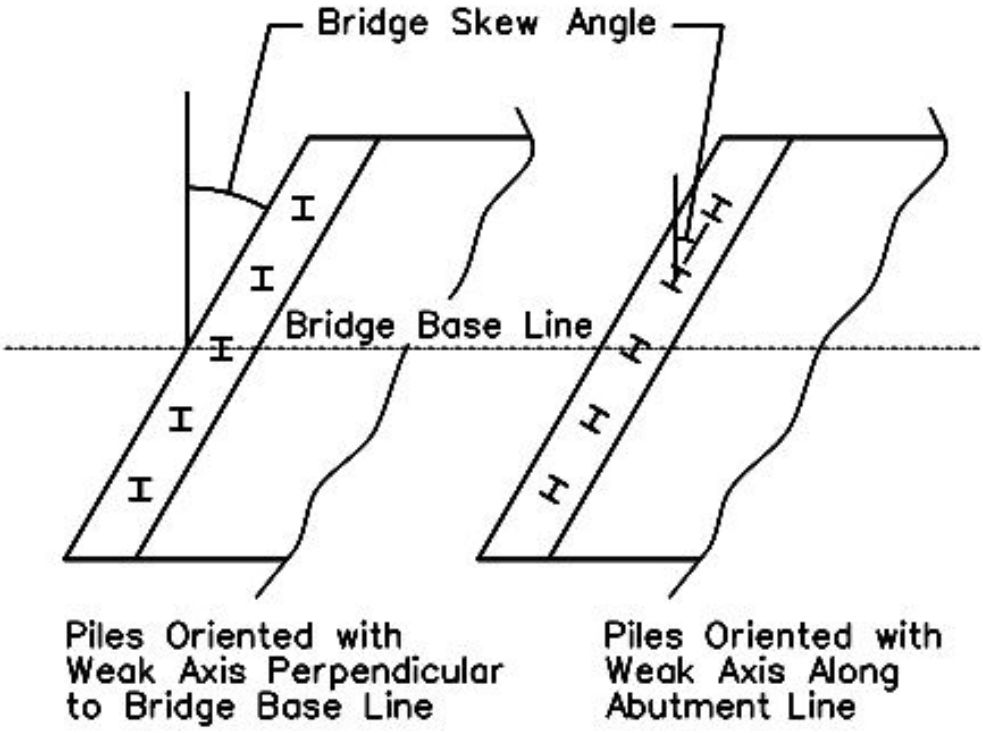

Figure 3-7 Pile orientation in skewed bridges (Najib 2002; Najib and Amde 2010)

The results of this investigation indicate as the skew increases from 0 to 30 degrees pile stresses increase only 3 percent when pile webs are perpendicular to the roadway and bridge centerline and 38 percent when pile webs are parallel to the abutment line. When the skew increases from 0 to 60 degrees, the increases in pile stresses are 13 percent and 63 percent respectively. Consequently, Najib (2002) recommends a maximum skew of 30 degrees for integral abutment bridges.

Effect of skew on soil pressures behind abutments

Soil pressures behind skewed integral abutments are non-uniform (Crovo 1998). In fact, soil pressures are greatest at the obtuse sides (Hassiotis et al. 2006). This is due to the rotation of the abutment wall about the vertical axis, which tends to push the obtuse side into the soil and pull the acute side away. However, the pressure at the acute side can still be positive because of the overall elongation of the bridge.

Elgaaly et al. (1992) and Sandford and Elgaaly (1993) observed stresses on the upper part of the abutment wall at the obtuse corner of a 20-degree skewed Forks Bridge in Maine that were nearly three times those at the acute corner. They also noted that the pressures caused by thermal expansion were of the same magnitude or higher than the live load response. During periods of expansion, the pressures on the obtuse side increased four to six times the cold weather value, whereas the pressures on the acute side increased only two to three times. These differences occurred seasonally as a result of long-term temperature changes and were relatively unaffected by short-term variations, indicating that the difference was not a reflection of non-uniform temperatures in the structure.

The live load response of integral bridges also appears to cause higher stresses at the obtuse corner of skewed integral bridges. Elgaaly et al. (1992) observed that the soil pressure near the obtuse corner side of the abutment wall increased while the acute side soil pressure decreased during live load tests. Dagher, Elgaaly, and Kankam (1991) concluded that the shear and moments from primary loads (dead and live loads) were relatively high near the obtuse corner of the slab. They also reported slab cracking near the obtuse corner of another integral bridge in Maine.

Thomas (1999) measured lower abutment strains at the obtuse angle side of a 30-degree skewed bridge when compared to the acute angle side. Although the soil pressure behind the abutment wall was not measured, the lower abutment strains indicate that there was more restraint against longitudinal movement at the obtuse side and, therefore, higher soil pressures at the obtuse side.

Effect of skew on the seismic performance of integral abutment bridges

Itani and Pekcan (2011) conducted an investigation on a simple-span bridge with integral abutments using different skew angles. The results of the analyses showed that the variation of skew causes significant changes in the bridge dynamic characteristics in terms of periods and mode shapes. In addition, the translational modes in skewed bridges are highly coupled between the longitudinal and the transverse translation. As a result of the coupling nature of the two horizontal directions, the longitudinal bridge response is affected by transverse loading.

Shamsabadi and Yan (2008) developed three-dimensional finite element models to study the response of skewed integral abutment bridges subject to earthquake excitations. The study indicates that because the center of the mass of the superstructure and the center of stiffness of the abutment of skewed bridges do not coincide, the inertia loading on the

bridge causes bridge rotation about its vertical axis, which can cause excessive transverse movement.

Effect of skew on condition rating of integral abutment bridges

Alampalli and Yannotti (1998) inspected and rated 30 steel superstructure bridges with integral abutments at varying skews. Their research assigned a numerical rating to the condition of the bridge deck, the approach slab, and the abutment stem. They used the New York State condition rating system that assigns a number to every structural element based on the amount of visible deterioration/distress observed during inspection. Analysis of the condition ratings of the bridges indicated that the greater the skew of the bridge deck, the lower the condition ratings were for the deck, approach slab, and abutment stem. Field inspections of 84 steel and concrete integral bridges in New York State concluded that steel integral bridges performed better than concrete integral bridges for skew less than 30 degrees. However, both steel and concrete integral bridges performed poorly with skews greater than 30 degrees.

Acceptable skew angles

Researchers do not seem to agree on a limit for skew angles for integral bridges. However, literature indicates that skew angles greater than 15 to 20 degrees cause forces sufficient to move the abutments (Sayers 2000). Burke (1994) showed that skews greater than 15 degrees cause instability. Hoppe and Gomez (1996), and Najib (2002) suggest limiting the bridge skews to less than 30 degrees to mitigate pile overstress. Soltani and Kukreti (1992) indicate that sharp skews are problematic to both conventional and integral abutment bridges. Doust (2011) pinpoints to the fact that when a bridge has a large length-to-width ratio, a small skew can cause a huge rotation in the bridge structure. Kunin and Alampalli (1999) constructed a table of the limiting skew angles used by state agencies (Table 3-1). The table indicates that the majority of states limit the skew angle of integral bridges to 30 degrees. The responses to the survey on integral abutment bridges conducted as part of this study (Chapter 4) indicate that the majority of states limit the skew angle of integral abutment bridges to 30 degrees. However, five states; California, Colorado, Idaho, Hawaii, and Tennessee report no limit on skew while the state of Indiana has no limitation for skew for only cast-in-place concrete superstructures.

3.2.3. Curvature

Curvature is problematic for bridges of all types, including integral abutment bridges. Kaufmann and Alvarez (2011) indicate that the bridge ends of curved integral bridges, in addition to longitudinal displacements, also undergo transverse displacements and rotations around the vertical axis. Thus, the maximum horizontal displacement of the bridge occurs at the edge of the bridge, rather than in the bridge axis. Harvey (2012) reports that there are serious concerns on whether integral abutments supported on steel H-piles oriented in weak-axis bending can accommodate the unbalanced abutment thrusts due to thermal effects. In his opinion, this may only be an acceptable solution if the curvature is slight. Consequently, he cautions against using integral bridges with flexible abutments on strongly-curved bridges. In fact, Kaufmann and Alvarez (2011) indicate that the current policy in Switzerland is to use rigid abutments for sufficiently-curved integral bridges. The survey on integral abutment bridges (Chapter 4) indicates that 26 states build integral abutments on curved alignment. However, those states allow construction of integral abutment bridges only on a slight curvature. Generally speaking, very little research on curved integral bridges has been conducted as of this moment.

Thanasattayawibul (2006) conducted a research on curved steel I-girder integral abutment bridges. As part of the research, he developed a three-dimensional nonlinear finite element analysis model in order to investigate the behavior of curved integral abutment bridges using a number of parameters. Among the findings is the fact that for curved integral abutment bridges up to 300 feet in length and in very stiff clay, larger radius is associated with lower abutment pile stresses. However, for curved integral abutment bridges longer than 300 feet and in all soil profiles, larger radius is associated with higher abutment pile stresses. Another finding is that curved integral abutment bridges with a larger radius achieve a larger pile stress reduction with the introduction of predrilled holes compared to curved integral abutment bridges of the same length, but smaller radius. Furthermore, stresses in the abutment piles can be reduced by introducing more spans within the bridge length. In addition, stresses in abutment piles oriented for weak-axis bending are smaller than the stresses in abutment piles oriented for strong-axis bending. However, the stresses in abutment piles remain the same regardless of whether the steel H-piles are designed as end-bearing or friction piles.

Doust (2011) conducted research on both steel and concrete curved integral abutment bridges. The research on curved steel integral abutment bridges pinpoints to a reduction in the magnitude of internal forces in the integral abutments as the radius of the curve is reduced (larger degree of curve) under the application of the most critical loading, that is, temperature contraction. In addition, the internal forces in the integral abutments were always smaller compared to those developed in the integral abutments of straight bridges of the same length. The research on curved concrete integral abutment bridges resulted in the finding that the bending moments in the piles of integral abutment bridges increase up to bridge lengths of 300 feet for small radii of curvature, then remain constant. In addition, the bending moments in the piles of highly-curved bridges remain constant as the curvature increases.

3.2.4. Soil-Structure Interaction

The complex soil-structure interaction mechanism involves relative movement between the integral abutment and adjacent retained soil. This movement is the result of natural seasonal thermal variations and is inherent in all integral abutment bridges (Lock 2002). The soil-structure interaction is difficult to predict because the reactive soil pressures are a nonlinear function of the magnitude of the displacement and deflected shape of the abutment wall, and the deflected shape of the wall is a function of soil pressures. The basic variables that affect the soil-structure interaction are the configurations of abutment walls, soil characteristics (primarily soil stiffness), and structure movement.

Abutment Movement

Abutment movement affects the magnitude and distribution of soil pressures, which has a significant influence on the behavior of integral abutment bridges. The term abutment movement includes the magnitude of both the longitudinal and lateral displacements of the abutment wall as well as its deflected shape. Abutment movement is the result of two effects: the thermal movement of the superstructure and the temperature-dependant volumetric expansion of the pile cap concrete. Thermal expansion of the superstructure pushes the abutment wall into the soil, which affects the magnitude of lateral earth pressure on the abutments, piles, diaphragms, and wingwalls, and causes movement of the approach slabs. On the other hand, the volumetric expansion of the pile cap concrete is small in comparison to the thermal expansion and contraction of the bridge and is usually ignored.

One of the factors that influence the deflected shape of the wall is the connection between the superstructure and the abutment. Research indicates that the typical continuity connection of the superstructure and abutment, where the superstructure is cast integrally with the abutment wall, is sufficiently rigid to prevent large rotations. Lawver et al. (2000) measured abutment rotations less than 0.06 degrees. This was further corroborated by evidence of double curvature in the piles which is expected when the abutment walls translate horizontally with little or no rotation. Thomas (1999) measured abutment rotations between 0.06 degrees and 0.075 degrees for both 15 degree and 30 degree skew bridges.

Differences in the abutment geometry at each end of an integral bridge may have an impact on the behavior of the bridge, but very little has been published on this topic. The Massachusetts Highway Department (Crovo 1998) reports that a difference in abutment heights causes an unbalanced lateral load resulting in sidesway at the abutments, which should be considered in the design of integral abutments.

Soil Pressures on Abutments

Soil pressures are secondary loads and their effects are described in section 3.2.1.

Soil Stiffness

Literature review indicates that soil stiffness is the most significant factor influencing soil pressures applied on the abutment system. Soil stiffness is a function of the compaction level of a soil. Denser soils have a higher stiffness than loose soils and provide more resistance to thermal movement than loose soils. They also apply higher lateral pressures on the abutment system, which introduces higher axial forces into the bridge superstructure (Fennema et al. 2005), causes more rotation of the abutment and therefore influences the moments in the superstructure. When soil is frozen its stiffness dramatically increases. Nilsson et al. conducted a bridge monitoring program and concluded that the stiffness of frozen soil is 10 to 20 times higher than the stiffness of unfrozen soil.

Cosgrove and Lehane (2003) investigated the effects of loose backfill placed adjacent to integral bridge abutments. They observed large increases in lateral stresses in the abutments attributed to the tendency of loose backfill to experience strain hardening due to repeated cyclic straining. These lateral stresses in the abutment exceed those that would be inferred from sand density variations alone. Consequently, Xu et al. (2007) recommend against using loose backfill behind integral abutments because it does not reduce the tendency to develop high earth pressures under cyclic loads. In addition, it produces larger settlements.

Other studies attempted to quantify the change in soil pressure when soils of varying densities are used. The Massachusetts Department of Transportation utilized a nonlinear three dimensional analysis to model a 150 feet steel girder integral abutment bridge supported on steel H piles oriented for weak-axis bending for a thermal loading increment of $\Delta T = +80°F$. The axial force and moment in the superstructure more than doubled when compaction was varied from the loose to dense soil compaction range (Crovo 1998). Field tests of the supporting piles indicated that the maximum moment in the piles increased by a factor of about 1.75 when dense soil was used in lieu of loose soil.

Construction Technology Laboratories (Oesterle et al. 1998) determined that in addition to soil compaction, backfill slope has a significant influence on soil pressures applied on the abutment system. A finite element analysis indicated that a decrease in soil compaction from 90 percent to 80 percent decreased the passive pressure by a factor of 2.5. A decrease in the slope of the in-situ soil behind the abutment wall prior to backfilling from 45 to 30 degrees decreased the passive soil pressure by a factor of two.

Soil stiffness has also a significant influence on the rotation of the abutment wall. Numerical analysis conducted by Ting and Faraji (1998) resulted in the abutment translating 35 percent less and rotating 67 percent more for dense backfill than for loose

backfill. Sayers (2000) attempted to match the abutment rotations from finite element models to those measured in the field, which were smaller than the model results. He applied a horizontal restraining force at the deck to represent the approach slab restraint, but the approach slab restraint had a negligible effect on abutment rotation. He reduced the temperature gradient through the superstructure and the result was a slight reduction in rotation. He reduced the coefficient of expansion between the deck and steel girders and the result was again a slight reduction in rotation. He used various linear pressure distributions other than the assumed triangular distribution and the computer model results remained unchanged. However, lowering the stiffness of the soils in a second model gave a good correlation with field measurements. This lead to the conclusion that in addition to influencing soil pressures applied on the abutment system, soil stiffness has a significant influence on the rotation of the abutment wall.

3.2.5. Soil-Pile Interaction

The interaction between the soil and the piles is similar to the interaction between the soil and the abutment wall. However, soil-pile interaction has much less influence on the behavior of the bridge than the soil-abutment interaction. Soil-pile interaction primarily influences the stresses in the piles. Soil stiffness has a significant impact on the stresses developed in the piles. In addition, pile deflection causes a reduction in the vertical load capacity of the piles, particularly in dense soils. Predrilled holes filled with loose granular soil are an effective solution to prevent reduction in pile load capacity.

Soil Stiffness

Research indicates that soil stiffness next to the piles does not significantly affect the stresses in the abutment wall and the superstructure. However, soil stiffness next to the piles has a significant effect in the stresses induced in the piles. Stiff soils have been shown to induce large bending stresses in piles. In addition, both the abutment wall-soil interaction and the pile-soil interaction affect the stresses in the piles. Furthermore, the pile stresses most affected by the soil stiffness are those towards the top of the pile.

The Massachusetts Department of Transportation showed through numerical analysis that the level of soil compaction adjacent to the piles has no significant influence on the wall or superstructure moments or deflections (Crovo 1998). However, when dense soil is present behind the abutment wall, a change from loose soil to dense soil at the level of the pile increases the pile moment by a factor of about 1.75. In all cases, the peak moment occurs at the abutment-pile interface.

A finite element study conducted by Faraji et al. (2001) indicates similar results. The magnitude of the axial force in the superstructure varied significantly depending on the compaction level of the soil behind the abutment wall, but was only slightly affected by the soil compaction next to the piles. However, compaction of the soil both next to the piles and behind the abutment had a significant influence in the moments in the steel H piles.

Other studies confirm the fact that the pile stresses most affected by the soil stiffness are those near the top of the pile. This is due to the fact that there is typically less lateral movement at the bottom of the pile than at the top of the pile. Jorgenson (1983) conducted a numerical study of piles oriented for strong-axis bending and found that doubling the modulus of subgrade reaction on the bottom half of a pile while holding the modulus of subgrade reaction at the top half of the pile constant had less than a five percent influence on the maximum moment. Numerical studies conducted by Kamel et al. (1995) indicate that the soil type along the bottom 50 feet of a 60-foot-long concrete pile with a hinged top has little influence in the pile stresses when using a 10-foot deep upper layer of loose sand. Laboratory pile tests conducted by Kamel et al. (1996) confirm the fact that maximum pile lateral displacements depend on the soil stiffness in the upper 10 feet of pile and that soil stiffness below this depth has a negligible effect.

Pile Capacity Reduction from Lateral Displacement

As piles deflect under abutment movement, their vertical load capacity is reduced. However, the relationship between pile head displacement and reduction of the vertical load carrying capacity of pile is not clear. This is due to the big number of parameters that influence the magnitude of pile displacement. This includes among others the stiffness of the soil surrounding the pile, stiffness of bridge deck, abutment height, bridge length, number and weight of trucks travelling over the bridge, and changes in temperature.

Research conducted at Iowa State University and reported by Amde et al. (1982) suggests that the vertical load capacity of displaced piles is reduced in very stiff soil because the soil is sufficiently stiff to force formation of a plastic hinge. The research indicates that the vertical load-carrying capacity of steel H piles is not significantly affected by lateral displacements of 2 inches in soft and stiff clay, and in loose, medium, and dense sands. However, in very stiff clay (average blow count of 50), piles fail by elastic-plastic buckling and their vertical load-carrying capacity is reduced by about 50 percent for a lateral displacement equal to 2 inches and 20 percent for a lateral displacement equal to 1 inch.

However, further development of design models by Greimann et al. (1984), Amde et al. (1988), and Greimann and Amde (1988) indicates that the vertical load capacity of piles is not significantly affected for lateral displacements of up to 4 inches for steel H piles and up to 2 inches for concrete and timber piles in six different soil types. Greimann and Amde report that both their design method and the finite element model predict only a slight reduction in the ultimate vertical load capacity of steel H piles oriented in both strong and weak axis bending for pile head deflections of up to 4 inches. The capacity was reduced in types of soils tested, but there was not a strong correlation between the magnitude of the reduction and the soil type. Their design method predicted that plastic buckling of piles becomes increasingly dominant over elastic buckling as the stiffness of the soil increases.

Predrilled Holes

For stiff soil conditions, predrilling oversize holes (Figure 3-8) and surrounding the piles with loose granular soil has emerged as an effective method to increase pile flexibility (Dunker and Liu 2007), reduce bending stresses in the piles and increase their vertical load capacity (Yang et al. 1985; Greimann et al. 1986; Greimann and Amde 1988; Crovo 1998; Faraji 1997; Najib 2002; Khodair and Hassiotis 2003).

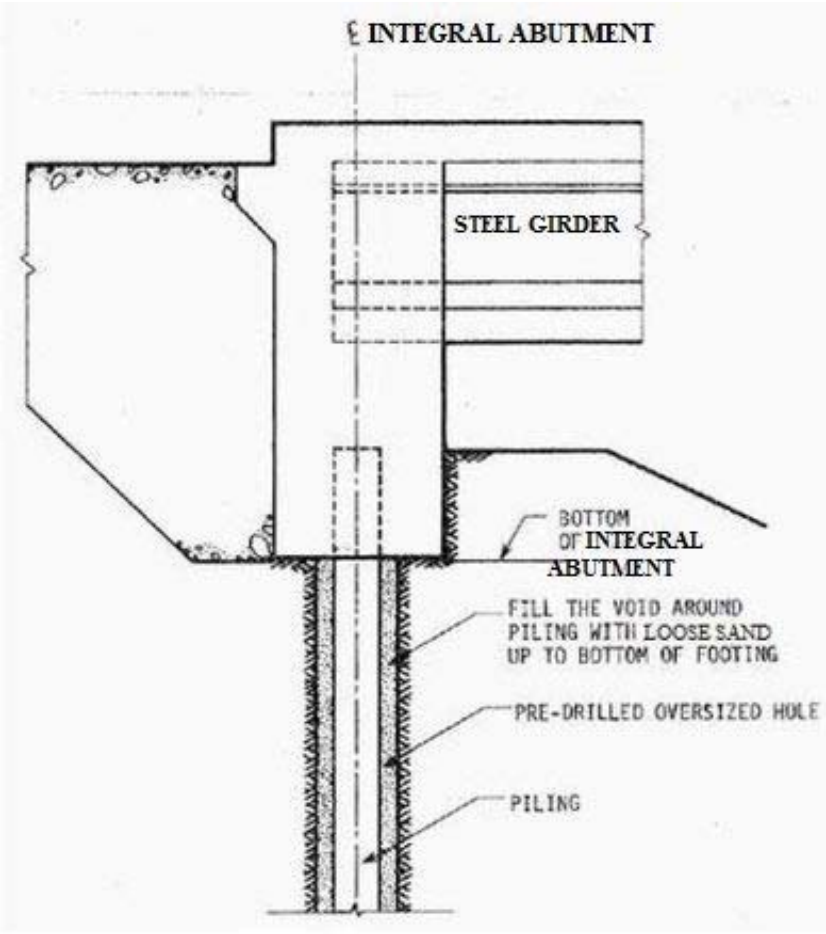

Figure 3-8 Predrilled hole detail (Yang et al. 1982)

Yang et al. (1985) demonstrated that predrilling holes to replace stiff soils with loose sand greatly increases the vertical load capacity of piles. The depth of predrilled holes was a significant factor. Using HP10x42 steel piles, 6 to 10 feet of depth was necessary to take full advantage of predrilling. Mourad and Tabsh (1998) report that the predrilled holes need to be 10 to 20 feet deep, measured from the pile head. Crovo (1998) and Wasserman (2001) report that the depth of predrilled holes should be at least 8 feet, Najib (2002), Thaanasarttayawibul et al. (2014), and Amde et al. (2014) suggest 9-feet-deep predrilled holes filled with loose sand, and Mistry (2005) recommends the use of 10-feet-deep predrilled holes. In addition, Crovo (1998) suggests that the diameter of predrilled holes should be 2 feet while Wasserman (2001) recommends that the diameter of

predrilled holes should be twice the equivalent diameter of the pile. The state of Vermont indicates that the diameter of predrilled holes shall be the diagonal dimension of the pile plus a minimum of 6 inches while the Massachusetts Department of Transportation stipulates that the diameter of the predrilled holes shall be 2'-6". Meanwhile, the state of Iowa makes the holes twice the equivalent diameter of the pile (Dunker and Liu 2007).

For HP sections, the equivalent diameter of the pile is equal to twice the length of the equivalent radius given by the expression (Figure 3-9)

$$R_{equiv.} = (b + h) / \pi$$

where

$R_{equiv.}$ is the equivalent radius of the HP steel section

b is the flange width of the HP steel section

h is the depth of the HP section

π is a mathematical constant that is the ratio of a circle's circumference to its diameter and is equal to 3.14

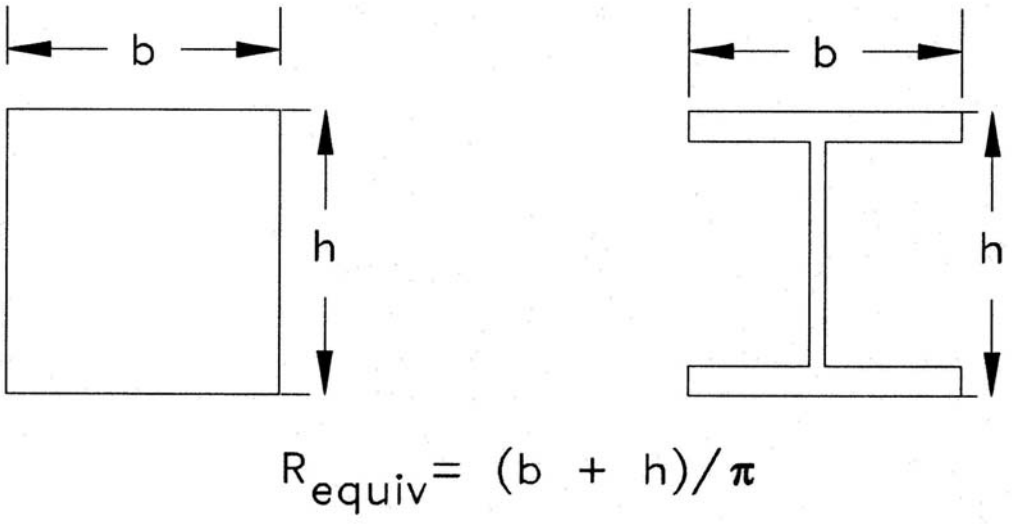

Figure 3-9 Equivalent radius of HP section

3.2.6. Flexibility of Substructure

The magnitude and distribution of stresses in an integral bridge depends on the flexibility of the substructure. Pile orientation, superstructure to substructure stiffness ratio, and the boundary conditions of the abutment system have a significant effect on the flexibility of the substructure. A properly-designed pile system can accommodate superstructure and abutment movement by flexure near its top and will be sufficiently strong to withstand passive soil pressures, pressures generated by traffic on the approach slab, and vertical loads. For integral abutment bridges, the most important issue is the ability of abutment piles to accommodate the expected translation, not the axial capacity.

Pile Orientation

The orientation of a pile in an integral abutment system has a significant effect on the stresses generated in the piles. Piles are oriented either in strong-axis bending (Figure 3-8) or in weak-axis bending (Figure 3-11). Although both methods have proven to be satisfactory (Wasserman and Walker 1996), the responses of the fifty state transportation departments to the survey on integral abutment bridges (Chapter 4) indicate that the majority of states orient integral abutment piles for weak-axis bending. The survey also indicates that a number of states orient their piles either in strong-axis bending or weak-axis bending depending on the specific situation of the bridge to be designed. This includes bridge length, soil stiffness, pile stiffness, and susceptibility of the bridge to potentially high seismic loads. Thus, some of the integral abutments in those states have their piles oriented in strong-axis bending and some in weak-axis bending.

Strong-axis bending

Strong-axis bending of a pile occurs when the web of the pile is parallel to the roadway and bridge centerline and perpendicular to the abutment centerline (Figure 3-10). Piles oriented for strong-axis bending are better able to resist flange buckling (Wasserman and Walker 1996). As a result, the 2011 New York State DOT Bridge Manual instructs engineers to investigate orienting the piles for strong-axis bending for bridges longer than 245 feet in lieu of developing a plastic hinge under weak-axis bending. Piles oriented in strong-axis bending perform better in terms of nonlinear response under seismic loads (Itani and Pekcan 2011) and provide more structural capacity (Bao and Rietz 2013). Furthermore, they have been shown to provide more rigidity for earthquake loads when liquefaction of the embankment soil is considered (Hassiotis et al. 2006). On the other hand, an analysis model created by the Massachusetts Department of Transportation (Crovo 1998) indicates that when piles are oriented for strong-axis bending, the pile moments and shears increase by a factor of two when the soil behind the abutment wall changes from loose to dense. Notable states that orient all their integral abutment piles for strong-axis bending include California, Nevada, and Tennessee.

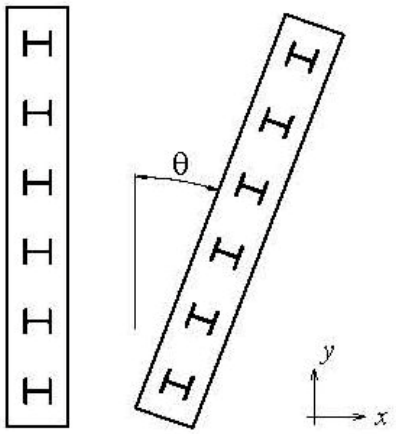

Figure 3-10 Strong-axis bending pile orientation

Weak-axis bending

Weak-axis bending of a pile occurs when the web of the pile is perpendicular to the roadway and bridge centerline and parallel to the abutment centerline (Figure 3-11). Arsoy et al. (2002) report that steel H-piles oriented in weak-axis bending are the best pile type for support of integral abutment bridges. However, piles oriented in weak-axis bending offer less resistance to movement and as a result may subject the piles to cyclic axial and flexural stresses that approach, equal or exceed the yield strength of the steel (Amde et al. 1982; Jorgenson 1983). This can lead to the formation of a plastic hinge at the pile section near the pile head under critical combinations of weak-axis pile bending orientation, stiff soils, and long bridge length (Huang et al. 2008). Because of the potential for formation of a plastic hinge, several states use compact sections for piles oriented for weak-axis bending. On the other hand, orienting the piles in weak-axis bending, reduces the stresses in the abutment wall and the superstructure. Research by Thippeswamy and GangaRao (1995) indicates that the orientation of piles has a significant impact on the stresses in the superstructure. Weak-axis bending of piles resulted in stresses at the superstructure and abutment joint that were three times lower than the stresses developed when the piles were oriented for strong-axis bending. Models developed by Amde et al. (1987) predicted a 20 percent increase in pile pre-load, a 10 percent increase in girder axial load, and a 20 percent increase in superstructure stresses when piles were oriented for strong-axis bending instead of weak-axis bending. Huang et al. (2008) confirms the fact that orienting the piles in strong-axis bending increases the stresses in the superstructure. The survey on integral abutment bridges (Chapter 4) indicates that the majority of states orient all their integral abutment piles for weak-axis bending. This includes among others the states of Iowa, Maine, Massachusetts, Minnesota, Missouri, New Jersey, Pennsylvania, Vermont, and Virginia.

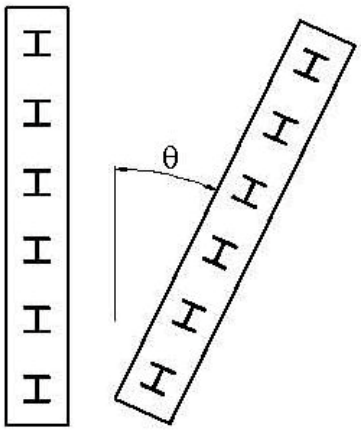

Figure 3-11 Weak-axis bending pile orientation

Superstructure to Substructure Stiffness Ratio

The ratio of the superstructure stiffness to the substructure stiffness has a significant impact on the magnitude and distribution of forces and moments in the bridge system. This is due to the fact that when the ratio is high the magnitude of the temperature-induced displacements are almost unaffected by the stiffness of the integral abutment piles. Under this scenario, the stiffest piles and the most flexible piles are subject to essentially the same displacement (Duncan and Arsoy 2003). The ratio is lower for bridges with longer spans and/or stiff abutments and piles. As the superstructure to abutment stiffness ratio decreases, the effects of continuous frame action are becoming more pronounced. For bridges with short spans and/or flexible substructures, the superstructures tend to behave more like a simply supported structure.

Flexible substructures tend to relieve some of the tensile stress in the deck at the abutment, but increase tensile stresses at midspan. Thippeswamy and GangaRao (1995) conducted a numerical analysis of five steel girder integral bridges with varying skew and pile orientations. The effects of dead load, live load, creep, shrinkage, temperature gradient, settlement, and earth pressures were examined for spread footings and pile systems with varying stiffness. For more flexible pile supported abutments, tensile stresses in the bridge deck at the abutment caused by dead and live loads were reduced significantly. Overall, the stress from combined loads at the abutment joint was two-and-a-half times lower for piles than for stiff spread footing systems. The compressive stresses from combined loads at midspan were reduced, but the tensile stresses in the steel girders increased significantly. In fact, the bottom tensile stress in flexible systems exceeded the allowable stress in the steel. More flexible systems also had tensile stresses from dead loads nearly twice that for stiff systems in the superstructure at the intermediate piers. Creep, settlement, and temperature gradient stresses were also affected by the substructure stiffness. Creep reduced top tensile stresses at the abutment

up to 40 percent for a very stiff spread footing and reduced stresses 10 percent for the systems on piles. Stresses in stiff footing systems at the superstructure and abutment joint due to temperature gradients were nearly double the stresses for flexible systems. Settlement stresses were also considerable for stiff footings and very small for flexible systems. At the foundation level, large stresses developed in the stiff footings. Total stresses from creep, temperature gradient, shrinkage, and settlement in the piles and more flexible spread footings were considered negligible.

Thippeswamy et al. (1994) used a two-dimensional frame model to study the effects of varying superstructure to substructure stiffness ratio, among other variables, on the moments within the structure. The superstructure to substructure stiffness ratio had a significant influence on the magnitude of the moments developed in the bridges. The moments at midspan of the superstructure due to dead and live load increased as the substructure became more flexible while the moment due to temperature gradients decreased. The moment at the footing and at midspan of the superstructure due to earth pressure became increasingly negative as the flexibility of the substructure increased. Finally, the magnitude of the moment in the footing due to a one-inch settlement decreased. Settlement moments were negligible at midspan.

Boundary Conditions

Piles are usually considered fully fixed at the pile cap and fixed or free to rotate at the pile tip. Although piles have typically been constructed integrally with the abutment wall, researchers have experimented with pinned head connections. There may be some advantage to this because it may lead to lower bending stresses in the piles. Numerical analysis of concrete piles conducted by Kamel et al. (1995) confirmed that piles with fixed heads had significantly higher bending stresses than piles with hinged heads for a constant lateral deflection regardless of the soil density. In addition, Husain and Bagnariol (1996) indicate that if the connection is fixed, plastic bending moments may develop at the pile top due to thermal movements and effect of vehicular traffic and may result in the formation of a plastic hinge.

Although bending stresses may be lower in pinned head piles, the axial load capacity of the piles could decrease. Models developed by Greimann et al. (1984) resulted in a 10 percent reduction in the axial load capacity of steel H-piles with a fixed head at a lateral displacement of four inches. However, the axial load capacity was reduced 20 percent for a pinned head pile at a lateral displacement of four inches. Contrary to these results, Mourad and Tabsh (1998) found that the axial load capacity in the piles was unaffected by changing the connection from fixed to pinned.

Frosch et al. (2009) conducted a research on the response of integral abutment bridges to seismic loading. They concluded that full fixity with a 24-inch pile embedment in the abutment provides enhanced behavior for seismic considerations. In addition, they discourage the use of "pin" detail because its performance under dynamic load is uncertain.

Burke (1987) and Mistry (2005) suggest that the pile should be embedded into the abutment pile cap approximately two pile diameters (or widths) to achieve pile fixity. Similarly, the 2003 Federal Highway Administration report FHWA NHI-04-041 indicates that a pile needs to be embedded 2 to 3 times its diameter into the pile cap to develop full fixity. Crovo (1998) as well as Dunker and Abu-Hawash (2005) suggest that projecting the piles 2 feet into the abutment ensures pile fixity. This conclusion is confirmed by a 2009 research report prepared by CTC & Associates LLC and the research unit of the Wisconsin Department of Transportation indicating that most states require a minimum pile embedment of 2 feet into the integral abutment to assure pile fixity. The report also indicates that the state of Oregon relates the minimum pile embedment with pile size. As a result, the embedment length for HP10X42 and HP12X53 piles is 20 inches; the embedment length for HP12X74 and HP14X89 piles is 24 inches; and the embedment length for HP14X117 piles is 27 inches.

The fixity condition at the base of the pile does not appear to have a significant influence on the overall behavior of the pile because the piles usually have sufficient embedment depth to develop double curvature. The fixity of the base of the pile may be a concern when the pile is shallow or the soil is loose. For abutment walls without piles, the fixity of the base of the abutment wall footing appears to have only a small influence on the stresses in the superstructure. A frame model studied by (Thippeswamy et al. 1994) showed that fixing the base of the abutment caused a slight reduction in the superstructure moments at midspan and at the supports due to primary loads. The moment due to earth pressure at the support switched from negative to positive. Frame models by Dahger et al. (1991) also indicated that the degree of fixity does not affect the moments and shears in the superstructure.

3.2.7. Foundation Systems

The typical foundation for integral abutment bridges is a single row of vertical piles. Although steel H-piles are most frequently used to support integral abutments, cast-in-place concrete piles, prestressed concrete piles, steel pipe piles (open ended or concrete filled), drilled shafts, and spread footings are also used by states as indicated by the survey on integral abutment bridges (Chapter 4). The survey also indicates that several states use different foundation systems for integral abutments depending on soil conditions within the various geographic regions of the state.

Steel H-piles are by far the most-commonly-used pile type to support integral abutments (Dunker and Liu 2007) and the best pile type for support of integral abutment bridges if oriented in weak-axis bending (Arsoy et al. 2002). Experimental data from Arsoy et al. (1999, 2002) showed that steel H-piles supporting integral bridges can withstand cyclic loading as long as the total stress induced in the piles does not exceed the yield strength of the steel. Although the steel H-piles can be either end bearing or friction piles, the majority of states use bearing piles in integral abutments (GangaRao et al. 1996). Olson et al. (2009) suggest that using higher grade steel such as 50 ksi in lieu of 36 ksi allows for an increase of the present bridge length limits and skew of integral abutment bridges. This confirmed a parametric study conducted by Dunker and Abu-Hawash (2005) suggesting that an increase in pile specified yield strength from 36 Ksi to 50 Ksi can double the limits on integral abutment bridge lengths currently in place in the state of Iowa.

Prestressed concrete piles are also used to support integral abutments. Cyclic tests conducted by Oesterle et al. (1998) on steel H-piles and prestressed concrete piles showed that both were able to sustain the applied vertical load throughout the tests. However, the prestressed concrete piles sustained damage that was considered unacceptable. Research conducted by Arsoy et al. (2002) determined that prestressed concrete piles are too stiff to support integral abutments. Under repeated lateral loads, tension cracks developed in the piles at the location of the connection of those piles to the integral abutment, which resulted in a significant reduction of their vertical load capacity. As a result, they discourage their use for the support of integral abutments.

Kamel et al. (1996) investigated the use of prestressed concrete piles in integral abutment bridges. The researchers studied the lateral load versus lateral displacement relationships for both prestressed concrete piles and steel H-piles. The steel H-piles experienced greater lateral displacements than that of the prestressed concrete piles before the allowable moment strength was developed for a cross section of the pile. Laboratory tests of piles in loose sand, which is sometimes placed in prebored holes for integral abutment piles, revealed that the density of the sand had a significant effect on the lateral displacements of both types of piles. The lateral displacements of a pile head were dependent on the lateral stiffness of the soil against the upper 10 feet of the pile length. The lateral stiffness of the soil below this depth had a negligible effect on the lateral

displacement at the pile head. This behavior was observed for both the prestressed concrete piles and the steel H-piles.

Burdette et al. (2007) performed a series of lateral load tests at the University of Tennessee to investigate the behavior of integral abutments supported by prestressed concrete piles. The tests were performed over a period of three years. Four abutments were tested and the results indicated that prestressed concrete piles are appropriate for use in integral abutment bridges. The results also indicated that the Tennessee Department of Transportation design criterion of 1.0 inch horizontal displacement in each direction is conservative. This research confirmed previous research conducted by Burdette et al. (2004), which indicated that prestressed concrete piles are appropriate for use in integral abutment bridges and that the Tennessee Department of Transportation design criteria are conservative. While no specific recommendation of maximum allowable displacement was formulated through the research, a value of displacement of as much as 1.5 inches appears to be reasonable.

Huang et al. (2008) performed a parametric study of concrete integral abutment bridges using cast-in-place concrete piles. Their recommendation is to use cast-in-place concrete piles to support integral abutment bridges only for lengths up to 150 feet because their relatively large bending stiffness can cause large superstructure concrete stresses during temperature changes. This is in line with the practice in the state of New York where cast-in-place concrete piles are only used when the integral abutment bridge length is 160 feet or less (Yannotti et al. 2005). Others (Harvey 2012), advise against the use of cast-in-place concrete piles as a foundation for integral abutments in high-seismic zones.

Steel pipe piles, either open ended or filled with concrete, are also used to support integral abutments. Concrete-filled pipe piles are more ductile than prestressed concrete piles and have greater resistance to local buckling than steel H-piles. They also have large moment and shear capacity (Coduto 1994; Hooper et al. 1999). Sites most suitable for pipe piles include soft clays, silts and loose to medium dense sands underlain by dense-bearing granular material (Prakash and Sharma 1990). Pipe piles can be driven closed end or open end; they are typically economical in the range of 40 to 80 feet and can carry loads as high as 250 kips (Prakash and Sharma 1990). Harvey (2012) reports that steel pipe piles with concrete infill have uniform stiffness in all directions and are the foundation of choice in the earthquake-prone area of British Columbia, Canada. His experience indicates that steel pipe piles with concrete infill provide adequate seismic capacity, yet are fairly flexible if the thermal strains are modest. In addition, a single row of pipe piles achieves both a higher bearing capacity and a higher seismic shear capacity compared to a single row of HP10 piles. Finally, in contrast to H piles, steel pipe piles with concrete infill are not prone to twisting or installation damage in cobbly or bouldery subgrade. Others (Arsoy et al 2002) disagree and discourage the use of pipe piles for the support of integral abutments on the grounds that for a given displacement stresses in an integral abutment supported by pipe piles are always higher compared to stresses in integral abutments supported by steel H-piles. Consequently, according to Arsoy et al. (2002), this increases both the likelihood of abutment distress and the chance that the abutment would fail prior to the pipe piles if one of the two were to fail.

Drilled shafts are not as flexible as H-piles, therefore are rarely used to support integral abutments. The main exception is the state of Hawaii where steel piles have to be imported, corrosion tends to be severe, and steel H-piles have low buckling capacity in scour-susceptible soils (Ooi et al. 2010)

Research indicates that using integral abutments founded on spread footings results in high stresses in the superstructure and that should be limited to bridges with small movements. The fifth edition of AASHTO LRFD Bridge Design Specifications section 11.6.1.3 stipulates that integral abutments shall not be constructed on spread footings founded or keyed into rock unless one end of the span is free to displace longitudinally. The same stipulation exists in the British Columbia Ministry of Transportation Bridge Standards and Procedures Manual (2007). On the other hand, spread-footing integral abutments supported, but not keyed into, rock have been successfully utilized for bridges with up to 0.25 inches of total movement (Wasserman and Walker 1996). Matsushima (2003) argues that in active fault locations, integral abutments supported or keyed into rock, should not be constructed because the vertical fault displacement under the span will cause severe and extensive cracking of the integral abutment bridge as evidenced by the 1999 Chichi Taiwan earthquake.

A critical area in the performance of integral bridges is the bridge reaction to settlements. Spread footings appear to be more susceptible to larger settlement stresses than piles (Ng et al. 1998; Thippeswamy and GangaRao 1995).

3.2.8. Approach Slabs

It is common practice to build an approach slab integrally with the abutment to span the backfill behind the abutment wall. The primary function of the approach slab is to provide a smooth transition between the fixed superstructure and the roadway pavement in order to avoid a "bump" at the end of the bridge. The "bump" is not a significant safety problem; rather it is an expensive maintenance issue. Approach slabs constructed with a joint at the bridge abutment have a tendency to shift towards the flexible approach pavement because of the continual cyclic movement of the bridge and debris infiltration (Sanford and Elgaaly 1993). Moving the joint to the roadway end of the approach slab eliminates shifting of the approach slab off of the slab seat, reduces water infiltration of the backfill and prevents erosion of the abutment backfill or freeze/thaw damage resulting from saturated backfill. Properly-constructed approach slabs also eliminate pressure on the abutment wall from expansion of approach pavement, which has been known to cause severe abutment and pier damage (Arsoy et al. 1999; Xanthakos 1995; Burke 1987).

Others contest the need for approach slabs. Lock (2002) cites evidence that an approach slab is unnecessary and that regular maintenance of the bridge surface is sufficient to accommodate the soil settlement below the approach roadway. Horvath (2000) notes that if an approach slab is used, the slab will eventually crack in flexure due to the cumulative effects of backfill soil settlement and traffic compaction.

A survey conducted by Hoppe (1999) indicates that with the exception of Maryland and Kentucky, all 39 states that responded to the survey are using an approach slab to minimize differential settlement effects and provide a smooth transition from the highway pavement to bridge deck (Greimann et al. 2008). Similar results were obtained in the survey on integral abutment bridges conducted as part of this study (Chapter 4). The survey indicates that 38 out of the 41 states that build integral abutment bridges use approach slabs; Maryland, Virginia, and Arkansas being the exceptions. The overwhelming use of approach slabs is in agreement with the FHWA Technical Advisory T5140.13 (1980) on integral construction that suggests "approach slabs are needed to span the area immediately behind integral abutments to prevent traffic compaction of material where the fill is partially disturbed by abutment movement."

Approach slab details

The level of performance of the approach slab is based upon many factors, including: (1) approach slab dimensions, (2) steel reinforcement, (3) the use of a sleeper slab, and (4) the type of connection between the approach slab and the bridge.

Approach slabs constructed with a joint at the bridge abutment have a tendency to shift towards the flexible approach pavement due to continual thermal cycling of the bridge and the infiltration of debris into the joints between the approach slabs and the bridge decks (Burke 1987). This situation allows drainage to penetrate the joints and erode the

abutment backfill and deteriorate the bearing seat of the approach slab. When approach slabs lose support, they behave like cantilever beams supported on the abutment. Bending moments develop in this section. Since approach slabs are not designed to carry these moments, cracking in the approach slabs develops. As a result, Stewart (1985) suggests that the approach slab should be doweled into the backwall to ensure a watertight joint. In addition, the slab should be cantilevered over the wingwalls to minimize surface water infiltration beneath the approach slabs resulting from the differential movement between the approach slabs and wingwalls (Maberry and Camp 2005). Wasserman and Walker (1996) encourage the use of a rigid connection between the approach slab and the abutment to prevent a shifting of the approach slab from its support. In addition, FHWA Technical Advisory T5140.13 (1980) states that the approach slab should be anchored with reinforcing steel to the superstructure.

There are two techniques to connect the approach slab to the bridge (Kunin and Alampalli 2000). The first technique is to connect the approach slab to the bridge through extension of the bridge deck rebar (Figure 3-12). The second technique uses reinforcing steel to connect the approach slab to the integral abutment (Figure 3-13).

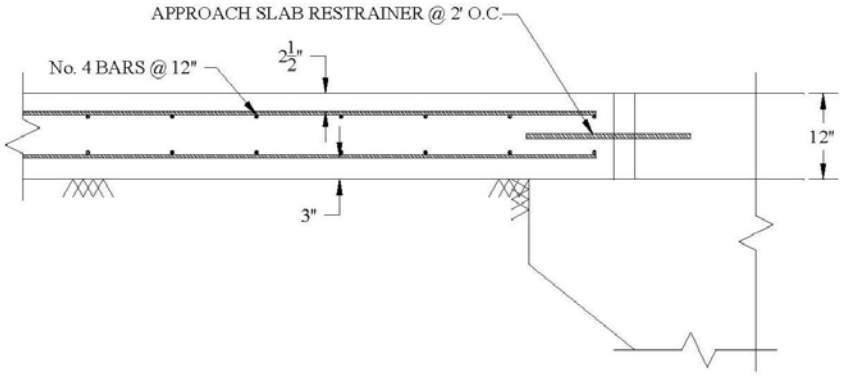

Figure 3-12 Connection of approach slab to bridge deck (standard Nevada detail)

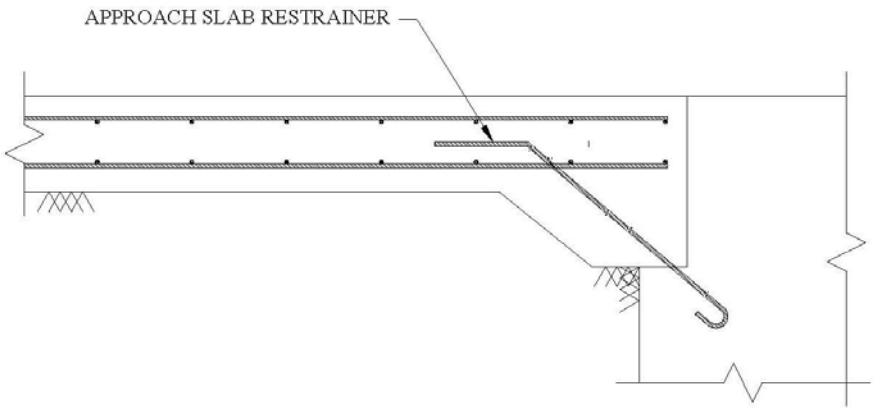

Figure 3-13 Connection of approach slab to integral abutment (standard Ohio detail)

For the connection of approach slab and roadway pavement, Mistry (2008) recommends the use of sleeper slabs as a means to avoid or minimize cracking and settlement at the approach slab/roadway pavement joint (Figure 3-14). The intent of the joint seal in Figure 3-14 is to absorb thermal strains that occur at the far end of the approach slab from the pavement and the bridge. However, Harvey (2012) warns that this detail is costly and requires maintenance because the seal element can be easily damaged by traffic, debris, or freezing conditions. Consequently, he recommends the use of inexpensive mastic-filled saw cut joint, which intercepts pavement cracks.

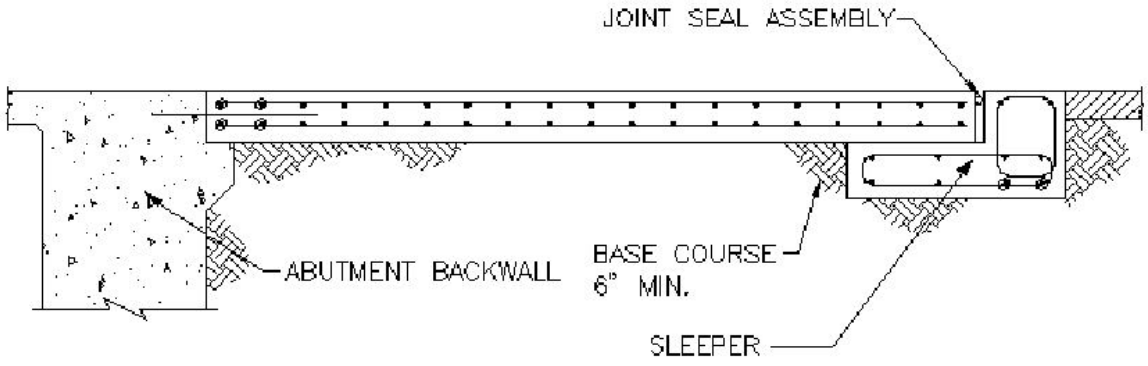

Figure 3-14 Sleeper slab at the connection of approach slab and roadway pavement

Approach slab dimensions

The length of the approach slab is often based on experience, approximate calculations or derived from finite element simulations. In general, the length of an approach slab is compatible with the expected settlement. As a result, longer approach slabs are used in cases involving very soft foundation soils and/or high embankments.

Stewart (1985) suggests using approach slabs 30 ft long supported on select backfill material having a maximum plasticity index (PI) of 15, fewer than 40 percent fines, and 95 percent compaction. Briaud et al. (1997) recommend that approach slabs be designed to span various lengths; typically 13 to 23 feet. Thiagarajan et al. (2010) recommend approach slabs having a length of 20 feet and thickness 12 inches for new construction. According to Arsoy et al. (1999), "it is often argued that the length of the approach slabs should be made two to three times the height of the abutment." This argument follows from the rationale that displacing an abutment causes movement of a wedge of the backfill with a height equal to the height of the abutment and a length equal to $\tan(45+\Phi/2)$, which is about twice the height of the abutment; φ is the angle of internal friction of the fill. However, a finite element analysis conducted by Arsoy et al. (1999) indicates that the length of the settlement zone extends to about three and one-half times the height of the abutment.

Surveys conducted by Hoppe (1999) and Thiagarajan et al. (2010) indicate that the majority of states are using 20-feet-long approach slabs. The shortest reported length is 10 feet and the longest 40 feet. The reported thickness of the slabs varies from 8 inches for a 15-feet-long approach slab to 17 inches for a 30-feet-long approach slab. Approach slabs with length of 20 feet have a thickness that varies between 9 and 15 inches with 12 inches be the most common.

Longitudinal slope of the approach slab

The primary function of the approach slab is to provide a gradual transition between the fixed superstructure and the roadway pavement in order to avoid a "bump" at the end of the bridge. Ideally, the longitudinal slope of the approach slab should match the longitudinal slope of the bridge. In most cases, however, this is not possible because the slope of the approach slab should also match the slope of the roadway on the other end of the approach slab. Then, there is the issue of rider comfort. As a result, there should be a limit in the difference in slope between the slopes of fixed bridge/approach slab and between approach slab/roadway. According to Briaud et al. (1997), the maximum allowable change in slope should be 1/200 of the approach slab length, based on studies by Wahls (1990) and Stark et al. (1995). This critical settlement gradient was also referred by Long et al. (1998) and is used by several states as a threshold value to initiate maintenance procedures on bridge approach areas. Others (Albajar et al. 2005) establish a threshold value of 1.5 inches of vertical settlement as the starting point of maintenance procedures (Puppala et al. 2008).

Impacts of superstructure length on the approach slab

Alampalli and Yannotti (1998) noted that there is a direct and significant correlation between the condition of the approach slabs and the length of steel superstructure integral bridges. They note an inverse relation between the length of steel superstructures and approach slab ratings; the longer the steel superstructure, the lower the approach slab ratings. Washington State reports problems with approach slabs when the integral bridge length exceeds 350 feet.

Impacts of approach slab on the bridge

Greimann et al. (2008) investigated the impacts that approach slabs have on the bridge. They found that tying the approach slab to the bridge induces longitudinal and transverse abutment displacements as well as girder forces; moments and axial forces. Induced abutment displacements range from a maximum positive displacement to a maximum negative displacement while induced girder forces include compressive axial forces and both positive and negative moments. However, the reference makes no comparison between the magnitude of induced and existing girder forces and abutment displacements. Furthermore, there is no reference to any changes in abutment or girder design as a result of the additional forces induced in the bridge.

3.2.9. Wingwalls

Wingwalls are located at the ends of a bridge and their function is to retain the approach roadway embankment. There are two types of wingwalls; independent and cantilever wingwalls. Independent wingwalls are separated from the abutment with an expansion or construction joint while cantilever wingwalls are built integral with the abutment. Wingwalls are considered part of the bridge substructure only if they are integral with the abutment. Thus, only cantilever wingwalls are considered part of the bridge substructure. Although cantilever wingwalls are not the primary load-carrying members of the integral bridges, their connection to the integral abutment might have an impact on the magnitude and distribution of forces throughout the bridge structure (White 2008).

Depending on their orientation with respect to the abutment wall, cantilever wingwalls are classified as cantilevered inline wingwalls (Figure 3-15), cantilevered U-shaped wingwalls (Figure 3-16), or cantilevered flared wingwalls (Figure 3-17). Cantilevered inline wingwalls are inline extensions of the abutment wall. Cantilevered U-shaped wingwalls are parallel to the roadway centerline. Cantilevered flared wingwalls have an orientation that lies between an inline and a U-shaped wingwall.

The orientation of cantilever wingwalls has a significant influence because as the wingwall orientation changes from parallel to perpendicular to the abutment, the soil becomes more confined. According to Chu (2010), wingwalls parallel to abutments take the least time to build and provide the least disturbance to existing slope embankment. He also states that wingwalls at an angle to abutments offer the most economical solution among the three orientations in terms of material cost. Research has confirmed that the U-shaped wingwall orientation produces the greatest confining effect, which increases the earth pressure on the wingwalls to the level of at-rest pressures (Harvey 2012) and by as much as a factor of 2 on the abutments (Crovo 1998). However, despite the increase in the magnitude of earth pressures, U-shaped wingwalls have the benefit of reducing approach fill settlements (Arsoy et al. 1999) and provide a support for the traffic barriers (Harvey 2012).

Wingwalls also affect not only the magnitude, but also the distribution of loads in the bridge structure. Mourad and Tabsh (1998) studied the effect of adding U-shaped wingwalls and changing their length. Only live loads were considered in the analysis. For bridges without wingwalls, the analysis showed that the applied live load was distributed more uniformly among the piles under the abutment walls. Pile axial stresses were larger when a wingwall was in place, but decreased as the wingwall length increased because the moment arm was longer over a constant applied moment. The pile under the end of the wingwall farthest from the abutment was always in tension. The abutment wall-wingwall system did not behave as a rigid block under the applied truck loads, so the piles at the corners of the substructure were not always the most heavily loaded.

A different behavior is observed when bridge movement is considered. The wingwalls provide resistance to bridge expansion and also resist the tendency of the abutment to

rotate as the bridge expands. Compressive axial forces are developed in the wingwall piles that resist the vertical abutment rotation. This may result in axial strains that are much larger than the predicted axial strains in the abutment piles (Sayers 2000).

The influence of cantilever wingwalls and their orientation is further complicated for skewed bridges as well as bridges on a horizontally-curved alignment.

White (2008) conducted a survey on wingwall types used by states. Out of the thirty states that responded to the survey, only 10 states use flared wingwalls. By contrast, 24 states use U-shaped wingwalls, and 19 states use inline wingwalls. According to the survey, very few states use piles beneath the wingwalls. In fact, only the state of Wisconsin uses piles beneath flared wingwalls, five states use piles underneath U-shaped wingwalls, and six states use piles underneath inline wingwalls. The survey on integral abutment bridges conducted as part of this study (Chapter 4) indicates similar responses to both issues, that is, types of wingwalls and wingwall foundations used by states.

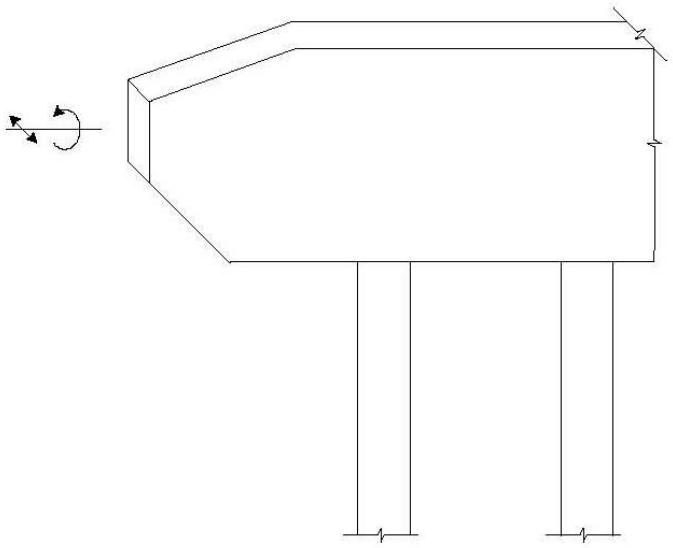

Figure 3-15 Cantilevered inline wingwall (White 2008)

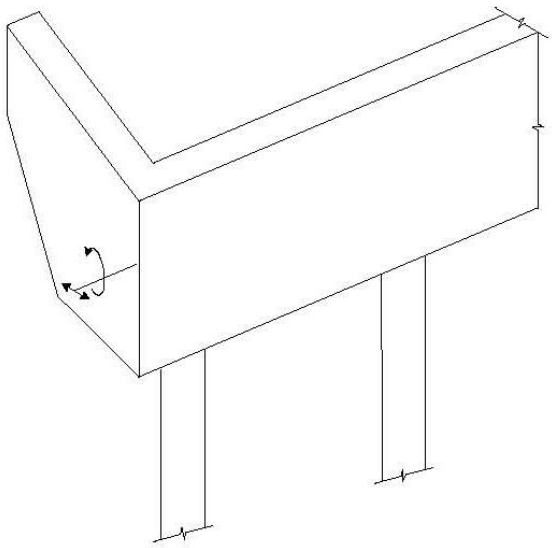

Figure 3-16 Cantilevered U-shaped wingwall (White 2008)

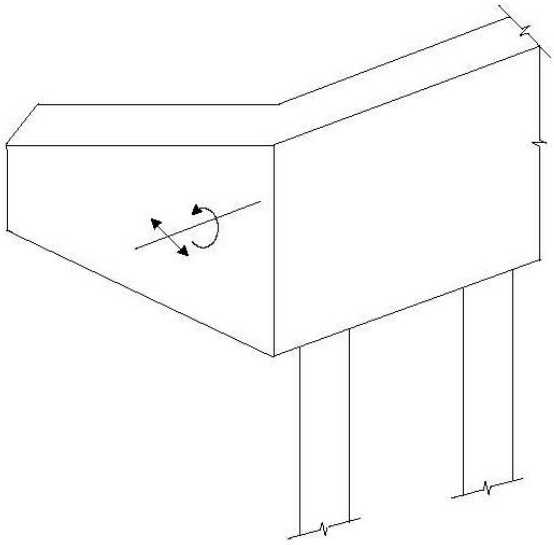

Figure 3-17 Cantilevered flared wingwall (White 2008)

3.2.10. Bridge length and movement limitations

One of the main reasons for the increasing use of integral abutment bridges by states is their economic advantage over conventional bridges. Consequently, using the integral abutment concept to longer bridges will produce more economic benefits. As a result, the question arises about the length limit of integral abutment bridges.

Arsoy et al. (1999) assert that the maximum length of an integral bridge is very difficult to determine. Many researchers agree that a thorough understanding of the complex soil – structure interaction of an integral bridge is necessary in order to expand the current limits on the lengths of integral bridges.

Dicleli and Albhaisi (2003) used a low-cycle fatigue damage model for the piles to define the maximum length limits of integral bridges. They calculated the maximum strain amplitude a steel pile can sustain and retain a service life of 75 years. Accordingly, they recommend maximum bridge lengths of 490–870 feet for concrete superstructures on cold climates and 590–1050 feet for concrete superstructures on moderate climates. For steel superstructures the bridges length range is between 260–475 feet for cold climates and 410–720 feet for moderate climates.

Wasserman (2007) indicates that the length limit of integral abutment bridges should be determined by the longitudinal displacement that an abutment and piles can withstand without sustaining damage that threatens serviceability. According to Wasserman, integral abutments can accommodate 2 inches of movement at each end.

Kunin and Alampalli (1999) conducted a survey to ascertain bridge length and movement limitations allowed by states. The findings are shown in Table 3-1. Iinterestingly enough, several states built integral abutment bridges having lengths longer than the limits indicated in the survey. For example, Colorado built a 1,044 feet steel integral abutment bridge (limit is 300 ft) and a 952 feet cast-in-place integral abutment bridge (limit is 500 ft). Tennessee built a 1,175 feet precast concrete integral abutment bridge (limit is 800 ft) and a 525 feet steel integral abutment bridge (limit is 430 ft).

Table 3-1 Maximum allowable limits (Kunin and Alampalli 1999)

State or Prov.	Thermal movement (cm)	Length (m)			Skew angle (deg)	Tolerance for pile location (cm)	Height (m)	
		Steel girder	Pre-cast concrete girder	Cast-in-place concrete girder			Abutment	Stem
AK	–	–	61.0	–	30	7.6	–	–
AR	–	91.5	91.5	–	15	Per specs	No limit	No limit
CA	1.3	31.1	50.9	50.9	21	10.2	4.3	2.7
CO	10.2	91.5	183.0	152.5	No limit	15.2	No limit	No limit
GA	No limit	No limit	No limit	No limit	30	No specs	No limit	No limit
IL	No limit	83.9	114.4	114.4	30	Standard	No limit	No limit
IA	Limited by length	Undet.	152.5	152.5	30	7.6	0.9 to 1.5	Length dependent
KS	5.1	91.5	152.5	152.5	45	7.6	By design	By design
KY	No limit	91.5	122.0	122.0	30	15.2	No limit	0.9 m min. pile cap
ME	9.5	90.0	150.0	150.0	25	5.1	3.6	–
MD	2.5	–	18.3	–	30	15.2	3.1 to 4.6	3.1
MA	Not defined	99.1	99.1	99.1	30	7.6	Minimize	Minimize
MI	No limit	No limit	No limit	No limit	30	15.2	–	–
MN	No limit	61.0	61.0	61.0	20	No specs	1.0	1.0
NV	2.5	76.3	122.0	122.0	20- 45	–	Design	Design
NH	3.8	45.8	24.4	–	10	–	–	–
NY	Limited by length	140.0	140.0	140.0	30	2.5	–	0.3 to 0.6
ND	Limited by length	122.0	122.0	48.8	30	No specs	3.7	1.5 to 1.8
OK	–	91.5	122.0	–	0	15.2	3.1	1.8
OR	No limit	No limit	No limit	No limit	45	No specs	No limit	No limit
PA	5.1	91.5–122	122.0	Not used	20	–	–	–
QC	No limit	–	78.1	–	20°15′	5.0	3.0	1.9
SD	Limited by length	106.8	213.5	213.5	30	15.2	No limit	–
TN	5.1	130.8	244.0	244.0	No limit	No specs	–	No limit
VT	Limited by length	24.4	–	–	15	Standard	No limit	No limit
VA	3.8	91.5/45.8	152.5/79.3	–	30	7.6	No limit	No limit
WA	No limit	Not used	106.8	61.0	30	15.2	–	3.7
WV	5.1	Movement is limited, not length			30	7.6	No limit	No limit
WY	5.0	100.0	No limit	100.0	45	2.0	No limit	No limit
Max.	**No limit**	**No limit**	**No limit**	**No limit**	**No limit**	**Per specs**	**No limit**	**No limit**
Min.	**1.3**	**24.4**	**18.3**	**48.8**	**No skew**	**2.0**	**0.9**	**0.3**

3.2.11. Type of Superstructure

Typical integral abutment bridge superstructures consist of a concrete deck supported by steel I-beams, concrete I-beams, concrete bulb tees, concrete spread box beams, or hybrid composite beams. Olson et al. (2009) report that the use of steel versus concrete girders has only a secondary effect on the performance of the abutments and foundations, and for practical purposes can be considered to be the same. A survey conducted by Kunin and Alampalli (1999) indicates that 13 states report no difference in the performance of steel and concrete girder bridge superstructures. Colorado reports that steel bridges experience some cracking and spalling in the bearing areas of the abutment diaphragm. However, New York observes less deck cracking on steel girder bridges (Alampalli and Yannotti 1998). Kansas notes that steel girders move more and that concrete girders shrink. Oregon states that bridges with prestressed or post-tensioned concrete experience creep shortening after construction. However, none of the states report any structural problems with any type of superstructure in use.

3.2.12. Construction Sequence

Successful implementation of integral abutment bridges requires attention to construction sequence and good guidance to the contractor in the contract documents (Harvey and Kennedy 2002). According to Wasserman and Walker (1996) appropriate construction sequence is necessary to reduce the effects of thermal movements on fresh concrete and control moments induced into the supporting pile system. This is due to the fact that the abutments and superstructures of integral bridges are rigidly connected and any differential movement of the separate elements can damage fresh concrete. This is of particular concern for integral bridges with steel girders. As a result, Wasserman (2007) recommends a certain construction sequence when constructing steel bridges with integral abutments.

Husain and Bagnariol (1996) note that backfill shall be placed simultaneously behind both abutments keeping the height of the backfill approximately the same. In addition, backfill behind the abutment shall not be placed until the deck has reached 75 percent of the specified concrete strength.

The British Columbia Ministry of Transportation Bridge Standards (2007) section 8.11.2.1.3 states that concrete placement sequence for integral abutments shall be given special consideration to reduce stresses induced by deflection of the girders. Thus, the full width and length of deck shall be cast prior to end diaphragms being cast integral with the abutment.

Lee (2007) suggests a construction sequence composed of six steps illustrated in Figures 3-18 thru 3-23.

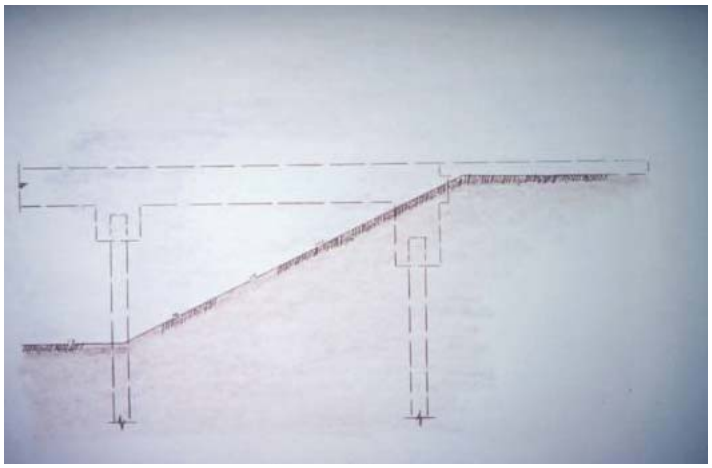

Figure 3-18 Step 1: Placement of abutment embankment

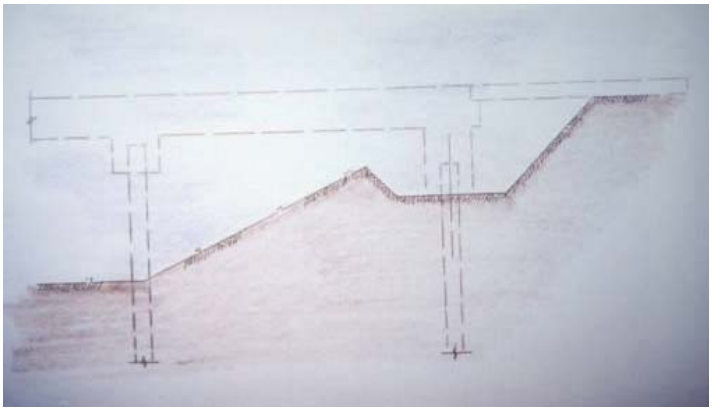

Figure 3-19 Step 2: Excavation for abutment pile cap

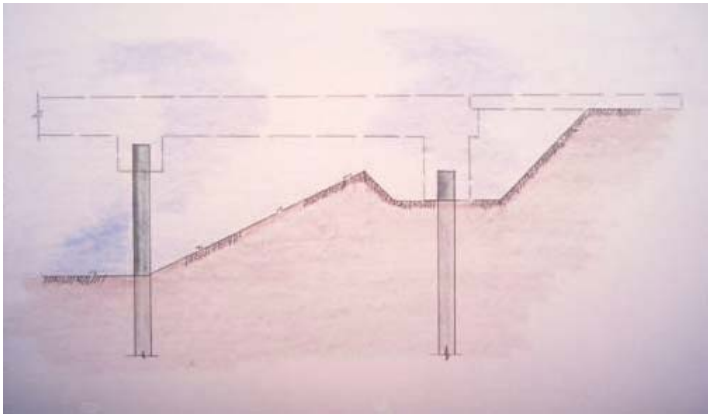

Figure 3-20 Step 3: Driving of integral abutment piles

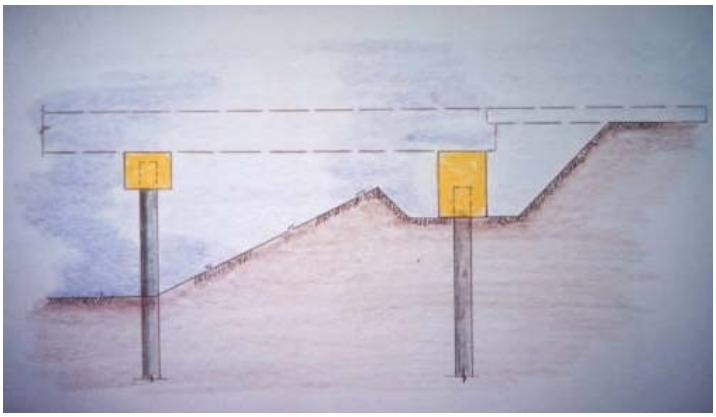

Figure 3-21 Step 4: Construction of integral abutment pile cap

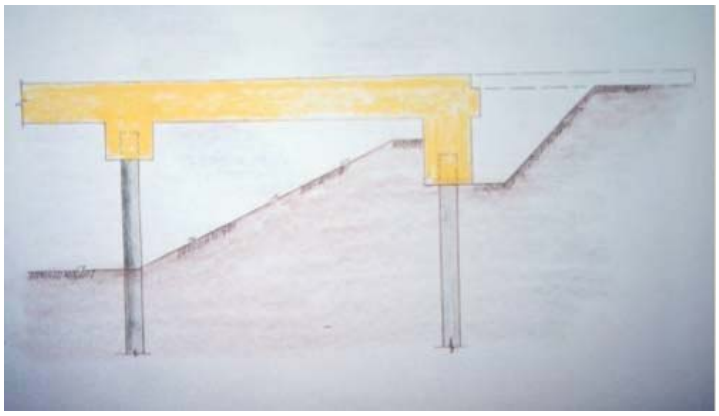

Figure 3-22 Step 5: Construction of deck slab and end diaphragm at abutment

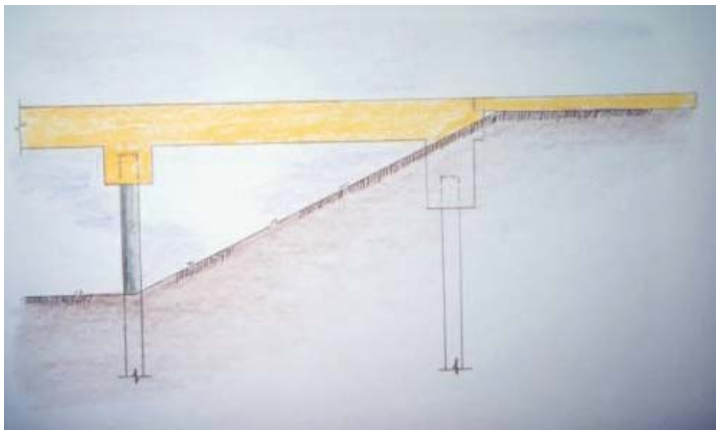

Figure 3-23 Step 6: Placement of backfill and construction of approach slab

Chapter 4

Survey on Integral Abutment Bridges

4.1. Introduction

Integral abutment bridges are used in the United States for decades starting in the 1920s. A testament of their excellent performance over the years is the fact that the current policy of the majority of states is to build integral abutment bridges whenever possible. In fact, forty-one states are now using integral abutment bridges. This is due to the fact that integral abutment bridges cost less to construct and maintain compared to conventional bridges. However, despite their success and acceptance by both federal and state transportation agencies as well as the engineering community in general, nationally-accepted design specifications for integral abutment bridges do not exist. Neither the AASHTO LRFD Bridge Design Specifications nor the AASHTO Standard Specifications contain detailed design criteria for integral abutment bridges. Instead, states have developed their own design guidelines for integral abutment bridges.

This chapter presents the findings of a survey of the fifty state transportation departments on the subject of integral abutment bridges. The survey was conducted as part of this research study is divided into two parts: The first part of the survey relates to the design parameters used by the fifty states to design integral abutment bridges. The second part of the survey focuses on the status of use, problems, and costs associated with the use of integral abutment bridges in all fifty states.

The responses to the survey indicate that forty-one states are using integral abutment bridges. The nine states that do not use integral abutments are: Alabama, Alaska, Arizona, Delaware, Florida, Louisiana, Mississippi, Texas, and Washington.

4.2. Survey Questions Related to Design Parameters of Use of Integral Abutment Bridges

This part of the survey focuses on the design parameters used by the fifty state transportation departments across the United States. The survey questions relate to the type of superstructure, alignment, skew, bridge length, foundation type, pile orientation, structural assumptions for the ends of girders and top of piles, secondary lateral load effects on pile stresses, pile bending stresses, backfill material, use of approach slabs and their connection to integral abutments, types of wingwalls and wingwall foundations. Forty-seven states responded to this part of the survey; Montana, Rhode Island, and South Carolina didn't respond.

Type of superstructure

The FHWA Bridge Programs National Bridge Inventory (NBI) Data indicates that all fifty states have bridges with steel, prestressed concrete, and cast-in-place concrete superstructure. However, the state responses indicate that only 98 percent of the 41 states that build integral abutments have steel superstructures, 93 percent prestressed concrete and 63 percent cast-in-place concrete superstructure (Figure 4-1). Hawaii is the only state not using a steel superstructure while Connecticut, Montana, and Nevada are the three states that do not use prestressed concrete superstructures with integral abutment bridges.

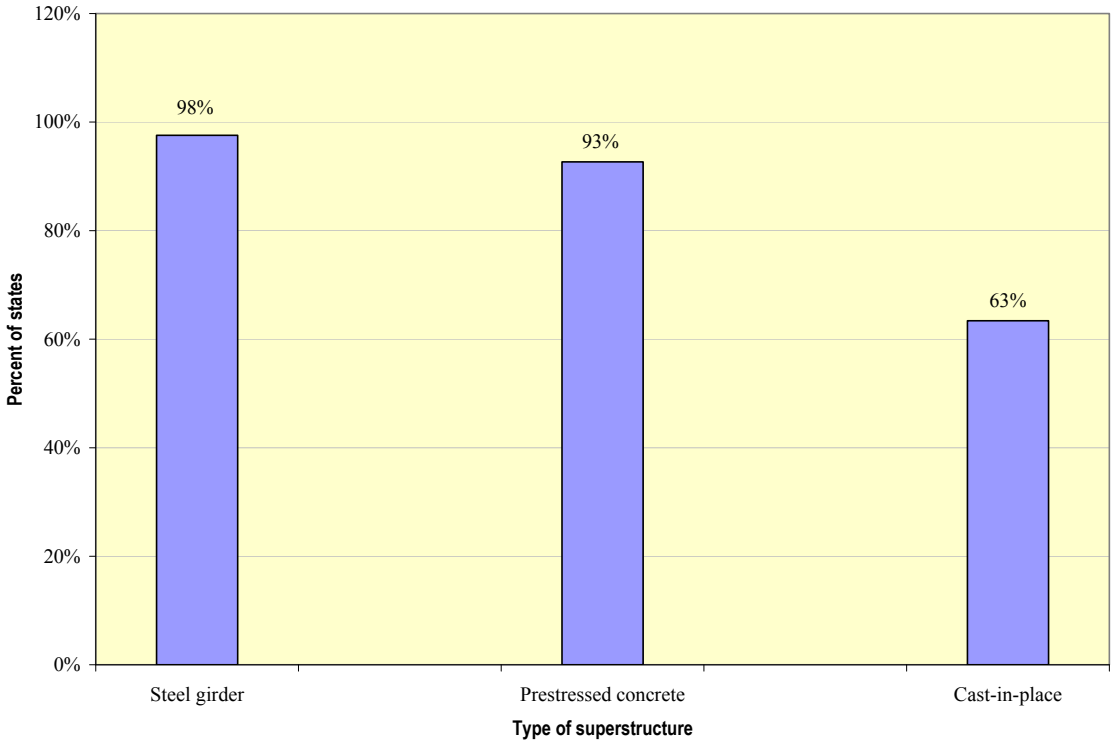

Figure 4-1 Type of superstructure for integral abutment bridges

Alignment

All forty-one states build integral abutment bridges on straight alignment. However, curvature is problematic for bridges of all types, including integral abutment bridges. In addition, research on the use of integral abutments on curved alignment is very limited. The states' responses indicate that only twenty-six states or 63 percent build integral abutment bridges on curved alignment (Figure 4-2). The responses to this question represent a major change compared to the 2004 survey on integral abutment bridges conducted by the Federal Highway Administration (FHWA), which indicated that only seven states had integral abutment bridges on curved alignment (Maruri and Petro 2004).

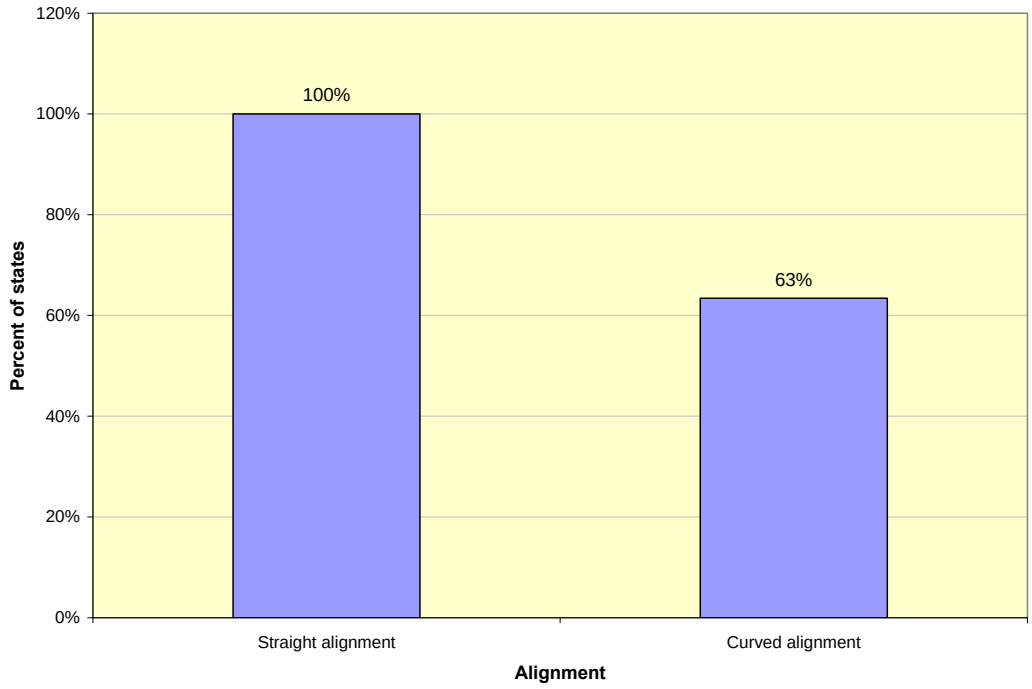

Figure 4-2 Alignment

Skew

Skew is a challenge for both conventional bridges and integral abutment bridges. However, the skew of integral bridges is a concern to structural engineers because of the effect of skew on soil pressures behind abutments. It appears that soil pressures from thermal loads and live loads are greatest at the obtuse sides of skewed integral abutment bridges. The states' responses to this question (Figure 4-3) indicate that the majority of states limit the skew to either 30 or 45 degrees for all three types of superstructure. Five states; California, Colorado, Idaho, Hawaii, and Tennessee have no limit on skew for all three types of superstructure. In addition, the state of Indiana has no limitation for skew only for the case of cast-in-place concrete superstructure.

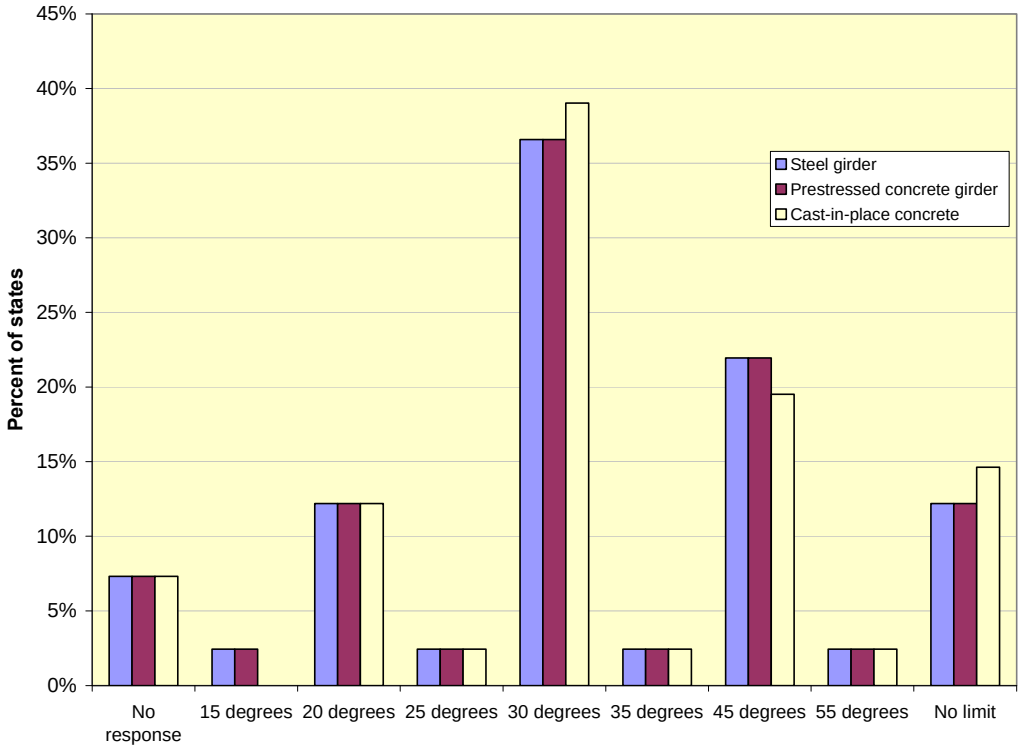

Figure 4-3 Maximum skew angle for integral abutment bridges

Bridge length

One of the main reasons for the increasing use of integral abutment bridges is their economic advantage over conventional bridges, which includes both construction and maintenance cost savings. Consequently, increasing the length limits of integral abutment bridges will yield economic benefits. The critical question is the optimum length limit of integral abutment bridges.

The states' responses to the question of length limit of their integral abutment bridges for a given skew are provided in Tables 4-1, 4-2, and 4-3: Table 4-1 provides information on integral abutment bridges built with a steel superstructure, Table 4-2 provides information on integral abutment bridges built with a prestressed concrete superstructure, and Table 4-3 provides information on integral abutment bridges built with a cast-in-place concrete superstructure. However, several states allow the construction of integral abutment bridges with lengths exceeding the limiting values provided that an appropriate rigorous detailed structural analysis is performed.

Table 4-1 Integral abutment bridge length limits (ft) with steel girder superstructure

	Skew is 0 degrees	Skew is between 0 and 15 degrees	Skew is between 15 and 30 degrees	Skew is over 30 degrees
Arkansas	No response	No response	No response	No response
California	400	400	400	400
Colorado	No limits	No limits	No limits	No limits
Connecticut	No response	No response	No response	No response
Georgia	300	300	300	300
Hawaii	No limits	No limits	No limits	No limits
Idaho	350	350	350	350
Illinois	310	310	310	
Indiana	500	500	500	250
Iowa	400	367	333	300
Kansas	300	300	250	200
Kentucky	500	500	500	500
Maine	200	200	200	
Maryland	150	150	150	
Massachusetts	350	350	350	
Michigan	300	300	300	
Minnesota	300	300	220	100
Missouri	500	500	500	500
Montana	No response	No response	No response	No response
Nebraska	No response	No response	No response	No response
Nevada	No response	No response	No response	
New Hampshire	No response	No response	No response	No response
New Jersey	300	300	300	
New Mexico	200	200	200	
New York	330	330	330	330
North Carolina	300	300	300	
North Dakota	400	386	346	
Ohio	400	400	400	
Oklahoma	350	300	300	
Oregon	No response	No response	No response	No response
Pennsylvania	390	390	130	90
Rhode Island	350	350	350	
South Carolina	240	240	240	
South Dakota	350	350	350	
Tennessee	No limits	No limits	No limits	No limits
Utah	300	300	300	
Vermont	145	145		
Virginia	300	225	150	
West Virginia	No response	No response	No response	
Wisconsin	150	150		
Wyoming	350	350	350	350

Table 4-2 Integral abutment bridge length limits (ft) with prestressed concrete superstructure

	Skew is 0 degrees	Skew is between 0 and 15 degrees	Skew is between 15 and 30 degrees	Skew is over 30 degrees
Arkansas	No response	No response	No response	No response
California	400	400	400	400
Colorado	No limits	No limits	No limits	No limits
Connecticut	No response	No response	No response	No response
Georgia	500	500	500	500
Hawaii	No limits	No limits	No limits	No limits
Idaho	650	650	650	650
Illinois	410	410	410	
Indiana	500	500	500	250
Iowa	575	525	475	425
Kansas	500	500	400	300
Kentucky	500	500	500	500
Maine	330	330	330	
Maryland	110	110	110	
Massachusetts	600	600	600	
Michigan	400	400	400	
Minnesota	300	300	220	100
Missouri	600	600	600	600
Montana	No response	No response	No response	No response
Nebraska	No response	No response	No response	No response
Nevada	No response	No response	No response	
New Hampshire	No response	No response	No response	No response
New Jersey	300	300	300	
New Mexico	135	135	135	
New York	330	330	330	330
North Carolina	400	400	400	
North Dakota	400	386	346	
Ohio	400	400	400	
Oklahoma	350	300	300	
Oregon	No response	No response	No response	No response
Pennsylvania	590	590	130	90
Rhode Island	600	600	600	
South Carolina	300	300	300	
South Dakota	700	700	700	
Tennessee	No limits	No limits	No limits	No limits
Utah	300	300	300	
Vermont	145	145		
Virginia	500	375	250	
West Virginia	No response	No response	No response	
Wisconsin	300	300		
Wyoming	350	350	350	350

Table 4-3 Integral abutment bridge length limits (ft) with cast-in-place concrete superstructure

	Skew is 0 degrees	Skew is between 0 and 15 degrees	Skew is between 15 and 30 degrees	Skew is over 30 degrees
Arkansas	No response	No response	No response	No response
California	400	400	400	400
Colorado	No limits	No limits	No limits	No limits
Connecticut	No response	No response	No response	No response
Georgia	500	500	500	500
Hawaii	No limits	No limits	No limits	No limits
Idaho	650	650	650	650
Illinois				
Indiana	500	500	500	500
Iowa	400	367	333	300
Kansas	500	500	400	300
Kentucky	500	500	500	500
Maine	330	330	330	
Maryland				
Massachusetts	600	600	600	
Michigan	400	400	400	
Minnesota	300	300	220	100
Missouri	600	600	600	600
Montana	No response	No response	No response	No response
Nebraska	No response	No response	No response	No response
Nevada	No response	No response	No response	
New Hampshire	No response	No response	No response	No response
New Jersey				
New Mexico	170	170	170	
New York				
North Carolina				
North Dakota				
Ohio				
Oklahoma				
Oregon	No response	No response	No response	No response
Pennsylvania				
Rhode Island	600	600	600	
South Carolina				
South Dakota	300	300	300	
Tennessee	No limits	No limits	No limits	No limits
Utah				
Vermont	No response	No response		
Virginia				
West Virginia	No response	No response	No response	
Wisconsin	300	300	300	
Wyoming	350	350	350	350

The data from Tables 4-1, 4-2, and 4-3 for zero skew are plotted in Figure 4-4

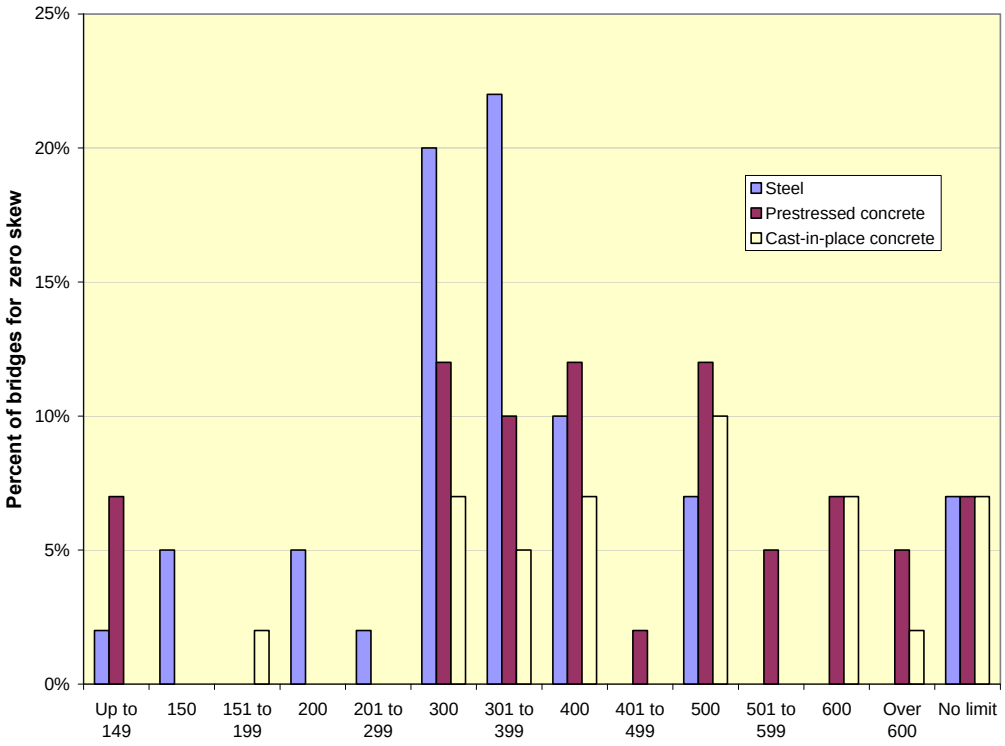

Figure 4-4 Bridge length limits (ft) for zero skew

The data from Tables 4-1, 4-2, and 4-3 are also combined to calculate the average bridge length limits (Figure 4-5) and standard deviation for various skew angles (Figure 4-6).

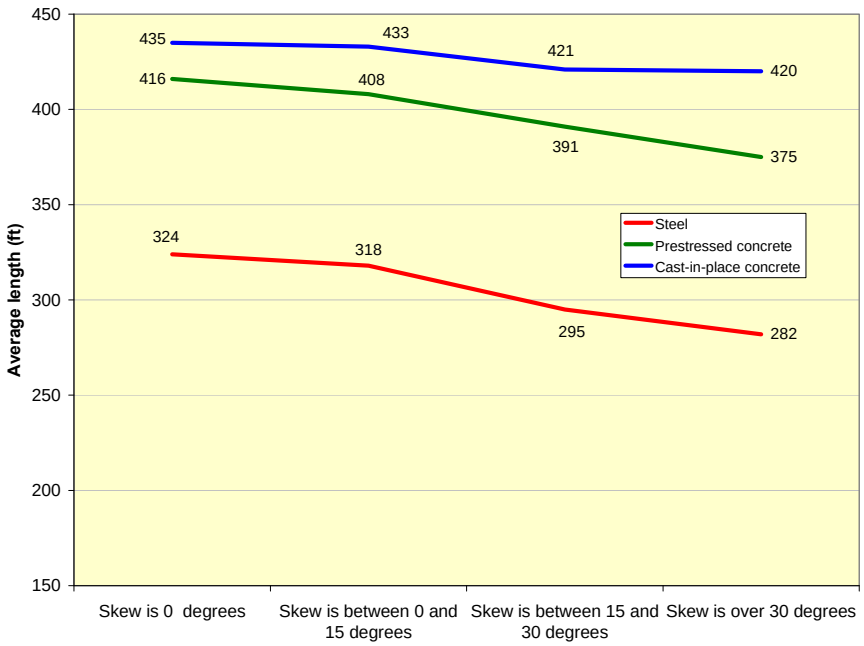

Figure 4-5 Average bridge length limits (ft) for various skew angles

Figure 4-6 Standard deviation for various skew angles

Using the normal distribution curve for each average bridge length limit and corresponding standard deviation, three cases were investigated (Table 4-4) for various skew angles and for all three materials, that is, steel, prestressed concrete, and cast-in-place concrete:

Case 1: Percent of states having bridge length limits within 10 percent of the average bridge length limit

Case 2: Percent of states having bridge length limits within 25 percent of the average bridge length limit

Case 3: Percent of states having bridge length limits within 50 percent of the average bridge length limit

Table 4-4 Normal distribution curve results

	Steel superstructure				Prestressed concrete superstructure				Cast-in-place concrete superstructure			
	Skew 0	Skew 0 - 15	Skew 15-30	Skew over 30	Skew 0	Skew 0 - 15	Skew 15 - 30	Skew over 30	Skew 0	Skew 0 - 15	Skew 15 - 30	Skew over 30
Case 1	27%	26%	20%	15%	22%	21%	20%	17%	25%	25%	23%	20%
Case 2	61%	60%	48%	36%	51%	50%	47%	41%	58%	57%	54%	48%
Case 3	91%	91%	80%	65%	83%	83%	80%	71%	89%	89%	86%	80%

The results in Table 4-4 prove that there is a wide variation in bridge length limits among states for all three materials.

Foundation types

The typical foundation for integral abutment bridges is a single row of vertical piles. Although steel H-piles are most frequently used to support integral abutments, cast-in-place piles, prestressed concrete piles, and steel pipe piles (open ended or concrete filled) are also used by several states.

The states' responses indicate that 40 out of the 41 states that build integral abutment bridges use steel H-piles as their foundation system; the exception is the state of Hawaii. In fact, Hawaii and Utah are using drilled shafts as one of the foundation types for their integral abutments. Spread footings are the most common foundation type for integral abutments in the state of Nevada, which is the only state that reported use of spread footings. In addition, Iowa reported use of timber piles since around 1965; however, they rarely use timber piles nowadays. The integral abutment foundation types used by states are shown in Figure 4-7.

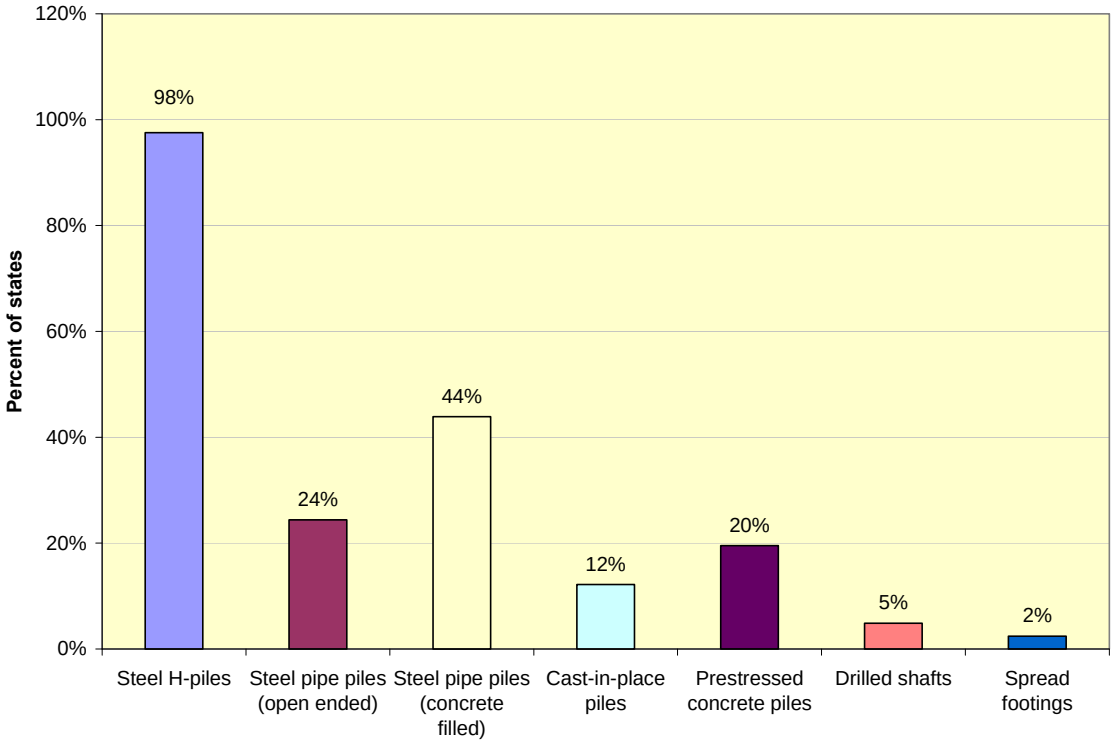

Figure 4-7 Types of foundations for integral abutment bridges

Pile orientation

The orientation of a pile in an integral abutment system has a significant effect on the stresses generated in the piles. States orient the piles supporting their integral abutments for either strong-axis or weak-axis bending.

Strong-axis bending of a pile occurs when the web of the pile is parallel to the centerline of the beam (Figure 3-8). Weak-axis bending of a pile occurs when the web of the pile is perpendicular to the centerline of the beam (Figure 3-9).

The states' responses indicate that 31 percent of states using piles to support their integral abutments orient the piles for strong-axis bending, 56 percent orient the piles for weak-axis bending, and another 13 percent orient their piles in both strong-axis and weak-axis bending.

Structural assumptions for the ends of girders

In general, the connection between the beams and the abutment is assumed to be simply supported for superstructure analysis and design. However, it is in some cases desirable to take advantage of the frame action in the superstructure design by assuming some degree of fixity. This, however, requires careful engineering judgment because of the uncertainty in the degree of fixity. The states' responses indicate that 77 percent of the respondents assume a pin connection at the ends of the girders. Furthermore, 33 percent assume fixity, 10 percent assume that the girder ends are partially restrained by piles, 8 percent assume that the girder ends are partially restrained by soil, and 5 percent make some other assumption. Overall, 39 out of the 41 states that use integral abutment bridges responded to this question.

Structural assumptions for the top of piles

The states' responses with regard to the structural assumptions for the top of the piles were mixed. Thirty-nine out of the 41 states using integral abutment bridges responded to this question. Thirty-eight percent of the respondents assume a pin at the top of the pile, while 51 percent assume fixity, 8 percent assume partial restraint by girder, 15 percent assume a partial restraint by soil, and 8 percent make another assumption.

Secondary lateral load effects on piles stresses

Depending on whether the loading can lead to a progressive collapse of a bridge, loadings are classified either as primary or secondary loads. Primary loads are the dead and superimposed dead load, live load, and seismic load. Secondary loads are the thermal load, creep, shrinkage, settlement load, and soil pressures.

The survey question relates to which of the secondary lateral loads; thermal load, creep, shrinkage, and soil pressures is accounted by states in the calculation of stresses in the piles. The states' responses indicate that only 28 out of the 41 states using integral abutment bridges account for these secondary lateral loads. In other words, almost one-third of the states using integral bridges do not consider the effects of thermal load, creep, shrinkage, and soil pressures in the determination of stresses in integral abutment piles. The responses of the 28 states that account for the effects of these loads are shown in Figure 4-8. In addition, two states; Montana, and South Carolina indicate that thermal load, creep, shrinkage, and soil pressures are accounted for in the calculation of pile stresses whenever the state limitations are exceeded; for example, when the bridge length or skew exceeds the bridge length limit or skew limit set by the state. In these instances, the secondary lateral loads are a part of the detailed structural analysis of the integral abutment bridge that includes calculation of pile stresses.

In reference to the temperature range used for the calculation of thermal load, two-thirds of the respondents follow the AASHTO Specifications; the rest uses local meteorological data.

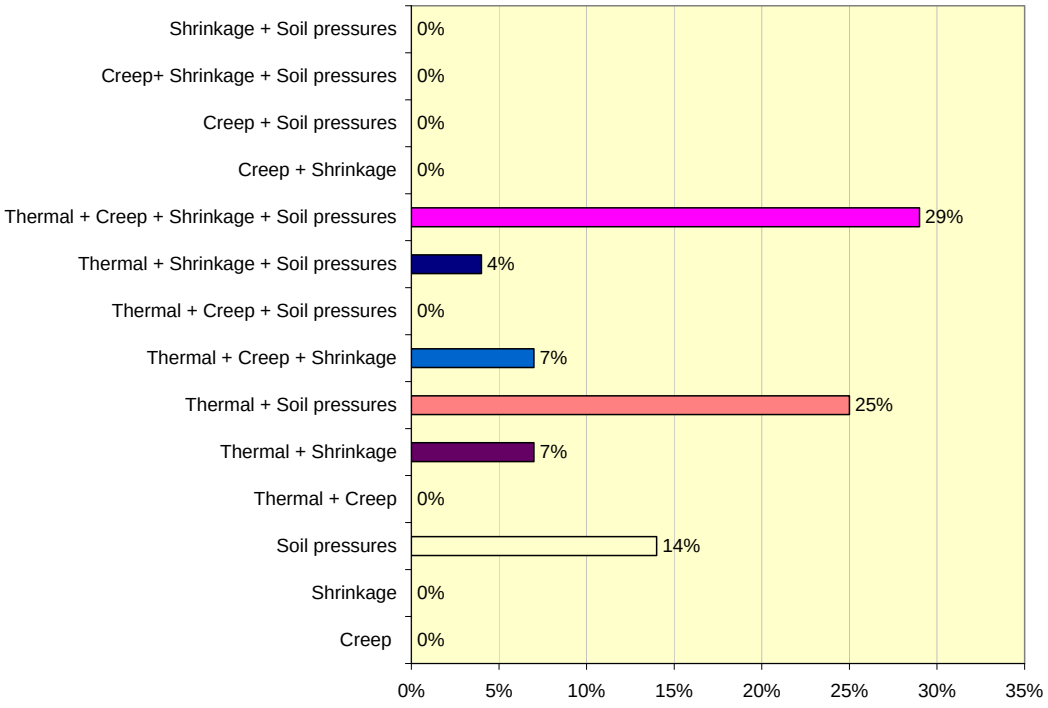

Figure 4-8 Secondary lateral loads accounted for in pile design

Pile bending stresses

The issue of pile bending stresses and their effects on pile performance was one of the survey questions. The question was answered by 37 of the 41 states that use integral abutment bridges. A significant percentage of the respondents, 46 percent, indicate that they neglect or assume that pile bending stresses do not affect pile performance. However, 22 percent of the respondents assume the location of pile inflection point and analyze the pile as a bending member, while 14 percent calculate pile bending stresses using other methods. In addition, 18 percent of the respondents assume the location of pile inflection point and analyze the pile as a bending member in combination with other methods.

Interestingly, only seven states account for the fact that using predrilled holes around piles reduces bending stresses in the piles. This is despite the fact that all states use predrilled holes around piles and research indicates that in stiff soil conditions, predrilling oversize holes and surrounding the piles with loose granular soil is an effective method to reduce bending pile stresses and increase their vertical load capacity.

Backfill material

The type of backfill material and its compaction level defines the stiffness of the soil behind the abutment. Research indicates that soil stiffness has the most influence than any other factor on soil pressures applied on to the abutment system. Compacted soils have higher stiffness than loose soils. As a result, they provide more resistance to thermal movement than loose soils and also apply higher pressures on the abutment system. This introduces higher axial forces into the bridge superstructure, causes more rotation of the abutment and therefore influences the moments in the superstructure.

The states' responses to the question of backfill material indicate that the vast majority of the states; 33 out of 38 respondents or 87 percent, use compacted backfill. However, five states or 13 percent do not use a compacted backfill; this includes the state of Illinois that uses uncompacted porous granular embankment, the state of Kentucky that uses granular free-draining material, the state of South Carolina that uses coarse aggregate, and the states of Montana and West Virginia that use select backfill.

Use of approach slabs and their connection to integral abutments

It is a common practice to build an approach slab integrally with the abutment to span the backfill behind the abutment wall. The primary function of the approach slab is to provide a gradual transition between the fixed superstructure and the roadway pavement in order to avoid a “bump” at the end of the bridge.

The states' responses indicate that approach slabs are used by 38 out of the 41 states using integral abutment bridges; this corresponds to 93 percent of the states. However, three states or 7 percent of the states do not use approach slabs. This includes the states of Arkansas, Maryland, and Virginia where approach slabs are only used where dictated by traffic volumes.

With regard to the question of connection between the approach slab and the integral abutment, 30 out of the 38 states using approach slabs use a doweled or tied connection to connect the approach to the integral abutment, 4 states do not provide any connection between the approach slab and the integral abutment, and 4 states didn’t respond to the question. The states that provide no connection between the approach slabs and the integral abutment are the states of Georgia, Iowa, Wisconsin, and Wyoming.

Types of wingwalls and their foundations

Wingwalls are necessary components of integral abutment bridges to retain the fill that supports the roadway. Depending on their orientation with respect to the abutment wall, wingwalls are classified as cantilevered in-line wingwalls, cantilevered U-wingwalls, or

cantilevered flared wingwalls. They can be either rigidly attached to the integral abutment or be independently supported and not rigidly attached to the integral abutment. Cantilevered in-line wingwalls are in-line extensions of the abutment wall. Cantilevered U-wingwalls are parallel to the roadway centerline. Cantilevered flared wingwalls have an orientation that lies between an in-line and a U-wingwall.

The states' responses indicate that cantilevered in-line wingwalls and cantilevered U-wingwalls are the dominant types of wingwalls used by the states (Figure 4-9). However, all six types of wingwalls are used; a number of states use more than one type of wingwall.

With regard to the issue of piles under the wingwalls of integral abutment bridges, 46 percent or 19 states don't use piles, 37 percent or 15 states use piles and 17 percent or 7 states didn't respond to the question. However, 8 out of the 15 states that use piles under the wingwalls do so under certain conditions; for example, when the wingwall has certain length or use piles only under certain types of wingwalls. For example, the state of California uses piles only with wingwalls longer than 20 feet and Missouri with wingwalls longer than 22 feet. The state of Kansas uses piles only under in-line wingwalls, while the state of New Jersey does not use piles under flared wingwalls. In addition, the state of Hawaii uses piles only under the independently-supported wingwalls.

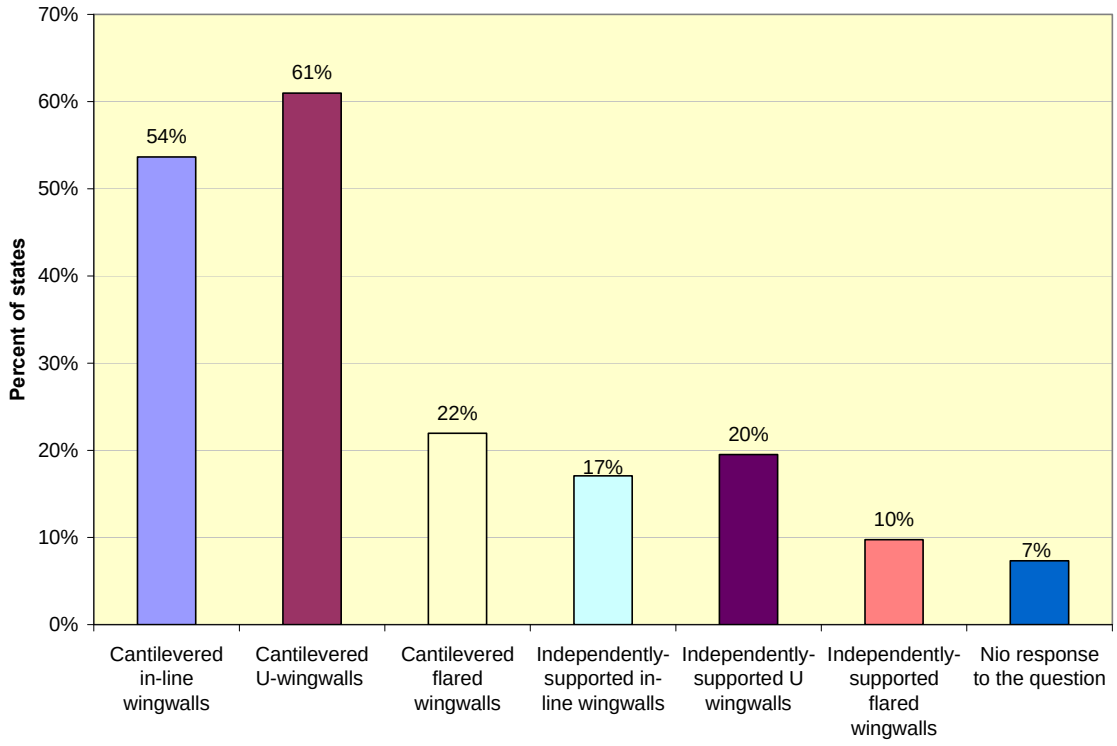

Figure 4-9 Types of wingwalls used with integral abutment bridges

4.3. Survey Questions Related to Status of Use, Problems, and Costs of Integral Abutment Bridges

This part of the survey focuses on three issues: (1) status of use of integral abutment bridges, (2) problems associated with integral abutment bridges, and (3) construction and maintenance costs of integral abutment bridges compared to conventional bridges. Forty-seven states responded to this part of the survey; Montana, Rhode Island, and South Carolina didn't respond.

Alabama

The state of Alabama never used and has no plans to build integral abutment bridges.

Alaska

The state of Alaska never allowed nor disallowed integral abutment bridges on a formal level. There is no written policy one way or the other with regard to integral abutments. However, the Alaska Department of Transportation does not typically use integral abutments for a couple of reasons: First, the thermal ranges can be quite extreme – in the interior regions of the state temperatures range from minus 60 degrees Fahrenheit in the winter to 90 degrees above zero in the summer. Second, foundation issues: Integral abutment bridges accommodate thermal expansion and contraction through the foundation piles rotating or bending in the soil. In Alaska, the soils are frozen in the winter, which prevents the piles from rotating. In addition, many of the bridge sites contain soils with boulder or prone to liquefaction. This requires the use of open-ended pipe piles, which tend to be much stiffer than H-piles.

The combination of a large thermal range in the state along with frozen ground conditions, led the Alaska Department of Transportation to the conclusion that the use of integral abutments does not offer much benefit to the state. As a result, they discontinued their use in 2000.

Arizona

The state of Arizona built its first integral abutment bridges in 1975. Having built 50 bridges, they decided to discontinue their use because longitudinal movements caused approach slab settlements. This condition required extensive and costly repairs. The last integral bridge in the state of Arizona was built in 1996.

Arkansas

The state of Arkansas built its first integral abutment bridges in 2001 in order to eliminate deck joints. The state has limited experience with integral bridges with only 30 integral abutment bridges built as of this moment. Because of the small number of integral bridges in service, the state of Arkansas is unable to assess their performance at this point of time. However, they found that while the construction cost of integral abutment bridges is slightly higher compared to conventional bridges, maintenance cost is lower.

California

The state of California built its first integral abutment bridges in 1950. Since then, more than 1,000 integral bridges have been built in the state. California reports three major benefits with the use of integral abutments: (1) lower construction costs compared to conventional bridges, (2) lower maintenance costs compared to conventional bridges, and (3) better energy absorption for seismic forces. Problems include need for continuous maintenance of approaches because of settlements at paving notch and along wingwalls. In addition, the state reports water intrusion between the abutments and the approaches that causes damages to the approach slab and pavement.

Colorado

The state of Colorado pioneered the use of integral abutment bridges in 1920. Nowadays, the majority of new bridges built in the state of Colorado are integral abutment bridges. The Colorado Department of Transportation reports lower construction and maintenance costs for integral abutment bridges compared to conventional bridges. In addition to being the first state to build integral abutment bridges, the state of Colorado has the longest steel girder integral abutment bridge in the United States with a length of 1,044 ft and the longest cast-in-place concrete integral abutment bridge with a length of 952 ft. However, the Colorado Department of Transportation reports a number of minor to moderate problems with the use of integral abutments: (1) a few integral abutments exhibit distress at the seat level, (2) a few integral abutments exhibit distress at the interface with the girder, (3) a few integral abutment bridges exhibit distress at the connection of the wingwalls to the abutments, (4) consistent problems with the approach fill when the approach slabs are long, that is, approach slabs having a length of 25 to 33 feet. (5) consistent problems with the approach fill when there are no expansion joints at the ends of the approach slabs, (6) pavement distress at the ends of the approach slabs of longer structures when the approach slabs have no expansion joints at their ends, and (7) pavement distress at the ends of the approach slabs caused by a combination of leaking expansion joints at their ends and general approach settlement.

Connecticut

The state of Connecticut built its first integral abutment bridges in 1995. The state has built only a small number of integral abutment bridges so far and reports no significant problems. Furthermore, they report savings in both construction and maintenance costs.

Delaware

The state of Delaware never used and has no plans to build integral abutment bridges.

Florida

The state of Florida tried integral abutments in the late 1980s and gained no benefit with their use. Although the integral abutment eliminated the joint at the abutment, a joint was needed behind the approach slab. In addition, on several occasions, a double approach slab detail with a buried cap between the two slabs was required. Because Florida receives no snowfall, deicing salts are not used. Consequently, there was no benefit to further continue the use of integral abutments and the practice was discontinued in the late 1990s.

Georgia
The state of Georgia built its first integral abutment bridges in 1970 and continues to use them occasionally when the situation warrants. Although Georgia has no problems with integral abutment bridges, it reports higher construction cost and same maintenance costs compared to conventional bridges.

Hawaii
The state of Hawaii built its first integral abutment bridges in 2001. It reports no problems with their use. In addition, it reports lower construction cost and same maintenance costs as conventional bridges.

Idaho
The state of Idaho built its first integral abutment bridges in 1970. The state uses integral abutment bridges in order to eliminate deck joints. Idaho reports no problems with the use of integral abutment bridges. In addition, it reports lower construction and maintenance costs for integral bridges compared to conventional bridges.

Illinois
The state of Illinois began the use of integral abutment bridges in 1986. The state uses integral abutment bridges in order to eliminate joints in the deck, which leak over time and accelerate corrosion. Illinois reports no problems with the use of integral abutment bridges. Although the state has built more than 1,000 integral abutment bridges, it has plans to further expand the parameters of their use through research. This is due to the fact that the state incurs lower construction and maintenance costs for integral bridges compared to conventional bridges.

Indiana
The state of Indiana began the use of integral abutment bridges in 1978. The state uses integral bridges in order to eliminate the damage caused by leaking deck joints. The state reports same construction and lower maintenance costs for integral abutment bridges compared to conventional bridges. Indiana has no problems with the use of integral abutments at this moment. However, in the past, cracking occurred in the deck when the contractor poured the bent and the deck in one pour. This practice is no longer allowed by the Indiana Department of Transportation.

Iowa
The state of Iowa reports excellent performance with the use of integral abutment bridges. Iowa uses integral abutments since 1965 and reports no problems with their use. In fact, it reports lower construction and maintenance costs compared to conventional bridges. In addition, the state of Iowa indicates that the majority of the new bridges built in the state are integral abutment bridges. As a result, more than 1,000 integral bridges have been already built in the state.

Kansas
The state of Kansas began the use of integral abutment bridges in 1935. As a result, Kansas has already built more than 1,000 integral abutment bridges. The state uses integral abutment bridges in order to eliminate deck joints and associated problems. It reports same construction and less maintenance cost compared to conventional bridges. The state also reports that when integral abutments were combined in the past with Mechanically Stabilized Earth (MSE) walls, the moments caused the wall to distress. As a result, the Kansas Department of Transportation decided to stop using MSE walls with integral abutments. Instead, MSE walls are now combined with semi-integral abutments with no problems reported.

Kentucky
The state of Kentucky began the use of integral abutment bridges in 1970. The state uses integral abutment bridges because in their opinion is the most economical type of substructure. In fact, the state of Kentucky reports that both construction and maintenance costs for integral bridges are lower compared to conventional bridges. The state also reports no problems with the use of integral abutment bridges.

Louisiana
The state of Louisiana reports that integral abutment bridges have never been explored in the state because of the unique soft soil conditions of the state and the complexity of the pile–soil interaction in integral abutment bridges. However, Louisiana reports use of semi-integral abutment bridges in the state since 1989.

Maine
The state of Maine began the use of integral abutment bridges in 1988. The state uses integral abutment bridges because both construction and maintenance costs for integral bridges are much lower compared to conventional bridges. The state reports that sometimes the 1.75:1riprap slope in front of the abutment slumps over time. As a result, riprap covers only the bottom of the abutment. Consequently, there is a concern that air and water have direct path to the top of the integral abutment piles.

Maryland
The state of Maryland built its first integral abutment bridges in 1990 in order to eliminate deck joints. The state reports no problems with the use of integral abutment bridges. It also reports higher construction, but lower maintenance costs for integral abutment bridges compared to conventional bridges.

Massachusetts
Massachusetts began the use of integral abutment bridges in 1930 and as a result became the second state after Colorado that used this type of bridge construction. It reports no problems with the use of integral abutment bridges.

Michigan
The state of Michigan began the use of integral abutment bridges in 1991. The state uses integral abutment bridges in order to eliminate joints on the superstructure. It reports

lower construction costs for integral abutment bridges compared to conventional bridges. However, they need more time to evaluate and compare the relative maintenance costs between integral and conventional bridges. The state reports some pavement distress and occasional substructure distress of integral abutment bridges.

Minnesota

The state of Minnesota began the use of integral abutment bridges in 1960. The state uses integral bridges in order to reduce the need for bridge maintenance. They report lower construction and maintenance costs for integral abutment bridges compared to conventional bridges. In addition, they report that currently have no problems with integral bridges. However, in the past, they had leakage problems when the approach panel was not anchored to the integral abutment.

Mississippi

The state of Mississippi tried integral abutments in the 1940s and discontinued their use in the 1950s. As stated by the Mississippi Department of Transportation, the decision to discontinue the use of integral abutment bridges was made because of expansive soil problems on integral bridges.

Missouri

The state of Missouri began the use of integral abutment bridges in 1969. According to Maruri and Petro (2004) Missouri has more than 4,000 integral abutment bridges, which represents the largest number of integral bridges among all states. The state uses integral bridges in order to keep open-deck joints to a minimum due to cost and maintenance concerns. In fact, the state reports lower construction and maintenance costs for integral abutment bridges compared to conventional bridges. However, they report problems in instances when the integral end bents are founded on rock; in this case the abutment beam/diaphragm is designed to slide on a concrete footing. In the likely case that the bridge gets too long and the fill is too rigid, movement is restricted. As a result, the beam/diaphragm may be cracked. In fact, the state of Missouri reports an occasion in which the beam/diaphragm developed cracks and warped as a result of the conditions just described.

Montana

The state of Montana uses integral abutment bridges for decades. However, the Montana Department of Transportation didn't respond to this survey. Consequently, there is no information on any problems that the state of Montana may experience with the use of integral abutment bridges.

Nebraska

The state of Nebraska began the use of integral abutment bridges in 1977. The state reports higher construction and same maintenance costs for integral abutment bridges compared to conventional bridges. It also reports that when tie rods are not used between wingwalls, wingwalls pull away from abutment causing the fill behind the abutment to spill out.

Nevada
The state of Nevada began the use of integral abutment bridges in 1978. The state uses integral abutment bridges because both construction and maintenance costs for integral bridges are much lower compared to conventional bridges. The state reports no problems with integral abutment bridges. In fact, they underscore the fact that integral abutments are the most economical and prevalent type of bridge construction in the state in the last 30 years.

New Hampshire
The state of New Hampshire began the use of integral abutment bridges in 1992. The state uses integral bridges in order to have the joints away from the bridge. However, they have difficulty identifying locations that in their opinion are good candidates for integral abutment bridges. The state reports same construction and lower maintenance costs for integral abutment bridges compared to conventional bridges. In addition, they are not aware of any problems related to integral abutment bridges in their state.

New Jersey
The state of New Jersey began the use of integral abutment bridges in 1988. The state uses integral bridges in order to eliminate deck joints and reduce construction and maintenance costs. In fact, the state reports lower maintenance costs for integral abutment bridges compared to conventional bridges. However, they don't provide any comparison of construction costs between integral abutment bridges and conventional bridges because "in New Jersey the cost of a foundation with and without piles is significantly different." In addition, the New Jersey Department of Transportation reports no problems with the use of integral abutment bridges.

New Mexico
The state of New Mexico began the use of integral abutment bridges in the 1950s. The state uses integral bridges because of their proven good performance and to eliminate the joint in the deck at the abutments. The state reports lower construction and maintenance costs for integral abutment bridges compared to conventional bridges. New Mexico reports spalling of the abutment diaphragms at expansion bearings when the extruded polystyrene that separates the abutment diaphragm and the abutment cap is not present or is too thin to provide girder rotation. According to the New Mexico Department of Transportation, the separation between the diaphragm and cap is needed at expansion abutments to allow girder rotation and prevent spalling of the cap or diaphragm.

New York
The state of New York began the use of integral abutment bridges in 1980. The state uses integral bridges in order to eliminate deck joints and improve durability. New York reports lower construction and maintenance costs for integral abutment bridges compared to conventional bridges. They also report no incidents of abutment or girder distress. However, they note minor problems: (1) Moderate cracking of approach and deck slabs at the ends of the span. This has been improved by modifying the detail; eliminating reinforcing bars that run continuously through the approach and deck slabs, (2) Some twisting of bridges on high skews, and (3) Unequal deflections of stage-constructed

integral bridges; this is taken care by introducing a closure pour in the abutments to allow the deflection from the slab pour in the second stage to be equal to the deflection in the stage-one beams. The New York State Department of Transportation underscores the fact that their integral abutment bridges "perform very well."

North Carolina

The state of North Carolina began the use of integral abutment bridges in 2006. The state uses integral bridges in order to eliminate deck joints and reduce maintenance. Because integral abutment bridges is a new practice in North Carolina, the state is not in a position to compare construction and maintenance costs of integral bridges and conventional bridges. The North Carolina Department of Transportation reports no performance problems with integral abutment bridges. However, they note a few constructability questions regarding placement of approach fill so that cranes can sit closer to the bridge when setting girders.

North Dakota

The state of North Dakota began the use of integral abutment bridges in 1960. The state uses integral bridges in order to eliminate deck joints. North Dakota reports lower construction and maintenance costs for integral abutment bridges compared to conventional bridges. They also report no problems with integral abutment bridges.

Ohio

The state of Ohio began the use of integral abutment bridges in 1935. The state uses integral bridges because of their lower construction and maintenance costs compared to conventional bridges. The Ohio Department of Transportation reports no problems with integral abutment bridges.

Oklahoma

The state of Oklahoma began the use of integral abutment bridges in 1980. The state reports lower construction and maintenance costs for integral abutment bridges compared to conventional bridges. The Oklahoma Department of Transportation reports that the only problem with the use of integral abutments bridges is settlement of the approach slabs.

Oregon

The state of Oregon began the use of integral abutment bridges in 1940. The state uses integral bridges because in their opinion provide a cost-effective solution. In fact, Oregon reports lower construction and maintenance costs for integral abutment bridges compared to conventional bridges. The Oregon Department of Transportation reports no problems with integral abutment bridges.

Pennsylvania

The state of Pennsylvania began the use of integral abutment bridges in 1946. The state uses integral bridges because of their low cost, economy of foundation, speed of construction, and in order to eliminate deck joints. Pennsylvania reports lower construction and maintenance costs for integral abutment bridges compared to

conventional bridges. They also report no known issues with the performance of integral abutments.

Rhode Island

The state of Rhode Island uses integral abutment bridges. However, the Rhode Island Department of Transportation didn't respond to this survey. Consequently, there is no information on any problems that the state of Rhode Island may experience with the use of integral abutment bridges.

South Carolina

The state of South Carolina uses integral abutment bridges. However, the South Carolina Department of Transportation didn't respond to this survey. Consequently, there is no information on any problems that the state of South Carolina may experience with the use of integral abutment bridges.

South Dakota

The state of South Dakota began the use of integral abutment bridges in 1948. The state uses integral bridges in order to eliminate joints in the deck and reduce long-term maintenance costs. In fact, South Dakota reports lower construction and maintenance costs for integral abutment bridges compared to conventional bridges. The South Dakota Department of Transportation reports that they no longer have any problems with the use of integral abutment bridges in the state. They note that in the past they had a small bit of spalling at the abutments around girders in some of the early skewed integral abutments with prestressed girders. The problem was eliminated by using some perform around the girders.

Tennessee

The Tennessee Department of Transportation reports excellent performance and uses the expression "success rate is 98 percent or better" to describe their experience with integral abutment bridges. The first integral abutment bridges in the state of Tennessee were built in 1965. The state uses integral bridges to improve structure efficiency and service life. Construction and maintenance costs for integral abutment bridges are lower compared to conventional bridges. In addition, the state of Tennessee indicates that the majority of new bridges built in the state are integral abutment bridges. As a result, more than 2,000 integral abutment bridges exist in the state. In fact, the state of Tennessee has the longest precast concrete integral abutment bridge in the United States with a length of 1,175 ft. The Tennessee Department of Transportation reports no problems with the use of integral abutment bridges.

Texas

The state of Texas is not using integral abutment bridges. According to Texas Department of Transportation "The soil conditions in most of Texas are such that drilled shafts or prestressed concrete piling are required. Very few structures, less than 10 percent, have conditions where steel piling and therefore integral abutments could be used. Steel piling is seldom used in Texas due to its cost when compared to prestressed concrete piling. This makes integral abutments uncompetitive from a cost standpoint in

Texas geotechnical and bidding environments." However, integral abutment bridges were built on rare occasions in the state of Texas. According to Texas Department of Transportation, an integral abutment bridge was built in far west Texas in 1994. The site-specifics were rare and allowed the use of steel H-piling on sandy soil. Although the integral abutment bridge is performing well, the state gained no economic or performance advantage by using an integral abutment bridge over its conventional practice. As a result, the practice was discontinued.

Utah

The state of Utah began the use of integral abutment bridges in 1984. The state uses integral bridges in order to eliminate deck joints and improve seismic performance. Utah reports much higher construction costs and much lower maintenance costs for integral abutment bridges compared to conventional bridges. The Utah Department of Transportation reports that integral abutment bridges are "mostly working really well." At the same time, they report some pulling away from the backwall of prestressed concrete girder integral abutment bridges. However, they don't observe any pulling away from the backwall of steel girder integral abutment bridges. In addition, they observe deck cracking in the vicinity of the integral abutments.

Vermont

The state of Vermont began the use of integral abutment bridges in 1981. The state uses integral bridges in order to eliminate deck joints and bearings. According to the Vermont Department of Transportation, integral abutment bridges are environmentally friendly and reduce construction site impacts. Vermont reports lower construction and maintenance costs for integral abutment bridges compared to conventional bridges. In addition, the Vermont Department of Transportation reports no problems with the use of integral abutment bridges in the state. Furthermore, they underscore the fact that integral bridges are their first choice for bridges.

Virginia

The state of Virginia began the use of integral abutment bridges in 1982. The state uses integral bridges in order to eliminate deck joints and therefore reduce life-cycle maintenance costs. Virginia reports lower construction and maintenance costs for integral abutment bridges compared to conventional bridges. The Virginia Department of Transportation also reports that they have successfully solved a number of problems with their integral abutment bridges (1) Rotations of skewed integral abutment bridges induced by soil-structure interactions; the rotations are now resisted by providing a "buttress force" in a variety of ways, and (2) Cracking of the approach slab; the problem was dealt by changing the approach slab connection detail. The original connection consisted of straight bars that extended from the deck into the approach slab in the plane of the top mat of reinforcement. When settlements occurred (as would be expected when an approach slab is used), the approach slab acted as a cantilever and cracking occurred at the ends of the connection bars. The connection detail was changed so that the reinforcing bars pass through the point of rotation, thereby allowing the rotation of the approach slab, while maintaining the connection.

Washington

The state of Washington built its first integral abutment bridges in 1965. Having built more than 1,000 integral abutment bridges in the state, the Washington Department of Transportation decided in the year 2000 to switch to semi-integral abutment bridges. In their view, semi-integral abutments are more economical than integral abutments. In addition, they allow the structure to move during a seismic event, which results in reduction of seismic forces.

West Virginia

The state of West Virginia began the use of integral abutment bridges in 1994. The state uses integral abutment bridges in order to eliminate abutment joints and associated problems when joints leak. West Virginia reports lower construction costs for integral abutment bridges compared to conventional bridges. As far as maintenance costs is concerned, their experience indicates higher costs for integral abutment bridges compared to conventional bridges for short-term maintenance, but much lower costs for long-term maintenance. This is due to the fact that in the short term many West Virginia integral abutment bridges exhibit cracking at the ends of their approach slabs when nominal thresholds are exceeded.

Wisconsin

The state of Wisconsin began the use of integral abutment bridges in 1960. The state uses integral bridges to avoid deck joints, which may leak and damage the substructure. Wisconsin reports lower construction and maintenance costs for integral abutment bridges compared to conventional bridges. They also report no problems with integral abutment bridges.

Wyoming

The state of Wyoming began the use of integral abutment bridges in 1957. The state uses integral bridges in order to eliminate deck joints and reduce maintenance. Wyoming reports lower construction and maintenance costs for integral abutment bridges compared to conventional bridges. The Wyoming Department of Transportation indicates that the integral abutment bridges in the state perform very well and without any problems. In addition, they refer to integral abutment bridges as their “conventional type of bridge.” The state of Wyoming has already built more than 1,000 integral abutment bridges.

Summary of Responses

The responses to this part of the survey indicate that forty-one states are using integral abutment bridges and nine states do not use integral abutments. Out of the nine states that do not use integral abutment bridges, three states (Alabama, Delaware, Louisiana) never used integral abutments, three states (Alaska, Arizona, Mississippi) discontinued their use due to serious problems, and three states (Florida, Texas, Washington) discontinued their use either because they realized no performance advantage over their conventional practice (Florida, Texas) or they concluded that semi-integral abutments offer more advantages compared to integral abutments (Washington). The status of use of integral abutment bridges is illustrated in Figure 4-10

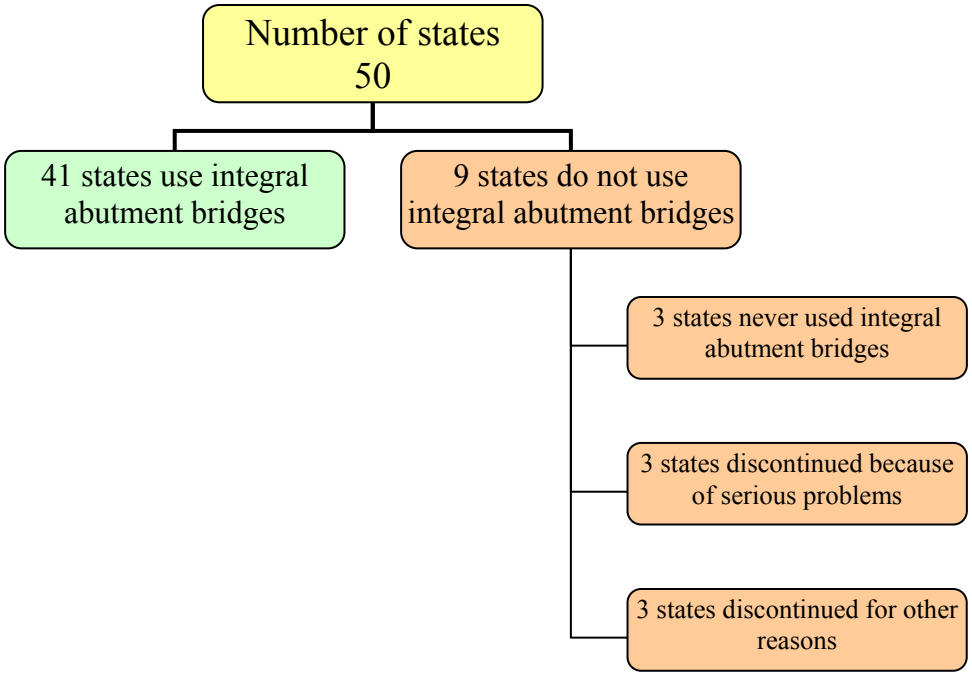

Figure 4-10 Status of use of integral abutment bridges

The responses also indicate that twenty-five states have no problems with the use of integral abutment bridges. In addition, twelve states (California, Colorado, Maine, Michigan, Missouri, Nebraska, New Mexico, New York, North Carolina, Oklahoma, Utah, West Virginia) report either minor or moderate problems with the use of integral abutment bridges. Four states (Indiana, Kansas, South Dakota, Virginia) had moderate problems with integral abutment bridges in the past; they found a solution to their problems and report no problems at this moment. However, three states (Alaska, Arizona, and Mississippi) had serious problems with integral abutment bridges; as a result, discontinued their use. The status of problems with integral abutment bridges is illustrated in Figure 4-11

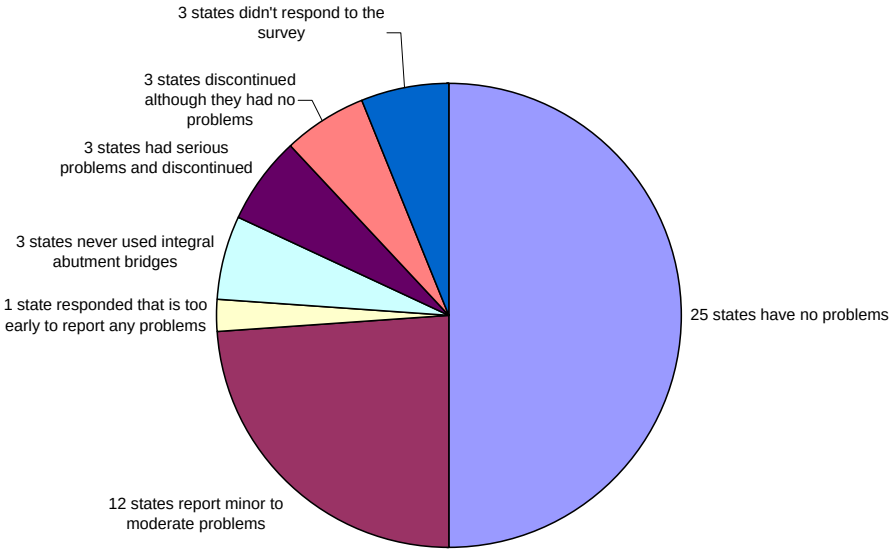

Figure 4-11 Status of problems with integral abutment bridges

The responses with regard to the issue of construction costs of integral abutment bridges compared to conventional bridges indicate a lower construction cost in twenty-seven states, higher construction cost in five states (Arkansas, Georgia, Maryland, Nebraska, Utah), and same construction cost in three states (Indiana, Kansas, New Hampshire). The status of comparative construction costs of integral abutment bridges and conventional bridges is illustrated in Figure 4-12.

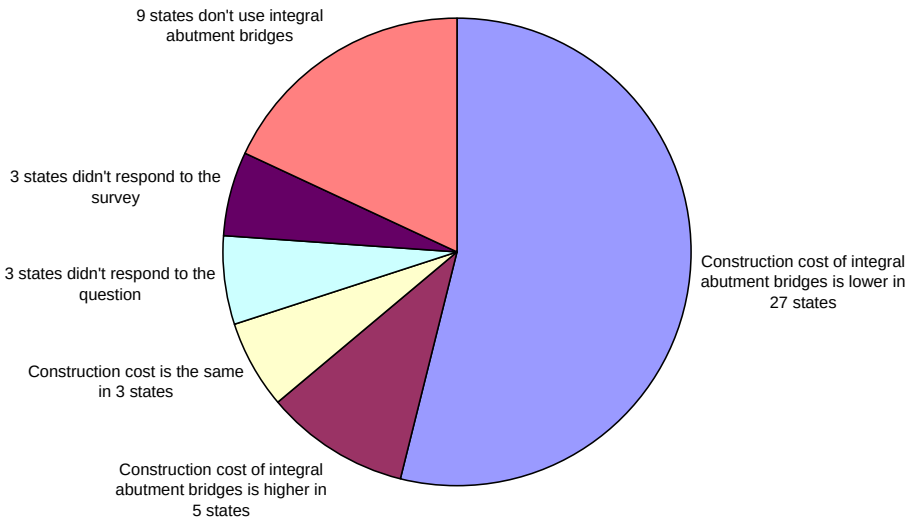

Figure 4-12 Status of comparative construction costs of integral abutment and conventional bridges

The responses with regard to the issue of maintenance costs of integral abutment bridges compared to conventional bridges indicate a lower maintenance cost in thirty-two states, and same maintenance cost in three states (Georgia, Hawaii, and Nebraska). Interestingly, no state reports a higher maintenance cost with the use of integral abutment bridges. The status of comparative maintenance costs of integral abutment bridges and conventional bridges is illustrated in Figure 4-13.

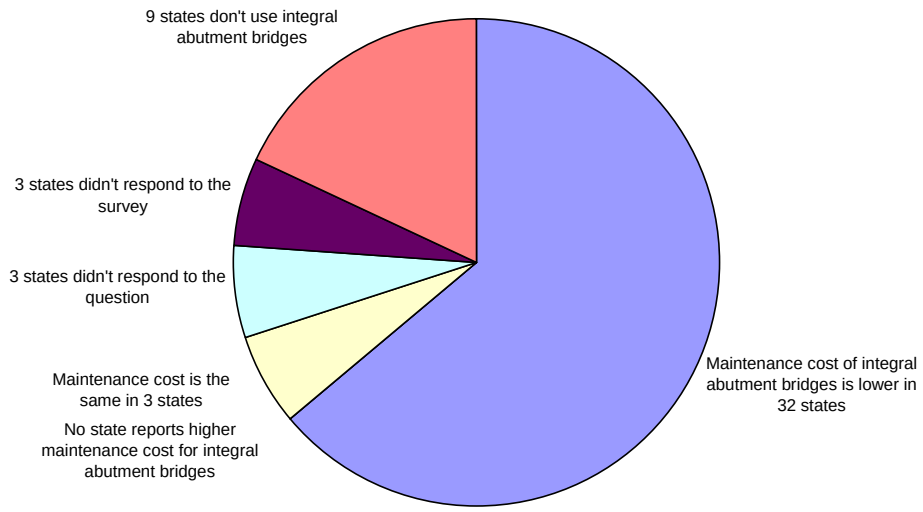

Figure 4-13 Status of comparative maintenance costs of integral abutment and conventional bridges

Chapter 5

Selection of Parameters for the Parametric Studies

Using the knowledge gained from the literature review (chapter 3) and the survey on integral abutment bridges (chapter 4), Table 5-1 presents a list of all parameters used in past integral abutment bridge research studies as well as design practice. The selected options for the parametric studies are identified among the listed options. The parametric studies are described in chapter 6.

Table 5-1 Parameters for the research study on wingwall configurations

Options or Limitations	Comments	Options for the research study
Bridge layout		
Single span		Yes
Continuous spans with integral piers	Harvey (2012) states that concrete superstructures are usually built with integral piers while steel superstructures are supported on piers with bearings	No
Continuous with bearings on piers		Yes. For this study, intermediate supports representing the bridge piers are modeled as roller supports
Bridge length		
Project specific	The survey on integral abutment bridges (Table 4-1) indicates a bridge length limit of 500 feet for steel integral bridges with no skew in all but three states, which impose no limit on bridge length. This includes the state of Colorado with the longest steel girder integral abutment bridge in the United States; its length is 1,044 feet. By definition, the length of a single	100 to 1200 feet

	span integral abutment bridge is equal to the distance between abutment centerlines (Figures 1-13 and 1-15).For continuous span bridges, bridge length is the sum of the span lengths of the bridge.	
Roadway width		
Function of number of lanes needed to accommodate present and future traffic demand	It is the sum of the width of all traffic lanes plus the width of shoulders, if any. The majority of bridges have two, three, or four lanes	Two-12-feet lanes plus two 6-feet shoulders* = 36 feet
		Four-12-feet lanes plus two 6-feet shoulders* = 60 feet
* According to the AASHTO *A Policy on Geometric Design of Highways and Streets* (2004), the range of minimum shoulder width is 4 to 12 feet for freeways and 2 to 8 feet for arterials, collectors, and local roadways		
Bridge width		
Depends on roadway width and provision of sidewalks for pedestrians or bicycles	It is the transverse dimension that is equal to the sum of roadway width plus width of sidewalk or bicycle lanes, if any, and width of parapets	Use a 2-feet wide parapet at each bridge end with no provision for sidewalks or bicycle lanes
		Bridge width=36+4=40 ft for two-lane bridges
		Bridge width=60+4=64 ft for four-lane bridges
Span configuration		
Single span	Number of spans is a function of bridge length	Yes
Multiple-span continuous		Yes

End-Span ratio		
The selected end-span ratio shall not cause uplift issues at the end span supports	According to the NYSDOT Bridge Manual Article 3.5.3 Table 3-2, the ratio of spans for two-span bridges is 1.0:1.0, for three-span bridges is 0.75:1.0:0.75, and for four-span bridges is 0.8:1.0:1.0:0.8. Harvey (2012) states that 0.7 to 0.8 end-span ratio is a common practice in Canada for three and four-span bridges. The intent of those provisions is to have nearly equal maximum positive moments in all spans	All bridges have spans of equal length to minimize effects of dead load
Span length		
Depends primarily on bridge length, type of bridge, and superstructure material	Maruri and Petro (2004) indicate a range of 65 to 300 feet for steel integral abutment bridges	100 feet (typical)
Span length to Girder depth ratio		
Satisfy live load deflection requirements stipulated by national and state bridge engineering codes and specifications	The AASHTO LRFD Bridge Design Specifications Article 2.5.2.6.3 Table 2.5.2.6.3-1 stipulate a span length to girder depth ratio of 25 for simple spans and 31.25 for continuous spans. The NYSDOT Bridge Manual Article 3.5.3 Table 3-2 stipulates a maximum ratio of 30 for continuous spans with an optimum ratio of 27.5	Maximum span length to girder depth ratio satisfies both AASHTO and NYSDOT Bridge Manual stipulations.
Type of bridge deck		
Reinforced concrete	Use of open steel grid, concrete-filled steel grid, and timber bridge decks is unsuitable for integral abutment bridges (GangaRao et al. 1996)	Yes
Open steel grid		No
Concrete filled steel grid		No
Timber		No

<table>
<tr><td colspan="3">Bridge deck slab thickness</td></tr>
<tr><td colspan="3">9.5 inches</td></tr>
<tr><td colspan="3">Deck concrete material properties</td></tr>
<tr><td colspan="3">Compressive strength f'c = 4,000 psi
Modulus of elasticity E = 3605 ksi
Poisson's ratio ν = 0.2
Coefficient of thermal expansion a = 0.0000060/^{0}F</td></tr>
<tr><td colspan="3">Type of integral abutment bridge superstructure</td></tr>
<tr><td>Steel I-beams</td><td rowspan="5"></td><td>Yes</td></tr>
<tr><td>Concrete I-beams</td><td>No</td></tr>
<tr><td>Concrete bulb tees</td><td>No</td></tr>
<tr><td>Concrete box beams</td><td>No</td></tr>
<tr><td>Hybrid composite beams</td><td>No</td></tr>
<tr><td colspan="3">Steel girder material properties</td></tr>
<tr><td>ASTM A709 Grade 36
Fy = 36 ksi</td><td rowspan="2">Common practice is to use Grade 50 steel for primary members and Grade 36 steel for secondary members</td><td rowspan="2">ASTM A709 Grade 50
Fy = 50 Ksi
Modulus of elasticity
E = 29,000 Ksi
Poisson's ratio ν = 0.3
Coefficient of thermal expansion
a=0.0000065/^{0}F</td></tr>
<tr><td>ASTM A709 Grade 50
Fy = 50 ksi</td></tr>
<tr><td colspan="3">Steel girder structural shapes</td></tr>
<tr><td>Rolled shapes composite with the bridge deck</td><td rowspan="4">Common practice is to use rolled shapes for simple spans up to 100 feet and continuous spans up to 120 feet; plate girders are used beyond those span ranges</td><td>Yes</td></tr>
<tr><td>Rolled shapes noncomposite with the bridge deck</td><td>No</td></tr>
<tr><td>Plate girders composite with the bridge deck</td><td>Yes</td></tr>
<tr><td>Plate girders noncomposite with the bridge deck</td><td>No</td></tr>
</table>

<table>
<tr><th colspan="4">Girder spacing</th></tr>
<tr><td rowspan="2">Girder spacing is a function of slab thickness</td><td colspan="2" rowspan="2">A thicker deck slab accommodates a wider girder spacing. Using a 9.5 inch thick deck slab, most states stipulate a maximum girder spacing of 12 feet. A wider girder spacing with fewer girders results in a more economical bridge design compared to closer girder spacing with more girders</td><td>8'-6" for two-lane bridges</td></tr>
<tr><td>9'-6" for four-lane bridges</td></tr>
<tr><th colspan="4">Overhang width</th></tr>
<tr><td rowspan="2">Determined such that the moments and shears in the exterior girder are similar to those in the interior girder. In addition, the positive and negative moments in the deck slab are balanced</td><td colspan="2" rowspan="2">A common rule of thumb is to make the overhang approximately 35 to 50 percent of girder spacing</td><td>3'-0" for two-lane bridges resulting in a ratio of 35.3 percent</td></tr>
<tr><td>3'-6" for four-lane bridges resulting in a ratio of 36.8 percent</td></tr>
<tr><th colspan="4">Number of girders</th></tr>
<tr><td rowspan="2">Depends on bridge width, girder spacing, and vertical clearance requirements.</td><td colspan="2" rowspan="2">The fewest number of girders in the cross section provides the most economical bridge.

Most states require a minimum of 4 girders and a maximum of 12 girders in the cross section</td><td>5 girders for two-lane bridges</td></tr>
<tr><td>7 girders for four-lane bridges</td></tr>
<tr><th colspan="4">Cross frame material properties</th></tr>
<tr><td colspan="2">ASTM A709 Grade 36
Fy = 36 ksi</td><td rowspan="2">Common practice is to use Grade 50 steel for primary members and Grade 36 steel for secondary members</td><td rowspan="2">ASTM A709 Grade 50
Fy = 50 Ksi
Modulus of elasticity
E = 29,000 Ksi
Poisson's ratio ν = 0.3
Coefficient of thermal expansion
a=0.0000065/^{0}F</td></tr>
<tr><td colspan="2">ASTM A709 Grade 50
Fy = 50 ksi</td></tr>
</table>

Cross frame spacing		
Spacing of cross frames shall satisfy the requirements of the AASHTO Specifications	A rule of thumb, based on previous editions of the AASHTO Specifications, is to use a maximum cross frame spacing of 25 feet	Maximum cross frame spacing is 25 feet
Skew		
Any skew	There are limitations on skew (chapter 4)	Zero skew
Horizontal curvature		
Any degree of curvature	There are limitations on horizontal alignment (chapter 4)	Zero degree of curvature
Integral abutment material		
Reinforced concrete		
Integral abutment concrete material properties		
Compressive strength f'_c = 4,000 psi Modulus of elasticity E = 3605 ksi Poisson's ratio ν = 0.2 Coefficient of thermal expansion a = 0.0000060/^{0}F		
Integral abutment height		
Integral abutments are limited to a certain height because of concerns about the magnitude of earth pressures exerted on the abutments	Harvey (2012) states that integral abutments are deeper than the superstructure by about 3 to 5 feet. Typical integral abutment heights are 7 to 15 feet	Integral abutment height= Slab thickness + girder depth + (3 to 5) feet Typical span length = 100' therefore for a span/depth ratio of 25 → Girder depth = 100'/25 = 4'-0" Minimum abutment height = 9.5" + (4'-0") + (3'-0") = 7'-9.5"

<table>
<tr><td colspan="3">Difference in height between the two integral abutments</td></tr>
<tr><td colspan="3">The height of both integral abutments is the same</td></tr>
<tr><td colspan="3">Difference in elevation at the top of integral abutments</td></tr>
<tr><td colspan="3">Top elevation of both integral abutments is the same</td></tr>
<tr><td colspan="3">Length of integral abutments</td></tr>
<tr><td colspan="3">The length of an integral abutment is equal to bridge width</td></tr>
<tr><td colspan="3">Thickness of integral abutment walls</td></tr>
<tr><td>A minimum thickness is required to assure that the piles will yield prior to any abutment wall failure</td><td>Most states use a cross section of 3 feet</td><td>3'-0"</td></tr>
<tr><td colspan="3">Backfill soil behind integral abutments</td></tr>
<tr><td rowspan="3">Well-graded, free-draining granular material (Amde et al. 1987; White 2012) compacted to 95 percent to eliminate backfill settlement (Fu 2008)</td><td rowspan="3"></td><td>Dense sand with angle of internal friction Φ = 45° (Figures 6-1 and 7-3)</td></tr>
<tr><td>Medium dense sand with angle of internal friction Φ = 37° (Figures 6-1 and 7-3)</td></tr>
<tr><td>Loose sand with angle of internal friction Φ = 30° (Figures 6-1 and 7-3)</td></tr>
</table>

Foundation type for integral abutments		
Steel H-piles	The survey on integral abutment bridges (Figure 4-7) indicates that steel H piles is the most common foundation type for integral abutments	Yes
Prestressed concrete piles		No
Cast-in-place concrete piles		No
Steel pipe piles open ended		No
Steel pipe piles filled with concrete		No
Drilled shafts		No
Spread footings		No
Pile type under integral abutments		
End bearing piles	Maruri and Petro (2004) indicate that 67 percent of states use bearing piles to support integral abutments. Thanasattayawibul (2006) indicates that there is only a minor difference in the magnitude of integral abutment pile stresses between end bearing and friction pile types. According to Komurka (2014), end bearing H-piles are good applications for cohesive soils while friction piles are a marginal application	Yes
Friction piles		No
Integral abutment pile material properties		
ASTM A 709 Grade 36 Fy=36 ksi	Dunker and Abu-Hawash (2005) and Olson et al. (2009) suggest that using higher grade steel such as 50 ksi in lieu of 36 ksi allows for longer integral abutment bridges	ASTM A709 Grade 50 Fy = 50 Ksi Modulus of elasticity E = 29,000 Ksi Poisson's ratio $\nu = 0.3$ Coefficient of thermal expansion $a=0.0000065/^{0}F$
ASTM A 709 Grade 50 Fy=50 ksi		

Size of integral abutment piles		
The most commonly-used steel H-pile sections for bridges are: HP14X117 HP14X102 HP14X89 HP12X84 HP12X74 HP12X53 HP10X57 HP10X42 HP8X36	Piles oriented in weak-axis bending offer less resistance to movement and as a result may subject the piles to cyclic axial and flexural stresses that approach, equal or exceed the yield stress of the pile material (Amde et al. 1982; Jorgenson 1983). This might lead to the formation of a plastic hinge at the pile section near the pile head under critical combinations of weak-axis pile bending orientation, stiff soils, and long bridge length (Huang et al. 2008)	There are only two steel H-pile sections that satisfy the provisions of AASHTO LRFD Bridge Design Specifications Article 6.12.2.2.1 and are capable of developing a fully plastic stress distribution and may be used where plastic hinge formation is expected. These sections are HP10X57 and HP12X84 (MassDOT 2009) Use HP10X57 pile section for this study
Integral abutment pile arrangement		
Single row of vertical piles	Integral abutment foundation consists of a single row of vertical piles	Yes
Single row of battered piles		No
Multiple rows of vertical piles only		No
Multiple rows of vertical and battered piles		No
Multiple rows consisting of rows with vertical piles and rows with battered piles		No

<table>
<tr><th colspan="3">Integral abutment pile spacing</th></tr>
<tr><td rowspan="3">There are limits, both minimum and maximum, on pile spacing and distance from center of pile to the edge of the integral abutment wall</td><td rowspan="3">The AASHTO LRFD Specifications Article 10.7.1.2 stipulate a minimum pile spacing of 2.5 pile diameters or 2'-6" and a minimum distance of 9" from the side of any pile to the nearest edge of the pile cap

The NYSDOT Bridge Manual Article 11.1.4.2 stipulates a minimum pile spacing of 3 pile diameters or pile widths and a maximum pile spacing of 9 feet . In addition, they stipulate a minimum distance of 1'-6" from the center of a pile to the nearest footing edge and a 9" minimum distance from the edge of a pile to the nearest footing edge</td><td>Use 6'-0" pile spacing with 2'-0" distance from the center of a pile to the nearest edge of the integral abutment wall</td></tr>
<tr><td>For 2-lane bridges
6 spaces at 6'-0" + 2' +2' = 40 feet equal to bridge width</td></tr>
<tr><td>For 4-lane bridges
10 spaces at 6'-0"+2'+2' = 64 feet equal to bridge width</td></tr>
<tr><th colspan="3">Number of integral abutment piles</th></tr>
<tr><td rowspan="2">It is a function of integral abutment length and pile spacing</td><td rowspan="2"></td><td>7 piles for 2-lane bridges</td></tr>
<tr><td>11 piles for 4-lane bridges</td></tr>
<tr><th colspan="3">Integral abutment pile length</th></tr>
<tr><td>Minimum length of piling is required to ensure that the pile has adequate flexibility to accommodate the abutment movement</td><td>Piles shall be driven through at least 10 to 15 feet of overburden (Burke 1993; Hoppe and Gomez 1996)</td><td>Soil profile (Figure 6-2) indicates pile length = 40 ft (bottom of abutment to pile tip)+2 ft (pile penetration into the abutment for fixity)= 42 ft</td></tr>
</table>

<table>
<tr><th colspan="3">Integral abutment pile orientation</th></tr>
<tr><td>Weak-axis bending</td><td rowspan="2">Both the literature review (Chapter 3) and the survey on integral abutment bridges (Chapter 4) indicate that states orient abutment piles in both strong and weak-axis bending. However, the majority of states orient integral abutment piles in weak-axis bending</td><td rowspan="2">Weak-axis bending</td></tr>
<tr><td>Strong-axis bending</td></tr>
<tr><td colspan="3"> 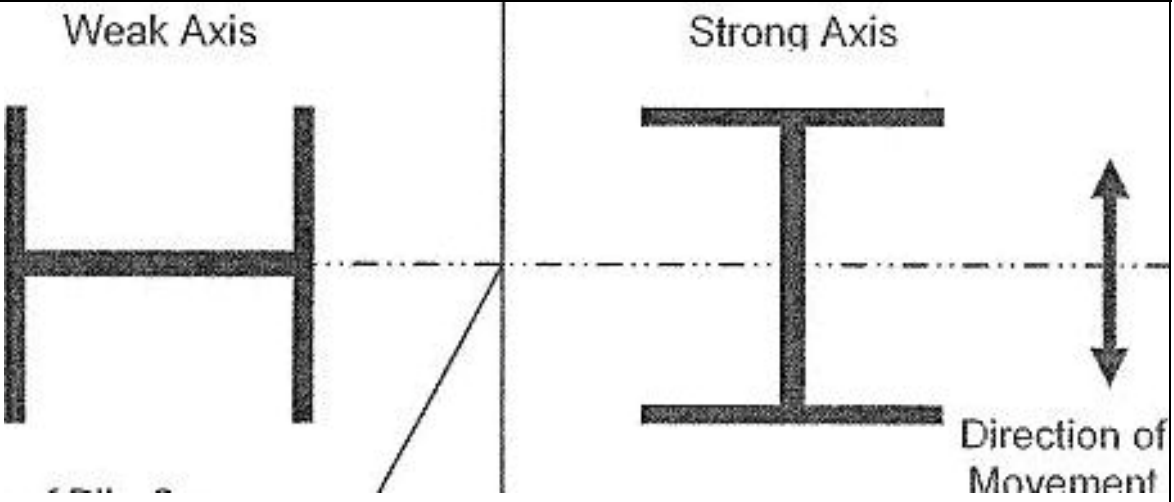
</td></tr>
<tr><th colspan="3">Pile connection to integral abutment</th></tr>
<tr><td>Fixed connection</td><td rowspan="2">Fixed connection provides for higher axial load pile capacity (Greimann et al. 1984) and enhanced behavior for seismic considerations (Frosh et al. 2009)

FHWA NHI-04-041 indicates that a pile needs to be embedded 2 to 3 times its diameter or width into the pile cap to develop full fixity</td><td rowspan="2">Fixed connection by projecting the piles 2'-0" into the integral abutment</td></tr>
<tr><td>Hinged connection</td></tr>
</table>

<table>
<tr><td colspan="3">Pile connection at pile tip</td></tr>
<tr><td>Fixed connection</td><td rowspan="2">The boundary condition (hinge or fixed) at the base does not appear to have a significant influence on the overall performance of the pile due to the restraining effect of the soil (Erhan and Dicleli 2009)</td><td>Yes</td></tr>
<tr><td>Defined translational and rotational degrees of freedom</td><td>No</td></tr>
<tr><td colspan="3">Use of predrilled holes</td></tr>
<tr><td>No predrilled holes around the piles</td><td rowspan="2">Use of predrilled holes of adequate depth around the piles and filling the holes with loose granular soil after pile driving is used as a means to increase pile flexibility, reduce bending stresses in the piles and increase their vertical load carrying capacity (Yang et al. 1985; Greimann et al. 1986; Greimann and Amde 1988; Faraji 1997; Najib 2002; Khodair and Hassiotis 2003). However, according to White (2012) a potential issue with predrilled holes is that, over time, the back and forth movement of the abutment stem will compact the soil around the piles, and the results will approach that of non-drilled holes. The length of time required to reach this level of compaction depends on the native soil properties as well as the magnitude and frequency of movement.</td><td rowspan="2">Use 9'-0" deep predrilled holes based on the results of a research study conducted at the University of Maryland (Najib 2002) and investigate the case of no predrilled holes as an extreme worse-case scenario</td></tr>
<tr><td>Use predrilled holes around the piles for certain depth</td></tr>
<tr><td colspan="3">Diameter of predrilled holes</td></tr>
<tr><td>Larger than the equivalent diameter of the steel H-pile section</td><td>Crovo (1998) suggests that the diameter of predrilled holes should be 2 feet. Wasserman (2001) recommends that the diameter of predrilled holes should be twice the equivalent diameter of the pile (Figure 3-9). The state of Iowa makes the holes twice the equivalent diameter of the pile (Dunker and Liu 2007) while the state of Massachusetts stipulates that the diameter of the predrilled holes should be 2'-6"</td><td>Effect of presence of predrilled holes filled with appropriate material is reflected in the soil properties in the vicinity of predrilled holes as shown in the soil profile in Figure 6-2</td></tr>
</table>

Backfill material in the predrilled holes		
Several options are employed; the most common are the following: • Loose sand • Pea stone gravel • Dense gravel • Bentonite		Effect accounted in the three-dimensional nonlinear finite element analysis in terms of soil properties. Refer to the soil profile in Figure 6-2 for soil properties in the vicinity of predrilled holes
Depth to bedrock		
Sites with shallow depth to bedrock are not good candidates for integral abutment bridges	Depth to bedrock is identified by soil borings. Use of integral abutments is not an option where the depth to bedrock is considered shallow, less than 13 feet from the ground surface (Hartt et al. 2006) or where piles cannot be driven through at least 10 to 15 feet of overburden (Burke 1993; Hoppe and Gomez 1996)	Depth to bedrock is greater than 15 feet from the ground as shown in the soil profile in Figure 6-2
Ground slope		
Horizontal ground	The lateral resistance of flexible piles decreases as the ground level changes from horizontal to slope (Begum and Muthukkumaran 2008)	Yes
Sloping ground		No
Type of soil at the site		
The type of soil present at the site is one of the parameters used to assess whether the site is a good candidate for an integral abutment bridge	Soil profile is identified by soil borings taken at selected site locations	A soil profile, which indicates that the site is suitable for an integral abutment bridge is used for this research study

Soil type at integral abutment locations		
Knowledge of the type of soil present at abutment locations is required	Soil profile at potential integral abutment locations is identified by soil borings	Refer to the soil profile in Figure 6-2. The same soil profile is used at both integral abutments
Water table elevation		
Water elevation is considered in combination with the type of soil present at the site and abutment locations in particular	Water table elevation is identified on soil borings. A free-draining material is commonly used as backfill, therefore no hydrostatic lateral pressures are assumed on the integral abutments	The abutment backfill is a free-draining material. Consequently, no hydrostatic or expansive forces are exerted on the integral abutments
Scouring potential at the site		
There is scouring potential at the site	Sites with scouring potential are not good candidates for integral abutment bridges	No
There is no scouring potential at the site		Yes
Liquefaction potential at the site		
There is liquefaction potential at the site	Sites with liquefaction potential are not good candidates for integral abutment bridges	No
There is no liquefaction scouring potential at the site		Yes
Wingwalls		
Cantilevered wingwalls	There are two types of wingwalls; independent and cantilever wingwalls. Independent wingwalls are separated from the abutment with an expansion or construction joint while cantilever wingwalls are built integral with the abutment. Thus, cantilever wingwalls are considered part of the bridge substructure and independent wingwalls are not considered part of the bridge substructure	Yes
Independent wingwalls		Yes. This is the case of bridges without wingwalls in the study

<table>
<tr><th colspan="3">Types of cantilever wingwalls based on orientation</th></tr>
<tr><td>Inline wingwalls</td><td rowspan="3">Depending on their orientation with respect to the abutment wall, cantilever wingwalls are classified as cantilevered inline wingwalls, cantilevered U-shaped wingwalls, or cantilevered flared wingwalls</td><td>Yes</td></tr>
<tr><td>Flared wingwalls</td><td>Yes</td></tr>
<tr><td>U-shaped wingwalls</td><td>Yes</td></tr>
<tr><td colspan="3"> 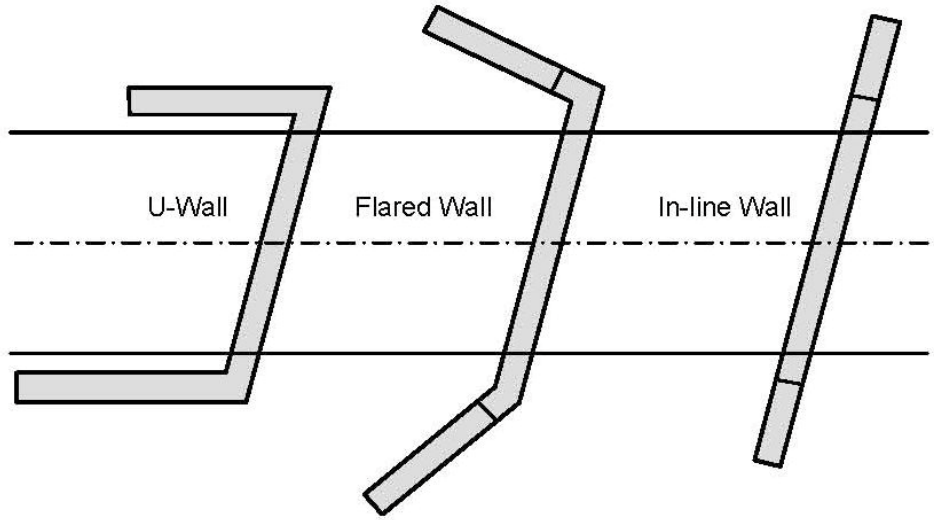
</td></tr>
<tr><th colspan="3">Cantilevered wingwall material</th></tr>
<tr><td colspan="3">Reinforced concrete</td></tr>
<tr><th colspan="3">Cantilevered wingwall concrete material properties</th></tr>
<tr><td colspan="3">Compressive strength f'_c = 4,000 psi
Modulus of elasticity E = 3605 ksi
Poisson's ratio ν = 0.2
Coefficient of thermal expansion a=0.0000060/^{0}F</td></tr>
<tr><th colspan="3">Height of cantilevered wingwalls</th></tr>
<tr><td>Maximum height of cantilevered wingwalls is limited to the height of integral abutments</td><td>Height of cantilevered wingwalls may taper along its length to meet the various groundwork slopes required around the structure (White 2012)</td><td>Height of wingwalls constant and equal to height of abutment in order to determine the most severe effects on the superstructure and piles</td></tr>
</table>

<table>
<tr><th colspan="4">Length of cantilevered wingwalls</th></tr>
<tr><td>The minimum length of cantilevered wingwalls is 2 feet.</td><td colspan="2">States stipulate maximum length of cantilevered wingwalls based on past experiences and performance, not research. In practice, wingwall length is limited to 25 feet; at that point there is a joint and then the wall is defined as a retaining wall.</td><td>Length of cantilever wingwalls is defined in Figure 5-1 for all three orientations. Wingwall lengths ranging from 8 to 24 feet are used for this study</td></tr>
<tr><th colspan="4">Thickness of cantilevered wingwalls</th></tr>
<tr><td>Wingwalls with no special foundation support</td><td colspan="2"></td><td>1'-6"
(Figure 5-1)</td></tr>
<tr><th colspan="4">Backfill soil behind cantilevered wingwalls</th></tr>
<tr><td rowspan="3">Well-graded, free-draining granular material (Amde et al. 1987; White 2012) compacted to 95 percent to eliminate backfill settlement (Fu 2008)</td><td colspan="2" rowspan="3"></td><td>Dense sand (Figure 7-3)</td></tr>
<tr><td>Medium dense sand (Figure 7-3)</td></tr>
<tr><td>Loose sand (Figure 7-3)</td></tr>
<tr><th colspan="4">Type of cantilevered wingwall foundation</th></tr>
<tr><td colspan="2">Steel H-piles</td><td rowspan="8">The survey on integral abutment bridges (Chapter 4) shows that states use either steel H-piles or no special foundation for cantilevered wingwalls</td><td>No</td></tr>
<tr><td colspan="2">Prestressed concrete piles</td><td>No</td></tr>
<tr><td colspan="2">Cast-in-place concrete piles</td><td>No</td></tr>
<tr><td colspan="2">Steel pipe piles open ended</td><td>No</td></tr>
<tr><td colspan="2">Steel pipe piles filled with concrete</td><td>No</td></tr>
<tr><td colspan="2">Drilled shafts</td><td>No</td></tr>
<tr><td colspan="2">Spread footings</td><td>No</td></tr>
<tr><td colspan="2">No special foundation support</td><td>Yes</td></tr>
</table>

Loads		
DC-Dead load of all the components of the superstructure, both structural and nonstructural	The behavior of an integral abutment bridge depends on the extent of temperature variation. According to Harvey and Kennedy (2002), daily and seasonal temperature variations have the greatest influence on the behavior of integral abutment bridges. This is due to the fact that in integral abutment bridges, the soil behind the abutment wall provides restraint against thermal expansion. As a result, large thermal stresses are induced in the various elements of the integral abutment bridge (National Steel Bridge Alliance 2005) Doust (2011) compared the magnitude of stresses induced in the piles of integral abutments by each loading. He concluded that the most critical loadings are the temperature expansion and temperature contraction due to seasonal temperature variation. The two temperature variations were applied as uniform temperature loading	Uniform temperature load TU due to seasonal variation using the temperature range for cold climate stipulated in the AASHTO LRFD Specifications for steel structures. The choice of cold climate lies in the fact that integral abutment bridge construction yields more economic benefit when used in those geographical areas where the climate is defined as "cold climate". In addition, using the temperature ranges stipulated for cold climate will produce more conservative results compared to the results that would have been produced using the temperature ranges for moderate climate.
DW-Dead load of wearing surfaces and utilities		
EL-Locked-in or residual force effects resulting from the construction process, including the secondary forces from post-tensioning(which are not gravitational dead loads)		
EV-Vertical pressure of earth fill		
EH-Horizontal earth pressure		
ES-Earth pressure from a permanent earth surcharge such as an embankment		
DD-Downdrag		
LL-Vehicular live load		
PL-Pedestrian live load		
IM-Vehicular dynamic load allowance		
LS-Live load surcharge		
BR-Vehicular braking force		
CE-Vehicular centrifugal force from vehicles on a curved roadway		

WA-Water load resulting from differential water levels, stream flow or buoyancy		
WS-Wind load on structure		
WL-Wind load on live load		
EQ-Earthquake load		
CT-Vehicular collision force on abutments or piers due to vehicles or trains		
CV-Vessel collision force due to aberrant ships or barges		
IC-Ice load		
TU-Uniform temperature change due to seasonal variation		
TG-Temperature gradient due to exposure of the bridge to solar radiation		
SH-Shrinkage		
CR-Creep of concrete		
SE-Settlement effects due to settlement of substructure units on the superstructure		
FR-Friction forces on sliding surfaces from structure movements		
Structural Analysis method		
Three-dimensional nonlinear finite element analysis		
Finite Element Analysis Software		
ANSYS Release 13.0 Academic Research Mechanical		

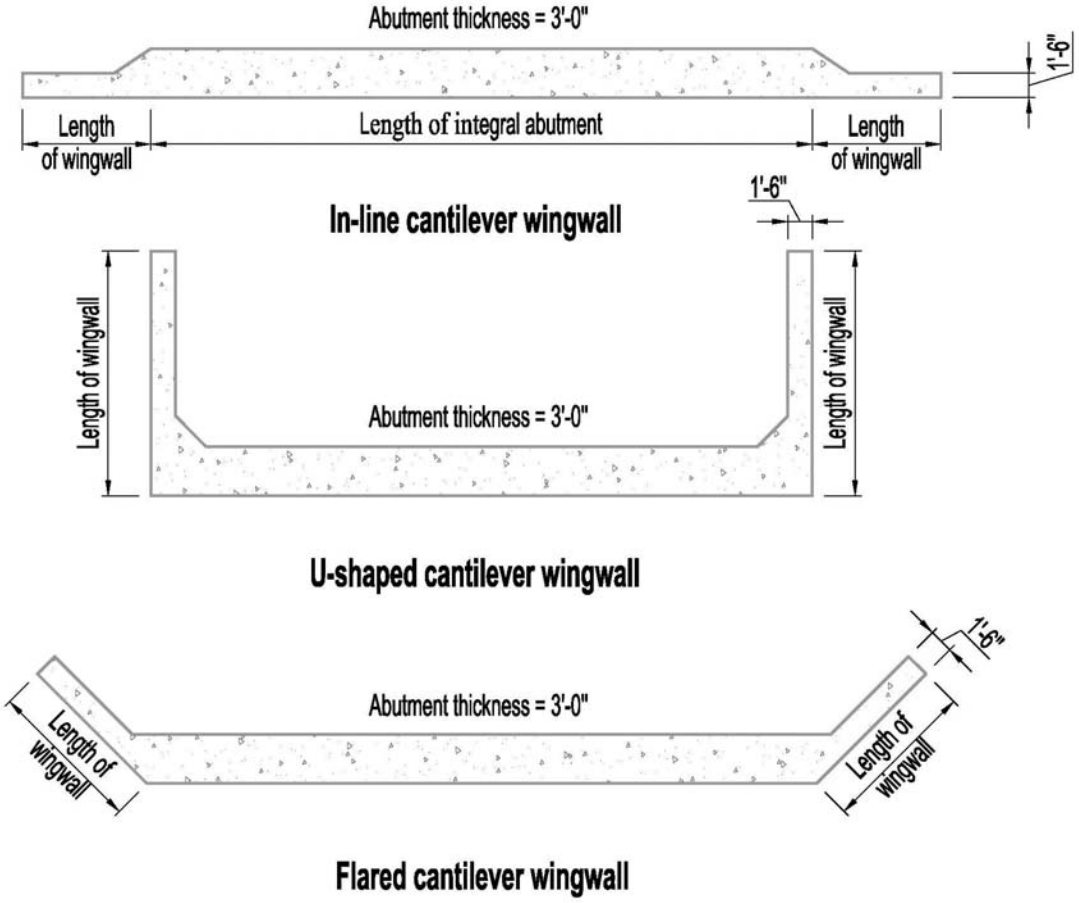

Figure 5-1 Definition of cantilever wingwall length

Chapter 6

Parametric Studies

6.1. Introduction

Parametric studies in structural engineering investigate the effects of certain parameters on the performance or behavior of a structure or structural element. This chapter describes the parametric studies conducted as part of this research study aim to investigate the effects of the various cantilever wingwall configurations on the behavior of integral abutment bridges.

6.2. Objective of the Parametric Studies

The objective of the parametric studies for this study is to identify problems or potential problems arising with the use of cantilever wingwalls in integral abutment bridge construction. Thus, the parametric studies focus on the effects of cantilever wingwalls on axial forces in the steel girders, stresses in the piles as well as cracking pattern and stresses in the reinforcing steel of integral abutments.

6.3. Parametric Studies

Table 5-1 lists the selected parameters for the parametric studies. Table 6-1 further elaborates on the selected parameters by identifying their value or range.

6.3.1. Bridge Length

Bridge length for the parametric studies varies from 100 to 1200 feet. The shortest bridge is a single-span 100-feet-long bridge and the longest is a 12-span 1200-feet-long bridge with 12 equal spans. The other bridge lengths used for the parametric studies are 200 feet, 300 feet, 400 feet, 600 feet, 900 feet, and 1200 feet.

The reasoning for the selection of these bridge lengths is explained below:

- The starting range of bridge length at which composite steel plate girder systems are preferred over rolled sections is 100 feet. In addition, Figure 1-6 indicates that 88.3 percent of in-service bridges in the United States have a maximum span of 100 feet or less.

- According to the NYSDOT Bridge Manual, multiple-span arrangements should be considered once the single span exceeds 165 feet. Using a typical 100 feet span, a 2-span arrangement equals 200 feet in length.

- The average steel girder integral abutment bridge length for bridges on zero skew is 324 feet (Figure 4-5). As a result, both the 300 and 400 feet bridge lengths are used in the parametric studies.

- The normal distribution curve in Figure 6-1 indicates that 99.7 percent of steel girder integral abutment bridges have lengths ranging from 39 to 609 feet. This is based on an average (mean) bridge length of 324 feet (Figure 4-5) and standard deviation equal to 95 feet (Figure 4-6) applicable to steel bridges with zero skew. As a result, the bridge length of 600 feet is included in the parametric studies.

- The bridge length of 900 feet is used as the mid point between the bridge lengths of 600 feet and 1200 feet already part of the parametric studies.

- The longest steel girder integral abutment bridge built in the United States has a length of 1044 feet. The bridge was built in the state of Colorado where there is no limit on bridge length for integral abutment bridges (Tables 4-1,4-2, and 4-3). The bridge length of 1200 feet used in the parametric studies is about 15 percent greater than the length of the 1044-feet-long bridge.

Steel Superstructure with zero skew		
Case	Percent of Bridges	Range of Bridge Length (feet)
Mean ± One Standard Deviation	68%	229 - 419
Mean ± Two Standard Deviations	95%	134 - 514
Mean ± Three Standard Deviations	99.7%	39 - 609

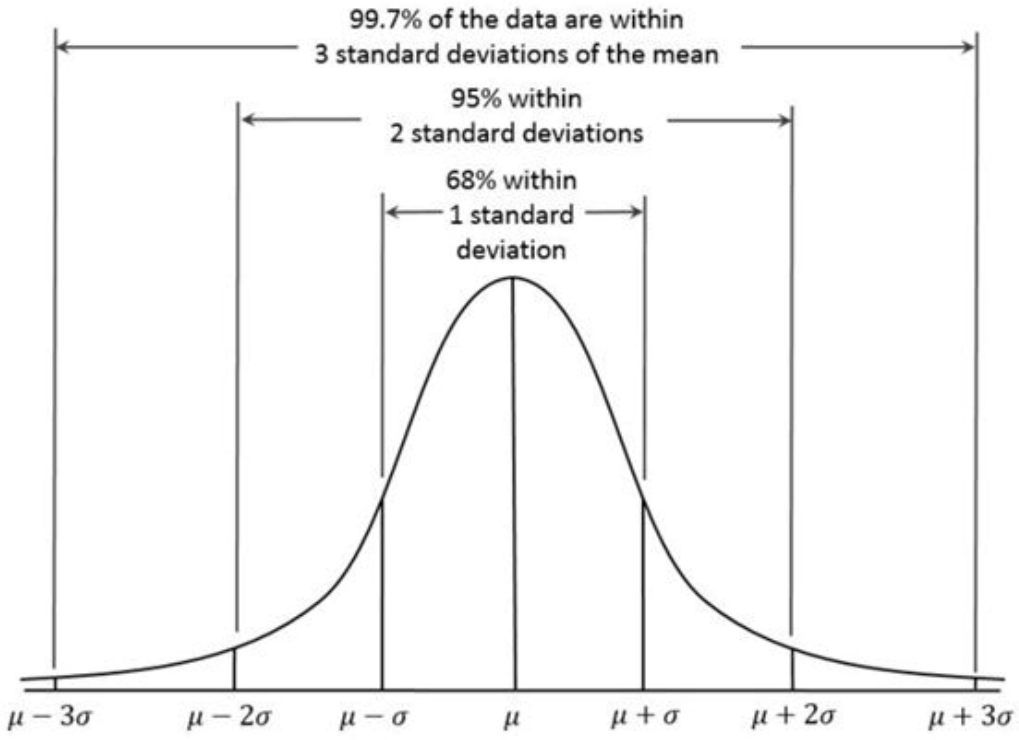

Figure 6-1 Normal distribution curve for length of steel girder integral abutment bridges

6.3.2. Span Layout

With the exception of the 100-feet long bridge, all bridges for the parametric studies are single multi-span units. All spans are equal and each measures 100 feet. The choice of this particular span layout lies in the fact that the bridges are analyzed for the load combination of dead plus temperature load. Consequently, using this span layout dead load effects are minimized and the effects of temperature load are emphasized.

6.3.3. Range and Values of Selected Parameters

The values and ranges of the selected parameters for the parametric studies are listed in Table 6-1. The selection of parameters was the subject of chapter 5 of this study.

Table 6-1 Range and values of selected parameters

Parameter	Value or Range
Bridge deck material properties	Compressive strength f'_c = 4,000 psi Modulus of elasticity E = 3605 ksi Poisson's ratio ν = 0.2 Coefficient of thermal expansion a = 0.0000060/^{0}F
Thickness of bridge deck	9.5"
Number of lanes	2 lanes
	4 lanes
Bridge width	40'-0" for 2-lane bridges
	64'-0" for 4-lane bridges

Overhang width	3'-0" for 2-lane bridges
	3'-6" for 4-lane bridges
Number of steel plate girders	5 girders for 2-lane bridges
	7 girders for 4-lane bridges
Steel plate girder spacing	8'-6" for 2-lane bridges
	9'-6" for 4-lane bridges
Steel plate girder size (based on a 125-feet span to have a deeper girder)* For simple spans (125x12)/25 = 57.6" For continuous spans (125x12)/30 = 50" The AASHTO LRFD Bridge Design Specifications Article 2.5.2.6.3 Table 2.5.2.6.3-1 stipulate a span length to girder depth ratio of 25 for simple spans and 31.25 for continuous spans. The NYSDOT Bridge Manual Article 3.5.3 Table 3-2 stipulates a maximum ratio of 30 for continuous spans with an optimum ratio of 27.5 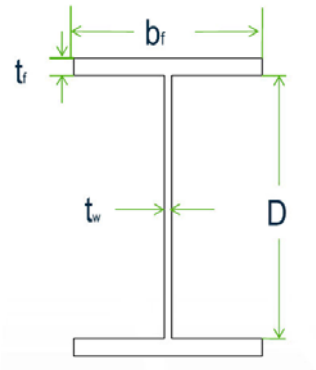 	Use Top flange 14"x1.5" Web 57"x 0.5" Bottom flange 14"x1.5" AASHTO LRFD 6.10.2.1. $D/t_w \leq 150$ where D = depth of web Thus, $(t_w)_{min} = D/150 = 57"/150 = 0.38"$ $t_w = 0.5" > 0.38"$ o.k. AASHTO LRFD equation 6.10.2.2-1 $b_f / 2t_f \leq 12$ $14"/2x1.5 = 14/3 = 4.7 < 12$ o.k AASHTO LRFD equation 6.10.2.2-2 $b_f \geq D/6$ where $D/6 = 57/6 = 9.5$ $b_f = 14 > 9.5$ o.k. AASHTO LRFD equation 6.10.2.2-3 $t_f \geq 1.1\ t_w$ where $1.1t_w = 1.1x0.5" = 0.55"$ $t_f = 1.5" > 0.55"$ o.k. AASHTO LRFD equation C6.l0.3.4-1 $b_{fc} \geq L/85$ where $L/85 = (100x12)/85 = 14"$ $b_{fc} = 14"$ o.k.

Steel plate girder material properties	ASTM A709 Grade 50 Fy = 50 Ksi Modulus of elasticity E = 29,000 Ksi Poisson's ratio $\nu = 0.3$ Coefficient of thermal expansion $a = 0.0000065/^0F$
Cross frame spacing	25'-0"
Cross frame size	W8X18
Cross frame material properties	ASTM A709 Grade 50 Fy = 50 Ksi Modulus of elasticity E = 29,000 Ksi Poisson's ratio $\nu = 0.3$ Coefficient of thermal expansion $a = 0.0000065/^0F$
Integral abutment concrete material properties	Compressive strength $f'_c = 4{,}000$ psi Concrete crushing stress = Compressive strength = 4,000 psi = UCS Concrete tensile cracking stress UTCS = $7 (f'_c)^{0.5} = 442$ psi Modulus of elasticity E = 3605 ksi Poisson's ratio $\nu = 0.2$ Coefficient of thermal expansion $a = 0.0000060/^0F$
Integral abutment reinforcing steel (rebar) material properties	ASTM A615 Grade 60 Yield strength Fy = 60 Ksi Modulus of elasticity E = 29,000 Ksi Poisson's ratio $\nu = 0.3$ Coefficient of thermal expansion $a = 0.0000065/^0F$
Integral abutment reinforcing steel (rebar) size and spacing	Vertical rebar outside face #9@6" Vertical rebar inside face #9@12" Horizontal rebar #9@12" EF (each face)

Integral abutment height** ** (9.5"+60"+36") = 105.5" = 8'-9.5"	9'-0"
Integral abutment wall thickness	3'-0"
Integral abutment foundation type	Steel H piles
Integral abutment pile type	End bearing piles
Integral abutment pile size	HP10X57
Integral abutment pile material properties	ASTM A709 Grade 50 Yield strength Fy = 50 Ksi Modulus of elasticity E = 29,000 Ksi Poisson's ratio $\nu = 0.3$ Coefficient of thermal expansion $a = 0.0000065/^{0}F$
Integral abutment pile spacing	6'-0"
Number of integral abutment piles	7 piles for 2-lane bridges
	11 piles for 4-lane bridges
Integral abutment pile orientation	Weak-axis bending
Integral abutment pile length	Total length 42'-0", which includes 2'-0" penetration into the integral abutment

Depth of predrilled holes around integral abutment piles	9'-0"
Cantilever wingwall concrete material properties	Compressive strength f'_c = 4,000 psi Concrete crushing stress = Compressive strength = 4000 psi = UCS Concrete tensile cracking stress UTCS = 7 (f'_c)^0.5 = 442 psi Modulus of elasticity E = 3605 ksi Poisson's ratio ν = 0.2 Coefficient of thermal expansion a = 0.0000060/^{0}F
Cantilever wingwall reinforcing steel (rebar) material properties	ASTM A615 Grade 60 Yield strength Fy = 60 Ksi Modulus of elasticity E = 29,000 Ksi Poisson's ratio ν = 0.3 Coefficient of thermal expansion a = 0.0000065/^{0}F
Cantilever wingwall reinforcing steel (rebar) size and spacing	Vertical rebar outside face #9@6" Vertical rebar inside face #9@12" Horizontal rebar #9@12" EF (each face)
Cantilever wingwall length	8'-0"
	12'-0"
	15'-0"
	18'-0"
	21'-0"
	24'-0"

Cantilever wingwall height	9'-0"
Cantilever wingwall thickness	1'-6"
Cantilever wingwall foundation type	No special foundation
Loads and Load Combinations	Dead Load + Temperature Load Uniform temperature load (TU) for cold climate as per AASHTO LRFD Specifications Table 3.12.2.1-1 for steel structures. Thus, the temperature range is from -30°F to 120°F or ΔT=150°F. The amount of thermal movement depends on the ambient temperature at which the girders are integrated with the abutments. Assuming the beams are set at either of the temperature extremes stipulated in AASHTO Table 3.12.2.1-1, the temperature range is 150°F Typically, however, in regions with cold climate, beams erected in the summer are integrated with the abutments at temperatures lower than 100°F and in the winter at temperatures higher than 32°F (Vermont Agency of Transportation Integral Abutment Bridge Design Guidelines) Consequently, maximum temperature variation is 100°F -(-30°F) = 130°F for thermal contraction and 120°F -32°F = 88°F for thermal expansion respectively. These two temperature variations are applied to the modeled bridges as uniform temperature loading

Backfill soil behind integral abutments and wingwalls, and soil profile around piles	The parametric studies investigate three cases of backfill soil behind the integral abutments and cantilever wingwalls. This includes: • Dense sand with γ = 130 pcf (Peck et al. 1974) and $\Phi = 45°$ (Meyerhof 1956) • Medium dense sand with γ=125 pcf (Peck et al. 1974) and $\Phi = 37°$ (Meyerhof 1956), • Loose sand with γ = 118 pcf (Peck et al. 1974) and $\Phi = 30°$ (Meyerhof 1956), as shown in Figures 6-2 and 7-3. The soil that extends from the bottom of the abutment to the pile tip consists of two layers: (1) the top 9 feet assumed to be loose sand as the predrilled hole filled with loose sand provides minimal soil restraint, and (2) very stiff clay that extends from the loose sand layer to the pile tip. According to Yang et al. (1982) in very stiff clay, the vertical load-carrying capacity of H piles is reduced by a much as 20 percent while they observe no significant reduction in the vertical load-carrying capacity of H piles in other types of soils that included soft clay, stiff clay, loose sand, medium sand, and dense sand. Consequently, use of very stiff clay provides for a conservative soil profile The soil properties for the loose sand are γ' = 55 pcf is the submerged unit weight of the soil and $\Phi = 30^{o}$ is the angle of internal friction (Figure 6-2) The soil properties for the very stiff clay are γ' = 65 pcf is the submerged unit weight of the soil, Cu = 5000 psf is the undrained cohesion of clay, and $\varepsilon_{50} = 0.005$ is the strain of clay at 50 percent of soil strength (Figure 6-2)

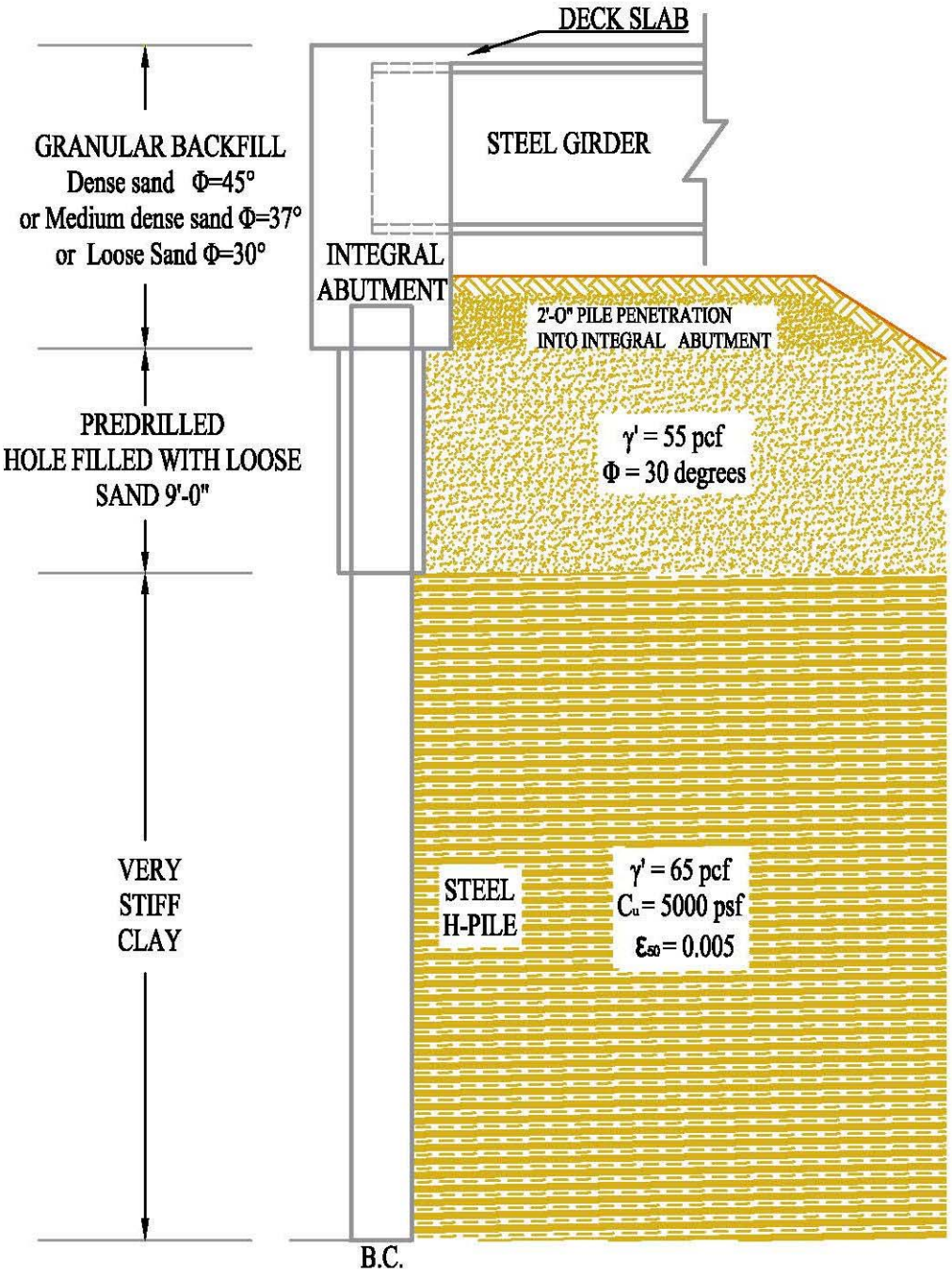

Figure 6-2 Soil profile

Chapter 7

Modeling of Soil-Structure Interaction

7.1. Introduction

Integral abutment bridges are structures whose loading conditions and deformations imposes stresses on the soil, which in turn deforms and as a consequence transmits back additional forces and deformations to the structure. The magnitude of the lateral earth pressure is a function of structure deformation and the structural response is dependent on the magnitude of the lateral earth pressure. The mutual dependence of soil and structure behavior is known as soil-structure interaction (SSI).

Soil-structure interaction (SSI) is the combined study of both the structure and the surrounding soil aim to predict the response of the soil to the loading of the structure as a function of deflection, and the corresponding response of the structure. In the case of integral abutment bridges, the movement of bridge abutments, due to thermal expansion and contraction of the bridge deck, creates passive and active soil conditions in the backfill. The soil reaction is nonlinear and varies with depth. The earth pressures are dependent on the stiffness of the soil and the amount and nature of the wall displacement, which can be a translation and/or rotation. This interdependency of the nature and amount of displacements both in the soil and the structure to the stresses created is the soil-structure-interaction problem for the case of integral abutment bridges and therefore explicitly accounted for in the modeling.

7.2. Lateral Earth Pressure

Soil is a complicated material that exhibits nonlinear behavior (Beresnev and Wen 1996), and shows anisotropic (Barden, 1963; Hoque et al., 1996; Gazetas, 1981) as well as time-dependent behavior when subjected to loads (Augustesen et al. 2004). Its stiffness modulus (both shear modulus G and Young's modulus E) is stress-dependent (Obrzud 2010) meaning all stiffnesses increase with pressure. Furthermore, soil behaves differently in primary loading, unloading, and reloading; undergoes plastic deformation; is inconsistent in dilatancy; and experiences small stiffness at very low strain levels and upon stress reversals (Kok et al. 2009).

The complexity of soil behavior has important consequences for all instances that involve soil-structure interaction (Jardine et al. 1986). This includes the analysis of integral abutment bridges where thermally-induced movements of the bridge superstructure

produces large deformations in the backfill behind the integral abutments and mobilizes lateral earth pressures behind both the abutments and the foundation piles (Arsoy et al. 2004). The magnitude of lateral earth pressure can be as low as the minimum active or as high as the maximum passive pressure (Figure 7-1).

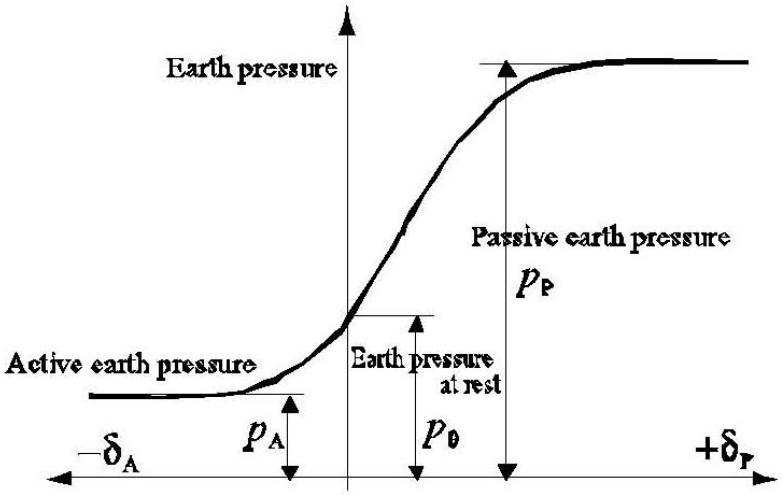

Figure 7-1 Relationship between displacement and earth pressure

Three categories of lateral earth pressure are exerted on an abutment wall (Figure 7-2):

- At-rest earth pressure: It is the lateral earth pressure exerted by the backfill on the wall when the wall experiences no lateral movement.
- Active earth pressure: It is the lateral earth pressure applied by the backfill on the wall when the wall moves outward from the soil. The lateral earth pressure starts to be reduced until it reaches its minimum value.
- Passive earth pressure: It is the lateral earth pressure developed within the backfill and occurs when the wall moves toward the backfill. The lateral earth pressure increases until it reaches its maximum value.

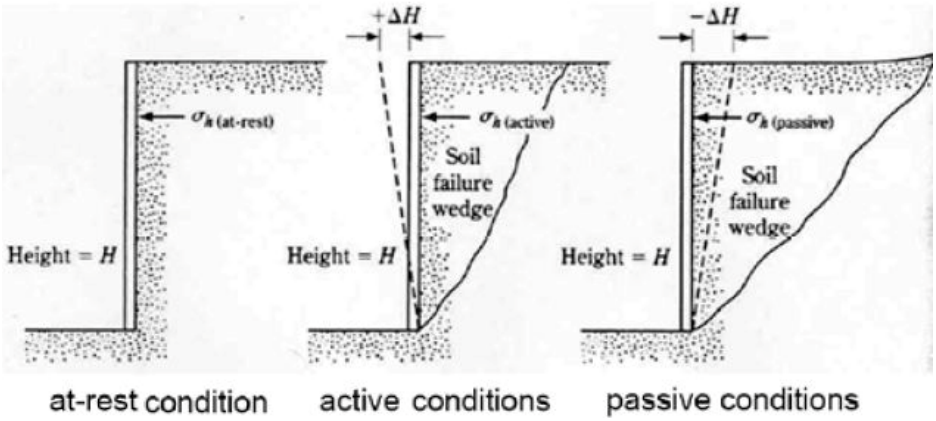

Figure 7-2 Categories of lateral earth pressure

Table 7-1 obtained through experimental data and finite element analyses (Clough and Duncan 1991) gives approximate magnitudes of wall movements required to reach minimum active and maximum passive earth pressure conditions. The tabulated data indicate that the movement required to reach the maximum passive pressure is about ten times as great as that required to reach the minimum active pressure for walls of the same height.

Table 7-1 Approximate horizontal displacement of a wall to activate active and passive earth pressure conditions (Clough and Duncan 1991)

Type of Backfill	Displacement Required to Reach Active Soil-Pressure, Δ_{active}/H	Displacement Required to Reach Passive Soil-Pressure, $\Delta_{passive}/H$
Loose sand	0.004	0.04
Medium-dense sand	0.002	0.02
Dense sand	0.001	0.01

- The value for the earth pressure coefficient (K) varies with wall displacement and eventually remains constant after sufficiently large displacement (Figure 7-3). The earth pressure coefficient (K) represents the ratio between lateral earth pressure and vertical earth pressure. Depending on the state of earth pressure, it is classified as coefficient of active earth pressure (Ka), coefficient of earth pressure at rest (Ko), or coefficient of passive earth pressure (Kp).
- The change in the magnitude of earth pressures also varies with the type of soil, that is, the magnitude of earth pressures in the dense sand change more quickly with wall movement compared to medium and loose sand (Figure 7-3).

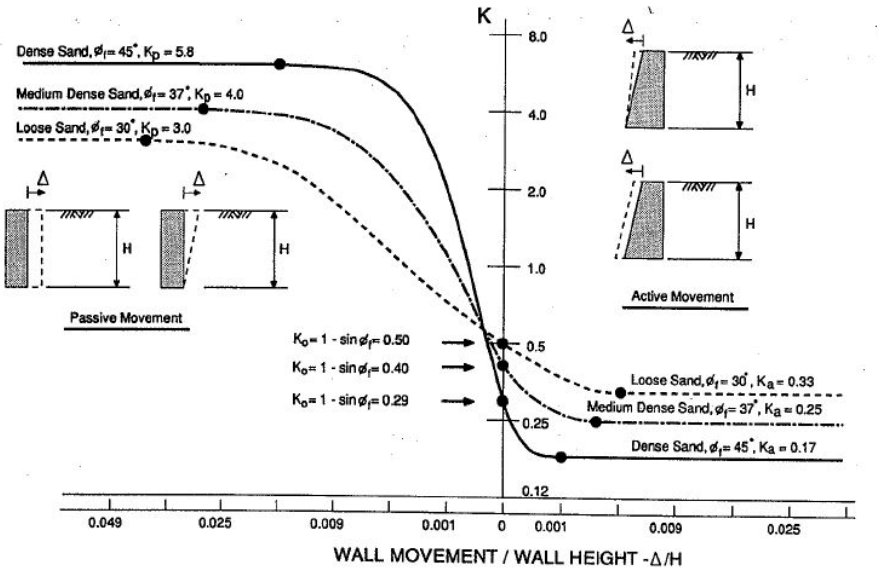

Figure 7-3 Relationship between wall movement and earth pressure (Clough and Duncan 1991)

7.3. Lateral Earth Pressure Theories

Lateral earth pressure theories in geotechnical engineering started to develop almost 300 years ago. Coulomb (1776) and Rankine (1857) developed theories to represent the actual earth pressures exerted on retaining structures. Caquot and Kerisel (1948) developed the more generally applicable log spiral theory, where the movements of walls are sufficiently large so that the shear strength of the backfill soil is fully mobilized, and where the strength properties of the backfill can be estimated with sufficient accuracy. These three classical earth pressure theories still occupy a dominant place in geotechnical engineering practice.

Sophisticated analyses of soil-structure interaction and wall-soil movements began in the 1960s with the development of finite difference and finite element analytical procedures. Sokolovski (1965) presented a method based on finite difference solution; Habibagahi and Ghahramani (1979) developed a solution for lateral earth pressure coefficients based on zero extension line theory; Chen and Liu (1991) and Soubra (2000) did experimental and theoretical researches and developed some theories and methods for the determination of passive earth pressures; Lancellotta (2002) developed an analytical solution on passive earth pressures.

The simultaneous advancement of geotechnical instrumentation equipment and monitoring procedures made the "observational method" of design (Peck 1969) popular and cost effective.

7.3.1. Classical Lateral Earth Pressure Theories

The three classical lateral earth pressure theories are: (1) Coulomb Theory, (2) Rankine Theory, and (3) Caquot and Kerisel Log Spiral Theory.

Coulomb Theory

The Coulomb Theory (1776), the first rational solution to the earth pressure problem, is based on the concept that the lateral force exerted on a wall by the backfill can be evaluated by analysis of the equilibrium of a wedge-shaped mass (also called failure zone) of soil bounded by the back of the wall, the backfill surface, and a surface of sliding through the soil. Coulomb's theory was derived according to the principle of force equilibrium. As a result, there is only one failure surface, which is a plane (Figure 7-4). The assumptions in this analysis are:

- There is friction between the wall and soil and this is included in computations by the use of the soil-wall friction angle (δ). In general, the soil-wall friction angle (δ) ranges from $\phi/2$ to $2\phi/3$, where ϕ is the friction angle of the soil
- Lateral earth pressure is not limited to vertical walls

- The resultant force is not necessarily parallel to the backfill surface due to the soil-wall friction angle (δ)
- The surface of sliding through the soil is a straight line.
- The full strength of the soil is mobilized to resist shear failure through the soil

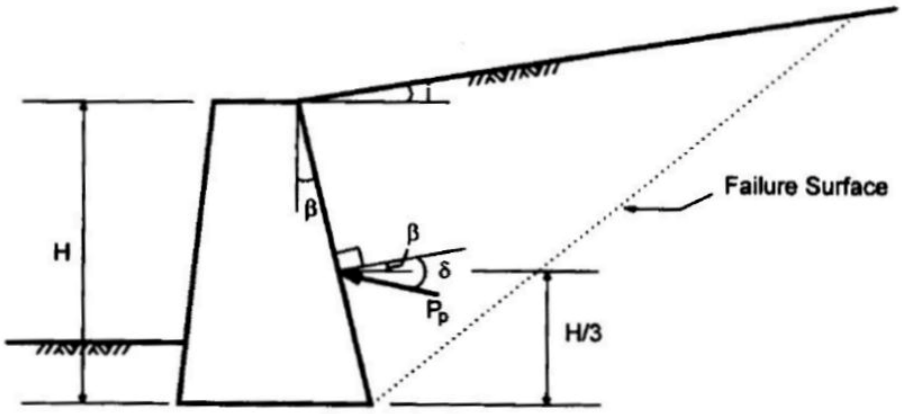

Figure 7-4 Coulomb theory for active and passive earth pressures

The mathematical expressions for the active and passive earth pressure coefficients are very complicated and are a function of the angle of the back of the wall, the soil-wall friction angle (δ), and the friction angle of the soil (ϕ). These expressions are available in tables and computer software.

Rankine Theory

The Rankine Theory developed in 1857 presents a simple procedure for computing the minimum active and maximum passive earth pressures. Rankine's earth pressure theory is based on the equilibrium of the strained soil meaning that soil at any point within the failure zone is indiscriminately at failure and thereby there are infinite failure surfaces (Figure 7-5). The theory predicts triangular active pressure distribution oriented parallel to the backfill surface for homogeneous cohesionless backfill and is based on the following assumptions:

- There is no friction or adhesion between the wall and soil
- Lateral pressure is limited to vertical walls, that is, 90 degrees with the horizontal
- Failure in the backfill occurs as a sliding wedge along an assumed failure plane defined by the friction angle of soil (ϕ)
- Lateral earth pressure varies linearly with depth and the resultant pressure is located one-third of the height above the base of the wall
- The resultant force is parallel to the backfill surface
- The full strength of the soil is mobilized to resist shear failure through the soil

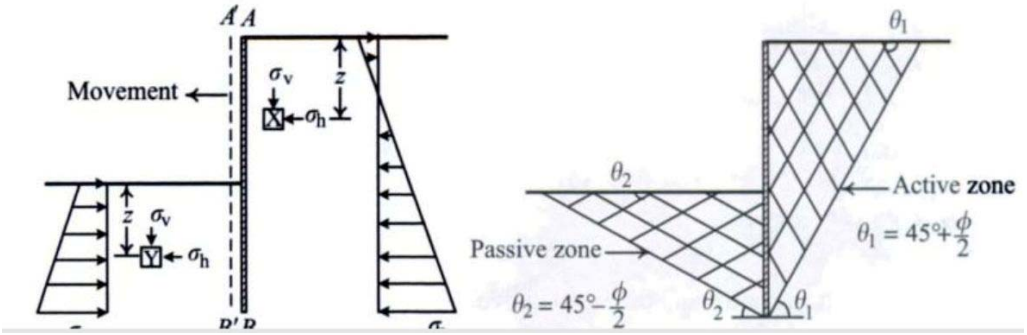

Figure 7-5 Rankine's earth pressure theory (Ou 2006)

Caquot and Kerisel Theory

Caquot and Kerisel developed in 1948 an advanced theory, called the log spiral theory, to account for a non-planar rupture surface. Thus, they used a logarithmic spiral to represent the rupture surface than a straight line (Figures 7-6 and 7-7). The mathematical equations developed to calculate the active and passive earth pressure coefficients are too complex to use; therefore, tables of earth pressure coefficients, or computer software are used instead.

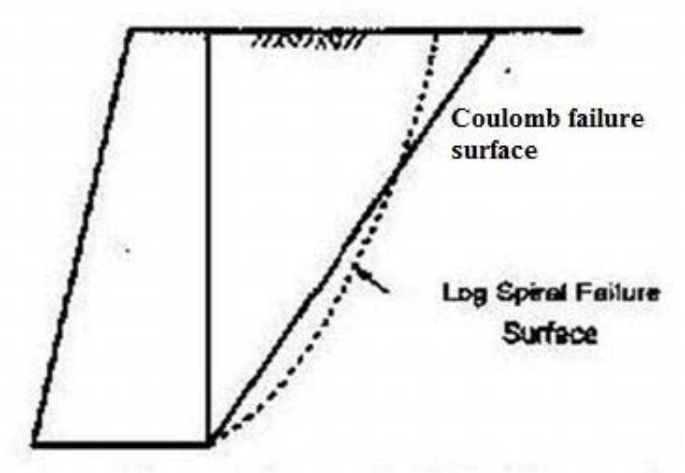

Figure 7-6 Comparison of logarithmic spiral and Coulomb's failure surfaces for active conditions (Clough and Duncan 1991)

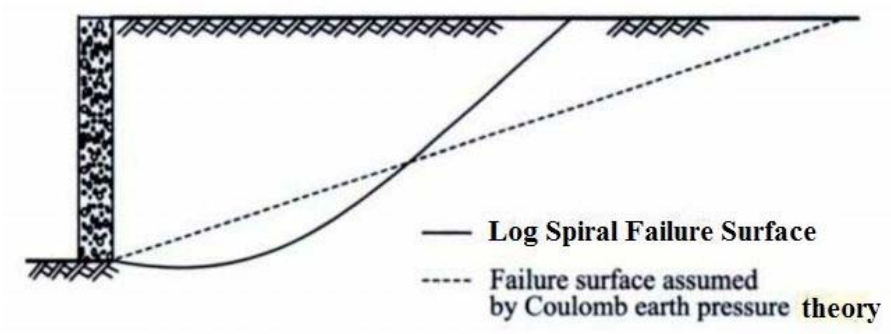

Figure 7-7 Comparison of logarithmic spiral and Coulomb's failure surfaces for passive conditions (Ou 2006)

Reliability of Classical Lateral Earth Pressure Theories

The reliability of any theory including all three classical lateral earth pressure theories depends on how close they match the actual field conditions. According to many studies and experiments (Peck and Ireland 1961; Rowe and Peaker 1965; Mackey and Kirk 1967; James and Bransby 1970; Rehnman and Broms 1972) the failure surfaces of both active and passive failure are both curved surfaces rather than planes. Consequently, the actual active and passive failure surfaces assumed by Caquot and Kerisel better represent the actual conditions. This is the reason why the coefficients of both the active and passive earth pressures derived from the Caquot and Kerisel theory are widely adopted in engineering practice; for example the NAVFAC DM 7.2 (1986).

Comparison of Classical Lateral Earth Pressure Theories

A comparison of the active and passive earth pressure coefficients of all three classical theories indicates the following:

- Both the active and passive earth pressure coefficients of Coulomb, Rankine, and Caquot-Kerisel theories are identical for the case of horizontal backfill surface and soil-wall friction angle (δ) equal to zero.
- As the friction angle of the soil (ϕ) increases, that is, the soil becomes stronger, the active earth pressure coefficients decrease resulting in a decrease in the active lateral earth pressure while the passive earth pressure coefficients increase resulting in an increase in the passive lateral earth pressure.
- For active pressure conditions, when the soil-wall friction angle (δ) is greater than zero, the Rankine coefficient is always the largest while the Coulomb and Caquot-Kerisel coefficients are close and almost identical for $\delta \leq 0.67\phi$
- For passive pressure conditions, when the soil-wall friction angle (δ) is greater than zero, the Rankine coefficient is the smallest and the Coulomb coefficient is the largest.

7.3.2. Other Earth Pressure Theories

In addition to the classical earth pressure theories, a number of other theories are used in geotechnical engineering practice. This includes:

Table 7-2 Other earth pressure theories

Active earth pressure theories	Passive earth pressure theories
Müller-Breslau theory (1906)	Müller-Breslau theory (1906)
Absi theory (Kerisel and Absi 1990)	Sokolovski theory (1965)
Mazindrani theory (1997)	Absi theory (Kerisel and Absi 1990)
	Mazindrani theory (1997)
	Lancellotta (2002)

7.3.3. Seismic Earth Pressures

Okabe (1926) and Mononobe and Matsuo (1929) developed the basis of analysis of seismic earth pressures on retaining structures that has become known as the Mononobe-Okabe (M-O) method. The M-O method is a direct extension of the static Coulomb theory and falls under the category of force-equilibrium methods that are based on pseudo-static analysis. In summary, the most commonly-used methods to analyze earth retaining structures under seismic conditions are force equilibrium methods based on

- Pseudo-static analysis
  - Okabe (1926)
  - Mononobe and Matsuo (1929)
  - Arrango (1969) described by Seed and Whitman (1970)
  - Choudhury et al. (2002)
  - Ortigosa (2005)

- Pseudodynamic analysis
  - Steedman and Zeng (1990)
  - Choudhury-Nimbalkar (2005)

- The displacement-based sliding block method by Richards and Elms (1979)

7.4. Lateral Earth Pressures on Bridge Abutments

Lateral earth pressure is one of the most important parameters for the analysis and design of bridge abutments. Although the classical earth pressure theories just described give no consideration to structural displacement, actual lateral earth pressures depend on the stress-displacement relationship (Figure 7-1). The mode of displacement of the abutment involves both translation and rotation (Hassiotis and Xiong 2007). Experiments conducted by Thomson and Lutenegger (1998), Fang et al. (1994), Sherif et al. (1982), Rowe (1954), and Terzaghi (1938) as well as studies by Shamsabadi et al. (2007), Arsoy (2004), Dicleli (2004), and Jung-Hee Hong (2003) show that both the deformation mode and the magnitude of the deformation affect the magnitude and distribution of the earth pressure. Several methods are employed to predict these nonlinear responses. This includes approximate solutions to displacement-dependent earth pressures developed by Shamsabadi and Yan (2008), Shamsabadi et al. (2007), Duncan and Mokwa (2001), Zhang et al. (1998), Chang (1997), Clough and Duncan (1991), and Bang (1984) as well as soil-structure-interaction such as in Winkler soil springs model or finite element analysis.

7.4.1. Lateral Earth Pressures on Integral Abutments

The magnitude and distribution of soil pressures exerted on integral abutments is a complex issue because soil pressures change significantly when the integral abutment moves due to seasonal and daily cycles of expansion and contraction of the bridge deck. Over time, the magnitude of soil pressures escalates due to densification of the retained soil (England and Dunstan 1994; Hassiotis et al. 2006; Hassiotis and Xiong 2007; Xu et al. 2007). The researchers indicate that the earth pressures behind integral abutments increase over time with expansion-contraction cycles and eventually reach states of stress close to full passive and active pressures (Xu et al. 2007) or higher than the usual design values (Hassiotis et al. 2006). Both the magnitude and distribution of soil pressures depends on the deflected shape of the abutment wall. Pressure distribution is inherently nonlinear despite the fact that a linear triangular soil pressure distribution along the height of the abutment wall in the opinion of many researchers adequately represents the soil pressure against the wall (Ting and Faraji 1998; Kunin and Alampalli 2000; Hassiotis and Xiong 2007; Kim and Laman 2010).

Design Curves

A number of design curves has been developed that relates the abutment movement to the magnitude of lateral earth pressure behind integral abutments. This includes the design curves developed by Clough and Duncan (1991) shown in Figure 7-3 that were adopted by the National Cooperative Highway Research Program (NCHRP) (Barker, et al., 1991), the design curves of the Canadian Foundation Engineering Manual (1992) shown in Figure 7-8, the design curves by Husain and Bagnaroil (1996) shown in Figure 7-9, and the design curve of the Massachusetts DOT Manual (2009) shown in Figure 7-10.

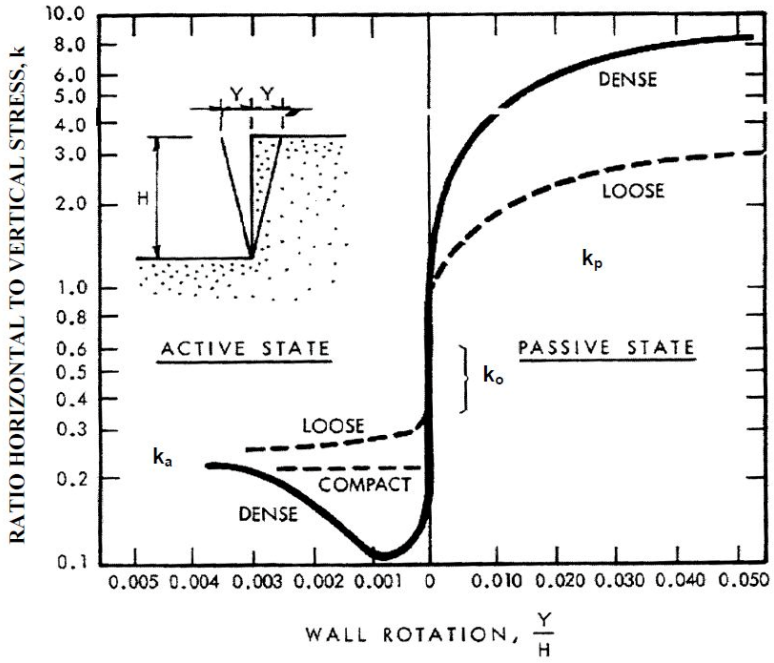

Figure 7-8 Canadian Foundation Engineering Manual (1992)

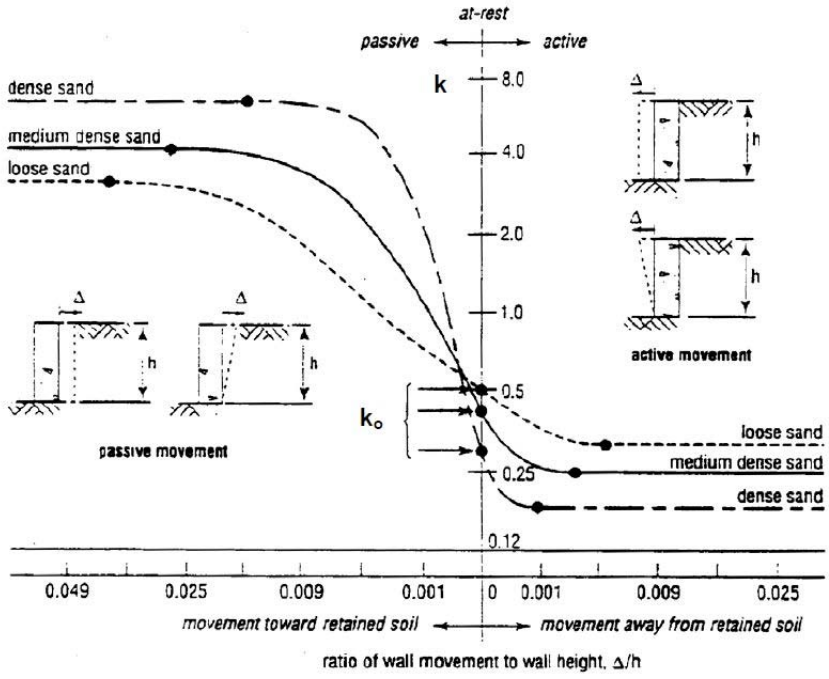

Figure 7-9 Husain and Bagnaroil (1996)

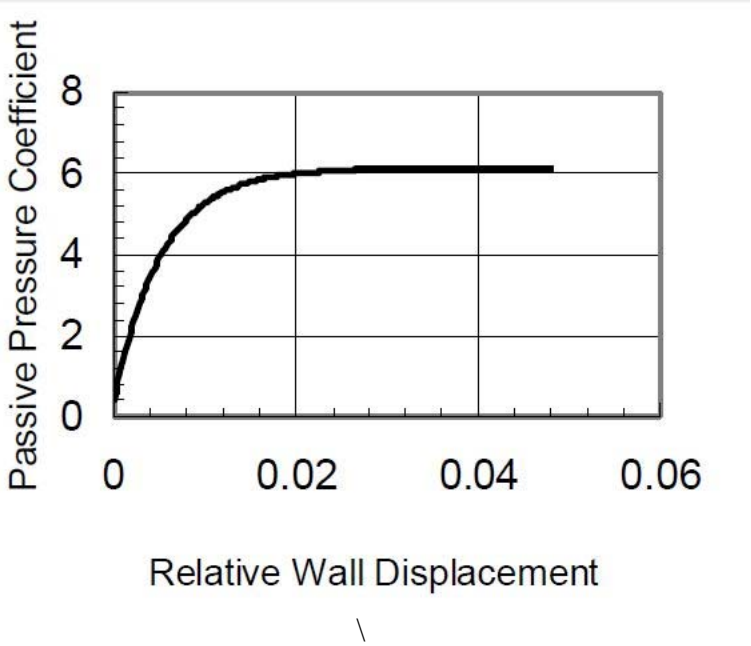

\

Figure 7-10 Massachusetts DOT Manual (2009)

Ting and Faraji (1998) compared soil pressures that were predicted by applying numerous design curves with soil pressures established by experimental studies. They concluded that the NCHRP design curve underestimates the ultimate, passive-soil pressure and overestimates the initial, lateral stiffness for dense and medium-dense sand. These researchers determined that the Canadian Foundation Engineering Manual (CFEM) design curve closely matched the experimental data for dense and medium sands. Ting and Faraji noted that both the NCHRP and CFEM design curves provide an accurate representation of the experimental data for a loose backfill. In addition, the researchers stated that a triangular, soil pressure distribution along the height of the abutment wall can adequately represent the soil pressure against the wall with this type of a displacement.

Hassiotis and Xiong (2007) investigated earth pressures behind integral abutments and concluded that for relatively short bridges, which experience small abutment displacements, the classic theories overestimate the passive pressure because a small displacement would produce pressures between passive and at-rest. In these cases, they suggest that the NCHRP proposed Kp value for dense sand should be used. For bridges that are long enough to produce displacements that guarantee the applicability of the classical theories, the NCHRP in their opinion seems to be overly conservative and overestimates the passive pressure coefficient. Instead, they suggest the use of a Rankine Passive Kp value, which should be calculated with a maximum internal friction angle for the soil, to simulate the densification due to the cyclic loading. A triangular stress distribution along the height of the integral abutment for both cases is also suggested.

Mathematical Expressions

Despite the fact that Arsoy (1999) and Jung-Hee Hong (2003) report that a simple and reliable way of predicting the exact relationship between the earth pressure coefficient and abutment movement is still unavailable, a number of equations is available in literature that relates the expected earth pressure coefficient by a given abutment displacement. This includes the following mathematical expressions:

- Canadian Foundation Engineering Manual formula
- Husain and Bagnaroil formula
- Clough and Duncan formula
- Massachusetts DOT Manual formula
- British Code 42 (BA42) formula

Canadian Foundation Engineering Manual Formula

The magnitude of the actual earth pressure coefficient (K_h) that depends on wall movement, for dense sand condition (Φ=45º), is equal to

$$K_h = 33.26 \left(\frac{d}{H}\right)^{0.44} \qquad (7.1)$$

where
d = abutment displacement
H = abutment height
Φ = angle of internal friction of soil

Husain and Bagnaroil Formula

Applicable to integral abutment bridges, the magnitude of the actual earth pressure coefficient (K_h) that depends on wall movement, for dense sand condition (Φ=45º), is equal to

$$K_h = 10.72 \left(\frac{d}{H}\right)^{0.37} \qquad (7.2)$$

where
d = abutment displacement
H = abutment height
Φ = angle of internal friction of soil

Clough and Duncan Model Formula

Dicleli (2004) developed an expression applicable to integral abutment bridges for the earth pressure coefficient, K, based on Clough and Duncan's model. Thus, the earth pressure coefficient, K, as a function of the top displacement, Δ, of the abutment towards the backfill is expressed as follows:

$$K = K_o + m\left(\frac{\Delta}{H}\right)^n \qquad (7.3)$$

where
Ko = at rest earth pressure coefficient = 1-sinΦ
H = height of the abutment
m and n are constants to be determined
Φ = angle of internal friction of soil

Massachusetts DOT Manual formula

In the design of integral abutments, Massachusetts uses a magnitude of lateral earth pressure that depends on the movement of the abutment. The value is assumed to be somewhere between at-rest conditions and passive pressures. According to the Massachusetts DOT manual (2009), the earth pressure coefficient (K_h) is equal to

$$K_h = 0.43 + 5.7[1 - e^{-190(\Delta/H)}] \qquad (7.4)$$

where
Δ = abutment displacement
H = abutment height

British Code 42 (BA42) formula

Hassiotis and Xiong (2007) report a formula from the British Code BA42 applicable to the design of integral abutment bridges that proposes an earth pressure coefficient equal to:

$$K_h = K_o + \left(\frac{\Delta}{0.03H}\right)^{0.6} K_p \qquad (7.5)$$

where

K_o = at rest earth pressure coefficient = 1-sinΦ
Δ = displacement of the abutment
H = height of the abutment
K_p = passive earth pressure coefficient = (1+sinΦ)/(1-sinΦ)
Φ = angle of internal friction of soil

Comparison of various methods

Alizadeh et al. (2010) conducted a study to compare the displacements at the top of the abutment using the formulas from the Canadian Foundation Engineering Manual (equation 7.1), Husain and Bagnaroil (equation 7.2), Massachusetts DOT Manual (equation 7.4), and the British Code (equation 7.5) to the displacements at the top of the abutment for the case of free expansion and the case of displacements at the top of the abutment calculated using finite element analysis and a backfill with angle of internal friction equal to 45 degrees.

The comparison indicated that all four methods yield displacements at the top of the abutment that range in-between the displacement value of free expansion and that of the finite element analysis. It also indicated that the British Code is the closest method to the finite element analysis.

The study also indicated an average difference of 8.44 percent between the displacement at the top of the abutment during free expansion and the finite element analysis results. This finding confirms the work of other researchers (Girton et al. 1991; Elgaaly et al. 1992; Lawver et al. 2000) who concluded that the soil restraint does not significantly reduces the expansion of integral abutment bridges.

Plotting the displacement and temperature variation values in Tables 2, 3, and 4 from Alizadeh et al. (2010) in terms of abutment displacement to height ratio (Δ/H) versus temperature variation (ΔT) in Figure 7-11, we observe that in order to reach the Δ/H ratio (0.01) required for development of full passive pressures for dense sand (Table 7-1) the temperature variation should be in the upper range of temperature variation stipulated in the AASHTO Specifications for cold climate. The results in Figure 7-11 confirm the presence of passive earth pressures behind integral abutments. They also confirm the validity and conservatism of the various methods just described; their validity is confirmed by the fact that the Δ/H values obtained lie between those of finite element analysis and free expansion and the conservatism is confirmed by the fact that they are closer to the free expansion case than the analytical method.

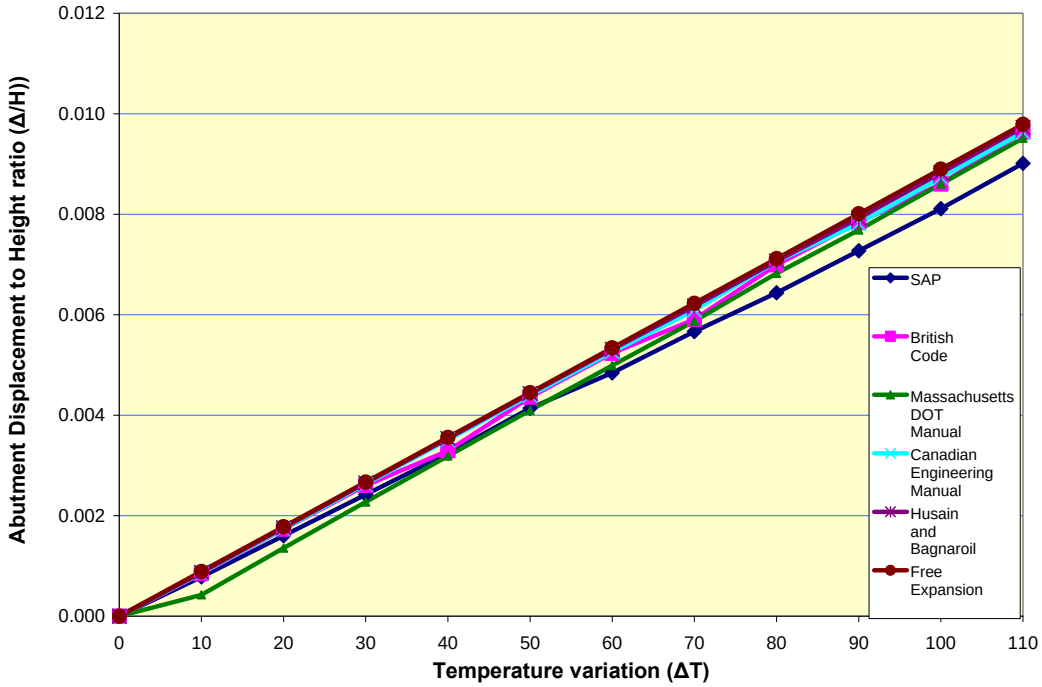

Figure 7-11 Comparison of abutment displacement to height ratio (Δ/H) versus temperature variation (ΔT) using various methods

In reference to the earth pressure distribution behind integral abutments, there is a wide difference of opinion among researchers. Hassiotis and Xiong (2007) suggest a triangular stress distribution (Figure 7-12) along the height of the integral abutment using the Rankine Kp values for "long bridges" and the Clough and Duncan (1991) Kp values (Figure 7-3) for "short bridges".

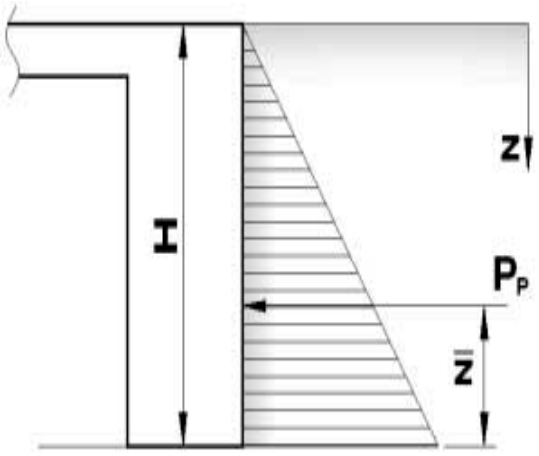

Figure 7-12 Earth pressure distribution according to Hassiotis and Xiong (2007)

The Swedish Bridge Code is using the earth pressure distribution shown in Figure 7-13 that suggests an increased pressure beyond the earth pressure at rest with a maximum value at abutment mid height.

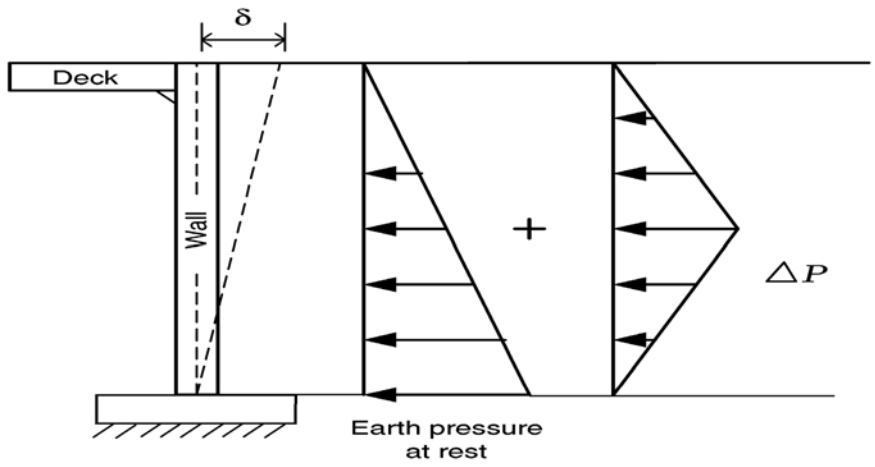

Figure 7-13 Earth pressure distribution according to the Swedish Bridge Code

The British Code BA42 suggests the earth pressure distribution shown in Figure 7-14 while Sanford and Elgaaly (1993) suggest the earth pressure distribution shown in Figure 7-15.

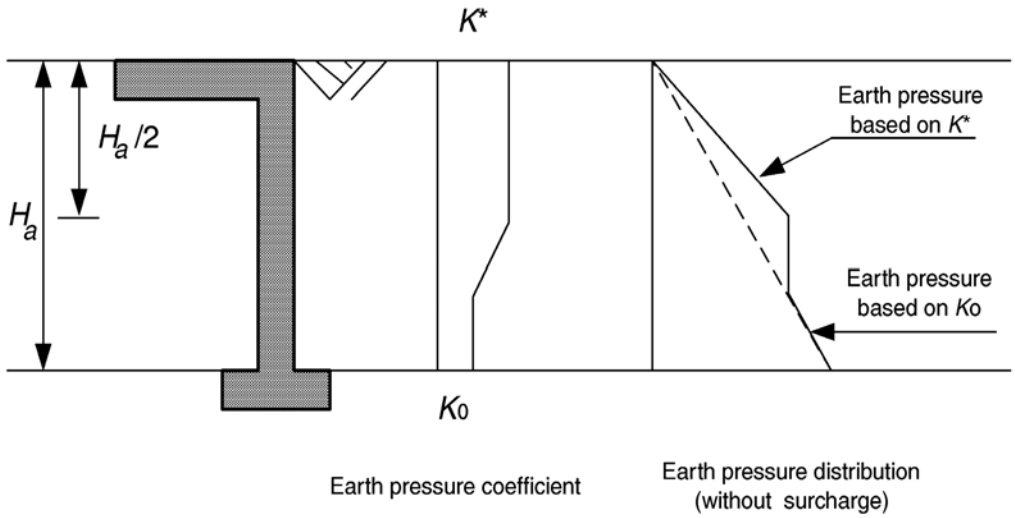

Figure 7-14 Earth pressure distribution according to the British Code BA42

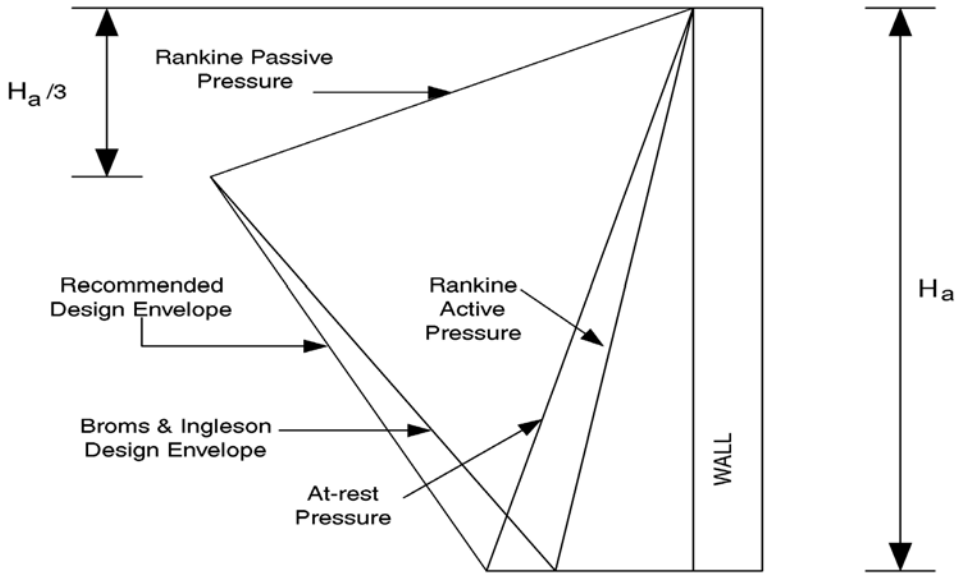

Figure 7-15 Earth pressure distribution according to Sanford and Elgaaly (1993)

A numerical example using the material properties shown in Figure 7-16 from Flener (2004) is used to develop the graph in Figure 7-17 that depicts the earth pressure distribution behind abutments according to the references mentioned earlier, that is,

- Hassiotis and Xiong (2007) triangular earth pressure distribution based on Rankine passive pressure
- Hassiotis and Xiong (2007) triangular earth pressure distribution based on Clough and Duncan (Figure 7-3) passive earth pressure coefficients
- Sanford and Elgaaly (1993)
- Swedish Bridge Code
- British Code BA42

The numerical example is carried out for a displacement $\Delta = 0.04$ m

Material properties	values
ϕ (° C)	38.3
γ_s (kN/m^3)	19.0
K_0	0.38
K_a	0.3
K_p	4.2
Wall height, H_a (m)	6.0

Figure 7-16 Parameters used for the derivation of Figure 7-17 that depicts earth pressure distribution from various sources (Flener 2004)

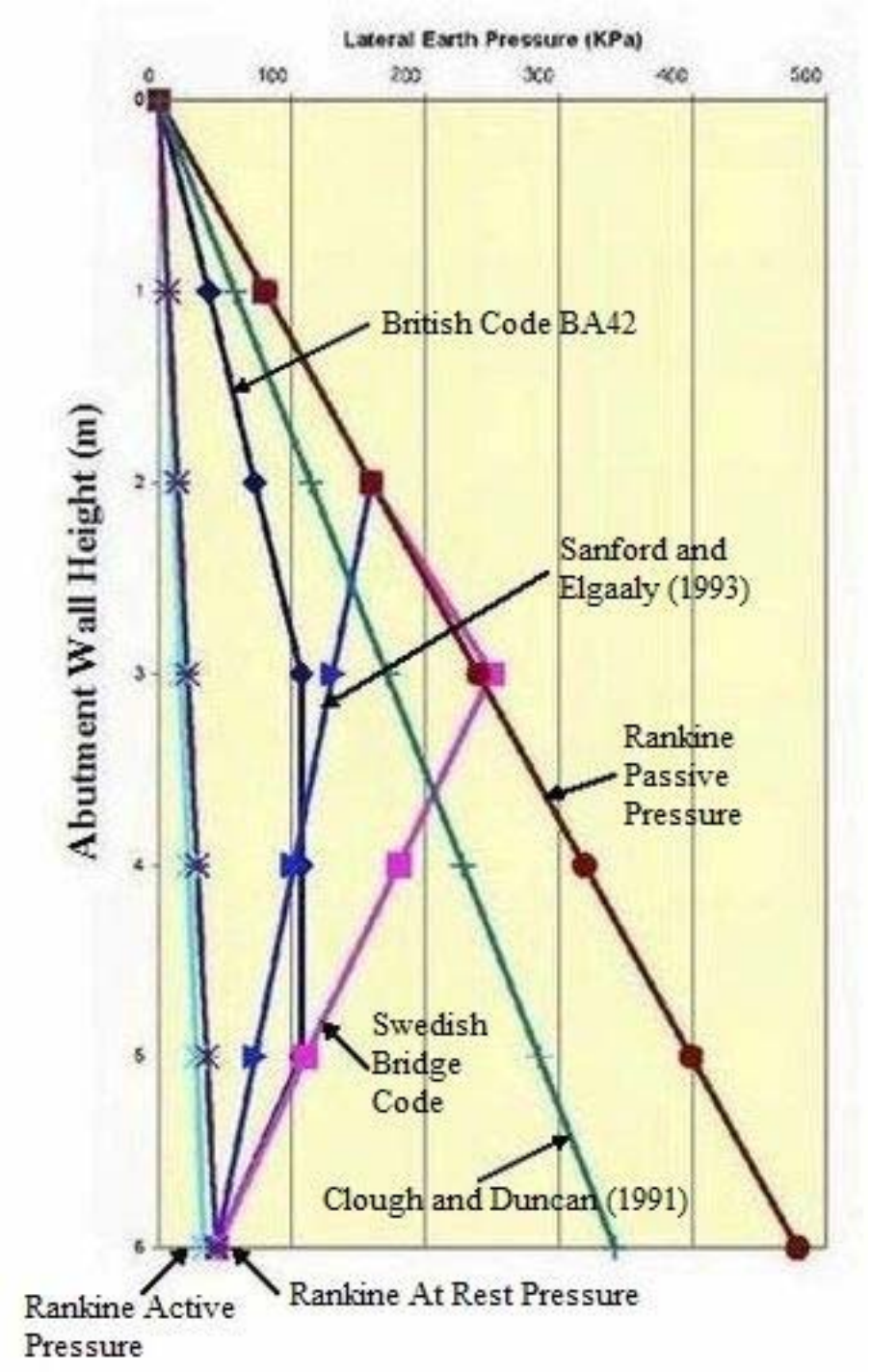

Figure 7-17 Comparison of earth pressure distributions behind bridge abutments from different sources

7.5. Soil Constitutive Models

Constitutive models are mathematical material models that simulate various kinds of material behavior, such as isotropic and orthotropic elasticity, plasticity, viscoelasticity, hyperelasticity, anisotropic hyperelasticity, and viscoplasticity. These constitutive models can be used to simulate various kinds of materials such as metals, concrete, plastics, soil, rubber, and glass. The importance of constitutive modeling lies in the fact that soil constitutive models can predict the response of soil structures under critical combinations of load taking into account the actual characteristics of the soil under such loads (Sridhanya et al. 2008). Actual behavior of soils is very complicated and it shows a great variety of behavior when subjected to different conditions. As a result, a number of soil constitutive models have been proposed by several researchers to describe several aspects of soil behavior for the purpose of applying these models in finite element modeling for geotechnical engineering applications. Although a number of soil constitutive models exist to describe the soil material behavior, there is no soil constitutive model available that can completely describe the complex behavior of soils under all conditions.

According to Brinkgreve (2005) there are five basic aspects of soil behaviour. The first aspect is the influence of water on the behaviour of the soil from the effective stresses and pore pressures. Second aspect is the factor which influences the soil stiffness such as the stress level, stress path (loading and unloading), strain level, soil density, soil permeability, consolidation ratio, and the directional-dependant stiffness (stiffness anisotropy) of the soil. The third aspect is the irreversible deformation as a result of loading. Fourth aspect is the factor that influences soil strength such as loading speed of the tested specimen, age and soil density, undrained behavior, consolidation ratio, and directional dependant shear strength (strength anisotropy). The fifth aspect includes other factors such as compaction, dilatancy, and preconsolidation stress.

In addition to soil behavior, its failure in three-dimensional state of stress is extremely complicated. Numerous criteria have been devised to explain the condition for failure of a material under such a loading state. This includes two, three, four, and five-parameter models. An example of two-parameter model is the Mohr-Coulomb model.

In general, the selected soil constitutive model should be able to represent the behavior of soil material under a wide range of conditions, its material parameters can be determined from standard laboratory tests, and be simple in computational application meaning mathematical modeling and computational simulation.

7.5.1. Most Commonly Used Soil Constitutive Models

There is a large variety of soil constitutive models available to represent the stress-strain and failure behavior of soils. All these models inhibit certain advantages and limitations which largely depend on their application. The most commonly used soil constitutive models are discussed. This includes the following models:

- Mohr Coulomb model
- Duncan-Chang Hyperbolic model
- Drucker-Prager model and Extended Drucker-Prager model
- Cam Clay model and Modified Cam Clay model
- Plaxis Hardening Soil model

7.5.1.1. Mohr Coulomb Model

Mohr-Coulomb model as shown in Figure 7-18 is an elastic-perfectly plastic model, which is often used to model soil behaviour in general and serves as a first-order approximation (Sallam 2009). In general stress state, the model's stress-strain behaves linearly in the elastic range, with two defining parameters from Hooke's law (Young's modulus, E and Poisson's ratio, ν). There are two parameters to define the failure criteria (friction angle, ϕ and cohesion, c) and also a parameter to describe the flow rule (dilatancy angle, ψ which comes from the use of non-associated flow rule which is used to model a realistic irreversible change in volume due to shearing).

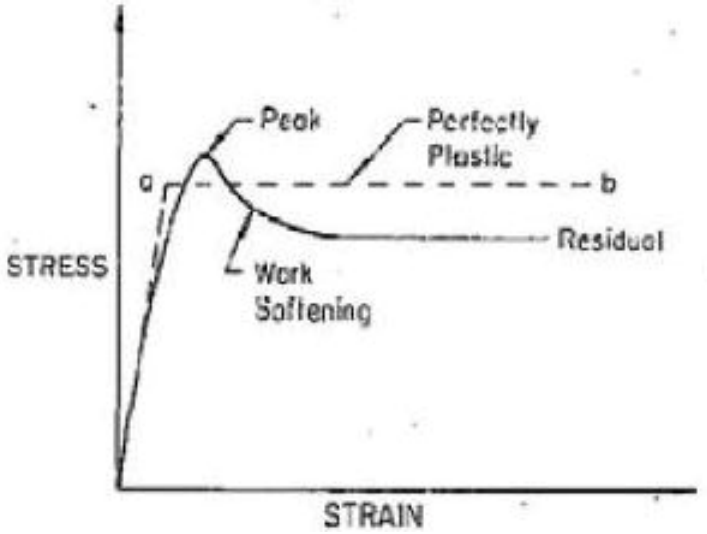

Figure 7-18 Elastic-perfectly plastic assumption of Mohr-Coulomb model (Kok et al. 2009)

The Mohr-Coulomb model is a simple and applicable to three-dimensional stress space model (Figure 7-19) with only two strength parameters to describe the plastic behavior. Kok et al. (2009) stated that this model performs well in regards of strength behaviour. Researchers have indicated by means of true triaxial tests that stress combinations causing failure in real soil samples agree quite well with the hexagonal shape of the failure contour (Goldscheider, 1984). Mohr-coulomb model has been the basis for most of sophisticated and enhanced constitutive models (Tabatabaei 2010; Brinkgreve 2005; Kok et al. 2009). The validity of Mohr-Coulomb model is well established and documented for many soils.

This model is well suited to analyze the stability of dams, slopes, embankments and shallow foundations.

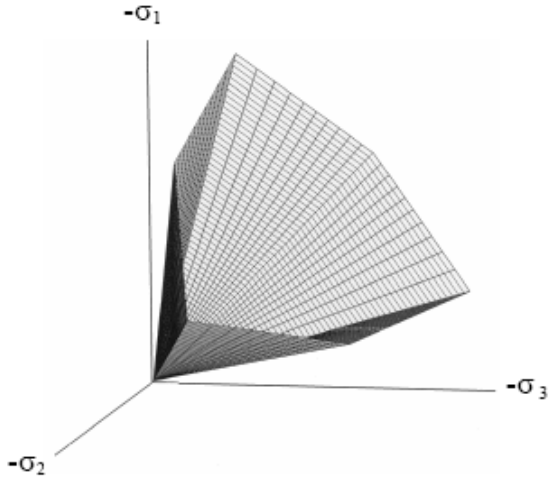

Figure 7-19 The Mohr-Coulomb yield surface in principal stress space

7.5.1.2. Duncan-Chang Hyperbolic Model

The Duncan-Chang Hyperbolic constitutive model (Duncan and Chang 1970) is widely used for the modelling of soil behavior. It is capable of modelling the three most important soil characteristics; nonlinearity, stress-dependant, and inelastic behavior of cohesive and cohesionless soils. It was first used by Kondner ((Duncan and Chang 1970; Brinkgreve 2005; Kok et al. 2009) to model the stress-strain behavior of soils. The Duncan-Chang model is an incremental nonlinear stress-dependant model, which is also known as the hyperbolic model (Duncan and Chang 1970).

Duncan-Chang model is widely used as its soil parameters can be easily obtained directly from standard triaxial test. It is a simple, yet obvious enhancement to the Mohr-Coulomb model. In this respect, this model is preferred over the Mohr-Coulomb model. Failure itself is described by means of the Mohr-Coulomb failure criterion, but this is not

properly formulated in the plasticity framework. As a result, dilatancy cannot be described. This model captures soil behavior in a very tractable manner on the basis only two stiffness parameters and is very much appreciated for practical modeling. The major inconsistencies of this type of model is that, in contrast to the elastoplastic type of model, a purely hypoelastic model cannot consistently distinguished between loading and unloading. In addition, the model does not account for the intermediate principal stress σ_2 and does not consider the volume change due to changes in shear stress (shear dilatancy). The model is unsuitable for collapse load computations in the fully plastic range and is mainly intended for quasi-static analysis (Duncan et al. 1980). Nevertheless, Duncan-Chang model was quoted by Brinkgreve (2005) as the improved first order model for geotechnical engineering application in general. In fact, Duncan and Mokwa (2001) demonstrated that the hyperbolic model accurately predicts the passive earth pressures in numerical model/test comparisons.

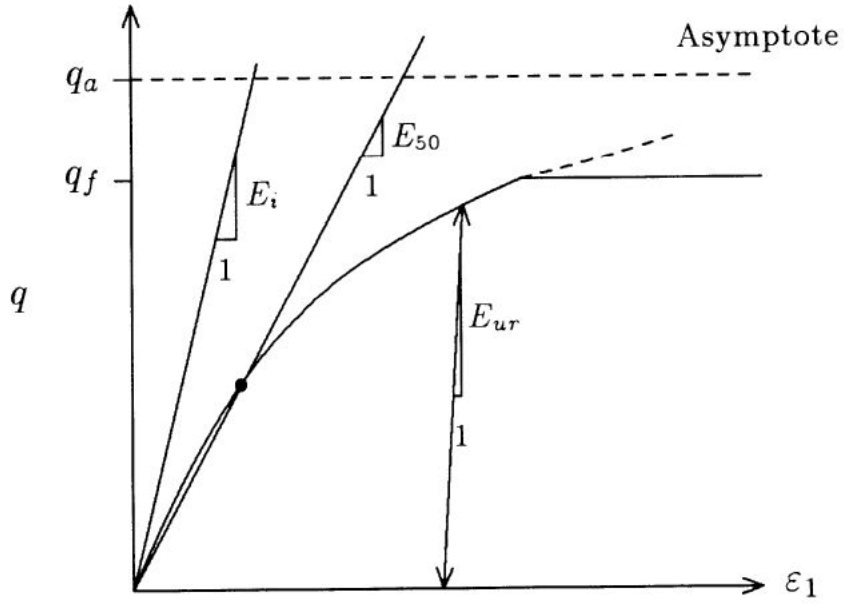

Figure 7-20 Hyperbolic stress-strain relation in primary loading for a standard drained triaxial test (Schanz et al. 1999)

7.5.1.3. Drucker-Prager Model and Extended Drucker-Prager Model

The Drucker-Prager model is an isotropic elastoplastic soil constitutive model proposed by Drucker and Prager (1952) to describe the stress–strain behavior of pressure-dependent materials such as soil, rock, and concrete. Also known as the extended Von Mises model, it can be used to simulate the behavior of granular soil materials such as sand and gravel. The Drucker-Prager model is an approximation of the Mohr-Coulomb model where the hexagonal shape of the failure cone is being replaced by a simple cone known as the Drucker-Prager model (Drucker and Prager 1952). The Mohr-Coulomb failure surface has corners (Figure 7-21), and therefore it is not mathematically convenient for use particularly for three-dimensional problems unlike the Drucker-Prager yield criterion that is more convenient from the view of numerical efficiency. The Drucker–Prager yield criterion is a pressure-dependent model for determining whether a material has failed or undergone plastic yielding. The criterion was introduced to deal with the plastic deformation of soils. In general, the Drucker-Prager model shares the same advantages and limitations with the Mohr-Coulomb model (Brinkgreve 2005; Kok et al. 2009).

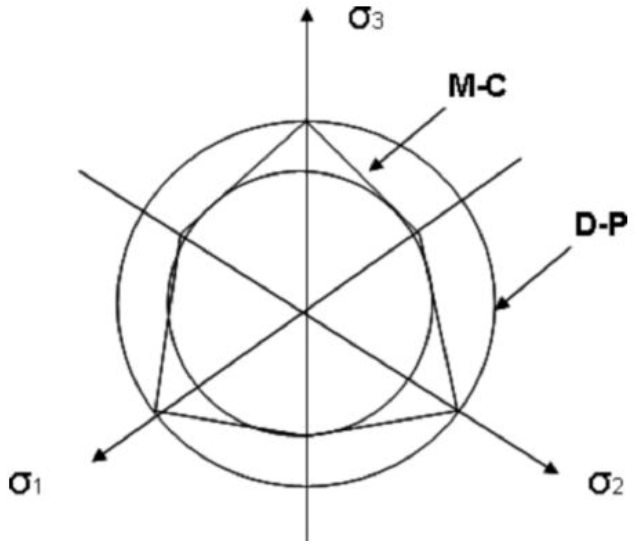

Figure 7-21 Mohr-Coulomb (M-C) and Drucker–Prager (D-P) models in the deviatoric plane

The deviatoric plane (also known as π plane) is a plane where the stresses are expressed in terms of the three principal stresses σ_1, σ_2, and σ_3 (Figure 7-22).

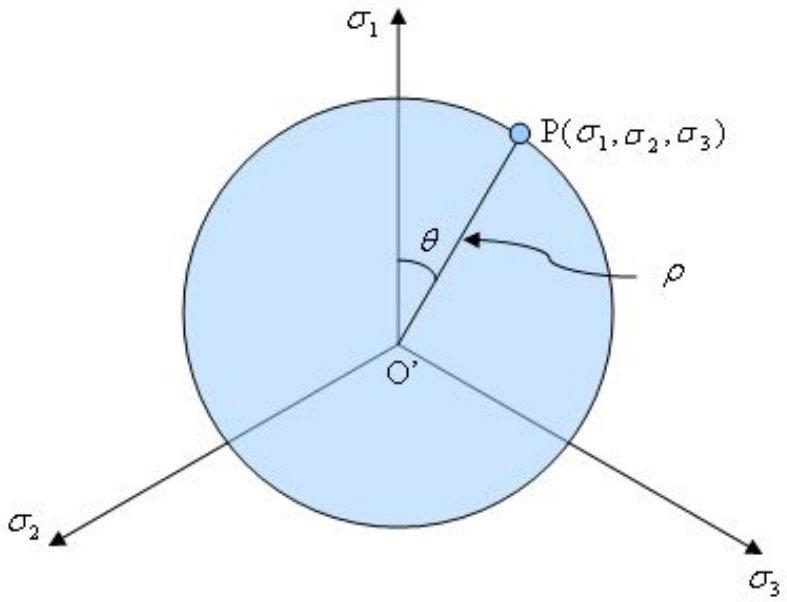

Figure 7-22 Deviatoric plane

The Extended Drucker-Prager model is also used to model frictional materials, which are typically granular-like soils and rock, and exhibits pressure-dependent yield meaning that the material becomes stronger as the pressure increases. Unlike the Classical Drucker-Prager model, the yield surface of the Extended Drucker-Prager model is not a circle (Figure 7-23) and differs from the classical model in that it includes strain-hardening behavior - the Classical basic Drucker-Prager model assumes perfectly plastic behavior.

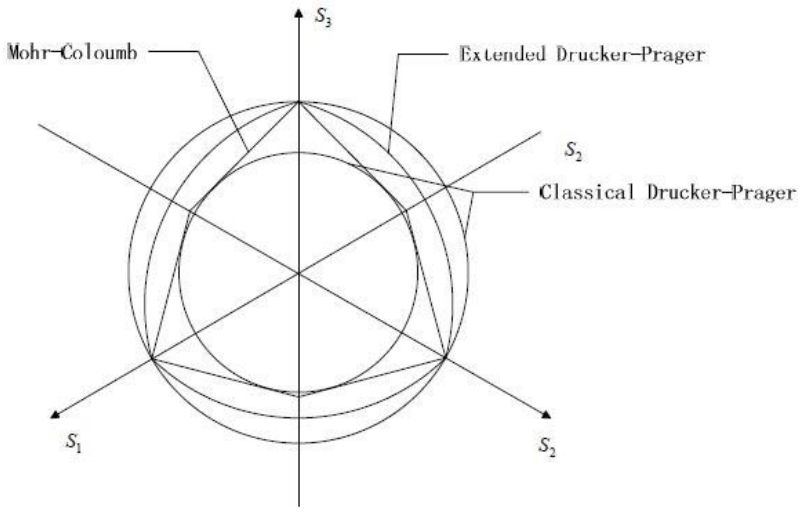

Figure 7-23 Mohr-Coulomb, Drucker–Prager, and Extended Drucker-Prager models in the deviatoric plane

7.5.1.4. Cam Clay Model and Modified Cam-Clay Model

The Cam Clay (Roscoe et al. 1958) and Modified Cam Clay (Roscoe and Burland, 1968) soil constitutive models were developed at Cambridge University in the United Kingdom and belong to a category of soil models called critical state models - a soil is said to be in critical state when it undergoes large shear deformations at constant volume and constant shear and normal effective stress (Schofield and Wroth 1968). According to Wood (1991), critical state soil mechanics is about the importance of considering volume changes as well as changes in effective stresses when trying to understand soil behavior. A locus of critical states of all shear tests on a soil is called a Critical State Line (CSL) and is shown in Figure 7-24 where p = mean stress and q = deviatoric stress.

According to Gens and Potts (1988), the materials modeled by critical state models appear to be mostly limited to saturated clays and silts, while stiff overconsolidated clays do not appear to be generally modeled with critical state formulations. The critical state also had been much less successful for modeling granular materials due to its inability to predict observed softening and dilatancy of dense sands and the undrained response of very loose sands.

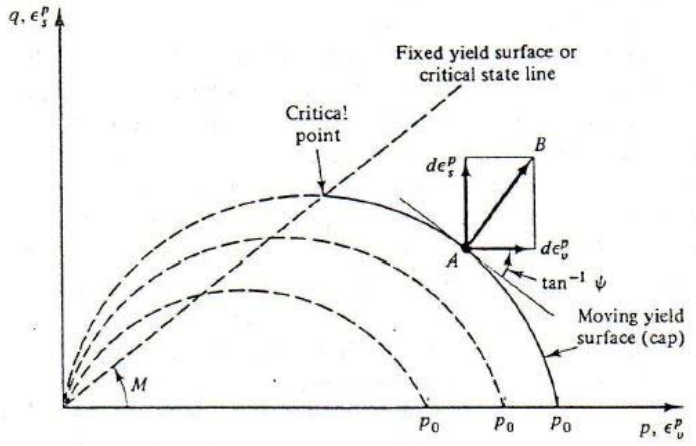

Figure 7-24 Critical State Line (Utomo et al. 2007)

The Cam Clay model was the first elastoplastic model applicable to deformation analysis of ground and describes soil behavior under both shear loading and consolidation (Nakai 2007). The model is simple and involves only a few parameters. It predicts the stress-strain behavior of normally (NC) and lightly overconsolidated (OC) clays, but has several limitations (Koh 2010): (1) does not take into account the anisotropy of soil, (2) cannot predict the stress-strain response of overconsolidated clay and that of sand (dilative soil), and (3) overestimates the failure stress on the dry side.

While both the Cam-Clay (CC) and the Modified Cam-Clay (MCC) model three important aspects of soil behavior: (1) strength, (2) volume changes, and (3) critical states their difference lies in the shape of the yield surface; the yield surface of the original Cam

Clay Model is described by a logarithmic spiral shape while the yield surface of the modified Cam Clay Model is described by an ellipse (Figure 7-25).

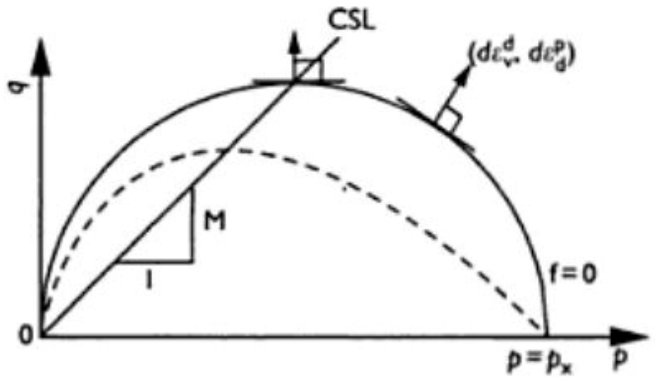

Figure 7-25 Yield surface of Cam Clay (dotted line) and Modified Cam Clay (solid line) (Matsuoka and Sun 2006)

The Modified Cam-clay is an elastic plastic strain hardening model where the nonlinear behavior is modeled by means of hardening plasticity. Research conducted by Utomo et al. (2007) indicates that the MCC model is able to simulate the mechanical behavior of normally consolidated clays satisfactorily, but fails to predict the mechanical behavior of heavily overconsolidated clays. In addition, using the MCC model to simulate the mechanical behavior of heavily overconsolidated clays would lead to a conservative design, which would result in a much lower strength compared to the actual strength of the heavily overconsolidated clays. This model is more suitable to describe deformation than failure especially for normally consolidated soft soils. The model also performs best in applications involving loading conditions such as embankments or foundations.

7.5.1.5. Plaxis Hardening Soil Model

The Hardening Soil model (Schanz and Vermeer 1998) is an advanced nonlinear model formulated in the framework of the classical theory of plasticity. The model simulates the behavior of both soft and stiff soils. Unlike elastoplastic models, the yield surface of hardening plasticity models is not fixed in principal stress space, but it can expand due to plastic straining caused by deviatoric loading and compression. Shear hardening is used to model irreversible strains due to deviatoric loading and compression hardening is used to model irreversible plastic strains due to primary compression in oedometer loading and isotropic loading (Plaxis Material Models Manual). The yield contour of the model in principal stress space is shown in Figure 7-26. Other characteristics of this model include the stress dependency of soil stiffness (means that all stiffnesses increase with pressure), elastic unloading and reloading, and failure described by means of the Mohr Coulomb model, that is, in terms of the friction angle, ϕ, the cohesion, c, and dilatancy angle, ψ.

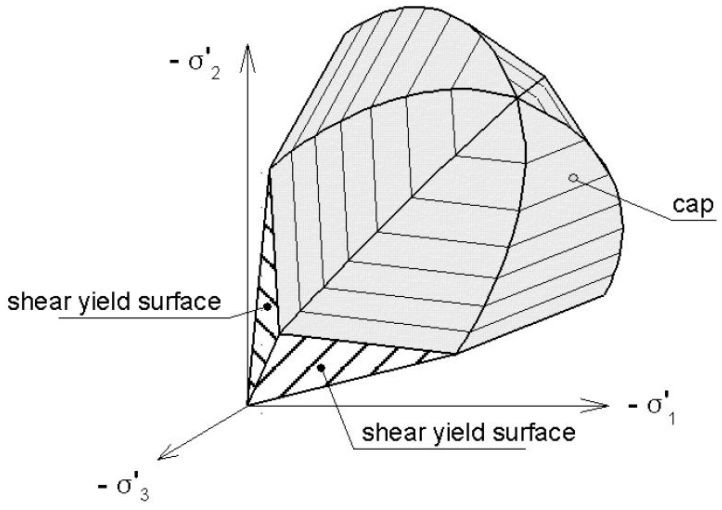

Figure 7-26 Representation of total yield contour of the Hardening Soil Model in principal stress space for cohesionless soil (Schanz et al. 1999)

With respect to its stiffness behavior, the model involves a formulation for stress dependant stiffness, similar as the one used in the original hyperbolic model (Duncan and Chang 1970). However, this model supersedes the Duncan-Chang model by far by using the theory of plasticity rather than the theory of elasticity, including soil dilatancy, and introducing a yield cap. (Figure 7-26). In this model, the magnitude of soil deformations is described using three different stiffnesses (Figure 7-27): (1) triaxial loading stiffness (E_{50}) due to primary deviatoric loading, (2) triaxial unloading-reloading stiffness (E_{ur}), and (3) oedometer loading stiffness modulus (E_{oed}) due to primary compression.

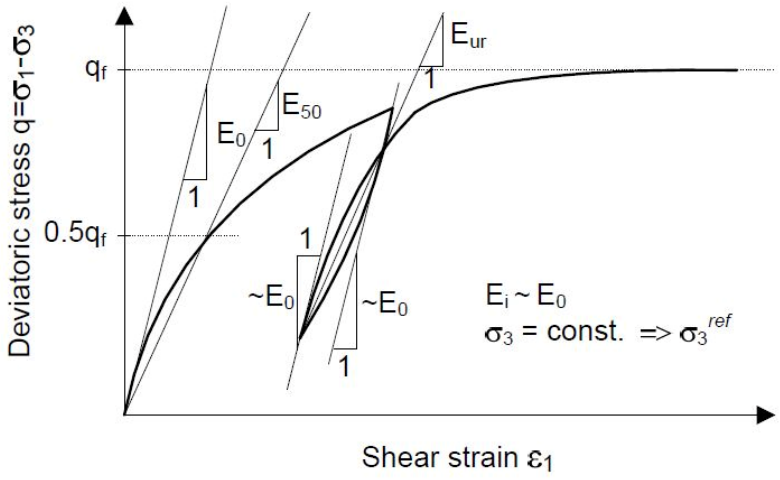

Figure 7-27 Stiffness parameters used in the Hardening Soil model (Obrzud 2010)

The limitations of this soil constitutive model lie in the fact that the model does not include anisotropic strength of stiffness, or time-dependant behaviour (creep). In addition, its capabilities for dynamic applications are limited.

7.5.2. Selection of Soil Constitutive Model

Constitutive models are mathematical models that describe the stress-strain behavior of soils and provide a framework for understanding how soil will behave under different loading conditions. They are implemented in finite element and finite difference codes for use in numerical analyses. There are many soil constitutive models of varying levels of complexity available; the most commonly-used soil models were described in the previous section.

The choice of soil constitutive model is the most important issue in the process of creating a finite element model for a geotechnical application (Brinkgreve and Engin 2013). The selection of a constitutive model should be based on an evaluation of the capabilities and limitations that the model has to describe the essential features of soil behavior for the application at hand. In that respect, the constitutive model provides the qualitative description of soil behavior, whereas the parameters in the model are used to quantify the behavior. The composition of the model plus parameters can be regarded as the "artificial soil" that is used in the finite element model, which should be representative for the real soil behavior in the application (Brinkgreve and Engin 2013).

In selecting a constitutive model for soil, Wood (1991) suggests that for engineering purposes, a relatively simple model like the Modified Cam Clay model can be modified and levels of complexity added as necessary in order to provide insight into particular problems. Wroth and Houlsby (1985) suggest that in order for a constitutive model to be useful in solving engineering problems, it should be simple and reflect the physical behavior of the soil. Duncan (1994) states that for constitutive models to be practical, it should be possible to obtain the model parameters values in a simple manner from conventional soil tests.

Duncan (1994) states that simple elasticity models, such as the hyperbolic model, can be applied for stable structures where deformations are small, orientation of stresses are constant, and for fully drained or completely undrained conditions. For accurate predictions of stress-strain behavior near failure and for undrained pore pressures due to application of total stress external loads, Duncan (1994) states that more complex elastoplastic models, such as the Cam Clay model, should be used. Duncan (1994) reviewed almost 2000 papers related to geotechnical applications of constitutive models or finite element modeling. He observed that commonly used models are the hyperbolic model (Duncan and Chang 1970), Modified Cam Clay model (Roscoe and Burland 1968), and versions of the Cam Clay model (Roscoe et al. 1958). (Wood 1991) confirms that the Modified Cam Clay model is more widely used than the Cam Clay model.

Studies have explored constitutive models and found that isotropic elastoplastic models such as Mohr-Coulomb and Drucker-Prager are sufficiently accurate (Chen and Saleeb 1983; Hibbitt et al. 1998). Mohr-Coulomb and Drucker-Prager are the most widely used soil constitutive models in geotechnical engineering practice because of their simplicity and the fact that their parameters are easy to obtain. This includes both the plastic

parameters (cohesion, friction angle, dilatancy angle) and the elastic parameters (Young's Modulus and Poisson's ratio). On the other hand, Mohr-Coulomb and Drucker-Prager models are conservative and do not contain modern concepts of soil modelling. For example, a precise deformation prediction requires the application of more advanced soil constitutive models, like the Plaxis Hardening model that approximates the stress-strain relation more accurately. The choice of a constitutive model depends on many factors, but in general, it is related to the type of analysis required to perform, expected precision of predictions, and available knowledge of soil (Obrzud 2010). It should always be remembered that no matter how complex the selected soil constitutive model is, it is only a simplification of the real soil behaviour (Brinkgreve and Engin 2013). As a result, certain features of anticipated soil behavior can't be captured by the selected model.

7.5.3. Soil Constitutive Models for Integral Abutment Bridges

Literature review reveals that currently there is no soil constitutive model available that captures all elements of soil behavior associated with soil behind integral abutment bridges. Consequently, whenever researchers and engineers employ any of the available soil constitutive models to model soil behavior behind integral abutment bridges, certain aspects of the anticipated soil behavior would not be captured or well replicated. For example, Horvath (2000) states that the hyperbolic model has some significant shortcomings with regard to modeling the way soil is loaded in the integral abutment bridge problem. This is due to the fact cyclic loadings are known to be an important aspect of soil behavior in integral abutment bridge problems. An important aspect of cyclic soil loading is the accumulation of plastic strains due to the inherent hysteretic behavior of soil (England 1994; England and Dunstan 1994; England et al. 1995). However, according to Horvath (2000) the hyperbolic model does not do a good job of replicating hysteretic behavior.

As part of the effort to develop a soil constitutive model suitable for both design and research of soil-structure interaction applicable to integral abutment bridges, Xu (2005) developed a soil constitutive model that works well for a single element of soil behind an abutment (Banks et al. 2008). The model includes granular soil and cyclic loading associated with integral abutment bridges, that is, thermal cycling. Thus, Xu (2005) carried out radial strain controlled triaxial tests on granular soil under cyclic loading and developed a mathematical model that reproduced the soil behavior and programmed it in the Finite Difference Method (FDM) program, FLAC. The mathematical model compared favorably with published and field data at element level. This shows that the model works well for a single element of soil behind an abutment (Figure 7-28).

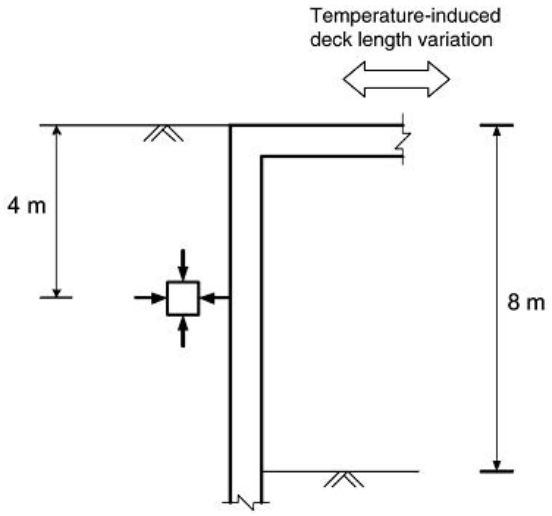

Figure 7-28 The location of the representative soil element behind a typical integral abutment (Bloodworth et al. 2012)

The next frontier in developing a soil constitutive model for integral abutment bridges is to extend the current model from a single element to an entire integral bridge soil-structure system. This will lead to the creation of a soil constitutive model capable of capturing all important features of granular soil behavior under both monotonic and cyclic loadings. The new soil constitutive model shall be also validated by testing to confirm the accuracy of its predictions.

7.6. Modeling of Soil-Structure Interaction

Soil-structure interaction (SSI) is the combined study of both the structure and the surrounding soil aim to predict the response of the soil to the loading of the structure as a function of deflection, and the corresponding response of the structure. In other words, the structure with its loading conditions imposes stresses and forces on the soil, which in turn deforms and as a consequence transmits back additional forces and deformation to the structure. The process continues until full equilibrium of the soil-structure system is established. However, the behavior of the structure and the soil are profoundly different. Although modelling for structural analysis and geotechnical analysis address different concerns, the modeling of soil-structure interaction should be able to complement each other to provide reliable analytical results.

7.6.1. Soil-Structure Modeling Approaches

There are three modeling approaches commonly employed by researchers in the area of soil-structure interaction:

- Winkler Springs method
- Interface Element method
- Contact Analysis method

7.6.1.1. Winkler Springs Method

Winkler (1867) introduced the concept of spring constant in which springs, known as Winkler springs, represent the load-deformation behavior of a soil-structure system such as a longitudinal bridge abutment-backfill system or a system of flexible foundation, such as a raft foundation, and the soil underneath. In this elastic soil model, the soil medium is represented by a system of identical but mutually independent, closely spaced, discrete and linearly-elastic springs (Figure 7-29). This model is known to be the simplest mathematical formulation to replicate the soil behavior in soil-structure interaction.

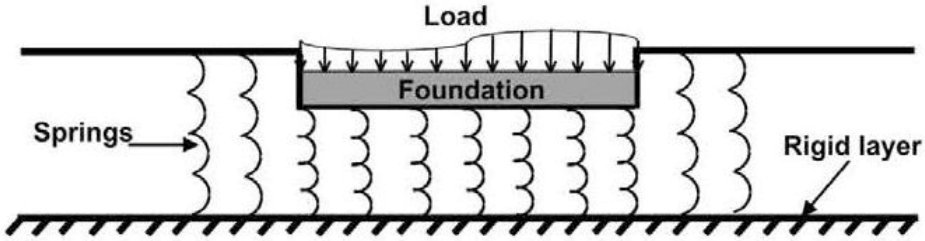

Figure 7-29 Winkler Spring Model

The soil medium is represented by springs whose stiffness equals to Ks, known as the coefficient of subgrade reaction, and its magnitude is equal to the ratio of contact pressure (P) at any given point and settlement (y) produced by load application at that point (equation 7.6).

$$K_s = \frac{P}{y} \qquad (7.6)$$

The Winkler model, however, is based on simplifying assumptions and has certain limitations (Marto et al. 2012). One of the limitations of it lies in the fact that this model cannot transmit the shear stresses, which are derived from the lack of spring coupling (Sadrekarini and Akbarzad 2009). In addition, the model assumes a linear or elastic stress-strain behavior. Fact is, soil behavior is not elastic and can be better replicated with the use of soil constitutive models (Gouw 2001).

.

The Winkler spring model was first introduced for the analysis of rigid plates, but during the following decades the theory was expanded to include the computation of stresses in flexible foundations (Terzaghi 1955). In the area of soil-foundation interaction, many researchers have utilized this model. This includes Biot (1937), Terzaghi (1955), Vlassov and Leontev (1966), and Vesic (1961) among others (Table 7-3).

Table 7-3 Common relations for Ks (Sadrekarini and Akbarzad 2009)

Researcher	Mathematical Expression
Biot (1937)	$k_s = \frac{0.95 E_s}{B(1-\nu_s^2)}\left[\frac{B^4 E_s}{(1-\nu_s^2)EI}\right]^{0.108}$
Terzaghi (1955)	For sands $k_s = k_{s1}\left(\frac{B+1}{2B}\right)^2$ For clays $k_s = k_{s1}\frac{1}{B}$
Vlassov and Leontev (1960)	$k_s = \frac{E_s(1-\nu_s)}{(1+\nu_s)(1-2\nu_s)}\left(\frac{\mu}{2B}\right)$
Vesic (1961)	$k_s = \frac{0.65 E_s}{B(1-\nu_s^2)}\sqrt[12]{\frac{E_s B^4}{EI}}$

where

Es = modulus of elasticity of soil

Vs = Poisson's ratio of soil

B = footing width

EI = flexural rigidity of footing

ks1 = the coefficient of subgrade reaction of soil for a plate 1 foot wide

μ = non-dimensional soil mass per unit length

Since 1920, the theory of subgrade reaction has also been used for computing stresses in piles and sheet piles, which are acted on by horizontal forces above the ground surface. In this case, the ratio between the contact pressure and displacement of pile is referred to as the coefficient of horizontal subgrade reaction, Kh (Terzaghi 1955). Matlock et al. (1978) initiated the use of the Winkler model to analyze problems of laterally-loaded pile foundations. Rajashree (2001) and Pranjoto and Pender (2003) further substantiated the use of the Winkler Spring method to model laterally-loaded pile foundations. Faraji et al. (2001) used this approach to analyze the nonlinear behaviour of an integral abutment bridge. In that study, the soil medium was idealized with nonlinear elastic springs. In fact, the Winkler Spring method is being used by the vast majority of researchers in the area of integral abutment bridges to model soil-structure interaction.

Although using the Winkler Spring method to model soil behavior is a simplification due to the fact that the physical behaviour of soil is not well replicated, this method is acceptable for computational purposes when structural response is the main quantity of interest; structural response is a reference to induced deflections and stresses within the structure.

7.6.1.2. Interface Element Method

In soil-structure interaction, the soil-structure interface is represented by interface elements. Several kinds of interface elements have been developed to model the behavior of the interface under certain loading conditions. When an interface element is developed for a particular problem, an appropriate constitutive relationship must be adopted. The constitutive relationship should be capable of modeling the interface response under the expected loading conditions.

Interface elements were first introduced by Goodman, Taylor, and Brekke (1968) for finite element analysis of jointed rock masses. They were soon extended to soil-structure interaction (SSI) analyses of retaining walls by Clough and Duncan (1971) and Duncan and Clough (1971). The adoption of interface elements represented a significant improvement over previous methods, which assumed either of two conditions: a perfectly rough interface with no slip between soil and structure, or a perfectly smooth interface with no shear stresses developed (Clough and Duncan 1971).

The element developed by Goodman, Taylor, and Brekke (1968) is commonly referred to as the **zero thickness interface element**. The basic idea was to introduce a constitutive model for an interface of zero thickness (Wang et al. 2003). This constitutive model may

be elastic, rigid-plastic, or elastic-plastic (Goodman et al. 1968; Wang et al. 2003; Sekiguchi et al. 1990).

The zero thickness interface element consists of two four node quadrilateral elements which face each other. (Figure 7-30)

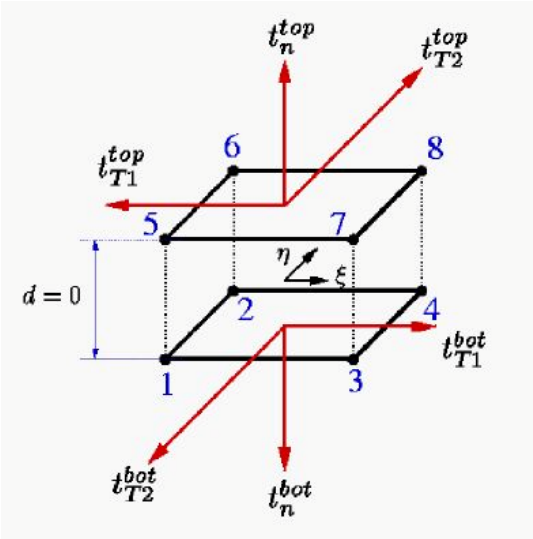

Figure 7-30 Goodman's zero thickness interface element (Mayer and Gaul 2008)

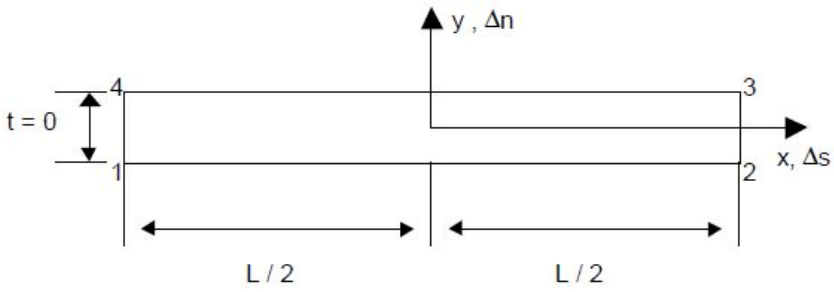

$$K = \frac{1}{6}\begin{pmatrix} 2ks & 0 & ks & 0 & -ks & 0 & -2ks & 0 \\ 0 & 2kn & 0 & kn & 0 & -kn & 0 & -2kn \\ ks & 0 & 2ks & 0 & -2ks & 0 & -ks & 0 \\ 0 & kn & 0 & 2kn & 0 & -2kn & 0 & -kn \\ -ks & 0 & -2ks & 0 & 2ks & 0 & ks & 0 \\ 0 & -kn & 0 & -2kn & 0 & 2kn & 0 & kn \\ -2ks & 0 & -ks & 0 & ks & 0 & 2ks & 0 \\ 0 & -2kn & 0 & -kn & 0 & kn & 0 & 2kn \end{pmatrix}$$

Figure 7-31 Goodman's zero thickness interface element and stiffness matrix (Gomez 2000)

In the derivation of the joint element stiffness matrix, Goodman et al. (1968) used a very simple constitutive law consisting of constant values for both the shear stiffness and the normal stiffness:

$$k_n \Delta_n = \sigma_n \quad (7.7)$$

$$k_s \Delta_s = \tau \quad (7.8)$$

where

k_n = normal interface stiffness

Δ_n = displacement normal to the interface

σ_n = normal stress acting on the interface

k_s = interface shear stiffness

Δ_s = displacement along the interface

τ= interface shear stress

In this formulation, coupling effects between tangential and normal displacements along the interface are excluded, as evidenced by zero off diagonal elements in the stiffness matrix (Figure 7-31).

A continuous development of improved joint elements has taken place since the original formulation by Goodman et al. (1968). Heuze and Barbour (1982) presented a zero-thickness axisymmetric joint element for finite element analyses of footings on rock, underground openings, and excavations, where dilation effects play an important role. Although no coupling terms are included in the formulation of the element, the dilation-induced normal stresses are determined explicitly based on the stiffness of the surrounding rock and the dilation angle. Yuan and Chua (1992) presented a more general formulation of the Heuze and Barbour (1982) axisymmetric element.

Matsui and San (1989) proposed an elastoplastic joint element to model interface behavior of rock joints. It accounts for the generation of normal stresses during shear, due to fully restrained dilation of the joint, in a way similar to that of Heuze and Barbour (1982).

Desai et al. (1984) and Zaman et al. (1984) presented the **thin layer interface element**. This element is based on the idea that interface behavior is controlled by a narrow band of soil adjacent to the interface with different properties from those of the surrounding materials. The thin layer interface element (Figure 7-32) has a finite thickness (Mayer and Gaul 2008) and it is described by solid elements (Qian et al. 2013). It is treated

mathematically as any other element of the finite element mesh and is assigned special constitutive relations. The Desai et al. (1984) thin layer element prevents overlapping between structural and geological materials due to its finite thickness. Desai et al. (1986) implemented the thin layer element in interaction analyses of grouted anchors-soil systems.

Wong et al. (1989) implemented a three-dimensional version of the thin layer interface element for soil-structure interaction analyses of drilled shafts under generalized loading.

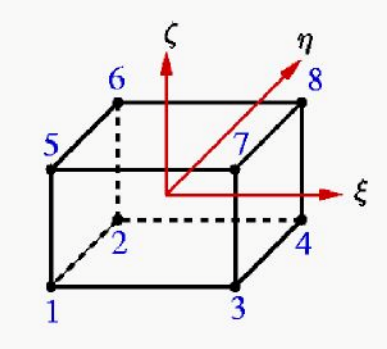

Figure 7-32 Thin layer interface element (Mayer and Gaul 2008)

Applicability of zero thickness and thin layer interface elements

According to Hu (2004) the interface element derived from the relationship of relative nodal displacement and stresses proposed by Goodman et al. (1968) is one of the most commonly used interface elements. However, zero thickness elements are prone to errors in normal stress and deformation calculations. This is due to the fact that a very large normal stiffness is assumed to avoid overlapping between two side materials with very different characteristics (for example soil and structure) when the interface is subjected to compression (Yin et al. 1995; Hu 2004). This is due to the fact that compared with the interfaces between metals and rocks and other solid materials, the soil-structure interface has a more sophisticated behavior. Soil-structure interfaces are frequently met in geotechnical engineering and include shallow foundations, deep foundations, tunnels, and earth retaining structures among others. However, the zero thickness interface element is applicable to situations where two similar materials are jointed. Mayer and Gaul (2008) state that the zero thickness element is more appropriate to model solid-on-solid contact in finite element analyses than the thin layer element.

.

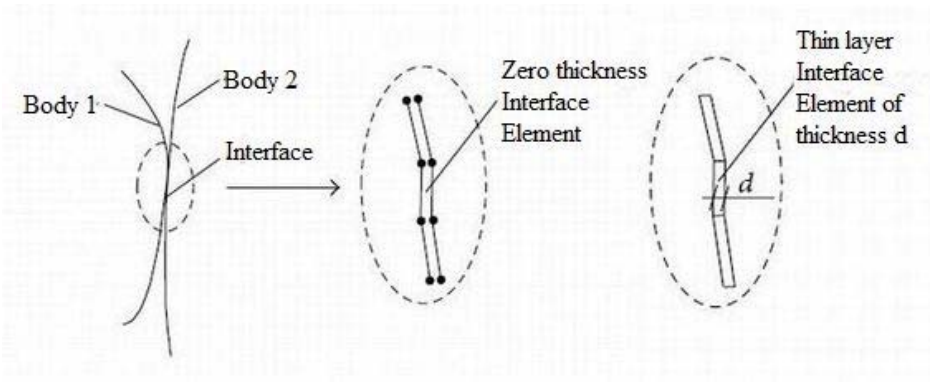

Figure 7-33 Comparison of zero thickness and thin layer interface elements

Use of the thin layer element primarily depends on the thickness of the interface. It is shown in Pande and Sharma (1979) and Desai et al. (1984) that the thin layer element thickness d must be chosen relative to the element lengths l_1 and l_2. Pande and Sharma (1979) define the aspect ratio (A.R.) as equal to

$$\text{A.R.} = \frac{\max(\ell_1, \ell_2)}{d} \tag{7.9}$$

Furthermore, Desai et al. (1984) suggest using thin layer elements having an aspect ratio of less than 100. Zienkiewicz et al. (1970), Zaman (1985), and Griffiths (1985) point out to the fact that when the aspect ratio varies in the range of 10 to 100, slippage is modeled quite accurately. Others (Wei 2009) suggest that shear tests should be carried out to determine the thickness of thin-layer interface.

The issue over the thickness of the thin layer element stems from the fact that for vanishing thickness ($d \rightarrow 0$), the determinant of the Jacobian matrix [J] tends to zero ($\det([J]) \rightarrow 0$). With a determinant of zero, the Jacobian [J] cannot be inverted and the strain-displacement matrix [B] can therefore not be calculated.

$$[J] = \begin{bmatrix} \ell_1/2 & 0 & 0 \\ 0 & \ell_2/2 & 0 \\ 0 & 0 & d/2 \end{bmatrix} \tag{7.10}$$

The thin layer element method has been successfully applied to jointed rock masses (Zienkiewicz et al. 1970), buried pipes (Desai et al. 1984), interaction of foundation and soil masses (Zaman 1985; Griffiths 1985), and grouted anchors-soil systems (Desai et al. (1986).

Both the zero thickness and the thin layer interface elements can be implemented to model nonlinear elastic, viscoelastic, and elastoplastic behavior (Mayer and Gaul 2008). However, both the zero thickness and the thin layer interface elements are limited to small deformations (Qian et al. 2013).

Interface Constitutive Models

A number of interface constitutive models have been developed by various researchers. Depending on the type of analysis performed, the interface behavior may be represented by a quasi-linear or a nonlinear model. Quasi-linear models consider a constant value of stiffness over a range of interface displacements, until yield is reached. After yield, a low constant value of stiffness is usually assigned to the interface. Quasi-linear models have been used by Goodman et al. (1968); Desai et al. (1986); Matsui and San (1989); and Wong et al. (1989).

In nonlinear models, the interface shear stress-displacement relationship is represented by a mathematical function of higher degree. The interface shear stiffness changes during shear, depending on the magnitude of the displacement and any other factor included in the model. Nonlinear models have been used by Clough and Duncan (1971); Zaman et al. (1984); and Desai et al. (1985) among others.

The hyperbolic model for soil behavior developed by Duncan and Chang 1970 was extended to interfaces by Clough and Duncan (1969, 1971) and implemented into the Goodman et al. (1968) joint element formulation. It has been used extensively in soil-structure interaction analyses and design of earth retaining structures (Ebeling et al. 1993; Ebeling and Mosher 1996; Ebeling, Peters, and Mosher 1997; Ebeling and Wahl 1997; and Ebeling, Pace, and Morrison 1997). The model provides satisfactory results to the interface response under monotonic loading at constant normal stress. Other advantages of the Clough and Duncan (1971) interface hyperbolic model are: (1) nonlinearity of the interface shear stress-displacement relationship is well represented, (2) the hyperbolic parameters have a clear physical meaning, and (3) the method is easy to implement in soil-structure interaction analyses. On the other hand, the Clough and Duncan (1971) interface hyperbolic model has some important limitations regarding its use in soil-structure interaction analyses of earth retaining structures. This includes the fact that the hyperbolic formulation does not model displacement softening of the interface and does not include any coupling effects between shear and normal displacements. It has not been extended to cases in which the shear and normal stresses both change, and it has not been fully implemented for cases of cyclic loading and shear stress reversals.

Gomez et al. (2000) extended the soil-structure interface hyperbolic model past the Clough and Duncan version and demonstrated its reasonableness for soil-structure interaction problems.

Zaman et al. (1984) developed a constitutive model for cyclic loading of interfaces. It is based on a polynomial formulation that includes the effects of the number of cycles, amplitude of shear displacements, and normal stress on interface response.

Desai et al. (1985) presented a modified Ramberg-Osgood model for interfaces under cyclic loading. The model accounts for shear stress reversals, hardening or degradation effects with number of load cycles, normal stress, relative density of the sand, and

maximum displacement amplitude. Uesugi and Kishida (1985) observed that the modified Ramberg-Osgood model yields inconsistent results for shear stresses close to failure.

In all the interface models described previously, the interface yield stress is determined by the Mohr-Coulomb criterion (Goodman et al. 1968; Clough and Duncan 1971; Zaman et al. 1984; Desai et al. 1986; and Wong et al. 1989). However, coupling between normal and shear deformations is not included in any of the constitutive formulations previously described.

All commercial finite element and finite difference codes have interface elements. Most used constitutive model for these interface elements, for the modeling of earth retaining structures, is the Clough and Duncan (1971) interface hyperbolic model.

7.6.1.3. Contact Analysis Method

Modeling of soil-structure interaction involves contact between two separate bodies. For example, for the case of integral abutment bridges it involves contact between the integral abutment and the surrounding soil. The interaction between contact surfaces consists of two components: one normal to the surfaces and one tangential to the surfaces. The tangential component behavior is described in terms of relative motion (sliding) of the surfaces and frictional shear stresses. The normal component behavior is described in terms of bearing and gapping.

In finite element analysis, contact conditions are a special class of discontinuous constraint, allowing forces to be transmitted from one part of the model to another (Hibbitt et al. 2002). The constraint is discontinuous because it is applied only when the two surfaces are in contact. When the two surfaces separate, no constraint is applied. Contact analysis is performed with the use of contact (gap) elements and its purpose is to detect when the two surfaces are in contact and apply the contact constraints accordingly. Similarly, the analysis must be able to detect when two surfaces separate and remove the contact constraints. The purpose of contact simulations in finite element analysis is to identify the areas on the surfaces that are in contact and to calculate the contact pressures generated between the two surfaces. Detection of the contact is the key issue in the contact analysis method.

When surfaces are in contact, they usually transmit shear as well as normal forces across their interface. Thus, the analysis should take into consideration the frictional forces, which resist the relative sliding of the surfaces. This is accomplished with the use of the coefficient of friction to characterizes the frictional behavior between the surfaces in contact.

The Coulomb friction model is a common friction model used to describe the interaction of contact surfaces. The model quantifies the frictional behavior between the contact surfaces using a coefficient of friction, μ. The tangential motion is zero until the surface traction reaches a critical shear stress value, $\tau_{crit.}$,which depends on the normal contact pressure, according to the following equation:

$$\tau_{crit.} = \mu\rho \qquad (7.11)$$

where

$\tau_{crit.}$ = critical shear stress

μ = coefficient of friction

ρ = contact pressure between the two surfaces

The two contact surfaces can carry shear stresses up to a certain magnitude across their interface before they start sliding relative to each other. The Coulomb friction model (Figure 7-34) defines this critical shear stress as $\tau_{crit.}$ at which the sliding of the surfaces start as fraction of the contact pressure, p, between the surfaces. The Coulomb friction model assumes isotropic friction and for the case of soil-structure surface interaction this can be assumed to be the case. Also, for the case of soil structure interaction, the effect of the temperature on the friction constant is usually ignored.

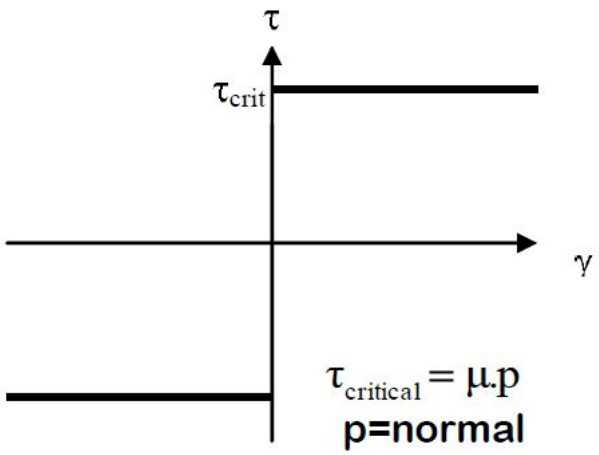

Figure 7-34 Coulomb friction model (Hibbitt et al. 2002)

Comparison of Interface Element Method and Contact Analysis Method

Both the interface element and the contact analysis methods are used by researchers to investigate soil-structure interaction problems. The important phenomena at the interface are relative motion (sliding) and shear resistance (tangential behavior), and bearing and gapping (normal behavior). Zero thickness elements have been around for years and found to be very appropriate to model solid-on-solid contact (Mayer and Gaul 2008). Furthermore, zero thickness elements using a Mohr-Coulomb failure criterion have been shown to model interface behavior of retaining walls with good accuracy, but numerical stability issues emerge in some problems (Day and Potts 1994). Thin layer elements have also been used to model jointed rock masses (Zienkiewicz et al. 1970), buried pipes (Desai et al. 1984), foundation-soil interaction (Zaman 1985; Griffiths 1985), and grouted anchors-soil systems (Desai et al. (1986). However, thin layer elements require a constitutive model for implementation. Conversely, experiments and simple lab tests are performed on the soil and the interface to obtain various parameters such as the normal and tangential stiffnesses. Both the zero thickness and the thin layer interface elements are limited to small deformations (Qian et al. 2013).

Interface elements were initially developed for rock joints, and typically use normal and tangential stiffnesses to model the pressure transfer and friction at the interface. Because they have to be predefined and their topology remains unchanged with time, they are only suitable for predefined interfaces with small deformations (Sheng et al. 2007). However, in problems such as pile installation, soil anchors, structural foundations under eccentric loading, retaining walls, geotextile reinforcements in embankments and retaining structures, the soil-structure interfaces undergo large deformations, large frictional sliding as well as surface separation and reclosure, and are highly variable during the loading procedure (Sheng et al. 2007). Consequently, these interfaces cannot be modeled properly using simplified boundary conditions or traditional interface elements. These simplifications often lead to inaccurate predictions of the real soil behavior and are only possible when the surfaces are always in contact. Soil-structure interaction that involves large deformation, surface separation and reclosure is better represented by frictional contact using the contact analysis method.

Qian et al. (2013) conducted a comparative study on interface element (zero thickness and thin layer elements) and contact analysis methods in the analysis of high concrete-faced rockfill dams. To investigate the accuracy and limitations of each method, the simulation results were compared in terms of the dam deformations, contact stresses along the interface, stresses in the concrete face slab, and separation of the concrete face slab from the cushion layer. The predicted dam deformations and slab separation were also compared with in-situ observation data. The results proved that the interface element method has its limitations in predicting contact stresses, slab separations and stresses in the concrete face slab when a large slip occurs. The study concluded that the contact analysis method is the best numerical method to model soil-structure interaction whether the separation is finite or not and that for contact problems involving large separation or slipping, the contact analysis method shall be used over the interface element method.

7.7. Modeling of Soil-Structure Interaction of Integral Abutment Bridges

An extensive review of previous research studies on integral abutment bridges show that the vast majority of researchers employ the Winkler Springs method to model soil-structure interaction, that is, the interaction between the integral abutment and the backfill. Although use of the Winkler Springs method to model soil behavior is a simplification due to the fact that the physical behaviour of soil is not well replicated, this model is acceptable for computational purposes when the structural response is the main focus of the research.

Most researchers use the Winkler Springs method by means of the information presented in Figure 7-3 that describes the relationship between wall movement and earth pressure (Clough and Duncan 1991). Based on the earth pressure coefficients presented in Figure 7-3, for an abutment of height H, unit weight of soil γ, internal friction angle of soil Φ, and for springs of selected tributary area and located at different depths along the height of the abutment wall, force-displacement curves such as the curve shown in Figure 7-35 are derived and used in the finite element models.

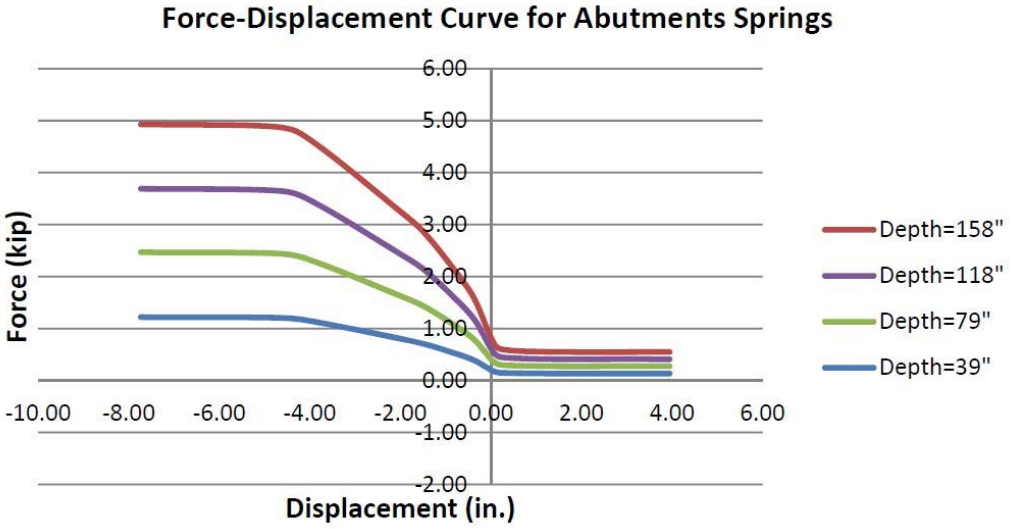

Figure 7-35 Use of the Winkler Springs method by Doust (2011)

Arsoy et al. (2002) used the Interface Element method to model soil-structure interaction during the course of their experimental and analytical investigations of piles and abutments of integral bridges. The investigations used finite element meshing combined with zero thickness interface elements (Figure 7-36) along with the use of a soil constitutive model such as Mohr-Coulomb, Drucker-Prager, Duncan-Chang Hyperbolic, and Cam Clay (Bentler et al. 1999). The results from the analytical investigations compared well to the experimental results.

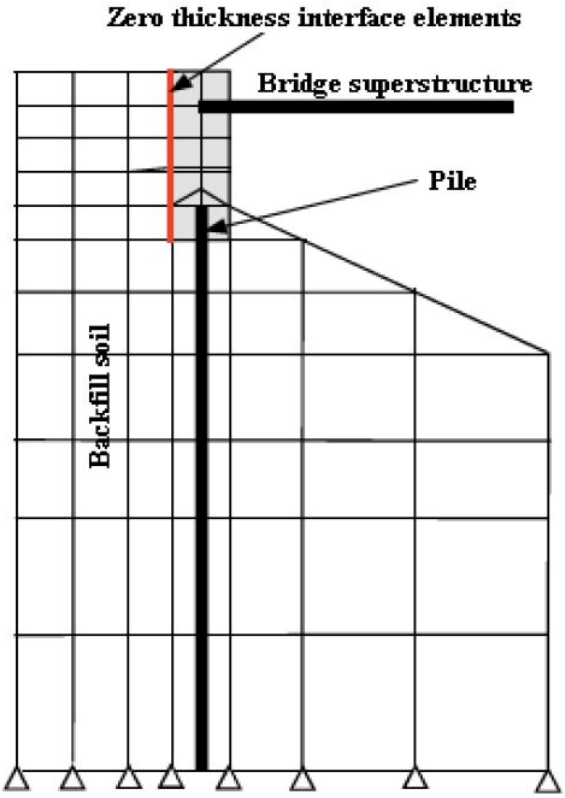

Figure 7-36 Use of the Interface Element method by Arsoy et al. (2002)

Bao and Rietz (2013) used the Contact Analysis method to model seismic soil-structure interaction in integral abutments bridges supported on HP steel piles. The Drucker-Prager (D-P) soil constitutive model was used to model the granular soil embankment in the finite element analysis along with ANSYS contact elements to simulate the contact surface between the concrete abutment walls and the soil embankment.

Issues with the modeling of soil-structure interaction of integral abutment bridges

It is generally accepted that daily and seasonal temperature changes cause the decks of integral abutment bridges to expand during temperature increases and to contract during temperature decreases (Figure 7-37). This process causes movement of the integral abutments and mobilizes passive soil pressures behind the abutments with the potential to form permanent soil displacements. As the abutments move away from the backfill, a gap may form between the abutments and the backfill. Development of such soil gaps around the abutments significantly reduces the soil-structure resistance, which may lead to a reduction of the lateral load capacity of the bridge structure (Kyle 2006).

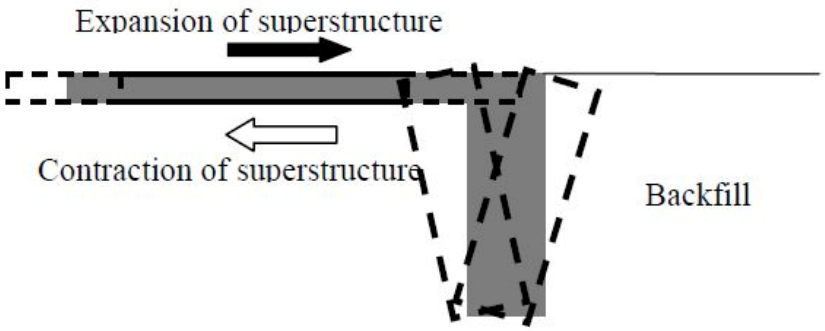

Figure 7-37 Integral abutment movement due to thermal expansion and contraction (David and Forth 2011)

Under purely elastic conditions within the soil, the lateral displacements of the bridge structure and the soil are equal. However, soil has a very limited ability to take tension and it is likely that separation (gaps) may occur near the top of the structure (Figure 7-38). This separation or gap may cause large compression stresses to develop in front of the structure and tensile stresses behind the structure. This is very likely to happen as a result of thermal expansion and contraction (David and Forth 2011). The cyclic nature of loading will cause the structural element to move in and out of contact with the soil as it moves laterally.

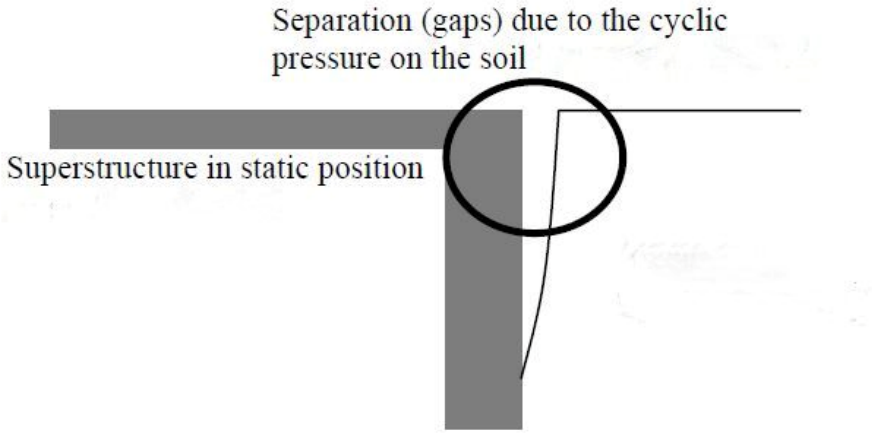

Figure 7-38 Gap between the integral abutment and backfill due to cyclic pressure on the soil over period of time (David and Forth 2011)

Consequently, thermal expansion and contraction in internal abutment bridges potentially creates a gap between the integral abutment and backfill, which should be considered in the modeling of soil-structure interaction. This can be achieved with the use of the Contact Analysis method that involves use of contact elements - these elements can detect contact, which is the key issue in the Contact Analysis method.

7.8. Modeling of Soil-Structure Interaction for this Research Study

The Winkler Springs method is used for the modeling of soil-structure interaction in this study. This is due to the fact that the focus of this research is on the structural response of the bridge, not on soil deformations or the impacts on adjacent structures, both of which will necessitate the use of a soil constitutive model in combination with interface or contact elements. For these reasons, the Winkler Springs method is the most appropriate method for the modeling of soil-structure interaction for the parametric studies of this research study. Although there is a potential for a gap formation between the integral abutments and the backfill as a result of thermal cyclic loading, use of the Contact Analysis method is not required for this research study for a number of reasons. This includes, among others, the lack of a soil constitutive model specific to integral abutment bridges and the fact that the Contact Analysis method is a work in progress; the combination of these two factors would produce results as approximate as the use of the Winkler Springs method. In addition, the number of parametric studies needed to investigate the effects of the various cantilever wingwall configurations on the behavior of integral abutment bridges, which is the focus of this study, does not bode well with the use of the Contact Analysis method. Furthermore, the use of Contact Analysis method may be more appropriate to structures such as dams or seawalls where the effects of gap formation are more pronounced.

Force-Displacement Curves

The force-displacement relationships for this study are derived by means of the graphs shown in Figure 7-3, which predicts the relationship between wall movement and earth pressure (Clough and Duncan 1991) for dense sand, medium dense sand, and loose soil during active and passive movements. Figure 7-39 shows the force-displacement relationship for the 9-feet high abutment used in this study with medium dense sand used as backfill soil material. The graph is derived using the coefficients of earth pressure, K, and the internal friction angle of 37 degrees from Figure 7-3 along with a unit weight of 125 pcf. Nonlinear Winkler springs using the COMBIN39 element from the ANSYS element library are employed to model the soil response behind the integral abutments and the cantilevered wingwalls.

Figure 7-3 indicates that development of maximum passive earth pressure requires displacement of the abutment wall in the range of 0.03 of its height for the case of medium dense sand. Thus, for the 9-feet high abutments, development of maximum passive pressures behind the abutments requires an abutment displacement equal to $\Delta=(0.03)(9x12)=3.24$ inches. This is illustrated in Figure 7-39.

The curve in Figure 7-39 also shows that the springs have very low stiffness when the abutments move away from the backfill (active movement). Conversely, spring stiffness

is much higher when the abutment is being pushed into the backfill during bridge expansion (passive movement).

The same interaction curve (Figure 7-39) used to simulate the soil-structure interaction behind the integral abutments with medium dense sand as backfill material is used to simulate the soil-structure interaction behind the cantilevered wingwalls. In other words, Figure 7-39 applies to both the integral abutments and the cantilevered wingwalls.

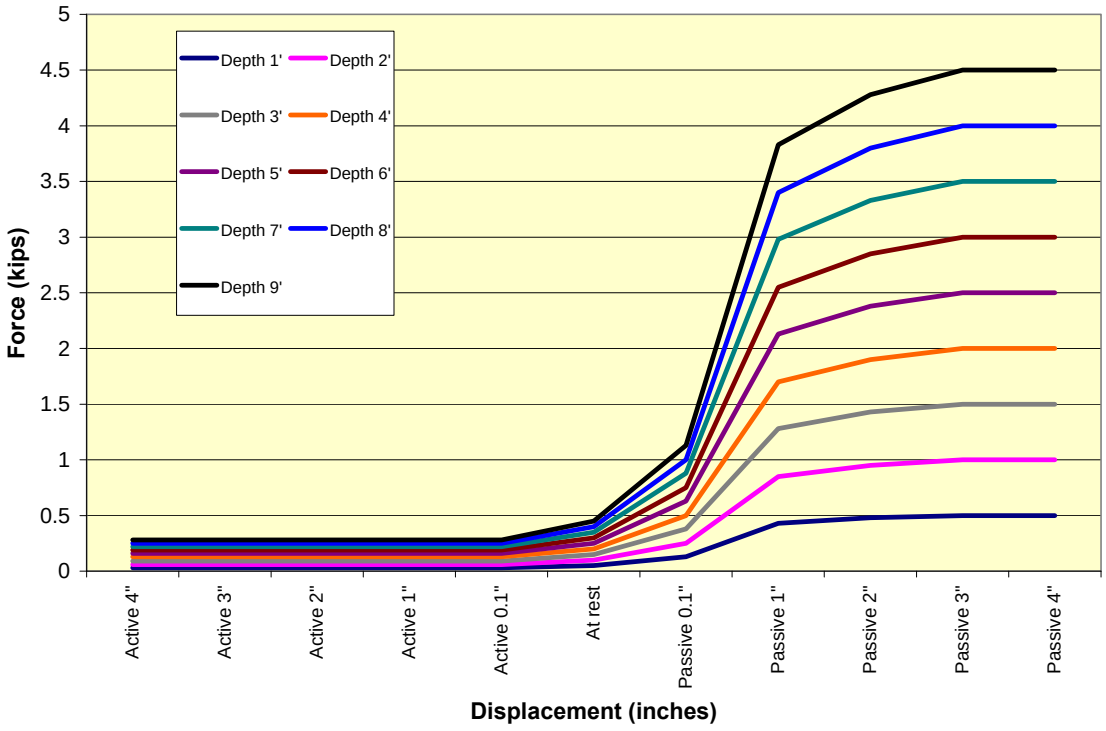

Figure 7-39 Force-Displacement curves for the 9-feet high integral abutment with medium dense sand as the backfill soil material

Chapter 8

Modeling of Soil-Pile Interaction

8.1. Introduction

Modeling of soil-pile interaction is critical for integral abutment bridges. Superstructure movement due to temperature changes, creep, shrinkage, earthquake and braking forces is primarily horizontal translation. Integral abutment bridges accommodate superstructure movement by flexure of the piling and use of cycle-control (expansion) joints at the roadway end of the approach slabs. As a result, bending stresses directly related to the combined stiffness of the piles and the surrounding soil are induced in the piles. Determination of the magnitude of induced bending stresses requires the inclusion of the stiffness of the soil in the modeling of the integral abutment bridge. Soil-pile interaction is modeled by attaching springs at selected nodes along the length of the piles. The stiffness of these springs represents the stiffness of the soil around the piles. Spring stiffnesses serve as input to the finite element models developed in order to perform the parametric studies described in chapter 6.

8.2. Modeling of Soil-Pile Interaction

Spring stiffnesses are determined from three types of soil resistance versus displacement curves. These curves, which are also referred to as soil-pile interaction curves, are derived from soil parameters. All three types of curves assume nonlinear soil behavior and define the soil-pile interaction at every point along the pile length. The three types of soil-pile interaction curves are:

- lateral soil resistance-displacement curves, known as P-y curves
- longitudinal load-slip curves, known as f-z curves
- pile tip load-settlement curves, known as q-z curves

The P-y curves are a soil model that describes the behavior of the soil surrounding laterally-loaded piles. These curves describe the relationship between the horizontal resistance of the soil at a depth z along the pile length and the corresponding horizontal displacement of the pile at that depth. The quantity P is the soil resistance per unit length of pile. It acts in same direction as the deflection y, but opposite in sign. The quantity y is the horizontal displacement of the pile at a specific point along the length of the pile. P-y curves are assumed to have the same response in both tension and compression because the piles have similar resistance when they move for an equal distance in either direction.

The P-y curves are the most important of the three types of soil-pile interaction curves for modeling the behavior of laterally-loaded piles.

The f-z curves describe the relationship between the vertical skin frictional resistance (vertical force per unit length of pile) of the soil at a depth z along the pile length and the relative vertical displacement between the pile and the soil at that depth.

The q-z curves describe the relationship between the bearing resistance (vertical force on the effective pile-tip area) at the pile tip and the vertical settlement of the pile tip. For end bearing piles, q-z curves may be neglected.

Nonlinear springs (Figure 8-1) in both orthogonal directions are attached at each node along the length of the piles to model the stiffness of the soil around the piles. Spring spacing varies along the length of the piles. Generally, the upper one-third of the pile has the most significant contribution in the lateral soil reaction (Washington State DOT Bridge Design Manual 2011) and is the region where significant moments and displacements do occur. As a result, a finer mesh is usually employed at the top one-third of the piles in order to provide sufficient accuracy with the simulation. Considering however, the capabilities of the ANSYS Release 13.0 Academic Research Mechanical software, a fine mesh of 3 by 3 inches was used throughout the entire length of the piles.

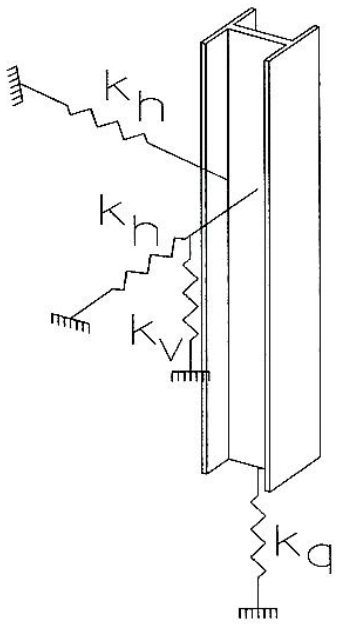

Figure 8-1 Soil springs for soil-pile interaction (Thanasattayawibul 2006)

Spring stiffnesses K_h, Kv, and Kq, which are used as input in the ANSYS structural analysis models are calculated using the mathematical expressions in Tables 8-5 and 8-6.

8.3. Modified Ramberg-Osgood Model

Research conducted by Amde et al (1982), Greimann et al (1984), Greimann and Amde (1988) utilized an idealized model based on the modified Ramberg-Osgood model to approximate the load-displacement curves for the modeling of the nonlinear pile-soil interaction. The parameters needed for the model are calculated from the soil and pile properties. The modified Ramberg-Osgood model is used to approximate all three types of load-displacement curves.

The modified Ramberg-Osgood P-y curve is expressed mathematically using the equation

$$p = \frac{k_h y}{\left[1 + \left[\frac{y}{y_u}\right]^n\right]^{1/n}} \qquad (8.1)$$

$$y_u = \frac{p_u}{k_h} \qquad (8.2)$$

where

Kh is the initial lateral stiffness of the soil in ksf

P is the lateral soil resistance in klf

Pu is the ultimate lateral soil resistance at depth z along the pile length in klf

n is a dimensionless shape parameter. The effect of the shape parameter on the modified Ramberg-Osgood equation is shown in Figure 8-3

y is the lateral displacement of the pile in inches

yu is the lateral displacement of the pile in inches that is associated with an elastic-plastic soil material when the resistance P equals the resistance Pu

Figure 8-2 presents a comparison between the modified Ramberg-Osgood curve and a typical P-y curve. The figure shows that the typical P-y curve simplifies the nonlinear soil behavior with the use of an elastoplastic curve. This curve has two parts: (1) elastic portion, which is defined with a slope equal to the secant soil modulus for the case of clay, and initial soil modulus for the case of sand, and (2) plastic portion, which is the ultimate soil resistance per unit length of pile, Pu.

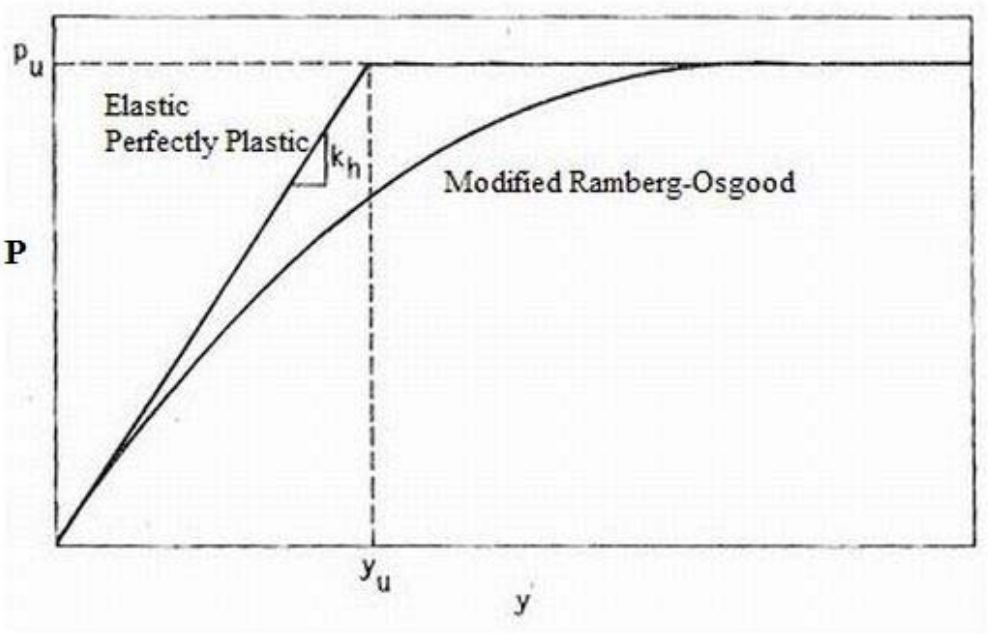

Figure 8-2 Modified Ramberg-Osgood P-y curve (Amde et al. 1987)

Figure 8-3 presents a non-dimensional form of the modified Ramberg-Osgood P-y equation in terms of P/Pu versus y/yu. The graph clearly indicates the effect of shape parameter n in the modified Ramberg-Osgood P-y equation (8.1).

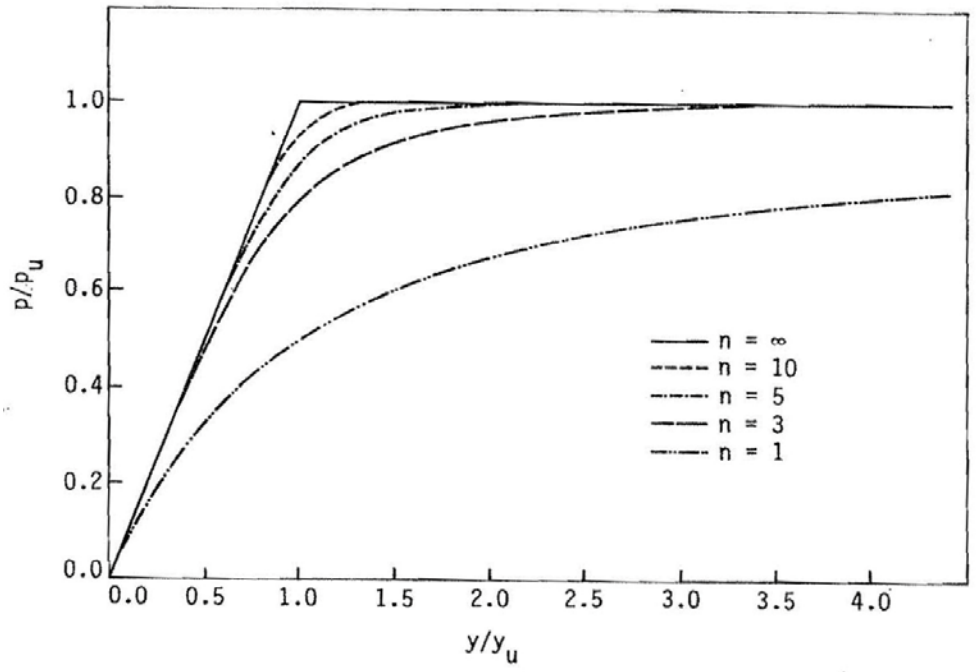

Figure 8-3 Non-dimensional form of the modified Ramberg-Osgood P-y equation (Amde et al. 1987)

Amde et al. (1987) developed mathematical expressions for both the modified Ramberg-Osgood f-z and q-z curves. The mathematical expression for the f-z curve is shown as Eq. (8.3) and for the q-z curve as Eq. (8.7). Both expressions apply for $Z \leq Zc$. For $Z > Zc$ Vijayvergiya (1977) recommends equations (8.4) and (8.8).

$$f = f_{max}\left(2\sqrt{\frac{z}{z_c}} - \frac{z}{z_c}\right) \qquad (8.3)$$

$$f = f_{max} \qquad (8.4)$$

where, f is the friction force mobilized at the pile/soil interface at displacement z, in Klf

f_{max} is the maximum friction force mobilized at the pile/soil interface expressed in Klf and calculated using the expressions in Table 8-2

Z is the vertical pile displacement in inches

Zc is the vertical pile displacement needed to mobilize the maximum friction force f_{max}
= 0.40 in. (0.033 ft) for sand
= 0.25 in. (0.021 ft) for clay

The non-dimensional form of Eq. (8.3) is shown as Eq.(8.5) and presented in Figure 8-4

$$\frac{f}{f_{max}} = 2\sqrt{\frac{z}{z_c}} - \frac{z}{z_c} \qquad (8.5)$$

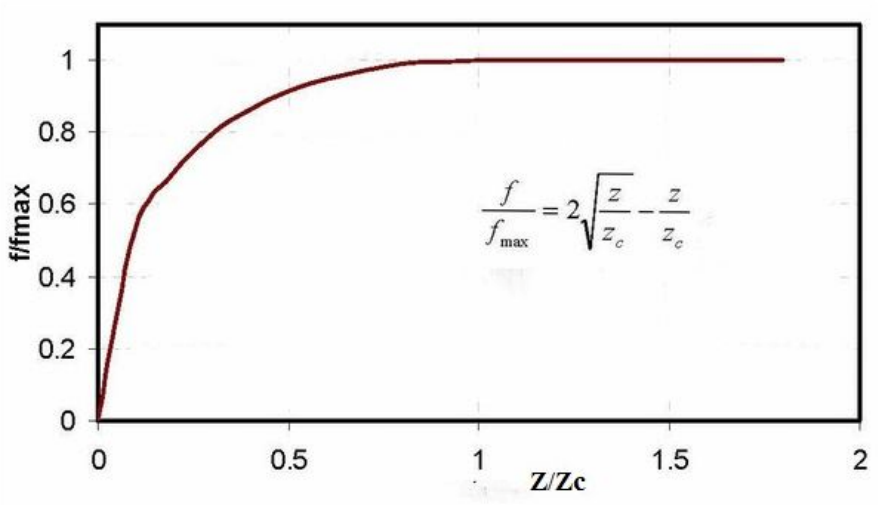

Figure 8-4 Non-dimensional form of the modified Ramberg-Osgood f-z equation (Vijayvergiya 1977)

In addition, Mosher (1984) developed an expression (Eq. 8.6) in which the friction force f is related to the displacement Z in terms of the initial vertical stiffness of the soil K_v and the maximum friction force f_{max} mobilized at the pile/soil interface.

$$f = \frac{z}{\frac{1}{k_v} + \frac{z}{f_{max}}} \qquad (8.6)$$

The expression (Eq. 8.6) is presented in Figure 8-5 in the form of f/f_{max} versus Z relationship

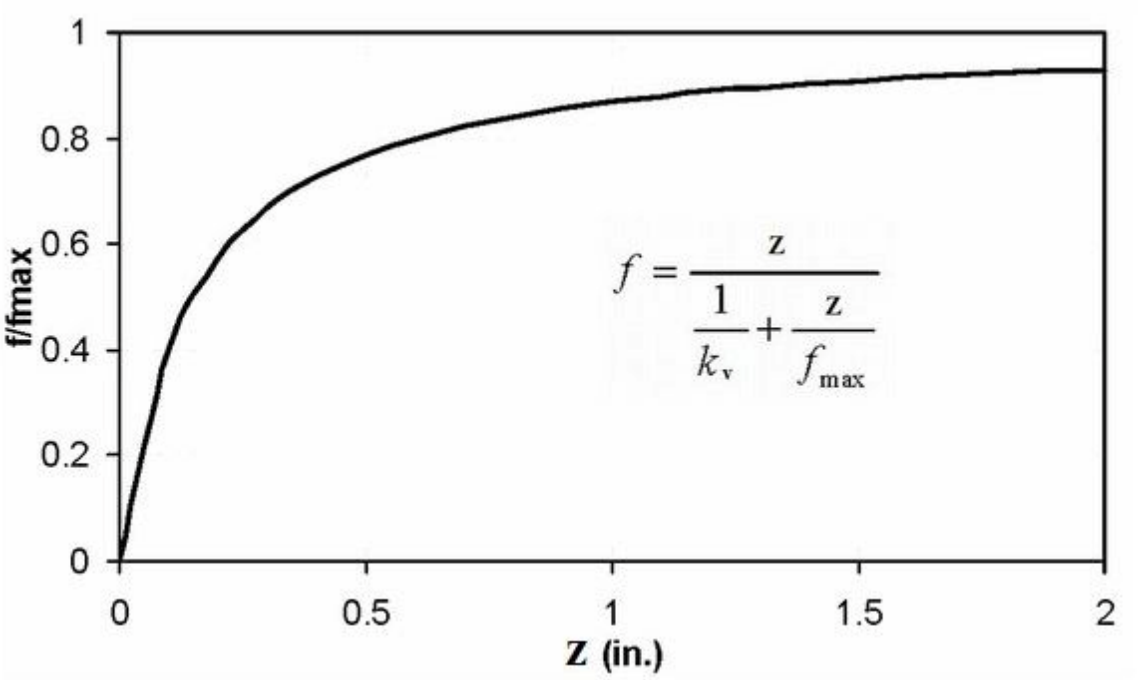

Figure 8-5 f-z curve (Mosher and Dawkins 2000)

The mathematical expression for the modified Ramberg-Osgood q-z curve developed by Amde et al. (1987) is shown as Eq. (8.7) and applies for $Z \leq Zc$ while for $Z > Zc$ Vijayvergiya (1977) recommends Eq. (8.8).

$$q = q_{max}\left(\frac{z}{z_c}\right)^{1/3} \qquad (8.7)$$

$$q = q_{max} \qquad (8.8)$$

where, q is the soil resistance mobilized at the pile tip at pile tip displacement Z, in Ksf

q_{max} is the maximum soil resistance at the pile tip expressed in ksf and calculated using the expressions in Table 8-3

Z is the pile tip displacement in inches

Zc is the pile tip displacement needed to mobilize the maximum soil resistance at the pile tip q_{max}
= 0.40 in. (0.033 ft) for sand
= 0.25 in. (0.021 ft) for clay

8.4. Analytical Forms of Soil-Pile Interaction Curves

The following tables present the analytical forms of the three load-displacement curves for soft clay, stiff clay, very stiff clay, and sand.

- Table 8-1 presents the analytical forms of P-y curves
- Table 8-2 presents the analytical forms of f-z curves
- Table 8-3 presents the analytical forms of q-z curves

Table 8-1 Analytical forms of P-y curves (Greimann et al. 1984)

Case	n	P_u (Use Lesser Value)	k_h
Soft Clay, Static Load	1.0	$P_u = 9C_uB$ $P_u = (3+\frac{\gamma}{C_u}x+\frac{0.5}{B}x)C_uB$	$\frac{p_u}{y_{50}}$
Stiff Clay, Static Load	1.0	$P_u = 9C_uB$ $P_u = (3+\frac{\gamma}{C_u}x+\frac{0.5}{B}x)C_uB$	$\frac{p_u}{y_{50}}$
Very Stiff Clay, Static Load	2.0	$P_u = 9C_uB$ $P_u = (3+\frac{\gamma}{C_u}x+\frac{2.0}{B}x)C_uB$	$\frac{p_u}{2y_{50}}$
Sand, Static Load	3.0	$P_u = \gamma x[B(k_p-k_a)+\eta+\mu]$ $P_u = \gamma x(k_p^3+2k_p^2k_o\tan\phi-k_a)B$ $\eta = xk_p\tan\alpha\cdot\tan\beta$ $\mu = xk_o\tan\beta(\tan\phi-\tan\alpha)$	$\frac{J\gamma x}{1.35}$

where

B is the pile width (ft)

Cu is the undrained cohesion of clay = 97.0N + 114.0 expressed in psf

J is an empirical dimensionless soil parameter that is taken as
= 200 for loose sand
= 600 for medium sand
= 1500 for dense sand

Ka is the coefficient of active earth pressure = (1-sinΦ)/(1+sinΦ)

Ko is the coefficient of at rest earth pressure = (1-sinΦ)

Kp is the coefficient of passive earth pressure = (1+sinΦ)/(1-sinΦ)

x is the depth from the top surface of soil (Figure 2-10) in feet

y_{50} is the displacement at one-half of the ultimate soil reaction
= $2.5B\varepsilon_{50}$ for soft and stiff clay
= $2.0B\varepsilon_{50}$ for very stiff clay

a is a soil parameter
= $\Phi/2$ for medium or dense sand
= $\Phi/3$ for loose sand

β is a soil parameter = $45^{o} + \Phi/2$

γ is the effective unit soil weight (kcf)

ε_{50} is the strain of clay at 50 percent of soil strength. According to Matlock (1970)
= 0.02 for soft clay
= 0.01 for medium clay
= 0.005 for stiff clay

Φ is the angle of internal friction of the soil in degrees

Table 8-2 Analytical forms of f-z curves (Amde et al. 1987)

Case	Basic *f-z* Curve Equations	f_{max} (klf)	
		H Piles	Others
Clay (Static Load)	$\frac{f}{f_{max}} = 2\sqrt{\frac{z}{z_c}} - \frac{z}{z_c}$	The least of: $2(d+b_f)c_u$ $2(d+2b_f)c_a$ $2(dc_u + b_f c_a)$	The lesser of: $l_g c_a$ $l_g c_u$
Sand (Static Load)	$\frac{f}{f_{max}} = 2\sqrt{\frac{z}{z_c}} - \frac{z}{z_c}$	$0.04N(d+2b_f)$	$0.04Nl_g$

where

Ca is the adhesion between soil and pile = aCu (psf)

Cu is the undrained cohesion of clay = 97.0N + 114.0 (psf)

N is the average standard penetration test (SPT) blow count

Z is the vertical pile displacement in inches

Zc is the vertical pile displacement needed to mobilize the maximum friction force f_{max}
= 0.40 in. (0.033 ft) for sand
= 0.25 in. (0.021 ft) for clay

a is the shear strength reduction factor (Figure 8-6). The lower curve applies to steel H-piles

b_f is the flange width of steel H-pile section expressed in ft

d is the depth of the steel H-pile section expressed in ft

f is the friction force mobilized at the pile/soil interface at displacement Z, in Klf

f_{max} is the maximum friction force mobilized at the pile/soil interface expressed in Klf

lg is the gross perimeter of the pile (ft)

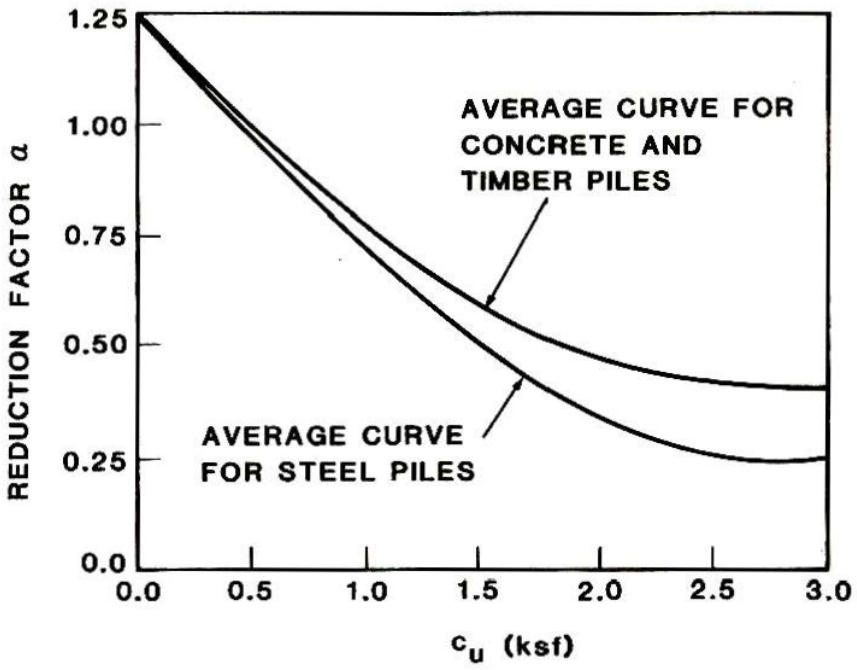

Figure 8-6 Shear strength reduction factor (Tomlinson 1957)

Table 8-3 Analytical forms of q-z curves (Amde et al. 1987)

Case	Basic q-z Curve Equation	q_{max} (ksf)
Clay (Static Load)	$\frac{q}{q_{\max}} = \left(\frac{z}{z_c}\right)^{1/3}$	$9c_u$
Sand (Static Load)	$\frac{q}{q_{\max}} = \left(\frac{z}{z_c}\right)^{1/3}$	$8N_{corr}$

where

Cu is the undrained cohesion of clay = 97.0N + 114.0 expressed in psf

N is the average standard penetration test (SPT) blow count

Ncorr is the corrected standard penetration test (SPT) blow count at pile tip depth
= N (uncorrected) if N is equal or less than 15
= 15 + 0.5(N-15) if N is greater than 15

q is the soil resistance mobilized at the pile tip at pile tip displacement Z, in Ksf

qmax is the maximum soil resistance at the pile tip expressed in ksf

Z is the pile tip displacement in inches

Zc is the pile tip displacement needed to mobilize the maximum soil resistance at the pile tip qmax
= 0.40 in. (0.033 ft) for sand
= 0.25 in. (0.021 ft) for clay

Table 8-4 summarizes the equations developed by Amde et al. (1987) to calculate the spring stiffnesses Kh, Kv, and Kq where Kh is the initial lateral stiffness of the soil (ksf), Kv is the initial vertical stiffness of the soil at depth z along the pile length (ksf), and Kq is the initial vertical stiffness of the soil at the pile tip (kcf).

Table 8-4 Spring stiffnesses Kh, Kv, and Kq (Amde et al. 1987)

Curve Type	Soil Type	Calculated		Used	
		$k_{(h,\,v,\,q)}$	n	$k_{(h,\,v,\,q)}$	n
p-y	Soft Clay	$0.669\frac{P_u}{y_{50}}$	1.5	$\frac{P_u}{y_{50}}$	1.0
	Stiff Clay	$0.915\frac{P_u}{y_{50}}$	1.07	$\frac{P_u}{y_{50}}$	1.0
	Very Stiff Clay	$0.539\frac{P_u}{y_{50}}$	2.56	$\frac{P_u}{2y_{50}}$	2.0
	Sand	-	-	$\frac{J\gamma x}{1.35}$	3.0
f-z	All Soils	$7.32\frac{f_{\max}}{z_c}$	1.33	$10\frac{f_{\max}}{z_c}$	1.0
q-z	All Soils	$7.32\frac{q_{\max}}{z_c}$	1.33	$10\frac{q_{\max}}{z_c}$	1.0

Explanation of symbols in Table 8-4 is provided in earlier pages of this chapter.

The mathematical equations presented in Tables 8-1 to 8-4 are used to calculate the Ramberg-Osgood parameters for both HP10X57 and HP12X84 piles in loose sand and very stiff clay that comprise the soil profile (Figure 6-2). The results are summarized in Tables 8-5 and 8-6 and the calculations are presented in Appendix B. The section properties of the steel H-pile sections are taken from the AISC Manual of Steel Construction.

Table 8-5 Ramberg-Osgood parameters for HP10X57 and HP12X84 piles in loose sand

Properties and Parameters		**HP10X57**	**HP12X84**
Soil Properties	Blow count N	5	5
	Effective, saturated unit weight γ_{sat} (pcf)	55	55
	Dry unit weight γ_{dry} (pcf)	90-125	90-125
	Angle of friction Φ (degrees)	30	30
Ramberg-Osgood P-y curve Parameters	n	3.0	3.0
	Saturated conditions Pu (klf)	$0.069x^2 + 0.125x$ for $x \leq 20$ feet 1.49x for $x > 20$ feet	$0.069x^2 + 0.15x$ for $x \leq 24$ feet 1.8x for $x > 24$ feet
	Saturated conditions K_h (ksf)	8.15x	8.15x
Ramberg-Osgood f-z curve Parameters	n	1.0	1.0
	Saturated conditions f_{max} (klf)	0.507	0.615
	Saturated conditions K_v (ksf)	152	185
Ramberg-Osgood q-z curve Parameters	n	1.0	1.0
	Saturated conditions q_{max} (ksf)	40	40
	Saturated conditions Kq (kcf)	12,000	12,000

Table 8-6 Ramberg-Osgood parameters for HP10X57 and HP12X84 piles in very stiff clay

Properties and Parameters		HP10X57	HP12X84
Soil Properties	Blow count N	50	50
	Effective, saturated unit weight γ_{sat} (pcf)	65	65
	Dry unit weight γ_{dry} (pcf)	120-140	120-140
	Undrained cohesion Cu (psf)	5000	5000
Ramberg-Osgood P-y curve Parameters	n	2.0	2.0
	Saturated conditions Pu (klf)	12.75 + 10.06x for x ≤ 2'-6" 38.25 for x > 2'-6"	15.375 + 10.07x for x ≤ 3'-0" 46.13 for x > 3'-0"
	Saturated conditions K_h (ksf)	2250	2250
Ramberg-Osgood f-z curve Parameters	n	1.0	1.0
	Saturated conditions f_{max} (klf)	6.33	7.69
	Saturated conditions K_v (ksf)	3043	3697
Ramberg-Osgood q-z curve Parameters	n	1.0	1.0
	Saturated conditions q_{max} (ksf)	45	45
	Saturated conditions Kq (kcf)	21,635	21,635

8.5. Soil-Pile Interaction Curves

The Ramberg-Osgood parameters in Tables 8-5 and 8-6 are used to plot the soil-pile interaction curves for this research study. The soil-pile interaction curves are listed in Table 8-7.

Table 8-7 List of soil-pile interaction curves for the research study

Curve	Pile size	Soil type	Figure
P-y	HP10X57	loose sand	8-7
P-y	HP12X84	loose sand	8-8
P-y	HP10X57 HP12X84	very stiff clay	8-9
f-z	HP10X57 HP12X84	loose sand	8-10
f-z	HP10X57 HP12X84	very stiff clay	8-11
f/fmax - z	HP10X57 HP12X84	loose sand	8-12
f/fmax - z	HP10X57 HP12X84	very stiff clay	8-13
q-z	HP10X57 HP12X84	loose sand	8-14
q-z	HP10X57 HP12X84	very stiff clay	8-15
q/qmax - z	HP10X57 HP12X84	loose sand	8-16
q/qmax - z	HP10X57 HP12X84	very stiff clay	8-17

Looking at the soil profile (Figure 6-2) and using a 3 feet minimum cover over the bottom of the integral abutment (Figure 2-10), then the height of the soil profile from the top surface of soil to the pile tip elevation is 3'+9'+31' = 43'. Consequently, the P-y curves in Figures 8-7, 8-8, and 8-9; f-z curves in Figures 8-10 and 8-11; and q-z curves in Figures 8-14 and 8-15 are used as input in the analysis.

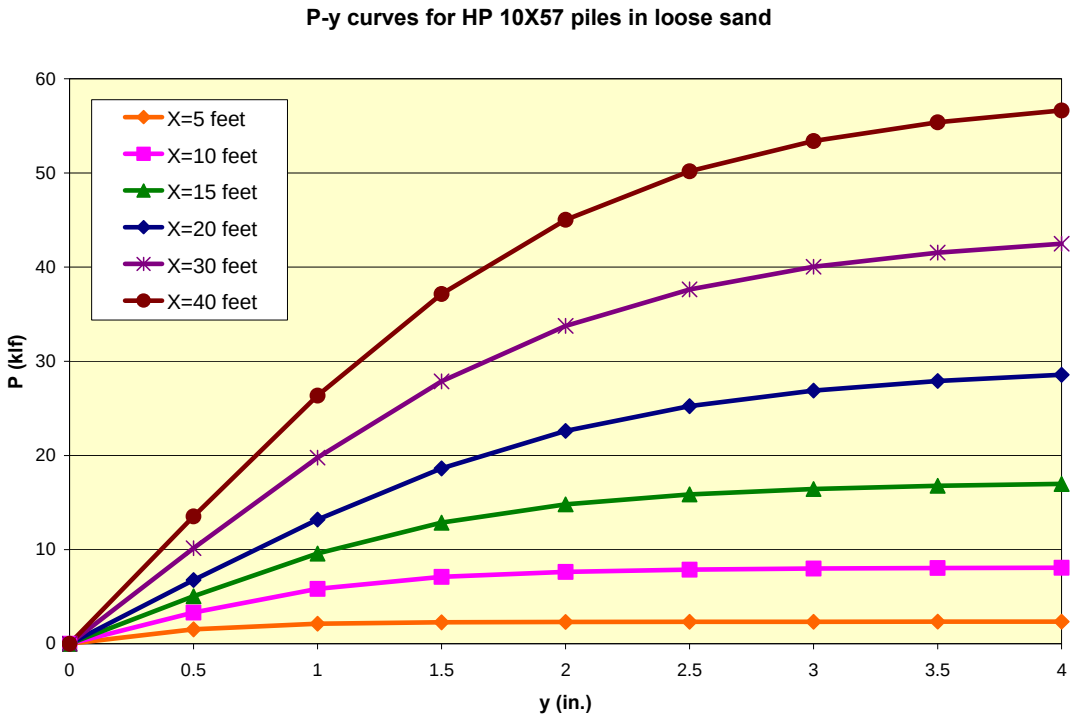

Figure 8-7 P-y curves for HP10X57 piles in loose sand

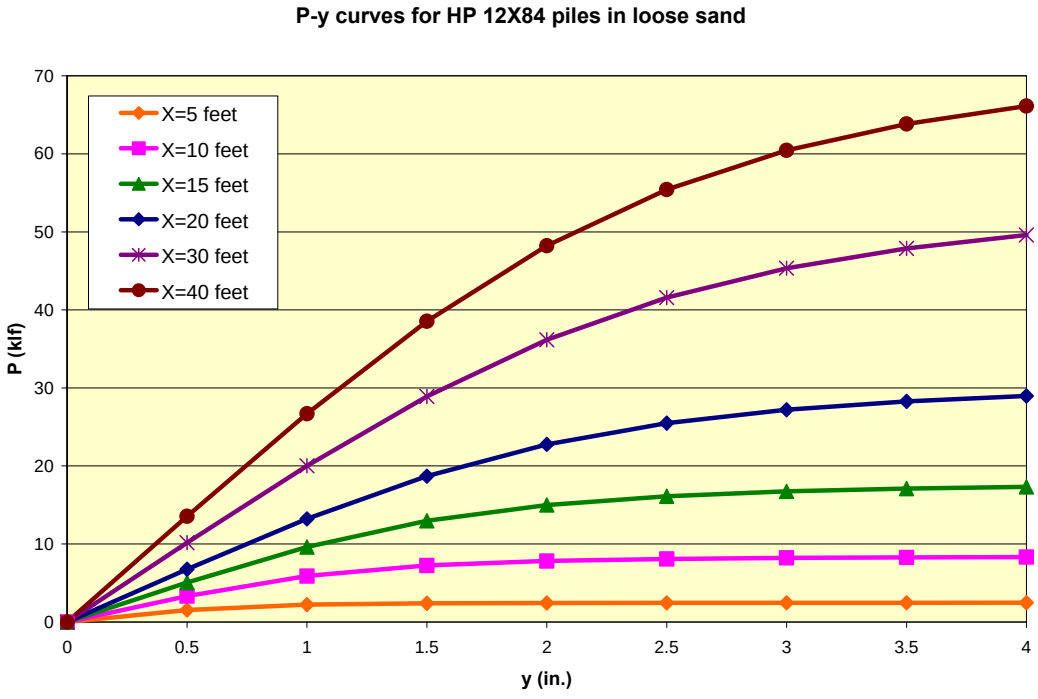

Figure 8-8 P-y curves for HP12X84 piles in loose sand

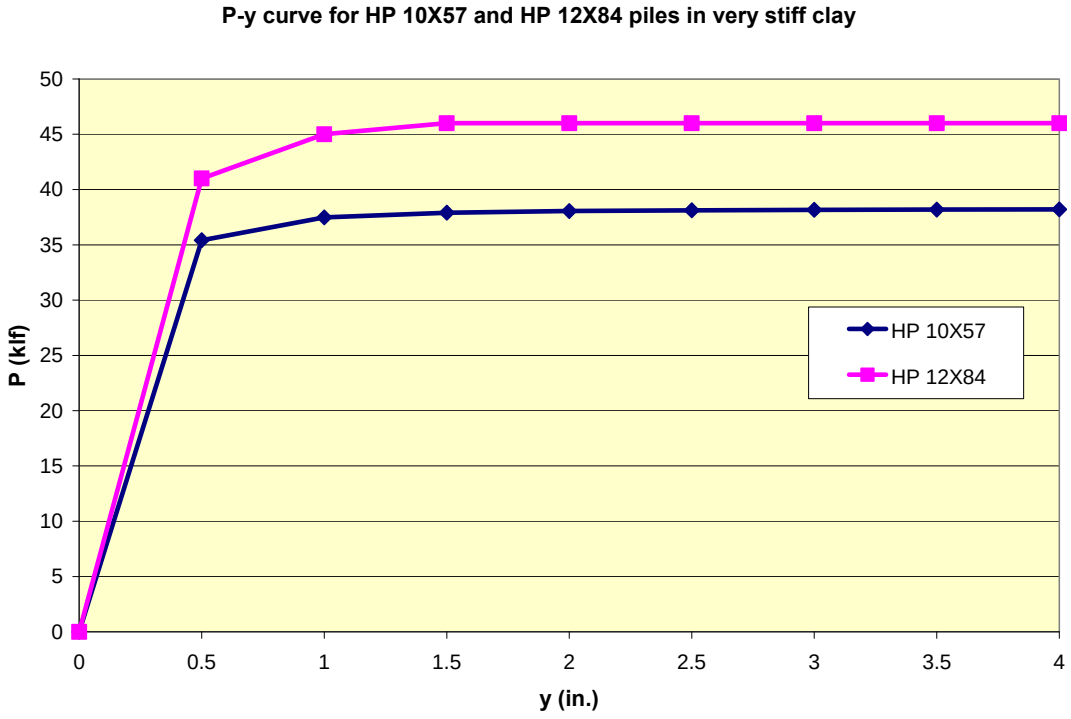

Figure 8-9 P-y curve for HP10X57 and HP12X84 piles in very stiff clay

For both f-z and q-z curves, the maximum value of displacement Z plotted correspond to ratio of Z/Zc=4 for both loose sand and very stiff clay. This amounts to 1.60" for loose sand and 1" for very stiff clay. A vertical displacement of magnitude Zc is the amount of movement needed to mobilize the maximum friction force f_{max} (f-z curves) and the maximum soil resistance at the pile tip q_{max} (q-z curves).

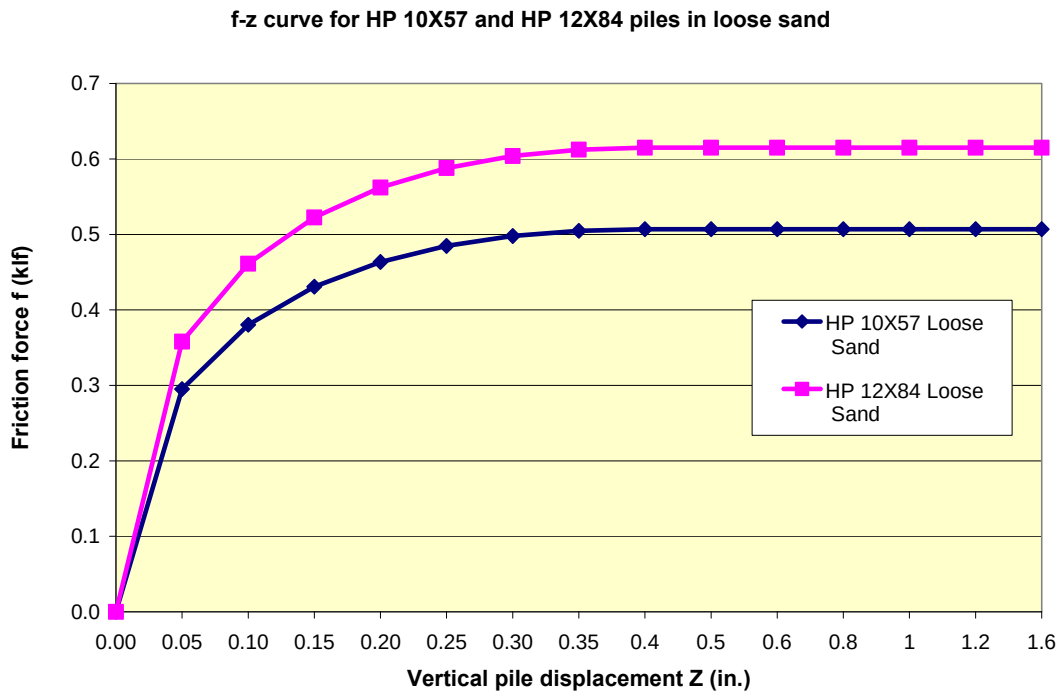

Figure 8-10 f-z curve for HP10X57 and HP12X84 piles in loose sand

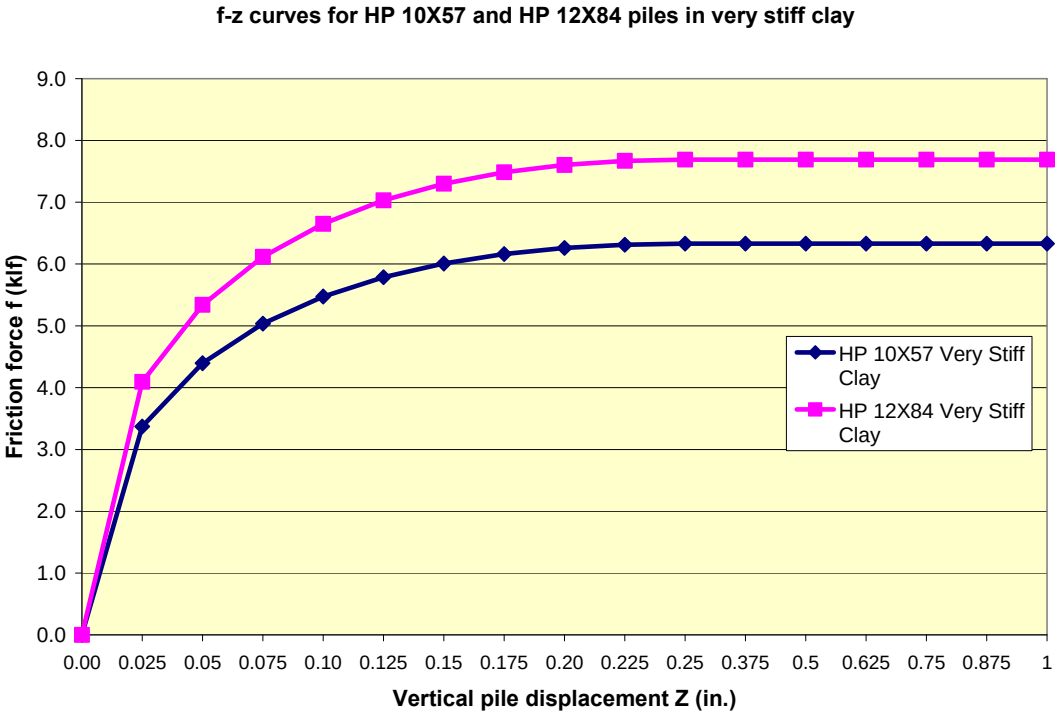

Figure 8-11 f-z curve for HP10X57 and HP12X84 piles in very stiff clay

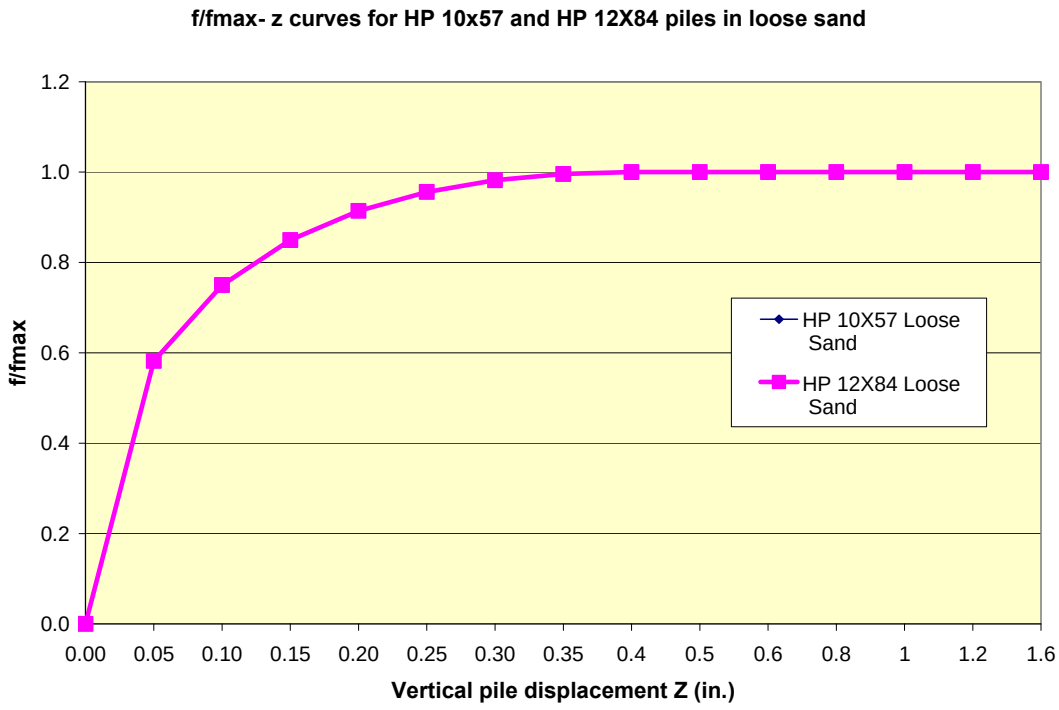

Figure 8-12 f/fmax - Z curve for HP10X57 and HP12X84 piles in loose sand

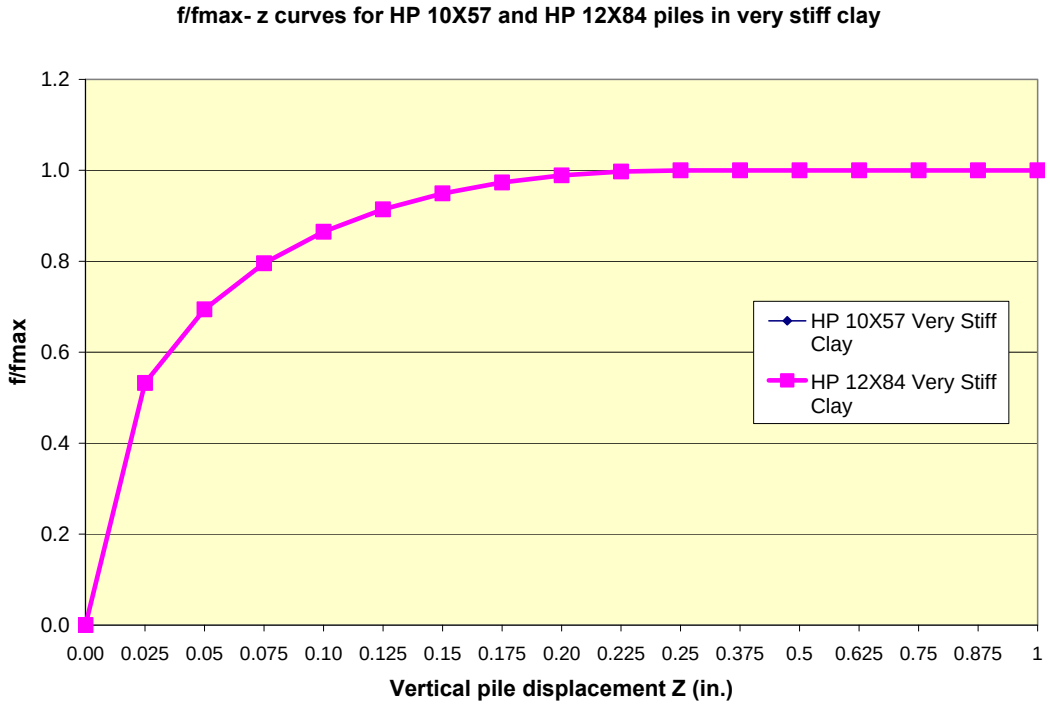

Figure 8-13 f/fmax - Z curve for HP10X57 and HP12X84 piles in very stiff clay

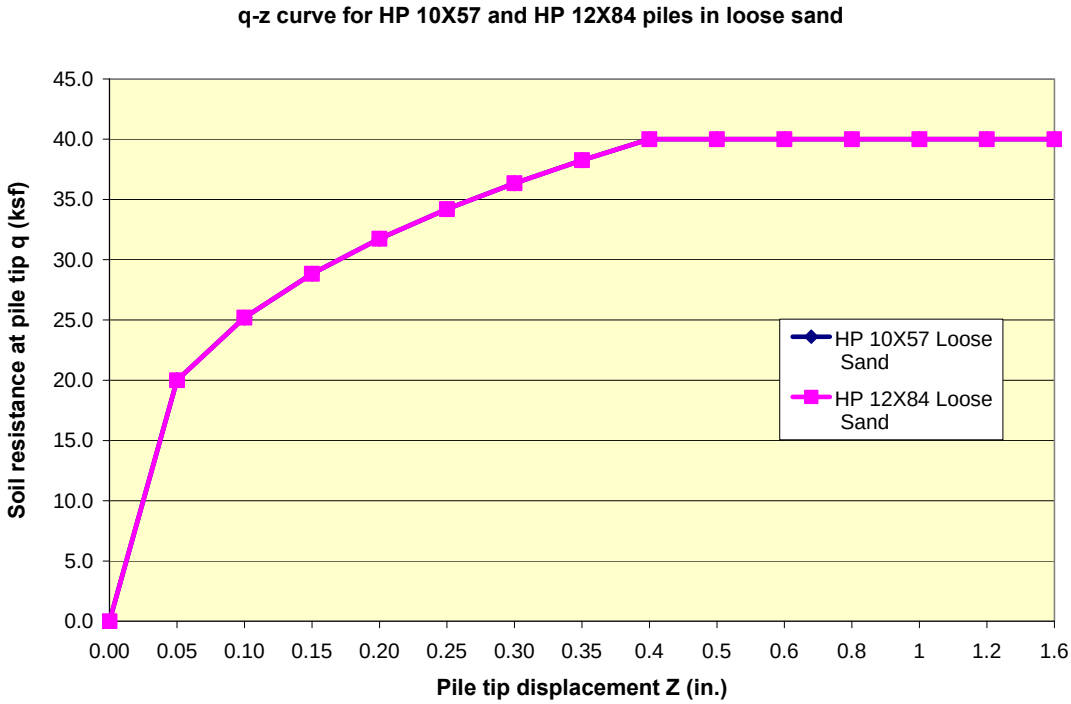

Figure 8-14 q-z curve for HP10X57 and HP12X84 piles in loose sand

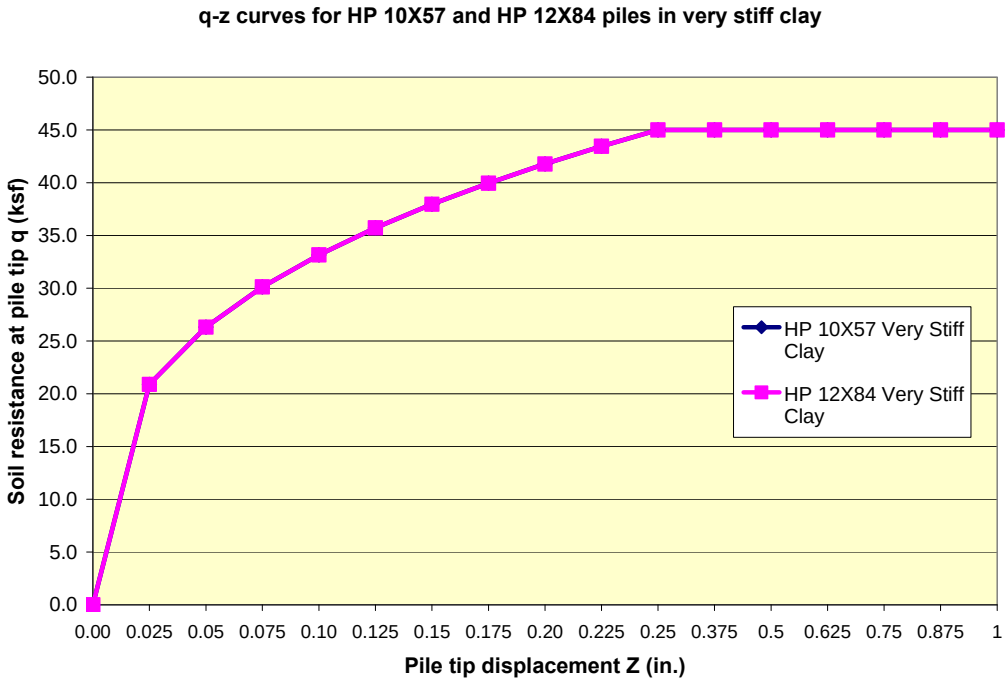

Figure 8-15 q-z curve for HP10X57 and HP12X84 piles in very stiff clay

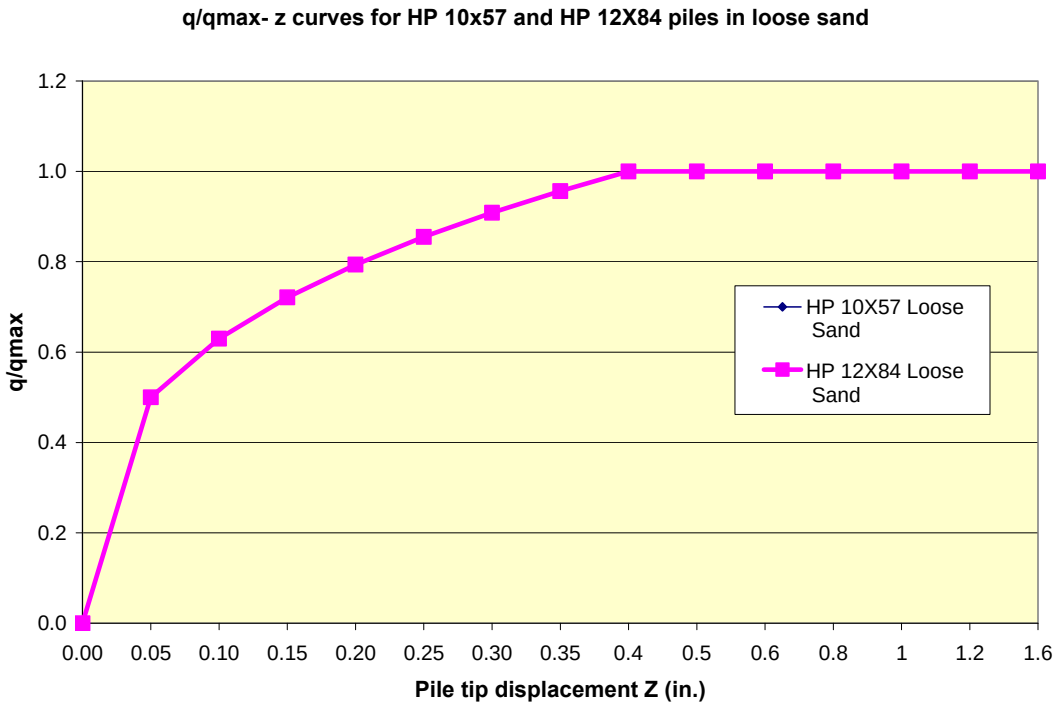

Figure 8-16 q/qmax - Z curve for HP10X57 and HP12X84 piles in loose sand

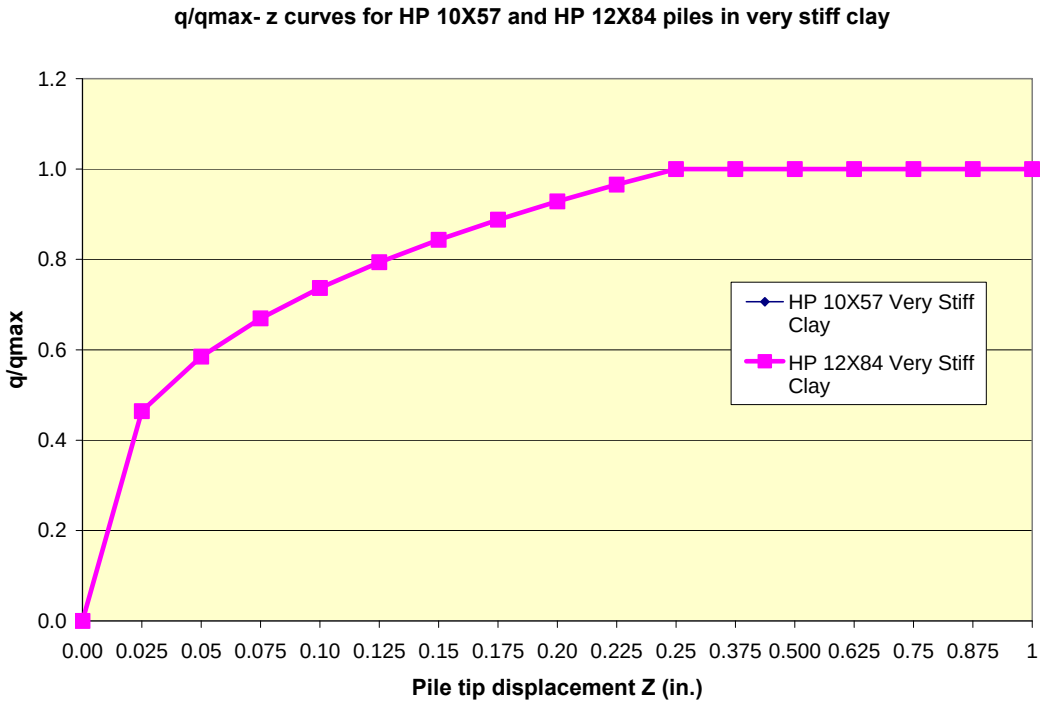

Figure 8-17 q/qmax - Z curve for HP10X57 and HP12X84 piles in very stiff clay

Chapter 9

Structural Modeling and Analysis

9.1. Introduction

Structural modeling is the mathematical representation of a structure. It includes geometry, boundary conditions, and loading. Structural analysis is the determination of displacements, stresses, strains, and forces induced in a structure under various load effects. Structural analysis is also the most common application of the finite element method. In fact, there are seven types of structural analyses available in ANSYS, which is the finite element analysis software used in this study.

This chapter elaborates on both the structural modeling as well as the types of structural analyses performed as part of the parametric studies for this research.

9.2. Finite Element Analysis Three-Dimensional Models

Considering the purpose of structural analysis, three-dimensional modeling is used in order to obtain the required level of response accuracy.

9.2.1 Modeling Approach

A series of three-dimensional models was created using the ANSYS finite element analysis software. The three-dimensional finite element models incorporate the entire bridge structure, which includes the bridge superstructure, substructure, foundation, and soil. Because only end bearing piles are used, the models are fixed at the base of the piles. The soil around the piles and behind the abutments and the wingwalls is modeled as nonlinear spring elements. Bridge piers are modeled as roller supports. This assumption is conservative for the estimation of abutment displacements and represents typical construction with the use of elastomeric bearings (Frosch et al. 2009). Model geometry and element properties are discussed in the following sections. Typical finite element models used in this study are shown in Figures 9-4 to 9-7.

9.2.2 Geometric Models

Geometric models are created using the information presented in chapter 6. This includes bridge length and width; number and length of spans; abutment shape and dimensions; wingwall shape and dimensions; girder shape, size, length, and spacing; and pile shape, size, length, and spacing.

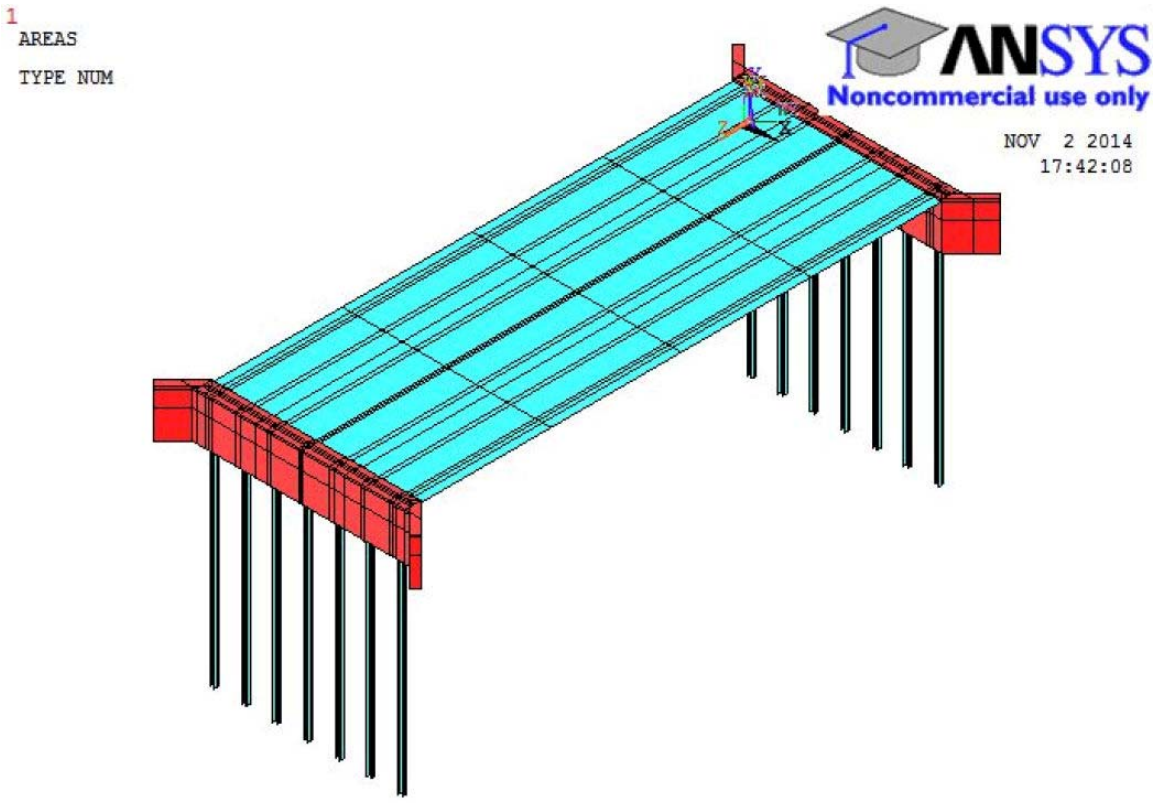

Figure 9-1 Geometric model of an integral abutment bridge with flared cantilever wingwalls

9.2.3 ANSYS Elements used in Structural Analyses

Table 9-1 illustrates the ANSYS elements used in the finite element analysis models. The description of the elements is covered in more detail in the "ANSYS Element Reference 2009".

Table 9-1 ANSYS elements used in the finite element analysis models

Element Type	Element Number	Description of Element	Shape
Beam	BEAM188	Structural 3-D 2-Node Beam 2 nodes 3-D space DOF: UX, UY, UZ, ROTX, ROTY, ROTZ	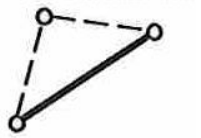
Solid	SOLID45	3-D Structural Solid 8 nodes 3-D space DOF: UX, UY, UZ	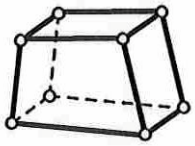
Solid	SOLID65	3-D Reinforced Concrete Structural Solid 8 nodes 3-D space DOF: UX, UY, UZ	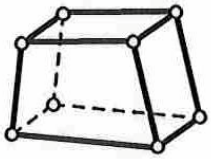
Link	LINK8	Structural 3-D Spar (or Truss) 2 nodes 3-D space DOF: UX, UY, UZ	
Multipoint Constraint Element	MPC184	Rigid beam with two nodes and six degrees of freedom at each node (UX, UY, UZ, ROTX, ROTY, ROTZ).	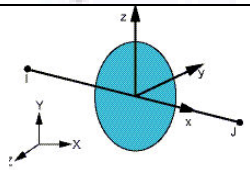
Shell	SHELL181	4-Node Structural Shell 4 nodes 3-D space DOF: UX, UY, UZ, ROTX, ROTY, ROTZ	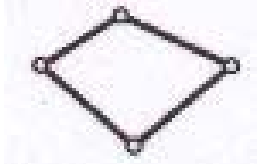
Combination	COMBIN39	Combination Nonlinear Spring 2 nodes 3-D space DOF: UX, UY, UZ, ROTX, ROTY, ROTZ PRES, TEMP	

BEAM188 is suitable for analysis of slender to moderately thick beam structures. The element is based on Timoshenko beam theory, which accounts for shear deformation effects. BEAM188 is a three-dimensional linear, quadratic, or cubic beam element. It has two nodes; each node has six degrees of freedom. The degrees of freedom at each node include translations in x, y, and z directions, and rotations about the x, y, and z directions. The element is well-suited for linear, large rotation, and/or large strain nonlinear applications. Elasticity, plasticity, creep, and other nonlinear material models are supported. A cross section associated with this element type can be a built-up section referencing more than one material; for example, an I-section made of three materials. It is worth pointing out that ANSYS beam elements are based either on the Bernoulli or Timoshenko beam theories. While bending stresses are accounted on both beam theories, shear stresses are only accounted in Timoshenko beam theory. As a result, Bernoulli beam elements exhibit a stiffer behavior, therefore less deflection, compared to Timoshenko beam elements.

SOLID45 is a three-dimensional brick (hexahedral) element used to model isotropic solid structures. The element is defined by eight nodes having three degrees of freedom at each node. The degrees of freedom at each node include translations in x, y, and z directions. Consequently, 24 nodal displacements and 24 nodal forces must be considered. The size of the stiffness matrix that relates the nodal displacement vector with the nodal forces vector is [24x24]. The element has plasticity, creep, stress stiffening, large deflection, and large strain capabilities.

SOLID65 is a nonlinear concrete element that is used in three-dimensional modeling with or without steel reinforcing bars. This element is specifically designed to handle reinforced or plain concrete behavior and is also capable of cracking in tension and crushing in compression. Thus, in concrete applications, the solid capability of the element is used to model the concrete while the rebar capability is available for modelling reinforcement behavior. This is accomplished by inputting the reinforcing volume ratio. The element is defined by eight nodes having three degrees of freedom at each node. The degrees of freedom at each node include translations in x, y, and z directions. Up to three different rebar specifications may be defined. The concrete element is similar to the SOLID45 element with the addition of special cracking and crushing capabilities. The most important aspect of this element is the treatment of nonlinear material properties. The concrete is capable of cracking in three orthogonal directions, crushing, plastic deformation, and creep. The rebars are capable of tension and compression, but not shear. They are also capable of plastic deformation and creep.

The multi-point constraint element MPC184 is used to model the composite action between the concrete deck and the steel girders. Multi-point constraint elements establish geometric relationships that have to be met by the displacements of certain nodes of the structure in order to avoid displacement incompatibility between elements.

LINK8 is used to model steel reinforcing bars. This is a three-dimensional spar element with two nodes. The degrees of freedom at each node include translations in x, y, and z directions. This element is capable of plasticity, creep, swelling, and stress stiffening effects.

SHELL181 is one of the newest ANSYS elements. It offers state-of-the-art element technology be it linear or nonlinear analysis with emphasis on ease of use. It is suitable for analysis of thin to moderately thick shell structures. The element has 4 nodes; each node has six degrees of freedom. The degrees of freedom at each node include translations in x, y, and z directions, and rotations about the x, y, and z axes. SHELL181 is well-suited for linear, large rotation, and/or large strain nonlinear applications. Change in shell thickness is accounted for in nonlinear analyses.

COMBIN39 is a unidirectional nonlinear spring element with a nonlinear force-deflection capability that can be used in different types of analysis. The element has longitudinal or torsional capability in 1-D, 2-D, or 3-D applications. Consequently, it behaves as either an axial spring or a rotational spring. The use of the nonlinear COMBIN39 spring element is appropriate for this study because the behavior of both the backfill and foundation soils is nonlinear in nature. In addition, temperature loading induces significant abutment and pile lateral displacements.

Table 9-2 ANSYS elements' representation of bridge structural elements

Bridge Structural Elements and boundary conditions	ANSYS Element
Deck slab	SHELL181
Steel girders	BEAM188
Connection of deck slab to steel girder	MPC184
Abutment	SOLID45 SOLID65 is used in nonlinear concrete model LINK8 is used to model steel reinforcing bars in nonlinear concrete model
Steel Piles	SHELL181
Wingwall	SOLID45 SOLID65 is used in nonlinear concrete model LINK8 is used to model steel reinforcing bars in nonlinear concrete model
Soil-pile interaction	COMBIN39
Soil-structure (abutment/wingwall) interaction	COMBIN39

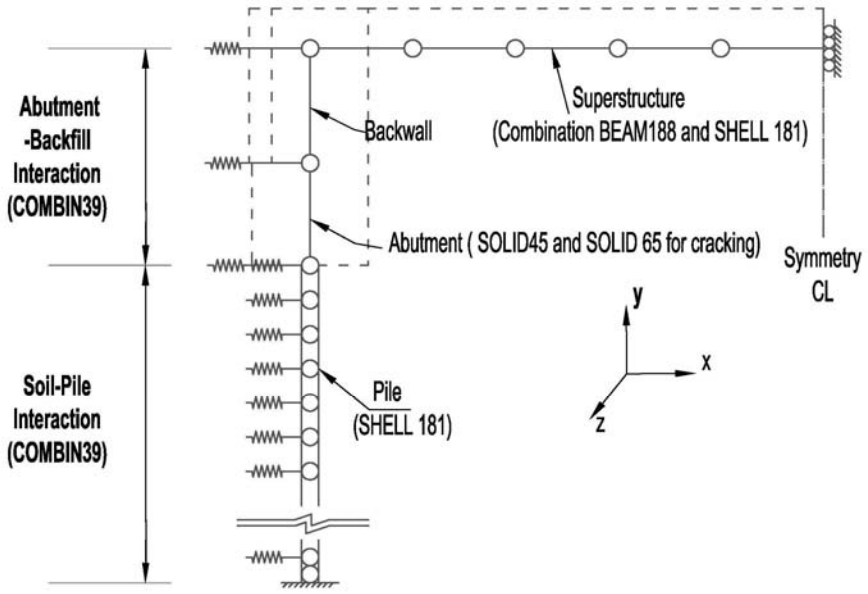

Figure 9-2 Schematic of integral abutment bridge finite element analysis model

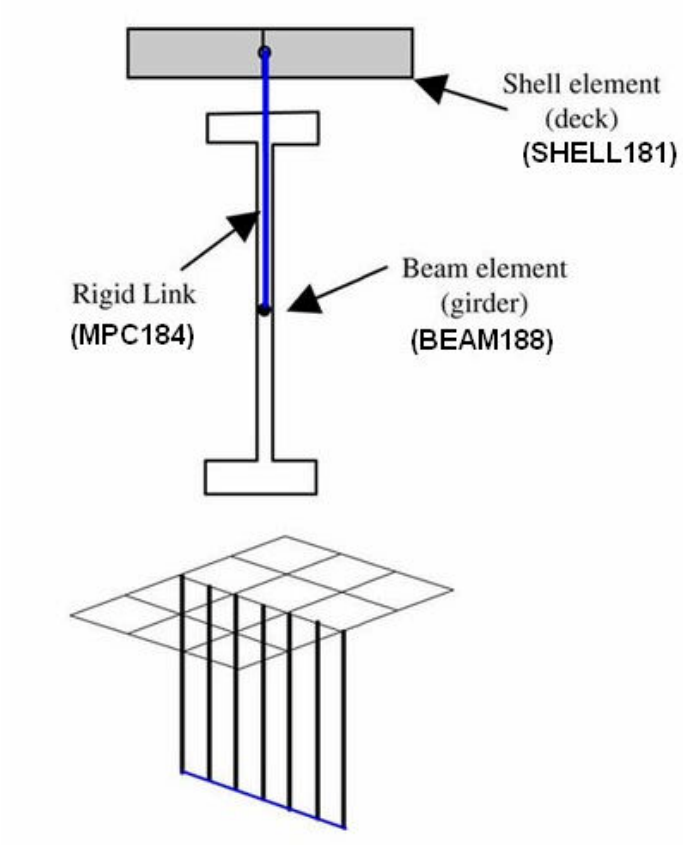

Figure 9-3 Schematic of connection of steel girder to deck slab (Chung and Sotelino 2006)

9.2.4 Element Size

As an initial step, a finite element analysis requires meshing of the model. In other words, the model is divided into a number of small elements, and after loading, stress and strain are calculated at integration points of these small elements (Bathe 1996). An important step in finite element modeling is the selection of the mesh density. A convergence of results is obtained when an adequate number of elements is used in a model.The element sizes used in all ANSYS finite element models of this study are summarized in Table 9-3

Table 9-3 Element size of structural elements in ANSYS models

Structural Element	Element Size (inches)
Deck slab	12
Abutment	6
Wingwall	6
Piles	3

The structures analyzed as part of this study varied widely in size ranging from a 100-feet-long bridge without cantilever wingwalls to a 1200-feet-long bridge with 24-feet long cantilever wingwalls. The size of the finite element models of these structures is expressed in terms of number of nodes and elements and is shown in Table 9-4. Please note that taking advantage of the symmetry of the bridge, half of the entire bridge was used for the ANSYS nonlinear concrete models in order to reduce CPU time.

Table 9-4 Size of smallest and largest ANSYS finite element models

Model Size	100-feet-long Bridge without Cantilever Wingwalls	1200-feet-long Bridge with 24-feet-long Cantilever Wingwalls
Number of Nodes	73,993	238,919
Number of Elements	65,315	215,203

9.2.5 Finite Element Models

Figures 9-4 to 9-11 show the view of the finite element models constructed as part of the structural analysis. This includes a model with no cantilever wingwalls (Figure 9-4) as well as models with inline, flared, and U-shaped cantilever wingwalls (Figures 9-5, 9-6, and 9-7). In addition, Figures 9-8 to 9-11 present views of the deck slab and girders' finite element mesh (Figure 9-8), pile finite element mesh (Figure 9-9),soil-structure and soil-pile interaction (Figure 9-10), and temperature load during thermal expansion (Figure 9-11).

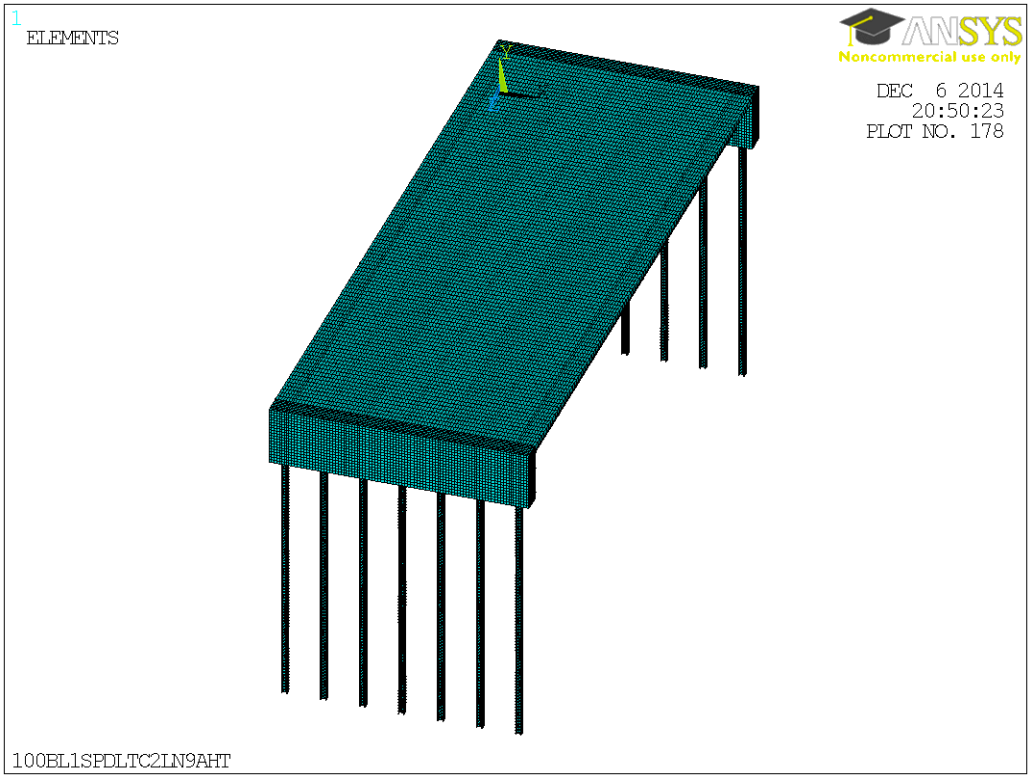

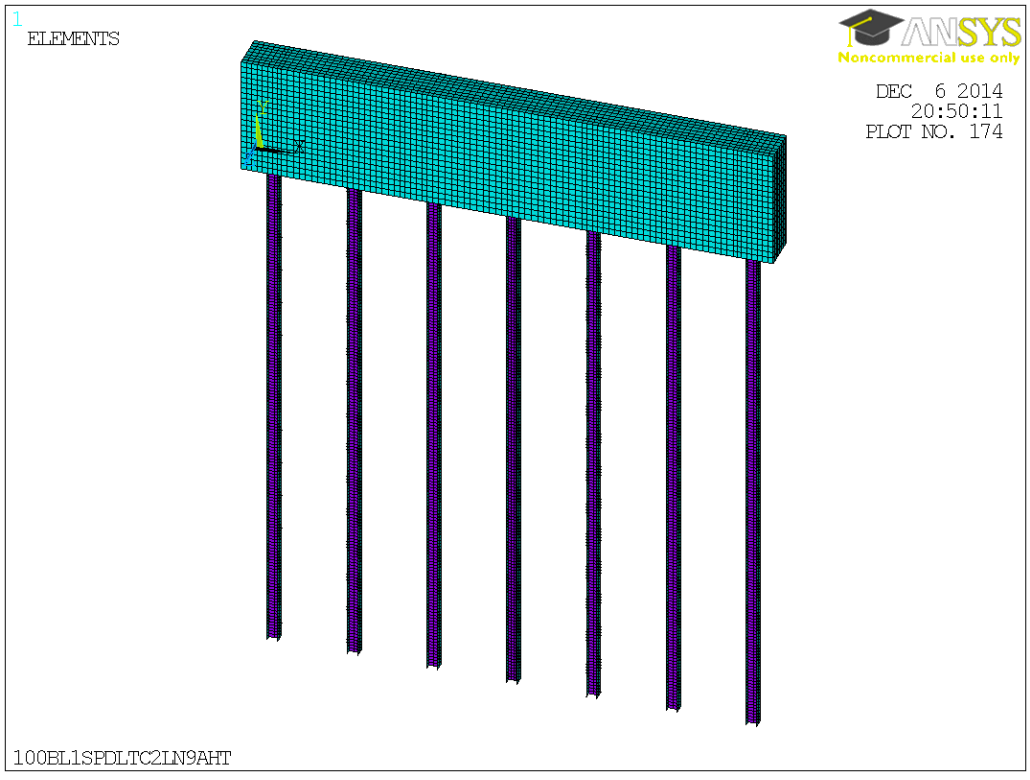

Figure 9-4 Finite element model of an integral abutment bridge with no cantilever wingwalls

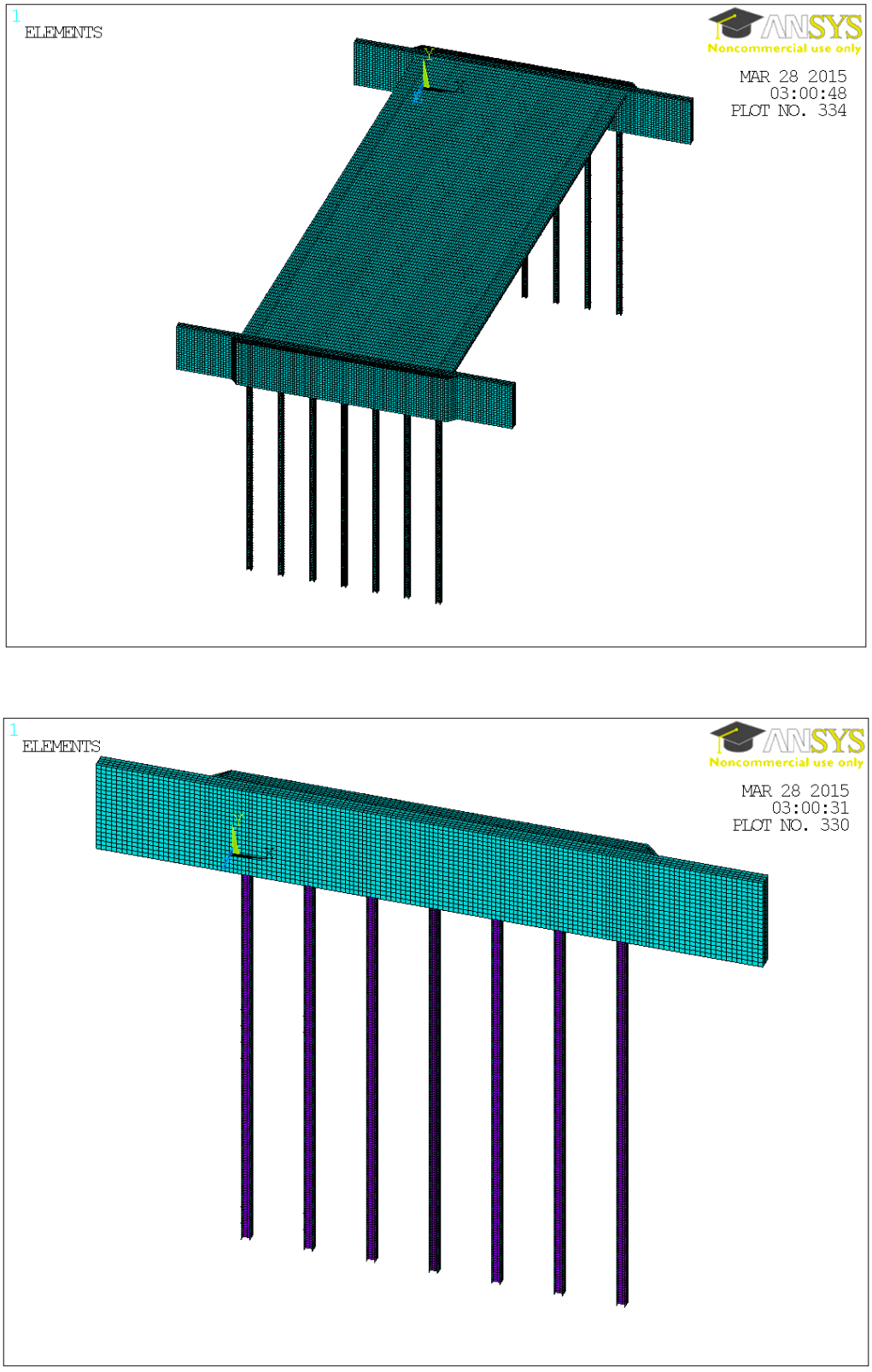

Figure 9-5 Finite element model of an integral abutment bridge with inline cantilever wingwalls

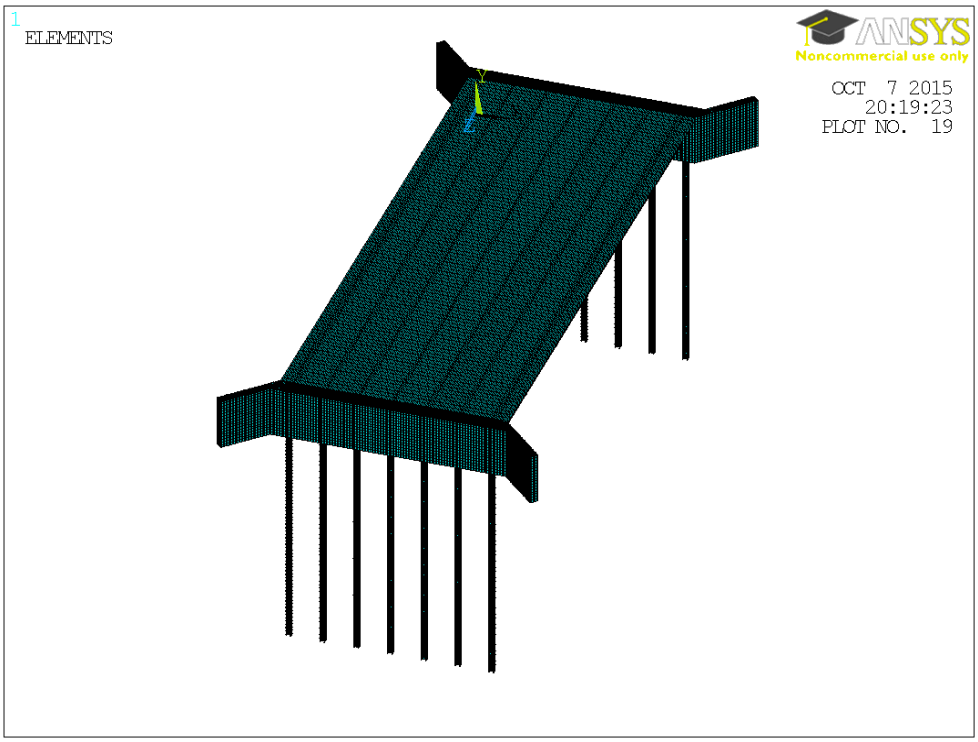

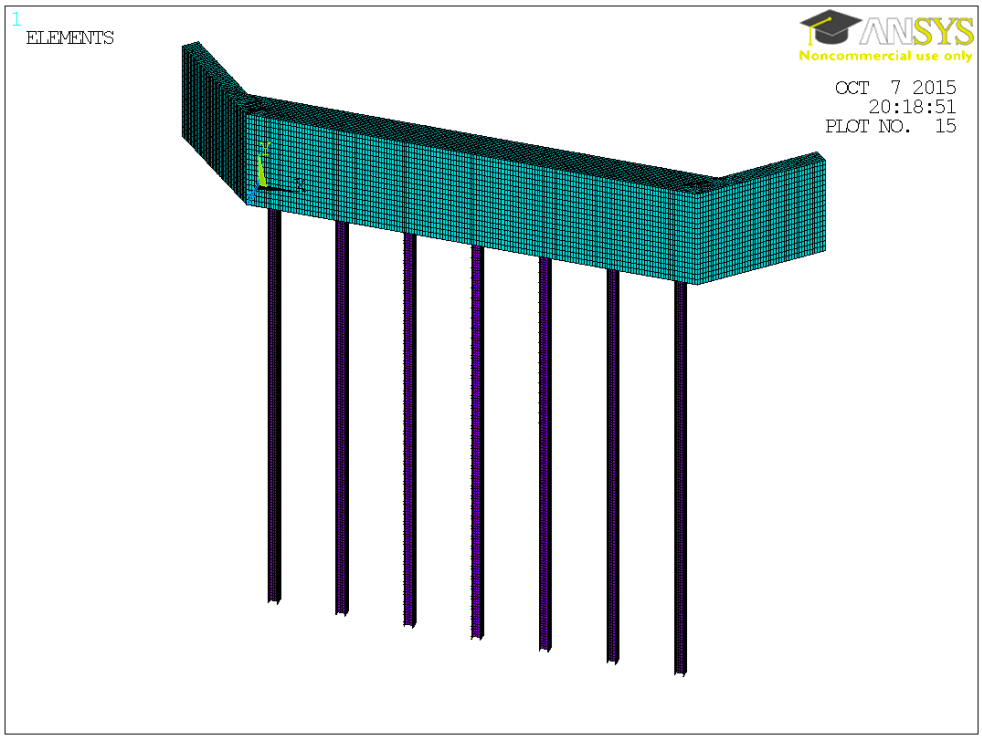

Figure 9-6 Finite element model of an integral abutment bridge with flared cantilever wingwalls at 45 degrees

Figure 9-7 Finite element model of an integral abutment bridge with U-shaped cantilever wingwalls

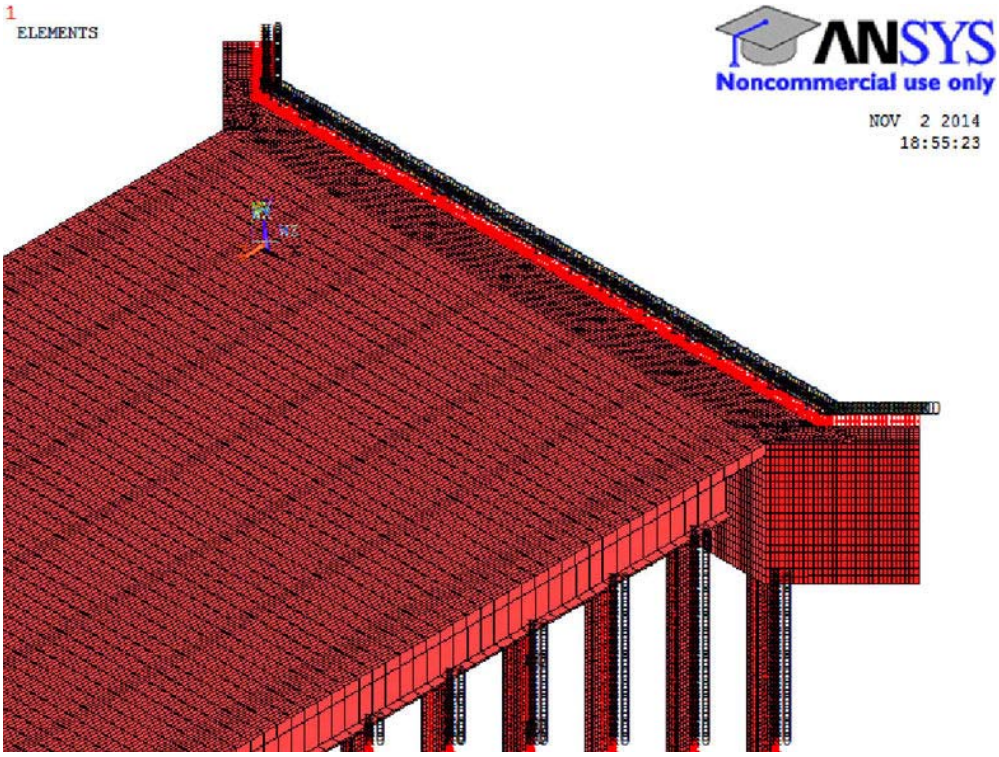

Figure 9-8 View of deck slab and steel girders' finite element mesh

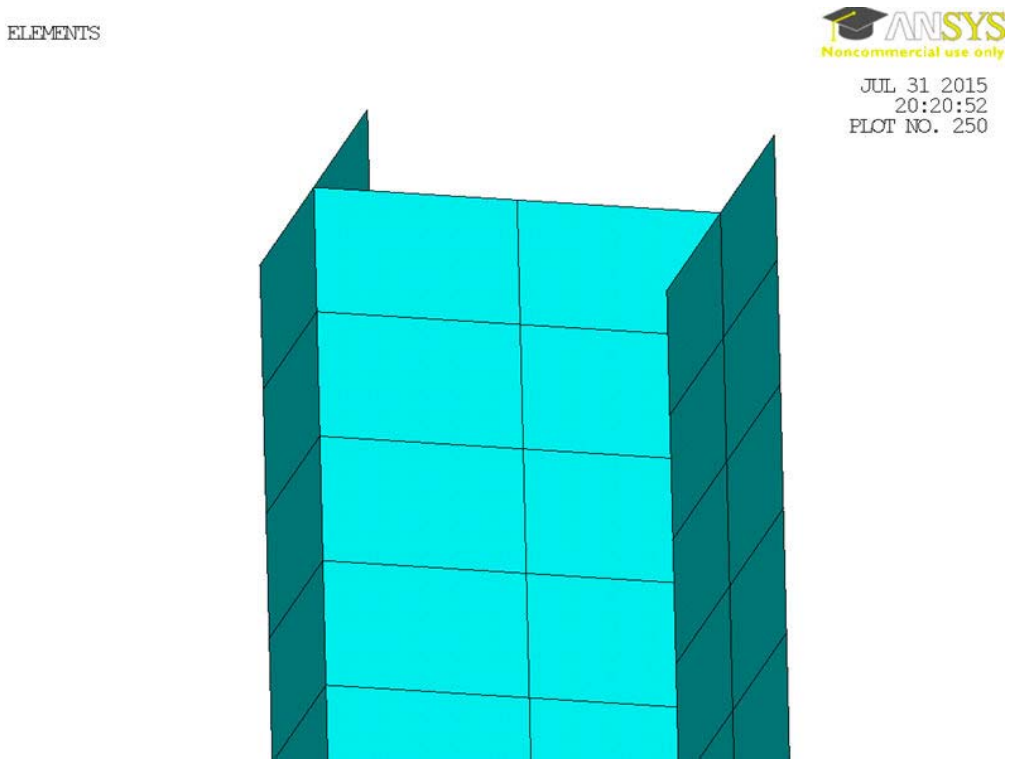

Figure 9-9 View of pile finite element mesh

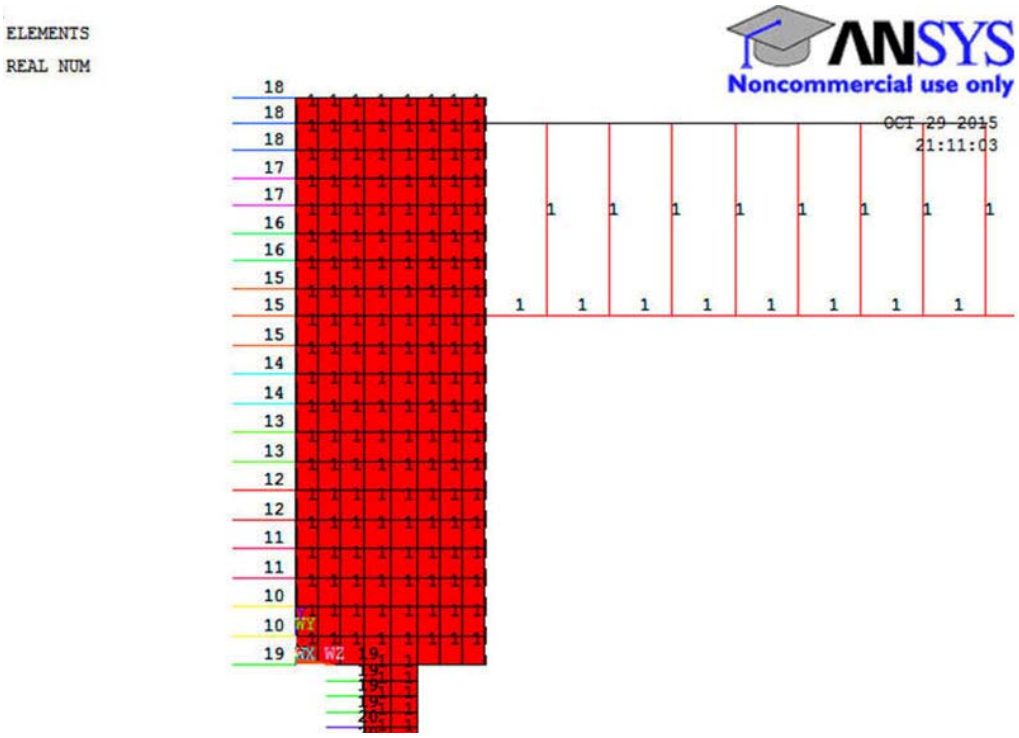

Figure 9-10 View of soil-structure and soil-pile interaction

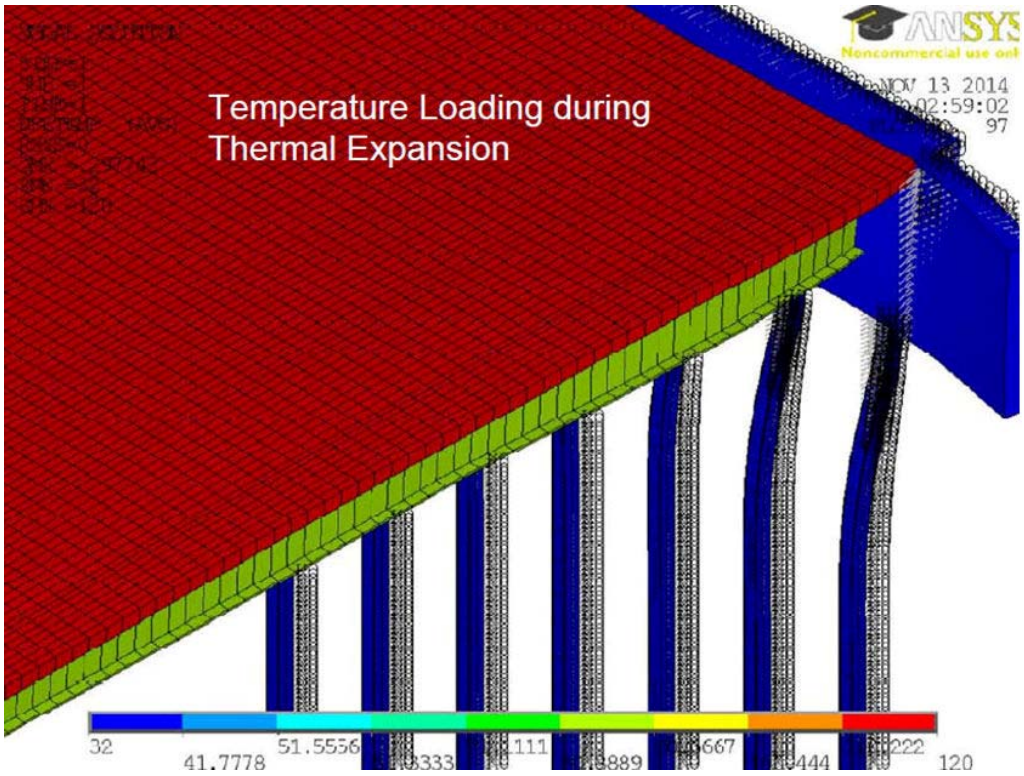

Figure 9-11 View of temperature load during thermal expansion

9.3. Structural and Material Modeling

The structural elements of the bridge are modeled as linear elements while the soil adjacent to the piles and behind the abutments and wingwalls is modeled as nonlinear springs. This is a condensed description of the three-dimensional model of a 2-lane bridge:

- The superstructure consists of a concrete slab in composite action with five steel girders spaced at 8'-6" and cross frames spaced at 25 feet.

- The deck slab is modeled using shell elements and the steel girders as beam elements. The intermediate piers are treated as roller supports.

- The integral abutments and cantilever wingwalls are modeled using solid elements. The soil behind the abutments and wingwalls as well as around the piles is modeled as nonlinear springs.

- Seven steel piles spaced at 6 feet with full fixity are connected to each integral abutment allowing full moment transfer. Piles are modeled using shell elements with common node for pile and the abutment wall.

For the case of 4-lane bridges, the bridge model includes seven steel girders spaced at 9'-6" and eleven steel piles spaced at 6 feet.

The analysis is performed using the ANSYS Release 13 Mechanical APDL to create input files. APDL stands for ANSYS Parametric Design Language, a scripting language that allows users to parameterize the model and automate tasks.

9.4. Nonlinear Structural Analysis - Plasticity Model

Nonlinear structural analysis for the piles is warranted once the stresses in the piles exceed the yield strength of the material. This is accomplished using the appropriate plasticity material model in ANSYS to describe the nonlinear material behavior. The selection of the appropriate material model requires familiarity with the basics of plasticity including:

- Selection of strain-rate-independent versus rate-dependent models
- Selection of yield criterion
- Selection of hardening rule

9.4.1. Plasticity Model Theory

When a ductile material experiences stresses beyond the elastic limit, it will yield, acquiring large permanent deformations. Plasticity refers to the elastoplastic behavior of a material that has been loaded beyond its yield strength. Such material would remain permanently deformed after unloading. Plasticity can further be described as rate independent or rate dependent. Rate independent means plastic strain is assumed to develop instantaneously, that is, independent of time.

Plasticity theory provides a mathematical relationship that characterizes the elastoplastic response of materials. There are three ingredients in the rate-independent plasticity theory: the yield criterion, flow rule, and the hardening rule.

9.4.1.1. Rate-Independent Plasticity

If the material response is not dependent on the rate of loading or deformation, the material is said to be rate-independent. Most metals exhibit rate-independent behavior at temperatures below half of the metal's melting-point temperature (Ramanan 2006) - the melting point temperature of low carbon steel (defined as carbon content equal to or less than 0.20 percent) is 2700°F.

Rate-independent plasticity is characterized by the irreversible straining that occurs in a material once a certain level of stress is reached. The plastic strains are assumed to develop instantaneously, that is, independent of time. Several options are available to characterize different types of material behaviors:

a) Bilinear Kinematic Hardening (BKIN)
b) Multilinear Kinematic Hardening (MKIN)
c) Bilinear Isotropic Hardening (BISO)
d) Multilinear Isotropic Hardening (MISO)
e) Anisotropic (ANISO)
f) Drucker-Prager (DP)

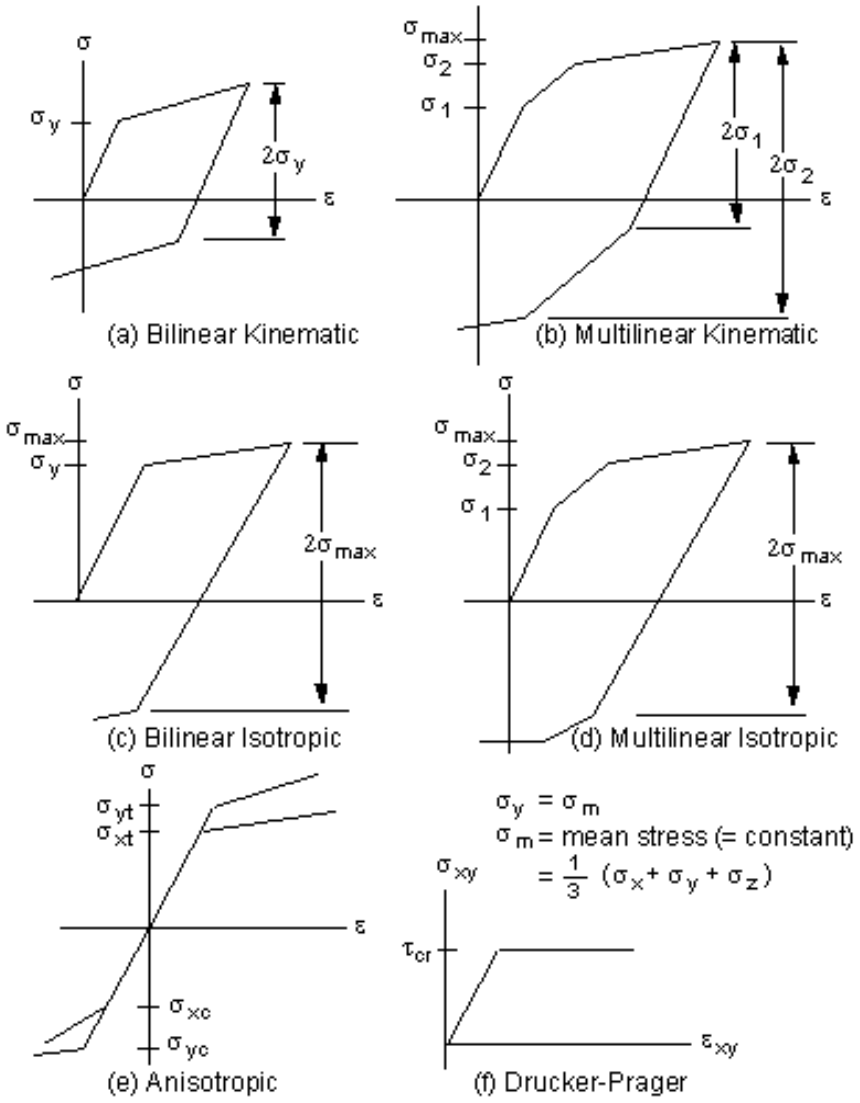

Figure 9-12 Stress-strain behavior of each of the plasticity options (ANSYS Mechanical APDL and Mechanical Applications Theory Reference 2010)

9.4.1.2. Yield Criterion

The yield criterion determines the stress level at which yielding of a material is initiated. Yield criterion does not imply failure; the essence of yielding in piles, if experienced, it is a way of accommodating thermal displacements without resorting to other means such as expansion joints.

Determination of plastic deformation, that is, yielding, in a simple bar loaded with a uniaxial tensile load is only a matter of calculating the uniaxial stress and comparing it with the yield strength of the material. In contrast, in an elastic body that is subject to a system of loads in three dimensions, a complex three-dimensional system of stresses is developed. At any point within the body there are stresses acting in different directions, and the direction and magnitude of stresses changes from point to point. These stresses are called principal stresses and can be calculated at any point. Von Mises found that, even though none of the principal stresses exceeds the yield stress of the material, it is possible for yielding to result from the combination of stresses. The von Mises criterion is a formula for combining these three stresses into an equivalent stress, which is then compared to the yield stress of the material. The equivalent stress is called the von Mises equivalent stress and when its magnitude exceeds the yield stress, yielding occurs. The mathematical derivation of the von Mises equivalent stress is illustrated below:

Any state of stress can be decomposed into a hydrostatic (or mean) stress σ_m and a deviatoric stress s, according to

$$\begin{bmatrix} \sigma_{11} & \sigma_{12} & \sigma_{13} \\ \sigma_{21} & \sigma_{22} & \sigma_{23} \\ \sigma_{31} & \sigma_{32} & \sigma_{33} \end{bmatrix} = \begin{bmatrix} \sigma_m & 0 & 0 \\ 0 & \sigma_m & 0 \\ 0 & 0 & \sigma_m \end{bmatrix} + \begin{bmatrix} s_{11} & s_{12} & s_{13} \\ s_{21} & s_{22} & s_{23} \\ s_{31} & s_{32} & s_{33} \end{bmatrix}$$

where hydrostatic or mean stress σ_m is the average of the three principal stresses $\sigma_1, \sigma_2, \sigma_3$

$$\sigma_m = \frac{\sigma_{11} + \sigma_{22} + \sigma_{33}}{3}$$

The plastic behavior of materials is often independent of a hydrostatic stress and this feature necessitates the study of the deviatoric stress. Since the hydrostatic stress remains unchanged with a change of coordinate system, the principal directions of stress coincide with the principal directions of the deviatoric stress, and the decomposition can be expressed with respect to the principal directions as

$$\begin{bmatrix} \sigma_1 & 0 & 0 \\ 0 & \sigma_2 & 0 \\ 0 & 0 & \sigma_3 \end{bmatrix} = \begin{bmatrix} \sigma_m & 0 & 0 \\ 0 & \sigma_m & 0 \\ 0 & 0 & \sigma_m \end{bmatrix} + \begin{bmatrix} s_1 & 0 & 0 \\ 0 & s_2 & 0 \\ 0 & 0 & s_3 \end{bmatrix}$$

Consequently, the second invariant of the deviatoric stress can be expressed either as

$$J_2 = \tfrac{1}{2}\left(s_1^2 + s_2^2 + s_3^2\right)$$

or in terms of principal stresses as

$$J_2 = \frac{1}{6}\left[(\sigma_1 - \sigma_2)^2 + (\sigma_2 - \sigma_3)^2 + (\sigma_3 - \sigma_1)^2\right]$$

The yield criterion determines the stress level at which yielding is initiated. For multi-component stresses, this is represented as a function of the individual components, which can be interpreted as an equivalent stress σ_e. When the equivalent stress is equal to a material yield stress σ_y, the material will develop plastic strains.

The von Mises equivalent stress is defined as $\sigma_e = \sigma_y$ where

$$\sigma_e = \sqrt{3J_2}$$

Therefore, $3J_2 = (\sigma_e)^2$

$2(\sigma_e)^2 = 6J_2$ where J_2 is given in the expression in the previous page.

The von Mises equivalent stress σ_e derived as

$$\sigma_e = \sqrt{\frac{1}{2}\left[(\sigma_1 - \sigma_2)^2 + (\sigma_2 - \sigma_3)^2 + (\sigma_3 - \sigma_1)^2\right]}$$

When von Mises equivalent stress σ_e exceeds the uniaxial material yield strength σ_y, general yielding will occur.

If plotted in three-dimensional principal stress space, the von Mises yield surface is a circular cylinder. The figure shows that the cylinder is aligned with the axis $\sigma_1 = \sigma_2 = \sigma_3$. It means that only stresses that deviate from this axis contribute to the von Mises stress calculation.

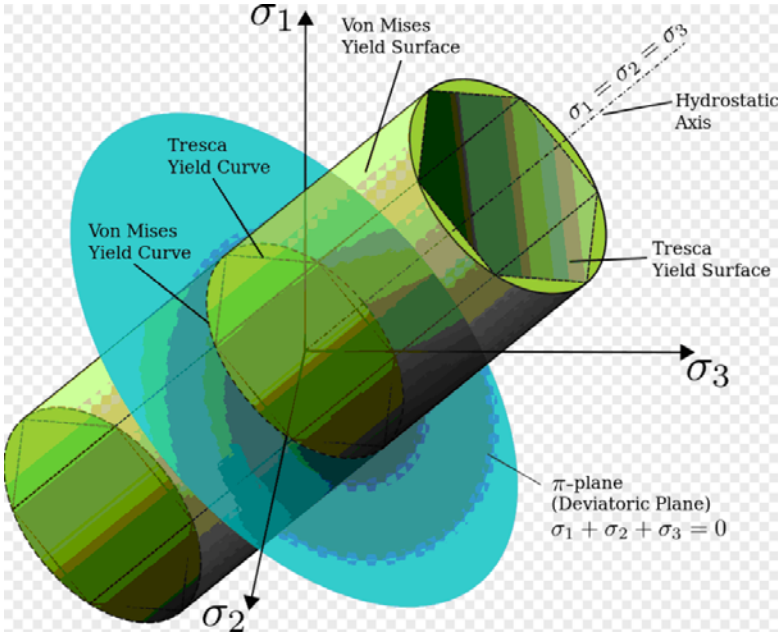

Figure 9-13 Von Mises criterion for different stress conditions (Wikipedia)

Figure 9-14 also shows Tresca's maximum shear stress criterion (dashed line). Tresca's yield surface is circumscribed by von Mises's meaning that it predicts plastic yielding already for stress states that are still elastic according to the von Mises criterion. This implies that as a model for plastic material behavior, Tresca's criterion is more conservative than von Mises's criterion. In fact, according to Ansys.net Newsletter (2002), the Tresca criterion is, at most, about 15 percent more conservative than the von Mises criterion.

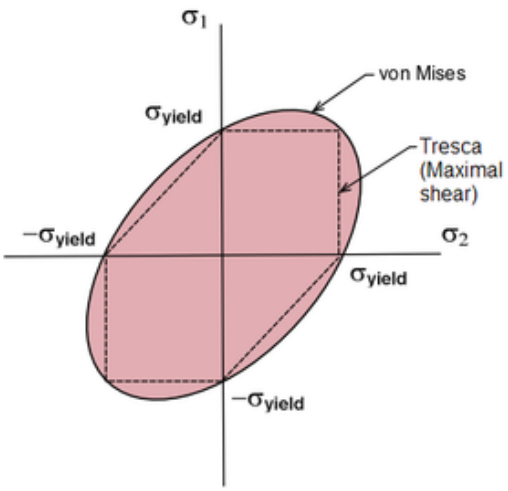

Figure 9-14 Comparison between Von Mises and Tresca criteria (Wikipedia)

9.4.1.3. Flow Rule

Flow rule, also known as plastic straining, states that the movement of the yield surface is directly dependent on the plastic strain increment (ANSYS Mechanical APDL and Mechanical Applications Theory Reference 2010).

The plastic strain increment is obtained by multiplying the plastic multiplier with the plastic potential gradient as shown in the equation

$$d\epsilon^{PL} = \lambda\{\frac{\partial Q}{\partial \sigma}\}$$

where:

ϵ^{PL} = plastic strain
λ = plastic multiplier
Q = plastic potential
σ = stress

The plastic multiplier indicates the magnitude of plastic deformation and it changes with loading. The plastic potential gradient indicates the direction of plastic straining. The plastic potential gradient indicates the direction of plastic straining

In associative flow rule, which is the type of flow rule pertaining to bilinear isotropic hardening behavior, the plastic potential gradient is normal to the yield surface. Since plastic potential gradient is directional, thus the plastic strain increment is also normal to the yield surface.

9.4.1.4. Hardening Rule

Plasticity occurs after a material has yielded. For the one-dimensional case, yielding happens at a single value of stress known as the yield stress. For more complex stress states, the von Mises criterion, is commonly used to compared with the uniaxial yield stress. Regardless of the method used, the singular valued uniaxial yield strength becomes a yield curve in the two-dimensional case and a yield surface in the three-dimensional case.

The hardening rule describes how the yield surface changes in shape as yielding occurs. The hardening rule also determines when the material will yield again if the loading is continued or reversed. There are two basic hardening rules to prescribe the modification of the yield surface:

- Isotropic hardening: the yield surface size changes, but the center axis and the general shape of the yield surface do not change (Figure 9-15). Isotropic hardening is used for large-strain analyses of metals, but is not meant for cyclic loading.

- Kinematic hardening: The yield surface remains constant in size and translates in the direction of yielding (Figure 9-17). Unlike isotropic hardening, kinematic hardening is used for small-strain applications and is meant for cyclic loading.

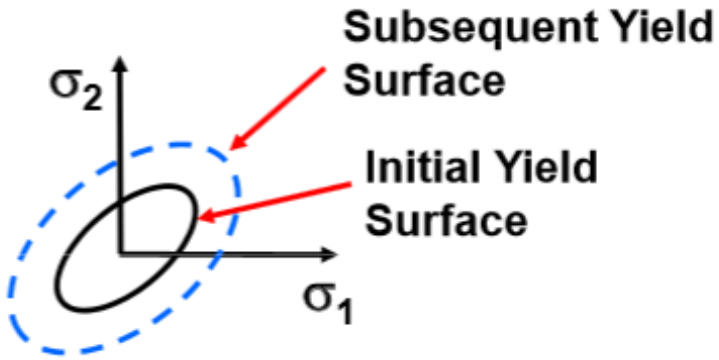

Figure 9-15 Isotropic hardening rule (ANSYS Training Material 2010)

The stress-strain behavior for isotropic hardening is shown in Figure 9-16. The figure enables an understanding of what occurs during a loading and reverse loading cycle. It shows that the subsequent yield in compression is equal to the highest stress attained during the tensile phase. In other words, the compressive and tensile yield strengths are increasing together by the same amount.

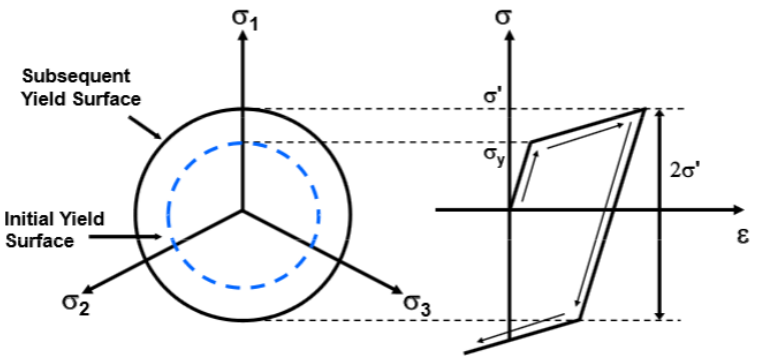

Figure 9-16 Stress-strain diagram of isotropic hardening behavior (ANSYS Training Material 2010)

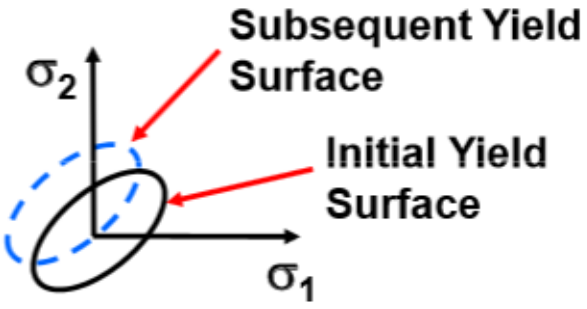

Figure 9-17 Kinematic hardening rule (ANSYS Training Material 2010)

The stress-strain behavior for kinematic hardening is shown in Figure 9-18. The figure shows that the subsequent yield in compression is decreased by the amount that the yield stress in tension increased, so that a $2\sigma_y$ difference between the yields is always maintained. In other words, the sum of the compressive and tensile yield strengths is constant.

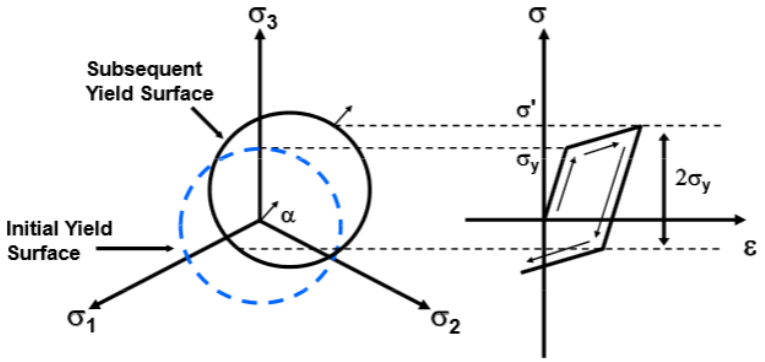

Figure 9-18 Stress-strain diagram of kinematic hardening behavior (ANSYS Training Material 2010)

The primary differences in isotropic and kinematic hardening material model are summarized and tabulated in Table 9-5

Table 9-5 Differences between isotropic and kinematic hardening

Isotropic Hardening	Kinematic Hardening
Yield surface grows equally in all directions and remains centered about its initial location as the material hardens	Yield surface remains constant in size and shifts in location
Absolute value of compressive yield surface is always equal to tensile yield stress	If a specimen is first loaded and deformed in uniform tension, then the load is removed and the specimen is loaded in compression, the compressive yield stress will be less than the initial tensile yield stress.
Recommended for large-strain analyses of metals (greater than 5 to 10 percent of true strain)	Recommended for small-strain analyses of metals
Recommended for proportional, non-cyclic loading	Recommended for non-proportional cyclic loading

In conclusion, the choice of hardening law, yield criterion, and stress-strain curve representation is dependent on the material used and expected loading conditions. As long as the constitutive model adequately describes the material within the strain range of interest that constitutive model should provide useful results in simulation.

9.4.2. Modeling of Plasticity in ANSYS for this study

The plasticity behavior of the piles has been simplified into a bilinear isotropic hardening behavior with the use of ANSYS capabilities. Studying it in ANSYS is much like a transient problem.

- Instead of time steps, used load steps
- Used elements that support plasticity
- Defined stress-strain curve

9.4.2.1. Definition of elastic material properties

- Structural
- Linear
- Elastic
- Isotropic
  - Elastic modulus (see Table 6-1)
  - Poisson's ratio (see Table 6-1)
  - Coefficient of thermal expansion (see Table 6-1)

9.4.2.2. Definition of plastic parameters

- Structural
- Nonlinear
- Inelastic
- Rate Independent
- Isotropic hardening plasticity
- Von Mises plasticity
- Bilinear isotropic hardening

  Yield stress σ_y (see Table 6-1)

  Tangent modulus E_T (see Appendix C)

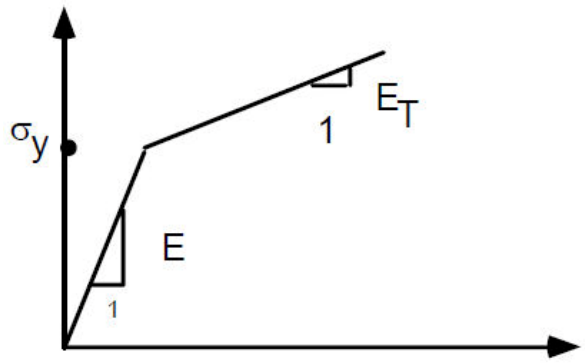

Figure 9-19 Definition of bilinear isotropic hardening material in ANSYS

9.4.2.3. Nonlinear Solution

ANSYS employs the "Newton-Raphson" approach to solve nonlinear problems. In this approach, the total load applied to a finite element model is subdivided into a series of load increments. The load increments are applied over several load steps.

Prior to each solution, the Newton-Raphson method evaluates the out-of-balance load vector, which is the difference between the restoring forces (the loads corresponding to the element stresses) and the applied loads. The program then performs a linear solution, using the out-of-balance loads, and checks for convergence. If convergence criteria are not satisfied, the out-of-balance load vector is re-evaluated, the stiffness matrix is updated, and a new solution is obtained. This iterative procedure continues until the problem converges (ANSYS Mechanical APDL Structural Analysis Guide 2010).

The arc-length method causes the Newton-Raphson equilibrium iterations to converge along an arc, thereby often preventing divergence, even when the slope of the load versus deflection curve becomes zero or negative. This iteration method is represented schematically in Figure 9-20

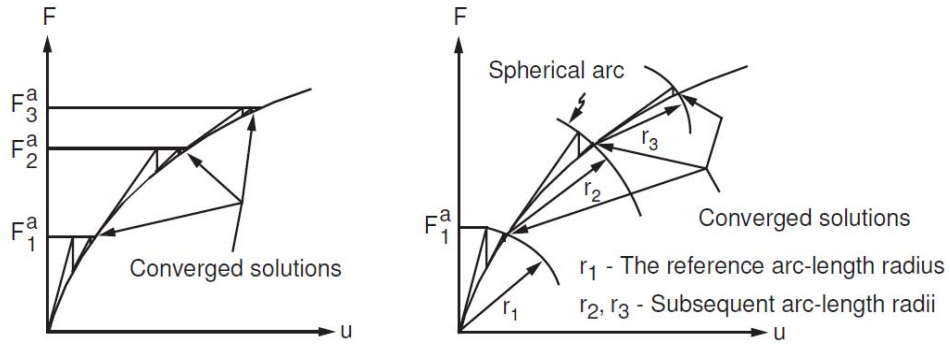

Figure 9-20 Traditional Newton-Raphson Method versus Arc-Length Method (ANSYS Mechanical APDL Structural Analysis Guide 2010)

In conclusion, a nonlinear analysis is organized into three levels of operation:

- The "top" level consists of the load steps that you define explicitly over a "time" span. Loads are assumed to vary linearly within load steps for static analyses.
- Within each load step, you can direct the program to perform several solutions (substeps or time steps) to apply the load gradually.
- At each substep, the program performs a number of equilibrium iterations to obtain a converged solution.

Figure 9-21 illustrates a typical load history for a nonlinear analysis.

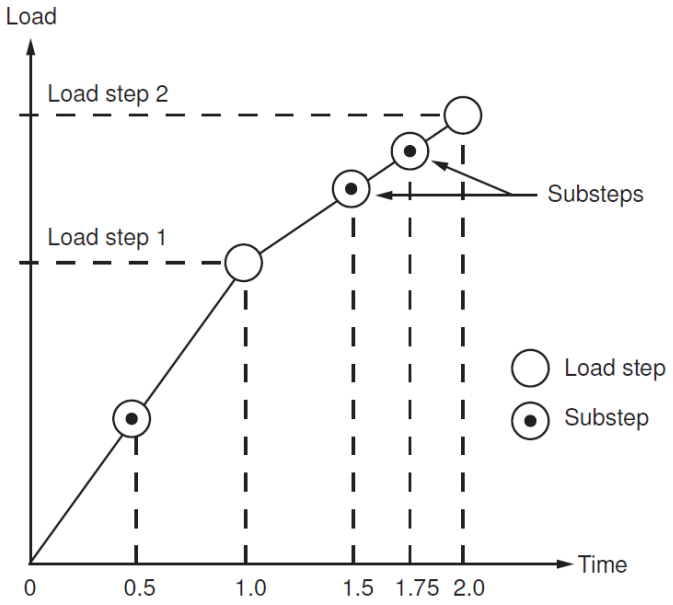

Figure 9-21 Load steps, substeps, and time (ANSYS Mechanical APDL Structural Analysis Guide 2010)

In this study, for the steel pile shell elements, convergence criteria were based on force. A force convergence tolerance of 0.5 percent was specified in the analysis.

9.4.2.4. Output from Plasticity Analysis

The output from plasticity analysis is provided by means of the following two plots:

- The contour of the von Mises equivalent stress SEQV
- The contour of the equivalent plastic strain EPEQ

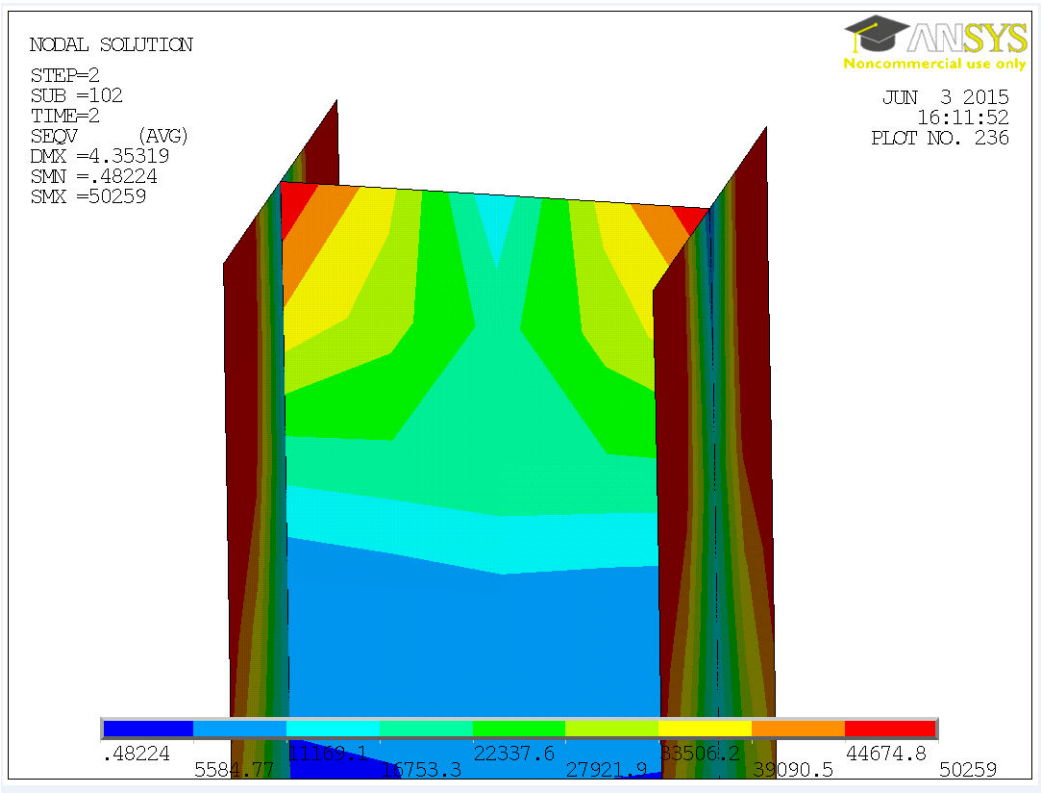

Figure 9-22 Contour of the von Mises equivalent stress SEQV for the case of 1200-feet-long bridge with 10-feet flared cantilever wingwalls

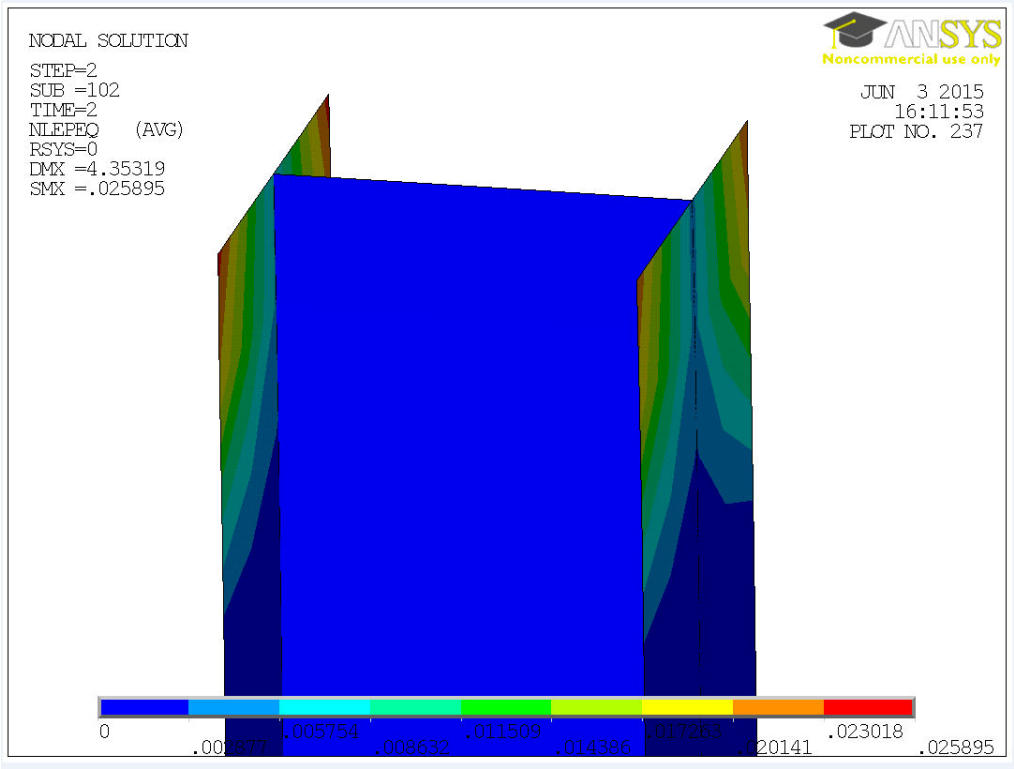

Figure 9-23 Contour of the equivalent plastic strain EPEQ for the case of 1200-feet-long bridge with 10-feet flared cantilever wingwalls

9.5. Nonlinear Structural Analysis - Concrete Model

Reinforced concrete structures are largely employed in engineering practice in a variety of situations and applications. In most cases these structures are designed following simplified procedures. Although traditional empirical methods remain adequate for ordinary design of reinforced concrete members, the wide dissemination of computers and the development of the finite element method have provided means for analysis of much more complex systems in a much more realistic way.

Development of a model for the behavior of concrete is a challenging task. Concrete is a quasibrittle material and has different behavior in compression and tension. The tensile strength of concrete is typically 8 to 15 percent of the compressive strength (Shah et al. 1995). Figure 9-24 shows a typical stress-strain curve for normal weight concrete (Bangash 1989).

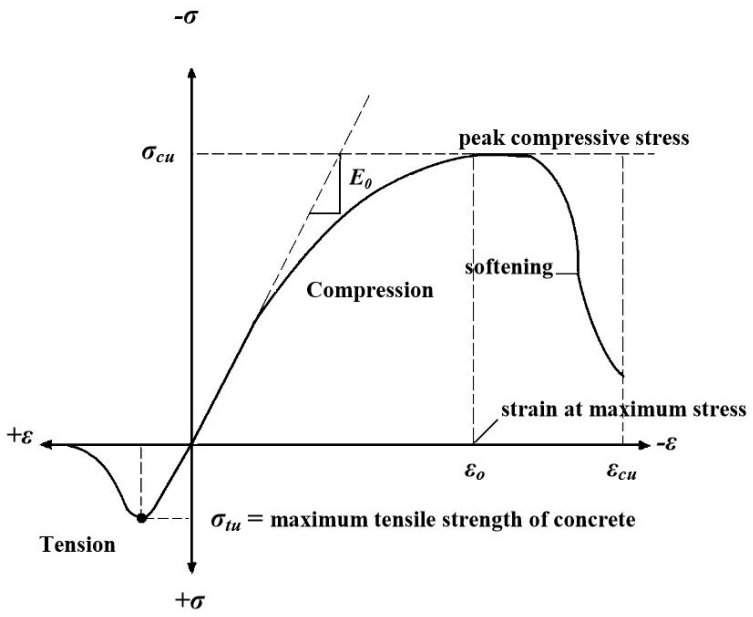

Figure 9-24 Typical uniaxial compressive and tensile stress-strain curve for concrete (Bangash 1989)

In compression, the stress-strain curve for concrete is linearly elastic up to about 30 percent of the maximum compressive strength. Above this point, the stress increases gradually up to the maximum compressive strength. After it reaches the peak compressive stress σ_{cu}, the curve descends into a softening region, and eventually crushing failure occurs at an ultimate strain ε_{cu}. In tension, the stress-strain curve for concrete is approximately linearly elastic up to the maximum tensile strength. After this point, the concrete cracks and the strength gradually decreases to zero (Bangash 1989).

The main obstacle to finite element analysis of reinforced concrete structures is the difficulty in characterizing the material properties. The challenges include not only having a model that represents the material behavior adequately, but also one that is reliable and efficient since concrete cracking, crushing and softening is highly nonlinear. Much effort has been spent in search of a realistic model to predict the behavior of reinforced concrete structures. Due mainly to the complexity of the composite nature of the material, proper modelling of such structures is a challenging task. In fact, a unique and complete constitutive model for reinforced concrete is still lacking.

9.5.1. Academic Research Applications of the Nonlinear ANSYS Concrete Model

In addition to practical applications, the nonlinear ANSYS concrete model is widely used in academic research.

Barbosa and Riberio (1998) used ANSYS to investigate the possibilities of performing nonlinear finite element analysis of reinforced concrete structures using ANSYS concrete model. They compared the nonlinear modeling of reinforced concrete members with discrete and smeared reinforcement. Two different models were developed for the same beam. Concrete was defined with SOLID65. In the first model, LINK8 bar was used as discrete reinforcement element. In the second model, steel reinforcement was modeled as smeared concrete element, defined according to the volumetric proportions of steel and concrete. Each model was analyzed several times using four different material models. Based on their analysis, the results of the load-displacement curves were very similar for both discrete and smeared reinforcement. The differences exhibited at the load greater than the service load when the effects of material modeling led to the difference in the nonlinear behavior and ultimate load capacity. They concluded that despite the relative simplicity of the analyzed structure and of the employed models, satisfactory prediction of the response of reinforced concrete structures may be obtained.

Padmarajaiah and Ramaswamy (2002) investigated the prestressed concrete with fiber reinforcement. They used spring elements to model the interface behavior between the concrete and reinforcement. They found that the crack pattern predicted by ANSYS is in close agreement with the experimental results.

Kachlakev et al. (2001) developed linear and nonlinear finite element method models for a reinforced concrete bridge that had been strengthened with fiber reinforced polymer composites using ANSYS. The results predicted by the model were in agreement with measurements from full-size laboratory beams and the actual bridge. A comparison using model results showed that the structural behavior of the bridge before and after strengthening was nearly the same for legal loads.

Fanning (2001) developed finite element models of reinforced and posttensioned beams using ANSYS. He concluded that the optimum modelling strategy is to model the primary reinforcing in a discrete manner.

Wolanski (2004) performed finite element analysis of reinforced and prestressed concrete beams using ANSYS and compared to experimental results. The FEA results predicted very closely the failure load measured during experimental testing.

Ibrahim and Mubarak (2009) used ANSYS to predict the ultimate load and maximum deflection at midspan of continuous concrete beams, which were prestressed using external tendons. This model accounted for the influence of the second-order effects in externally prestressed members. The results predicted by the model were in good agreement with experimental data.

Dahmani et al. (2010) compared the discrete and smeared reinforcement models and concluded that the discrete reinforcement model gives more accurate results compared to the smeared reinforcement model.

Wahyuni et al. (2013) used ANSYS to study the crack propagation of lightweight sandwich reinforced concrete (LSRC) beams under bending. The numerical model showed the crack in the area of AAC blocks which associated with the brittle failure of LSRC beams. The crack propagation of the beams analyzed by ANSYS was in agreement with the results from the experimental investigation.

9.5.2. The Concrete Material Model in ANSYS

The concrete material model in ANSYS is capable of predicting failure for both cracking and crushing failure modes. This is accomplished by implementation of the William and Warnke (1975) material model in ANSYS, which requires definition of the following parameters:

- Shear transfer coefficient for an open crack
- Shear transfer coefficient for a closed crack
- Uniaxial tensile cracking stress (f_t)
- Uniaxial crushing stress (f_c)
- Biaxial crushing stress (f_{cb})
- Ambient hydrostatic stress state (σ_h)
- Biaxial crushing stress under the ambient hydrostatic stress state (f_1)
- Uniaxial crushing stress under the ambient hydrostatic stress state (f_2)

The shear transfer coefficients for open and closed cracks are used to consider the retention of shear stiffness in cracked concrete. The value of 0 represents an open crack (complete loss of shear transfer) while the value of 1.0 represents a closed crack (no loss of shear transfer).

The uniaxial tensile cracking stress is based upon the modulus of rupture and is denoted as f_t. This value is determined using the expression

$$f_r = 7.5\sqrt{f_c'}$$

The uniaxial crushing stress in the ANSYS model is based on the uniaxial unconfined compressive strength f'_c and is denoted as f_c

The biaxial crushing stress refers to the ultimate biaxial compressive strength f'_{cb} and is denoted as f_{cb}

The ambient hydrostatic state is denoted as σ_h and is defined as

$$\sigma_h = \frac{1}{3}(\sigma_{xp} + \sigma_{yp} + \sigma_{zp})$$

where σ_{xp} , σ_{yp} , and σ_{zp} are the principal stresses in the x, y, and z directions.

The biaxial crushing stress under the ambient hydrostatic stress state refers to the ultimate compressive strength for a state of biaxial compression superimposed on the hydrostatic stress. It is denoted as (f_1).

The uniaxial crushing stress under the ambient hydrostatic stress state refers to the ultimate compressive strength for a state of uniaxial compression superimposed on the hydrostatic stress state. It is denoted as (f_2).

According to William and Warnke (1975) when the stress states satisfy the condition

$$|\sigma_h| \leq \sqrt{3}\, f_c$$

the following three expressions are true

$f_{cb} = 1.2\, f_c$

$f_1 = 1.45\, f_c$

$f_2 = 1.725\, f_c$

Since f_{cb} , f_1, and f_2 are now expressed in terms of f_c it means that the failure surface can be defined with only two parameters, that is, the uniaxial tensile cracking stress (f_t) and the uniaxial crushing stress (f_c). This is shown in the three-dimensional failure surface for concrete (Figure 9-25).

The failure surface represents a three-dimensional failure surface for states of stress that are biaxial or nearly biaxial (ANSYS Mechanical APDL and Mechanical Applications

Theory Reference 2010). The most significant nonzero principal stresses are in the x and y directions, represented by σ_{xp} and σ_{yp} respectively. Three failure surfaces are shown as projections on the σ_{xp} - σ_{yp} plane. The mode of failure is a function of the sign of σ_{zp} (principal stress in the z direction). For example, if σ_{xp} and σ_{yp} are both negative (compressive) and σ_{zp} is slightly positive (tensile), cracking would be predicted in a direction perpendicular to σ_{zp} . However, if σ_{zp} is zero or slightly negative, the material is assumed to crush (ANSYS Mechanical APDL and Mechanical Applications Theory Reference 2010).

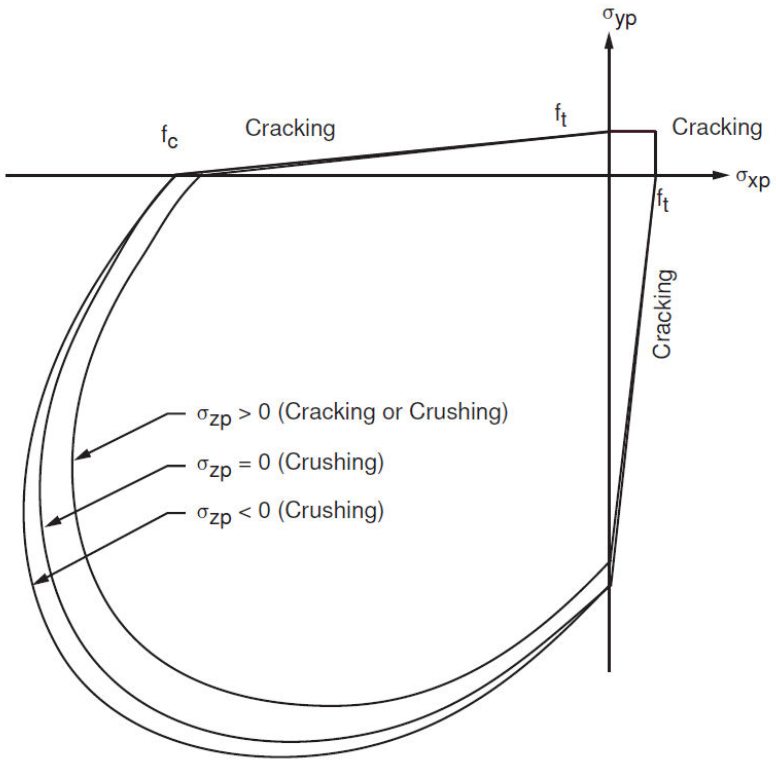

Figure 9-25 Three-dimensional failure surface for concrete (ANSYS Mechanical APDL and Mechanical Applications Theory Reference 2010)

The SOLID65 element in ANSYS requires both linear isotropic and multilinear isotropic material properties to properly model concrete. The multilinear isotropic material uses the von Mises failure criterion along with the William and Warnke (1975) model to define the failure of the concrete. The linear isotropic material properties are expressed in terms of the elastic modulus and the Poisson's ratio while the multilinear isotropic material properties are expressed in terms of the uniaxial tensile cracking stress (f_t) and the uniaxial crushing stress (f_c) that defined the concrete failure surface shown in Figure 9-25. The input for the SOLID65 element is summarized in Table 9-7.

9.5.3. Modeling of Concrete using Finite Elements

The numerical simulation of concrete fracture was initiated in the late 1960s by Ngo and Scordelis (1967) and Rashid (1968) who introduced the discrete crack and smeared crack models respectively. The discrete crack model is aimed at simulating the initiation and propagation of dominant cracks. In contrast, the smeared crack model is based on the idea that in concrete, due to its heterogeneity and the presence of reinforcement, many small cracks nucleate, which only in a later stage of the loading process link up to form one or more dominant cracks. Since each individual crack is not numerically resolved, the smeared crack model captures the deterioration process through a constitutive relation, thus smearing out the cracks over the continuum (De Borst et al. 2004).

9.5.3.1. Discrete Crack Models

According to the discrete crack approach to concrete fracture, a crack is introduced as a geometric entity. This is implemented by letting a crack grow when the nodal force at the node ahead of the crack tip exceeds a certain tensile strength criterion. Then, the node is split into two nodes and the tip of the crack is assumed to propagate to the next node. When the tensile strength criterion is violated at this node, it is split and the procedure is repeated, as shown in Figure 9-26.

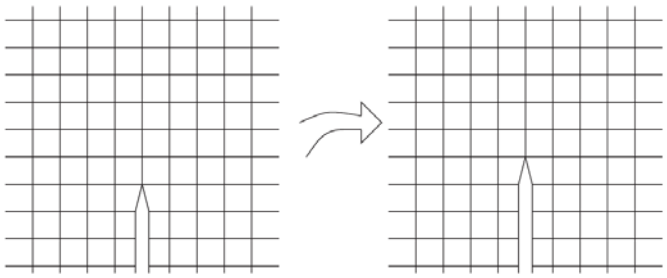

Figure 9-26 Early discrete crack modelling (De Borst et al. 2004)

This method is theoretically more suitable to capture the failure localization. On the other hand, an adaptive remeshing technique is required to account for phenomena such as progressive failure (Jendele et al. 2001). In addition, cracks are forced to propagate along element boundaries, so that a mesh bias is introduced. As a result, a computational difficulty, namely, the continuous change in topology, is inherent in the discrete crack approach and is to a certain extent even aggravated by remeshing procedures (De Borst et al. 2004). Consequently, discrete models are very demanding in the sense that they require development of a rather complex software package, in which the finite element model is tightly coupled with the geometrical model (Jendele et al. 2001).

9.5.3.2. Smeared Crack Models

According to the smeared crack approach, the nucleation of one or more cracks in the volume that is attributed to an integration point is translated into deterioration of the stiffness and strength at that integration point. Generally, when the combination of stresses satisfies a specified criterion; for example, the principal tensile stress exceeds the ultimate tensile strength, a crack is initiated. This implies that at the integration point where the stress, strain, and history variables are monitored, the isotropic stress-strain relation is replaced by an orthotropic elasticity-type relation with the n; s-axes being axes of orthotropy; n is the direction normal to the crack and s is the direction tangential to the crack (De Borst et al. 2004). The early form of the isotropic stress-strain relation was:

$$\begin{pmatrix} \sigma_{nn} \\ \sigma_{ss} \\ \sigma_{ns} \end{pmatrix} = \begin{bmatrix} 0 & 0 & 0 \\ 0 & E & 0 \\ 0 & 0 & 0 \end{bmatrix} \begin{pmatrix} \varepsilon_{nn} \\ \varepsilon_{ss} \\ \varepsilon_{ns} \end{pmatrix}$$

Suidan and Schnobrich (1973) found that the use of this equation induces convergence difficulties as well as unrealistic and distorted crack patterns. For this reason, a reduced shear modulus βG ($0 \leq \beta \leq 1$) was inserted into the matrix as shown below:

$$\begin{bmatrix} 0 & 0 & 0 \\ 0 & E & 0 \\ 0 & 0 & \beta G \end{bmatrix}$$

Furthermore, the use of the shear retention factor β not only reduces numerical difficulties, but also improves the capability of fixed smeared crack models because it can be regarded as a representation of some effects of aggregate interlocking and friction within the crack. Fixed and rotating crack is a reference to the ability of the crack to propagate along a fixed axis, or at an angle to the axis of the previous crack. If the direction of the crack is known, then fixed smeared crack models are used; otherwise rotating smeared crack models should be used.

The matrix was further refined to its current form with the introduction of the factor μ with the intent to achieve a gradual decrease (as opposed to sudden drop) from maximum tensile strength σ_{tu} to zero on crack initiation (Figure 9-24).

$$\begin{bmatrix} \mu E & 0 & 0 \\ 0 & E & 0 \\ 0 & 0 & \beta G \end{bmatrix}$$

The smeared crack approach has been shown to be mesh sensitive. In fact, a number of researchers (Barzegar and Maddipudi 1997; Shah et al. 1995) suggest that when using smeared crack models the concrete element size should be two to three times greater than the maximum aggregate size in order to correctly and realistically model the actual cracks.

9.5.3.3. Uses of Discrete and Smeared Crack Models

Jendele et al. (2001) analyzed a number of plain and reinforced concrete structures using both discrete and smeared crack models, then compared the results with experimental evidence. Their recommendations based on both the experiments as well as their professional experience regarding the use of discrete and smeared crack models in finite element analysis of concrete structures are summarized in Table 9-6

Table 9-6 Recommendations for use of discrete and smeared crack models (Jendele et al. 2001)

Crack Path	Plain Concrete Structures	Reinforced Concrete Strictures
Known crack path	discrete or smeared	smeared
Unknown crack path	discrete or smeared	combined or smeared

According to the authors, the smeared crack model is currently the most appropriate finite element analysis tool for concrete structures overall. However, the discrete model is the preferred choice for the analysis of structures made of plain or slightly reinforced concrete. The authors also point out to one of the structures analyzed, that is, a reinforced concrete wall subjected to shear load at its top. The analysis that involved concrete cracking, crushing, and reinforcement yielding proved, in their opinion, the superiority of the smeared crack model.

The combined model mentioned in Table 9-6 is a combination of smeared crack model to model distributed cracking and concrete crushing while the discrete cracks are inserted into the areas where a major crack is expected on the basis of engineering judgment (Jendele et al. 2001).

9.5.4. Modeling of Steel Reinforcement using Finite Elements

There are two ways to model steel reinforcement in nonlinear analysis. The first option is the discrete reinforcement modeling and the second option is the smeared reinforcement modeling of the steel reinforcement.

The discrete reinforcement modeling option requires explicit modeling of the rebar in order to capture yield or slippage of individual bars or both. The steel reinforcement is simulated as spar elements with geometric properties similar to the original reinforcing. These elements are connected to the concrete mesh nodes and hence the concrete and the steel reinforcement share the same nodes (Vasudevan and Kothandaraman 2011). The discrete reinforcement modeling option is considered to be more convergent than the smeared reinforcement modeling option as it subtracts the area of steel from the total area of concrete, which is the actual scenario. Compared to the smeared reinforcement modeling option, this option requires a finer mesh due to the explicit modeling of the rebar.

The smeared reinforcement modeling option does not require explicit modeling of the rebar and therefore a much coarser mesh can be defined. This option provides the independent nonlinear response, but does not calculate rebar stresses. The rebar element effectively sits on top of the existing concrete elements, and thus uses the same nodes as the underling concrete elements. The rebar is added to the SOLID65 elements as a percent of element area in various directions. In other words, the steel is embedded in the concrete and behaved as one unit, which is not the actual case.

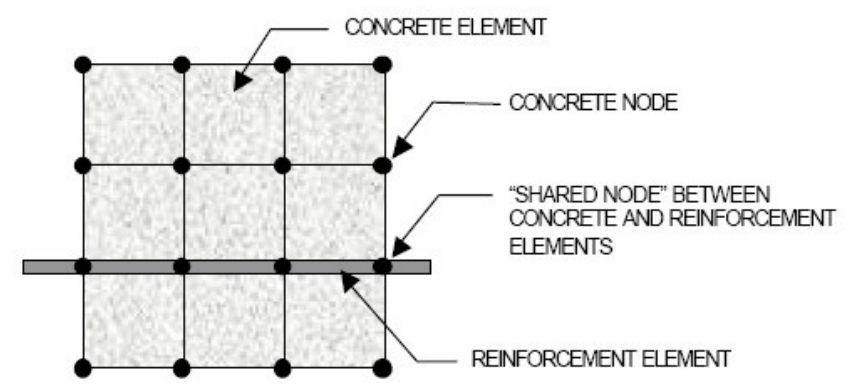

Figure 9-27 Idealization of rebar in concrete with discrete reinforcement modeling (Tavarez 2001)

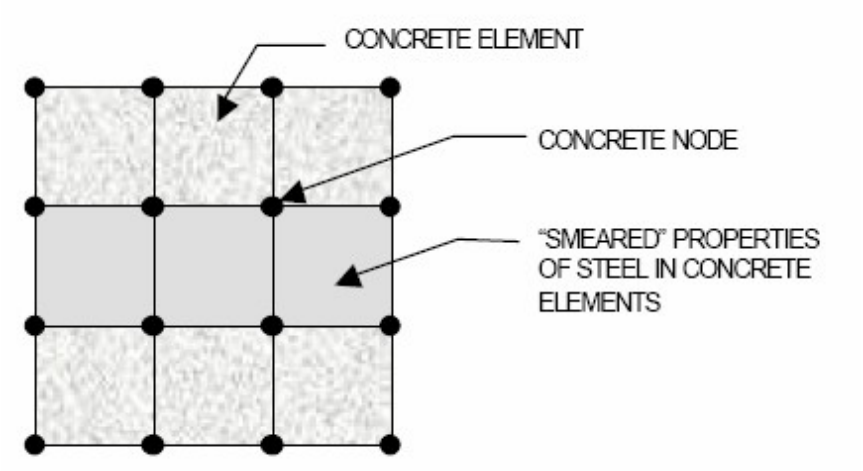

Figure 9-28 Idealization of rebar in concrete with smeared reinforcement modeling (Tavarez 2001)

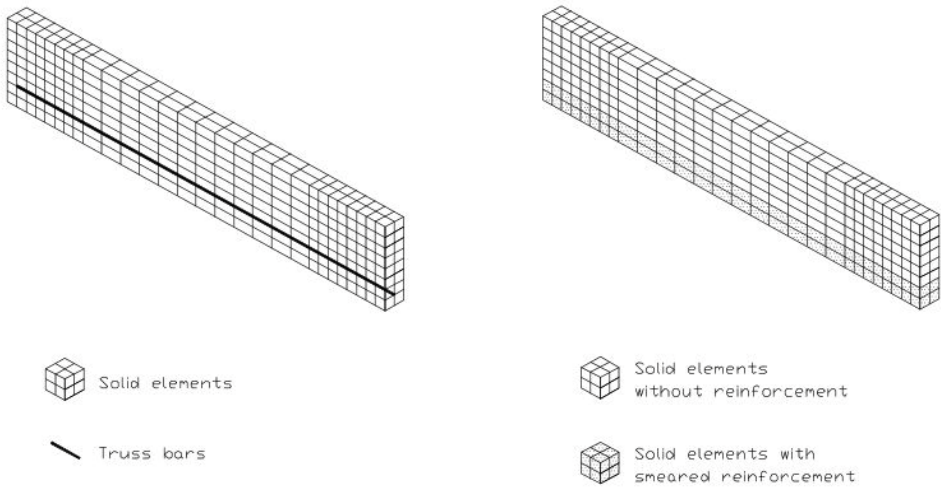

Figure 9-29 Finite element meshes with discrete and smeared reinforcement (Barbosa and Riberio 1998)

9.5.5. Finite Element Modeling using the ANSYS Concrete Model for this Study

For the modeling of concrete using finite elements, smeared crack models is the only option available in the ANSYS concrete model. Discrete crack models are not available in ANSYS. Consequently, the smeared crack approach is used in this analysis for the concrete. For the steel reinforcement, two options are available: (1) discrete reinforcement models, and (2) smeared reinforcement models. Along with cracking, the objective of this analysis is the determination of stresses in the rebar and capturing of the yield. This is only available with the use of discrete reinforcement models. As a result, the discrete reinforcement model is used in this analysis.

9.5.5.1. Definition of elastic and plastic properties

The concrete is modeled with the three-dimensional eight noded solid isoparametric element, SOLID65. Input data include the shear transfer coefficients for open and closed cracks discussed in section 9.5.2., the elastic modulus, Poisson's ratio, uniaxial crushing stress, and the uniaxial tensile cracking stress. The concrete properties are summarized in Table 9-7.

It is worth mentioning that only solid elements support the concrete model in ANSYS. This is considered a major limitation for more extensive use of ANSYS for reinforced concrete analysis.

The three-dimensional spar element LINK8 is used to model the steel reinforcement. The stress-strain curve for the steel reinforcement is bilinear isotropic (Figure 9-30). Input material properties include the elastic modulus and the Poisson's ratio. The stress-strain curve is defined in terms of the yield stress $f_{y,}$ and the tangent modulus $E_{T.}$ The steel reinforcement properties are summarized in Table 9-7.

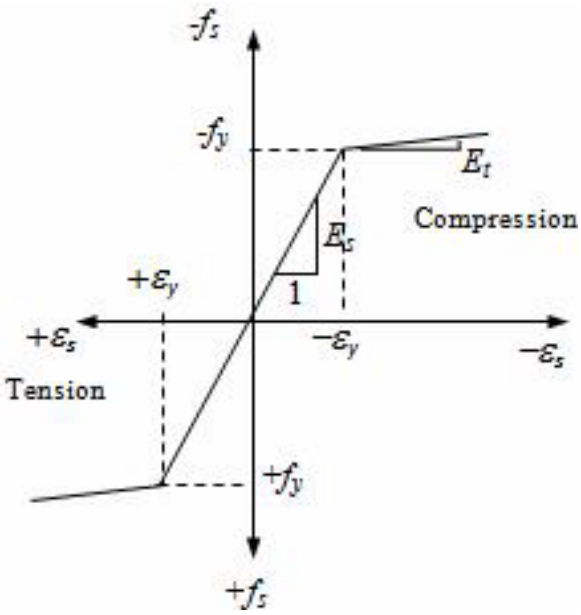

Figure 9-30 Stress-strain curve for steel reinforcement

The use of the discrete method to model the steel reinforcement requires definition of the real constants for the LINK8 element. This includes the cross sectional area of reinforcement and the initial strain (ANSYS Element Reference 2009). Their values are summarized in Table 9-8. A value of zero is entered for the initial strain because there is no initial stress in the reinforcement.

At the beginning of FE model development, a reasonable mesh and a convergence study are needed to obtain a reliable model. Convergence of the solution is achieved when an adequate number of elements is used in a model. Because the smeared crack approach has been shown to be mesh sensitive (Kachlakev et al. 2001), too fine of a mesh may cause numerical instability. Conversely, if the mesh is too coarse, the analysis will not be sufficiently accurate. Barzegar and Maddipudi (1997), and Shah et al. (1995) suggest that the concrete element size should be two to three times greater than the maximum aggregate size to correctly and realistically model the actual cracks. Assuming a 2-inch maximum nominal aggregate size, the 6-inch element size used for the abutments and wingwall is appropriate. In addition, use of 6-inch elements matches the rebar spacing of 6 and 12 inches respectively.

In a nonlinear reinforced concrete analysis, the shear transfer coefficients must be defined. Two shear transfer coefficients, one for open cracks and other for closed ones, are used to consider the retention of shear stiffness in cracked concrete. The value of 0 represents an open crack (complete loss of shear transfer) and the value of 1.0 represents a closed crack (no loss of shear transfer). For the case of open cracks, several researchers (Barzegar and Maddipudi 1997; Huyse et al. 1994; Najjar et al. 1997) suggest the use of a value in the range of 0.05 to 0.5, rather than 0.0, to prevent numerical difficulties. In this analysis, a value of 0.9 is used for the shear transfer coefficient for closed cracks and a value of 0.1 is used for the shear transfer coefficient for open cracks.

Table 9-7 Material properties defined in the ANSYS concrete model

ANSYS Element and Model	Material Properties	
SOILD65 (concrete) Smeared crack model	Linear isotropic concrete properties	
	Elastic modulus EX	3605 ksi
	Poisson's ratio PRXY	0.20
	Multinear isotropic concrete properties	
	Shear transfer coefficient for an open crack STCUC	0.1
	Shear transfer coefficient for a closed crack STCCC	0.9
	Uniaxial tensile cracking stress UTCS	474 psi
	Uniaxial crushing stress UCS	4,000 psi
LINK8 (steel reinforcement) Discrete reinforcement model	Linear isotropic steel reinforcement properties	
	Elastic modulus EX	29,000 ksi
	Poisson's ratio PRXY	0.30
	Bilinear isotropic hardening (BISO) steel reinforcement properties	
	Yield stress f_y	60 ksi
	Tangent modulus E_T	2900 psi (Wolanski 2004)

Table 9-8 Real constants for steel reinforcement

Element Type	Real Constant	Quantity
LINK8 (vertical reinforcement)	Cross sectional area (in^2)	2.0 in^2
	Initial strain (in./in.)	0
LINK8 (horizontal reinforcement)	Cross sectional area (in^2)	1.0 in^2
	Initial strain (in./in.)	0

9.5.5.2. Nonlinear Solution

The approach described in section 9.4.2.3. for the nonlinear solution of the plasticity model applies to the concrete model as well. For this analysis, in order to achieve the most efficient convergence, a large number of intermediate solution steps was used coupled with both force and displacement convergence criteria as well as adequate number of elements in the model.

9.5.5.3. Output from Nonlinear Concrete Analysis

The output from the nonlinear concrete analysis is provided by means of the following two plots:

- The cracking pattern in the integral abutment and cantilever wingwalls
- The stresses in the rebar of both integral abutment and cantilever wingwalls

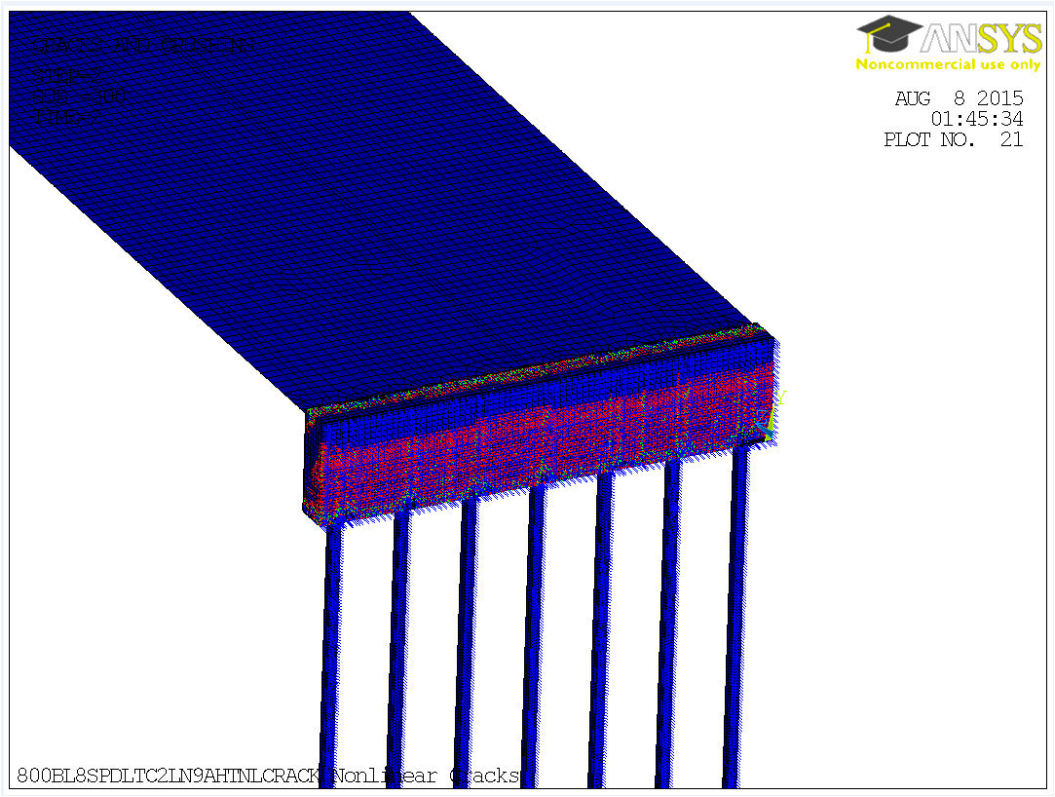

Figure 9-31 Cracking pattern in the integral abutment of an 800-feet-long bridge during temperature expansion (DL+TE)

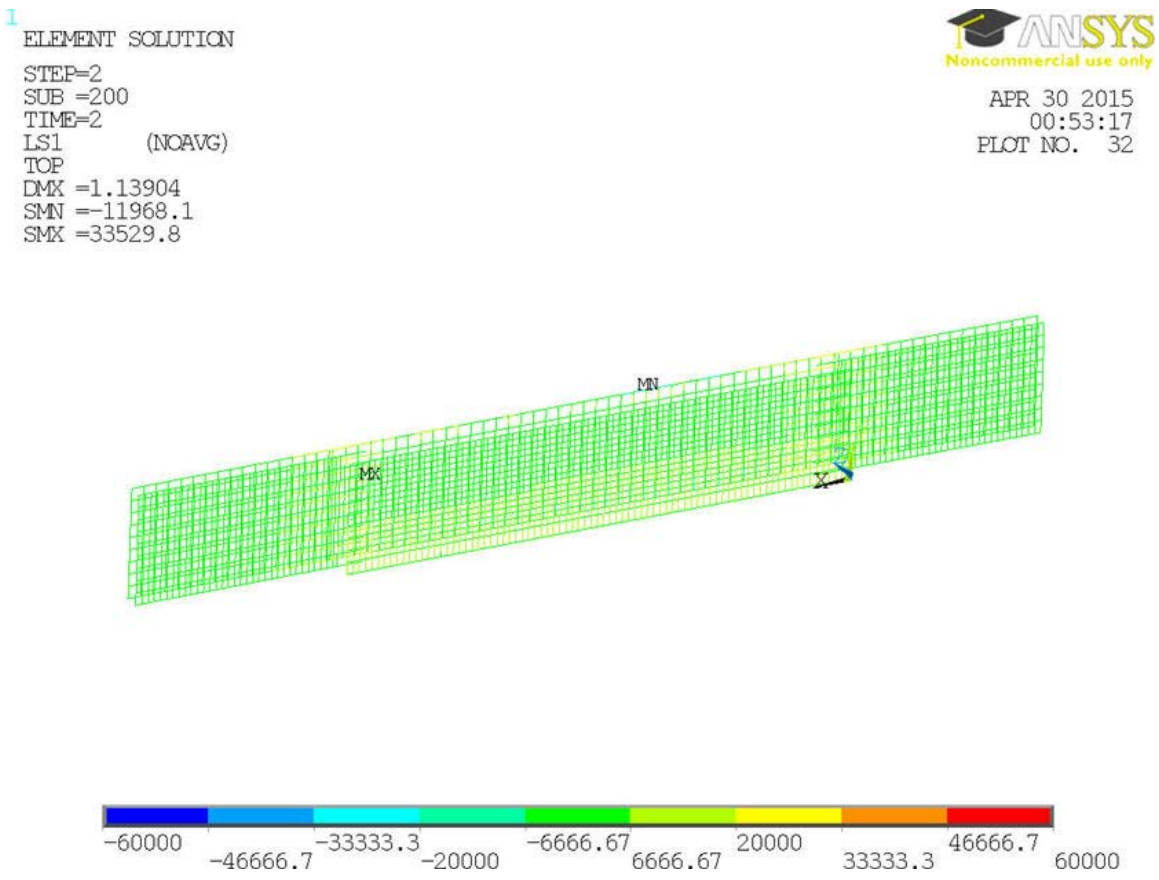

Figure 9-32 Stresses in the abutment and wingwall rebar of a 400-feet-long bridge with 16-feet-long wingwalls during temperature contraction (DL+TC)

9.6. Validation of Finite Element Models

Validation is the process of determining the degree to which a model and its associate data are an accurate representation of the real world from the perspective of the intended uses of the model. In other words, validation answers the question whether the right model has been built.

The results from the finite element analysis models developed for this study match closely the results of an experimental program conducted by Huang et al. (2004, 2008). The program was developed by the University of Minnesota from November 1996 to February 2004 and included instrumentation of integral abutment bridges with cantilever wingwalls.

In addition, the finite element models produced similar results to a previous research conducted at the University of Maryland by Najib (2002). The research indicated that the most effective depth for predrilled holes is 9 feet.

Chapter 10

Results of Parametric Studies

10.1. Introduction

This chapter presents the results of the parametric studies described in chapters 6 and 9. The parametric studies were performed with the use of the finite element program ANSYS. The models were built using the ANSYS Parametric Design Language (APDL), which is a scripting language used to automate tasks and build models in terms of parameters (variables). The analyses results are documented in such a way that meaningful conclusions are drawn on the effects of cantilever wingwall configurations on the integral abutment piles, integral abutments, and bridge superstructure. The severity of the effects of cantilever wingwalls on those bridge elements is compared to the effects of other parameters that influence the behavior of integral abutment bridges. This includes the type of backfill soil (dense sand, medium dense sand, loose sand) behind the integral abutments and cantilever wingwalls, use or no use of predrilled holes at the top nine feet of piles, and bridge length.

The effects on integral abutment piles are expressed in terms of the stresses introduced into the piles. The effects on the integral abutments are expressed in terms of the stresses introduced into the abutments' reinforcing steel as well as the cracking pattern developed in the abutment walls. The effects on the bridge superstructure are expressed in terms of axial forces introduced into the steel girders.

10.2. Effects of Cantilever Wingwalls on Pile Stresses

The results of the analyses indicate that the magnitude of stresses in the piles is a function of a number of parameters. The piles in the parametric studies are always oriented in weak-axis bending and the parameters included in these studies are the following:

- Type of cantilever wingwalls
- Use of predrilled holes
- Type of backfill soil behind integral abutments and cantilever wingwalls
- Loading
- Bridge length

Three types of cantilever wingwalls are investigated: (1) inline wingwalls, (2) flared wingwalls at 45 degrees, and (3) U-shaped wingwalls. Detailed information is provided in Tables 5-1 and 6-1 as well as in Figure 5-1.

Integral abutments are designed and built with predrilled holes at the top nine feet of piles. However, the danger of predrilled holes is that, over time, the back and forth movement of the abutment stem will compact the soil around the piles, and the results will approach that of nondrilled holes. The length of time required to reach this level of compaction is unknown and depends on the native soil properties, the magnitude and frequency of movement and the length of predrilled holes. Considering this possibility, this study considers both cases (a) predrilled holes, and (b) no predrilled holes at the top nine feet of piles. Consequently, although integral abutments are designed and built with predrilled holes, it is very likely that over the years a situation in-between the two scenarios will develop.

Three types of backfill soil behind the abutments and wingwalls are investigated. This includes (1) dense sand, (2) medium dense sand, and (3) loose sand. The soil profile is shown in Figure 6-2 and more details on the three soil types are included in Table 6-1. The soil around the piles remains always unchanged and as shown in Figure 6-2.

Two types of loadings are investigated. This includes temperature expansion (TE) and temperature contraction (TC) each combined with dead load (DL). The two loadings are denoted as DL+TE and DL+TC respectively.

Table 10-1 uses the bridge length at which pile plasticity is first generated as a metric to compare the effects of using predrilled holes during temperature contraction. The results are shown graphically in Figure 10-1.

Table 10-2 uses the bridge length at which pile plasticity is first generated as a metric to compare the effects of using predrilled holes during temperature expansion. The results are shown graphically in Figure 10-2.

Table 10-1 Bridge length at onset of pile plasticity during temperature contraction No predrilled holes Vs predrilled holes comparison

	DL+TC - No Predrilled Holes			DL+TC with predrilled holes		
	Dense Sand	Medium Dense Sand	Loose Sand	Dense Sand	Medium Dense Sand	Loose Sand
No Cantilever Wingwalls	120	122	124	422	430	438
Inline Wingwalls 0 Degrees	77	77	77	298	303	308
Flared Wingwalls 45 Degrees	85	87	88	277	283	289
U-Shaped Wingwalls 90 Degrees	114	114	115	371	372	374

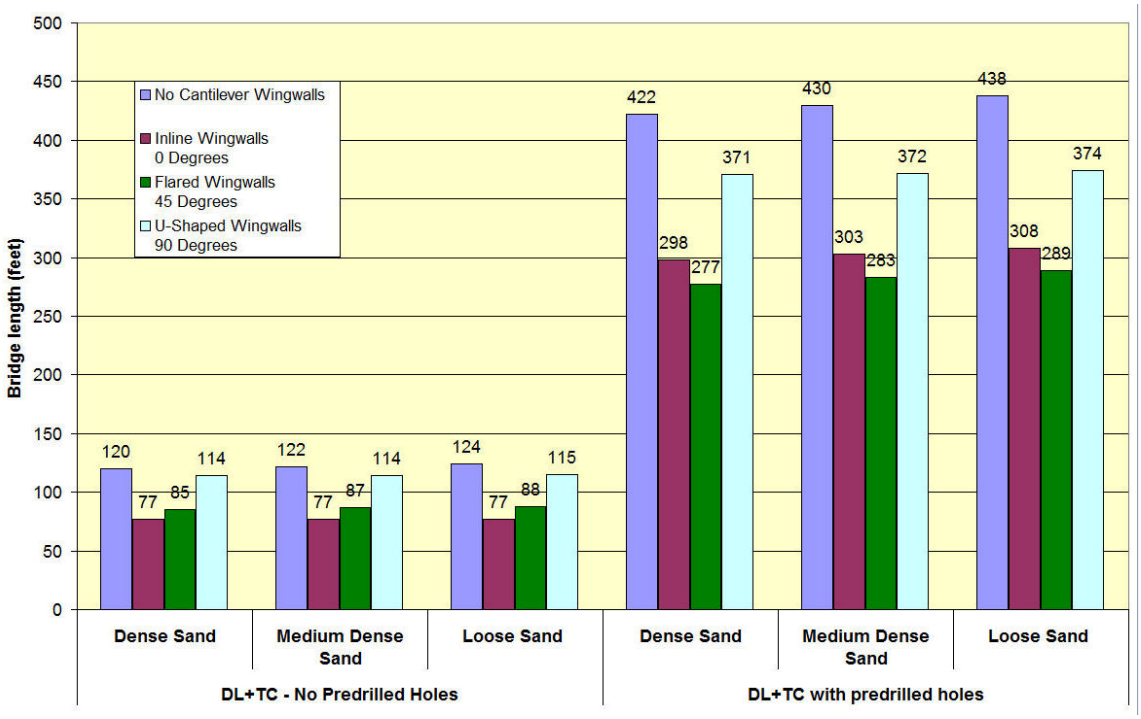

Figure 10- Bridge length at onset of pile plasticity during temperature contraction No predrilled holes Vs predrilled holes comparison

Table 10-2 Bridge length at onset of pile plasticity during temperature expansion No predrilled holes Vs predrilled holes comparison

	DL+TE - No Predrilled Holes			DL+TE with predrilled holes		
	Dense Sand	Medium Dense Sand	Loose Sand	Dense Sand	Medium Dense Sand	Loose Sand
No Cantilever Wingwalls	236	213	200	-	-	1191
Inline Wingwalls 0 Degrees	119	113	110	-	750	612
Flared Wingwalls 45 Degrees	185	159	149	-	-	952
U-Shaped Wingwalls 90 Degrees	195	185	180	-	-	941

(Use of hyphen in the table implies no pile plasticity is generated up to a bridge length of 1200 feet)

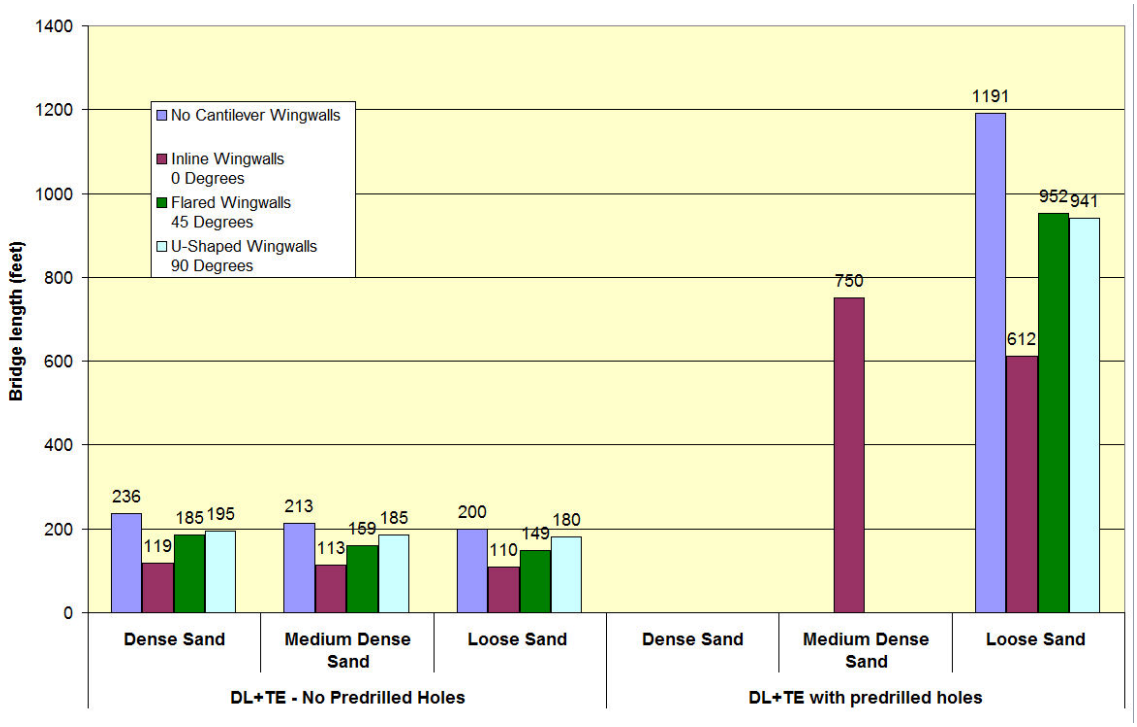

Figure 10-2 Bridge length at onset of pile plasticity during temperature expansion No predrilled holes Vs predrilled holes comparison

Table 10-3 uses the bridge length at which pile plasticity is first generated as a metric to compare the effects of temperature contraction to those of temperature expansion on pile stresses when predrilled holes are used at the top nine feet of piles. The results are shown graphically in Figure 10-3.

Table 10-4 uses the bridge length at which pile plasticity is first generated as a metric to compare the effects of temperature contraction to those of temperature expansion on pile stresses when no predrilled holes are used at the top nine feet of piles. The results are shown graphically in Figure 10-4.

Table 10-3 Bridge length at onset of pile plasticity with predrilled holes - DL+TC Vs DL+TE comparison

	DL+TC with predrilled holes			DL+TE with predrilled holes		
	Dense Sand	Medium Dense Sand	Loose Sand	Dense Sand	Medium Dense Sand	Loose Sand
No Cantilever Wingwalls	422	430	438	-	-	1191
Inline Wingwalls 0 Degrees	298	303	308	-	750	612
Flared Wingwalls 45 Degrees	277	283	289	-	-	952
U-Shaped Wingwalls 90 Degrees	371	372	374	-	-	941

(Use of hyphen implies no pile plasticity is generated up to a bridge length of 1200 feet)

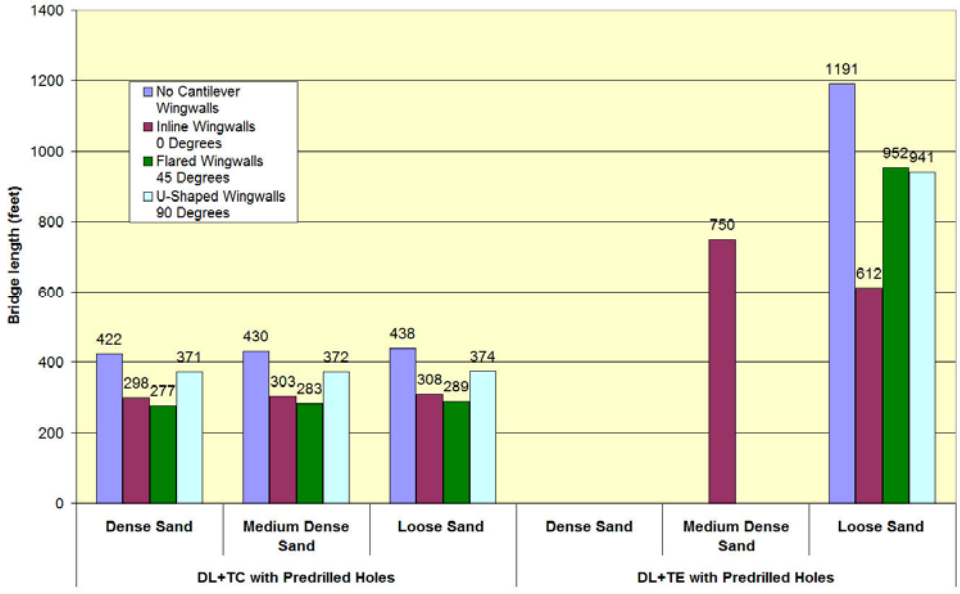

Figure 10-3 Bridge length at onset of pile plasticity with predrilled holes - DL+TC Vs DL+TE comparison

Table 10-4 Bridge length at onset of pile plasticity - No predrilled holes - DL+TC Vs DL+TE comparison

	DL+TC - No Predrilled Holes			DL+TE - No Predrilled Holes		
	Dense Sand	Medium Dense Sand	Loose Sand	Dense Sand	Medium Dense Sand	Loose Sand
No Cantilever Wingwalls	120	122	124	236	213	200
Inline Wingwalls 0 Degrees	77	77	77	119	113	110
Flared Wingwalls 45 Degrees	85	87	88	185	159	149
U-Shaped Wingwalls 90 Degrees	114	114	115	195	185	180

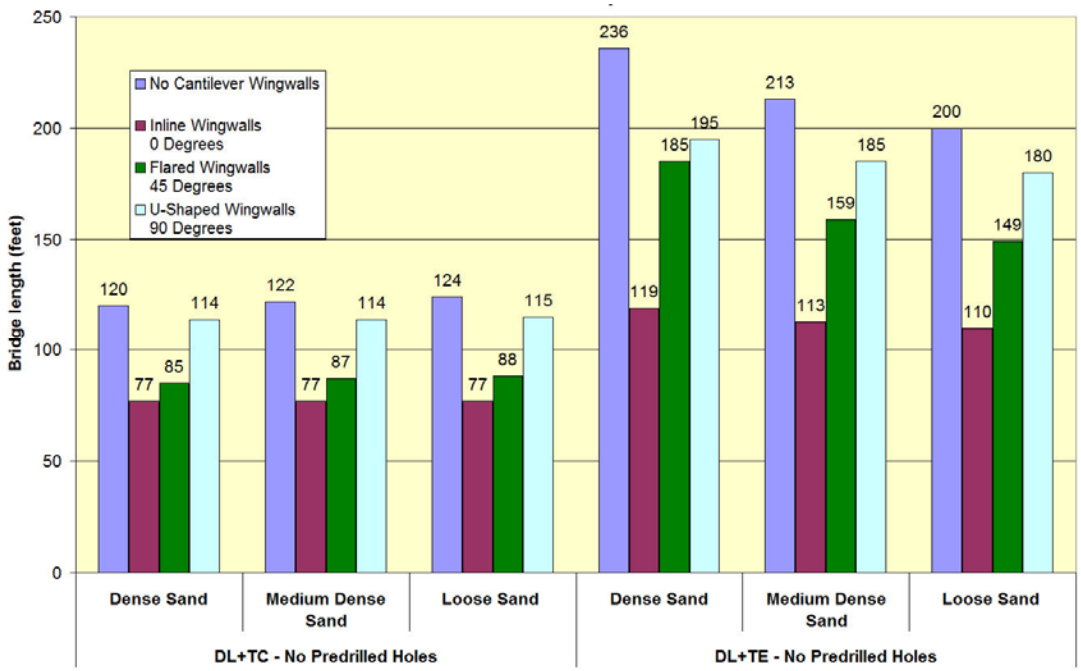

Figure 10-4 Bridge length at onset of pile plasticity - No predrilled holes - DL+TC Vs DL+TE comparison

Conclusions

- Higher piles stresses are induced during thermal contraction rather than during thermal expansion. This is the result of wider temperature variation during temperature contraction compared to temperature variation during temperature expansion (temperature ranges are defined in Table 6-1). In addition, active soil pressures are aligned and in the same direction as the temperature-induced loading. Therefore, the resulting deformation in combination with the gravity forces acting on the piles (P-Δ effect) produces higher pile stresses during temperature fall. During temperature expansion, as the approach fill is pushed by the abutment, it tends to move the foundation soil in the same direction. This is beneficial as far as pile stresses is concerned because the foundation soil is moving in the same direction as the piles. The result is lower stresses in the piles during temperature expansion rather than during temperature contraction.

- Addition of any type of cantilever wingwall (inline, flared or U-shaped) has an effect on pile stresses. Cantilever wingwalls perpendicular to the traffic (inline wingwalls) induce the most stresses and plasticity in the piles.

- Comparison of the effects of cantilever wingwalls, predrilled holes, and backfill soil on pile stresses, leads to the conclusion that the most critical parameter by far is the use of predrilled holes followed by the use of cantilever wingwalls and type of backfill soil.

- The most critical combination of parameters on pile stresses occurs during temperature contraction when no predrilled holes are used in combination with inline cantilever wingwalls and dense sand as backfill soil. In this instance, yielding in the piles occurs at a bridge length of 77 feet.

- During temperature contraction, plasticity in the piles of integral abutments with predrilled holes and no cantilever wingwalls is generated at bridge lengths between 422 and 438 feet depending on the type of backfill soil. Addition of cantilever wingwalls induces plasticity in the piles at bridge lengths between 277 and 374 feet depending on the cantilever wingwall orientation and type of backfill soil.

- Not using predrilled holes at the top nine feet of piles has a very serious effect on pile stresses. The results indicate that when no predrilled holes are used, plasticity in the piles of integral abutments without cantilever wingwalls is generated at bridge lengths between 120 and 124 feet depending on the type of backfill soil. However, when predrilled holes are used, pile plasticity is generated between 422 to 438 feet as stated in the previous paragraph. Addition of any type of cantilever wingwall (inline, flared or U-shaped) to bridges with no predrilled holes results in generation of plasticity in the piles at bridge lengths ranging from 77 to 115 feet. Using predrilled holes with any type of cantilever wingwall results in generation

of pile plasticity at bridge lengths between 277 and 374 feet as stated in the previous paragraph.

- During temperature expansion, plasticity in the piles is generated at bridge lengths substantially longer compared to those obtained during temperature contraction. This applies to all cases including use or not of predrilled holes or cantilever wingwalls in combination with any type of backfill soil. This is due to the fact that higher piles stresses are induced during thermal contraction rather than during thermal expansion.

Table 10-1 and Figure 10-1 indicate that during temperature contraction when predrilled holes are used, no cantilever wingwalls exist, and medium dense sand is used as backfill soil, pile plasticity is first generated at 430 feet. Considering this case as a metric, a comparison of pile plasticity generated at 430 and 1200 feet for all three types of cantilever wingwalls (inline, flared, and U-shaped) is made. The comparison also includes a 1200-feet-long-bridge with no cantilever wingwalls. The results are shown in Figure 10-5 expressed in terms of percentage increase in equivalent plastic strain (EPEQ).

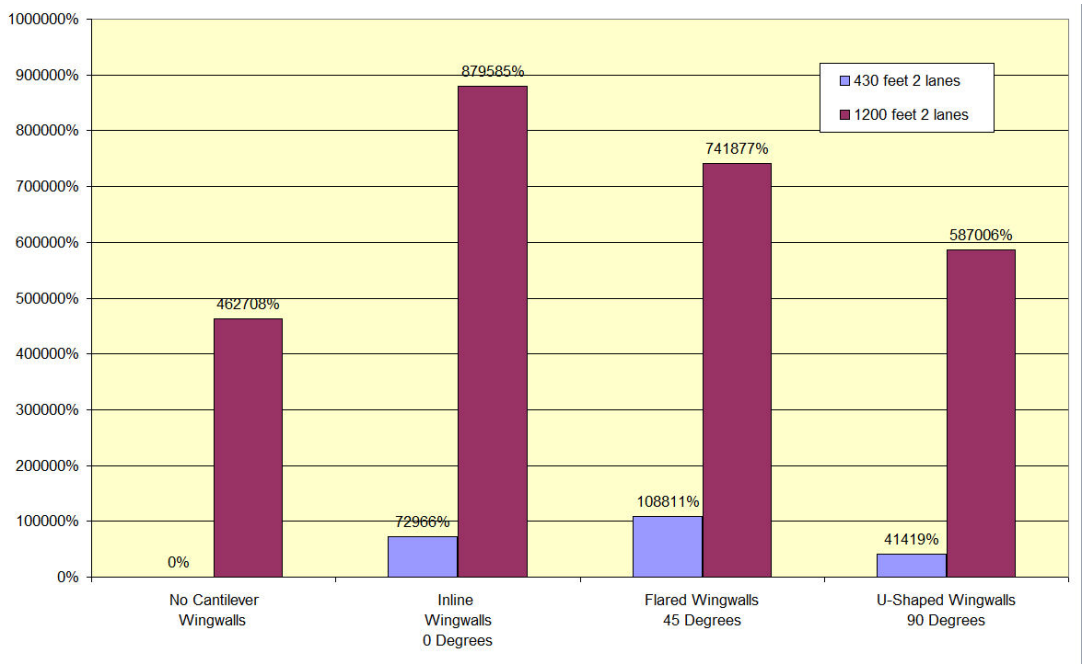

Figure 10-5 Percentage increase in equivalent plastic strain EPEQ for 2-lane bridges 430-feet bridge Vs 1200-feet bridge

Conclusion

- The results indicate that the most critical cantilever wingwall configuration is the inline cantilever wingwall.

Knowing that inline cantilever wingwalls induce the most stresses and plasticity in the piles, I calculated the equivalent plastic strain (EPEQ) in inline cantilever wingwalls for the cases of predrilled holes and no predrilled holes with all three types of backfill soil. The intent is to get the most critical case with the use of inline cantilever wingwalls. The results are summarized in Table 10-5 and shown in Figures 10-6 and 10-7 respectively.

Table 10-5 Comparison of equivalent plastic strain EPEQ in a 1200-feet-long bridge No predrilled holes Vs predrilled holes comparison

Equivalent Plastic Strain EPEQ						
	Soil Type					
	Dense sand		Medium dense sand		Loose sand	
	No cantilever wingwalls	24 feet Inline wingwalls	No cantilever wingwalls	24 feet Inline wingwalls	No cantilever wingwalls	24 feet Inline wingwalls
Predrilled holes	0.017207	0.035977	0.016152	0.032793	0.015321	0.030422
No predrilled holes	0.142444	0.197337	0.131808	0.186144	0.123957	0.177180

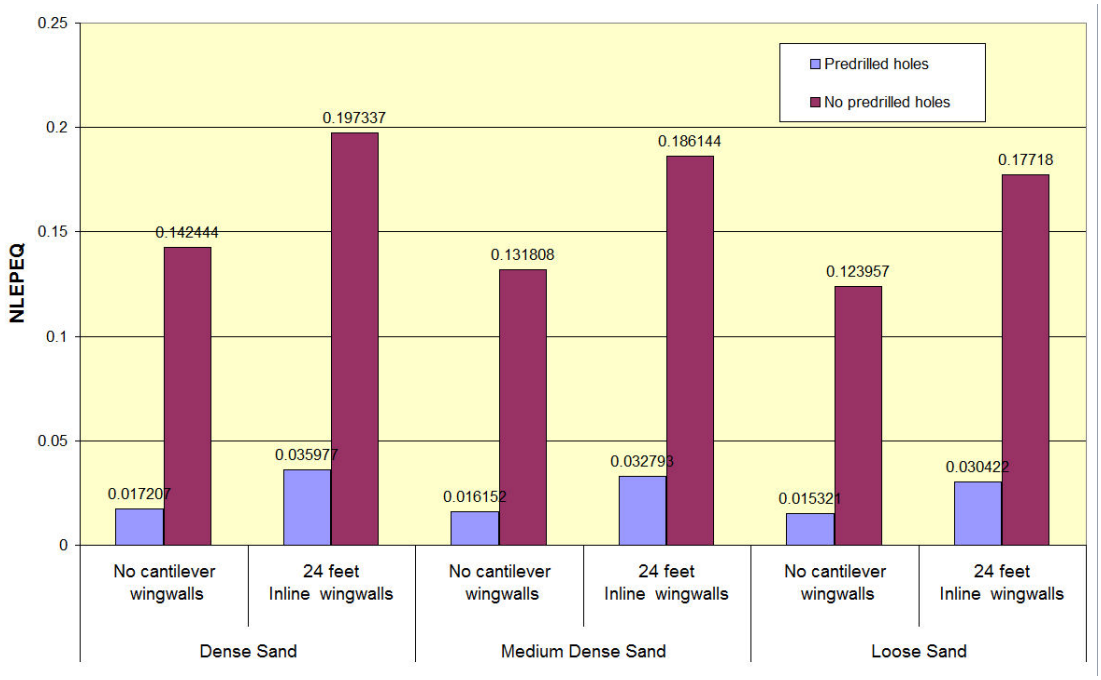

Figure 10-6 Comparison of equivalent plastic strain EPEQ in a 1200-feet-long bridge No predrilled holes Vs predrilled holes comparison

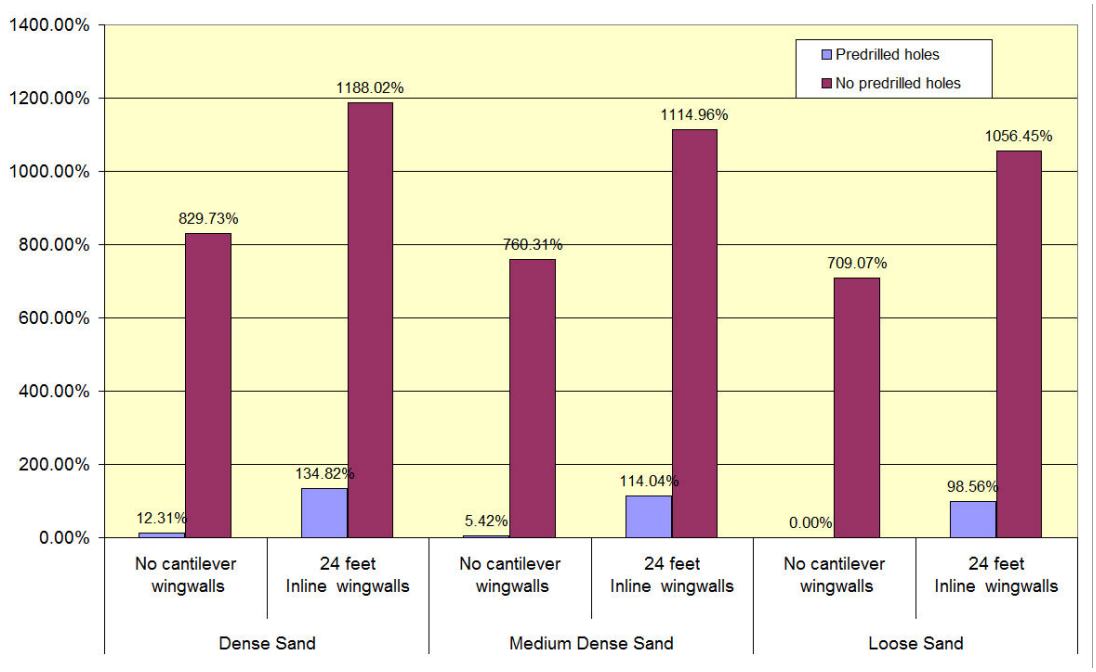

Figure 10-7 Percentage increase in equivalent plastic strain EPEQ in a 1200-feet-long bridge No predrilled holes Vs predrilled holes comparison

Conclusion

- The results indicate that the most critical inline cantilever wingwall configuration occurs with dense sand backfill soil and no predrilled holes.

For the most critical combination of parameters, that is,

- Temperature contraction (DL+TC)
- 1200-long-bridge
- 24-feet-long inline cantilever wingwalls
- No predrilled holes
- Dense sand backfill soil

the output from plasticity analysis is provided by means of the following two plots:

- The contour of the von Mises equivalent stress SEQV
- The contour of the equivalent plastic strain EPEQ

shown in Figures 10-8 and 10-9 respectively.

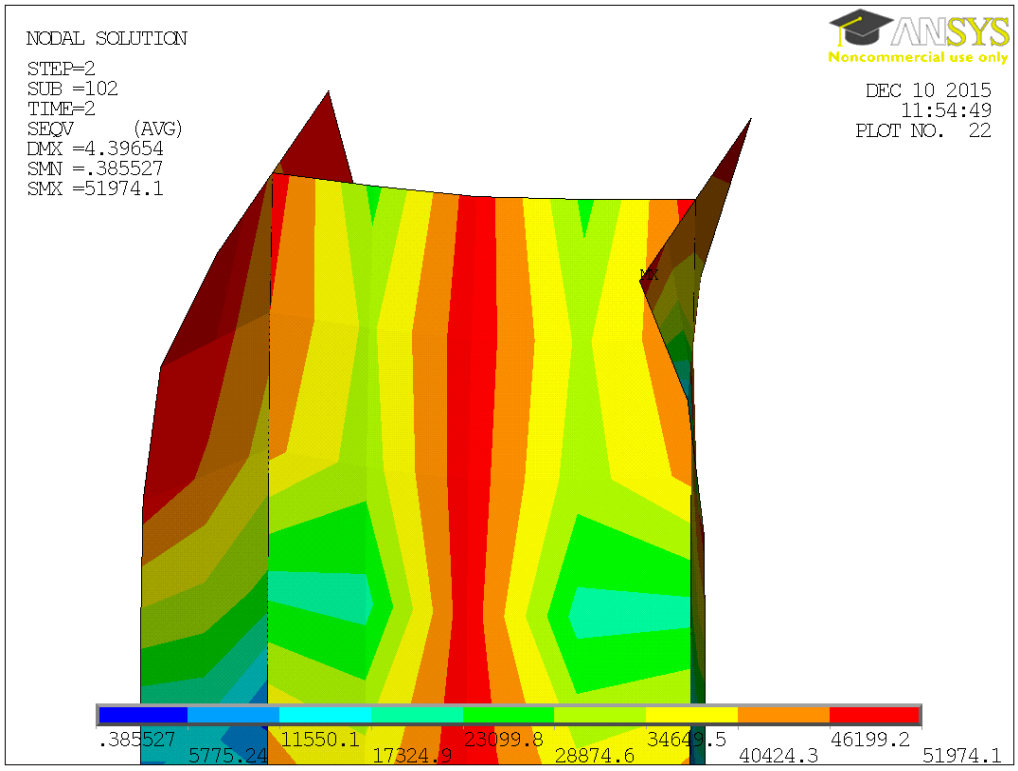

Figure 10-8 Contour of the Von Mises equivalent stress SEQV for piles for the most critical combination of parameters during temperature contraction DL+TC

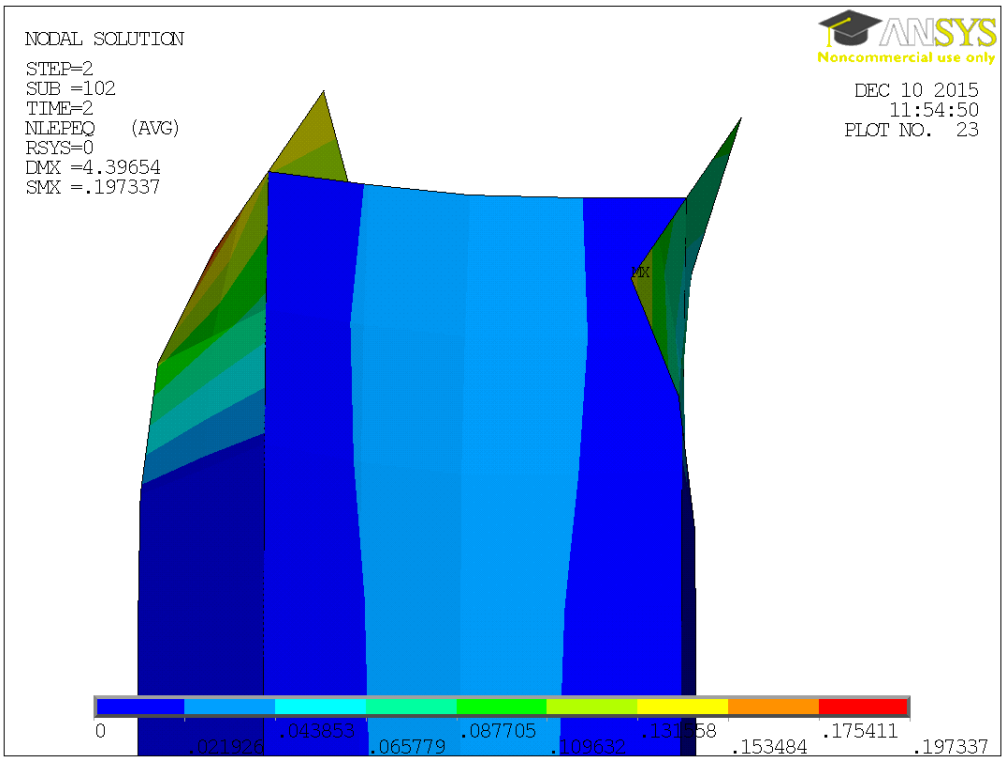

Figure 10-9 Contour of the equivalent plastic strain EPEQ for piles for the most critical combination of parameters during temperature contraction DL+TC

Conclusion

- The results indicate that no plastic hinge is formed near the pile head even under the most critical combination of parameters. This includes orientation of piles in weak-axis bending, presence of stiff soil around piles with no predrilled holes at the top nine feet of piles, maximum bridge length of 1200 feet, use of inline cantilever wingwalls with a maximum length of 24 feet, dense sand backfill soil behind the abutments and wingwalls during temperature contraction.

A comparison of the values of equivalent plastic strain EPEQ in the piles of 2-lane and 4-lane bridges is performed in order to detect any differences. This is due to the fact that for two-lane bridges backfill soil pressures acting on the wingwalls account for a larger portion of the total soil pressure acting on the combined abutment/wingwall length. The results are summarized in Table 10-6 and shown in Figure 10-10.

Table 10-6 Comparison of 2-lane bridges Vs 4-lane bridges in terms of equivalent plastic strain EPEQ in the piles

	No Cantilever Wingwalls	Inline Wingwalls 0 Degrees	Flared Wingwalls 45 Degrees	U-Shaped Wingwalls 90 Degrees
Piles with predrilled holes and medium dense sand backfill soil				
430 feet 2 lanes	0.00000349	0.00255	0.003801	0.001449
430 feet 4 lanes	0.00000212	0.001867	0.004001	0.001008
1200 feet 2 lanes	0.016152	0.030701	0.025895	0.02049
1200 feet 4 lanes	0.016091	0.025941	0.026137	0.019182

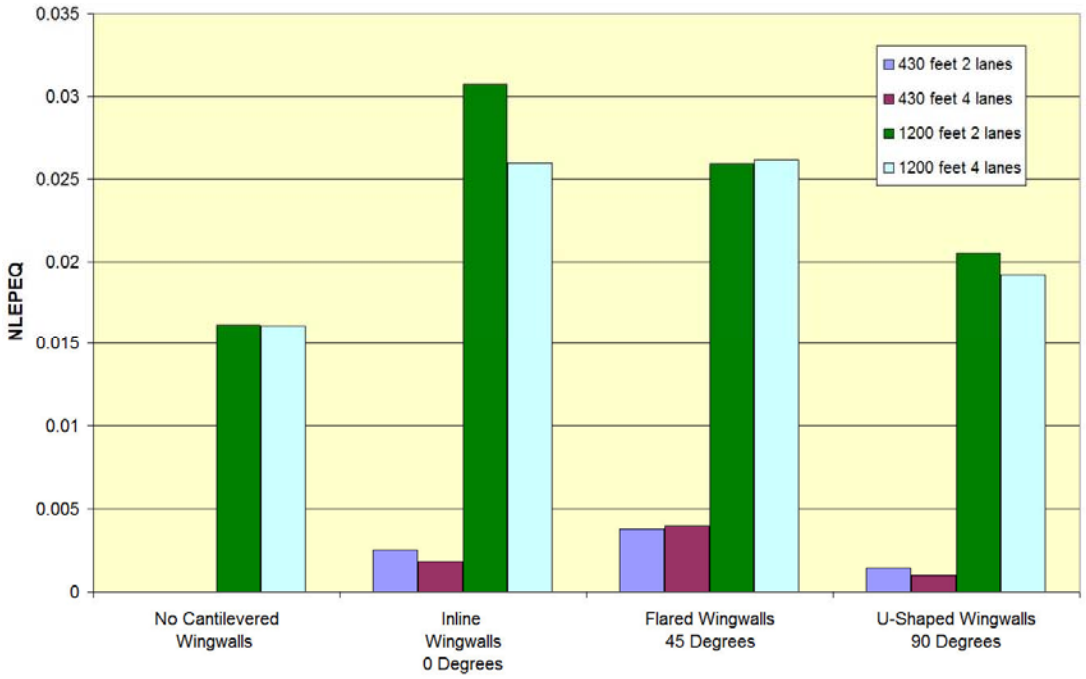

Figure 10-10 Comparison of 2-lane bridges Vs 4-lane bridges in terms of equivalent plastic strain EPEQ in the piles

Conclusion

- Pile stresses in bridges with two lanes are slightly higher compared to bridges with four lanes. This is due to the fact that for two-lane bridges backfill soil pressures acting on the wingwalls account for a larger portion of the total soil pressure acting on the combined abutment/wingwall length.

10.3. Cracking Pattern in Integral Abutments

The ANSYS concrete material model has the capability to predict cracking of concrete in tension and crushing in compression. Cracking and crushing are determined by a failure surface (Figure 9-25). Once the failure surface is surpassed, concrete cracks if any principal stress is tensile while crushing occurs if all principal stresses are compressive. The failure surface in ANSYS is based on the William and Warnke (1975).

The results of the parametric studies indicate progressive cracking of concrete, but no crushing. In reference to cracking the intent of this study is to identify cracking patterns, not to perform detailed cracking analysis. The evolution of cracking pattern in the integral abutments with increasing bridge length is shown in Figures 10-11 and 10-12. Figure 10-11 presents the evolution of cracking pattern in integral abutments with predrilled holes at the top nine feet of piles Figure 10-12 presents the evolution of cracking pattern in integral abutments with no predrilled holes at the top nine feet of piles. In both figures, the cracking pattern is shown for the following bridge lengths: 300 feet, 400 feet, 600 feet, 800 feet, 1000 feet, and 1200 feet.

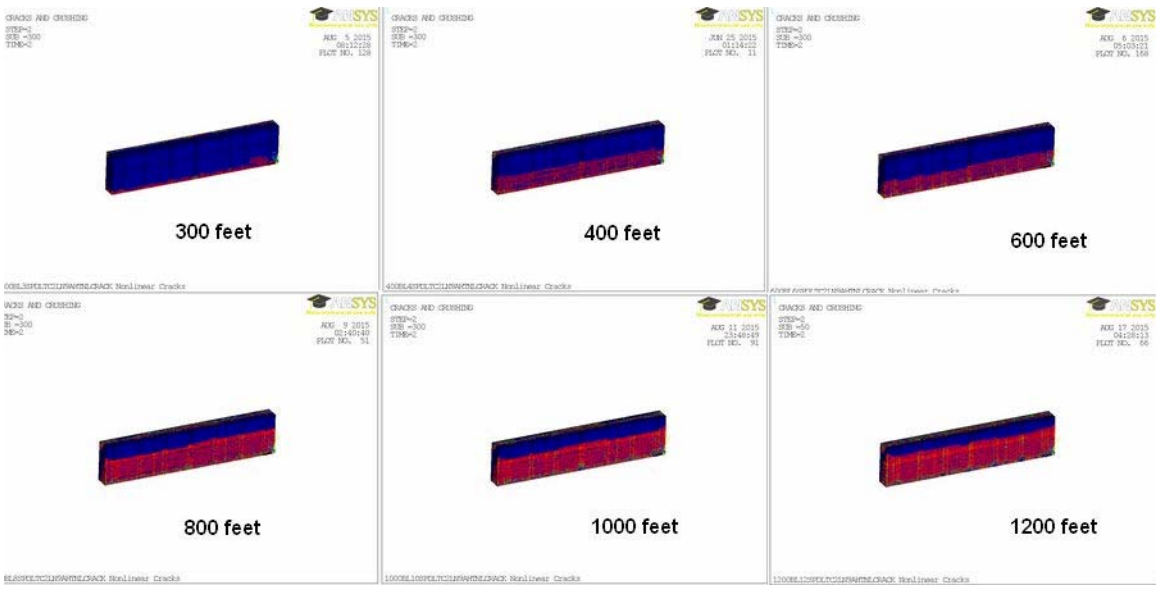

Figure 10-11 Evolution of cracking pattern in integral abutments with predrilled holes at top nine feet of piles

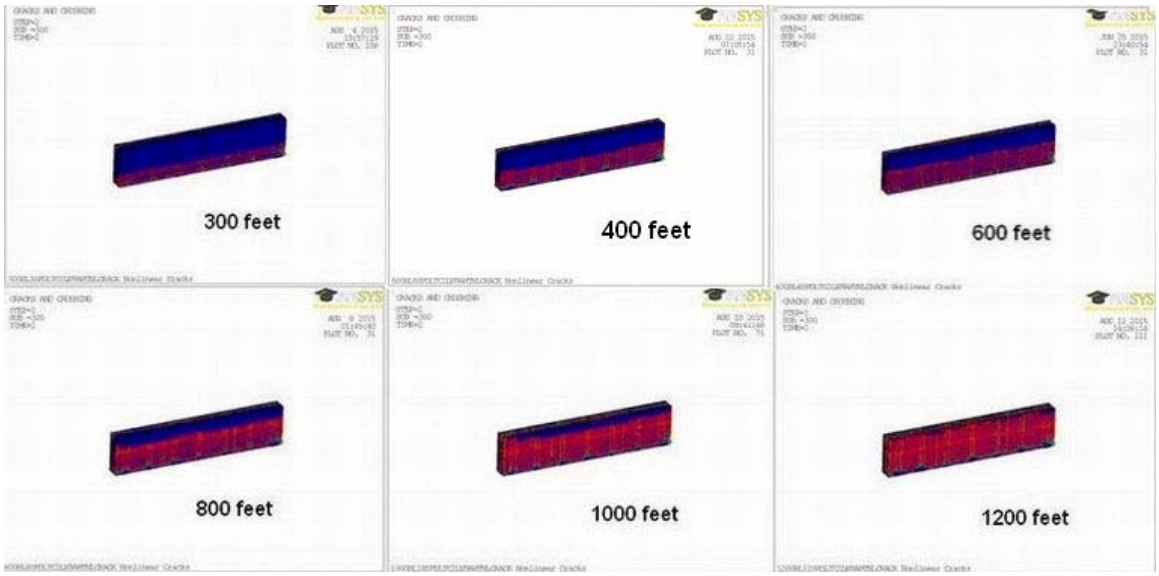

Figure 10-12 Evolution of cracking pattern in integral abutments with no predrilled holes at top nine feet of piles

Conclusions

- For the same bridge length, extent of cracking in integral abutments is more widespread when no predrilled holes are used at the top nine feet of piles compared to the case in which predrilled holes are used at the top nine feet of piles.

- Moderate amount of cracking is first observed in the integral abutments at a bridge length of 300 feet when no predrilled holes are used and at 400 feet bridge length when predrilled holes are used at the top nine feet of piles.

- Significant amount of cracking is first observed in the integral abutments at a bridge length of 400 feet when no predrilled holes are used and at 800 feet bridge length when predrilled holes are used at the top nine feet of piles.

- Both moderate and especially significant amounts of cracking point to a bridge maintenance issue. Failure to address this issue might lead to corrosion of the rebar and subsequent loss of strength.

- A number of states impose limitations on the length of cantilever wingwalls apparently because of cracking in the abutments. However, cracking occurs due to thermal expansion with increasing bridge length, not because of presence of cantilever wingwalls.

Figure 10-13 presents the extent of cracking in a 1200-feet-long bridge with 24-feet-long inline cantilever wingwalls.

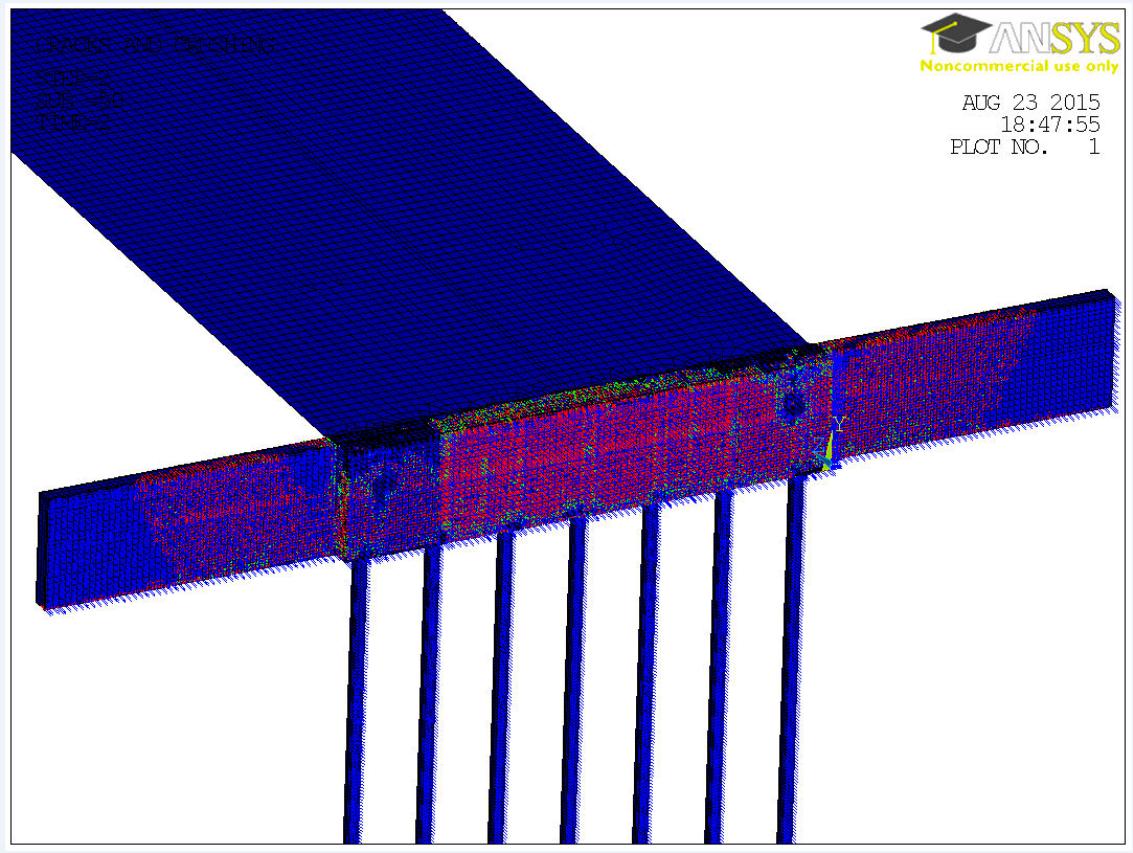

Figure 10-13 Cracking in a 1200-feet-long bridge with 24-feet-long inline cantilever wingwalls

10.4. Stresses in the Reinforcing Steel of Integral Abutments with no Cantilever Wingwalls

Modeling of steel reinforcement using finite elements in ANSYS can be performed using either the discrete reinforcement modeling option or the smeared reinforcement modeling option. The purpose of this analysis is to determine the stress in the rebar and capture the yield, which is only possible using the discrete modeling option. Thus, the discrete modeling option is used. Using this option, the steel reinforcement is simulated as spar elements (Figure 10-14) with geometric properties similar to the original reinforcing. These elements are connected to the concrete mesh nodes and hence the concrete and the steel reinforcement share the same nodes (Figure 9-27). Figure 10-14 shows a close up of the reinforcement modeled in a discrete manner in the integral abutment using LINK8 spar elements.

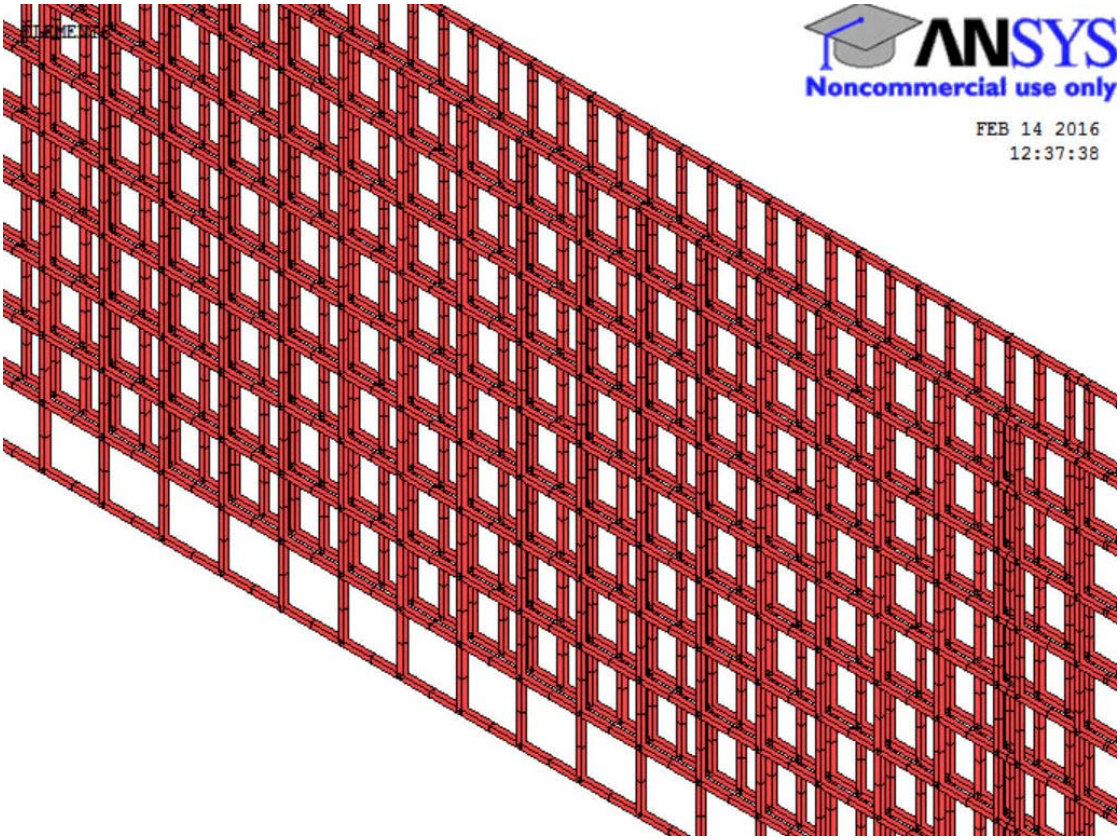

Figure 10-14 Abutment rebar modeled with LINK8 spar elements

Table 10-7 summarizes the results obtained for the maximum stress in the abutment reinforcing steel for bridges built with no cantilever wingwalls during temperature expansion (DL+TE). The bridges vary in length from 100 feet to 1200 feet and the backfill soil is medium dense sand. The results include a case in which predrilled holes are used at the top nine feet of piles and a case in which predrilled holes are not used. All results are shown in Figure 10-15.

Table 10-7 Maximum stress in the integral abutment reinforcing steel during temperature expansion with medium dense sand backfill soil and no cantilever wingwalls

Bridge length (feet)	Maximum Rebar Stress in the Abutment (psi) with predrilled holes	Maximum Rebar Stress in the Abutment (psi) No predrilled holes
100	6082	7761
200	17325	19042
300	26098	30673
400	33529	36196
600	48223	54964
950	58697	59689
1000	60004	60012
1200	60021	60027

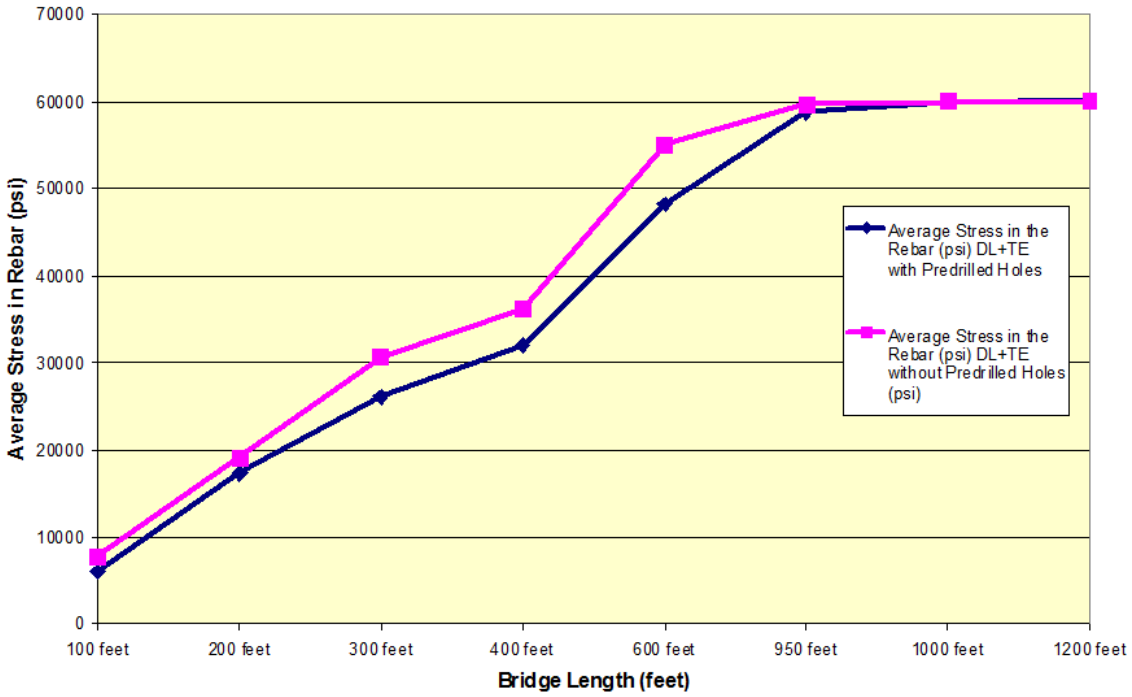

Figure 10-15 Maximum stress in the integral abutment reinforcing steel during temperature expansion with medium dense sand backfill soil and no cantilever wingwalls

Figure 10-16 shows the location of the maximum stress in the reinforcing steel for the case of a 1000-feet-long bridge in which predrilled holes are used at the top nine feet of piles.

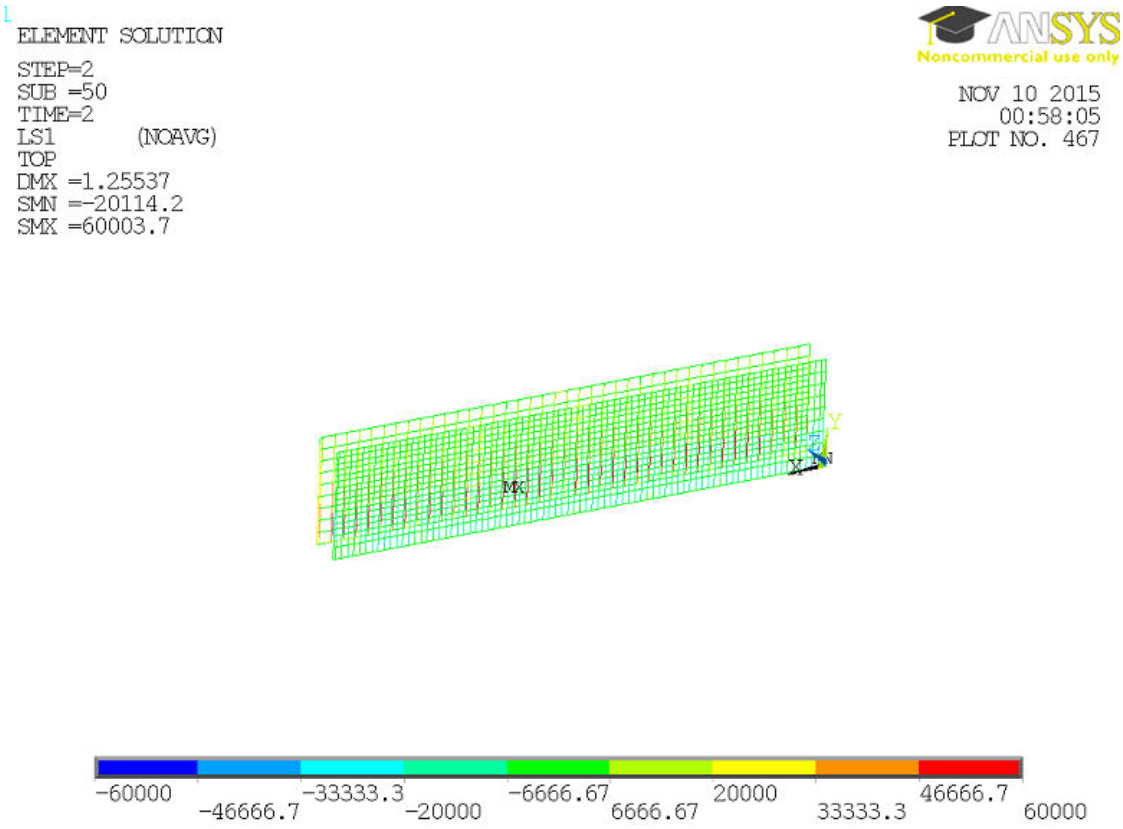

Figure 10-16 Stress in the integral abutment reinforcing steel of 1000-feet-long bridge during temperature expansion with predrilled holes and medium dense sand backfill soil, but no cantilever wingwalls

Table 10-8 summarizes the results obtained for the maximum stress in the abutment reinforcing steel for bridges built with no cantilever wingwalls during temperature contraction (DL+TC). The bridges vary in length from 100 feet to 1200 feet and the backfill soil is medium dense sand. The results include a case in which predrilled holes are used at the top nine feet of piles and a case in which predrilled holes are not used. All results are shown in Figure 10-17.

Table 10-8 Maximum stress in the integral abutment reinforcing steel during temperature contraction with medium dense sand backfill soil and no cantilever wingwalls

Bridge length (feet)	Maximum Rebar Stress in the Abutment (psi) with predrilled holes	Maximum Rebar Stress in the Abutment (psi) No predrilled holes
100	11923	14622
200	13397	17127
300	16128	21219
400	18688	27243
600	21108	33168
800	23567	41297
1000	28702	49102
1200	33770	53034

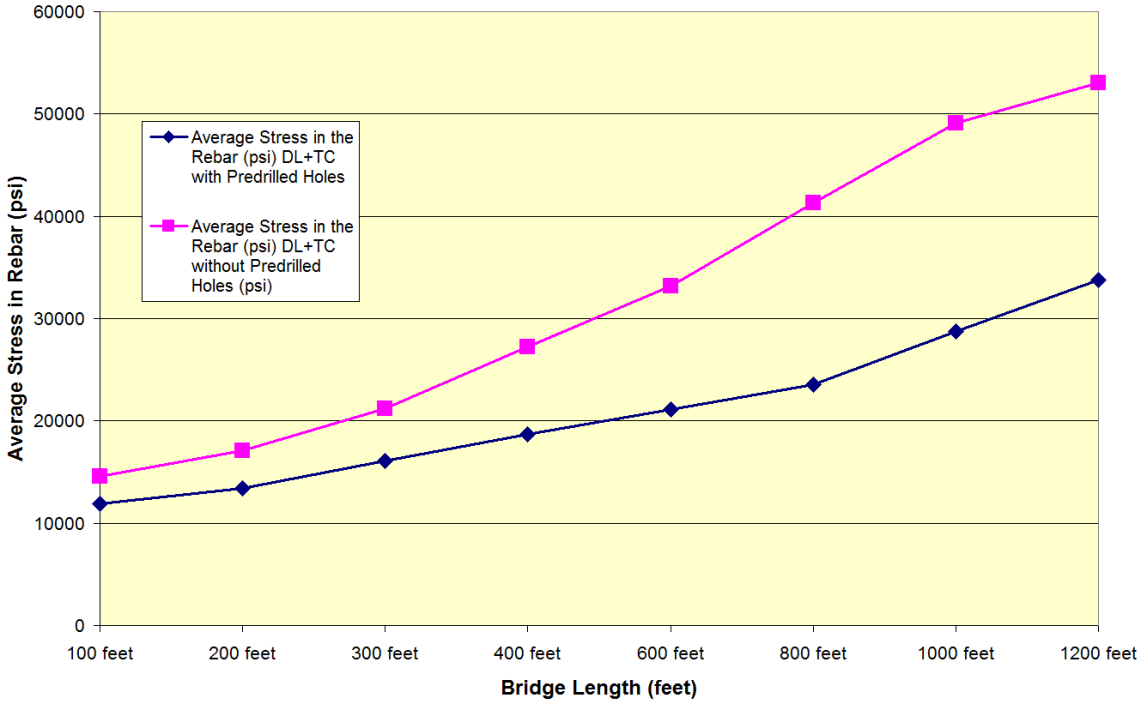

Figure 10-17 Average stress in the integral abutment reinforcing steel during temperature contraction with medium dense sand backfill soil and no cantilever wingwalls

Conclusions

- Stresses in the reinforcing steel during temperature expansion reach yield at a bridge length of 1000 feet with medium dense sand backfill soil. When dense sand is used as a backfill soil, stresses in the reinforcing steel reach yield at 900 feet. When loose sand is used as a backfill soil, stresses in the reinforcing steel reach yield at 1100 feet. In comparison, stresses in the reinforcing steel during temperature contraction do not reach yield even at the maximum bridge length of 1200 feet with any of the three types of backfill soil. This is explained by the fact that the magnitude of passive pressures on the abutments during temperature expansion is more severe than the magnitude of active pressures on the abutments during temperature contraction. Dense sand backfill soil induces the highest stresses in the reinforcing steel followed by medium dense sand and loose sand. This is due to the fact that it has the highest coefficient of passive earth pressure (Kp) and unit weight (γ).

- The effect of use predrilled holes on rebar stresses is more pronounced during temperature contraction rather than during temperature expansion. This is due to the fact that during temperature rise and for longer bridges, the magnitude of passive pressures on the abutments is comparable in magnitude to the magnitude of pressures imposed by the very stiff clay on the piles. Conversely, during temperature fall, the magnitude of active soil pressures applied on the abutments is small compared to the magnitude of pressures exerted by the very stiff clay on the piles.

- During both temperature expansion and temperature contraction, the location of maximum stress in the reinforcing steel is always at the bottom of the abutment.

10.5. Stresses in the Reinforcing Steel of Integral Abutments with Inline Cantilever Wingwalls

Because inline cantilever wingwalls induce higher bending stresses in the abutment walls compared to flared and U-shaped wingwalls, stresses in the reinforcing steel in the abutments are investigated for the case of integral abutments with inline cantilever wingwalls. The intent is to determine the bridge length at which yielding in the reinforcing steel might occur under various scenarios. This include use of predrilled holes, type of backfill soil, and length of inline cantilever wingwalls. The results are described below and summarized in Table 10-9. The table also includes similar results for integral abutment bridges with no cantilever wingwalls described in the previous section.

- When medium dense sand is used as a backfill material behind the integral abutments, stresses in the abutment reinforcing steel reach the level of yield stress of 60 ksi during temperature rise and a bridge length of 1000 feet. This occurs with and without predrilled holes at the top nine feet of piles. Adding inline cantilever wingwalls on both sides of the integral abutment along with predrilled holes around the top nine feet of piles, yielding of in the reinforcing steel is reached at a bridge length between 1000 and 1200 feet depending on the exact shape of the wingwall. While rectangular wingwalls are used in this study in order to determine the most severe effects on the bridge superstructure, in practice, most wingwalls are tapered. Using tapered wingwalls, however, less backfill soil pressures are exerted on the wingwalls compared to rectangular-shaped wingwalls. Consequently, yielding of the rebars will occur at a bridge length between 1000 and 1200 feet. In comparison, using inline cantilever wingwalls on both sides of the abutment without predrilled holes at the top nine feet of piles, yielding of the rebars is reached at a bridge length between 1000 and 1100 feet.

- When dense sand is used as a backfill material behind the integral abutments, stresses in the abutment reinforcing steel reach the level of yield stress of 60 ksi during temperature rise and a bridge length of 900 feet. This occurs with and without predrilled holes around the top nine feet of piles. Adding inline cantilever wingwalls on both sides of the integral abutment, with and without predrilled holes around the top nine feet of piles, yielding of reinforcing steel occurs at a bridge length between 900 feet and 1100 feet depending on the exact shape of the wingwall.

- When loose sand is used as a backfill material behind the integral abutments, stresses in the abutment reinforcing steel reach the level of yield stress of 60 ksi during temperature expansion and a bridge length of 1100 feet. This occurs with and without predrilled holes around the top nine feet of piles. Adding inline cantilever wingwalls on both sides of the integral abutment along with predrilled holes around the top nine feet of piles, yielding of reinforcing steel is reached between 1100 and 1200 feet for wingwalls with length up to 8 feet. For longer wingwalls and with predrilled holes around the top nine feet of piles, yielding of

reinforcing steel is reached at a bridge length between 1100 and a bridge length longer than 1200 feet. In comparison, using inline cantilever wingwalls on both sides of the abutment without predrilled holes around the top nine feet of piles, yielding of the reinforcing steel is reached at a bridge length between 1100 and 1200 feet for all wingwall lengths.

- Stresses in the reinforcing steel in the abutment do not reach the level of yield stress during temperature contraction because the magnitude of active soil pressures acting on the integral abutment is not significant enough to cause yielding of the reinforcing steel. This occurs with all three types of soil backfill material; dense sand, medium dense sand, and loose sand with and without predrilled holes around the top nine feet of piles. The addition of inline wingwalls for the case of falling temperatures increases the stresses in the reinforcing steel, but not enough to reach the level of yield stress with and without predrilled holes at the top nine feet of piles.

Table 10-9 Bridge length (feet) at onset of yielding of reinforcing steel

<table>
<tr><th colspan="5">Temperature Expansion (DL+TE)</th></tr>
<tr><th rowspan="2">Backfill soil</th><th colspan="2">Bridges with no cantilever wingwalls</th><th colspan="2">Bridges with inline cantilever wingwalls</th></tr>
<tr><td>With Predrilled holes</td><td>No Predrilled holes</td><td>With Predrilled holes</td><td>No Predrilled holes</td></tr>
<tr><td rowspan="2">Dense sand</td><td rowspan="2">900</td><td rowspan="2">900</td><td>8 ft WW→1100</td><td>8 ft WW→1100</td></tr>
<tr><td>24 ft WW→1100</td><td>24 ft WW→1100</td></tr>
<tr><td rowspan="2">Medium dense sand</td><td rowspan="2">1000</td><td rowspan="2">1000</td><td>8 ft WW→1200</td><td>8 ft WW→1100</td></tr>
<tr><td>24 ft WW→1200</td><td>24 ft WW→1100</td></tr>
<tr><td rowspan="2">Loose sand</td><td rowspan="2">1100</td><td rowspan="2">1100</td><td>8 ft WW→1200</td><td>8 ft WW→1200</td></tr>
<tr><td>24 ft WW→ No rebar yielding observed up to and including 1200'</td><td>24 ft WW→1200</td></tr>
<tr><th colspan="5">Temperature Contraction (DL+TC)</th></tr>
<tr><td colspan="5">During temperature contraction the stress in the rebar does not reach the level of yield stress for bridges with lengths up to 1200 feet in all cases. This includes bridges with no cantilever wingwalls as well as wingwalls up to 24 feet in length with and without predrilled holes. The results are true with all three types of backfill soil: dense sand, medium dense sand, and loose sand.</td></tr>
</table>

Figure 10-18 shows the location of the maximum stress in the reinforcing steel for the case of a 1100-feet-long bridge with 24-feet-long inline cantilever wingwalls during temperature expansion. The backfill soil is dense sand and there are predrilled holes at the top nine feet of piles.

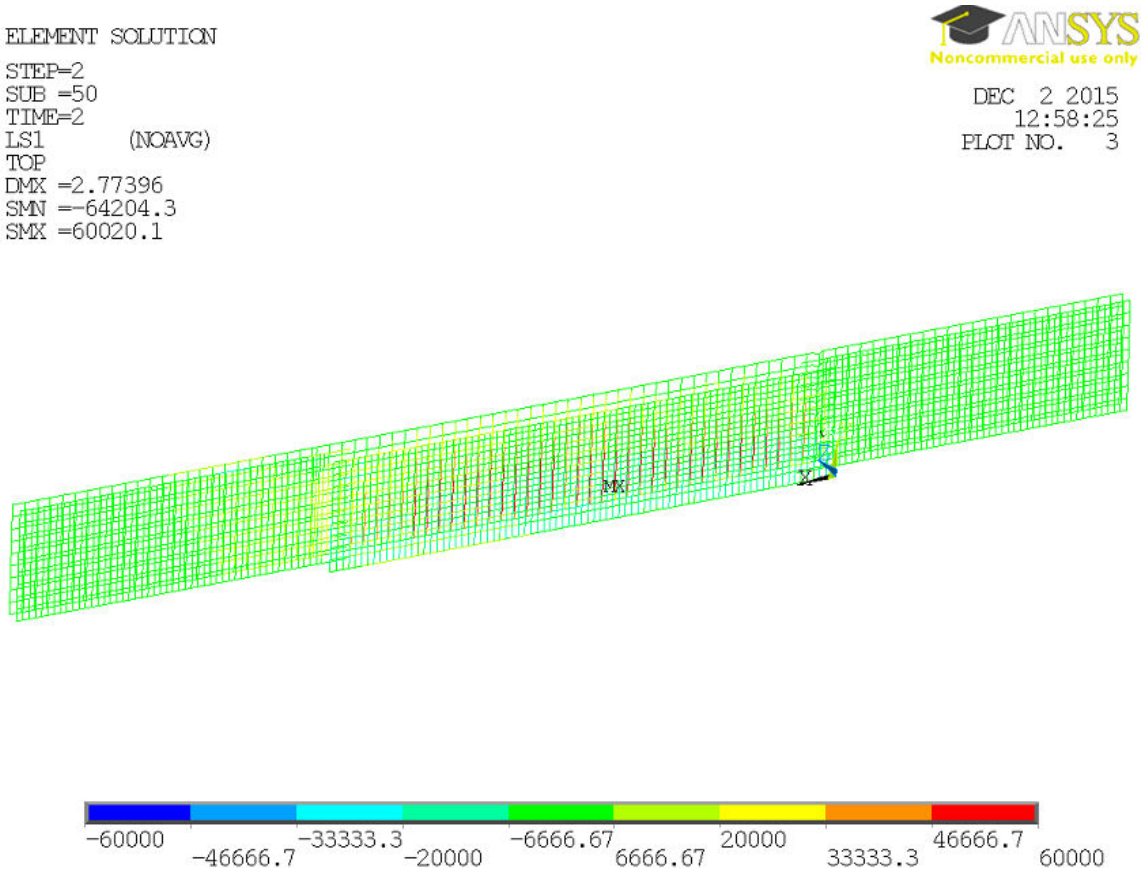

Figure 10-18 Stress in the abutment and wingwall reinforcing steel of 1100-feet-long integral abutment bridge with dense sand backfill soil, predrilled holes at top nine feet of piles and inline cantilever wingwalls during temperature expansion

Conclusions

- During temperature expansion, stresses in the reinforcing steel reach the level of yield stress at a certain bridge length that is a function of use of cantilever wingwalls, length of cantilever wingwalls, type of backfill soil, and use of predrilled holes at the top nine feet of piles. In comparison, during temperature contraction, stresses in the reinforcing steel do not reach the level of yield stress under any scenario even at the maximum bridge length of 1200 feet. This is explained by the fact that the magnitude of passive pressures exerted on the abutments during temperature expansion is more severe than the magnitude of active pressures on the abutments during temperature contraction.

- Comparison of the effects of length of cantilever wingwalls, use of predrilled holes, and type of backfill soil on the stresses in the reinforcing steel leads to the conclusion that the most critical parameter is the type of backfill soil.

- The most critical combination of parameters on stresses in the reinforcing steel occurs during temperature expansion with dense sand as a backfill soil and no inline cantilever wingwalls. In this instance, yielding in the reinforcing steel occurs at a bridge length of 900 feet.

- The location of maximum stress in the reinforcing steel during temperature expansion is at the intersection of integral abutments and the 24-feet-long cantilever wingwalls for bridge lengths up to 400 feet. Beyond the 400-feet bridge length, the location of maximum stress in the reinforcing steel is at the base of the abutment. This is due to the fact that for longer bridges the effect of bridge length is more severe than the effect of wingwall length on stresses in the reinforcing steel.

10.6. Effects of Cantilever Wingwalls on Bridge Superstructure

The effects of cantilever wingwalls on the bridge superstructure are expressed in terms of the magnitude of axial forces introduced into the steel girders. These effects are investigated using all three types of cantilever wingwalls (inline, flared, and U-shaped) with all three types of backfill soil (dense sand, medium dense sand, and loose sand) for both the case in which there are predrilled holes at the top nine feet of piles and for the case that no predrilled holes are used at the top nine feet of piles. Bridge length ranges from 100 to 1200 feet as described in detail in chapter 6. Loadings include temperature expansion (DL+TE) and temperature contraction (DL+TC) as described in table 6-1.

The results indicate significant effects only during temperature expansion. The most severe effects occur with the maximum wingwall length of 24 feet. During temperature contraction, use of cantilever wingwalls does not lead to introduction of significant axial forces into the steel girders.

Figure 10-19 shows the variation in the magnitude of axial forces in the steel girders as bridge length increases from 100 to 1200 feet during thermal expansion with dense sand backfill soil and no predrilled holes at the top nine feet of piles for the following cases:

- integral abutment bridge with no cantilever wingwalls
- integral abutment bridge with inline cantilever wingwalls
- integral abutment bridge with flared cantilever wingwalls
- integral abutment bridge with U-shaped cantilever wingwalls

Figure 10-20 shows the percentage increase in the magnitude of girder axial forces as a result of use of cantilever wingwalls for all bridge lengths under consideration. This includes the following bridge lengths: 100 feet, 200 feet, 300 feet, 400 feet, 600 feet, 900 feet, and 1200 feet.

Figure 10-21 shows the variation in the magnitude of axial forces in the steel girders as bridge length increases from 100 to 1200 feet during thermal expansion with dense sand backfill soil and with predrilled holes at the top nine feet of piles for the following cases:

- integral abutment bridge with no cantilever wingwalls
- integral abutment bridge with inline cantilever wingwalls
- integral abutment bridge with flared cantilever wingwalls
- integral abutment bridge with U-shaped cantilever wingwalls

Figure 10-22 shows the percentage increase in the magnitude of girder axial forces as a result of use of cantilever wingwalls for all bridge lengths under consideration. This includes the following bridge lengths: 100 feet, 200 feet, 300 feet, 400 feet, 600 feet, 900 feet, and 1200 feet.

Figure 10-23 shows the variation in the magnitude of axial forces in the steel girders as bridge length increases from 100 to 1200 feet during thermal expansion with medium dense sand backfill soil and no predrilled holes at the top nine feet of piles for the following cases:

- integral abutment bridge with no cantilever wingwalls
- integral abutment bridge with inline cantilever wingwalls
- integral abutment bridge with flared cantilever wingwalls
- integral abutment bridge with U-shaped cantilever wingwalls

Figure 10-24 shows the percentage increase in the magnitude of girder axial forces as a result of use of cantilever wingwalls for all bridge lengths under consideration. This includes the following bridge lengths: 100 feet, 200 feet, 300 feet, 400 feet, 600 feet, 900 feet, and 1200 feet.

Figure 10-25 shows the variation in the magnitude of axial forces in the steel girders as bridge length increases from 100 to 1200 feet during thermal expansion with medium dense sand backfill soil and with predrilled holes at the top nine feet of piles for the following cases:

- integral abutment bridge with no cantilever wingwalls
- integral abutment bridge with inline cantilever wingwalls
- integral abutment bridge with flared cantilever wingwalls
- integral abutment bridge with U-shaped cantilever wingwalls

Figure 10-26 shows the percentage increase in the magnitude of girder axial forces as a result of use of cantilever wingwalls for all bridge lengths under consideration. This includes the following bridge lengths: 100 feet, 200 feet, 300 feet, 400 feet, 600 feet, 900 feet, and 1200 feet.

Figure 10-27 shows the variation in the magnitude of axial forces in the steel girders as bridge length increases from 100 to 1200 feet during thermal expansion with loose sand backfill soil and no predrilled holes at the top nine feet of piles for the following cases:

- integral abutment bridge with no cantilever wingwalls
- integral abutment bridge with inline cantilever wingwalls
- integral abutment bridge with flared cantilever wingwalls
- integral abutment bridge with U-shaped cantilever wingwalls

Figure 10-28 shows the percentage increase in the magnitude of girder axial forces as a result of use of cantilever wingwalls for all bridge lengths under consideration. This includes the following bridge lengths: 100 feet, 200 feet, 300 feet, 400 feet, 600 feet, 900 feet, and 1200 feet.

Figure 10-29 shows the variation in the magnitude of axial forces in the steel girders as bridge length increases from 100 to 1200 feet during thermal expansion with loose sand backfill soil and with predrilled holes at the top nine feet of piles for the following cases:

- integral abutment bridge with no cantilever wingwalls
- integral abutment bridge with inline cantilever wingwalls
- integral abutment bridge with flared cantilever wingwalls
- integral abutment bridge with U-shaped cantilever wingwalls

Figure 10-30 shows the percentage increase in the magnitude of girder axial forces as a result of use of cantilever wingwalls for all bridge lengths under consideration. This includes the following bridge lengths: 100 feet, 200 feet, 300 feet, 400 feet, 600 feet, 900 feet, and 1200 feet.

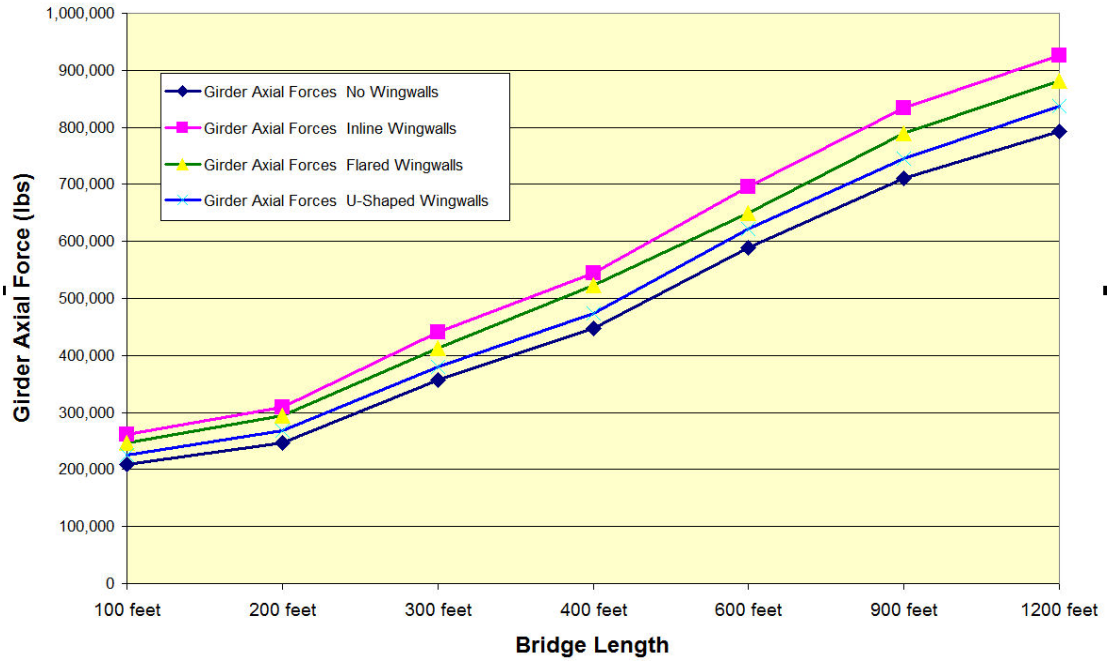

Figure 10-19 Girder axial forces during temperature expansion using dense sand backfill soil and no predrilled holes at the top nine feet of piles

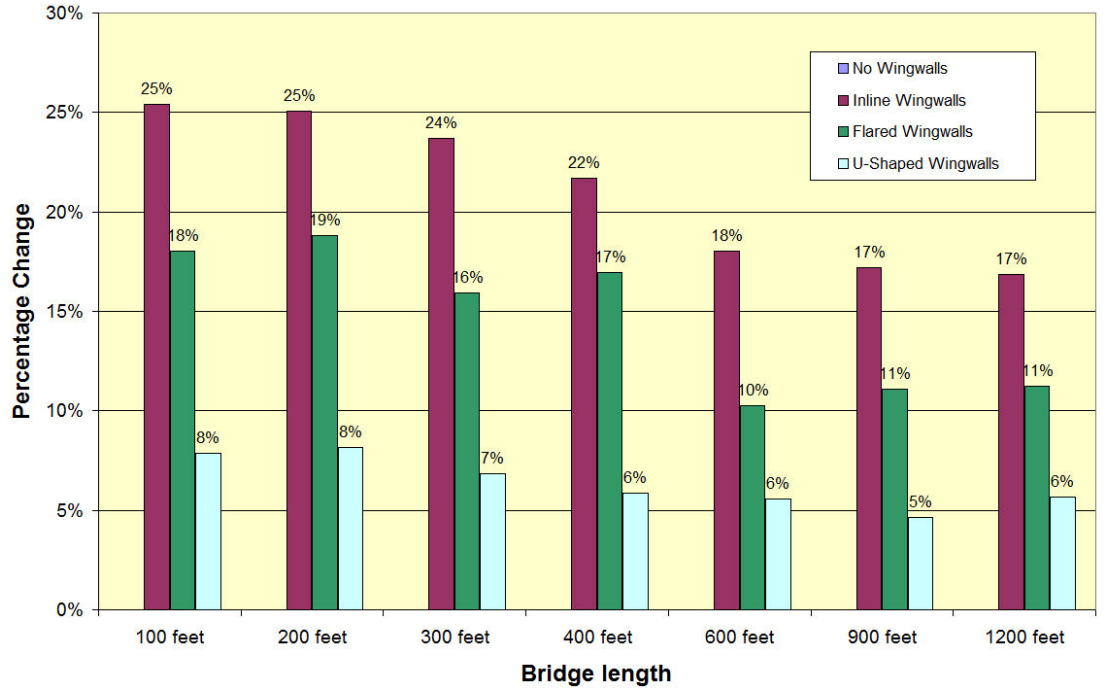

Figure 10-20 Percentage change in the magnitude of girder axial forces compared to bridges with no wingwalls during temperature expansion using dense sand backfill soil and no predrilled holes at the top nine feet of piles

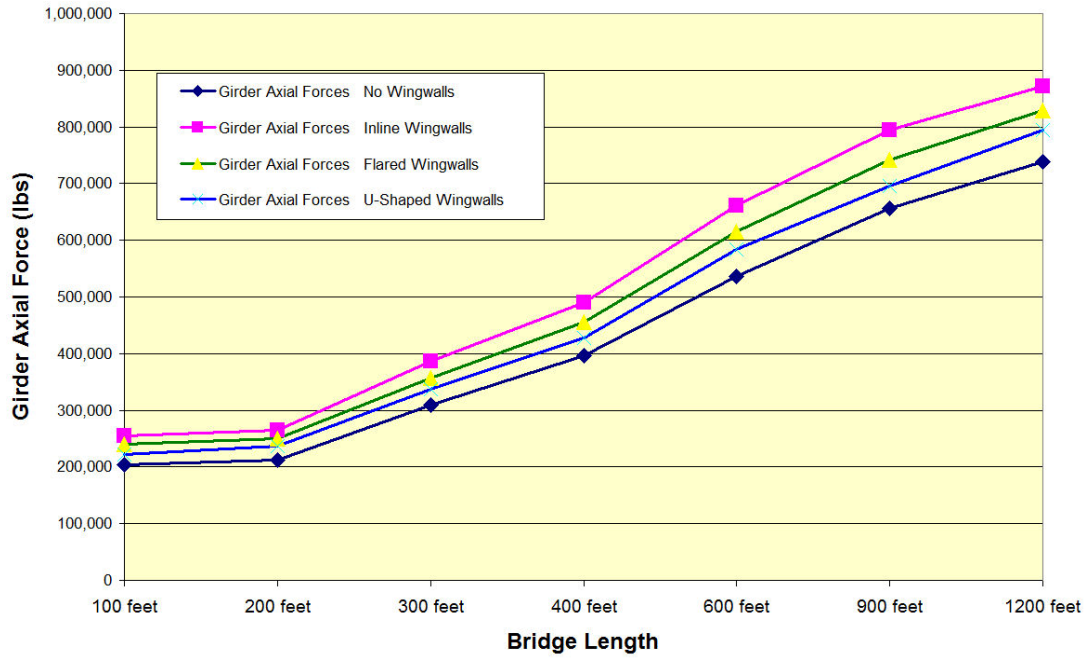

Figure 10-21 Girder axial forces during temperature expansion using dense sand backfill soil and predrilled holes at the top nine feet of piles

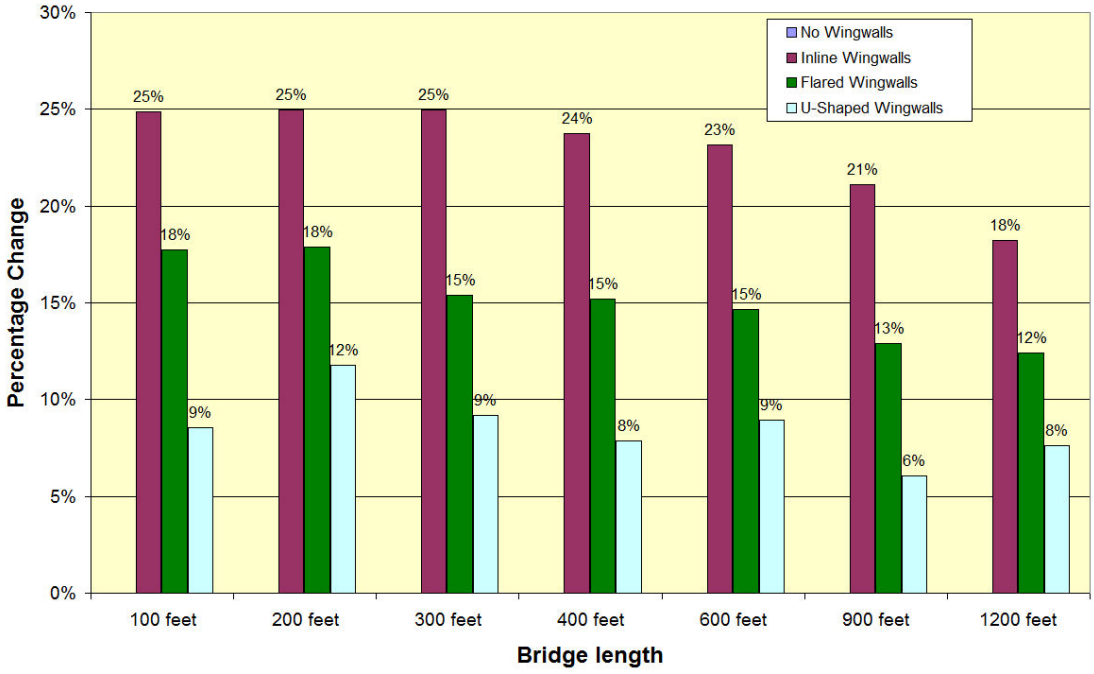

Figure 10-22 Percentage change in the magnitude of girder axial forces compared to bridges with no wingwalls during temperature expansion using dense sand backfill soil and predrilled holes at the top nine feet of piles

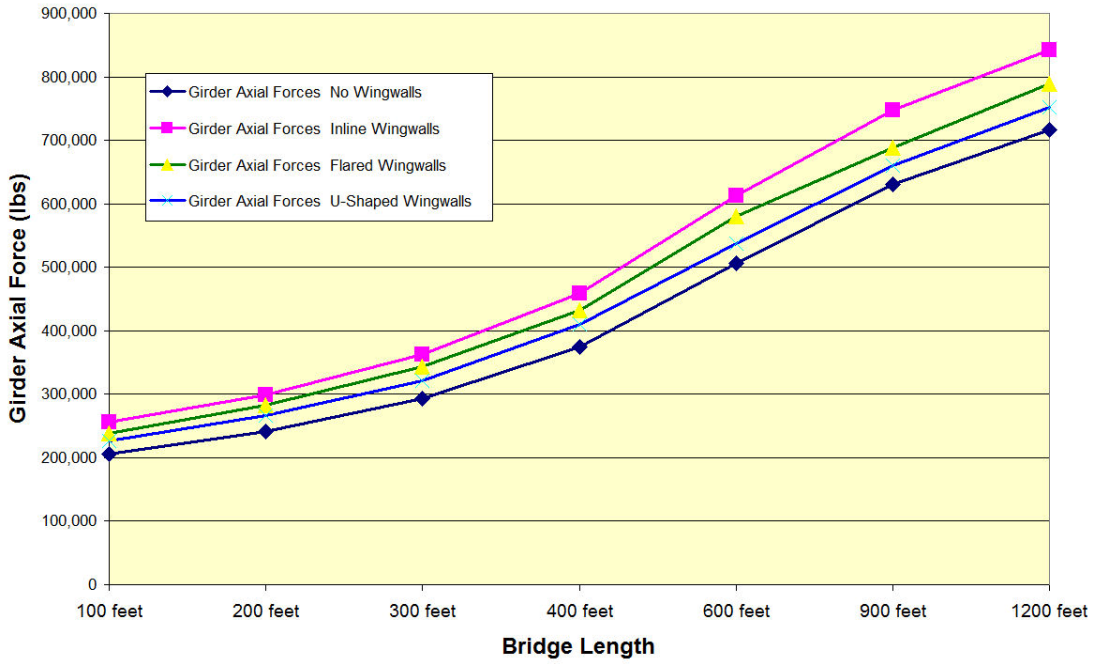

Figure 10-23 Girder axial forces during temperature expansion using medium dense sand backfill soil and no predrilled holes at the top nine feet of piles

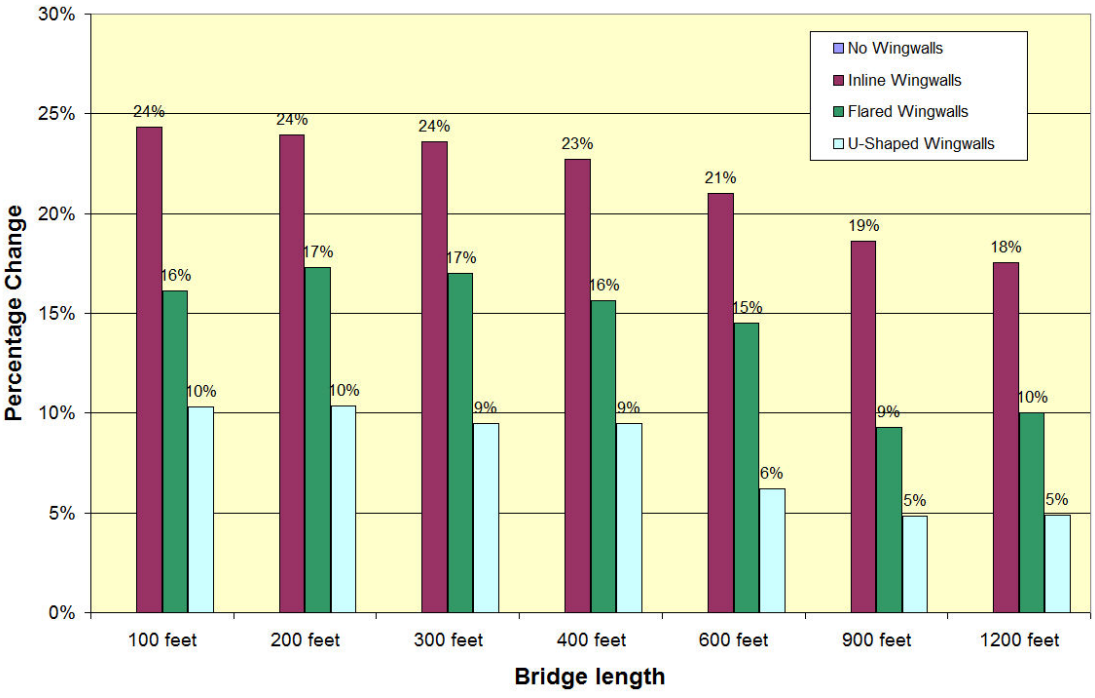

Figure 10-24 Percentage change in the magnitude of girder axial forces compared to bridges with no wingwalls during temperature expansion using medium dense sand backfill soil and no predrilled holes at the top nine feet of piles

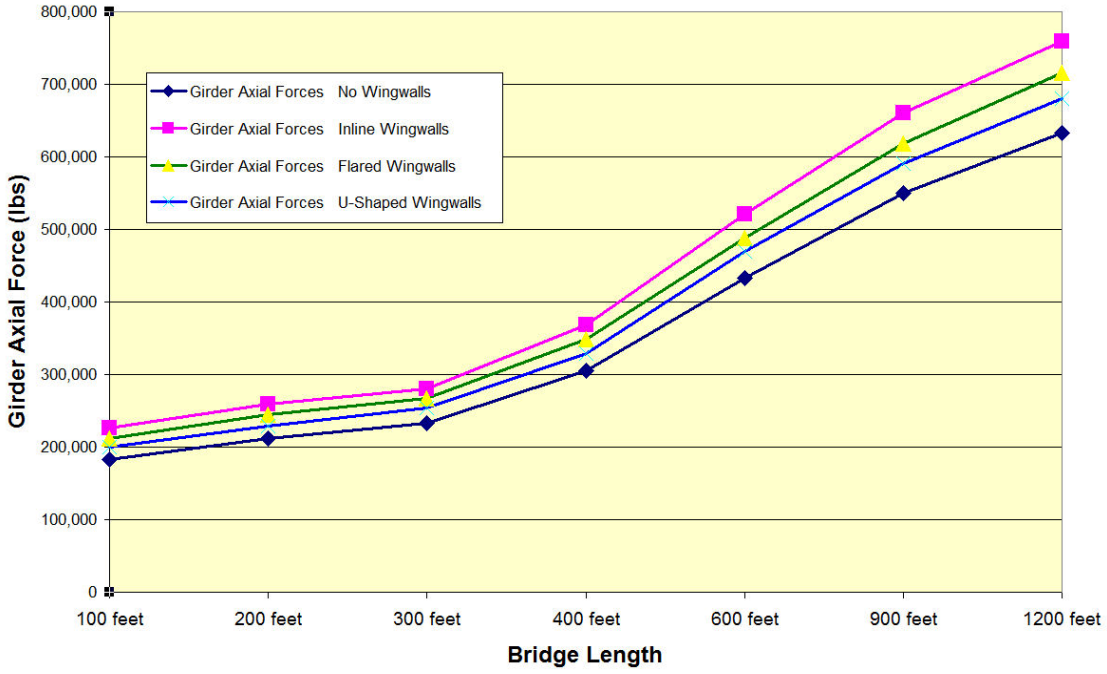

Figure 10-25 Girder axial forces during temperature expansion using medium dense sand backfill soil and predrilled holes at the top nine feet of piles

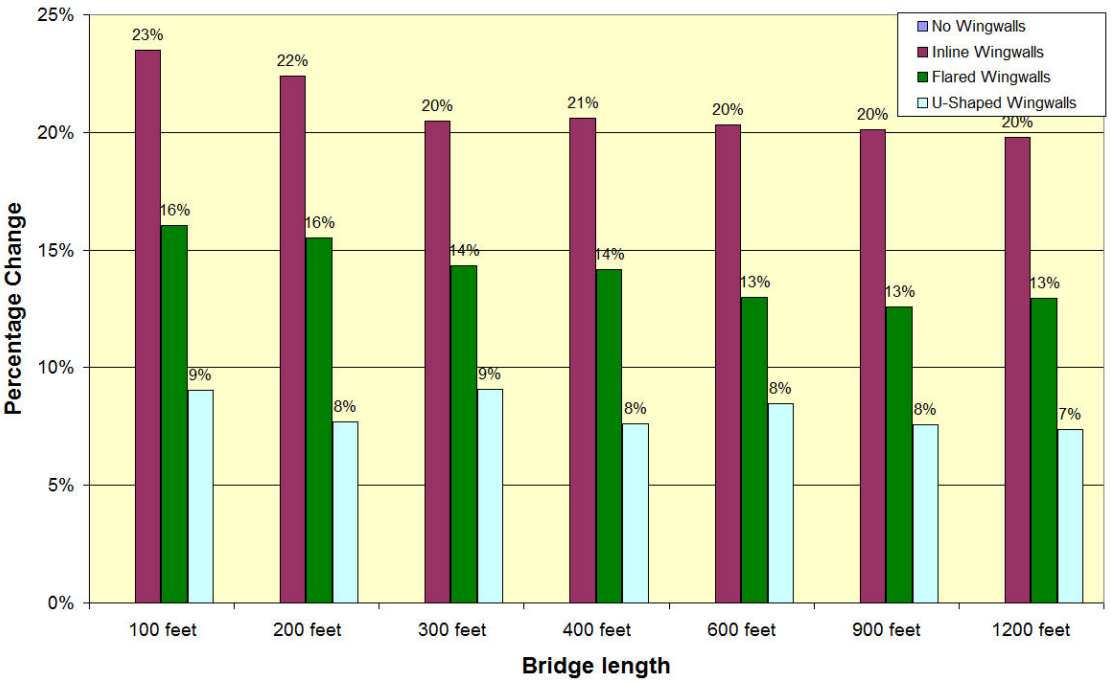

Figure 10-26 Percentage change in the magnitude of girder axial forces compared to bridges with no wingwalls during temperature expansion using medium dense sand backfill soil and predrilled holes at the top nine feet of piles

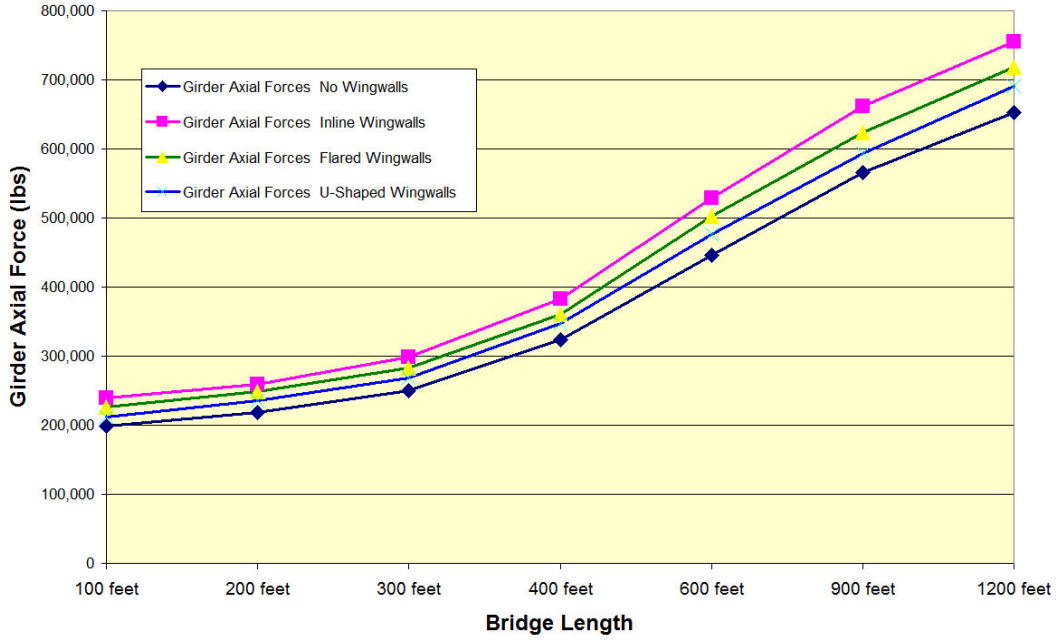

Figure 10-27 Girder axial forces during temperature expansion using loose sand backfill soil and no predrilled holes at the top nine feet of piles

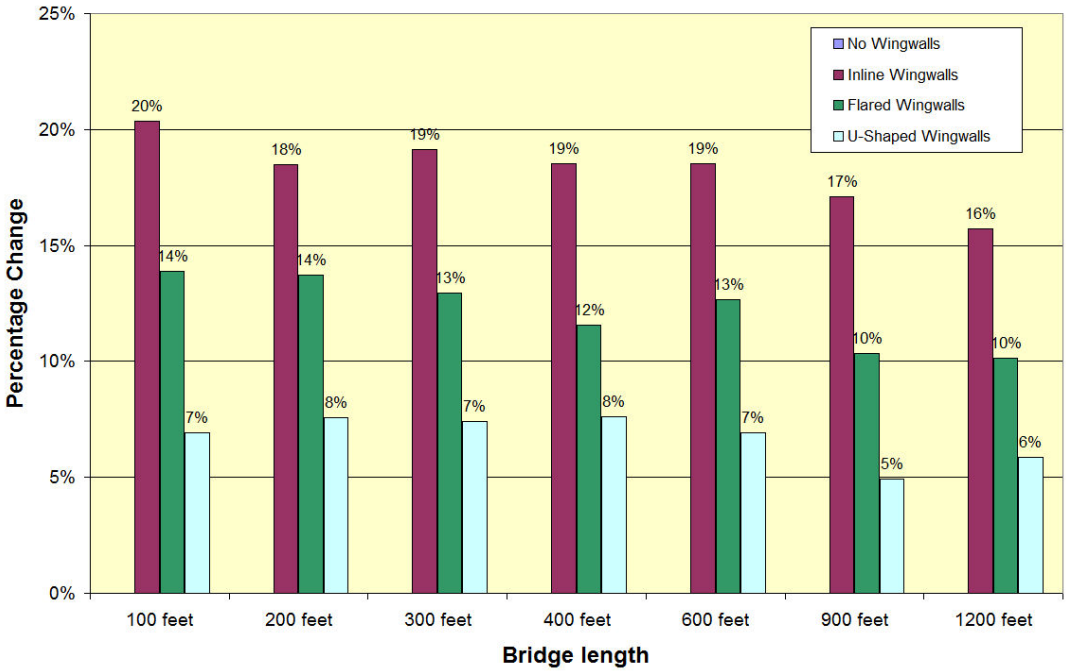

Figure 10-28 Percentage change in the magnitude of girder axial forces compared to bridges with no wingwalls during temperature expansion using loose sand backfill soil and no predrilled holes at the top nine feet of piles

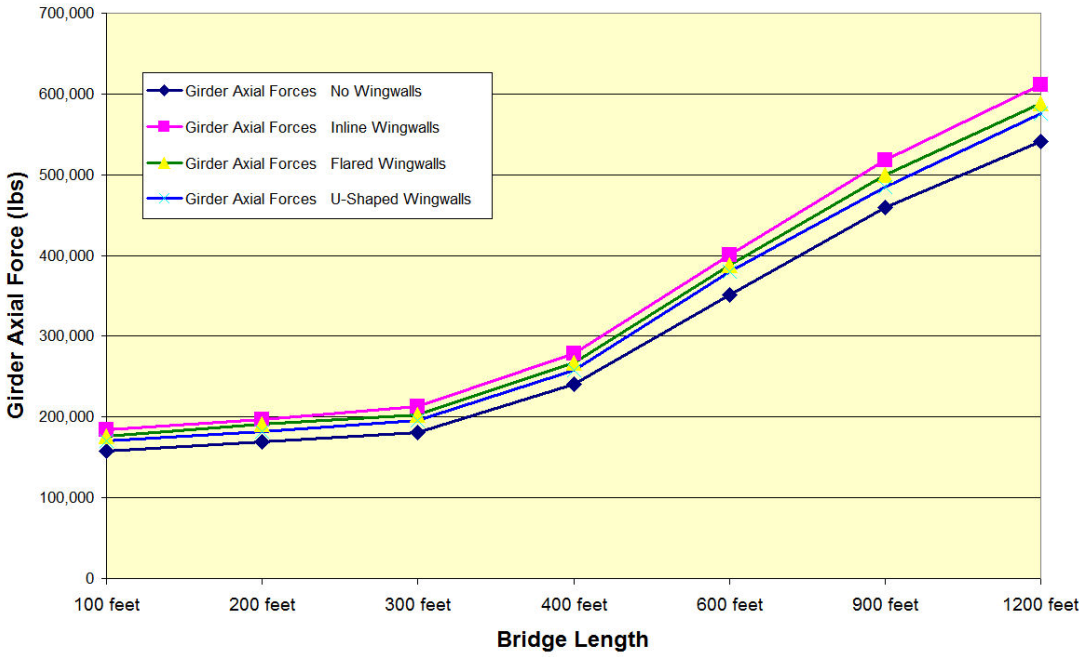

Figure 10-29 Girder axial forces during temperature expansion using loose sand backfill soil and predrilled holes at the top nine feet of piles

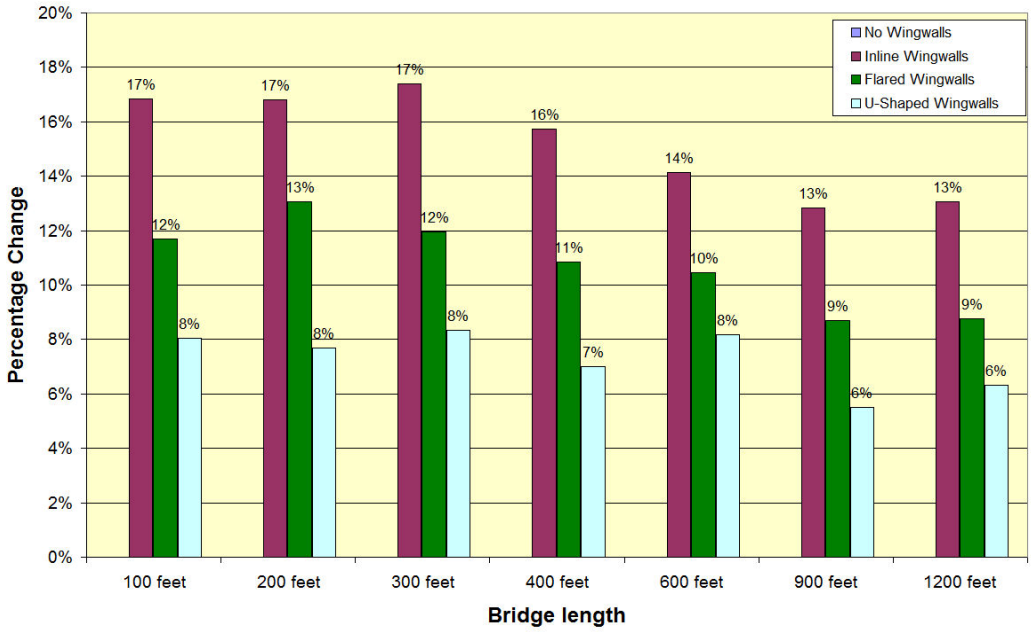

Figure 10-30 Percentage change in the magnitude of girder axial forces compared to bridges with no wingwalls during temperature expansion using loose sand backfill soil and predrilled holes at the top nine feet of piles

The results shown in Figures 10-20, 10-22, 10-24, 10-26, 10-28, and 10-30 are summarized in Table 10-10. The percentage values shown represent the average of all values for each type of wingwall in each of the figures. For example, for the case of inline cantilever wingwalls in Figure 10-20, average = [(25+25+24+22+18+17+17)/7] = 21.14%.

Table 10-10 Summary of percentage increase in the magnitude of axial forces introduced into the steel girders

	No Predrilled Holes			Predrilled Holes		
	Inline Cantilever Wingwalls	Flared Cantilever Wingwalls	U-Shaped Cantilever Wingwalls	Inline Cantilever Wingwalls	Flared Cantilever Wingwalls	U-Shaped Cantilever Wingwalls
Dense sand	21.14%	14.57%	6.57%	23.00%	15.14%	8.71%
Medium dense sand	21.86%	14.29%	7.71%	20.86%	14.14%	8.14%
Loose sand	18.29%	12.29%	6.86%	15.29%	10.86%	7.29%

Using an average value for each type of cantilever wingwall for both the case of presence of predrilled holes at the top nine feet of piles and the case of no predrilled holes at the top nine feet of piles, we can determine the effect of each type of cantilever wingwall on the magnitude of axial forces introduced into the girders. For example, for the case of inline cantilever wingwalls in Table 10-10 when no predrilled holes are used at the top nine feet of piles, [(21.14+21.86+18.29)/3] = 20.43%. The results are rounded to one decimal place and presented in Table 10-11.

Table 10-11 Effect of the three types of cantilever wingwalls on the magnitude of axial forces introduced into the steel girders

	No Predrilled Holes			Predrilled Holes		
	Inline Cantilever Wingwalls	Flared Cantilever Wingwalls	U-Shaped Cantilever Wingwalls	Inline Cantilever Wingwalls	Flared Cantilever Wingwalls	U-Shaped Cantilever Wingwalls
AVERAGE	20.4%	13.7%	7.0%	19.7%	13.4%	8.0%

Conclusions

Comparison of the results summarized in Table 10-11 indicates that the use of cantilever wingwalls has more impact on the magnitude of axial forces introduced into the steel girders than either the type of backfill soil or use of predrilled holes at the top nine feet of piles.

The results also indicate that using inline cantilever wingwalls results in higher axial forces into the steel girders than using either flared cantilever wingwalls or U-shaped cantilever wingwalls.

10.7. Ranking of Parameters on the Basis of their Impact on Bridge Elements

Evaluation of the results from the parametric studies indicate that the various parameters have different impact on the bridge elements under consideration. Table 10-12 provides a ranking of the impact of each of the parameters on the piles, reinforcing steel, and steel girders using a certain metric. The parameter with the most impact is ranked number 1, the parameter with the second most impact is ranked number 2 and so on.

The metric for the piles is the onset of plasticity and for the reinforcing steel is the onset of yielding. The metric for the steel girders is the percentage increase in the magnitude of axial forces introduced into the steel girders.

Table 10-12 Ranking of parameters on the basis of their impact on bridge elements

	Bridge Element		
	Piles	**Reinforcing Steel in Abutments**	**Steel Girders**
Metric	Onset of plasticity	Onset of yielding	Percentage increase in the magnitude of axial girder forces
Critical Load	Temperature Contraction (DL+TC)	Temperature Expansion (DL+TE)	Temperature Expansion (DL+TE)
Parameters	1. Use of predrilled holes	1. Bridge length	1. Bridge length
	2. Bridge length	2. Type of backfill soil	2. Use of cantilever wingwalls
	3. Use of cantilever wingwalls	3. Length of inline cantilever wingwall	3. Type of backfill soil
	4. Type of backfill soil	4. Use of predrilled holes	4. Use of predrilled holes

Chapter 11

Summary of Results, Conclusions, and Recommendations

This chapter presents a summary of the results described in detail in chapter 10. It follows with conclusions and recommendations for future research on the effects of cantilever wingwalls on the behavior of integral abutment bridges and integral abutment bridges in general.

Summary of Results

Effects of Cantilever Wingwalls on Pile Stresses

- Higher piles stresses are induced during thermal contraction rather than during thermal expansion. This is the result of wider temperature variation during temperature contraction compared to temperature variation during temperature expansion (temperature ranges are defined in Table 6-1). In addition, active soil pressures are aligned and in the same direction as the temperature-induced loading. Therefore, the resulting deformation in combination with the gravity forces acting on the piles (P-Δ effect) produces higher pile stresses during temperature fall. During temperature expansion, as the approach fill is pushed by the abutment, it tends to move the foundation soil in the same direction. This is beneficial as far as pile stresses is concerned because the foundation soil is moving in the same direction as the piles. The result is lower stresses in the piles during temperature expansion rather than during temperature contraction.

- Addition of any type of cantilever wingwall (inline, flared or U-shaped) has an effect on pile stresses. Cantilever wingwalls perpendicular to the traffic (inline wingwalls) induce the most stresses and plasticity in the piles. Thus, inline cantilever wingwalls is the most critical cantilever wingwall configuration.

- Comparison of the effects of cantilever wingwalls, predrilled holes, and backfill soil on pile stresses, leads to the conclusion that the most critical parameter among those three is by far the use of predrilled holes followed by the use of cantilever wingwalls. The type of backfill soil is the least critical.

- The most critical combination of parameters on pile stresses occurs with piles oriented in weak-axis bending during temperature contraction, presence of stiff soil around piles with no predrilled holes at the top nine feet of piles, use of inline

cantilever wingwalls, and presence of dense sand as backfill soil behind the abutments and wingwalls. This critical combination of parameters generates pile plasticity at a bridge length of 77 feet.

- No plastic hinge is formed in the piles even under the most critical combination of parameters on pile stresses. This includes a bridge length of 1200 feet in combination with 24-feet-long inline cantilever wingwalls, dense backfill soil, very stiff around the piles, and no predrilled holes at the top nine feet of piles.

- During temperature contraction, plasticity in the piles of integral abutments with predrilled holes and no cantilever wingwalls is generated at bridge lengths between 422 and 438 feet depending on the type of backfill soil. Addition of cantilever wingwalls induces plasticity in the piles at bridge lengths between 277 and 374 feet depending on the cantilever wingwall orientation and type of backfill soil.

- Not using predrilled holes at the top nine feet of piles has a very serious effect on pile stresses. The results indicate that when no predrilled holes are used, plasticity in the piles of integral abutments without cantilever wingwalls is generated at bridge lengths between 120 and 124 feet depending on the type of backfill soil. However, when predrilled holes are used, pile plasticity is generated between 422 to 438 feet as stated in the previous paragraph. Addition of any type of cantilever wingwall (inline, flared or U-shaped) to bridges with no predrilled holes results in generation of plasticity in the piles at bridge lengths ranging from 77 to 115 feet. Using predrilled holes with any type of cantilever wingwall results in generation of pile plasticity at bridge lengths between 277 and 374 feet as stated in the previous paragraph.

- During temperature expansion, pile plasticity is generated at bridge lengths substantially longer compared to those obtained during temperature contraction. This applies to all cases including use or not of predrilled holes or cantilever wingwalls in combination with any type of backfill soil. This is due to the fact that higher piles stresses are induced during thermal contraction rather than during thermal expansion.

- Pile stresses in bridges with two lanes are slightly higher compared to bridges with four lanes. This is due to the fact that for two-lane bridges backfill soil pressures acting on the wingwalls account for a larger portion of the total soil pressure acting on the combined abutment/wingwall length.

Cracking Pattern in Integral Abutments

- For the same bridge length, extent of cracking in integral abutments is more widespread when no predrilled holes are used at the top nine feet of piles compared to the case in which predrilled holes are used at the top nine feet of piles.

- Moderate amount of cracking is first observed in the integral abutments at a bridge length of 300 feet when no predrilled holes are used and at a bridge length of 400 feet when predrilled holes are used at the top nine feet of piles.

- Significant amount of cracking is first observed in the integral abutments at a bridge length of 400 feet when no predrilled holes are used and at a bridge length of 800 feet when predrilled holes are used at the top nine feet of piles.

- Both moderate and especially significant amounts of cracking point to a bridge maintenance issue. Failure to address this issue might lead to corrosion of the rebar and subsequent loss of strength.

- A number of states impose limitations on the length of cantilever wingwalls apparently because of cracking in the abutments. However, cracking occurs due to thermal expansion with increasing bridge length, not because of presence of cantilever wingwalls.

Stresses in the Reinforcing Steel in Integral Abutments with no Cantilever Wingwalls

- Stresses in the reinforcing steel during temperature expansion reach yield at a bridge length of 1000 feet with medium dense sand backfill soil. When dense sand is used as a backfill soil, stresses in the reinforcing steel reach yield at 900 feet. When loose sand is used as a backfill soil, stresses in the reinforcing steel reach yield at 1100 feet. In comparison, stresses in the reinforcing steel during temperature contraction do not reach yield even at the maximum bridge length of 1200 feet with any of the three types of backfill soil. This is explained by the fact that the magnitude of passive pressures on the abutments during temperature expansion is more severe than the magnitude of active pressures on the abutments during temperature contraction. Dense sand backfill soil induces the highest stresses in the reinforcing steel followed by medium dense sand and loose sand. This is due to the fact that dense sand has the highest coefficient of passive earth pressure (Kp) and unit weight (γ).

- The effect of use predrilled holes on rebar stresses is more pronounced during temperature contraction rather than during temperature expansion. This is due to the fact that during temperature rise and for longer bridges, the magnitude of

passive pressures on the abutments is comparable in magnitude to the magnitude of pressures imposed by the very stiff clay on the piles. Conversely, during temperature fall, the magnitude of active soil pressures applied on the abutments is small compared to the magnitude of pressures exerted by the very stiff clay on the piles.

- During both temperature expansion and temperature contraction, the location of maximum stress in the reinforcing steel is always at the bottom of the abutment.

Stresses in the Reinforcing Steel in Integral Abutments with Inline Cantilever Wingwalls

- During temperature expansion, stresses in the reinforcing steel reach the level of yield stress at a certain bridge length that is a function of use of cantilever wingwalls, length of cantilever wingwalls, type of backfill soil, and use of predrilled holes at the top nine feet of piles. In comparison, during temperature contraction, stresses in the reinforcing steel do not reach the level of yield stress under any scenario even at the maximum bridge length of 1200 feet. This is explained by the fact that the magnitude of passive pressures exerted on the abutments during temperature expansion is more severe than the magnitude of active pressures on the abutments during temperature contraction.

- Comparison of the effects of length of cantilever wingwalls, use of predrilled holes, and type of backfill soil on the stresses in the reinforcing steel leads to the conclusion that the most critical parameter among those three parameters is the type of backfill soil.

- The location of maximum stress in the reinforcing steel during temperature expansion is at the abutment/wingwall interface for bridge lengths up to 400 feet. Beyond the 400-feet bridge length, the location of maximum stress in the reinforcing steel is at the base of the abutment. This is due to the fact that for longer bridges the effect of bridge length is more severe than the effect of wingwall length on stresses in the reinforcing steel.

- When medium dense sand is used as a backfill material behind the integral abutments, stresses in the abutment reinforcing steel reach the level of yield stress during temperature expansion and a bridge length of 1000 feet. This occurs with and without predrilled holes at the top nine feet of piles. Adding inline cantilever wingwalls on both sides of the integral abutment along with predrilled holes around the top nine feet of piles, yielding of in the reinforcing steel is reached at a bridge length between 1000 and 1200 feet depending on the exact shape of the wingwall. While rectangular wingwalls are used in this study in order to determine the most severe effects on the bridge superstructure, in practice, most wingwalls are tapered. Using tapered wingwalls, however, less backfill soil

pressures are exerted on the wingwalls compared to rectangular-shaped wingwalls. Consequently, yielding of the rebars will occur at a bridge length between 1000 and 1200 feet. In comparison, using inline cantilever wingwalls on both sides of the abutment without predrilled holes at the top nine feet of piles, yielding of the rebars is reached at a bridge length between 1000 and 1100 feet.

- When dense sand is used as a backfill material behind the integral abutments, stresses in the abutment reinforcing steel reach the level of yield stress during temperature expansion and a bridge length of 900 feet. This occurs with and without predrilled holes around the top nine feet of piles. Adding inline cantilever wingwalls on both sides of the integral abutment, with and without predrilled holes around the top nine feet of piles, yielding of reinforcing steel occurs at a bridge length between 900 feet and 1100 feet depending on the exact shape of the wingwall.

- When loose sand is used as a backfill material behind the integral abutments, stresses in the abutment reinforcing steel reach the level of yield stress during temperature expansion and a bridge length of 1100 feet. This occurs with and without predrilled holes around the top nine feet of piles. Adding inline cantilever wingwalls on both sides of the integral abutment along with predrilled holes around the top nine feet of piles, yielding of reinforcing steel is reached between 1100 and 1200 feet for wingwalls with length up to 8 feet. For longer wingwalls and with predrilled holes around the top nine feet of piles, yielding of reinforcing steel is reached at a bridge length between 1100 and a bridge length longer than 1200 feet. In comparison, using inline cantilever wingwalls on both sides of the abutment without predrilled holes around the top nine feet of piles, yielding of the reinforcing steel is reached at a bridge length between 1100 and 1200 feet for all wingwall lengths.

- Stresses in the reinforcing steel in the abutment do not reach the level of yield stress during temperature contraction because the magnitude of active soil pressures acting on the integral abutment is not significant enough to cause yielding of the reinforcing steel. This occurs with all three types of soil backfill material; dense sand, medium dense sand, and loose sand with and without predrilled holes around the top nine feet of piles. The addition of inline wingwalls for the case of falling temperatures increases the stresses in the reinforcing steel, but not enough to reach the level of yield stress with and without predrilled holes at the top nine feet of piles.

Effects of Cantilever Wingwalls on Bridge Superstructure

- Wingwall size and orientation affects the magnitude of girder curvatures and axial forces introduced into the steel girders during temperature expansion. The largest axial forces occur with inline wingwalls due to the larger constraint imposed to the bridge expansion by the passive backfill soil pressures. In fact, using inline cantilever wingwalls there is a 20 percent increase in the magnitude of axial forces in the steel girders compared to 13 percent with flared cantilever wingwalls and 7 percent with U-shaped cantilever wingwalls respectively. The percentage increase in the magnitude of axial forces is larger when the ratio of wingwall to bridge length is higher. However, with longer bridges the magnitude of axial forces is much higher.

- During temperature fall, there is no effect on the magnitude of axial forces by the presence of any of the three types of cantilever wingwalls; inline, flared, or U-shaped, due to the low magnitude of active backfill soil pressures.

- The expansion and contraction of the deck and girders are not restrained by the substructure including the integral abutments and cantilever wingwalls, or the backfill soil because of the large axial stiffness of the deck and girders. The amount of expansion or contraction of the superstructure is a function of the bridge length and the coefficients of thermal expansion of steel and concrete.

- The type of backfill soil behind the integral abutments and cantilever wingwalls affects the magnitude of axial forces during temperature rise. Dense sand introduces higher axial forces into the bridge superstructure than medium sand or loose sand. This is due to the fact that the magnitude of passive earth pressures induced during thermal expansion increases with the density of backfill.

- The type of backfill soil behind the integral abutments and cantilever wingwalls does not contribute to the magnitude of the effects of cantilever wingwalls on the bridge superstructure during temperature fall. This is due to the fact that the magnitude of active soil pressures is not significant in any of the three types of soil backfill investigated in this study.

- Comparison of the impact of cantilever wingwalls, predrilled holes, and backfill soil on the magnitude of axial forces introduced into the steel girders, leads to the conclusion that the most critical parameter among the three is the use of cantilever wingwalls followed by the type of backfill soil, and use of predrilled holes. It is worth mentioning, however, that bridge length has more impact on the magnitude of axial forces introduced into the steel girders than all three parameters.

- The frictional effect of soil pressure on the flared and U-shaped cantilever wingwalls increases the restraint on end rotation of the girders.

Conclusions

Use of cantilever wingwalls with integral abutments has a modest impact on the behavior of integral abutment bridges. The effects include an increase in the magnitude of axial forces in the steel girders during thermal expansion and generation of pile plasticity at shorter bridge lengths compared to bridges built with independent wingwalls. In other words, for the same bridge length the stresses generated in the piles are higher when integral abutments are built with cantilever wingwalls than when independent wingwalls are built next to the integral abutments.

Cantilever wingwall orientation effects are more severe compared to the effects incurred due to increasing length of wingwalls. Cantilever wingwalls perpendicular to the traffic (inline wingwalls) have the most impact on the behavior of integral abutment bridges.

Parameters impacting the behavior of integral abutment bridges located on straight alignment and zero skew include the bridge length, temperature variation, type of backfill soil behind the abutments and the wingwalls, soil profile around piles, use of predrilled holes around the top nine feet of piles, pile orientation, span layout, abutment height, and use of cantilever wingwalls. Comparison of the effects of four of these parameters (bridge length, use of predrilled holes, use of cantilever wingwalls, and type of backfill soil) leads to the conclusion that the most critical parameter on the overall bridge behavior is the bridge length followed by the use of predrilled holes, use of cantilever wingwalls, and type of backfill soil. Thus, considering only these four parameters, the most severe combination for overall integral abutment bridge behavior occurs with long bridges, no predrilled holes at the top nine feet of piles, use of inline cantilever wingwalls, and presence of dense sand backfill soil behind the abutments and the wingwalls.

Ranking only the four parameters stated at the end of the previous paragraph (bridge length, use of predrilled holes, use of cantilever wingwalls, and type of backfill soil) based on their impact on the magnitude of stresses generated in the piles, the two most critical parameters are the use of predrilled holes and bridge length followed by the type of cantilever wingwall used and type of backfill soil (Table 10-12). It is worth mentioning that no plastic hinge is formed near the pile head even under the most critical combination o parameters.

Ranking the same four parameters based on their impact on the stresses in the abutment reinforcing steel, the two most critical parameters are the bridge length and type of backfill soil followed by the length of cantilever wingwalls and use of predrilled holes (Table 10-12).

Ranking again the same four parameters based on their impact on the magnitude of axial forces introduced in the steel girders, the two most critical parameters are the bridge length and type of cantilever wingwall followed by the type of backfill soil and use of predrilled holes (Table 10-12).

.

Significant amount of cracking is observed at the abutments at bridge lengths indicated in chapter 10. Its importance lies in the fact that failure to address this bridge maintenance issue might lead to corrosion of the reinforcing steel and subsequent loss of strength.

Cantilever wingwalls up to 25 feet can be used taking into consideration their effects on the steel girders and pile stresses. In fact, in practice, wingwalls whether cantilever or independent are limited to 25 feet. At that point, there is a joint and the rest of the wall is analyzed and designed as a retaining wall. Consequently, considering the state-of-practice, there should be no limitations on the length of cantilever wingwalls of integral abutment bridges.

Although wingwalls with lengths up to 25 feet can be used judging on their effects on other bridge elements, when their length exceeds 20 feet (particularly if only 18-inches thick), compaction pressures, over time, might cause excessive distortions. The damage will increase by expansion or seismic displacements or both. For these instances, unless the thickness of the wingwall increases, it is preferable to lengthen the bridge superstructure to minimize soil retention needs and thus minimize wingwall length. Using independent wingwalls is less preferable due to the need for complex joints to accommodate the differential movement of the integral abutment and the independent wingwalls.

Recommendations for Future Work

It is recommended that any future research on the subject of effects of cantilever wingwalls on the behavior of integral abutment bridges focuses on the following areas: curved and skew integral abutment bridges, bridges with deeper abutment heights, piles oriented in strong-axis bending, and bridge span layouts with a variety of span ratios.

In addition, AASHTO specifications are currently using the same load factor for temperature load for both conventional and integral abutment bridges. Taking into consideration that the temperature load is much more critical for integral abutment bridges than it is for conventional bridges, a future research might focus on calibration of an appropriate load factor for temperature load specifically for integral abutment bridges. This may be expanded to a load combination for the analysis and design of integral abutment bridges. In addition, future specifications should consider the merits of using site-specific temperature ranges instead of the current methodology of "cold climate" and "moderate climate" temperature ranges.

Appendix A

Integral Abutment Bridge Survey Questionnaire

1. Do you use integral abutment bridges in your state? Yes ….. No …..
   Primary reason for yes or no ……
   If the answer is no, skip the remainder of the questionnaire

2. What type of superstructure do you use with integral abutment bridges?
   Steel …….
   Prestressed concrete ……. ……
   Cast-in-place concrete ……...

3. Do you built integral abutments on
   Straight alignment …….
   Curved alignment …….

4. What is the limit for skew? ……...

5. What are the bridge length limits (in feet) for a given skew?

	0°	0°-15°	15°-30°	Skew >30°
Steel				
Prestressed concrete				
Cast-in-place concrete				

6. What type of piles do you use?
   Steel H-piles …….
   Steel pipe piles (open ended) …….
   Steel pipe piles (concrete filled) …….
   Cast-in-place piles …….
   Prestressed concrete piles …….

7. What is the pile orientation?
   Strong-axis bending (pile web is parallel to beam centerline) ……
   Weak-axis bending (pile web is perpendicular to beam centerline) ……

8. What type of structural assumption is made for the end of the girder?
   Pinned (moment is zero) ……..
   Fixed (rotation is zero) ……..
   Partially restrained by pile ..……...
   Partially restrained by soil …….
   Other assumption ……..

9. What type of structural assumption is made for the top of the pile?
   Pinned (moment is zero) ……..
   Fixed (rotation is zero) ……..
   Partially restrained by girder……...
   Partially restrained by soil …….
   Other assumption ……..

10. What loads do you include in the calculation of pile stress?
    Thermal ……
    Creep ……
    Shrinkage ……...
    Soil pressure on abutment face ……...

    If thermal load is included, what is the temperature range used?
    Per AASHTO Specifications ……..
    Local meteorological data ……

11. How is bending accounted for in the pile?
    Neglect or assume bending stresses do not affect pile performance ……...
    Assume location of pile inflection point and analyze pile as bending member ……
    Reduce bending by pre-drilled holes ……..
    Other ……...

12. What type of backfill material do you specify on the backside of the abutment?
    ……
    ……

13. Do you require the fill behind the abutment to be compacted?
    Yes ……
    No …….

14. How is the approach slab connected to the bridge abutments?
    Doweled or tied ……
    No connection ……
    Approach slab is not used …….

15. What type of wingwalls do you use with integral bridges?
    Cantilevered u-shaped wingwalls …….
    Cantilevered U- wingwalls …….
    Cantilevered flared wingwalls …….
    Independently-supported u-shaped wingwalls …….
    Independently-supported U- wingwalls …….
    Independently-supported flared wingwalls …….

16. Do you place piles beneath wingwalls?
    Yes ……..… No ……..

17. Briefly evaluate the performance of integral abutment bridges in your state compared to conventional bridges:
    Construction cost more ……less …… same ……..
    Maintenance cost more ……less …… same ……..

Appendix B

Calculation of Ramberg-Osgood Parameters for HP10X57 and HP12X84 Piles in Loose Sand and Very Stiff Soil

Appendix B presents the calculations performed in order to determine the Ramberg-Osgood parameters listed in Tables 8-5 and 8-6

- Ramberg-Osgood P-y curve parameters for HP10X57 piles in loose sand
- Ramberg-Osgood f-z curve parameters for HP10X57 piles in loose sand
- Ramberg-Osgood q-z curve parameters for HP10X57 piles in loose sand

- Ramberg-Osgood P-y curve parameters for HP12X84 piles in loose sand
- Ramberg-Osgood f-z curve parameters for HP12X84 piles in loose sand
- Ramberg-Osgood q-z curve parameters for HP12X84 piles in loose sand

- Ramberg-Osgood P-y curve parameters for HP10X57 piles in very stiff clay
- Ramberg-Osgood f-z curve parameters for HP10X57 piles in very stiff clay
- Ramberg-Osgood q-z curve parameters for HP10X57 piles in very stiff clay

- Ramberg-Osgood P-y curve parameters for HP12X84 piles in very stiff clay
- Ramberg-Osgood f-z curve parameters for HP12X84 piles in very stiff clay
- Ramberg-Osgood q-z curve parameters for HP12X84 piles in very stiff clay

Ramberg-Osgood P-y curve parameters for HP10X57 piles in loose sand

As per Table 8-1 for sand:

$P_u = \gamma' x[B(Kp - Ka) + xKp(tana)(tan\beta) + xKo(tan\beta)(tan\Phi - tana)]$ or

$P_u = \gamma' x[B(Kp - Ka) + n + \mu]$ where

$n = xKp(tana)(tan\beta)$

$\mu = xKo(tan\beta)(tan\Phi - tana)$

For loose sand → $\gamma' = 55$ pcf and $\Phi = 30^o$

For $\Phi = 30^o$ → $Ka = (1-sin\Phi)/(1+sin\Phi) = (1-sin30^o)/(1+sin30^o) = 0.5/1.5 = 0.33$

$Kp = (1+sin\Phi)/(1-sin\Phi) = (1+sin30^o)/(1-sin30^o) = 1.5/0.5 = 3.0$

$Ko = 1-sin\Phi = 1-0.5 = 0.5$

$a = \Phi/3$ ⇨ $tana = tan10^o = 0.176$

$\beta = 45^o + \Phi/2$ ⇨ $tan\beta = tan(45^o + \Phi/2) = tan60^o = 1.732$

$\therefore n = xKp(tana)(tan\beta) = 3x(0.176)(1.732) = 0.914x$

$n = 0.914x$

$\mu = x\ Ko(tan\beta)(tan\Phi - tana) = xKo(tan\beta)(tan30^o - tan10^o)$

$\therefore \mu = x(0.5)(1.732)(0.577 - 0.176) = 0.347x$

$\mu = 0.347x$

$P_u = \gamma' x[B(Kp - Ka) + n + \mu]$ where

$\gamma' = 55$ pcf

B =10.2" = 0.85' for HP 10X57 piles

$\therefore P_u = \gamma' x[B(Kp - Ka) + n + \mu] = 55x[(0.85)(3-0.33) + 0.914x + 0.347x]$

$= 55x[2.27 + 1.261x] = 124.85x + 69.36x^2$ or $0.125x + 0.069x^2$ in Kips

$P_u = 0.069x^2 + 0.125x$

The second equation in Table 8-1 for sand is:

$P_u = \gamma' x[(Kp)^3 + 2(Kp)^2 Ko(\tan\Phi) - Ka]B$

$= 55x[27 + (2)(9)(0.5)(0.577) - 0.33](0.85) = 1489.5x$ or $1.49x$ in Kips

$P_u = 1.49x$

Table 8-1 indicates that the smaller of the two expressions shall be used. This results in using

$P_u = 0.069x^2 + 0.125x$	**for $x \leq 20$ feet**
$P_u = 1.49x$	**for $x > 20$ feet**

$K_h = (J\gamma' x)/1.35$ where

J = 200 for loose sand and
γ' = 55 pcf

$\therefore K_h = (J\gamma' x)/1.35 = [(200)(0.055)x]/1.35 = 8.15x$

$K_h = 8.15x$

Ramberg-Osgood f-z curve parameters for HP10X57 piles in loose sand

As per Table 8-2 for sand:

$f_{max} = 0.04N(d + 2b_f)$ where

N =5
d = 9.99" =0.8325' for HP 10X57 piles
b_f =10.2" = 0.85' for HP 10X57 piles

$\therefore f_{max} = 0.04N(d + 2b_f) = 0.04(5)[0.8325 + (2)(0.85)] = 0.507$ klf

f_{max} =0.507 klf

As per Table 8-4 for all soils including sand:

$K_v = 10f_{max} /Zc$ where

f_{max} = 0.507 klf
Zc = 0.40 in. (0.0333 ft) for sand

$\therefore K_v = 10f_{max} /Zc = (10)(0.507)/(0.0333) = 152$ ksf

K_v = 152 ksf

Ramberg-Osgood q-z curve parameters for HP10X57 piles in loose sand

As per Table 8-3 for sand:

$q_{max} = 8N_{corr}$ where N_{corr} = N (uncorrected) if N is equal or less than 15
= 15 + 0.5(N-15) if N is greater than 15

$\therefore N_{corr} = 5$

$q_{max} = 8N_{corr} = (8)(5) = 40$ ksf

qmax = 40 ksf

As per Table 8-4 for all soils including sand:

$K_q = 10q_{max}/Z_c = (10)(40)/(0.0333) = 12{,}012$ say 12,000 kcf

K_v =12,000 kcf

Ramberg-Osgood P-y curve parameters for HP12X84 piles in loose sand

As per Table 8-1 for sand:

$P_u = \gamma' x[B(Kp - Ka) + xKp(tana)(tan\beta) + xKo(tan\beta)(tan\Phi - tana)]$ or

$P_u = \gamma' x[B(Kp - Ka) + n + \mu]$ where

$n = xKp(tana)(tan\beta)$

$\mu = xKo(tan\beta)(tan\Phi - tana)$

For loose sand → $\gamma' = 55$ pcf and $\Phi = 30^o$

For $\Phi = 30^o$ → $Ka = (1-sin\Phi)/(1+sin\Phi) = (1-sin30^o)/(1+sin30^o) = 0.5/1.5 = 0.33$

$Kp = (1+sin\Phi)/(1-sin\Phi) = (1+sin30^o)/(1-sin30^o) = 1.5/0.5 = 3.0$

$Ko = 1-sin\Phi = 1-0.5 = 0.5$

$a = \Phi/3$ ⇨ $tana = tan10^o = 0.176$

$\beta = 45^o + \Phi/2$ ⇨ $tan\beta = tan(45^o + \Phi/2) = tan60^o = 1.732$

$\therefore n = xKp(tana)(tan\beta) = 3x(0.176)(1.732) = 0.914x$

$n = 0.914x$

$\mu = xKo(tan\beta)(tan\Phi - tana) = xKo(tan\beta)(tan30^o - tan10^o)$

$\therefore \mu = x(0.5)(1.732)(0.577 - 0.176) = 0.347x$

$\mu = 0.347x$

$P_u = \gamma' x[B(Kp - Ka) + n + \mu]$ where

$\gamma' = 55$ pcf

B= 12.3"=1.025' for HP 12X84 piles

$\therefore P_u = \gamma' x[B(Kp - Ka) + n + \mu] = 55x[(1.025)(3-0.33) + 0.914x + 0.347x]$

$= 55x[2.737 + 1.261x] = 150.54x + 69.36x^2$ or $0.15x + 0.069x^2$ in Kips

$P_u = 0.069x^2 + 0.15x$

The second equation in Table 8-1 for sand is:

$P_u = \gamma' x[(Kp)^3 + 2(Kp)^2 Ko(\tan\Phi) - Ka]B$

$= 55x[27 + (2)(9)(0.5)(0.577) - 0.33](1.025) = 1796.3x$ or $1.8x$ in Kips

$P_u = 1.8x$

Table 8-1 indicates that the smaller of the two expressions shall be used. This results in using

$P_u = 0.069x^2 + 0.15x$ for $x \leq 24$ feet

$P_u = 1.8x$ for $x > 24$ feet

$K_h = (J\gamma' x)/1.35$ where

$J = 200$ for loose sand and
$\gamma' = 55$ pcf

$\therefore K_h = (J\gamma' x)/1.35 = [(200)(0.055)x]/1.35 = 8.15x$

$K_h = 8.15x$

Ramberg-Osgood f-z curve parameters for HP12X84 piles in loose sand

As per Table 8-2 for sand:

$f_{max} = 0.04N(d + 2b_f)$ where

N =5
d = 12.3" = 1.025' for HP 12X84 piles
b_f =12.3" = 1.025' for HP 12X84 piles

$\therefore f_{max} = 0.04N(d + 2b_f) = 0.04(5)[1.025 + (2)(1.025)] = 0.615$ klf

f_{max} =0.615 klf

As per Table 8-4 for all soils including sand:

$K_v = 10f_{max} /Zc$ where

f_{max} = 0.615 klf
Zc = 0.40 in. (0.0333 ft) for sand

$\therefore K_v = 10f_{max} /Zc = (10)(0.615)/(0.0333) = 185$ ksf

K_v = 185 ksf

Ramberg-Osgood q-z curve parameters for HP12X84 piles in loose sand

As per Table 8-3 for sand:

$q_{max} = 8N_{corr}$ where

N_{corr} = N (uncorrected) if N is equal or less than 15
= 15 + 0.5(N-15) if N is greater than 15

$\therefore N_{corr} = 5$

$q_{max} = 8N_{corr} = (8)(5) = 40$ ksf

qmax = 40 ksf

As per Table 8-4 for all soils including sand:

$K_q = 10q_{max}/Z_c = (10)(40)/(0.0333) = 12{,}012$ say 12,000 kcf

K_v =12,000 kcf

Ramberg-Osgood P-y curve parameters for HP10X57 piles in very stiff clay

As per Table 8-1 for very stiff clay P_u is the smallest of

$P_u = 9C_uB$
and
$P_u = [3 + (\gamma'/C_u)x + (2/B)x]C_uB$

$P_u = 9C_uB$ where

$C_u = 97.0N + 114.0 = (97)(50) + 114 = 4964$ psf say 5 ksf
$B = 10.2" = 0.85'$ for HP 10X57 piles

$\therefore P_u = 9C_uB = (9)(5)(0.85) = 38.25$ klf

$P_u = 38.25$ klf

$P_u = [3 + (\gamma'/C_u)x + (2/B)x]C_uB$ where

$\gamma' = 65$ pcf $= 0.065$ kcf

$C_u = 5$ ksf

$B = 10.2" = 0.85'$ for HP 10X57 piles

$\therefore P_u = [3 + (\gamma'/C_u)x + (2/B)x]C_uB = [3 + (0.065/5)x + (2/0.85)x](5)(0.85)$

$= [3 + 0.013x + 2.353x](4.25) = 12.75 + 10.06x$

$P_u = 12.75 + 10.06x$

The smaller of the two expressions shall be used. This results in using

$P_u = 12.75 + 10.06x$	**for $x \leq 2'\text{-}6"$**
$P_u = 38.25$	**for $x > 2'\text{-}6"$**

$K_h = P_u /(2)(y_{50})$ where

$y_{50} = 2.0B\varepsilon_{50}$ for very stiff clay = (2)(0.85)(0.005) = 0.0085

because B =10.2" = 0.85' for HP 10X57 piles
ε_{50} = 0.005 for very stiff clay (Figure 6-2)

$\therefore K_h = P_u /(2)(y_{50}) = (38.25)/(2)(0.0085) = 38.25/0.017 = 2250$ ksf

K_h = 2250 ksf

Ramberg-Osgood f-z curve parameters for HP10X57 piles in very stiff clay

As per Table 8-2 for clay, f_{max} is the least of:

$2(d + b_f)C_u$
$2(d + 2b_f)C_a$
$2(dC_u + b_f C_a)$

where

d = 9.99" =0.8325' for HP10X57 piles
b_f =10.2" = 0.85' for HP10X57 piles
C_u = 5 ksf
$C_a = aC_u$ where a = shear strength reduction factor from Figure 8-3.

By observation in Figure 8-3, for C_u = 5 ksf → a = 0.25

$\therefore$ $C_a = aC_u = (0.25)(5) = 1.25$ ksf

$\therefore$ $2(d + b_f)C_u = (2)(0.8325 + 0.85)(5) = 16.825$ klf
$2(d + 2b_f)C_a = (2)[0.8325 + (2)(0.85)](1.25) = 6.33$ klf ←
$2(dC_u + b_f C_a) = (2)[(0.8325)(5) + (0.85)(1.25)] = 10.45$ klf

By observation. The smallest value is 6.33 klf

f_{max} = 6.33 klf

As per Table 8-4 for all soils including very stiff clay:

$K_v = 10f_{max}/Z_c$ where

f_{max} = 6.33 klf
Z_c = 0.25 in. (0.0208 ft) for clay

$\therefore$ $K_v = 10f_{max}/Z_c = (10)(6.33)/(0.0208) = 3043$ ksf

K_v = 3043 ksf

Ramberg-Osgood q-z curve parameters for HP10X57 piles in very stiff clay

As per Table 8-3 for clay:

$q_{max} = 9C_u$ where

$C_u = 97.0N + 114.0 = (97)(50) + 114 = 4964$ psf say 5 ksf

$\therefore\ q_{max} = 9C_u = (9)(5) = 45$ ksf

qmax = 45 ksf

As per Table 8-4 for all soils including very stiff clay:

$K_q = 10q_{max}/Z_c = (10)(45)/(0.0208) = 21{,}635$ kcf

Kq =21,635 kcf

Ramberg-Osgood P-y curve parameters for HP12X84 piles in very stiff clay

As per Table 8-1 for very stiff clay P_u is the smallest of

$P_u = 9C_uB$
and
$P_u = [3 + (\gamma'/C_u)x + (2/B)x]C_uB$

$P_u = 9C_uB$ where

$C_u = 97.0N + 114.0 = (97)(50) + 114 = 4964$ psf say 5 ksf
$B = 12.3" = 1.025'$ for HP 12X84 piles

$\therefore P_u = 9C_uB = (9)(5)(1.025) = 46.13$ klf

$P_u = 46.13$ klf

$P_u = [3 + (\gamma'/C_u)x + (2/B)x]C_uB$ where

$\gamma' = 65$ pcf $= 0.065$ kcf

$C_u = 5$ ksf

$B = 12.3" = 1.025'$ for HP 12X84 piles

$\therefore P_u = [3 + (\gamma'/C_u)x + (2/B)x]C_uB = [3 + (0.065/5)x + (2/1.025)x](5)(1.025)$

$= [3 + 0.013x + 1.951x](5.125) = 15.375 + 10.07x$

$P_u = 15.375 + 10.07x$

The smaller of the two expressions shall be used. This results in using

$P_u = 15.375 + 10.07x$	**for $x \leq 3'\text{-}0"$**
$P_u = 46.13$	**for $x > 3'\text{-}0"$**

$K_h = P_u /(2)(y_{50})$ where

$y_{50} = 2.0B\varepsilon_{50}$ for very stiff clay = (2)(1.025)(0.005) = 0.01025

because B =12.3" = 1.025' for HP12X84 piles
ε_{50} = 0.005 for very stiff clay (Figure 6-2)

$\therefore K_h = P_u /(2)(y_{50}) = (46.13)/(2)(0.01025) = 46.13/0.0205 = 2250$ ksf

K_h = 2250 ksf

Ramberg-Osgood f-z curve parameters for HP12X84 piles in very stiff clay

As per Table 8-2 for clay, f_{max} is the least of:

$2(d + b_f)C_u$
$2(d + 2b_f)C_a$
$2(dC_u + b_f C_a)$

where

d = 12.3" = 1.025' for HP12X84 piles
b_f = 12.3" = 1.025' for HP12X84 piles
C_u = 5 ksf
$C_a = aC_u$ where a = shear strength reduction factor from Figure 8-3.

By observation in Figure 8-3, for C_u = 5 ksf → a = 0.25

$\therefore$ $C_a = aC_u = (0.25)(5) = 1.25$ ksf

$\therefore$ $2(d + b_f)C_u = (2)(1.025 + 1.025)(5) = 20.5$ klf
$2(d + 2b_f)C_a = (2)[1.025 + (2)(1.025)](1.25) = 7.69$ klf ←
$2(dC_u + b_f C_a) = (2)[(1.025)(5) + (1.025)(1.25)] = 12.813$ klf

By observation. The smallest value is 7.69 klf

f_{max} = 7.69 klf

As per Table 8-4 for all soils including very stiff clay:

$K_v = 10f_{max}/Z_c$ where

f_{max} = 7.69 klf
Z_c = 0.25 in. (0.0208 ft) for clay

$\therefore$ $K_v = 10f_{max}/Z_c = (10)(7.69)/(0.0208) = 3697$ ksf

K_v = 3697 ksf

Ramberg-Osgood q-z curve parameters for HP12X84 piles in very stiff clay

As per Table 8-3 for clay:

$q_{max} = 9C_u$ where

$C_u = 97.0N + 114.0 = (97)(50) + 114 = 4964$ psf say 5 ksf

$\therefore\ q_{max} = 9C_u = (9)(5) = 45$ ksf

qmax = 45 ksf

As per Table 8-4 for all soils including very stiff clay:

$K_q = 10q_{max}/Z_c = (10)(45)/(0.0208) = 21{,}635$ kcf

Kq =21,635 kcf

Appendix C

Calculation of Tangent Modulus for the Nonlinear Plasticity Model

Most nonlinear finite element analysis programs including ANSYS require the data to be in the form of "true stress" to "true strain" for finite element analysis. This is also the case for the nonlinear plasticity model used in this study. For this model, the true stress to true strain curve of low carbon steel is applicable to the steel piles.

The true stress to true strain curve of low carbon steel is shown in Figure C-1. The elastic modulus (E) and tangent modulus (E_T) are shown in Figure 9-19.

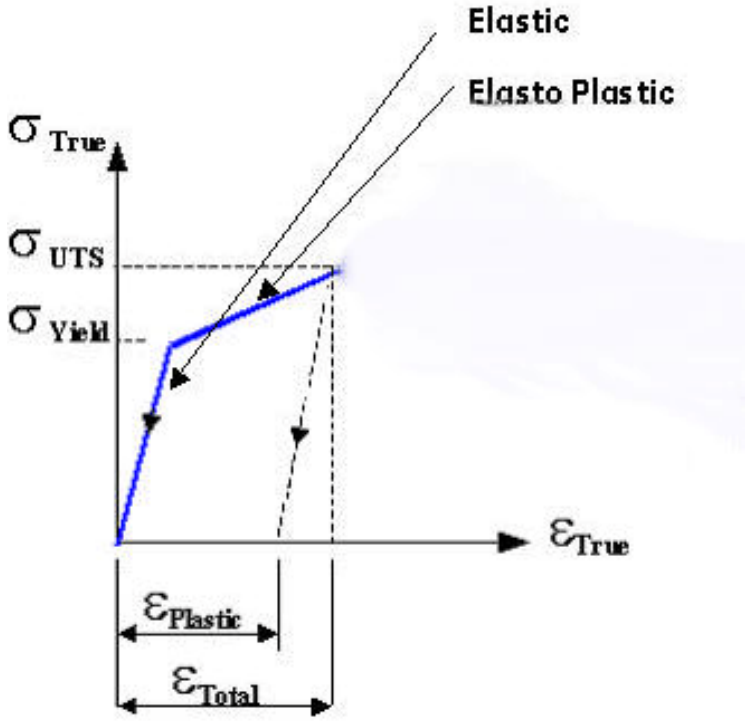

Figure C-1 True stress-true strain curve of low carbon steel

The data of engineering stress and strain of a typical ASTM A709 Grade 50 material are shown in Table C-1. This material is used for the steel piles.

Table C-1 Mechanical properties of ASTM A709 Grade 50

Material	Elastic Modulus (psi)	Poisson's Ratio	Yield Strength (psi)	Ultimate Tensile Strength (psi)	Elongation Percentage
ASTM A709	29×10^6	0.30	50,000	65,000	21%

Tangent Modulus (E_T) for the Steel Pile (Nonlinear Plasticity Model)

Tangent modulus (E_T) is defined as

$$\text{Tangent Modulus} = \frac{\text{(True stress at UTS – True Stress at Yield)}}{\text{(True Total Strain at UTS – True Total Strain at Yield)}}$$

where

True stress at yield = 50,000 psi

True total strain at UTS = $\varepsilon_{\text{true total}} = \ln(1+\varepsilon_{\text{engineering}}) = \ln(1+0.21) = \ln(1.21) = 0.19885$

True stress at UTS = (65,000 psi)(1.21) = 78,650 psi

True total strain at yield = $\varepsilon_{\text{elastic}}$ = (50,000 psi)/(29×10^6 psi) = 0.001724

$\therefore$ Tangent modulus = (E_T) = (78,650 - 50,000) / (0.19885 - 0.001724) = 145,339 psi

E_T =145,339 psi

References

Alampalli, S., and Yannotti, A. P.(1998). "In-Service Performance of Integral Bridges and Jointless Decks." *Structural Analysis and Design: Bridges, Culverts, and Pipes, Transportation Research Record*, No. 1624, pp. 1-7

Alampalli, S., and Yannotti, A. P.(June 1999). "Field Survey of Jointless Bridges for Design Improvements." *16th Annual International Bridge Conference*, Pittsburgh, PA

Alampalli, S., (November 2009). "National and New York State Highway Bridge Inspection," Presentation, MCEER/SUNY, Buffalo, NY

Albajar, L., Gascón, C., Hernando, A., and Pacheco, J. (2005). "Transiciones de Obra de Paso-Terraplén. Aproximación al Estado del Artey Experiencias Españolas." Asociación Técnica de Carreteras, Ministerio de Fomento.

Alizadeh, M.H., Rashid, A.R.K., Chik, Z., and Mirhosseiny, S.M. (2010). "Investigation of Abutment Displacement of a Full Height Integral Bridges in Dense Granule Backfill." *American Journal of Engineering and Applied Sciences*, Vol. 3, No.4, pp. 749-756

Allen, C.A. (March-April 2010). "Jointless Bridge Research Pays Dividends for Vermont." *Transportation Research News*, No. 267, pp.51-53

Amde, A.M., Greimann, L.F., and Yang, P.S. (1982). "Nonlinear Pile Behavior in Integral Abutment Bridges." Iowa State University, Ames, IA

Amde, A.M., Greimann, L.F. and Johnson, B. (1983). "Performance of Bridge Abutments." *Journal of the International Association for Bridge and Structural Engineering,* IABSE PERIODICA, pp.17-34

Amde, A.M., and Klinger, J.E. (1987). "Integral Bridge Design and Construction." Report FHWA/MD-87/04, Maryland Department of Transportation, Hanover, MD

Amde, A.M., Klinger, J.E., Mafi, M., Albrecht, P., White, J., and Buresli, M. (June 1987). "Performance and Design of Jointless Bridges." Contract No. DTFH61-85-C-00092, Department of Civil Engineering, University of Maryland, College Park, MD

Amde, A.M., and Greimann, L.F. (1988). "General Design Details for Integral Abutment Bridges." *Journal of Civil Engineering Practice*, BSCE/ASCE, Vol. 3, No. 2, pp. 7–20

Amde, A.M., Klinger, J.E., and White, E. (1988). "Performance of Jointless Bridges." *ASCE Journal of Performance of Constructed Facilities*, Vol. 2, No. 2, pp. 111-125

Amde, A.M., Greimann, L., and Yang, P. (1988). "End Bearing Piles in Jointless Bridges." *ASCE Journal of Structural Engineering*, Vol. 114, No. 8, pp. 1870-1884

Amde, A.M., Chini, S.A., Mafi, M. (1997). "Experimental Study of Piles in Integral Abutment Bridges." *International Journal of Geotechnical and Geological Engineering*, Vol. 15, Issue 4, pp. 343-355

Amde, A.M., Najib, R., and Paraschos, A. (2014). "Oversized Predrilled Holes in Skewed Integral Abutment Bridges" Proceedings 3rd World Conference on Applied Sciences, Engineering and Technology, Kathmandu, Nepal, pp. 18-24

American Association of State and Highway Transportation Officials (AASHTO) *Standard Specifications for Highway Bridges,* 17th Edition, 2002, Washington DC

American Association of State and Highway Transportation Officials (AASHTO) *A Policy on Geometric Design of Highways and Streets*, 5th Edition, 2004, Washington DC

American Association of State and Highway Transportation Officials (AASHTO) *LRFD Bridge Design Specifications*, 5th Edition, 2010, Washington DC

American Association of State and Highway Transportation Officials (AASHTO)/ National Steel Bridge Alliance (NSBA) Steel Bridge Collaboration, Task Group 13, *Guidelines for Steel Girder Bridge Analysis*, 1st Edition, 2011, Chicago, IL

American Concrete Institute (ACI) Committee 209, "Prediction of Creep, Shrinkage, and Temperature Effects in Concrete Structures." Farmington Hills, MI

American Institute of Steel Construction (AISC) *Manual of Steel Construction-Load and Resistance Factor Design*, Third Edition, 2001, Chicago, IL

ANSYS, Inc., "ANSYS Element Reference." Release 12.0, April 2009, Canonsburg, PA

ANSYS, Inc., "ANSYS Mechanical APDL and Mechanical Applications Theory Reference." Release 13.0, November 2010, Canonsburg, PA

ANSYS, Inc., "ANSYS Training Material." Release 13.0, November 2010, Canonsburg, PA

ANSYS, Inc., "ANSYS Mechanical APDL Structural Analysis Guide." Release 13.0, November 2010, Canonsburg, PA

Ansys.net Newsletter (2002). "Review of Yield/Failure Criteria." Canonsburg, PA

Arsoy, S., Barker, R.M., and Duncan, J.M. (1999). "The Behavior of Integral Abutment Bridges." Report VTRC 00-CR3, Virginia Transportation Research Council, Charlottesville, VA

Arsoy, S., Barker, R.M., and Duncan, J.M. (2002). "Experimental and Analytical Investigations of Piles and Abutments of Integral Bridges." Report VTRC 02-CR6, Virginia Transportation Research Council, Charlottesville, VA

Arsoy, S., Barker, R. M., Duncan, J. M. (2004). "Behavior of a Semi-Integral Bridge Abutment under Static and Temperature-Induced Cyclic Loading." *ASCE Journal of Bridge Engineering*, Vol. 9, No. 2, pp. 193-199

Augustesen, A., Liingaard, M., and Lade, P. (2004) "Evaluation of Time-Dependent Behavior of Soils." *International Journal of Geomechanics*, Vol. 4, No. 3, pp. 137-156

Bang, S. (March 1984). "Active Earth Pressure Behind Retaining Walls." *ASCE Journal of Geotechnical Engineering*, Vol. 111, No. 3, pp. 407-412

Bangash, M. Y. H., (1989). *Concrete and Concrete Structures: Numerical Modeling and Applications*, Elsevier Science Publishers Ltd., London, England

Banks, J., Bloodworth, A.G., Knight, T., and Young, J. (2008). "Integral Bridges - Development of a Constitutive Model for Soil Structure Interaction." *2008 Structures Congress - Crossing Borders*, Vancouver, Canada

Bao, Y., and Sture, S. (2010). "Application of a Kinematic-Cyclic Plasticity Model in Simulating Sand Liquefaction." *International Journal of Advances in Engineering Sciences and Applied Mathematics*, Vol. 2, Issue 3, pp. 119-124

Bao, Y., and Stein, S. (2011). "Numerical Modeling of Cyclic Mobility Based on Fuzzy-set Concepts in Plasticity Theory." *Computers and Geotechnics,* Vol. 38, Issue 3, pp. 375-382

Bao, Y., and Rietz, A. (2013). "Seismic Soil-Structure Interaction in Fully Integral Abutment Bridges with HP Steel Piles." *Proceedings of the 7th International Structural Engineering and Construction Conference*, Honolulu, HI

Barbaccia, T. G. (November 2014). "2014 Bridge Inventory." *Better Roads magazine*, Tuscaloosa, AL

Barbosa, A.F., Ribeiro, G.O. (1998). "Analysis of Reinforced Concrete Structures Using ANSYS Nonlinear Concrete Model." *Computational Mechanics*, pp. 1–7.

Barden, L. (1963). "Stress and Displacements in Cross-Anisotropic Soil." *Geotechnique*, The Institution of Civil Engineers, London, Vol. 13, pp. 198-210

Barker, R.M., Duncan, J.M., Rojiani, K.B., Ooi, P.S.K., Tan, C.K., and Kim, S.G. (1991) "Manuals for Design of Bridge Foundations." NCHRP National Cooperative Highway Research Program Report 343, *Transportation Research Board*, Washington, DC

Barzegar, F., Maddipudi, S. (1997) "Three-Dimensional Modeling of Concrete Structures." *ASCE Journal of Structural Engineering*, Vol. 123, No. 10, pp. 1339-1346

Bathe, K. J. (1996). *Finite Element Procedures*, Prentice-Hall, Inc., Upper Saddle River, NJ

Begum, N.A., and Muthukkumaran, K. (2008). "Numerical Modeling for Laterally Loaded Piles on a Sloping Ground." *12th International Conference of International Association for Computer Methods and Advances in Geomechanics (IACMAG)*, Goa, India

Bentler, D. J., Morrison, C. S., Esterhuizen, J. J. B., and Duncan, J. M. (1999). SAGE user's guide, Center for Geotechnical Practice and Research, Department of Civil Engineering, Virginia Tech, Blacksburg, VA

Beresnev, I. A., and K. L. Wen (December 1996). "Nonlinear Soil Response- A Reality?" Bulletin of the Seismological Society of America, Vol. 86, No.6, pp. 1964-1978

Biot, M. A. (1937). "Bending of Infinite Beams on an Elastic Foundation." *ASME Journal of Applied Mechanics*, Vol. 59, pp. A1-A7

Birkemoe, P. (2011). "Bridge Stability and Bracing." Presentation, *North American Steel Construction Conference*, Pittsburgh, PA

Bloodworth, A.G., Xu, M., Banks, J.R., and Clayton, CR.I. (2012). "Predicting the Earth Pressure on Integral Bridge Abutments." *ASCE Journal of Bridge Engineering*, Vol. 17, No. 2, pp. 371-381

Bonczar, C., Civjan, S., Brena, S., and DeJong, J. (June 2005). "Behavior of Integral Abutment Bridges: Field Data and Computer Modeling." Report No. SPRII.03.20, Department of Civil and Environmental Engineering, University of Massachusetts at Amherst, Amherst, MA

Briaud, J.L., James, R.W., and Hoffman, S.B. (1997). "Settlement of Bridge Approaches." National Cooperative Highway Research Program Synthesis of Highway Practice 234, *Transportation Research Board*, Washington, DC

Brinkgreve, R.B. J. (2005). *Selection of Soil Models and Parameters for Geotechnical Engineering Application*, Geotechnical Special Publication No.128, ACSE, pp. 69-98

Brinkgreve, R.B.J., and Engin, E. (2013). "Validation of Geotechnical Finite Element Analysis." *Proceedings of the 18th International Conference on Soil Mechanics and Geotechnical Engineering,* Paris, France, pp. 677-682

British Columbia Ministry of Transportation, *Bridge Standards and Procedures Manual, Volume 1, Supplement to CHBDC S6-06*, 2007, Vancouver, Canada

Burdette, E.G., Howard, C.S., Ingram, E.E., Goodpasture, D.W., and Deatherage, J.H. (May 22-26, 2004). "Behavior of Prestressed Concrete Piles Supporting Integral Abutments." *Structures Congress and Exposition*, Nashville, TN

Burdette, E.G., Deatherage, J.H., and Goodpasture, D.W. (2007). "Behavior of Laterally Loaded Piles Supporting Bridge Abutments-Phase II." Project Number TNSPR-RES1190, Tennessee Department of Transportation, Nashville, TN

Burke, M.P. (1987). "Bridge Approach Pavements, Integral Bridges and Cycle Control Joints." *Transportation Research Record,* No. 1113, pp. 54-65

Burke, M.P. (1990). "Integral Bridges." *Transportation Research Record,* No. 1275, pp. 53-61

Burke, M.P. (1993). "Integral Bridges: Attributes and Limitations." *Transportation Research Record,* No. 1393, pp. 1-8

Burke, M.P. (June 1993). "The Design of Integral Concrete Bridges." *Concrete International*, Vol. 15, No. 6, pp. 37-42

Burke, M. P. (1994). "Semi-Integral Bridges: Movements and Forces." *Transportation Research Record*, No. 1460, pp. 1-7

Burke, M. P., Jr. (1999). "Cracking of Concrete Decks and Other Problems with Integral-Type Bridges." *Transportation Research Record,* No. 1688, pp. 131-138

Burke, M. P., Jr. (2009). *Integral and Semi-Integral Bridges,* Wiley-Blackwell, Hoboken, NJ

Cakebread, T.J., (July 2011). "The Role of Finite Element Analysis in Bridge Assessment and Design." *6th New York City Bridge Conference*, New York, NY

Canadian Geotechnical Society. *Canadian Foundation Engineering Manual*, 3rd Edition, 1992, Richmond, British Columbia, Canada

Caquot, A., and Kerisel, J. (1948). *Tables for Calculations of Passive Pressure, Active Pressure, and Bearing Capacity of Foundations,* Gauthier-Villars, Paris, France

Chang, M.F. (August 1997). "Lateral Earth Pressures Behind Rotating Walls." *Canadian Geotechnical Journal*, Vol. 34, pp. 498-509

Chen, W., and Saleeb, A. (1983). *Constitutive Equations for Engineering Materials,* John Wiley & Sons, New York, NY

Chen W.F., and Liu, X.L. (1991). *Limit Analysis in Soil Mechanics,* Elsevier

Chen, Y. (1997). "Important Considerations, Guidelines, and Practical Details of Integral Bridges." *Journal Engineering Technology*, pp. 16–19

Chen, W.F., and Duan L. (2000). "Bridge Engineering." CRC Press, New York, NY

Choudhury, D., Subba Rao, K. S., and Ghosh, S. (2002). "Passive Earth Pressure Distribution under Seismic Conditions." *ASCE 15th Engineering Mechanics Conference*, Columbia University, New York, NY

Choudhury, D., and Nimbalkar, S. (2005). "Seismic Passive Resistance by Pseudo-Dynamic Method." *Geotechnique*, Vol. 55, No. 9, pp. 699-702

Chu, V.T.H. (2010). "200 Questions and Answers on Practical Civil Engineering Works." Second edition, http://inventcivil.com/2008/11/200-questions-and-answers-on-practical-civil-engineering-works

Chung, W., and Sotelino, E.D. (2006). "Three-Dimensional Finite Element Modeling of Composite Girder Bridges." *Journal of Engineering Structures*, Vol. 28, Issue 1, pp. 63-71

Clough, G. W., and Duncan, J. M. (1969). "Finite Element Analyses of Port Allen and Old River Locks." Report No. TE-69-3, U.S. Army Engineer Waterways Experiment Station, Vicksburg, MS

Clough, G. W., and Duncan, J. M. (1971). "Finite Element Analyses of Retaining Wall Behavior." *ASCE Journal of the Soil Mechanics and Foundations Division*, Vol. 97, No. 12, pp. 1657-1673

Clough, G. W. and Duncan, J. M. (1991). "Earth Pressures." *Foundation Engineering Handbook, 2nd edition*, Chapter 6, Edited by Hsai-Yang Fang, Van Nostrand Reinhold, New York, NY, pp. 223-235

Coduto, D.P. (1994). *Foundation Design Principles and Practices*, Prentice-Hall, Englewood Cliffs, NJ

Colorado Department of Transportation, *Bridge Design Manual*, 2002, Denver, CO

Cosgrove, E.F., and Lehane, B.M. (2003). "Cyclic Loading of Loose Backfill Placed Adjacent to Integral Abutment Bridges." *International Journal of Physical Modeling in Geotechnics*, Vol. 3, pp. 9-16

Coulomb, C. A. (1776). *Essai sur une Application des Regles de Maximis et Minimum a quelques Problemes de Statique Relatifs a l'Architecture,* Memoires de l' Academie Royale Des Sciences, Paris, France, Vol. 7, pp. 343-382

Crovo, D. S. (April 1998). "The Massachusetts Experience with Jointless Abutment Bridges." *15th Annual International Bridge Conference*, Pittsburgh, PA

CTC & Associates LLC, and Wisconsin Department of Transportation (WisDOT), *Pile/Footing Connections: A Survey of State Practice Transportation Research Report*, 2009, Madison, WI

Dagher, H. J., Elgaaly, M., and Kankam, J. (1991). "Analytical Investigation of Slab Bridges with Integral Wall Abutments." *Transportation Research Record,* No. 1319, pp. 115-125

Dahmani, L., Khennane, A., Kaci, S. (2010), "Crack identification in reinforced concrete beams using ANSYS software", Strength of materials, Vol. 42, No. 2, pp. 232-240
Das, B. M. (1994). *Principles of Geotechnical Engineering,* Third Edition, PWS Publishing Company, Boston, MA

David, T.K., and Forth, J.P. (2011). "Modelling of Soil-Structure Interaction of Integral Abutment Bridges." World Academy of Science, Engineering, and Technology, Year 7, Issue 78, pp. 1075-1080

Day, R. A. and Potts, D. M. (1994). "Zero Thickness Interface Elements-Numerical Stability and Application." *International Journal for Numerical and Analytical Methods in Geomechanics*, Volume 18, Issue 10, pp. 657-734

De Borst R., Remmers J.J.C., Needleman A., Abellan MA. (2004). "Discrete vs smeared crack models for concrete fracture: bridging the gap." *International Journal for Numerical and Analytical Methods in Geomechanics*, Vol. 28, pp. 583–607

Desai, C. S., Zaman, M. M., Lightner, J. G., and Siriwardane, H. J. (1984). "Thin-Layer Element for Interfaces and Joints." *International Journal for Numerical and Analytical Methods in Geomechanics*, Vol. 8, No. 1, pp. 19-43

Desai, C. S., Drumm, E. C., and Zaman, M. M. (1985). "Cyclic Testing and Modeling of Interfaces." *ASCE Journal of Geotechnical Engineering*, Vol. 111, No. 6, pp. 793-815

Desai, C. S., Muqtadir, A., and Scheele, F. (1986). "Interaction Analyses of Anchor-Soil Systems." *ASCE Journal of Geotechnical Engineering*, Vol. 112, No. 5, pp. 537-553

Dicleli, M., Eng, P., and Albhaisi, S.M. (2003). "Maximum Length of Integral Bridges Supported on Steel H-Piles Driven in Sand." *Engineering Structures,* Vol. 25, pp. 1491-1504

Dicleli, M. (2004). "Performance of Abutment-Backfill System under Thermal Variations in Integral Bridges Built on Clay." *Engineering Structures* , Vol. 26, pp. 949-962

Dicleli, M., and Erhan, S. (2008). "Effect of Soil and Substructure Properties on Live-Load Distribution in Integral Abutment Bridges." *ASCE Journal of Bridge Engineering*, Vol. 13, No. 5, pp. 527-539

Dicleli, M., and Erhan, S. (2009). "Live Load Distribution Formulas for Single-Span Prestressed Concrete Integral Abutment Bridge Girders." *ASCE Journal of Bridge Engineering*, Vol. 14, No. 6, pp. 472-486

Doust, E.S. (2011). "Extending Integral Concepts to Curved Bridge Systems." Ph.D. Thesis, University of Nebraska, Lincoln, NE

Drucker, D.C., and Prager, W. (1952). "Soil Mechanics And Plastic Analysis Or Limit Design." Quarterly of Applied Mathematics, Vol. 10, No. 2, pp 157-165

Duncan, J.M., and Chang, C.Y. (1970). "Nonlinear Analysis of Stress and Strain in Soils." *ASCE Journal of Soil Mechanics and Foundations Division*, Vol. 96, pp 1629-1653

Duncan, J. M., and Clough, G. W. (1971). "Finite Element Analyses of Port Allen Lock." *ASCE Journal of the Soil Mechanics and Foundations Division*, Vol. 97, No. 8, pp. 1053-1067

Duncan, J. M., Byrne, P., Wong, K. S., and Mabry, P. (1980). "Strength, Stress-Strain and Bulk Modulus Parameters for Finite Element Analysis of Stresses and Movements in Soil Masses." Report No. UCB/GT/80-01, Department of Civil Engineering, University of California, Berkeley, CA

Duncan, J. M. (1994). "The Role of Advanced Constitutive Relations in Practical Application." *Proceedings of the 12th International Conference on Soil Mechanics and Foundation Engineering,* New Delhi, India, Vol. 5, pp. 31-48

Duncan, J. M., and Mokwa, R. L. (2001). "Passive Earth Pressures: Theories and Tests." *Journal of Geotechnical and Geoenvironmental Engineering,* Vol. 127, No. 3, pp. 248-257

Duncan, J. M., and Arsoy, S. (2003). "Effect of Bridge-Soil Interactions on Behavior of Piles Supporting Integral Abutments." *Transportation Research Record*, No. 1849, pp. 91-97

Dunker, K. F., and Abu-Hawash, A. (August 2005). "Expanding the Use of Integral Abutments in Iowa." *Proceedings Mid-Continent Transportation Research Symposium*, Ames, IA

Dunker, K., and Liu, D. (2007). "Foundations for Integral Abutment Bridges." *ASCE Practice Periodical on Structural Design and Construction*, Vol. 12, No. 1, pp. 22-30

Ebeling, R. M., Mosher, R. L., Abraham, K., and Peters, J. F. (1993). "Soil Structure Interaction Study of Red River Lock and Dam No. 1 Subjected to Sediment Loading." Technical Report ITL-93-3, U.S. Army Engineer Waterways Experiment Station, Vicksburg, MS

Ebeling, R. M., and Mosher, R. L. (1996). "Red River U-Frame Lock No. 1 Backfill-Structure-Foundation Interaction." *ASCE Journal of Geotechnical Engineering*, Vol. 122, No. 3, pp. 216-225

Ebeling, R. M., and Wahl, R. E. (1997). "Soil-Structure-Foundation Interaction Analysis of New Roller-Compacted Concrete North Lock Wall at Mcalpine Locks." Technical Report ITL-97-5, U.S. Army Engineer Waterways Experiment Station, Vicksburg, MS

Ebeling, R. M., Pace, M. E., and Morrison, E. E. (1997). "Evaluating the Stability of Existing Massive Concrete Gravity Structures Founded on Rock." Technical Report REMR-CS-54, U.S. Army Engineer Waterways Experiment Station, Vicksburg, MS

Ebeling, R. M., Peters, J. F., and Mosher, R. L. (1997). "The Role of Nonlinear Deformation Analyses in the Design of a Reinforced Soil Berm at Red River U-Frame Lock No. 1." *International Journal for Numerical and Analytical methods in Geomechanics*, Vol. 21, pp. 753-787

Elbadry, M.M., and Ghali, A. (October 1983). "Temperature Variations in Concrete Bridges." *ASCE Journal of Structural Engineering*, Vol. 109, No. 10

Elgaaly, M., Sanford, T. C., and Colby, C. (1992). "Testing an Integral Steel Frame Bridge." *Transportation Research Record,* No. 1371, pp. 75-82

Emanuel, J. H., and Hulsey, J. L. (1977). "Prediction of the Thermal Coefficient of Expansion of Concrete." *Journal of the American Concrete Institute*, No. 74, pp. 149-155

England, G. L. (1994). *The Performance and Behaviour of Biological Filter Walls as Affected by Cyclic Temperature Changes,* ASCE Geotechnical Special Publication No. 42, pp. 57-76

England, G.L., and Dunstan, T. (1994). "Shakedown Solutions for Soil Containing Structures as Influenced by Cyclic Temperatures." *Proceedings of the 3rd Kerensky Conference; Global Trends in Structural Engineering*. Singapore, pp. 159-170

England, G. L., Dunstan, T., Tsang, C. M., Mihajlovic, N. and Bazaz, J. B. (1995). *Ratcheting Flow of Granular Materials, Static and Dynamic Properties of Gravelly Soils*, ASCE Geotechnical Special Publication No. 56, pp. 64-76

Erhan, S., and Dicleli, M. (2009). "Live Load Distribution Equations for Integral Bridge Substructures." *Engineering Structures,* Vol. 31, No. 5, pp. 1250-1264

Fang, Y.S., Chen, T.J., and Wu, B.F. (August 1994). "Passive Earth Pressures with Various Wall Movements." *ASCE Journal of Geotechnical Engineering*, Vol. 120, No. 8, pp. 1307-1323

Fanning, P. (2001). "Nonlinear Models of Reinforced and Post-tensioned Concrete Beams." *Electronic Journal of Structural Engineering*, (EJGE), Vol. 2

Faraji, S. (1997). "Behavior of Integral Abutment Bridges in Massachusetts." Project UMTC-96-5, Massachusetts Highway Department, Boston, MA

Faraji, S., Ting J.M., Crovo, D., and Ernest, H. (2001). "Nonlinear Analysis of Integral Abutment Bridges." *Journal of Geotechnical and Geoenvironmental Engineering*, Vol. 127, No. 5, pp 454-461

Federal Highway Administration (FHWA) *Integral, No-Joint Structures and Required Provisions of Movement, Technical Advisory T5140.13*, 1980, Washington, DC

Federal Highway Administration (FHWA) *Seismic Design of Highway Bridge Foundations Manual*, 1986, Volume 2, Report No. FHWA/RD-86/102, Washington, DC

Federal Highway Administration (FHWA) *Uncoated Weathering Steel in Structures, Technical Advisory T5140.22*, 1989, Washington, DC

Federal Highway Administration (FHWA) *LRFD Design Example for Steel Girder Superstructure Bridge*, 2003, Report No. FHWA NHI-04-041, Washington, DC

Federal Highway Administration (FHWA) *Comprehensive Design Example for Prestressed Concrete (PSC) Girder Superstructure Bridge with Commentary*, 2003, Report No. FHWA NHI-04-043, Washington, DC

Federal Highway Administration (FHWA) *Connection Details for Prefabricated Bridge Elements and Systems*, 2009, Report No. FHWA-IF-09-010, Washington, DC

Federal Highway Administration (FHWA) Bridge Programs National Bridge Inventory (NBI) Data http://www.fhwa.dot.gov/bridge/britab.cfm

Fennema, J.H., Laman, J.A., and Linzell, D.G. (2005). "Predicted and Measured Response of an Integral Abutment Bridge." *ASCE Journal of Bridge Engineering*, Vol. 10, No. 6, pp. 666-677

FLAC (Fast Lagrangian Analysis of Continua), Itasca Consulting Group, Inc FLAC, Minneapolis, MN, (2000)

Flener, E.B. (2004). "Soil-Structure Interaction for Integral Bridges and Culverts." Thesis, Department of Civil and Architectural Engineering, Structural Design and Bridge Division, Royal Institute of Technology, Stockholm, Sweden

Flores, D. I. (1994). "An Evaluation of Integral Abutment Behavior." Thesis, University of Washington, Seattle, WA

Frosch, R.J., Kreger, M.E., and Talbott, A.M. (2009). "Earthquake Resistance of Integral Abutment Bridges." Report No. FHWA/IN/JTRP-2008/11, Purdue University, West Lafayette, IN

Fu, C.C., (2008). "ENCE 717 Bridge Engineering - Abutment/Pier Design." The BEST Center, University of Maryland, College Park, MD

GangaRao, H., Thippeswamy, H., Dickson, B., and Franco, J. (1996). "Survey and Design of Integral Abutment Bridges." Workshop on Integral Abutment Bridges, Pittsburgh, PA

Gazetas, G. (August 1981). "Indentation of Anisotropic Halfspace by Yielding Circular Foundation." *ASCE Journal of the Engineering Mechanics Division*, Vol. 107, pp. 695-704

Gens, A., Potts, D.M. (1988). "Critical State Models in Computational Geomechanics." *Engineering Computations,* Vol. 5, Issue 3, pp 178-197

Girton, D.D., Hawkinson, T.R., and Greimann, L.F. (1991). "Validation of Design Recommendations for Integral-Abutment Piles." *ASCE Journal of Structural Engineering*, No. 117, pp. 2117–2134

Goel, R.K. (1997). "Earthquake Characteristics of Bridges with Integral Abutments." *ASCE Journal of Structural Engineering*, No. 123, pp. 1435–1443

Goldscheider M. (1984). True triaxial tests on dense sand. In: *Constitutive Relations for Soils*, Gudehus *et al.* editors., Grenoble, pp. 11–54

Gomez, J.E. (2000). "Development of an Extended Hyperbolic Model for Concrete to Soil Interfaces." Ph.D. dissertation, Virginia Tech, Blacksburg, VA

Gomez, J.E., Filz, G.M., and Ebeling, R.M. (2000). "Development of an Improved Numerical Model for Concrete-to-Soil Interfaces in Soil-Structure Interaction Analyses." Technical Report ITL-99-1, US Army Corps of Engineers

Gomez, J.E., Filz, G.M., and Ebeling, R.M (2000). "Extended Load/Unload/Reload Hyperbolic Model for Interfaces: Parameter Values and Model Performance for the Contact between Concrete and Coarse Sand." ERDC/ITL TR-00-7, US Army Corps of Engineers

Goodman, R. E., Taylor, R. L., and Brekke, T. L. (1968). "A Model for the Mechanics of Jointed Rock." *Journal of the Soil Mechanics and Foundations Division*, Vol. 94, No. 3, pp. 637-659

Gouw, T.L. (2001). "Notes on the Application of Spring Constant and Soil Structure Interaction Problem." Seminar on the Advancement and Trend in Soil Structural Engineering in The Third Millennium, Jakarta, Indonesia

Greimann, L. F., Amde, A. M., and Yang, P. S. (1983). "Skewed Bridges with Integral Abutments." *Transportation Research Record*, No. 903, pp. 64-72

Greimann, L.F., Yang, P.S., Edmunds, S.K., and Amde, A.M. (August 1984). "Final Report, Design of Piles for Integral Abutment Bridges." Engineering Research Institute, Department of Civil Engineering, Iowa State University, Ames, IA

Greimann, L.F., Amde, A.M., and Yang, P.S. (1986). "Nonlinear Analysis of Integral Abutment Bridges." *ASCE Journal of Structural Engineering,* Vol. 112, No. 10, pp. 2263-2280

Greimann, L.F., Abendroth, R.E., Johnson, D.E., and Ebner, P.B. (1987). "Pile Design and Tests for Integral Abutment Bridges." Final Report, Iowa Department of Transportation Project HR-273, Ames, IA

Greimann, L., and Amde, A. M. (1988). "Design Model for Piles in Jointless Bridges." *ASCE Journal of Structural Engineering*, Vol. 114, No. 6, pp. 1354-1371

Greimann, L., Phares, B., Faris, A., and Bigelow, J. (June 2008). "Integral Bridge Abutment-to-Approach Slab Connection." Report No. IHRB Project TR-530 & TR-539 Iowa State University, Ames, IA

Griffiths, D. V. (1985). "Numerical Modeling of Interfaces using Conventional Finite Elements." *Proceedings of the 5th International Conference on Numerical Methods in Geomechanics*, pp. 837-844, Nagoya, Japan.

Habibagahi, K., and Ghahramani, A. (1979). "Zero Extension Line Theory of Earth Pressure." *ASCE Journal of the Geotechnical Engineering Division*, Vol. 105, No. 7, pp. 881-896

Hartt, S.L., Sanford, T.C., and Davids, W.G. (August 2006). "Monitoring a Pile-Supported Integral Abutment Bridge at a Site with Shallow Bedrock. Phase II." Report No. ME 01-7, University of Maine, Orono, ME

Harvey, D.I., and Kennedy, D.W. (July 2002). "Integral Abutment Bridges-Design and Constructibility." *6th International Conference on Short and Medium Span Bridges*, Vancouver, Canada

Harvey, D.I. (2012). "Integral Abutment Bridges." harveyd@ae.ca, Associated Engineering, Burnaby, British Columbia, Canada

Hassiotis, S., and Roman, E.K. (June 2005). "A Survey of Current Issues on the use of Integral Abutment Bridges." *Bridge Structures*, Vol. 1, No. 2, pp. 81-101

Hassiotis, S., Khodair,Y., Roman, E.K., and Dehne, Y. (2006). "Evaluation of Integral Abutments." Report No. FHWA-NJ-2005-025, New Jersey Department of Transportation, Trenton, NJ

Hassiotis, S., and Xiong, K. (2007). "Deformation of Cohesionless Fill due to Cyclic loading." University Transportation Centers Program UTRC, SPR ID# C-05-03, Final Report, Department of Civil, Environmental and Ocean Engineering, Stevens Institute of Technology, Hoboken, N.J

Heuze, F. E., and Barbour, T. G. (1982). "New Models for Rock Joints and Interfaces." *ASCE Journal of the Geotechnical Engineering Division*, Vol. 108, No. 5, pp. 757-776

Hibbitt, Karlsson, & Sorensen, Inc. (1998). *ABAQUS Standard User's Manual*, Pawtucket, R.I

Hibbitt, Karlsson, & Sorensen, Inc. (2002). *ABAQUS Standard User's Manual*, Version 6.3, Pawtucket, R.I

Hooper, J.D., Roeder, C.W., Klemencic, R., and Nordquist, K. (January 1999). "Best of Both Worlds." Civil Engineering, pp. 40-42

Hoppe, E.J., and Gomez, J.P. (1996). "Field Study of an Integral Backwall Bridge." Report VTRC 97-R7, Virginia Transportation Research Council, Charlottesville, VA

Hoppe, E.J. (November 1999). "Guidelines for the Use, Design and Construction of Bridge Approach Slabs." Report VTRC 00-R4, Virginia Transportation Research Council, Charlottesville, VA

Hoque, E., Tatsuoka, F., and Sato, T. (1996). "Measuring Anisotropic Elastic Properties of Sand using a Large Triaxial Specimen" *Geotechnical Testing Journal*, Vol. 19, No. 4, pp. 411-420

Horvath, J.S. (2000). "Integral Abutment Bridges: Problems and Innovative Solutions Using EPS Geofoam and other Geosynthetics." Research Report No. CE/GE-00-2, Manhattan College, Bronx, NY

Hu, L. (2004). "Testing and Modeling of Soil-Structure Interface." *Journal of Geotechnical and Geoenvironmental Engineering*, Vol. 130, No. 8, pp. 851-860

Huang, J., French, C., Shield, C. (2004). "Behavior of Concrete Integral Abutment Bridges." Report No. MN/RC-2004-43, University of Minnesota, Minneapolis, MN

Huang, J., Shield, C.K., French, C.E.W. (2008). "Parametric Study of Concrete Integral Abutment Bridges." *ASCE Journal of Bridge Engineering*, Vol. 13, No. 5, pp. 511-526

Husain I, Bagnaroil D. (1996). "Integral Abutment Bridges." Structural Office Report SO-96-01, Structural Office, Ministry of Transportation, Ontario, Canada

Husain, I., and Bagnariol, D. (2000). "Design and Performance of Jointless Bridges in Ontario." *Transportation Research Record*, No. 1696, pp. 109-121

Huyse, L., Hemmaty, Y., and Vandewalle, L. (1994). "Finite Element Modeling of Fiber Reinforced Concrete Beams." Proceedings of the ANSYS Conference, Vol. 2, Pittsburgh, PA

Ibrahim, A.M., Mubarak, H.M. (2009). "Finite Element Modeling of Continuous Reinforced Concrete Beam with External Prestressing." *European Journal of Scientific Research*, Vol. 30, No. 1, pp. 177–186

Itani, A., and Pekcan, G. (2011). "Seismic Performance of Steel Plate Girder Bridges with Integral Abutments." Report No. FHWA-HIF-11-043, Department of Civil and Environmental Engineering, University of Nevada, Reno, NV

James, R.G., and Bransby, P.L. (1970). "Experimental and Theoretical Investigations of Passive Earth Pressure Problem." *Géotechnique*, Vol. 20, No. 1, pp. 17-37

Jardine, R. J., Porrs, D., Fouriea, B., and Burlandj, B. (1986). "Studies on the Influence of Nonlinear Stress-Strain Characteristics of Soil-Structure Interaction." *Geotechnique*, Vol. 13, No. 3, pp. 377-396

Jategaonkar, R., Jaeger, L.G. and Cheung, M.S. (1985). "Bridge Analysis using Finite Elements." Published by the Canadian Society for Civil Engineering

Jendele L, Cervenka J, Saouma V, Pukl R. (2001). "On the Choice between Discrete and Smeared Approach in Practical Structural FE Analyses of Concrete Structures." 4th International Conference on Analysis of Discontinuous Deformation Glasgow, United Kingdom, pp. 203-220

Jorgenson, J. L. (1983). "Behavior of Abutment Piles in an Integral Abutment in Response to Bridge Movements" *Transportation Research Record,* No. 903, pp. 72-78

Hong, J. H., Jung, J. H., You, S. K., and Yoon, S. J. (2003). "A Simplified Numerical Model for an Integral Abutment Bridge Considering the Restraining Effects Due to Backfill." Korea Concrete Institute (KCI) Concrete Journal, Vol. 15, No. 5, pp.759-767

Kachlakef, D., Miller, T, Yim, S., Chansawat, K., and Potisuk, T. (2001). "Finite Element Modeling of Reinforced Concrete Structures Strengthened with FRP Laminates." Final Report SPR 316, Oregon State University, OR

Kaufmann, W., and Alvarez, M. (2011). "Swiss Federal Roads Office Guidelines for Integral Bridges." *IABSE Structural Engineering International Journal*, Vol. 21, No. 2, pp. 189-194

Kamel, M. R., Benak, J. V., Tadros, M. K., and Jamshidi, M. (1995). "Application of Precast, Prestressed Concrete Piles in Integral Abutment Bridges." *Fourth International Bridge Engineering Conference,* Nebraska DOT, the Precast Concrete Associations of Nebraska, and the Center for Infrastructure Research University of Nebraska, Vol. 2, pp. 146-157

Kamel, M. R., Benak, J. V., Tadros, M. K., and Jamshidi, M. (1996). "Prestressed Concrete Piles in Jointless Bridges." *PCI Journal*; Nebraska Department of Roads, Pre-cast Concrete Association of Nebraska, and the Center for Infrastructure Research, University of Nebraska, pp. 56-67

Kerisel, J., and Absi, E. (1990). *Active and Passive Earth Pressure Tables*, Third edition, Balkema Publishers, Rotterdam, Netherlands

Khodair, Y., and Hassiotis, S. (July 16-18, 2003). "Analysis of Pile Soil Interaction." *ASCE 16th Engineering Mechanics Conference*, University of Washington, Seattle, WA

Kim, W., and Laman, J. A. (2010). "Numerical Analysis Method for Long-term Behavior of Integral Abutment Bridges." *Engineering Structures*, Vol. 32, Issue 8, pp. 2247-2257

Kim, W., and Laman, J. A. (2010). "Integral Abutment Bridge Response under Thermal Loading." *Engineering Structures*, Vol. 32, Issue 6, pp. 1495-1508

Knickerbocker, D., Basu, P.K., and Wasserman, E.P. (March 16-18, 2005). "Behavior of Two-Span Integral Bridges Unsymmetrical About the Pier Line." *FHWA Integral Abutment Jointless Bridges Conference*, Baltimore, MD

Koh, T. (2010). "Integration of Stress-Strain Rate Equations of CASM" *International Journal of Railway (IJR)*, Vol. 3, No. 4, pp. 117-122

Kok, S. T., Bujang, B.K., and Gue, S.S. (2009). "A Review of Basic Soil Constitutive Models for Geotechnical Application." *Electronic Journal of Geotechnical Engineering, (EJGE)*, Vol. 14

Komurka, W.E. (2014) "Driven Pile Types Comparison."
http://www.atlaspipepiles.com/images/Products/Pile-Types-Comparison1.pdf

Kunin, J., and Alampalli, S.(June 1999). "Integral Abutment Bridges: Current Practice in the United States and Canada." *Special Report 132, Transportation Research and Development Bureau*, New York State Department of Transportation, Albany, NY

Kunin, J., and Alampalli, S. (2000). "Integral Abutment Bridges: Current Practice in United States and Canada." *Journal of Performance of Constructed Facilities,* Vol. 14, No. 3, pp. 104-111

Kyle, R. M. (2006)). "Cyclic Lateral Load Behaviour of a Pile Cap and Backfill." *ASCE Journal of Geotechnical and Geoenvironmental Engineering*, Vol. 132, No.9, pp. 1143-1153

Lam, I.P., and Martin, G.R. (1986). "Seismic Design of Highway Bridge Foundations. Volume II Design Procedures and Guidelines." Report No. FHWA-RD-86-102, Washington, DC

Lancellotta R. (2002). "Analytical Solution of Passive Earth Pressure." *Geotechnique*, Vol. 52, No. 8, pp. 617-619

Lawver, A., French, C., and Shield, C. K. (2000). "Field Performance of Integral Abutment Bridge." *Transportation Research Record,* No. 1740, pp. 108-117

Lee, J. (2007). "Integral Abutment Bridges Design Background and Practice in US." Technical Seminar at Korea Expressway Corporation, Seoul, South Korea

Lock, R.J. (2002). "Integral bridge abutments." Masters in Engineering Project Report, CUED/DSOILS/STR320, University of Cambridge, United Kingdom

Long, J.H., Olson, S.M., and Stark, T.D. (1998). "Differential Movement at Embankment/Bridge Structure Interface in Illinois." *Transportation Research Board*, Washington, DC

Maberry, S., and Camp, J.D. (March 16-18, 2005). "New Mexico's Practice and Experience in Using Continuous Spans for Jointless Bridges." *FHWA Integral Abutment Jointless Bridges Conference*, Baltimore, MD

Mackey, R.D., and Kirk, D.P. (1967). "At rest, Active and Passive Earth Pressures." *Proceedings of the South East Asian Conference on Soil Mechanics and Foundation Engineering*, Bangkok, Thailand, pp. 187-199

Marto, A., Latifi, N., Janbaz, M., Kholghifard, M., Khari, M., Alimohammadi, P., and Banadaki, A.D. (2012). "Foundation Size Effect on Modulus of Subgrade Reaction on Sandy Soils." *Electronic Journal of Geotechnical Engineering, (EJGE)*, Vol. 17, pp. 2523-2530

Maruri, R., and Petro, S. (2004). "Integral Abutments and Jointless Bridges 2004 Survey Summary." Federal Highway Administration and Constructed Facilities Center at West Virginia University, Morgantown, WV

Massachusetts Department of Transportation (MassDOT), LRFD Bridge Manual, October 2009, Boston, MA

Matlock, H. (1970). "Correlations for Design of Laterally Loaded Piles in Soft Clay." Second Annual Offshore Technology Conference, Houston, TX, pp 577-594

Matlock, H., Bryant, L.M., and Foo, S.H.C. (June 1978). "Simulation of Lateral Pile Behaviour under Earthquake Motion." *ASCE Geotechnical Engineering Division Specialty Conference,* Pasadena, California, United States

Matsui, T., and San, K. C. (1989). "An Elastoplastic Joint Element with its Application to Reinforced Slope Cutting." *Soils and Foundations Journal*, Vol. 29, No. 3, pp. 95-104

Matsuoka, H., and Sun, D. (2006). *The SMP Concept-Based 3D Constitutive Models for Geomaterials*. Taylor & Francis

Matsushima, H. (2003). "Fault-Related Damages and Seismic Bridge Design; Application for 1999 Jiji Earthquake in Japan." *Journal of Earthquake Engineering (JSCE)*

Mayer, M., and Gaul, L. (2008). "Modeling of Contact Interfaces using Segment-to-Segment-Elements for FE Vibration Analysis." *2008 26th IMAC Conference and Exposition on Structural Dynamics*, Society for Experimental Mechanics (SEM), Orlando, FL

Mazindrani, Z.H., and Ganjali, M.H. (1997). "Lateral Earth Pressure Problem of Cohesive Backfill with Inclined Surface." *ASCE Journal of Geotechnical and Geoenvironmental Engineering*, Vol. 123, No. 2, pp. 110-112

Meyerhof, G.G. (1956). "Penetration Tests and Bearing Capacity of Cohesionless Soils." *ASCE Journal of the Soil Mechanics and Foundations Division*, Vol. 82, No.1, pp. 1-19

Mistry, V. (March 16-18, 2005). "Integral Abutment and Jointless Bridges." *FHWA Integral Abutment Jointless Bridges Conference*, Baltimore, MD

Mistry, V. (June 2-4, 2008). "Results of National Survey of Integral Abutments and Jointless Bridges." *International Bridge Conference*, Pittsburgh, PA

Minnesota Department of Transportation (MnDOT), *LRFD Integral & Semi-Integral Abutments LRFD Bridge Design Workshop,* 2007, Saint Paul, MN

Mononobe, N., and Matuo, H. (1929). "On the Determination of Earth Pressures during Earthquakes." *Proceedings World Engineering Conference*, Tokyo, Japan, Vol. 9, Paper No.388

Mosher, R. L.. (1984). "Load Transfer Criteria for Numerical Analysis of Axially Loaded Piles in Sand." US Army Engineering Waterways Experimental Station, Automatic Data Processing Center, Vicksburg, MS

Mosher, R. L., and Dawkins, W. P. (2000). "Theoretical Manual for Pile Foundations." Technical Report TR-00-5, U.S. Army Corps of Engineers, Washington DC

Moulton, L.K., GangaRao, H., and Halvorson, G.T. (1981). "Tolerable Movement Criteria for Highway Bridges." Report No. FHWA/RD-81/162, University of West Virginia, Morgantown, WV

Mourad, S., and Tabsh, S. W. (1998). "Pile Forces in Integral Abutment Bridges Subjected to Truck Loads." *Transportation Research Record*, No. 1633, pp. 77-83

Mourad, S., and Tabsh, S. W. (1999). "Deck Slab Stresses in Integral Abutment Bridges." *Journal of Bridge Engineering,* Vol. 4, No. 2, pp. 125-130

Müller-Breslau H. (1906). Erddruck auf Stutzmauern, Alfred Kroner, Stuttgart

Najib, R. (2002). "Integral Abutment Bridges with Skew Angles." Ph.D. Thesis, University of Maryland, College Park, MD

Najib, R., and Amde, A. M. (June 2010). "Effect of Pile Orientation in Skewed Integral Abutment Bridges." 27*th Annual International Bridge Conference*, Pittsburgh, PA

Najjar, S., Pilakoutas, K., and Waldron, P. (1997). "Finite Element Analysis of GFRP Reinforced Concrete Beams." *Proceedings of the Third International Symposium on Non-metallic (FRP) Reinforcement for Concrete Structures* , Sapporo, Japan, Vol. 2, pp. 519-526

Nakai, T. (2007). " Modeling of Soil Behavior Based on tij Concept." *13th Asian Regional Conference on Soil Mechanics and Geotechnical Engineering*, kolkata, India

National Steel Bridge Alliance (NSBA) Steel Bridge Design Handbook, 2005, Lincoln, NE

Ng, C. W., Springman, S. M., and Norrish, A. R. M. (1998). "Centrifuge Modeling of Spread-Base Integral Bridge Abutments." *Journal of Geotechnical and Geoenvironmental Engineering,* pp. 376-388

Nicholson, B.A., (1998). "Integral Abutments for Prestressed Beam Bridges." Prestressed Concrete Association, Leicester, United Kingdom

Nilsson, M., Eriksen, J., and Veljkovic, M. (July 2008). "Towards a Better Understanding of Behaviour of Bridges with Integral Abutments." *Composite Construction in Steel and Concrete VI International Engineering Conference*, Devil's Thumb Ranch, CO

New Jersey Department of Transportation (NJDOT), *Bridges and Structures Design Manual*, 5th edition, March 2010, Trenton, NJ

New York City Department of Transportation (NYCDOT), *New York City Bridges and Tunnels Annual Condition Report,* 2006, New York, NY

New York State Department of Transportation (NYSDOT), *Bridge Manual,* First edition, January 2008 with 2010,2011, and 2014 addendums, Albany, NY

New York State Department of Transportation (NYSDOT), *Bridge Design (BD) Sheets,* 2010, Albany, NY

Ngo, D. and Scordelis, A.C. (1967). "Finite Element Analysis of Reinforced Concrete Beams," Journal of ACI, Vol. 64, No. 3, pp. 152-163

Obrzud R.F. (2010). "On the use of the Hardening Soil Small Strain Model in Geotechnical Practice." *Numerics in Geotechnics and Structures*, Technical Report, edited by Zimmermann et al., Elmepress International, Lausanne, Switzerland

Oesterle, R.G., Tabatabai, H., Lawson, T.J., Refai, T.M., Volz, J.S., and Scanlon, A. (1998). "Jointless and Integral Abutment Bridges Summary Report." Construction Technology Laboratories, Skokie, IL

Okabe S. (1926). "General theory of earth pressure." *Journal of Japanese Society of Civil Engineering*, Vol. 12, No. 1

Olson, S.M., Long, J.H., Hansen, J.R., Renekis, D., and LaFave, J.M. (2009). "Modifications of IDOT Integral Abutment Design Limitations and Details." Report No. FHWA-ICT--09-054, University of Illinois at Urbana-Champaign, Urbana, IL

Ooi, P.K., Lin, X., and Hamada, H. (2010). "Numerical Study of an Integral Abutment Bridge Supported on Drilled Shafts." *ASCE Journal of Bridge Engineering*, Vol. 15, No. 1, pp. 19-31

Ortigosa, P. (2005). "Seismic Earth Pressure Including Soil Cohesion." *16th International Conference on Soil Mechanics and Geotechnical Engineering*, Osaka, Japan

Ou, C. Y. (2006). *Deep Excavations: Theory and Practice*, Taylor and Francis Group, London,, United Kingdom

Padmarajaiah, S.K. and Ramaswamy, A. (2002) "A Finite Element Assessment of Flexural Strength of Fiber Reinforced High Strength Concrete Prestressed Beams." *Journal of Cement and Concrete Composites*, Vol. 24, No. 2, pp. 229-241

Pande, G.N., Sharma, K.G. (1979) "On Joint/Interface Elements and Associated Problems of Ill-conditioning." *International Journal for Numerical and Analytical Methods in Geomechanics,* Vol. 3, Issue 3, pp. 293-300

Paraschos, A., and Amde, A.M. (Fall/Winter 2010), "State of the Art and State of Design of Integral Abutment Bridges" *Journal of Civil Engineering Practice*, Boston Society of Civil Engineers Section/ASCE, Vol. 25, No. 2, pp. 35-52

Paraschos, A., and Amde, A.M. (February 2011). "Integral Abutment Bridges-A survey on the status of use, problems and costs associated with integral abutment bridges" Better Roads magazine-digital edition

Peck, R.B., and Ireland, H.O. (1961). "Full Scale Lateral Load Test of a Retaining Wall Foundation." *5th International Conference on Soil Mechanics*, Paris, Vol. 2, pp. 453-458

Peck, R.B. (1969). "Advantages and limitations of the Observational Method in Applied Soil Mechanics." *Geotechnique*, Vol. 19, No. 2, pp. 171-187

Peck, R.B., Hanson, W.E. and Thornburn, T.H. (1974). *Foundation Engineering*, John Wiley & Sons, Inc., New York, NY

PLAXIS BV, Plaxis 3D Foundation Material Models Manual, Rhoon, Netherlands

Potgieter, I.C., and Gamble, W.L. (July/Aug 1989). "Nonlinear Temperature Distributions in Bridges at Different Locations in the United States." *PCI Journal,* Vol. 34, No. 4

Portland Cement Association (August 2008). "Material Usage and Condition of Existing Bridges in the U.S."

Prakash, S., and Sharma, H.D. (1990). *Pile Foundations in Engineering Practice*, John Wiley & Sons, Inc., New York, NY

Pranjoto, S., and Pender, M.J. (2003). "Gapping effects on the lateral stiffness of piles in cohesive soil." Proceedings of the Pacific Conference on Earthquake Engineering, Paper No. 96, Christchurch, New Zealand

Priestley, M.J.N., Seible, F., and Calvi, G.M. (1996). *Seismic Design and Retrofit of Bridges*, John Wiley & Sons, New York, NY

Puppala, J.A., Saride, S., Archeewa, E., Hoyos, R.L., and Nazarian, S. (August 2008). "Recommendations for Design, Construction and Maintenance of Bridge Approach Slabs." Report FHWA/TX-09/0-6022-1, University of Texas at El Paso, El Paso, TX

Qian, Xx., Yuan, Hn., Li, Qm., and Zhang, By. (2013). "Comparative Study on Interface Elements, Thin-Layer Elements, and Contact Analysis Methods in the Analysis of High Concrete-Faced Rockfill Dams." *Journal of Applied Mathematics*, Volume 2013, Article ID 320890, 11 pages

Rajashree, S. A. (2001). "Nonlinear Finite-Element Modeling of Batter Piles under Lateral Load." *Journal of Geotechnical and Geoenvironmental Engineering*, Vol. 127, No. 7, pp 604-612

Ramanan, L. (2006). "Simulation of Non-Linear Analysis in ANSYS." ANSYS 2006 India Users Conference

Rankine, W. (1857). "On the Stability of Loose Earth." Philosophical Transactions of the Royal Society of London, Vol. 147, pp. 9-27

Rashid, Y.R. (1968). "Analysis of Prestressed Concrete Pressure Vessels." Nuclear Engineering and Design, Vol. 7, No. 4, pp. 334-344

Rehnman S.E., and Broms B.B. (1972). "Lateral Pressure on Basement Wall: Results From Full-Scale Tests." *Proceedings 5th European Conference on Soil Mechanics and Foundation Engineering*, Vol. 1, pp. 189-197

Richard, R., and Elms, D.G. (1979). "Seismic Behavior of Gravity Retaining Walls." *ASCE Journal of Geotechnical Engineering*, Vol. 105, No. 4

Roscoe, K.H., Schofield, A.N., Wroth, C.P. (1958). "On the Yielding of Soils." *Géotechnique,* Vol. 8, Issue 1, pp. 22-53

Roscoe, K.H., and Burland, J.B. (1968). *On the generalized stress-strain behaviour of wet clay, Engineering plasticity*, Cambridge University Press, Cambridge, United Kingdom, pp. 535-609

Rowe, P. W. (1954). "A Stress-Strain Theory for Cohesionless Soil with Applications to Earth Pressure at Rest and Moving Walls." *Geotechnique*, The Institution of Civil Engineers, London, Vol. 4, No. 2, pp. 70-88

Rowe, P.W., and Peaker, K. (1965). "Passive Earth Pressure Measurements." *Géotechnique*, Vol. 15, No. 1, 57-78

Russell, H. G., and Gerken, L. J. (April 1994). "Jointless Bridges - the Knowns and Unknowns." *Concrete International*, pp. 44-48

Sadrekarimi, J., and Akbarzad, M. (2009). "Comparative Study of Methods of Determination of Coefficient of Subgrade Reaction." *Electronic Journal of Geotechnical Engineering, (EJGE),* Vol. 14, pp. 1-14

Sallam, A. (May 2009). "Application of Finite Element Analysis in Geotechnical Engineering." *Journal of Florida Engineering Society*, pp. 29-31

Sanford, T. C., and Elgaaly, M. (1993). "Skew Effects on Backfill Pressures at Frame Bridge Abutments." *Field Performance of Structures and Nondestructive Evaluation of Subsurface Infrastructure, Transportation Research Record,* No. 1415, pp. 1-10

Sayers, B. H. (2000). "Experimental and Analytical Study of Integral-Abutment Bridges." Iowa State University, Ames, IA

Schanz, T., and Vermeer, P.A. (1998). "Special Issue on Pre-failure Deformation Behaviour of Geomaterials." Géotechnique, Vol. 48, pp. 383-387

Schanz, T., Vermeer, P.A., and Bonnier, P.G. (January 1999). "The Hardening Soil Model Formulation and Verification." *Proceedings Plaxis Symposium* "Beyond 2000 in Computational Geotechnics." Amsterdam, Netherlands, Published by Balkema, pp. 281-296

Schofield, A.N., and Wroth, C.P. (1968). *Critical State Soil Mechanics,* McGraw-Hill, New York, NY

Seed, H.B., and Whitman, R.V. (1970). "Design of Earth Retaining Structures for Dynamic Loads." *Proceedings of the ASCE Specialty Conference on Lateral Stresses in the Ground and Design of Earth Retaining Structures*, pp. 103-147

Seible, F., Hegemier, G., Karbhari, V. M., Wolfson, J., Arnett, K., Conway, R., and Baum, J. D. (2008). "Protection of Our Bridge Infrastructure against Man-made and Natural Hazards." *Structure and Infrastructure Engineering*, Vol. 4, No. 6, pp. 415-429

Sekiguchi, K. R., Rowe, K., and Lo, K. Y. (1990). "Time Step Selection For 6-Noded Nonlinear Joint Element in Elasto-Viscoplasticity Analyses." *Computers and Geotechnics*, Vol. 10, No. 1, pp. 33-58

Shah, S. P., Swartz, S. E., and Ouyang, C. (1995). *Fracture Mechanics of Concrete*, John Wiley & Sons, Inc., New York, NY

Shamsabadi, A., Rollins, K. M., and Kapuskar, M. (2007). "Nonlinear Soil-Abutment-Bridge Structure Interaction for Seismic Performance-Based Design." *Journal of Geotechnical and Geoenvironmental Engineering,* Vol. 133, No. 6, pp. 707-720

Shamsabadi, A., and Yan, L. (2008). "Closed-Form Force-Displacement Backbone Curves for Bridge Abutment-Backfill Systems." *Proceedings of Geotechnical Earthquake Engineering and Soil Dynamics Congress IV Conference*, Sacramento, CA

Shamsabadi, A., and Yan, L. (October 2008). "Dynamic-Soil Abutment-Foundation-Structure Interaction of an Instrumented Skewed Bridge." *12th International Conference of International Association for Computer Methods and Advances in Geomechanics*, Goa, India

Sheng, D., Wriggers, P., and Sloan, S.W. (2007). "Application of Frictional Contact in Geotechnical Engineering." *ASCE International Journal of Geomechanics*, pp. 176-185

Sherif, M. A., Ishibashi, I., and Lee, C.D. (May 1982). "Earth Pressures Against Rigid Retaining Walls." *ASCE Journal of Geotechnical Engineering*, Vol. 110, No. 5, pp. 679-695

Shreedhar, R., Hosur, V., and Chappu, I. (November 2012). "Behavior of Integral Abutment Bridge with and without Soil Interaction." *International Journal of Scientific and Engineering Research (IJSER)*, Vol. 3, Issue 11

Siros, K. A., and Spyrakos, C. C. (1995). "Creep Analysis of Hybrid Integral Bridges." Steel, Concrete, and Wood Bridges, *Transportation Research Record,* No. 1476, pp. 147-154

Sokolovski, V.V. (1965). *Statics of Granular Media*, Pergamon Press, New York, NY

Soltani, A.A., and Kukreti, A.R. (1992). "Performance Evaluation of Integral Abutment Bridges." *Transportation Research Record*, No. 1371, pp. 17-25

Soubra, A.H. (2000). "Static and Seismic Passive Earth Pressure Coefficients on Rigid Retaining Structures." *Canadian Geotechnical Journal,* Vol. 37, No. 2, pp. 463-478

Sprinkel, M.M. (1978). "Systems Construction Techniques for Short Span Concrete Bridges." *Transportation Research Record 665: Bridge Engineering,* Vol. 2, Transportation Research Board, National Research Council, Washington D.C, pp. 226-227

Sridhanya K.V., Rajagopal K., and Lakshmana Rao, C. (2008). "Modelling of Degradation of Clayey Soils under Repeated Loading." *12th International Conference of International Association for Computer Methods and Advances in Geomechanics (IACMAG)*, Goa, India

Stark, T.D., Olson, S.M., and Long, J.H. (1995). "Differential Movement at the Embankment/Structure Interface: Mitigation and Rehabilitation." Report No. IAB-H1, Illinois Department of Transportation, Springfield, IL

Steedman, R.S., and Zeng, X. (1990). "The Influence of Phase on the Calculation of Pseudo-Static Earth Pressure on a Retaining Wall." *Geotechnique*, Vol. 40, No. 1, pp. 103-112

Stewart, C.F. (July 1985). "Highway Structure Approaches." Report No. FHWA-CA-SD-85-05, California Department of Transportation, Sacramento, CA

Suidan, M. and Schnobrich, W. C. (1973). "Finite Element Analysis of Reinforced Concrete." Journal of the Structural Division, ASCE, Vol. 99, No. 10, pp. 2109-2122

Tabatabaei, A. M. (2010). "A Simple Constitutive Model of Soil-structure Interface Using Soil Plasticity." *5th National Congress on Civil Engineering*, University of Mashhad, Mashhad, Iran

Tavarez, F.A., (2001). "Simulation of Behavior of Composite Grid Reinforced Concrete Beams Using Explicit Finite Element Methods." Master's Thesis, University of Wisconsin-Madison, Madison, WI

Terzaghi, K. (1938). "A fundamental Fallacy in Earth Pressure Calculations." *Journal of Boston Society of Civil Engineers*, Boston Society of Civil Engineers, Vol. 23, No. 2, pp. 71-88

Terzaghi, K. (1943). *Theoretical Soil Mechanics,* John Wiley & Sons, Inc, New York, NY

Terzaghi, K. (1955). "Evaluation of Coefficient of Subgrade Reaction." *Geotechnique*, Vol. 5, No. 4, pp. 297-326

Thanasattayawibul, N. (2006). "Curved Integral Abutment Bridges." Ph.D. Thesis, University of Maryland, College Park, MD

Thaanasarttayawibul, J., Amde, A.M., and Paraschos, A., (April 2014) "Effects of Bridge Length and Span Variations in Curved Integral Abutment Bridges" *Journal of Civil Engineering and Construction Technology,* Vol. 5, No. 1, pp. 1-10

Thiagarajan, G., Gopalaratnam, V., Halmen, C., Ajgaonkar, S., Ma, S., Gudimetla, B., and Chamarthi,R. (December 2010). "Bridge Approach Slabs for Missouri DOT. Looking at Alternative and Cost Efficient Approaches." Report OR11.009, University of Missouri, Kansas City, Kansas, MO and University of Missouri, Columbia, MO

Thippeswamy, H. K., Raju, P. R., and GangaRao, H. (1994). "Parametric Study of Single-Span Jointless Steel Bridges." *Transportation Research Record*, No. 1460, pp. 25-36

Thippeswamy, H. K., and GangaRao, H. (1995). "Analysis of In-Service Jointless Bridges." Steel, Concrete, and Wood Bridges, *Transportation Research Record*, No. 1476, pp. 162-170

Thomas, M. E. (1999). "Field Study of Integral Abutment Bridges." M.S. Thesis, Iowa State University, Ames, IA

Thomson, T. A., and Lutenegger, A. J. (1998). "Passive Earth Pressure Tests on Integral Bridge Abutment." *Proceedings of the 4th International Conference on Case Histories in Geotechnical Engineering*, pp. 733-739

Ting, J.M., and Faraji, S. (1998). "Streamlined Analysis and Design of Integral Abutment Bridges." Technical Report, Department of Civil and Environmental Engineering, University of Massachusetts, Lowell, MA

Tomlinson, M. J. (1957). "The Adhesion of Piles Driven in Clay Soils." *Proceedings of the 4th International Conference on Soil Mechanics and Foundation Engineering,* London, England, Vol. 2, pp. 66-71

Tonias, D.E. (1995). "Bridge Engineering: Design, Rehabilitation, and Maintenance of Modern Highway Bridges." McGraw-Hill, New York, NY

Uesugi, M., and Kishida, H. (1985). "Discussion: Cyclic testing and Modeling of Interfaces." *ASCE Journal of Geotechnical Engineering*, Vol. 113, No. 9, pp. 1086-1087

Utomo, P., Syakur, P., and Kikraz, H.R. (2007). "A Review on the Performance of Modified Cam Clay Model in Predicting the Mechanical Behaviour of Heavily Overconsolidated Clay." *Media Teknik Sipil Journal*, Vol. 7, No. 1, pp. 31-40

Vasudevan,G., and Kothandaraman, S. (2011). "Parametric study on Nonlinear Finite Element Analysis on flexural behavior of RC beams using ANSYS." *International Journal of Civil And Structural Engineering*, Vol. 2, No. 1, pp. 98-111

Vermont Agency of Transportation (VTrans), *Integral Abutment Bridge Design Guidelines*, Second edition, October 2008, Montpelier, VT

Vesic, A. B. (1961). "Beams on Elastic Subgrade and Winkler's Hypothesis." *Proceedings 5th International Conference on Soil Mechanic and Foundation Engineering*, Paris, France, pp. 845-850

Vijayvergiya, V. N. (1977). "Load-Movement Characteristics of Piles." *ASCE Proceedings Ports 77 Conference*, Vol. 2, pp. 269-286

Virginia Department of Transportation (VDOT) Integral/Jointless Bridges General Guidelines and Selection General Guidelines, 2007

Vlassov, V.Z., and Leontev, U.N. (1966). *Beams, Plates and Shells on Elastic Foundations,* Translated from Russian and published for NASA and the National Science Foundation by the Israel Program for Scientific Translations, Jerusalem, Israel

Wahls, H.E. (1990). "Design and Construction of Bridge Approaches." NCHRP Synthesis of Highway Practice, *Transportation Research Board*, No. 159, Washington, DC

Wahyuni, A. S., Vimonsatit, V., and Nikraz, H. (2012). "FEM modelling and analysis of reinforced concrete section with lightweight blocks infill." 22nd Australasian Conference on the Mechanics of Structures and Materials, Sydney, Australia, pp. 375-379

Walker, H. (March/April 2013). "Eliminating Bridge Joints - A Preservation Strategy." *HPC Bridge Views magazine*, Issue 70

Wang, J. G., Ichikawa, Y., and Leung, C. F. (2003). "A Constitutive Model for Rock Interfaces and Joints." *International Journal of Rock Mechanics and Mining Sciences*, Vol. 40, No. 1, pp. 41–53

Washington State Department of Transportation (WSDOT), *Bridges Design Manual*, Version M 23-50.06, July 2011, Olympia, WA

Wasserman, E. P., and Walker, J. H. (1996). "Integral Abutments for Steel Bridges." American Iron and Steel Institute, Vol. II, Chapter 5, Highway Structures Design Handbook

Wasserman, E.P. (September–October, 1999). "Tennessee State Route 50 Bridge over Happy Hollow Creek." *PCI Journal*, pp. 26-36

Wasserman, E.P. (May 2001). "Design of Integral Abutments for Jointless Bridges." *Structure magazine*, pp. 24–33

Wasserman, E.P. (April 19-20, 2007). "Integral Abutment Design Practices in the United States." *First U.S.-Italy Seismic Bridge Workshop*, Pavia, Italy

Wei, W. (2009). "Study on Shear Behaviour of Soil-Structure Interface." *International Conference on Engineering Computation*, pp. 127-130

White, H. (September 2008). "Wingwall Type Selection for Integral Abutment Bridges: Survey of Current Practice in the United States of America." *Special Report 154, Transportation Research and Development Bureau*, New York State Department of Transportation, Albany, NY

White, H. (2012). "Research on Integral Abutment Wingwalls." hwhite@dot.state.ny.us, New York State Department of Transportation, Albany, NY

Wikipedia https://en.wikipedia.org/wiki/Von_Mises_yield_criterion

William, K.J. and Warnke, E.P. (1975) "Constitutive model for the triaxial behavior of concrete." *Journal of the International Association for Bridge and Structural Engineering*, Zurich, Switzerland, Vol. 19, pp. 1-30

Winkler, E. (1867). Die Lehre von der Elastizitat und Festiget, Prague Czechaslovakia

Wiss, Janney, Elstner Associates, Inc. (2002). "Synthesis of technical information for Jointless Bridge Construction, Phase I Report."

Wolanski, A.J. (2004), "Flexural behavior of reinforced and prestressed concrete beams using finite element analysis." M.S.Thesis, Marquette University, WI

Wong, P. C., Kulhawy, F. H., and Ingraffea, A. R. (1989). "Numerical Modeling of Interface Behavior for Drilled Shaft Foundations under Generalized Loading." *Proceedings of Foundation Engineering Conference on Current Principles and Practices*, Evanston, IL, ASCE Geotechnical Special Publication 22, pp. 565-579

Wood, D. M. (1991). *Soil Behaviour and Critical State Soil Mechanics*, Cambridge University Press, Cambridge, United Kingdom

Wood, D. M., and Nash, D. (2000). "Earth Pressures on an Integral Bridge Abutment: A Numerical Case Study." *Soils and Foundations,* Japanese Society of Soil Mechanics and Foundation Engineering, Vol. 40, No. 6, pp. 23-38

Wroth, C. P., and Houlsby, G. T. (1985). "Soil Mechanics - Property Characterization and Analysis Procedures." *Proceedings of the 11th International Conference on Soil Mechanics and Foundation Engineering,* Vol. 1, pp. 1-57

Xanthakos, P. (1995). *Bridge Substructure and Foundation Design*, Prentice Hall PTR, Upper Saddle River, NJ

Xanthakos, P. (1996). *Bridge Strengthening and Rehabilitation*, Prentice Hall PTR, Upper Saddle River, NJ

Xu, M. (2005). "The behaviour of Soil Behind Full-Height Integral Abutments." Ph.D Thesis, University of Southampton, United Kingdom

Xu, M., Clayton, C.RI., and Bloodworth, A.G. (2007). "The Earth Pressure Behind Full-Height Frame Integral Abutments Supporting Granular Fill." *Canadian Geotechnical Journal*, Vol. 44, No. 3, pp. 284-298

Yannotti, A.P., Alampalli, S., and White, H.L. (March 16-18, 2005). "New York State Department of Transportation's Experience with Integral Abutment Bridges." *FHWA Integral Abutment Jointless Bridges Conference*, Baltimore, MD

Yang, P.S., Amde, A.M., and Greimann, L.F. (1982). "Nonlinear Finite Element Study of Piles in Integral Abutment Bridges Part 2." Final Report, Iowa Department of Transportation Project HR-273

Yang, P.S., Amde, A.M., and Greimann, L.F. (1985). "Effects of Predrilling and Layered Soils on Piles." *ASCE Journal of Geotechnical Engineering*, Vol. 111, No. 1, pp. 18-31

Yin, Zz., Zhu, H., Xu, Gh. (1995). "A Study of Deformation in the Interface between Soil and Concrete." *Journal of Computers and Geotechnics*, Vol. 17, pp. 75-92

Yuan, Z., and Chua, K. M. (1992). "Exact Formulation of Axisymmetric Interface-Element Stiffness Matrix." *ASCE Journal of Geotechnical Engineering*, Vol. 118, No. 8, pp. 1264-1271

Zaman, M. M., Desai, C. S., and Drumm, E. C. (1984). "Interface Model for Dynamic Soil-Structure Interaction." *ASCE Journal of Geotechnical Engineering*, Vol. 110, No. 9, pp. 1257-1273

Zaman, M. M. (1985). "Evaluation of Thin-Layer Element and Modeling of Interface Behavior in Soil-Structure Interaction." *Proceedings of the 5th International Conference on Numerical Methods in Geomechanics*, Nagoya, Japan, pp. 1797-1803

Zhang, J.M., Shamoto, Y., and Tokimatsu, K. (March 1998). "Evaluation of Earth Pressure under any Lateral Deformation." *Soils and Foundations*, Japanese Geotechnical Society, Vol. 38, No. 1, pp. 15-33

Zienkiewicz, O.C., Best, B., Dullage, C., and Stagg, K. G. (1970). "Analysis of Nonlinear Problems in Rock Mechanics with Particular Reference to Jointed Rock Systems." *Proceedings of the 2nd Congress of the International Society for Rock Mechanics,* Belgrade, Serbia, pp. 8-14